6-1986

Determination and Interpretation of Dispersion of Small Particles in Thermoplastics

Yoshiyuki Suetsugu
University of Tennessee - Knoxville

To the Graduate Council:

I am submitting herewith a dissertation written by Yoshiyuki Suetsugu entitled "Determination and Interpretation of Dispersion of Small Particles in Thermoplastics." I have examined the final electronic copy of this dissertation for form and content and recommend that it be accepted in partial fulfillment of the requirements for the degree of Doctor of Philosophy, with a major in Engineering Science.

James L. White, Major Professor

We have read this dissertation and recommend its acceptance:

Donald Bogue, John F. Fellers, J. E. Spruiell, L. C. Wadsworth

Accepted for the Council:

Carolyn R. Hodges

Vice Provost and Dean of the Graduate School

(Original signatures are on file with official student records.)

To the Graduate Council:

I am submitting herewith a dissertation written by Yoshiyuki Suetsugu entitled "Determination and Interpretation of Dispersion of Small Particles in Thermoplastics." I have examined the final copy of this dissertation for form and content and recommend that it be accepted in partial fulfillment of the requirements for the degree of Doctor of Philosophy, with a major in Polymer Engineering.

James L. White, Major Professor

We have read this dissertation
and recommend its acceptance:

Donald R. Bogue

John F. Fellers

J. E. Spruiell

L. C. Wadsworth

Accepted for the Council:

Vice Provost and
Dean of the Graduate School

DETERMINATION AND INTERPRETATION OF DISPERSION OF SMALL PARTICLES IN THERMOPLASTICS

A Dissertation

Presented for the

Doctor of Philosophy

Degree

The University of Tennessee, Knoxville

Yoshiyuki Suetsugu

June 1986

ACKNOWLEDGMENT

The author is grateful for the continuous advice and encouragement of his advisor, Professor James L. White, during the years of stay in the United States. He would also like to thank the Polymer Engineering Center at The University of Akron for making its facilities available to him.

Appreciation is also extended to Professor Thein Kyu for helpful comments on the small angle light scattering study.

The author also wishes to express his appreciation to Professor N. Nakajima and Dr. K. Min for precious discussions on mixing mechanisms.

Special appreciation is addressed to his colleagues, Mr. K. Kubota, Mr. Y. Morimoto, Mr. S. Montes, Mr. H. J. Kang, Mr. Y. Wang, and Mr. E. Maemura, for their devoted cooperation to the author.

Financial support for this research was provided by Ferro Corporation. The author is also grateful to the members of Ferro Corporation for useful suggestions and discussions.

Appreciation is also expressed to many other friends who made the life of the author in the United States valuable and interesting.

ABSTRACT

It is the purpose of the present research to characterize the particulate structure in the compounds for a range of small solid particulates. These include a wide range of calcium carbonates both in uncoated and coated modes, carbon blacks, uncoated and coated talc, mica, etc. The matrix polymers used are polystyrene and polypropylene.

The present research involves (i) development of methods and the interpretation of them to characterize the state of particles and their structure in plastics, (ii) to determine how these particulate structures are developed in the mixing process.

The primary particulate structure of concern is the state of dispersion. The methods of characterizing the particulates and the state of dispersion used in the present research include (i) sedimentation volume experiment, (ii) optical microscopy, (iii) scanning electron microscopy, (iv) small angle light scattering, and (v) electrical conductivity measurements.

The particulate structure in plastics covers a wide range in size and in quantity. Optical and scanning electron microscopy gives us direct information on particulate structures. The small angle light scattering technique is a new method of charactering the dispersion of small particulates. The primary structure of particulates characterized by these methods is the agglomerate.

Electrical conductivity measurements were used to determine the levels of dispersion for compounds of carbon black. The concept of three-dimensional network structures of particulates was developed associated with this experiment.

TABLE OF CONTENTS

CHAPTER PAGE

PAGE

LIST OF TABLES

TABLE PAGE

LIST OF FIGURES

FIGURE PAGE

FIGURE PAGE

FIGURE PAGE

FIGURE PAGE

FIGURE PAGE

FIGURE PAGE

FIGURE PAGE

FIGURE PAGE

FIGURE PAGE

FIGURE PAGE

FIGURE PAGE

CHAPTER I

INTRODUCTION

In the polymer industry, reinforcement with small particulates, such as calcium carbonate, carbon black, talc, etc., is often used to improve and modify the mechanical properties and performance of polymeric materials.

Many investigators have sought to characterize the state of dispersion of small particulates in compounds. Most earlier investigations are, however, limited to carbon black filled elastomer compounds.

It is the purpose in the present research to characterize the particulate structure in the compounds for a range of small solid particulates. These include a wide range of calcium carbonates both in uncoated and coated modes, carbon blacks, uncoated and coated talc, mica, etc. The matrix polymers used are polystyrene and polypropylene.

The present research involves (i) development of methods and the interpretation of them to characterize the state of particles and their structure in plastics, (ii) to relate this state of particles and interparticle structure to the mechanical behavior of the compounds, and (iii) to determine how these particulate structures are developed in the mixing process.

The primary particulate structure of concern is the state of dispersion. The methods of characterizing the particulates and the state of dispersion used in the present research include

(i) sedimentation volume experiment, (ii) optical microscopy, (iii) scanning electron microscopy, (iv) small angle light scattering, and (v) electrical conductivity measurements. Sedimentation volume experiments characterize interparticle interactions. Other methods characterize the state of dispersion.

The particulate structure in plastics covers a wide range in size and in quantity. Optical and scanning electron microscopy give us direct information on particulate structures. The primary structure of particulates characterized by these methods is the agglomerate.

The small angle light scattering technique is a new method of characterizing the dispersion of small particulates.

Electrical conductivity measurements were used to determine the levels of dispersion for compounds of carbon black. The concept of three-dimensional network structures of particulates was developed.

CHAPTER II

BACKGROUND

A. SEDIMENTATION VOLUME OF PARTICULATES

The sedimentation volumes of the small particulates in liquids reflect the characteristics of particle-particle interactions. The concept of sedimentation volume experiments and their relationship to rheological properties seem to be due to Freundlich et al. (F-5,F-7).

In 1934 Freundlich and Juliusburger (F-7) measured the sedimentation volumes of solnhofen slate (95-96% $CaCO_3$) and quartz powder with pure water and sea water in test tubes. They found that the mixture of the powder and liquid exhibited large sedimentation volume and possessed the rheological properties of plasticity and thixotropy.

Later Freundlich and Jones (F-5) carried out sedimentation volume experiments quite extensively. They employed a range of particulates including graphite, titanium dioxide, calcium carbonate, mica, etc. The determined the rheological properties of suspension in water, HCl, NaOH and NaCl vehicles as well as the sedimentation volumes. They pointed out that mixtures which exhibit large sedimentation volumes possess strong thixotropic and plastic properties.

B. OPTICAL AND ELECTRON MICROSCOPY CHARACTERIZATION OF SMALL PARTICLE FILLED COMPOUNDS

Optical and electron microscopy gives a direct picture of agglomeration and dispersion conditions. The details of individual aggregates and agglomerates can be determined. These methods, however, require tremendous labor to obtain reliable results. Recent developments of image analyzers reduce the amount of labor and human error. Most of the studies in this area have involved carbon black dispersed in rubber.

In 1951, Cohan and Watson (C-4) found carbon black to consist of chain-like aggregates with electron microscopy. This structure could occur by particle coalescence (fusion) during the formative stage in the furnace, where the fused chains form themselves. This fused persistent structure can be eliminated only by extreme methods, such as dry grinding or dry ball-milling of carbon black. The destruction of these coalesced agglomerates is irreversible. The primary aggregates tend to form larger units, so-called agglomerates. Agglomerates are transient structures formed by van der Waals attractive forces. Agglomerate structures can be destroyed by relatively small forces, such as the flow of matrix phase. This structure is reversible (V-4,V-5,V-7).

There have been some attempts which try to characterize the dispersion of filler in a matrix polymer by the microscopy method. Dannenberg (D-1) of Cabot observed the level of dispersion of various elastomers/carbon black compounds with a transmission electron

microscope. The compounds were prepared in a Banbury mixer and subsequently further dispersed in a roll mill. Rotor speed and mixing time were varied. It was reported that carbon black incorporation and dispersion appeared to take place simultaneously, and that chain-like aggregates were practically unchanged after mixing with elastomer.

Leigh-Dugmore (L-2) of Dunlop published methods for evaluating carbon black dispersion with an optical microscope. Thin frozen sections of vulcanized rubber were cut by glass knives and viewed under a light microscope with a micrometer ruled in squares in eyepiece. The magnification range was X70-100. The cross sections of black agglomerates on the sections were measured for a total area of coverage which can be used to derive the percent carbon black dispersion from the known volume fraction of black in the compound.

Stump and Railsback (S-9) developed an optical rating index with a set of standard photomicrographs rated 1 to 10 from a poor to an excellent dispersion. The cut surface of a vulcanized rubber was observed under a light microscope at the magnification of X30. This technique is referred to as the Phillips dispersion rating.

A further development in optical methods has been supported by Medalia (B-4,M-6). They prepared a set of standard photomicrographs arranged according to both the amount of undispersed carbon black and the average size of the agglomerates. The magnification for this technique is X77. In this rating method the letter indicates the size and the cipher the abundance of the undispersed agglomerate.

This two-way classification is more informative than earlier rating methods. This technique is called Cabot dispersion classification.

Heckman and Harling (H-6) observed carbon black aggregates with a transmission electron microscope. They found the graphitic layers oriented into the circumferential direction through aggregates.

Cembrola (C-3) of General Tire measured the dispersion of carbon black by an optical microscopy method (Phillips dispersion rating), surface roughness measurement and electrical conductivity. He found a correlation between the Phillips rating and electrical conductivity. He concluded that the Phillips rating works quite well at intermediate dispersions and loses sensitivity at very good dispersions. It was pointed out that the Phillips dispersion rating and the surface roughness analysis differ from the conductivity measurement in that they are sensitive to the undispersed filler.

There have been few other observations of disoersed particulates in polymer matrices.

Several authors have qualitatively observed the distribution of particles in rubber modified polymers (e.g., HIPS, ABS) by transmission electron microscopy (TEM) (A-1,A-3,M-22,O-2,S-1).

Aoki (A-1,A-3) and Münstedt (M-22) studied ABS (acrylonitrile butadiene styrene graft copolymer). Aoki (A-1,A-3) gave attention to contents of acrylonitrile (A) segments in the acrylonitrile-styrene (AS) molecules. When A contents of the AS molecules grafted on the butadiene phase are different from the A contents of the AS molecules

in the matrix (ungrafted) phase, the polybutadiene globules tend to form agglomerates after deformation in the molten state.

Münstedt (M-22) found that the rubber globules in ABS resine are more separated from each other and less continuous after shearing. He did not give the A contents.

C. ELECTRICAL CONDUCTIVITY OF SMALL PARTICLE FILLED COMPOUNDS

C.1. Experimental Studies of Electrical Conductivity of Small Particle Filled Compounds

Measurements of electrical conductivity for polymer/conductive filler compound is one of the unique techniques of characterizing dispersion. It is generally believed that a sequential structure (so-called three-dimensional network structure or connected chain) formed by conductive filler in compound increases electrical conductivity. This technique is useful especially when electrical conductivity of the filler is much higher than that of matrix polymer. Most of the polymeric resins have electrical conductivities of the order of 10^{-15} or lower. They may be regarded as the insulators in compounds. Examples of conductive fillers are carbon black, various metal particles, etc. The first publication of the electrical conductivities of such systems appears to be Dannenberg's (D-1) in 1952.

C.1.a. Effect of Filler and Matrix. Polley and Boonstra (P-5), in 1957, measured electrical conductivity of carbon black filled rubber compounds. It was reported that conductivity of

compounds sharply increase with loading level of carbon black. They employed carbon black after heat treatment at 1500°C as well as untreated black. Heat treated black compounds showed a conductivity which is 10^6 times higher than that of untreated black compounds, though there was no noticeable difference in the level of dispersion in electron micrographs. They measured the electrical conductivity during elongation. They reported that the conductivity first decreased and then increased as the sample elongated.

Voet et al. (V-2,V-4,V-5,V-6,V-7) measured electrical conductivity of various carbon black compounds to understand carbon black gel structure. They applied relatively low voltage such as 1 to 3 volt/cm or less to carbon black filled systems to avoid complications due to electron tunneling effects.

Voet and Cook (V-5) measured the electrical conductivity of SBR-polybutadiene vulcanizate/carbon black compounds during dynamic deformations. They found that the systems maintain high conductivities at low shear amplitude such as 10^{-3}. The conductivity decreases with increasing amplitude, then reaches a constant low value.

They interpreted the conductivity of carbon black filled elastomers based on the sequential structure of carbon black. They said that the reversible transient carbon black structure is nearly completely destroyed at moderate shear amplitudes such as 0.5, but was restored at lower amplitudes in a dynamic equilibrium between chain destruction and reformation.

Higher structure carbon blacks showed more rapid reformation of transient structure than lower structure blacks after the rest intervals of 24 hours. They suggested that the alignment of persistent structure of high structure blacks occurs at high amplitude. The storage modulus $G'(\omega)$ behaves in a similar manner to electrical conductivity as a function of amplitude, but has a maximum in the low amplitude region instead of at high constant values.

Later, Voet and Aboytes (V-4) gave more attention to the dual structure of carbon black, that is, irreversible fused persistent structure and reversible transient structure. They dispersed two types of carbon blacks, with persistent structure and without (destroyed by ball milling), into a mineral oil. Mineral oil and carbon black were sheared in a double cylindrical cell. The electrical conductivity was measured during shear deformation through the radial direction. It was concluded that the carbon black having no persistent structure formed less transient structure than the other. The conductivity of these systems decreased exponentially with increasing shear rate and reached a minimum constant value asymptotically.

The effect of chemical promoters have been studied (V-6). N-(2-methyl-2 nitropropyl)-4-nitrosoaniline (commercial name: Nitrol by Monsanto) was used as a chemical dispersion promoter in various elastomer/carbon black compounds. The electrical conductivity of the promoted system was remarkably lower than the other system, indicating such compounds formed fewer transient structures. Electron

micrographs of promoted compounds showed better dispersion than unpromoted ones. They argued that the decrease in electrical conductivity is ascribed to the formation of a highly insulating film around the carbon black particle, but not to the chemical interaction of the promoter with the elastomer, reducing its unsaturation, would affect the electrical conductivity of the vulcanizate.

Verhelst et al. (V-2) studied the effect of morphology and structure of carbon blacks on the electrical conductivity of vulcanizates. It was concluded that electrical conductivity of carbon black filled vulcanizates increase with increasing structure and decreasing size of carbon black. They found that most of carbon black compounds show an exponential increase of conductivity with increasing loading level. Ketjenblack EC compound possessed the highest electrical conductivity. They pointed out that the EC black owes its highest conductivity to an extremely low particle density caused by the presence of a large number of hollow-shell particles which was indicated by electron micrographs.

Verhelst et al. (V-2) measured electrical conductivity during uniaxial extension. It was shown that the conductivity of vulcanizates loaded with EC black was practically unaffected by deformation up to 150% in contrast to other blacks which showed substantial decreases of conductivity during extension.

They (V-2) stated that the above mentioned phenomena may be explained by the concept that the conductivity of these systems ascribed to the gap between particles or aggregates and is determined by a process of electron tunneling.

Sircar and Lamond (S-6) studied the effect of carbon black particle size distribution on electrical conductivity. They used three types of carbon blacks differing widely in particle size distribution, but close in electron micrograph surface area and DBP (bibutyl-phthalate) structure index. Broad particle size distribution increased conductivity at the same electron micrograph surface area and structure. They mentioned that this might be ascribed to the abundance of small particles compensating for a few large particles.

The influence of matrix polymers on the conductivity behavior has been studied intensively by Sumita et al (S-13). They employed high density polyethylene, low density polyethylene, polypropylene, nyloy-6, polystyrene, polymethyl methacrylate and SBR as the matrix polymers. Several types of carbon blacks were dispersed with a mixing roller. They reported that the critical volume fraction of carbon black above which the compound increases its conductivity very rapidly is dependent upon matrix polymer as well as types of carbon black. They found a correlation between critical volume fraction and interfacial tension. Critical volume fraction decreases with increasing interfacial tension.

Malliaris and Turner (K-10,M-1) published a unique study on conductivity behavior using powder of polymers and nickel. They mixed polyvinyl chloride (K-10) and low density polyethylene (M-1) powder with nickel powder and compacted at room temperature under a pressure of 1000 kg/cm^2. In the compacted sample, nickel powders were segregated at the boundary of polymeric powders, but did not

penetrate the polymeric powders. The critical volume fraction above which the conductivity increases rapidly was found to decrease with an increase in the ratio of polymeric powder size and metal powder size, R_p/R_m, throughout the range studied from 1 to 16. They presented a theoretical argument that the critical fraction of filler decreases as R_p/R_m ratio increases.

C.1.b. Effect of Mixing. Dannenberg (D-1), in 1952, measured the electrical conductivity of various elastomers/carbon black vulcanizates as a function of mixing conditions. A laboratory Banbury mixer was used to incorporate the black in the rubber, and the amount of mixing in the Banbury and subsequent roll-milling was adjusted to obtain various degrees of dispersion. Rotor speed and mixing time in the Banbury and mixing time in the roll mill were varied. A striking decrease in electrical conductivity was observed as the amount of mixing was increased. By comparing electro micrographs of compounds and electrical conductivity data, he pointed out that increased mixing might provide better distribution of the carbon black aggregates in the rubber matrix without change in size of aggregates.

In 1963 Boonstra and Medalia (B-5) made a more extensive study on electrical conductivity as a function of mixing condition. Carbon blacks were mixed with elastomers on a roll mill. A coaxial probe has been used to measure electrical conductivity of both uncured and cured compounds. Electrical conductivity most rapidly decreased

immediately after incorporation and was still decreasing after a total of 30 minutes of milling.

Boonstra and Medalia also determined the dispersion ratings of the same compounds according to the Cabot system (M-6). The dispersion rating obtained by the Cabot chart showed improvement of dispersion with mixing time and with decreasing conductivity. The relationship between electrical conductivity and Cabot rating was dependent upon types of carbon black. It was found that the conductivity of cured compounds is higher by a factor of 2-10 than the corresponding uncured compounds.

More recently, Henneka and Rotz (H-9) made an on-line measurement of electrical properties of rubber/carbon black compounds during mixing. They used a special mixing rotor which measures electrical properties perpendicular to the flow direction inside of two roll mill chamber. They mentioned that the electrical conductivity measured during mixing is a function of mixing time, rotor speed, carbon black concentration and type of carbon black. They compared the conductivity during mixing and after stopping the rotor for the same compounds. The conductivity increased with time after stopping the rotor. They suggested that this is presumably due to the disorientation of polymer molecules and filler particles during relaxation. They mentioned that the capacitance measured during the mixing process is not significantly affected by the amount of mixing, but is a sensitive function of the loading level of carbon black and type of carbon black.

Cembrola (C-3) measured the dispersion of carbon black in SBR-1500 by three different techniques: electrical conductivity measurement, Phillips dispersion rating, and surface roughness analysis. He employed a B. R. Banbury mixer. He concluded that the electrical conductivity method is relatively insensitive at the early stages of mixing but has a high sensitivity at intermediate and later stages. This method is directly influenced by the dispersed black. The method works only within a narrow range of volume loadings (35-75 phr, that is, 0.15-0.30 in volume fraction) and can only be used for small and intermediate particle size carbon blacks.

Some authors (C-3,H-9) reported that the conductivity appears to go through a maxima in the early stages of mixing, and then decreases slowly for the remainder of the test.

Henneka and Rotz (H-9) gave a brief explanation of this maxima in terms of the probability of forming conductive paths which is governed by size and distribution of filler agglomerates. Both explanations seem incomplete.

Cembrola (C-3) explained this behavior as follows. In the early stages of mixing, the black agglomerates are isolated with few through going paths for electrical conduction. The conductivity is governed by the gaps between agglomerates. As mixing proceeds, the agglomerates disappear, the distance of separation increases, but the conductivity of the matrix increases because of the increase of dispersed black. The maxima in conductivity arises as a result of these two opposing processes.

C.1.c. Effect of Temperature. The effect of temperature on the electrical conductivity of conductive filler compounds has been studied by a number of authors. Electric conductivities of materials are, in general, dependent upon temperature. Some materials possess increasing resistivity (not conductivity) with increasing temperature. Such material has a positive thermal coefficient (PTC). Others possess decreasing resistivity with increasing temperature. This is called a material with negative thermal coefficient (NTC). Most conductive filler compounds possess PTC in contrast to many polymers which show NTC.

Boonstra and Medalia (B-5) determined the activation energy of conductance. It was reported that the activation energy for SBR/carbon black compounds is 14.7-29.3 kJ/mol, the higher values being found for the better dispersions. The activation energies for EPDM compounds were found to be approximately 50% higher than those of SBR.

In a series of experiments, Meyer (M-9,M-10,M-11) looked for a correlation between the magnitude of the PTC effect and various physical characteristics of the polymers studied. It was shown that no correlation exists with heat of fusion, coefficient of thermal expansion, peak crystalline melting point or melting range. Glass transition temperature was directly related to the magnitude of the PTC effect. Meyer also showed that above the peak melting point, polymer degradation occurs, characterized by a rapid oxygen uptake

and a rapid decline of the PTC effect. In nitrogen, the decline was much slower.

Endo (E-3) suggested that the loss in PTC effect above melting temperature is due to flow of matrix.

Klasen and Kubat (K-7) suggested that at lower temperatures the carbon black structure is determined by the crystalline polymer phase. Above the melting temperature, the structure broke up, causing a more homogeneous particle distribution and a sharp increase in resistivity. At still higher temperatures, it was found that the resistivity of high PTC materials decreases. They suggested that this is due to the formation of new structures related with flow of matrix at higher temperatures.

Little has been published on high PTC effects found in noncrystalline polymers. Otsuki and Eguchi (O-4) disclosed high PTC effects in carbon black loaded butyl rubber and/or halogenerated butyl rubber. Wolfer (W-6) described high PTC effects in carbon black filled silicone polymers.

C.2. Theoretical Background of Electrical Conductivity for Bicomponent Systems

Heterogenious materials which are composed of a conductive element (or a conductive phase) and a nonconductive element (or a nonconductive phase) are of our concern here. Carbon black and metal powder filled polymeric materials are of this case. The carbon black and the metal powder are the conductive elements, and the polymeric resins are the nonconductive elements.

There are two distinguished mechanisms of the electrical conduction in such heterogeneous materials. One is the percolation mechanism and the other is the electron tunneling mechanism. The tunnel mechanism is based on more microscopic considerations than the percolation mechanism.

C.2.a. Percolation Theory. Percolation theory has been developed since the late 1950s. The first publication of this appears to be Broadbent and Hammersley (B-7) in 1957. Later percolation theory was employed to explain the conduction of electricity heterogeneous systems by Kirkpatrick (K-4,K-5,K-6), Pike and Seager (P-4), Straley (S-8) and Ohno (O-8).

The concept behind the percolation model is conveniently illustrated in a two-dimensional lattice with some of its sites occupied as shown in Figure II-1. The occupation of sites occur randomly. The occupied sites (+ symbols) tend to be more sequential with increasing the ratio of occupied sites. The occupied sites connect to form extended pathways, and finally form continuous channels that pervade the grid. When occupied sites are conductive, conduction is now allowed.

Two basic types of mechanisms may be distinguished. These are "bond percolation" and "site percolation." In the first, some known fraction of the bonds, distributed at random, are missing from the lattice, and current cannot flow through them. In the second, a known fraction of sites are assumed to be missing. The absence of a

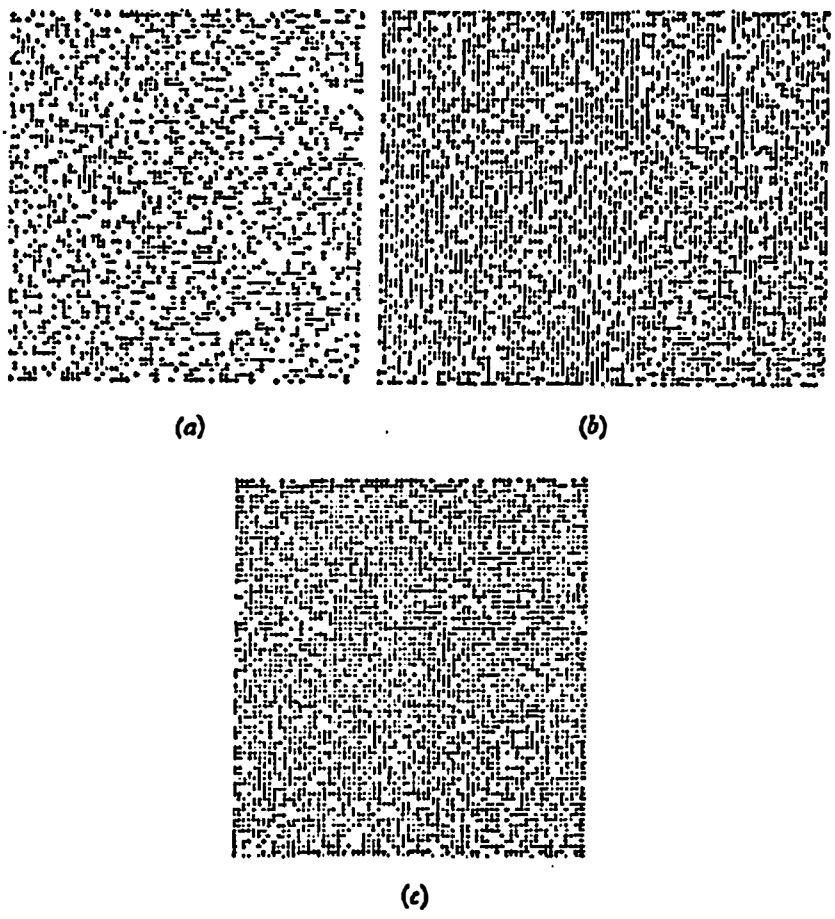

Figure II-1. Site percolation on the square lattice. (a) p smaller than p_c; (b) $p = p_c$; (c) p larger than p_c.

site implies that no current can flow through any of the bonds which join that site to its neighbors.

C.2.a.1. Critical Probability. In the 1960s, the critical probability, p_c, above which there is a nonzero probability of an element being a part of infinitely large cluster (or network) has been determined by various authors (D-10,D-11,E-2,F-8,F-9,O-1,R-6, S-2,S-18,V-8). p is defined as

$$p = \frac{\text{number of occupied sites (bonds)}}{\text{total number of sites (bonds)}} \qquad \text{(II-1)}$$

There are two basic approaches to obtain the critical probability. One is an exact series expansion for the mean cluster size (D-9,D-11,S-17,S-18), another is computer simulation by Monte Carlo methods (F-8,F-9,V-8). The critical probability obtained by various authors is shown in Tables II-1 and 2. The values are dependent upon the dimension and coordination number of the lattices used. p_c increases with decreasing number of dimension and coordination. It is clear that p_c for a one-dimensional lattice is 0.1.

Later, Scher and Zallen (S-2) introduced critical fraction ϕ_c (in their original paper, they use the word space-occupation probability density ρ) for site percolation, corresponding to the packing of sphere (in three dimensions) or circles (in two dimensions). ϕ is defined as

Table II-1. Critical Probability and Critical Fraction for Various Two-Dimensional Lattices (Site Percolation)

Lattice	Coordination Number n	Critical Probability p_c	Filling Factor f	Critical Fraction ϕ_c	Reference
Triangular	6	0.5000	0.9069	0.4534	H-1
		0.493±0.018		0.447±0.016	F-9
		0.51		0.46	D-11
		0.36		0.38	E-2
		(0.50		0.45)	
Square	4	0.59±0.02	0.7854	0.46±0.02	H-1
		0.581±0.015		0.456±0.011	F-9
		0.55		0.43	D-11
		0.48		0.38	E-2
		0.48		0.38	R-6
Kagomé	4	0.6527	0.6802	0.4440	H-1
Honey-Comb	3	0.70±0.02	0.6046	0.42±0.01	H-1
		0.688±0.017		0.416±0.01	F-9
		0.6-0.75		0.36-0.45	D-11
		0.49		0.30	E-2
				$\phi_c \simeq 0.44$	

Table II-2. Critical Probability and Critical Fraction for Various Three-Dimensional Lattices (Site Percolation)

Lattice	Coordination Number n	Critical Probability p_c	Filling Factor f	Critical Fraction ϕ_c	Reference
f.c.c.	12	0.195±0.01	0.7405	0.144±0.01	H-1
		0.204±0.008		0.151±0.006	F-9
		0.18		0.13	R-6
		0.195		0.144	S-17
		0.199		0.147	F-8
h.c.p.	12	0.195±0.01	0.7405	0.144±0.01	H-1
		0.199±0.008		0.147±0.006	F-8
b.c.c.	8	0.24±0.02	0.6802	0.163±0.01	H-1
		0.243		0.165	S-17
s.c.	6	0.31±0.02	0.5236	0.162±0.01	H-1
		0.325±0.023		0.170±0.012	F-8
		0.28		0.15	D-11
		0.28		0.15	R-6
		0.307		0.161	S-17
		0.325		0.170	F-8
				$\phi_c \approx 0.16$	

$$\phi = \frac{\text{total volume (area) occupied by sphere (circle)}}{\text{total volume (area) occupied by sphere (circle)} + \text{total matrix volume (area)}} \qquad \text{(II-2)}$$

In a three-dimensional lattice, ϕ is equivalent to the volume fraction of particles in compound.

It is evident that

$$\phi = f\ p \qquad \text{(II-3)}$$

where f is the filling factor for the lattice. It is quite significant that the critical fraction ϕ_c is not a function of coordination number but is always about 0.16 for a three-dimensional lattice and about 0.44 for the two-dimensional lattice. The critical fraction ϕ_c is calculated using the critical probability p_c obtained by various authors (Tables II-1 and II-2).

It may be interesting here to point out that White et al. (M-19,T-2,T-8) have pointed out that small particle filled polymer compounds tend to have yield stresses when volume fraction of filler is above 0.15. It is noteworthy that the critical volume fraction for yield stress agrees with critical volume fraction for infinitely large cluster (or network) in three dimensions.

C.2.a.2. Percolation Probability. The percolation probability, which denotes a probability of one ultimate particle being a part of infinitely large cluster or connected network, below and above threshold has been determined by several authors (D-2,D-3,F-8,F-9, K-4,K-5,K-6,R-5,S-8) more recently. Frisch et al. (F-8,F-9,V-8)

determined percolation probability P by numerical simulation (Monte Carlo method). Rudd and Frisch (R-5) have pointed out the asymptotic behavior of

$$P_{(p)} = k(p - p_c)^{\beta} \qquad \text{for } p > p_c \tag{II-4}$$

Values of exponent β obtained by Kirkpatrick (K-6) are summarized in Table II-3. These provide a good fit to the results obtained by computer simulation (K-5,K-6).

Table II-3. Values of Exponent β in Three-Dimensional Lattice

Lattice	β
s.c.	0.40-0.35
b.c.c.	0.40-0.30
f.c.c.	0.40-0.33

C.2.b. Percolation Theory and Electrical Conductivity of Small Particle Fitted Compounds

The electrical conductivity of random mix was considered by Kirkpatrick (K-4,K-5,K-6) by replacing occupied sites or bond with electric resistors. He determined the conductivity of the resistor network with the aid of Kirchhoff's current law.

$$\sum_j \sigma_{ij}(v_i - v_j) = 0 \tag{II-5}$$

where σ_{ij} is the conductance of the link between adjacent nodes i and j, v is the voltage at the nodes of each network.

He found (K-5,K-6)

$$G(p) = \frac{\sigma(p)}{\sigma(1)} = P_{(p)} \frac{D(p)}{D(1)} \qquad \text{(II-6)}$$

where

$$D(p)/D(1) = (p - p_c)^{1.1} \qquad \text{(II-7)}$$

where G(p) is normalized conductivity, $\sigma(p)$ is a conductivity at probability of occupancy p. The function D(p)/D(1) corresponds to a nonlinear relation between percolation probability and electric conductivity determined by numerical analysis.

Similarly, Straley (S-8) determined

$$\sigma \propto \sigma_1(p_c - p)^{-s} \qquad \text{for } p < p_c \qquad \text{(II-8)}$$

$$\sigma \propto \sigma_2(p - p_c)^{t} \qquad \text{for } p > p_c \qquad \text{(II-9)}$$

where σ_1 and σ_2 are conductances of matrix and conductive particle, respectively. The exponents s and t determined are 0.5 ± 0.1 and 1.75 → 0.1, respectively, for the three-dimensional site problem. t = 1.75 ± 0.1 is in good agreement with Kirkpatrick's result (K-5, K-6).

C.2.c. Electron Tunneling Theory. The electron tunneling theory concerns the mechanism of electric conduction microscopically compared with the percolation theory (B-2,F-1,H-10,H-11,S-3,S-5). Consider a heterogeneous material in which the conduction regions (or long conducting pathways) are separated by thin insulating barriers.

Quantum considerations show that the electrons which have a certain kinetic energy can pass through insulating barriers which have potential energies larger than the kinetic energy of electrons (B-2). Electron tunneling occurs and the heterogeneous material is regarded as conductive. The probability of breaking through of insulating barrier by electrons is known to show a drastic decrease with increasing the difference between the maxima of potential of barrier and the kinetic energy of electrons (B-2,S-5).

D. SMALL ANGLE SCATTERING

D.1. Experimental Studies of Small Angle Scattering from Small Particulates

Considerable efforts have been made to seek the structure of two-phase systems using small angle scattering methods.

In 1942, Biscoe and Warren (B-1) studied small angle x-ray scattering by three types of carbon blacks. The scattered intensity profiles of these carbon blacks in log I_s versus q angle plot were not linear but were curved in such a way that the slope increases with decreasing scattering angle. They determined the radius of gyration of 210 A for one of the carbon blacks they employed. This could be the size of the carbon black particles which fuse to an aggregate.

Later Riley (R-4) used an x-ray scattering method for an anthracite. The scattering patterns were very singular containing a ring. He suggested that there were particles in contact with one another in the carbon.

Jellinek et al. (J-2) in 1946 measured the scattered intensity of x-ray from an alumina and a carbon black. They determined the size distribution of these particulates by a graphical method.

In 1967, Hendus et al. (H-8) reported that the small angle x-ray diffraction patterns of SBS block copolymer showed discrete diffraction rings corresponding to a spacing of the same order as observed by electron microscopy.

Keller et al. (K-2) studied the structure of extruded SBS block copolymer with 25% polystyrene content with small angle x-ray diffraction. It was pointed out that an extruded sample has the long continuous polystyrene cylinders packed hexagonally along the extrusion direction.

Holland et al. (H-12) pointed out that the scattering of polarized light by randomly oriented, irregular, crystalline silica particles was well approximated by assuming assembled spherical particles with the same size distribution and refractive index. The scattering behavior of suspensions of particles of a few selected shapes has also been investigated and shown to be in reasonable agreement with that predicted for equivalent spheres.

Galanti and Sperling (G-1) determined the structure of the silicone rubber/silica system with the small angle light scattering method. The sizes of the scatterers determined by the small angle light scattering method were two orders of magnitude greater than the dimensions of the individual particles. They suggested that this is due to the agglomeration of filler in rubber. They used the Debye-

Bueche type correlation distances to obtain the sizes of the scatterers.

In 1970, Moritani et al. (M-20) used small angle light scattering for various styrene-isoprene block copolymers and acrylonitrile-butadiene-styrene (ABS) graft copolymers. They found that the correlation distances of the Gaussian type correlation function increases as the concentration of the dispersed spheres decreases, i.e., as the distances between the spheres increase. The size of the spherical domains determined from the Debye-Bueche type correlation distance reasonably agrees with the size of domains determined from electron micrographs.

Later, Tang and Witz (T-4) studied NaCl cubic particles. They concluded that the light scattering behavior of cubic particles can be approximated reasonably well by Mie scattering theory for spheres of equal volume within an error of ±4%. Uemura et al. (U-1,U-2) considered the light scattering from cylindrical objects based upon Mie and Rayleigh-Gans-Born theories.

Yamane (Y-1) studied the gelling process of silicon methoxide solution by means of small angle x-ray scattering. The small angle x-ray curves were analyzed using the Guinier's approximation (G-3, W-4) and Fankuchen's graphical method (F-2,J-1). He concluded that the small particles were first formed, and then they formed the secondary and tertiary agglomerates, step by step.

Matsumoto et al. (M-3) studied light scattering from agglomerated particles in suspension. They employed photosensitive

particles with photo-crosslinking reactions between particles which leads to persistent agglomeration. They reported that both $R_\theta/R_{\theta s}$ and τ/τ_s, where τ and τ_s denote relaxation times of agglomerated and nonagglomerated systems, respectively, increase with increasing irradiation time which promotes photo-crosslinking reaction.

Tabar, Hu and Stein (T-1) measured the radius of gyration for various high impact polystyrenes (HIPS) using Guinier's approximation. They also determined the elongation of the rubber phase during processing.

D.2. Theoretical Background for Small Angle Scattering

D.2.a. General. Considerable effort has been made to develop a theory of scattering to characterize the structure of two-phase or multi-phase systems.

One may proceed to develop scattering theory by presuming a system which satisfies Maxwell's equations both outside and inside the scattering object and the proper boundary conditions on surface of that object. The principal basis of scattering theory was given by Rayleigh (R-2) for dilute small homogeneous spheres which has a small diameter comparing with the wavelength of light.

Rayleigh (R-2) also presented an approximate theory for particles of any shape and size having a small relative refractive index. He applied this to homogeneous spheres, spherical shells, radially inhomogeneous spheres, as well as infinite cylinders. The full formulas for spheres were developed in latter papers by Raleigh (R-2,R-4).

Similar problems were considered by Thompson (T-5) for perfectly reflecting spheres and by Lorentz (L-7,L-8) for small absorbing spheres.

The solution for scattering by a large sphere is generally referred to as the Mie theory. Mie (M-13) was concerned not only with our exposition of the scattering formulas for a sphere but also with a variety of both computational and experimental aspects of the problem.

The scattered waves are coherent. Though incoherent (Compton) scattering will occur too, it can be neglected as only small angles are involved. Coherence means that the amplitudes are added, and the intensity is then given by the absolute square of the resulting amplitude. The amplitudes differ only by their phase, which depends on the position of the electron in space.

When electromagnetic waves are incident on an object, a path difference occurs between the incident beam and scattered beam. Due to this path difference, the scattered waves interfere, thus these waves mutually intensify or reduce their intensity.

The scattered intensity I_s may be

$$I_s = I_e \, F(\underline{q}) \quad F(\overset{*}{\underline{q}}) = I_e |F(\underline{q})|^2 \tag{II-10}$$

where I_e is the Thomson scattered intensity which is generally expressed as

$$I_e = I_o \frac{r_e^2}{r^2} \left[\frac{1 + \cos 2\theta}{2}\right] \tag{II-11}$$

and

$$\underset{\sim}{q} = \frac{2\pi}{} \sin\theta \qquad \text{(II-12)}$$

where 2θ is the scattering angle. $F(\underset{\sim}{q})$ is generally called structure amplitude of the system. We may obtain a general form of $|F(\underset{\sim}{q})|^2$ for the system where the electrons are continuously distributed.

$$|F(\underset{\sim}{q})|^2 = \int_v \rho(\underset{\sim}{r}_k)\, e^{-i(\underset{\sim}{q}\cdot\underset{\sim}{r}_k)}\, dv_k \cdot \int_v \rho(\underset{\sim}{r}_j)\, e^{i(\underset{\sim}{q}\cdot\underset{\sim}{r}_j)}\, dv_j$$

$$= \int_v \tilde{\rho}^2\, e^{i(\underset{\sim}{q}\cdot\underset{\sim}{r}_{ki})}\, dv_{kj} \qquad \text{(II-13)}$$

where

$$\tilde{\rho}^2 = \int_v \rho(\underset{\sim}{r}_j \sim \underset{\sim}{r}_{kj})\rho(\underset{\sim}{r}_i)\, dv_j \qquad \text{(II-14)}$$

Therefore the scattered intensity is given by

$$I_s = I_e \int_v \tilde{\rho}^2(\underset{\sim}{r})\, e^{-i(\underset{\sim}{q}\,\underset{\sim}{r})}\, dv \qquad \text{(II-15)}$$

or

$$I_s = I_e\, \rho^2 \int_0^\infty \overline{V}(r)\, \frac{\sin qr}{qr}\, 4\pi r^2 dr \qquad \text{(II-16)}$$

where ρ is the electron density and V is volume of scatterer.

D.2.b. Scattering from Isolated Particles. Scattering from isolated particles was considered by Rayleigh (R-2). He considered a dilute system in which identical particles of constant electron density ρ were embedded in a medium of constant ρ_0. Since the

particles are widely separated from each other, only a single particle needs to be considered. The scattered intensity from a single sphere which has radius of R_0, volume V and uniform density is given by (R-2).

$$I_s = I_e(\rho - \rho_0)^2 V^2 \left\{ 3 \frac{\sin q R_0 - q R_0 \cos q R_0}{(q R_0)^3} \right\}^2 \qquad \text{(II-17)}$$

Debye (D-4), in 1915, proposed a more general expression for scattered intensity. He assumed that the system is statistically isotropic and there is no correlation between two points separated widely enough. Distribution $\rho^2(\underset{\sim}{r})$ is dependent only upon the magnitude r of the distance. Phase factor $e^{-i\underset{\sim}{q}\cdot\underset{\sim}{r}}$ can be replaced by its average, taken over all directions of $\underset{\sim}{r}$. This is expressed by

$$\langle e^{-i\underset{\sim}{q}\cdot\underset{\sim}{r}} \rangle = \frac{\sin qr}{qr} \qquad \text{(II-18)}$$

Structure amplitude may be given by

$$F(q) = 4\pi \int_0^\infty \rho(r) \frac{\sin qr}{qr} v^2 \, d^r \qquad \text{(II-19)}$$

D.2.c. Guinier Approximation. Guinier (G-4,G-5) proposed an expression of the scattered intensity distribution for small qr values. He obtained

$$\frac{I_s(q)}{I_s(0)} = 1 - \frac{q^2 \langle r^2 \rangle}{6} + \frac{q^4 \langle r^4 \rangle}{120} - \cdots$$

$$\simeq 1 - \frac{q^2 \langle r^2 \rangle}{6}$$

$$\simeq 1 - \frac{R_g^2 q^2}{3}$$

$$\simeq K e^{-R_g^2 q^2/3} \qquad \text{(II-20)}$$

where R_g is a radius of gyration and K is a constant. This leads to

$$\ln I_s(q) = \ln K' - \frac{R_g^2 q^2}{3} \qquad \text{(II-21)}$$

The radius of gyration may be obtained from a slope in $\ln I_s(q)$ versus q^2.

D.2.d. Debye-Bueche Statistical Theory. The approaches previously mentioned as valid only when the geometrical shape of the scattering object is known. When the geometry of the scatterer is

unknown, scattering due to density fluctuations is more necessary to take into consideration.

Debye and Bueche (D-6), and Debye, Anderson and Bramberger (D-5) introduced correlation functions which denote the average of the product of two fluctuations at a distance r.

$$\gamma(r) = \langle \eta(\underset{\sim}{r}_1)\ \eta(\underset{\sim}{r}_2)\rangle / \langle \eta^2 \rangle \qquad \text{(II-22)}$$

where

$$r = |\underset{\sim}{r}_1 - \underset{\sim}{r}_2| \qquad \text{(II-23)}$$

η denotes the fluctuation from average electron density. Correlation function $\gamma(r)$ has the following properties:

$$\gamma(0) = 1 \qquad \text{(II-24)}$$

$$\lim_{r\to\infty} \gamma(r) = 0 \qquad \text{(II-25)}$$

Scattered intensity may be given as

$$I_s = I_e\ V\ \langle \eta^2 \rangle \int_v \gamma(\underset{\sim}{r}) e^{-i(\underset{\sim}{q}\cdot\underset{\sim}{r})} dv \qquad \text{(II-26)}$$

If the system is isotropic, $\gamma(\underset{\sim}{r})$ depends only on the distance r but not on the direction. We may rewrite Eq. (II-26) as

$$I_s = I_e V \langle \eta^2 \rangle \int_0^\infty \gamma(r) \frac{\sin qr}{qr} 4\pi r^2 \, dr \qquad \text{(II-27)}$$

Debye and Bueche (D-6) proposed the correlation function $\gamma(r)$ to be given by an exponential function

$$\gamma(r) = e^{-r/a} \qquad \text{(II-28)}$$

where a is known as correlation distance. Scattered intensity is then:

$$I_s = I_e V \langle \eta^2 \rangle \int_0^\infty e^{-r/a} \frac{\sin qr}{qr} 4\pi r^2 \, dr$$

$$= 8\pi I_e V \langle \eta^2 \rangle \frac{a^3}{(1 + a^2 q^2) q}$$

$$= K \frac{a^3}{(1 + a^2 q^2)^2} . \qquad \text{(II-29)}$$

The physical meaning of the correlation function (Eq. II-28) is that the probability of a point at a distance r in an arbitrary direction from a given point in the scatterer (or in the phase A) will itself also be in the scatterer (or in the phase A). The correlation distance a is a measure of the extension of the inhomogeneities (D-6).

Debye et al. (D-6) applied their correlation function to the Lucite and the glass samples in which the inhomogeneous phases are presumably of random shape and size.

E. SURFACE ANALYSIS

The method of surface analysis is similar to that of the microscopy discussed before. The difference between these methods is that the surface analysis employs relatively low magnification and observes entire roughness of the surface, although the microscopy, especially electron microscopy, pays more attention to observe the microstructure with high magnification.

One of the earliest applications of surface analysis to measure carbon black dispersion was reported by Wiegand (W-4) in 1926. He inspected freshly torn vulcanizate surfaces with hand lens. The technique is based on the diverting of the rupture path by agglomerates of black. This method was refined later using macrophotography along with comparative standards (S-14,S-15,S-16). The light microscope procedure using thin frozen sections of compounds is more quantitative than the torn surface method (L-2,T-6). Later some authors have introduced some techniques (E-1,J-2,V-1).

Recently Ebell and Hemsley (E-1) used DFRL (dark field reflected light) image to analyze the roughness of the surface of compounds. Oscilloscope traces from a line scan across the DFRL images were used to determine the goodness of dispersion in a quantitative manner. They concluded that the standard deviation of peak heights of oscilloscope traces is a better representative index of dispersion than Leigh-Dugmore dispersion rating (L-2) or Cabot dispersion rating, comparing these indices with the various rheological properties of the compounds. Vegvari et al. (V-1) used a similar

technique to determine the goodness of dispersion in carbon black filled rubber compounds. They mentioned a dispersion index derived from the surface roughness traces as follows:

$$DI = 100 - kf^2 \bar{h} \qquad \text{(II-30)}$$

where k is a proportionality constant based on the light microscope dispersion measurements, f is the frequency of roughness peaks per cm of rubber surface, $\bar{h}$ is the average peak height.

The surface analysis technique may be used to estimate the degree of dispersion roughly. However, it is not capable of determining details of the structure of dispersed phase.

The advantage and disadvantage of each measurement are summarized in Table II-4.

F. MECHANISM OF MIXING

Most of the publications on the mechanism of the mixing process have concerned mixing of elastomer compounds of elastomers and carbon black.

F.1. Experimental Studies of Mixing Process

Meder and May (M-8) gave their attention to the incorporation time of carbon black into oil extended SBR. They used Brabender Plastograph as a mixer. The transient Mooney viscosities of the compounds were measured. They found that the compounds in which the incorporation of carbon black take place slowly show a peculiar

Table II-4. Advantage and Disadvantage of the Measurement of Interparticle Agglomeration and Dispersion

Methods	Advantage	Disadvantage
Optical and Electron Microscopy	* Detail of the agglomeration and dispersion is clear	* On line measurement is impossible * Tremendous labor is required to get statistically reliable information
Electrical Conductivity	* On line measurement is possible	* Quantitative theory lacking * Reasonable conductivity difference between dispersed and matrix phase is required
Small Angle Light Scattering	* Theoretical basis is reasonably strong	* Experimental result may be insensitive to the overall shape of agglomerates * Some restrictions on experimental systems
Surface Analysis	* Measurement is relatively easy and rapid	* On line measurement is impossible * Quantitative theory lacking

transient Mooney viscosity. The transient Mooney viscosity shows minima and then increases again. They found that the difference between the maxima and minima of the Mooney viscosity is large when the incorporation process occurs slowly. The reason is not clear.

Tokita and White (T-10,T-11) classified the milling process of the elastomers into four regions. In region I, the elastomer is stiff and resists deformation, and breaks apart after passing through the nip region. In region II, the material is in the rubbery state, and is more easily deformed. An elastic band is formed around the roll. Milling and mixing are most effective in this region. In region III, the band loses tightness, tears easily, or sags. In region IV, a smooth band forms around the roll which is, however, not as elastic as in region II.

Tokita and Pliskin (T-9) and Dizon and Papazian (D-9) measured the transient torques and power consumptions during the mixing processes of the rubber and carbon black compounds in the Brabender and Banbury mixers. They related the characteristics of the transient torques and the steps of the mixing process, i.e., incorporation of filler, dispersion mixing, etc.

Dizon and Papazian (D-9) compared the total energy input with the levels of the dispersion of carbon black (based on the microscopy methods and electrical resistivity measurements) and with the mechanical properties of compounds such as the modulus, the tensile strength and the elongation to break. They found that at a certain level of energy input, both the level of the dispersion and the

mechanical properties of compounds reached plateaus. The total energy input determined to complete such plateaus was roughly 2100 MJ/m^3.

Freakley and Wan Idris (F-4) initiated flow visualization studies of polymeric fluids in an internal mixer using a model mixer with a polymethyl methacrylate window. The behavior of a silicone rubber was investigated.

Nakajima (N-1) considered the energy balance during the mixing process. He classified the total energy into four regions, that is, the energies for the comminution, the macroscopic homogenization, the incorporation and dispersion. He compared these with the power input during the mixing process.

Freakley et al. (F-3,F-4) and more recently Toki et al. (T-7) have followed the motion of elastomers in an internal mixer using strategically placed pressure transducers and following pressure variations with time.

White et al. (W-2) have determined the flow patterns in molten plastics in a two-dimensional single rotor mixer where a rotor moves past a fixed blade. They used several types of blades and found the formations of the vortice near the blades. The size and the location of vortices are dependent upon the types of polymers and the blades.

More recently Min et al. (M-15,M-16,M-17) have carried out the intensive studies of the flow visualization using an internal mixer (Haake Reocord). The front panel and a part of the chamber wall were replaced by glass plates and the flow of elastomer was video taped. They found the stagnant regions between two rotors for the elastomers which possess the small elongation to break.

F.2. Theoretical Background of Mixing Process

Few theoretical works appear to deal with the mixing process. These are mostly limited to dispersive mixing.

McKelvey (M-5) has considered the behavior of an agglomerate which consists of two identical ultimate particles in a simple shear flow. When a particle is located at the origin of the coordinate, the path of the other particle is

$$\left(\frac{x + y}{x_0 + y_0}\right)\left(\frac{y_0}{y}\right) = \exp\left[K\, y_0\left(1 - \frac{y}{y_0}\right)\right]$$

$$2R \leqslant r \leqslant r^* \qquad \text{(II-31)}$$

where

$$K = \frac{6\pi R\sigma}{F_a} \,. \qquad \text{(II-32)}$$

Here

(x_0, y_0) : initial location of a particle

(x, y) : location of a particle

R : radius of a particle

σ : shear stress

F_a : attractive force between two particles

r : center to center distance

r^* : critical center to center distance for the interaction force.

Later, in 1982, Hanas-Zioczower, Nir and Tadmor (M-2) have considered the process of dispersive mixing in the internal mixer. They assumed when hydrodynamic forces acting on the agglomerates

exceed cohesive forces in the agglomerates, the rupture of agglomerates occurs. This is the same as the assumption made by Bolen and Colwell (B-3).

Manas-Zloczower et al. (M-2) have proposed the volume fraction of agglomerates

$$Y_j = \frac{(xt^*)^j}{j!} e^{-xt^*} \qquad j = 0,1,2 \ldots m-1 \qquad \text{(II-33)}$$

where

$$t^* = \frac{t}{\bar{t}} . \qquad \text{(II-34)}$$

Here

Y_j : volume fraction of agglomerates which have experienced j times of rupture

j : number of ruptures which agglomerate experienced

t : mixing time

$\bar{t}$: mean residence time in the well mixed region of the mixer

x : fraction of broken agglomerates during one pass through the gap.

The size of the agglomerates which experienced j times of rupture is given by

$$D_j = 2^{-j/3} D_0 \qquad \text{(II-35)}$$

where D_0 is the size of the initial agglomerates.

We shall call their model of dispersion a rupture model.

In 1982, Shiga and Furuta (S-4) have proposed an onion model of dispersion. In their model, the ultimate particles are peeled off from the surface of the agglomerates when they pass through the high shear rate region. The volume fraction of the agglomerates is expressed by

$$C_n(d_s) \prod_{i=1}^{s} K_i = \sum_{j=0}^{n} P(n,j)\left(\frac{d_n}{d_{n-j}}\right)^3 C_0(d_{n-j}) \prod_{i=1}^{n-j} K_i \qquad \text{(II-36)}$$

where

$$K_i = \frac{d_i}{d_{i-1}} + \frac{\alpha}{3}\frac{d_{i-1}}{d_i^2} . \qquad \text{(II-37)}$$

Here

C_n : distribution function for the volume fraction of agglomerates after n revolutions of rotor

C_0 : initial distribution function for the volume fraction of agglomerates

s : critical number of peel-off

j : number of peel-off

d_j : size of agglomerates experienced j times of peel-off

α : constant.

CHAPTER III

MATERIALS AND SAMPLE PREPARATION

A. MATERIALS

Two polymer matrices were used in our investigation of dispersion. These were a polypropylene (Himont Profax 6523) and a polystyrene (Dow Styron 678D). According to the technical data furnished by the suppliers, M_w = 300,000 and M_n = 50,000 for polypropylene, and M_w = 240,000 and M_n = 80,000 for polystyrene.

A wide range of particulates are involved in this program. These cover a range of sizes, shapes, surface coatings, etc. We have used a total of 23 kinds of particulates. Specifically, they include five calcium carbonates, six stearic acid surface coated calcium carbonates, four carbon blacks, two types of glass beads, talc and silane treated talc, three wollastonites, and mica. Among these particulates, calcium carbonates cover the widest range of particle size.

The physical characteristics of the particles are summarized in Tables III-1 and III-2 as furnished by suppliers. Tables III-1 and III-2 represent isotropic particulates and anisotropic particulates, respectively. Average particle diameters mentioned in these tables were determined by transmission electron microscopy (TEM) by each supplier.

Table III-1. Characterization of Isotropic and Anisotropic Particles Studied in This Program

Type	Supplier	Grade	Density (g/cm^3)	BET Surface Area (m^2/g)	Average Diameter (μm)	Coating	DBP* Absorption ($cm^2/100g$)
Calcium Carbonate	Pfizer	Marble White 325	2.71	1.2	17	-	-
		Vicron	2.71	8.0	0.4	-	-
		Albaglos	2.71	8.0	0.4	-	-
		Multifex MM	2.71	20	0.07	-	-
		Phinyl 402	2.71	-	5.0	Stearic Acid	-
		Hi-Pflex	2.71	3.5	3.0	Stearic Acid	-
		Super-Pflex	2.71	6.0	0.5	Stearic Acid	-
		Ultra-Pflex	2.71	20	0.07	Stearic Acid	-
	Thompson Weinman	Atomite	2.71	2.8	3.0	-	-
		Kotamite	2.71	2.8	3.0	Stearic Acid	-
		Supercoat	2.71	7.7	1.0	Stearic Acid	-
Carbon Black	Huber	N990	1.8	8	0.32	-	42
		N326	1.8	80	0.026	-	71
		N351	1.8	78	0.028	-	121

Table III-1 (continued)

Type	Supplier	Grade	Density (g/cm^3)	BET Surface Area (m^2/g)	Average Diameter (μm)	Coating	DBP* Absorption ($cm^2/100g$)
Carbon Black	Continental Carbon	FEF-LS N542	1.8	-	0.045	-	-
Glass Bead	Ferro	PF-10-R	2.5	-	60?	-	-
		PF-10-S	2.5	-	60?	-	-

*Dibutylphthalate.

Table III-2. Characterization of Anisotropic Particles Studied in This Program

Type	Supplier	Grade	Density (g/cm^3)	BET Surface Area (m^2/g)	Average Diameter (μm)	Coating
Talc	Pfizer	CP 10-40	2.75	-	1.9	-
		Micro Pflex	2.75	-	1.5	Silane
Mica	English Mica	Micro Mica C-3000	2.84	-	(5-10)x0.5	-
Wollastonie	R. T. Vanderbilt	Vansil W-10	2.9	-	20	-
		Vansil W-20	2.9	-	11	-
		Vansil W-30	2.9	-	6	-

B. PREPARATION OF SAMPLES

The matrix polymer (polypropylene and polystyrene) and the particulates were mixed using both a two roll mill (Farrel Corp.) and an internal mixer (C. W. Brabender Plastograph). The rolls of the Farrel two roll mill have a diameter of 3 inches and 7 inches in length. Roll speeds during mixing were 20 ft/min and 6 ft/min for front and real rolls, respectively.

A C. W. Brabender internal mixer with CAM rotors is used. The capacity of mixing chamber is about 70 cm^3. The rotational speeds during mixing were 25 rpm and 50 rpm. Machine dimensions and mixing conditions are summarized in Table III-3. Figures III-1 and III-2 show the photographs of the two roll unit and the internal mixer used in this study. The CAM rotor is sketched in Figure III-3.

The compounding procedure was as follows. All fillers were dried in a vacuum oven at 100°C for 24 hours. The matrix polymer was first melted on the roll of two roll mill or in the chamber of the internal mixer. Filler was then added. The period to introduce filler into the matrix polymer phase is dependent upon the amount and types of fillers. The mixing times were determined from the instant that all filler had been taken into the polymer phase. This was determined by observations from the top of the internal mixer chamber. It should be noted that we did not start counting mixing time immediately after the filler was added, but after all filler was taken into the polymer phase. The mixing procedure is summarized in Figure III-4.

Table III-3. Machine Dimensions and Mixing Conditions

Method	Conditions
Two roll mill (TRM) (manufactured by Farrel)	Roll diameter - 3 inches Roll length - 7 inches Mill roll speeds Front - 20 ft/min Rear - 7 ft/min Nip distance - variable
Internal Mixer (IM) (manufactured by C. W. Barbender - Plastograph)	Rotor type - CAM Chamber capacity - 70 cm^3 Rotational speed - 25 rpm or 50 rpm Distance between rotor tip and chamber - 0.105 cm Rotor radius - 1.855 cm

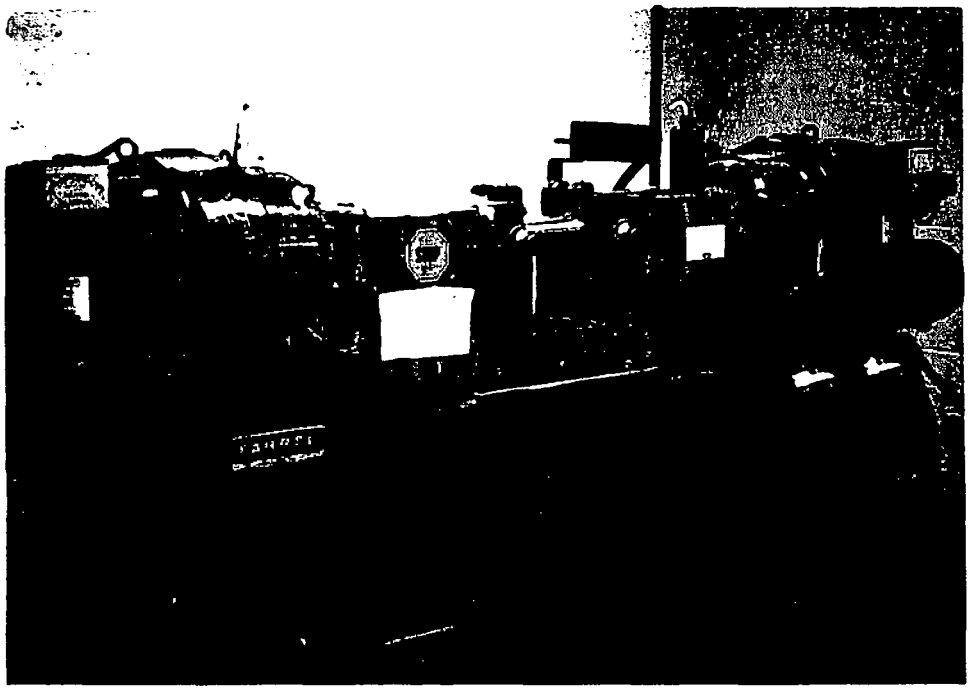

(a) Overall View

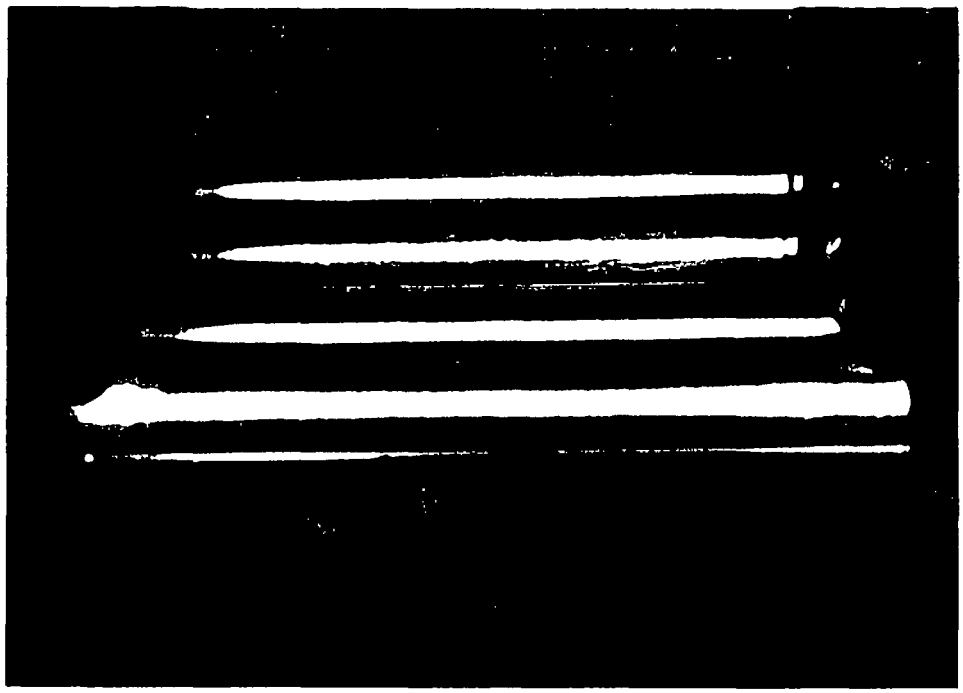

(b) Rollers

Figure III-1. Two roll mill. (Farrel)

(a) Overall View

(b) CAM Rotors

Figure III-2. Internal mixer. (C. W. Brabender Plastograph)

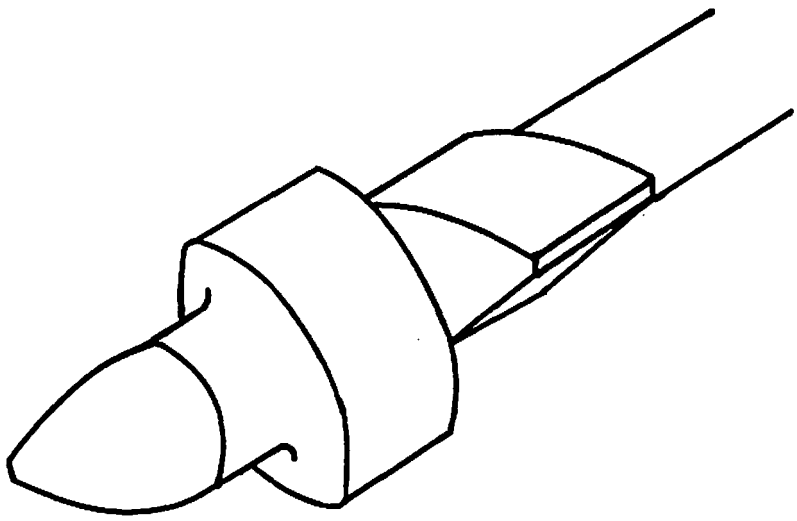

Figure III-3. Schematic drawing of CAM rotor.

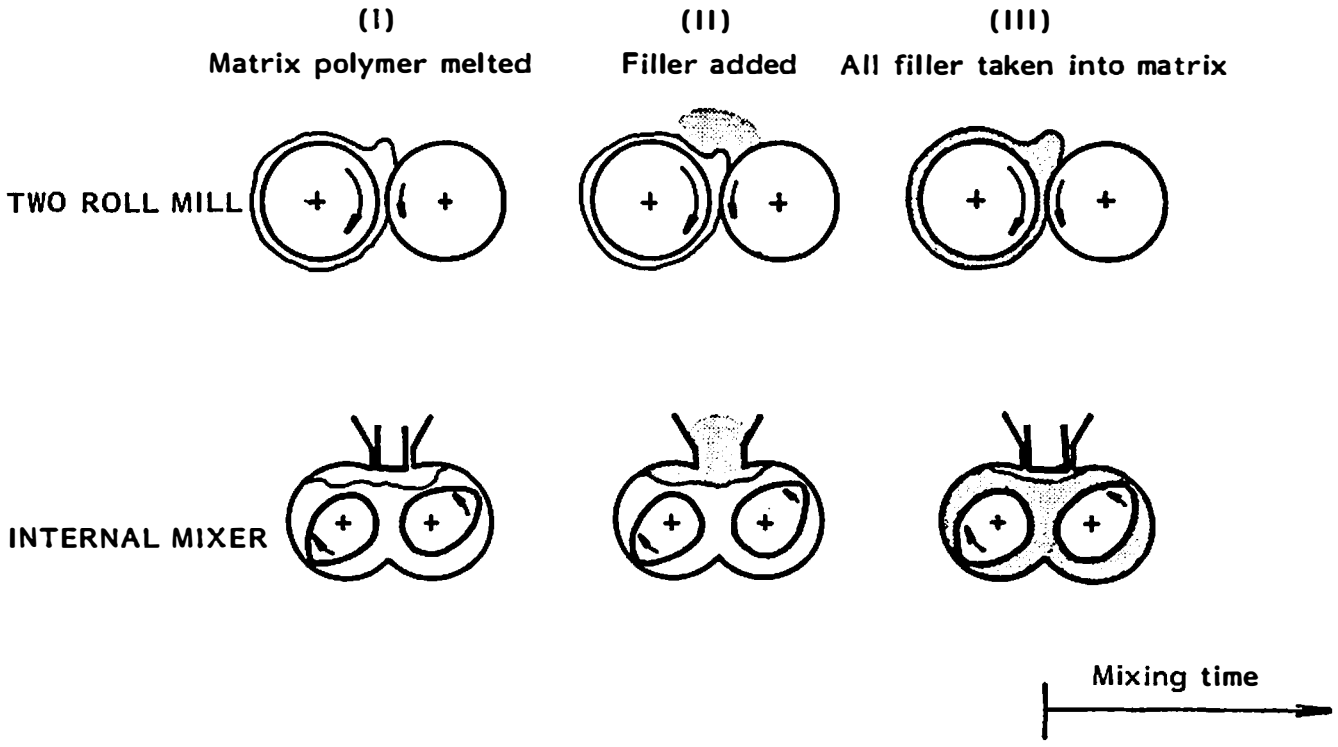

Figure III-4. Mixing processes in the present research.

The standard mixing temperatures in this study are 175°C for polypropylene, and 150°C for polystyrene. The mixing times were 20 minutes for two roll mill, and 0 to 20 minutes for the internal mixer.

The volume fraction of fillers was determined from

$$\phi = \frac{W_f/\rho_f}{W_f/\rho_f + (1 - W_f)/\rho_p} \qquad \text{(III-1)}$$

where W_f is the weight fraction of filler, ρ_f is the density of the filler, and ρ_p is the density of matrix polymer at 180°C. The volume fraction of the compounds prepared varied from 0.05 to 0.30.

Mixes were removed from mixers and broken into small pieces. These were compression molded at 200°C. The thickness of compression molded films was ∿100 μm for optical microscopy and for small angle light scattering (SALS), and 0.36 mm for the electric conductivity measurement. Ferro type stainless steel plates (Photo Materials Inc.) were used in the compression molding process to obtain a smooth surface. Films were quenched in water after compression molding.

Six types of ABS resins were employed to compare their rheological characteristics with the small solid particle filled polymer melts.

CHAPTER IV

RHEOLOGICAL PROPERTIES OF POLYMER MELTS AND THEIR COMPOUNDS

A. INTRODUCTION

This study contains an experimental study of the rheological behavior of polymer melts and their particle filled compounds. The materials include polystyrene, polypropylene, calcium carbonate filled polystyrene and ABS (acrylonitrile-butadiene-styrene block copolymer) resins which consist of SAN (styrene-acrylonitrile) thermoplastics with crosslinked polybutadiene glubules which have been grafted to the matrix during the polymerization process.

The measurements we present were obtained on a capillary rheometer (Monsanto Processability Tester) and in a cone-plate instrument (Rheometrics Mechanical Spectrometer). Steady state shear viscosity $\eta(\dot{\gamma})$ and dynamic measurements of storage and loss moduli $G'(\omega)$ and $G''(\omega)$ and dynamic viscosity $\eta'(\omega)$ have been determined. The measurements of $\eta(\dot{\gamma})$ include both the capillary rheometer and the cone-plate rheometer. $G'(\omega)$, $G''(\omega)$ and $\eta'(\omega)$ were determined by oscillating the cone relative to the plate in the cone-plate instrument. We also report extrudate swell behavior of calcium carbonate filled polystyrene compounds.

B. POLYMER MELTS

B.1. Results

Steady state viscosity behavior of unfilled polypropylene and polystyrene are given as a function of shear rate in Figure IV-1. The measurement temperatures are 175°C for polypropylene and 150°C, 180°C, and 210°C for polystyrene. Polystyrene changes viscosity drastically with temperature.

B.2. Discussion

These resins were used as matrix polymers to make small particle filled compounds. The standard mixing temperature during mixing both in a two roll mill and an internal mixer was 175°C for polypropylene and 150°C for polystyrene. We note that polystyrene has a greater viscosity than polypropylene at the mixing temperature.

C. CALCIUM CARBONATE FILLED THERMOPLASTICS

C.1. Results

The characteristics of the steady state shear viscosity of calcium carbonate filled polystyrene compounds are shown in Figures IV-2 through IV-4. The low shear rate viscosity data in these figures are quoted from the M.S. thesis by Suetsugu (S-10), and Suetsugu and White (S-11).

Figure IV-2 shows the steady state shear viscosity of the various uncoated calcium carbonate filled polystyrene compounds. The volume fractions ϕ of these compounds are 0.30 and the nominal

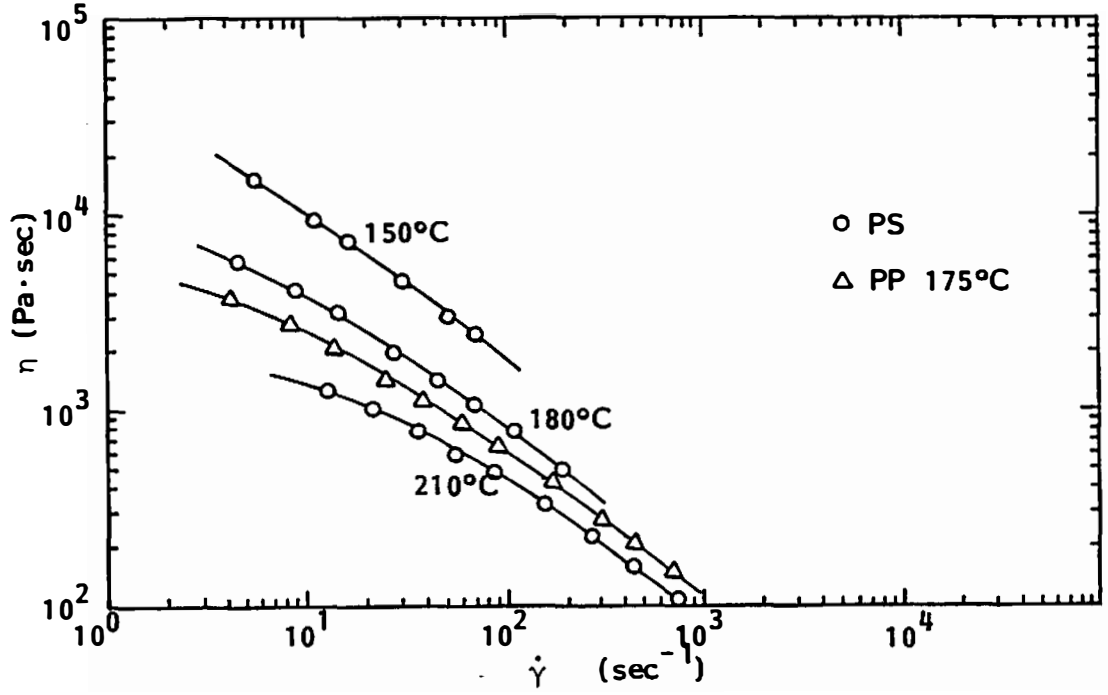

Figure IV-1. Steady shear viscosity as a function of shear rate for unfilled PP and PS.

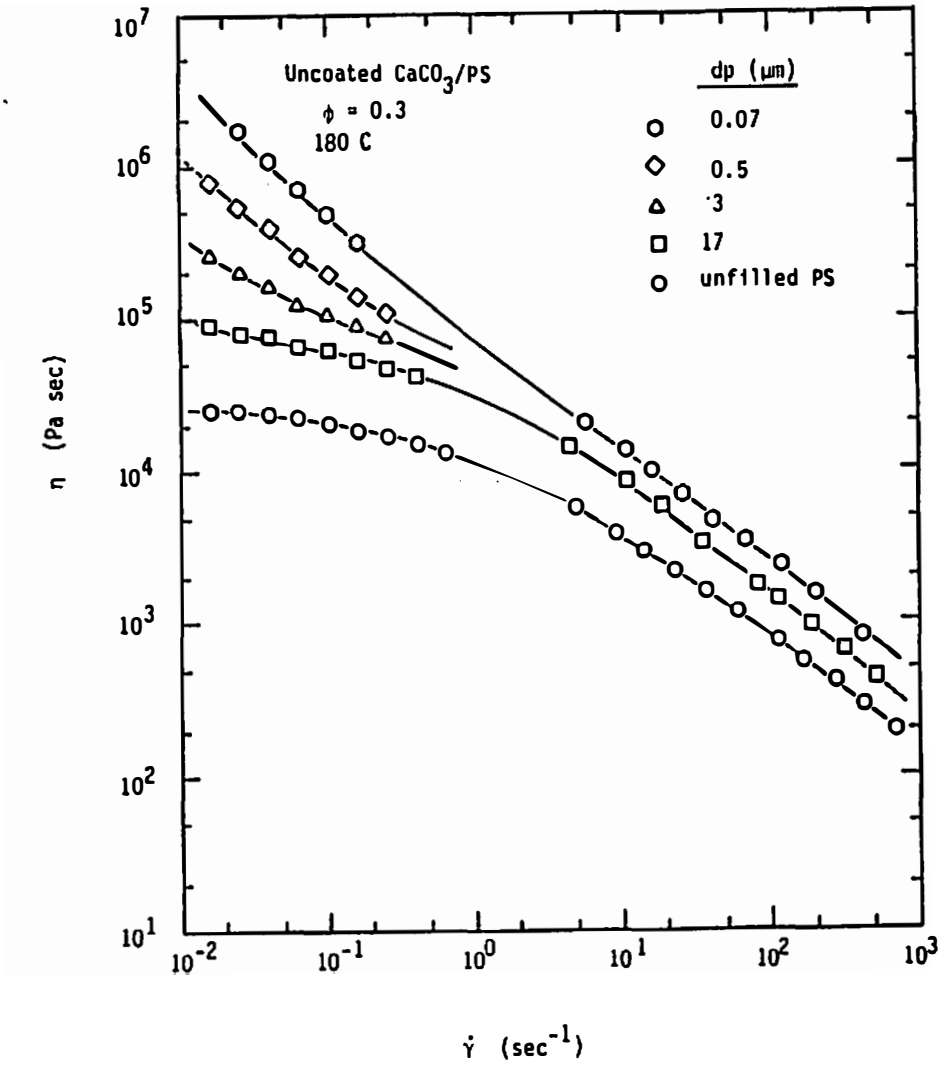

Figure IV-2. Shear viscosity of uncoated calcium carbonate filled polystyrene as a function of shear rate.

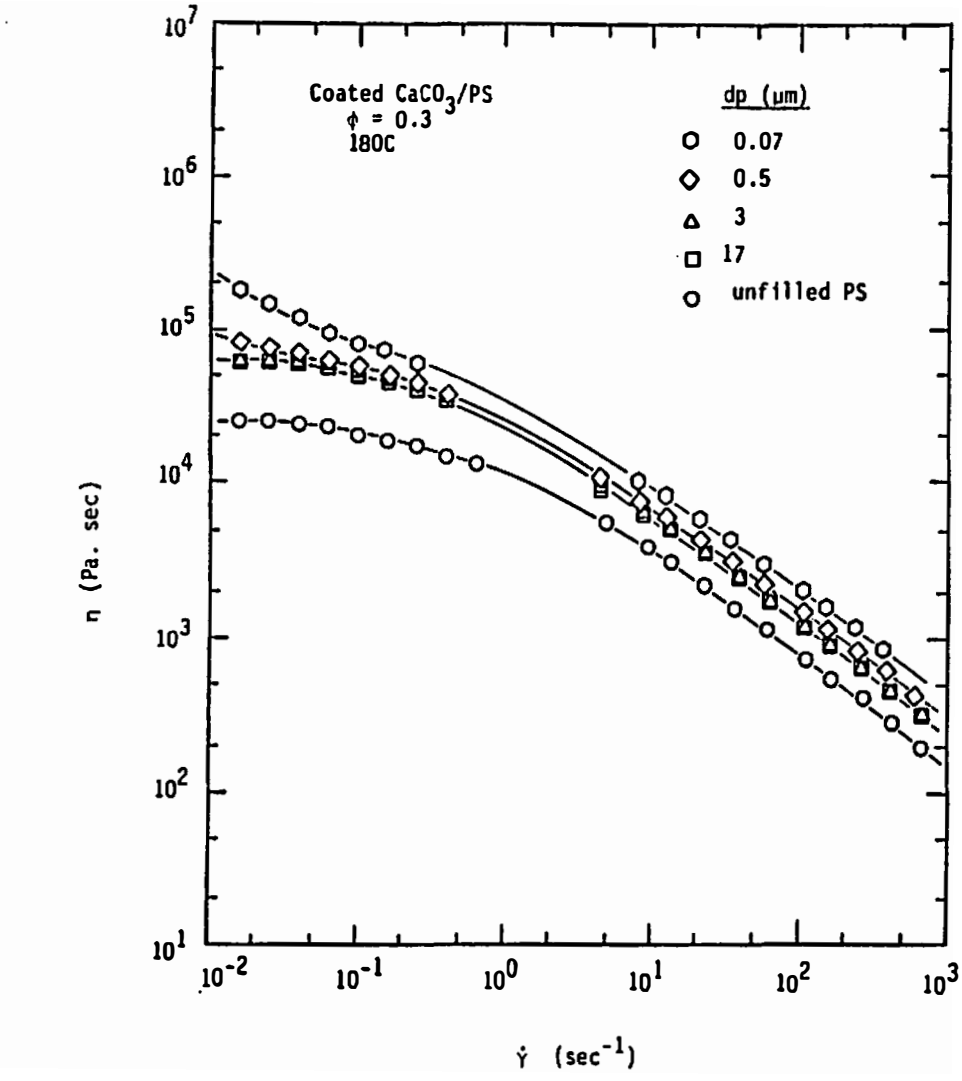

Figure IV-3. Shear viscosity of stearic acid coated calcium carbonate filled polystyrene as a function of shear rate.

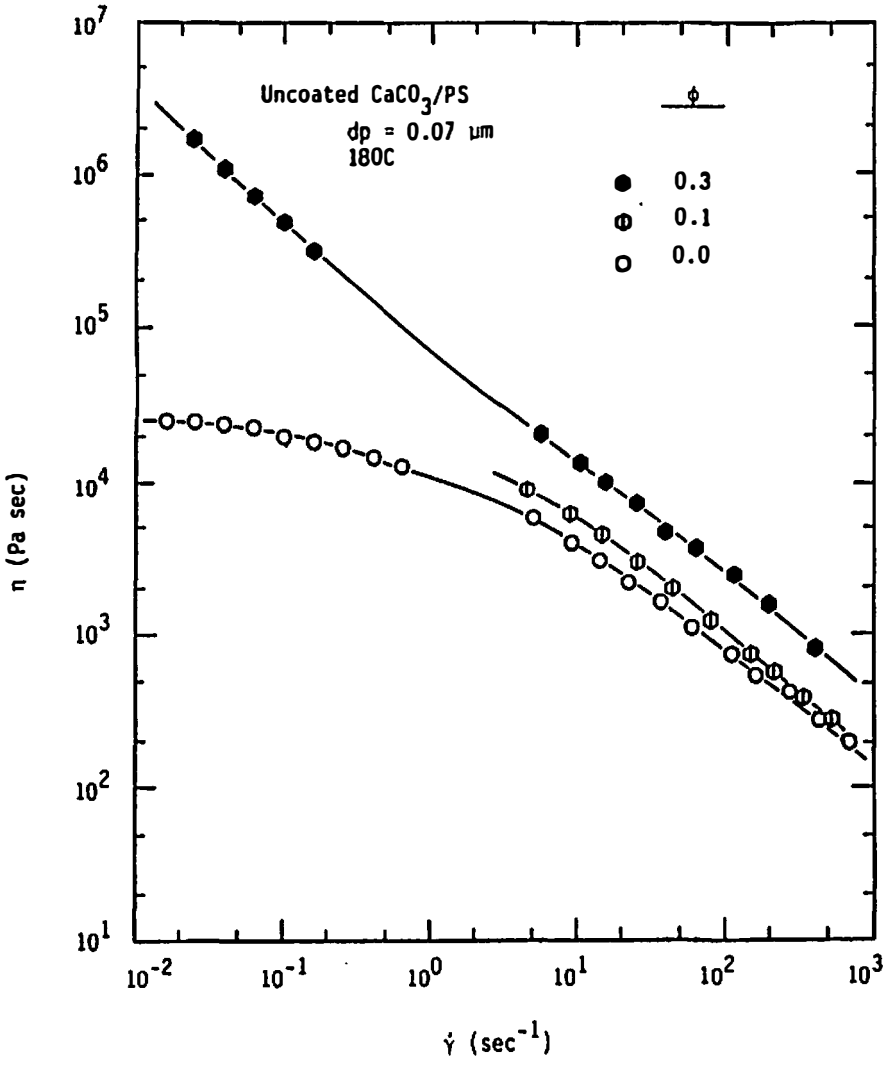

Figure IV-4. Shear viscosity of uncoated calcium carbonate filled polystyrene as a function of shear rate.

particle sizes of calcium carbonate are 0.07, 0.4, 3.0, and 17 μm. The measurement temperature is 180°C.

The unfilled polystyrene exhibits a Newtonian region at the low shear rate region. Uncoated calcium carbonate filled polystyrene compounds, however, show non-Newtonian behavior over all the shear rate range. The viscosity difference between the filled systems and the unfilled system is the greatest in the low shear rate region. This behavior is pronounced in the samples with the smaller average particle size. This indicates the existence of the yield stress.

Figure IV-3 shows the viscosity of stearic acid coated calcium carbonate filled polystyrene. Again volume fraction of filler is 0.30 for all compounds. It is clear that the stearic acid coating of calcium carbonate reduces the viscosity of compounds remarkably, especially in the low shear rate region. This implies that the yield stress is reduced remarkably by stearic acid coating.

The effect of volume loading level is shown in Figure IV-4 for uncoated calcium carbonate filled polystyrene with average particle size of 0.07 μm. Volume fractions of filler are 0.0, 0.10, and 0.30. (The low shear rate data are not plotted for ϕ = 0.10.) The shear viscosity is reduced with decreasing loading level of filler.

C.2. Discussion

The rheological properties of small particle filled polymer melts are strongly dependent upon the type, shape, size, volume fraction and surface coating of the filler. This was reported and

discussed extensively by the earlier authors (A-1,A-2,A-3,C-1,H-2,H-3, H-4,L-1,L-6,M-18,M-19,M-21,M-22,M-23,P-2,P-3,S-10,S-11,S-12,T-3).

The yield stress of the calcium carbonate/polystyrene compounds have been reported by Suetsugu and White (S-11). The yield stress decreases roughly inversely with increasing particle size. The stearic acid surface coating of calcium carbonate reduces the yield stress.

D. ABS RESINS

D.1. Results

Figures IV-5 through IV-7 exhibit the characteristics of ABS resins. Figure IV-5 shows the dynamic viscosity η' as a function of frequency. The content of rubber in ABS resins varies from 0.05 to 0.30. The Newtonian region in the low shear rate region disappears with increasing content of rubber.

The viscosity increases with increasing level of rubber globule. This behavior is pronounced in the low frequency region. ABS resins with high rubber content exhibit yield stresses (see Figure IV-5).

Storage moduli G' and loss moduli G" of ABS resins are exhibited in Figures IV-6 and IV-7, respectively. Both storage and loss moduli increases as rubber content increases. This is more pronounced in the low frequency region. The loss modulus of the highest rubber content ABS (ϕ = 0.30) shows a plateau in the low frequency region.

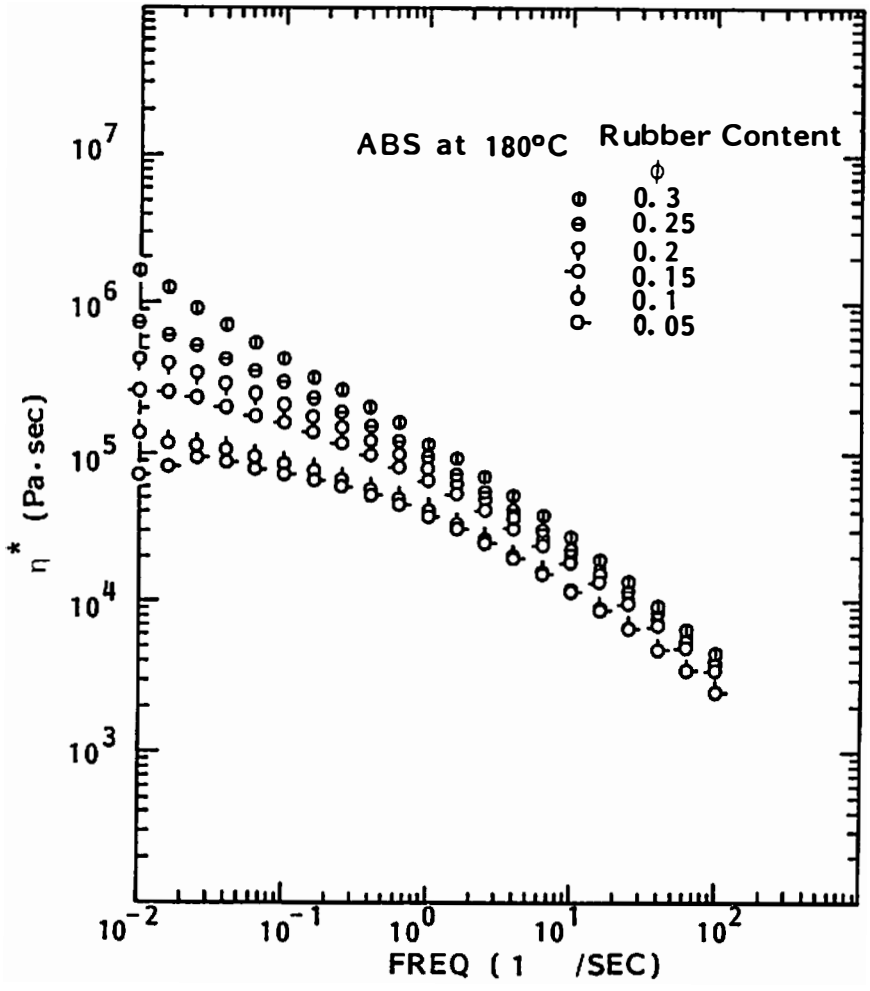

Figure IV-5. Dynamic viscosity as a function of frequency for ABS resins.

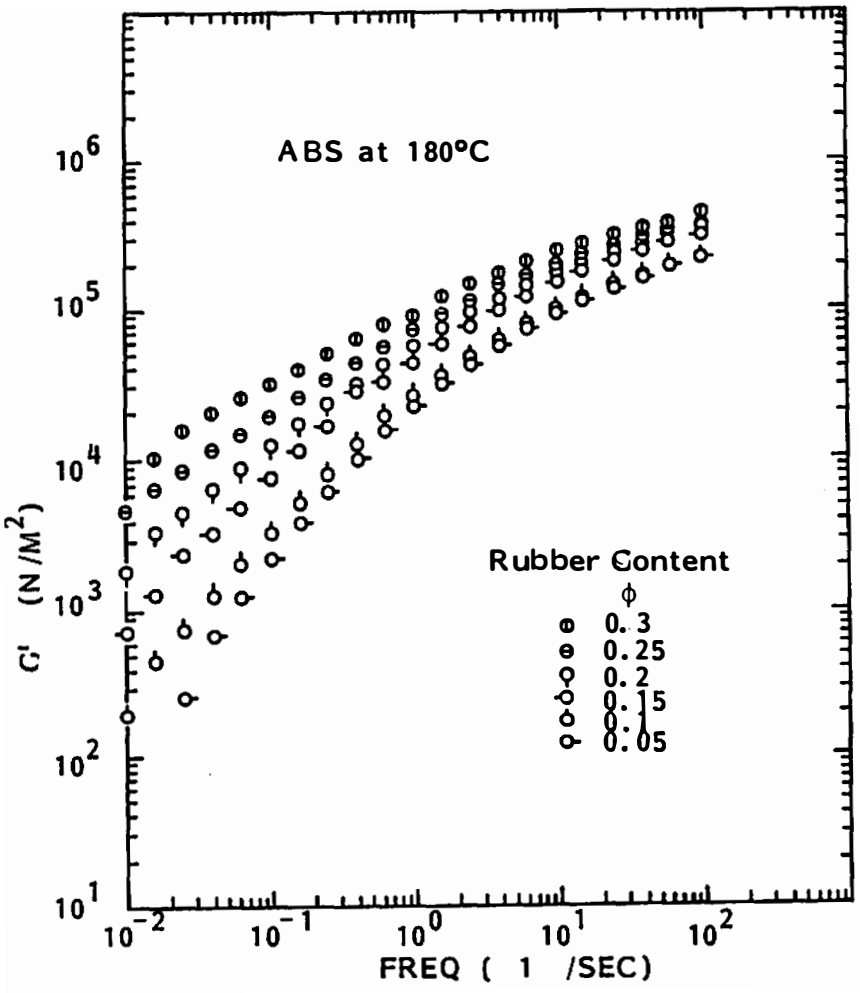

Figure IV-6. Storage modulus as a function of frequency for ABS resins.

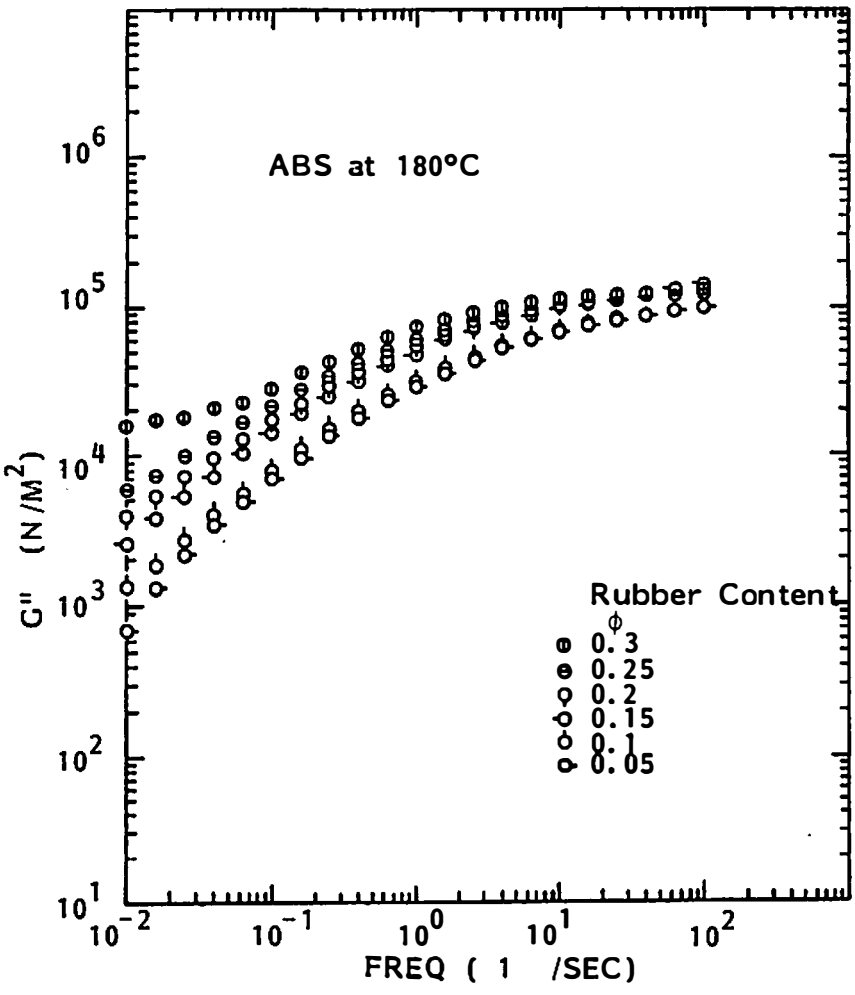

Figure IV-7. Loss modulus as a function of frequency for ABS resins.

D.2. Discussion

Steady state viscosities of various ABS resins are plotted as a function of shear stress in Figure IV-8. When the content of rubber globules is low, the viscosity is constant at low shear stress (low shear rate region) and possesses a Newtonian region. The viscosities tend to infinity at certain shear stresses, as the volume content of rubber increases. These asymptotic shear stresses are considered yield stresses.

The yield stresses have been obtained from Casson's plots (C-2). Casson's equation is:

$$\sigma_{12}^{1/2} = Y_f^{1/2} + k\dot{\gamma}^{1/2} \qquad \text{(IV-1)}$$

where σ_{12} is the shear stress, Y is the yield stress, and k is a constant.

Figure IV-9 shows Casson's plot for various ABS resins. This plot covers the low shear rate region only ($1 \times 10^{-2} < \dot{\gamma} < 1 \times 10^{-1}$). The yield stress is evaluated as an extrapolated value of σ_{12} to $\dot{\gamma} = 0$. The yield stress of lowest volume content ABS region ($\phi = 0.05$) is close to zero. The yield stress clearly increases with increasing content of rubber. The yield stresses of these ABS resins obtained by linear least square method are summarized in Table IV-1.

Suetsugu (S-10) proposed an empirical expression for the yield stress for small particle filled polymer melts of the form:

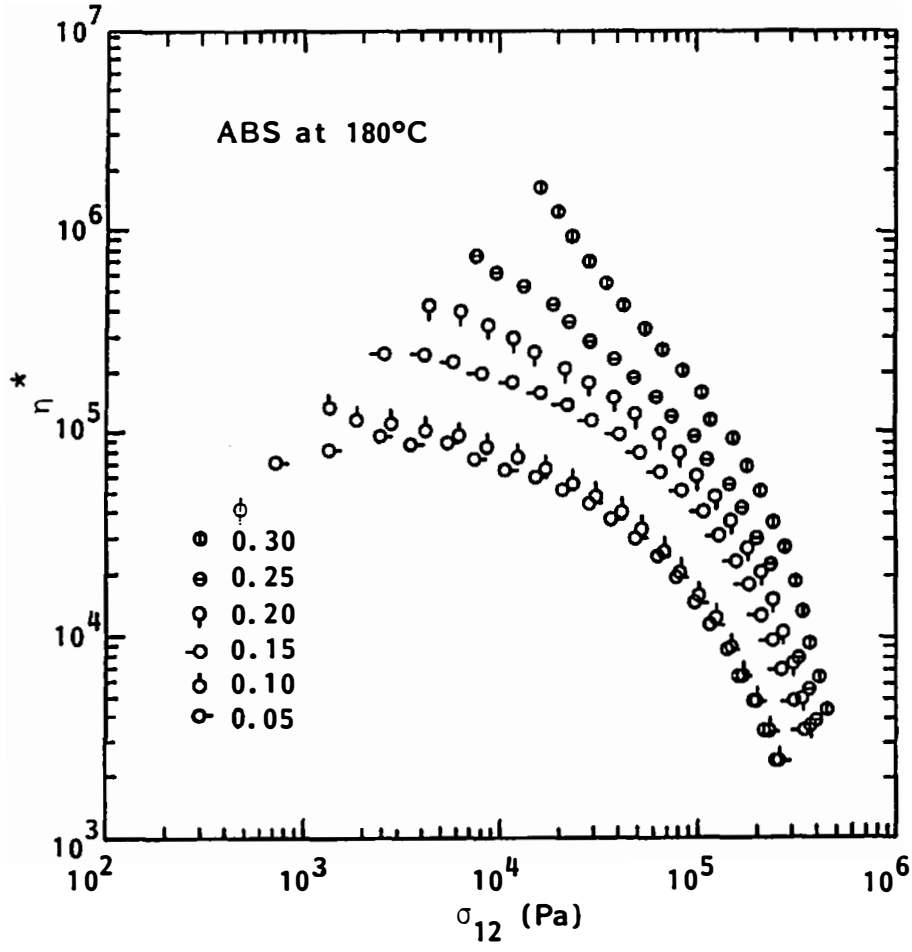

Figure IV-8. Viscosity as a function of stress for ABS resins.

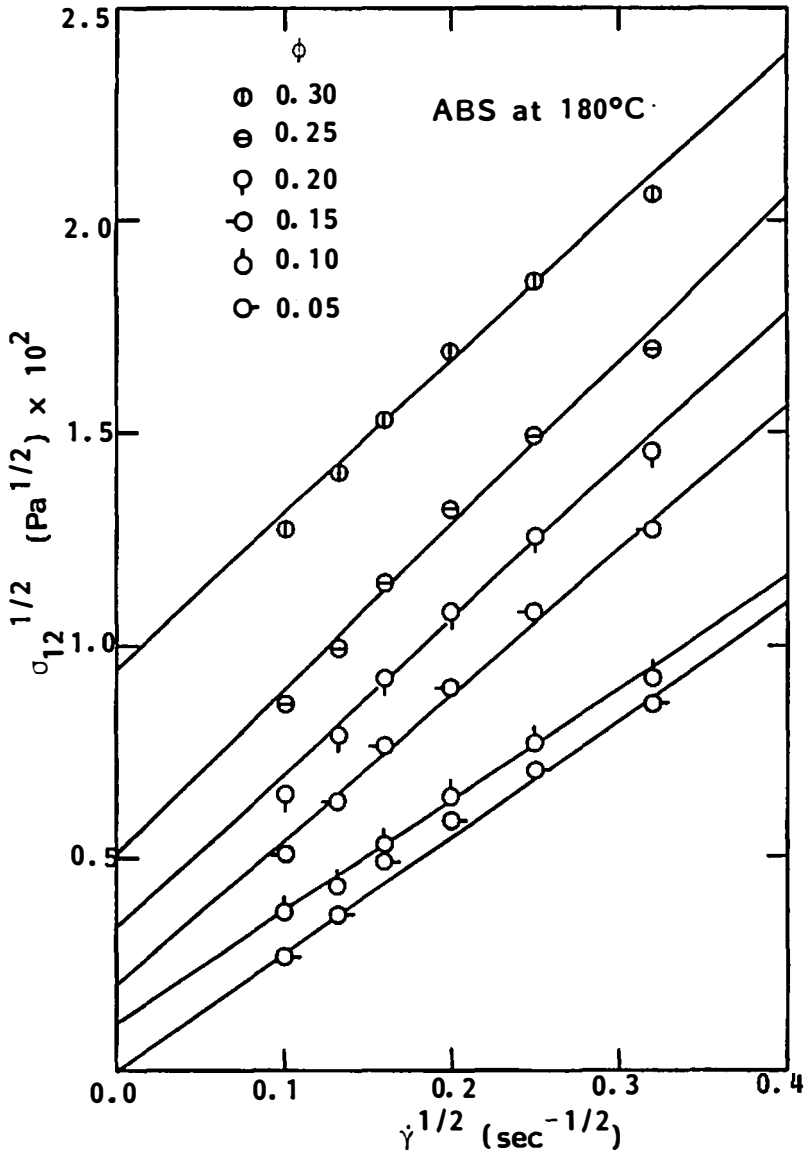

Figure IV-9. Casson's plot for ABS resins.

Table IV-1. Yield Stresses of ABS Resins with Various Rubber Content

Rubber Content ϕ (-)	Yield Stress Y_f (Pa)
0.05	~ 0
0.10	1.27×10^2
0.15	3.82×10^2
0.20	1.07×10^3
0.25	2.69×10^3
0.30	8.97×10^3

$$Y_f = c \frac{\phi^a}{dp^b} \qquad \text{(IV-2)}$$

where:

Y_f : steady state yield stress;

c : constant;

ϕ : volume fraction;

dp : particle diameter;

a,b : power indices.

The exponents a and b were determined for various filled systems (S-10). The above equation may be rewritten as:

$$\log Y_f = \log (c/dp^b) + a \log \phi \qquad \text{(IV-3)}$$

$\log Y_f$ versus $\log \phi$ has been given in Figure IV-10. Straight line shows a best fit with least square method. The experimental data is reasonably characterized by a straight line. A power index $b = 3.77$ is obtained.

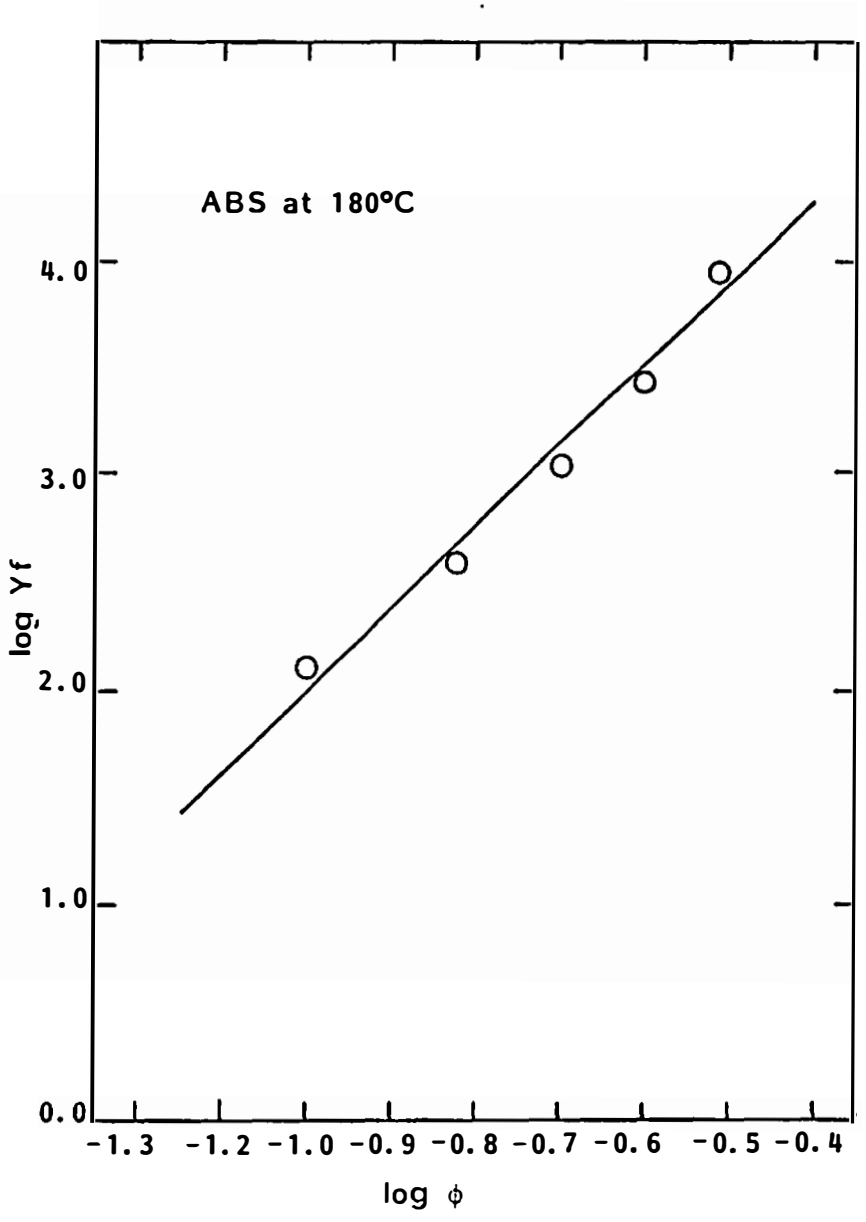

Figure IV-10. Yield stress as a function of volume fraction of rubber for ABS resins (log Yf vs. log ϕ).

$$Y_f = 5.89 \times 10^5 \cdot \phi^{3.77} \quad . \qquad \text{(IV-4)}$$

This is compared with earlier work by various authors in Table IV-2.

The experimentally obtained yield stresses Y_f is, however, better characterized in a semilogarithmic plot of log Y_f versus ϕ as shown in Figure IV-11. The agreement with a straight line is excellent. We obtain

$$Y_f = (1.58 \times 10^1) \times 10^{9.1 \cdot \phi} \quad . \qquad \text{(IV-5)}$$

The yield stress of a small particle filled system would then be characterized by

$$Y_f = c \frac{10^{a \cdot \phi}}{dp^b} \quad . \qquad \text{(IV-6)}$$

E. DIE SWELL

E.1. Results and Discussion

Extrudate swell d/D was determined for polystyrene/calcium carbonate compounds. Here d and D denote the diameter of the extrudate and capillary die, respectively.

Figures IV-12 and IV-13 exhibit extrudate swell as a function of shear stress at wall for the polystyrene/uncoated and coated calcium carbonate systems (dp = 17 μm and 0.07 μm, ϕ = 0.30). L/D (length/diameter of die) ratios are indicated in the figures. The extrudate swell shows a marked decrease with decreasing particle size.

Table IV-2. "a," "b" and "c" Values in Equation (IV-3) for Various Compounds

Sample	Average Particle Size (μm)	Volume Loading (vol%)	a	b	c	References
CB/PIB	0.02	9, 13	2.5	1.6*		Vinogradov et al. (V-3)
CB/PS	0.019	20, 25	7.2			Lobe and White (L-6)
CB/PS	0.045	20, 30	3.1			Tanaka and White (T-2)
CB/PS	0.045	20, 30	3.1			
Uncoated $CaCO_3$/PS	17, 3 0.5, 0.07	30	-	1.1	-	
Coated $CaCO_3$/PS	0.5, 0.07	30	-	0.9	-	
Glass Bead/PE	36	11.8, 19.2, 23.5	2.8	?	-	Kataoka et al. (K-9)
Glass Bead/PE	68.2	19.2, 25.2, 33.5	5.6			
Glass Balloon/PE	52.9	25.0, 30.2, 45.2	4.0	1.4**		
Glass Balloon/PE	73.8	23.0, 35.0, 42.0	2.1			
Silas balloon/PS	?	8 ∿ 55	2.6	-		Kataoka et al. (K-9)
ABS		0.05, 0.10, 0.15 0.20, 0.25, 0.30	3.77	-	-	The present work

*Evaluated for $0.25 \leqslant \phi \leqslant 0.3$. **Evaluated for $0.42 \leqslant \phi \leqslant 0.452$.

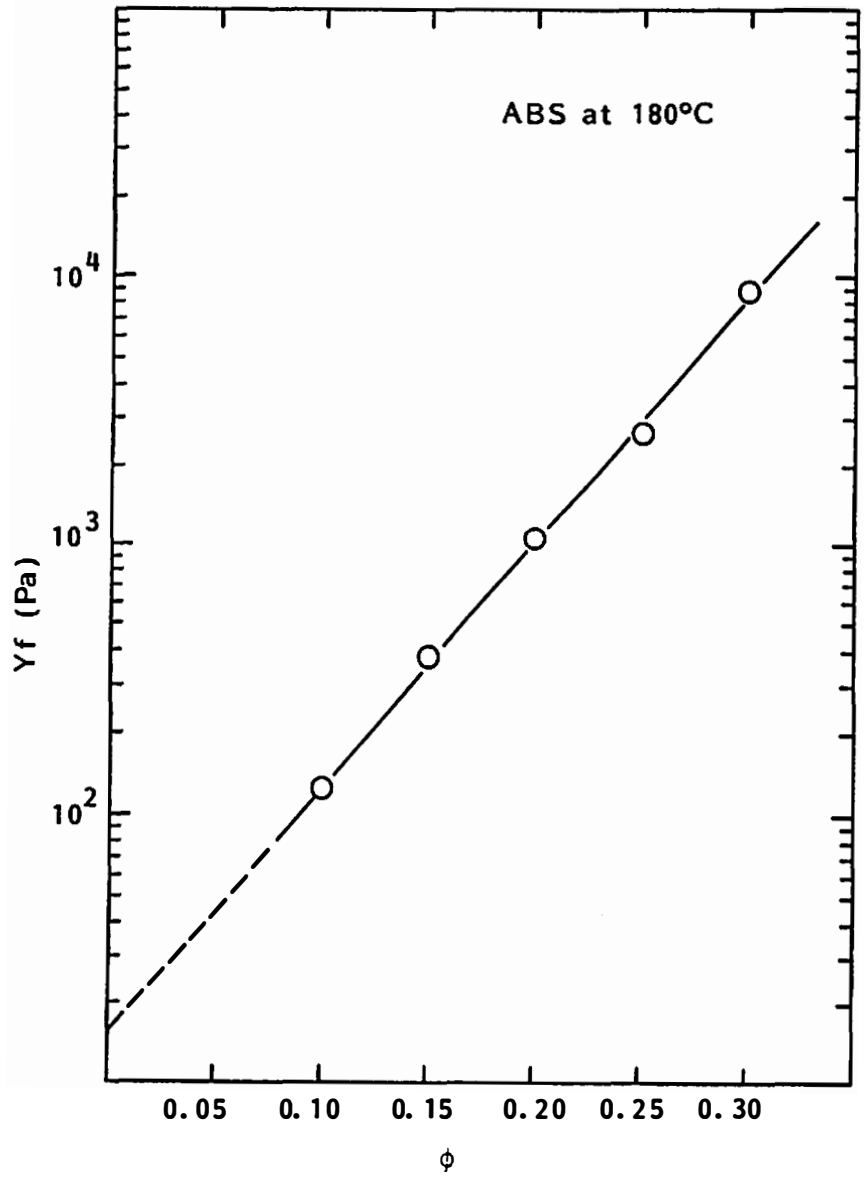

Figure IV-11. Yield stress as a function of volume fraction of rubber for ABS resins (log Yf vs. ϕ).

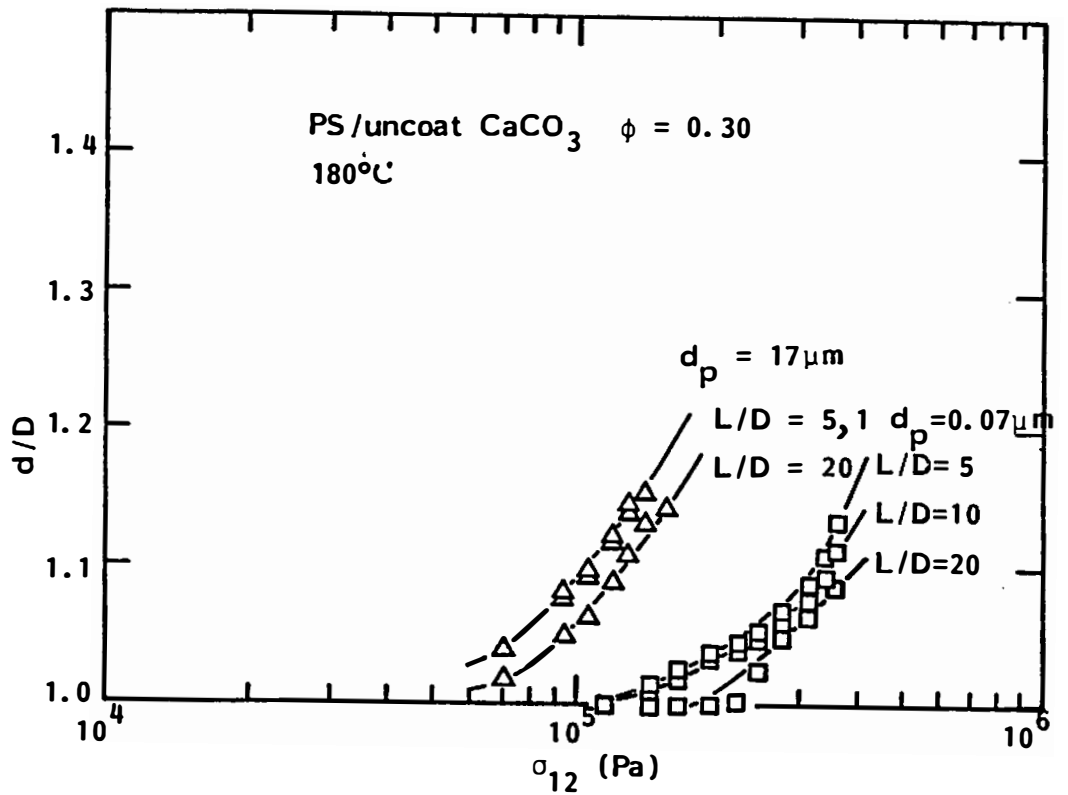

Figure IV-12. Die swell as a function of shear stress for PS/uncoat. $CaCO_3$.

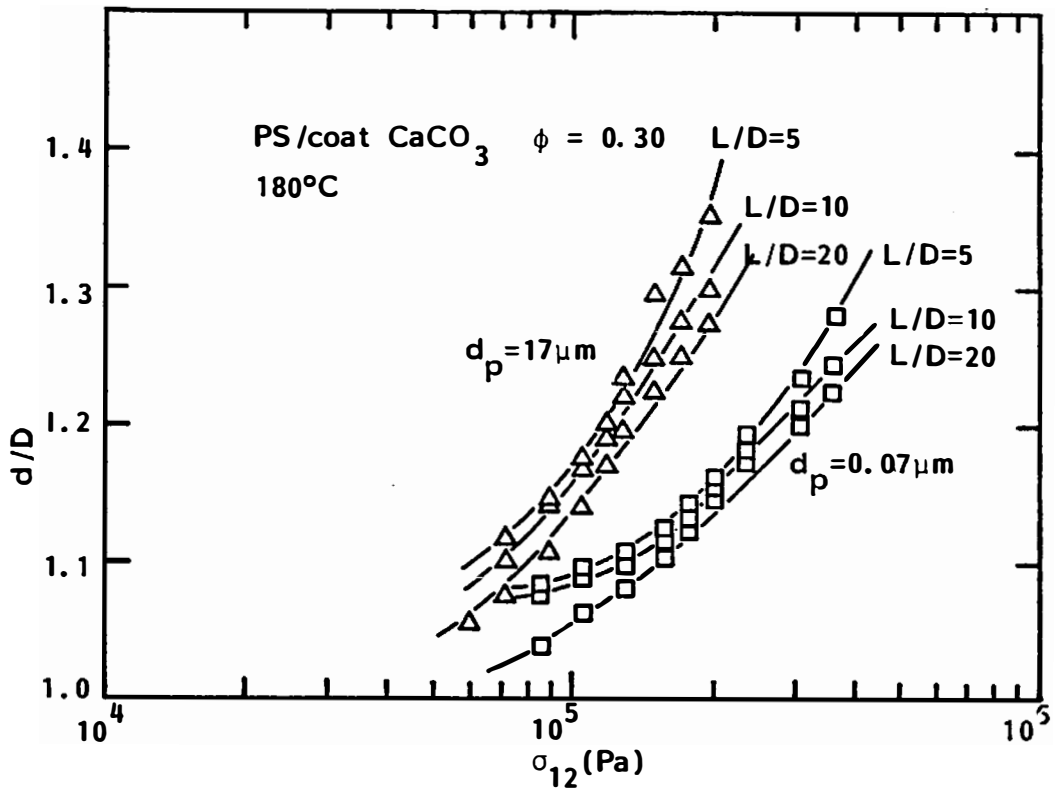

Figure IV-13. Die swell as a function of shear stress for PS/coat. $CaCO_3$.

Stearic acid coated calcium carbonate compounds exhibit greater swell than the uncoated compounds.

A strong correlation may be found with yield stresses of compounds. We may summarize the yield stresses previously obtained (S-10,S-11), and the extrudate swell of compounds as:

Extrudate Swell:	Coat, 17 μm	>	Unc, 17 μm	>	Coat, 0.07 μm	>>	Unc, 0.07 μm
Yield Stress (Pa)	~0	<	7.0×10^2	<	1.0×10^3	<<	3.8×10^4

CHAPTER V

SEDIMENTATION VOLUME EXPERIMENT

A. INTRODUCTION

The sedimentation volume experiment is one of the simplest methods of characterizing particle-particle interaction.

This method has a long history. It is described by Freundlich and Juliusbuger (F-7) in 1934. They mixed solnhofen slate (95-96% $CaCO_3$) and quartz powder with pure and seawater in test tubes. They found that the mixtures of powder and liquid which had a large sedimentation volume show rheological properties of plasticity and thixotrophy. Later Freundlich and Jones (F-5) carried out sedimentation volume experiments quite extensively. They used a range of particulates including titanium dioxide and graphite.

Unique rheological properties such as yield stress and thixotropic time dependent phenomenon of small particulate filled polymer melts appear to be strongly related to the interparticle interaction forces (S-10,S-11). As particle-particle interaction increases, the yield stress of melt compounds increases. Peculiar rheological properties of small particle filled polymer melts presumably result from the structure formed by particulates in the compound.

The magnitude of the sedimentation volume which is related to the particle-particle interaction forces may be relatable to the

ability to disperse particulates as well as the peculiar rheological properties of the compound.

B. EXPERIMENTAL PROCEDURE

The sedimentation volumes of various fillers were measured in the vehicle solvents. Toluene and hexane were chosen as the vehicles because of the similarities of their chemical structure to the matrix polymers employed in the present research. Toluene represents polystyrene:

Toluene: 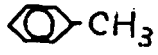

Polystyrene: 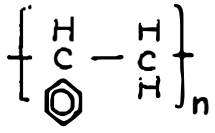

Hexane represents polypropylene:

Hexane: $CH_3(CH_2)_4CH_3$

Polypropylene: 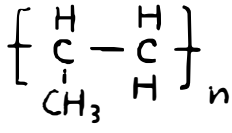

Fillers were dried in a vacuum oven at 100°C for a period of 24 hours, and were substantially weighed. Fillers and solvent were mixed in the test tubes (13 mm x 100 mm) for 20 minutes by hand-shaking. Test tubes were carefully cleaned with solvent in advance. Openings of the test tubes were sealed with rubber stoppers and teflon

film. The volume fraction of fillers used were 0.05 and 0.10. The total volume of filler and solvent in a test tube is 6.0 cm^3.

The test tubes were placed in stands on a laboratory table to observe sedimentation. The heights of the sedimented fillers were measured with a scale as a function of time.

This procedure was repeated at least three times for a single filler to obtain average values.

C. RESULTS

C.1. General and Definitions

Two types of representations have been used to describe the results of these experiments.

Relative Sedimentation Volume:

$$R = \frac{V_{sed}}{V_{bf}} \quad (-) \qquad \text{(V-1)}$$

Porosity of Structure:

$$\varepsilon = \frac{V_{sed} - V_{bf}}{V_{sed}} \times 100 \quad (\%) \qquad \text{(V-2)}$$

where V_{sed} denotes the sedimentation volume of filler and V_{bf} denotes the bulk filler volume. The function R is simply a ratio of sedimentation volume and bulk filler volume. The quantity ε means the percentage of the liquid phase in a total sediment.

We note that functions R and ε increase as the sedimentation volume increases.

The characteristics of these functions are as follows.

	Smallest Sedimentation Volume	Largest Sedimentation Volume
R:	$1/f$	$1/\phi$
ε:	$(1 - f) \times 100$	$(1 - \phi) \times 100$

where f is a fill factor of lattice and ε is a volume fraction of filler in suspension. We note the greatest sedimentation volume is equivalent to the total volume of suspension. Table V-1 summarizes the minima and maxima of these functions at the volume traction of 0.05 for various lattices.

Table V-1. Ranges of R and ε for Various Lattices at ϕ = 0.05

Lattice	f	R	ε
Simple Cubic (SC)	0.5236	1.91-20.0	47.6-95.0
Body Centered Cubic (BCC)	0.6803	1.47-20.0	32.0-95.0
Hexagonal Close-Packed (HCP)	0.7405	1.35-20.0	26.0-95.0

ϕ = 0.05.

C.2. Transients

The transient behaviors of the relative sedimentation volume function R are represented in Figures V-1 through V-4 for various particulates. The volume fraction of filler is 0.05 for all systems.

Figure V-1 shows the behavior of toluene/uncoated calcium carbonates suspensions. The nominal ultimate particle diameter varied

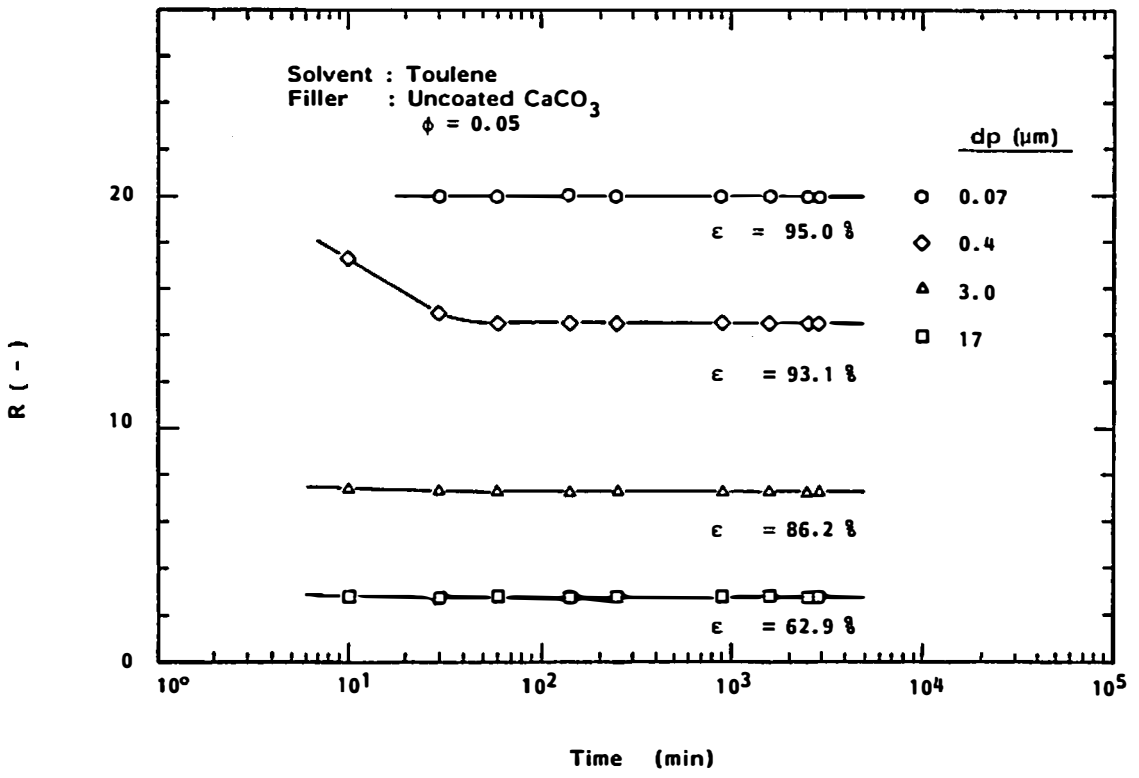

Figure V-1. R values as a function of time for uncoated $CaCO_3$ in toluene.

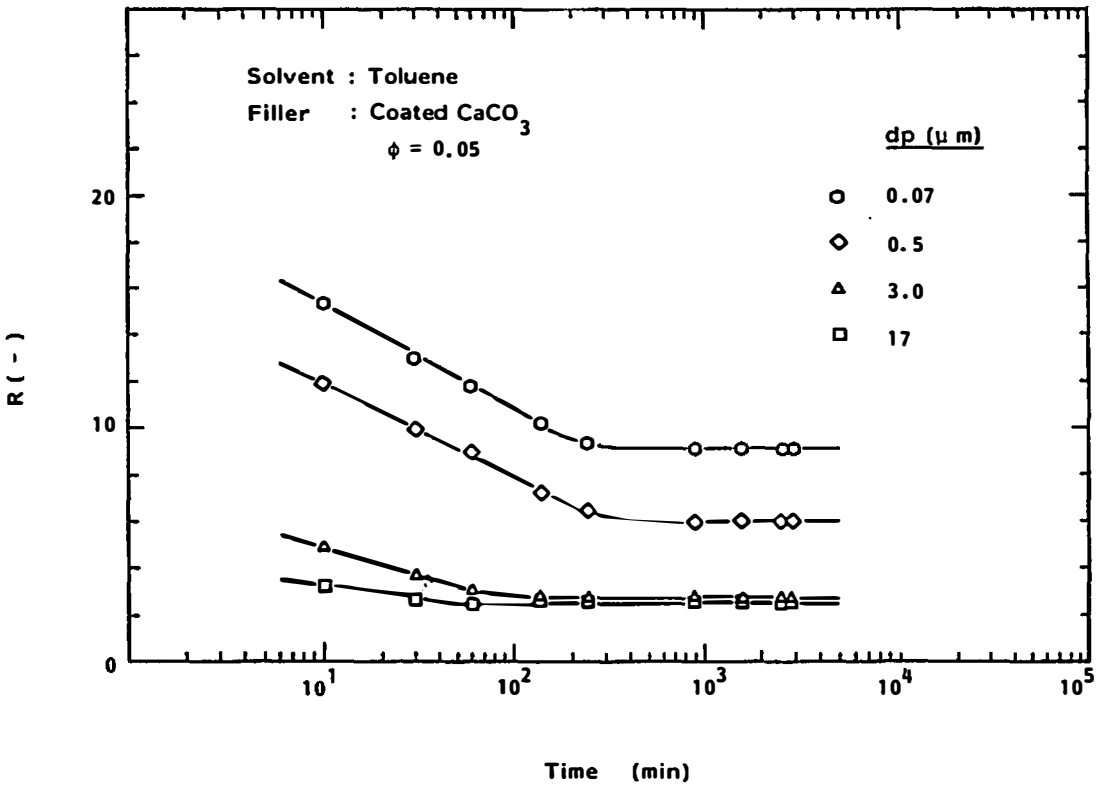

Figure V-2. R values as a function of time for coated $CaCO_3$ in toluene.

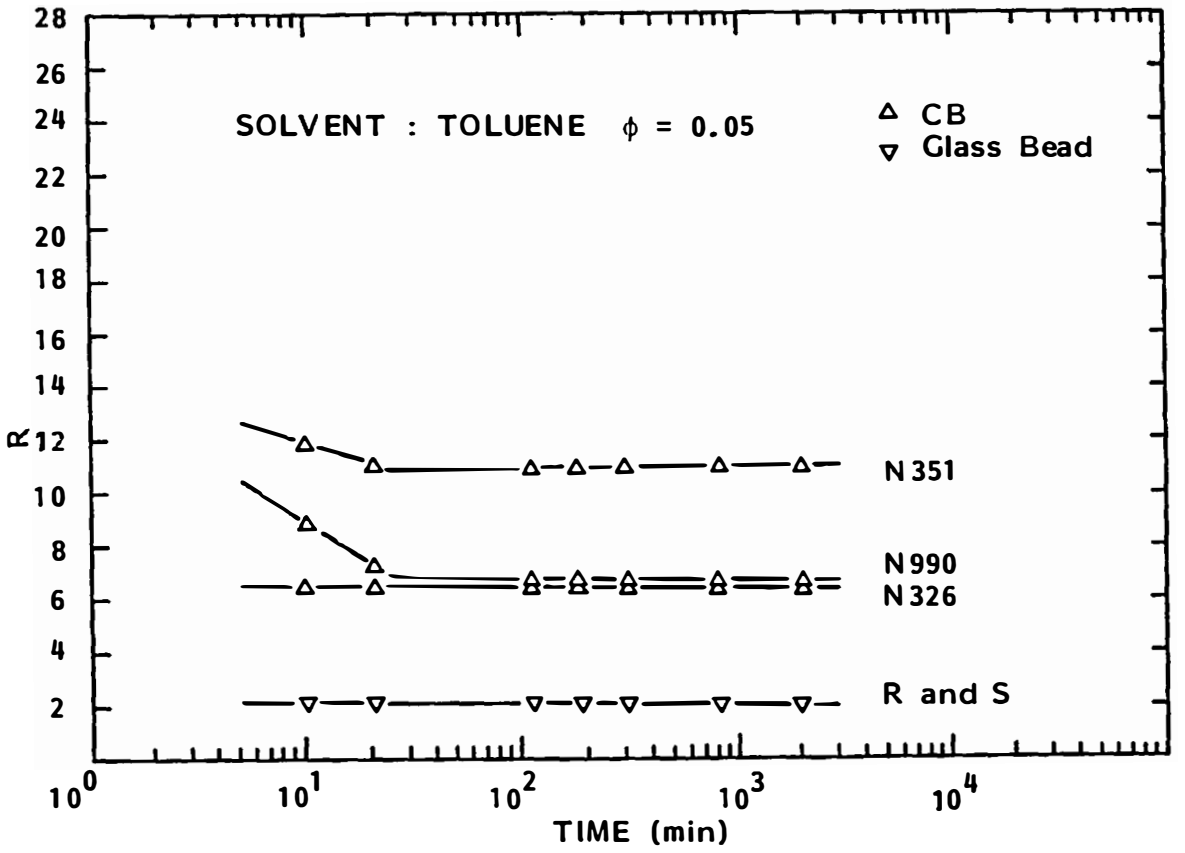

Figure V-3. R values as a function of time for carbon black and glass beads in toluene.

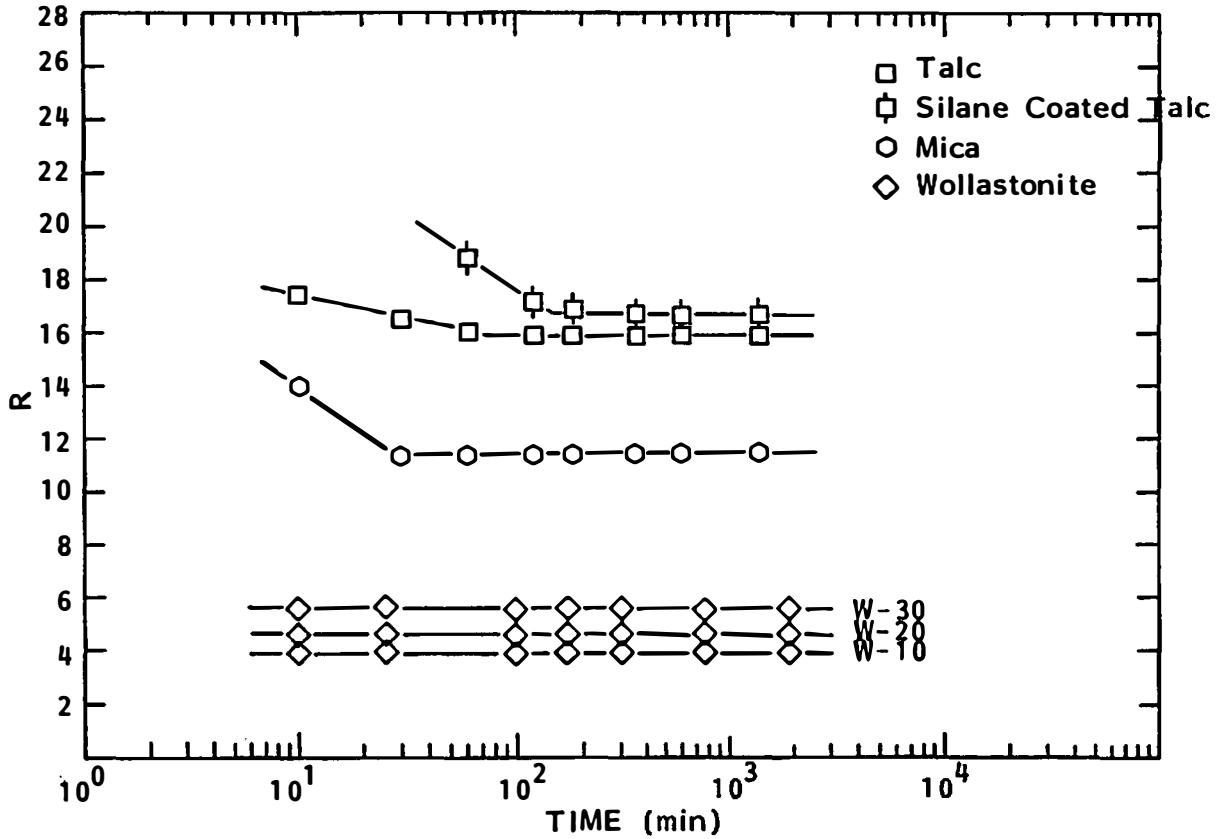

Figure V-4. R values as a function of time for talc, mica and wollastonite in toluene.

from 0.07 μm to 17 μm. It appears that the process of sedimentation terminates within 30 minutes after settling in the test tubes. Sedimentation volumes then maintain constant values. Sedimentation volumes are unchanged even after 50 hours.

The relative sedimentation volume increases with decreasing nominal ultimate particle size. It should be noted that the sedimentation volume of the smallest calcium carbonates is twenty times greater than the bulk filler volume. The porosity of its structure ε is indicated for all particulates. We note that more than 90% of sedimentation volumes of the two smallest uncoated calcium carbonates (dp = 0.07 and 0.4 μm) are occupied by liquid phase. These form highly porous structures.

Results of toluene/coated calcium carbonates systems are shown in Figure V-2. Stearic acid surface coated calcium carbonates take longer times than uncoated calcium carbonates to terminate the sedimentation process. It takes about 100 to 300 minutes for coated calcium carbonates. These again maintain constant sedimentation volumes for nearly 50 hours.

Smaller particulates show greater sedimentation volumes. Equilibrium values of R are, however, much smaller than those of uncoated calcium carbonates. Relative sedimentation volumes R for stearic acid surface coated calcium carbonates are less than 50% of R for uncoated calcium carbonates.

Figure V-3 shows the values of R for three types of carbon blacks and two types of glass beads in toluene. The sedimentation process for carbon blacks terminates within 30 minutes.

Two types of glass beads (dp = 60 μm) which have different surface treatments possess the same R values. The sedimentation process of these terminated right after the test tubes were set in the stand. The R values of these are as low as 2.

The transient behavior of relative sedimentation volume R for various anisotropic fillers is shown in Figure V-4. This includes talc, silane surface treated talc, mica and three types of wollastonites. Talc and mica have disc shapes and wollastonites have needle shapes. The sedimentation process of three types of wollastonite terminate within 10 minutes and these possess very low relative sedimentation volumes ranging 4 to 6 roughly.

C.3. Equilibrium

Figures V-5a and V-5b display photographs of sedimentation volume experiments for toluene/calcium carbonate systems at equilibrium state.

Figure V-5a shows the effect of particle size in toluene/uncoated calcium carbonate systems. Nominal particle diameters are included in the photograph. The volume fraction of filler is same for all samples and is 0.05. Sedimentation volume is strongly affected by particle size. Sedimentation volume rapidly increases as the size of particulates decreases.

Figure V-5b compares uncoated and stearic acid surface coated calcium carbonates for two different ultimate particle sizes. It is shown that stearic acid surface treatment reduces sedimentation volume at the same particle size.

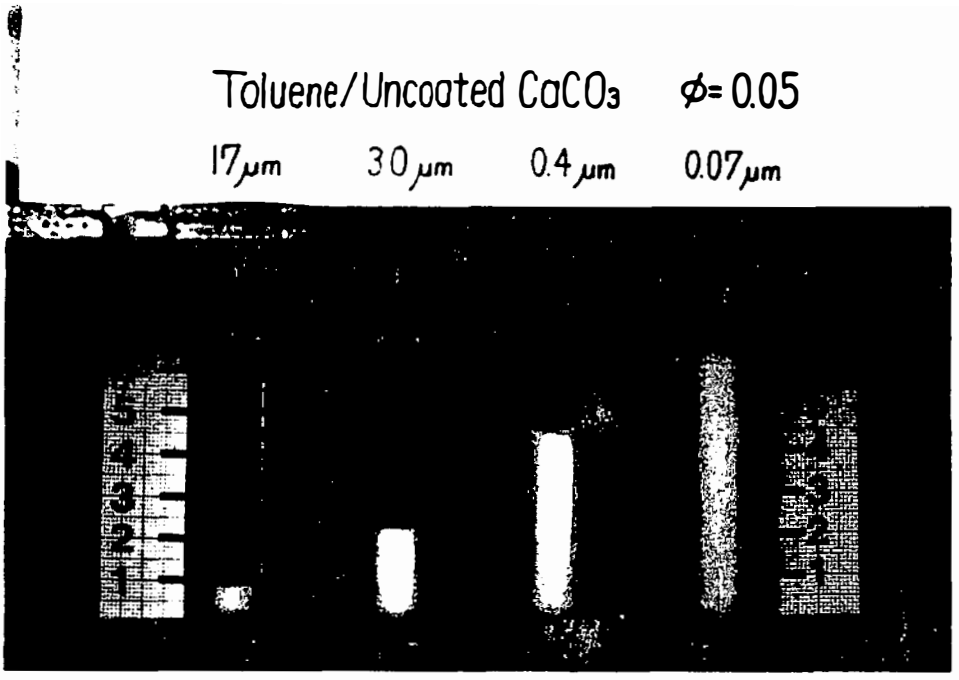

(a) Effect of particle size

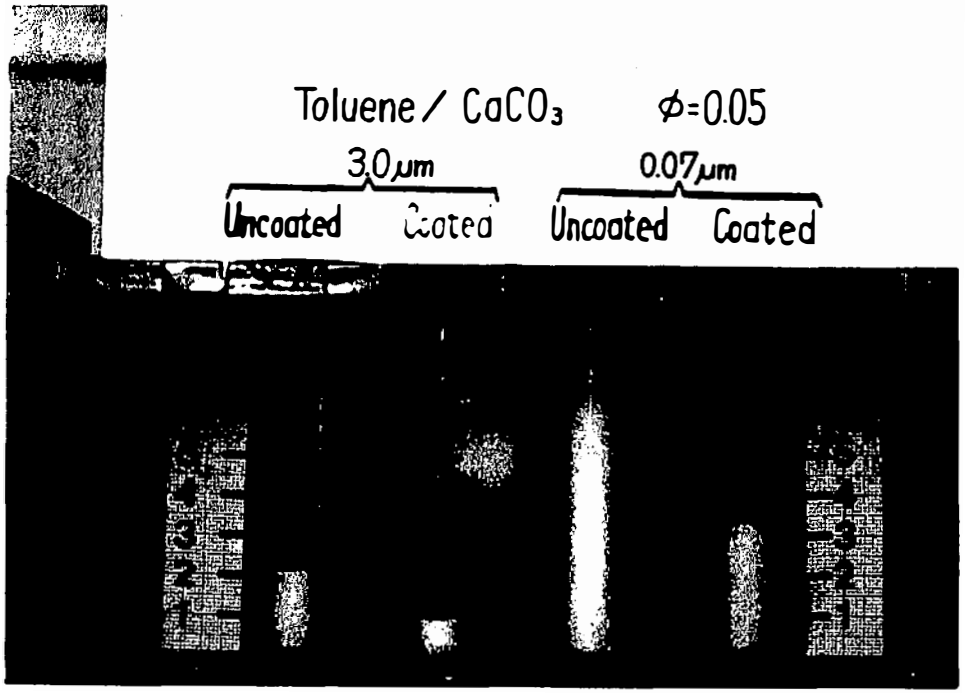

(b) Effect of surface coarting

Figure V-5. Photographs of sedimentation volume experiment at equilibrium state.

Figure V-6 compares relative sedimentation volume R at two different volume fractions, that is, 0.05 and 0.10. Values of R, in general, decrease slightly with increasing volume fraction of filler. The structure formed by particulates is more dense at greater volume fractions. This may be due to the smaller average distance between particulates in suspension at higher volume fractions. In addition, the structure of particulates may collapse more easily due to the weight of sedimented particulates as the height of sedimentation increases at higher volume fraction. (The height of sedimentation in a test tube is twice as large at ϕ = 0.10 when the value of R is constant for ϕ = 0.05 and 0.10.)

It is difficult to obtain values of R for some particulates at the 0.10 volume loading, that is, the transient and steady state values of R exceed 10 which is the maximum allowable value of R in our apparatus for ϕ = 0.10. These particulates include the two uncoated calcium carbonates (dp = 0.4 μm and 0.07 μm), talc and mica.

Figure V-7 shows relative sedimentation volume R as a function of nominal ultimate particle diameter dp for all isotropic particulates involved in this study. The volume fraction is 0.05 for all particulates. Both toluene and hexane data are contained in this figure. The type of vehicle solvents does not have a strong effect on sedimentation volumes.

The calcium carbonates have the greatest relative sedimentation volume R at constant nominal ultimate particle size. A strong correlation between relative sedimentation volume R and

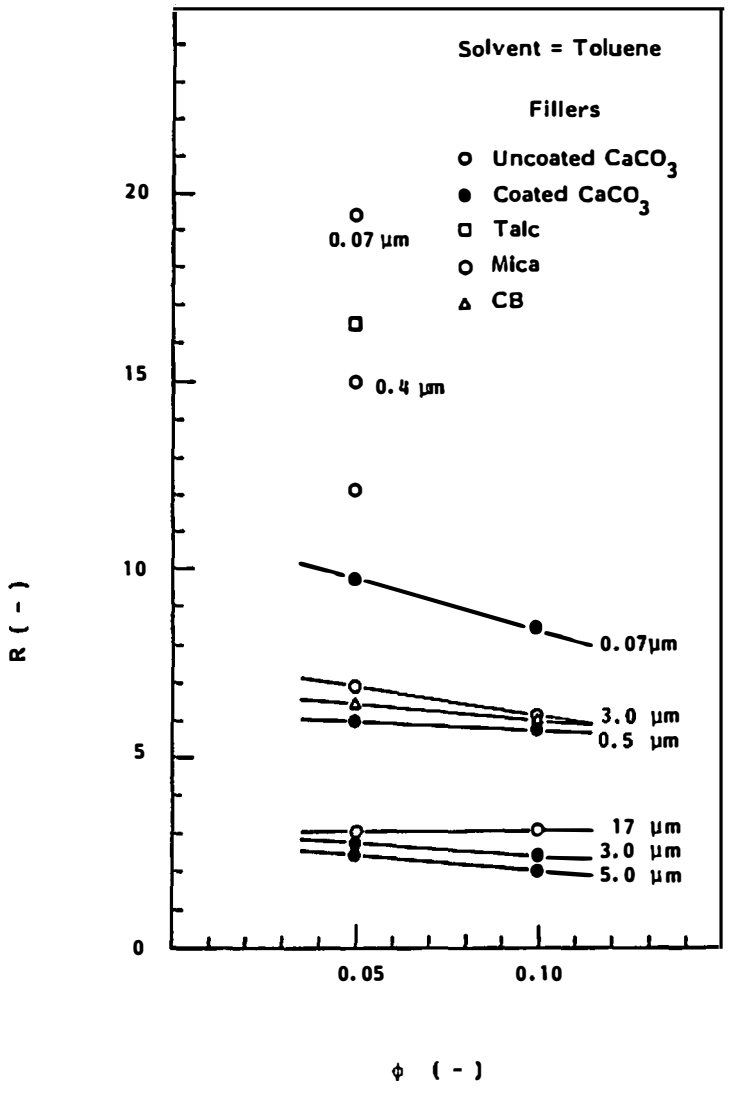

Figure V-6. R values as a function of volume fraction of fillers in toluene.

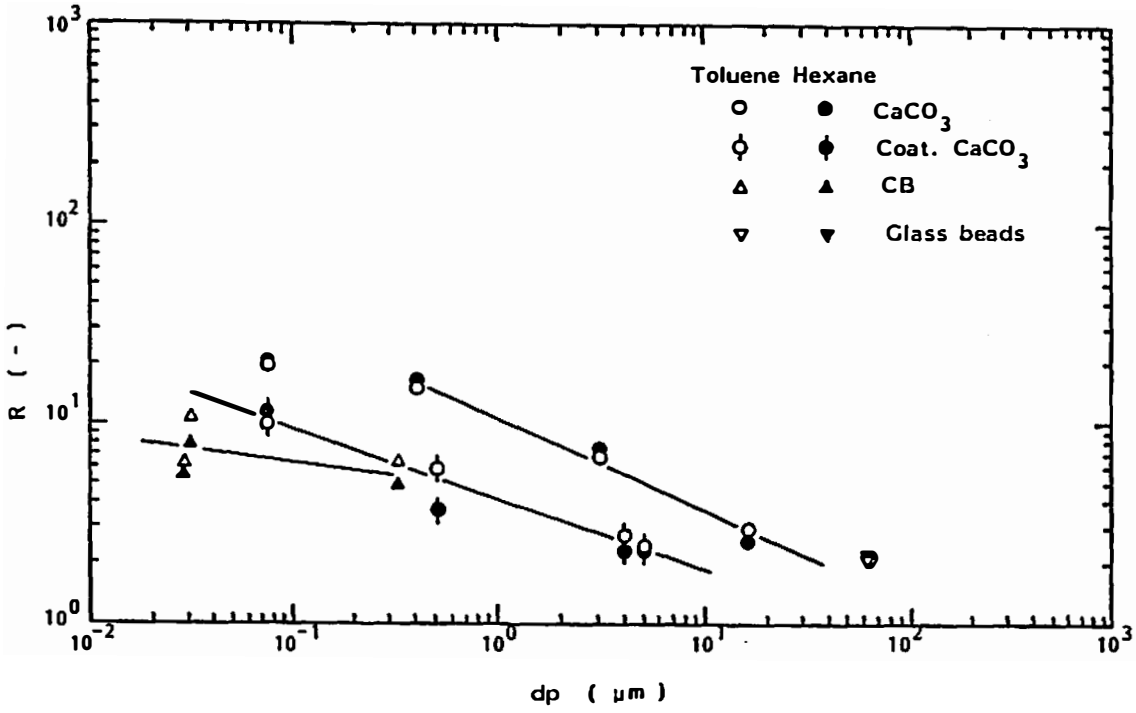

Figure V-7. Sedimentation volume R for isotropic particulates as a function of particle size.

ultimate particle size is found. As particle size decreases, sedimentation volume increases rapidly. The finest calcium carbonate (dp = 0.07 μm) shows a smaller relative sedimentation volume R than the extrapolated value with the three other sizes of uncoated calcium carbonates. This may be due to the restrictions of experiment. The upper limit of relative sedimentation volume is 20 at the volume fraction of 0.05. Volume of sedimentation becomes identical to the total volume of solvent and particulates at R = 20 for a suspension of ϕ 0.05.

The effect of stearic acid surface coating is clear. Surface treatment of calcium carbonates reduces relative sedimentation volume more than 50%. There is again a strong correlation between sedimentation volume and ultimate particle size. Relative sedimentation volume increases as ultimate particle size decreases.

Values of R for carbon blacks are smaller than for the coated calcium carbonates. It must be noted here that carbon black pellets probably are not completely destroyed by the agitation and carbon black pellets may still exist when sedimentation processes are initiated. It may be necessary to agitate carbon black suspension with ultrasonic vibrations to break up all pellets into the aggregates. One may expect that the relative sedimentation volume R of carbon black would increase further if the pellets break down to the individual "aggregate."

Two types of glass beads (dp = 60 μm) with different surface coatings (Ferro Corporation) show very small relative sedimentation

volumes. Those are about 2. Ferro Corporation reports that the glass beads of grade R have surface coating for polypropylene and other regimes and grade S glass beads has surface coating for polystyrene, etc. Small and identical relative sedimentation volumes of two types of glass beads are due to their large size. These have average diameter of 60 μm and are much larger than the other particulates.

The relative sedimentation volume R of glass beads, 2, is very close to the minimum value of R which was shown in Table V-1 in Section C.1, p. 79. This suggests that glass beads are packed into lattice structure, but do not form a three-dimensional porous network structure.

We compare the relative sedimentation volumes of anisotropic particulates with those of isotropic particulates in Figure V-8. R values of isotropic particulates are represented by the solid lines.

It should be noted that the largest dimension of anisotropic particles is adopted as an ultimate particle size dp in this figure. All anisotropic particulates show the greater relative sedimentation volume than isotropic particles. R of talc and mica (both have disc shapes) are larger than R of wollastonites (rod shape). The three types of sollastonites show clear effects of particulate size. The relative sedimentation volume decreases with increasing particulate size.

The effect of the silane surface coating of talc is not clear. Silane surface coating of talc may not be intended to reduce

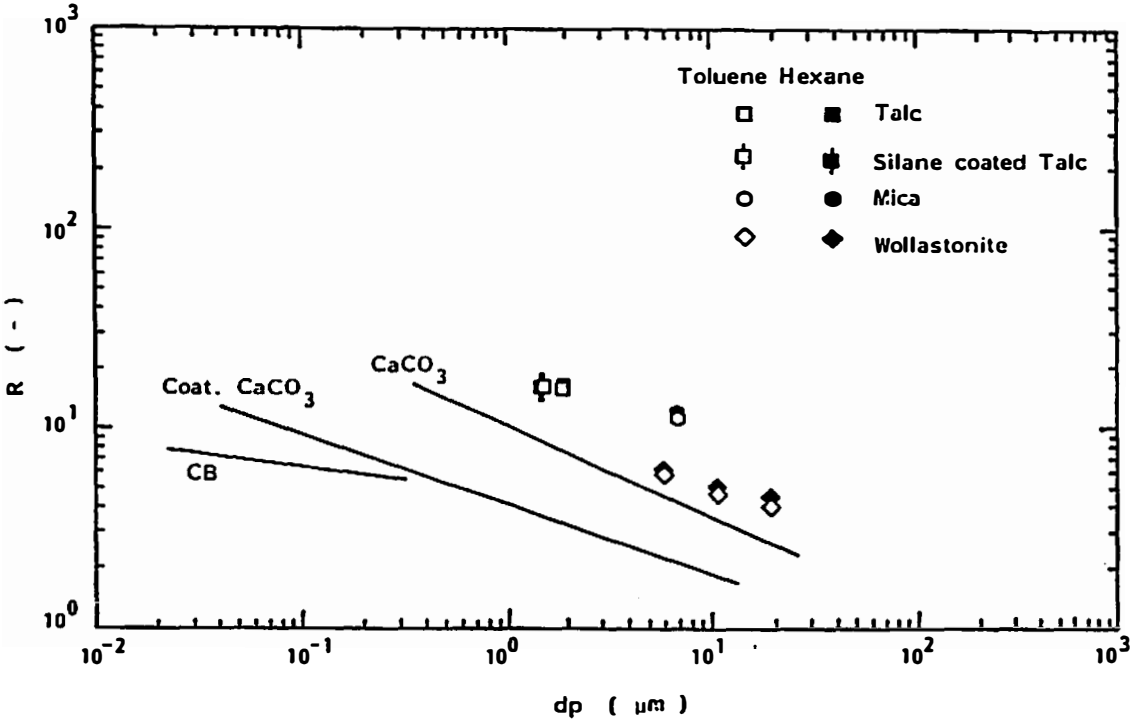

Figure V-8. Sedimentation volume R of anisotropic particulates as a function of particle size.

particle-particle interaction for a better dispersion, but it may be intended to improve polymer-particulate interactions to upgrade the mechanical properties.

Again, sedimentation volumes of anisotropic particulates are not strongly affected by the type of vehicle liquid.

Figures V-9 and V-10 represent porosity of structure ε, which has been defined in Eq. (V-2), as a function of ultimate particle size for isotropic and anisotropic particulates, respectively. Both toluene and hexane were used.

We note that the upper limit value of porosity of structure ε is 95%, that is, 95% of sedimentation volume is occupied by vehicle solvent and only 5% of sedimentation volume is occupied by particulates, for a volume fraction of 0.05.

The porosity of structure reaches an upper limit value of 95% as particle size decreases both for isotropic and anisotropic particles.

Small particulates, especially uncoated calcium carbonates, possess sediment porosity of greater than 90%.

D. DISCUSSION

D.1. Transient

Transient behavior of sedimentation is peculiar and is dependent upon the type and size of filler.

It stands to reason considering that the sedimentation process is governed by gravitational forces and particle-particle interaction forces. One may simplify the process of sedimentation as follows.

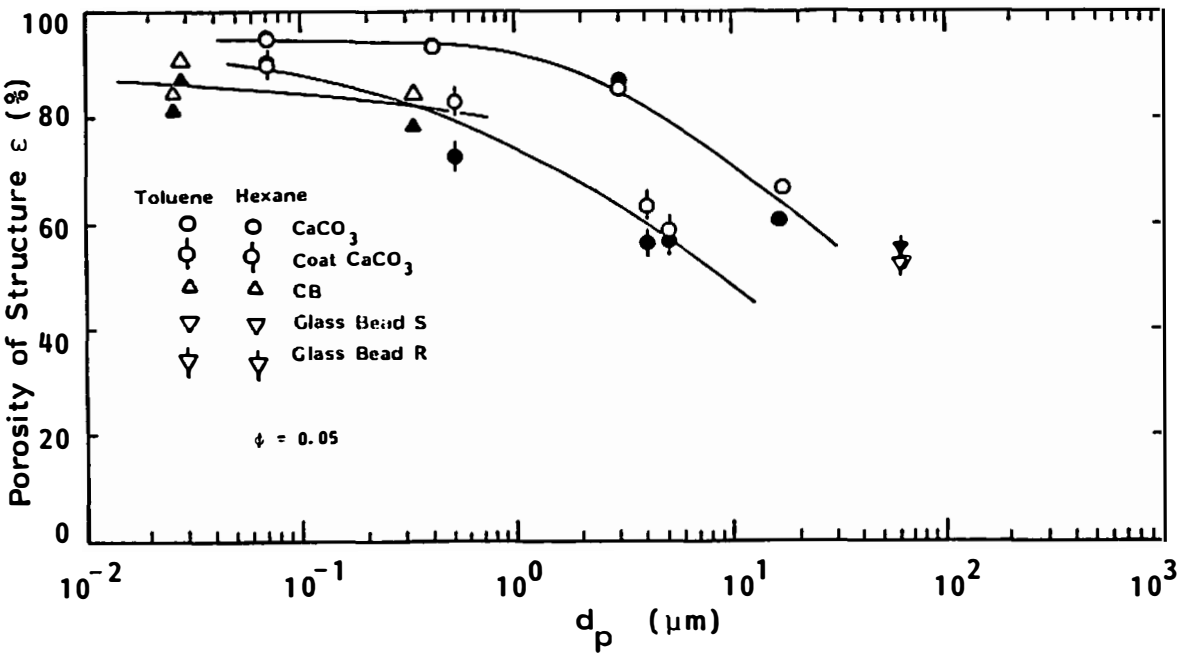

Figure V-9. Porosity of structure ε as a function of particle size for isotropic particulates.

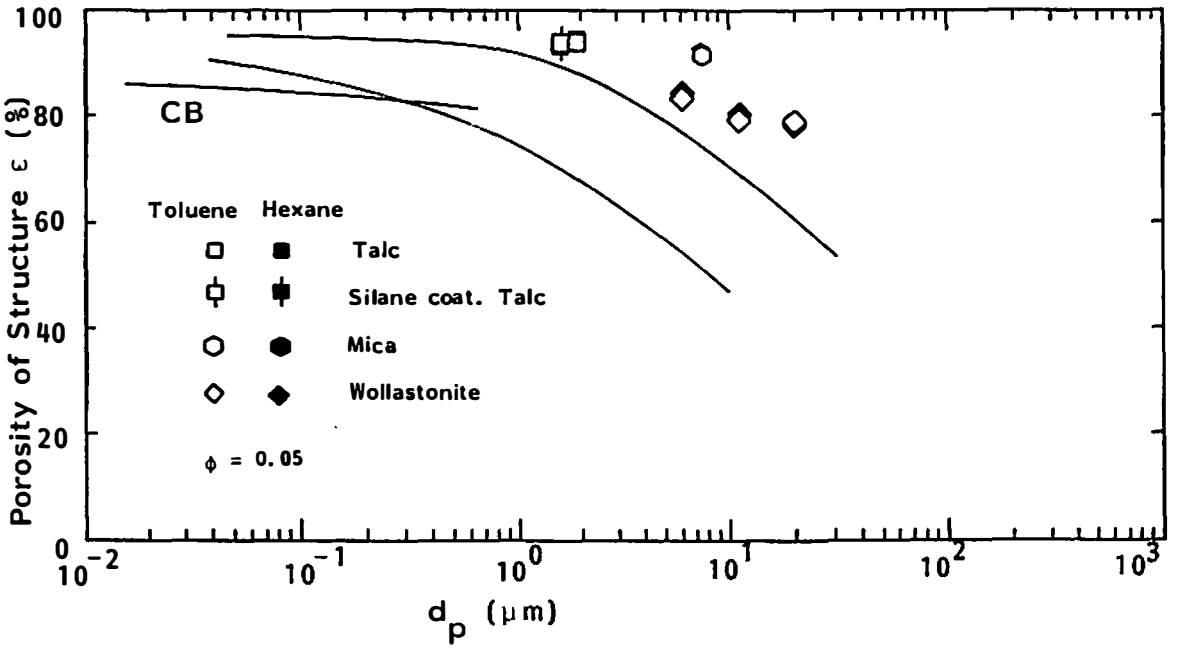

Figure V-10. Porosity of structure ε as a function of particle size for anisotropic particulates.

The first process which takes place right after stopping the agitation is the sedimentation of the individual particles. The distances between the particles are great enough so the particle-particle interaction is negligible. The gravitational force is dominant. Sedimentation of individual particles is governed by:

$$\frac{\pi}{6} dp^3(\rho_s - \rho_f)g = 3\pi\eta v_t\, dp \qquad (V\text{-}3)$$

where

dp : diameter of ultimate particle;

ρ_s : density of particle;

ρ_f : density of fluid;

g : gravitational acceleration (9.8 m/sec^2);

η : viscosity of fluid;

v_t : terminal velocity.

The left side of the equation represents the gravitational force and the right side is a well-known Stokes' law representing drag forces. This process occurs in the very early stage of sedimentation.

Freundlich and Jones ( ) pointed out that the reduction of sedimentation volume due to the sedimentation of independent particles is linear with time due to Eq. (V-3).

As the sedimentation of the individual particles progresses, interparticle distances decrease and particles start interacting each other. Particulates form a structure. This process would occur earlier if the particles possess stronger interaction forces. When particles possess weak interaction forces, the structure collapses

and reduces the sedimentation volume until it reaches an equilibrium and is well packed.

We may get the following empirical relation for a transient relative sedimentation volume:

$$R(t) = [R_{max} - R_{eq}]\exp(-t/\tau) + R_{eq} \qquad (V\text{-}4)$$

where R_{max} and R_{eq} denote the relative sedimentation volume at $t = 0$ and $t = \infty$ (equilibrium), respectively, and τ is a time constant. R_{max} corresponds to an initial relative sedimentation volume where the breakdown of structure begins.

The reduction of sedimentation volume of this process is not linear but an exponential function of time.

Curve fitting was carried out for coated calcium carbonates which show the distinct transient behavior. Figure V-11 compares the prediction of Eq. (V-4) to the experimental data. Good agreement was obtained.

Table V-2 summarizes R_{max}, R_{eq} and τ obtained for the toluene/coated calcium carbonate system. All values increase with decreasing ultimate particle diameter. The other systems possess relatively short termination periods. The above constants could not be accurately determined for such systems.

Tables V-3 and V-4 summarize the relative sedimentation volume R, porosity structure ε and termination period of sedimentation process t_s. Table V-3 represents isotropic particles. Calcium carbonates possess large relative sedimentation volume R and porosity of

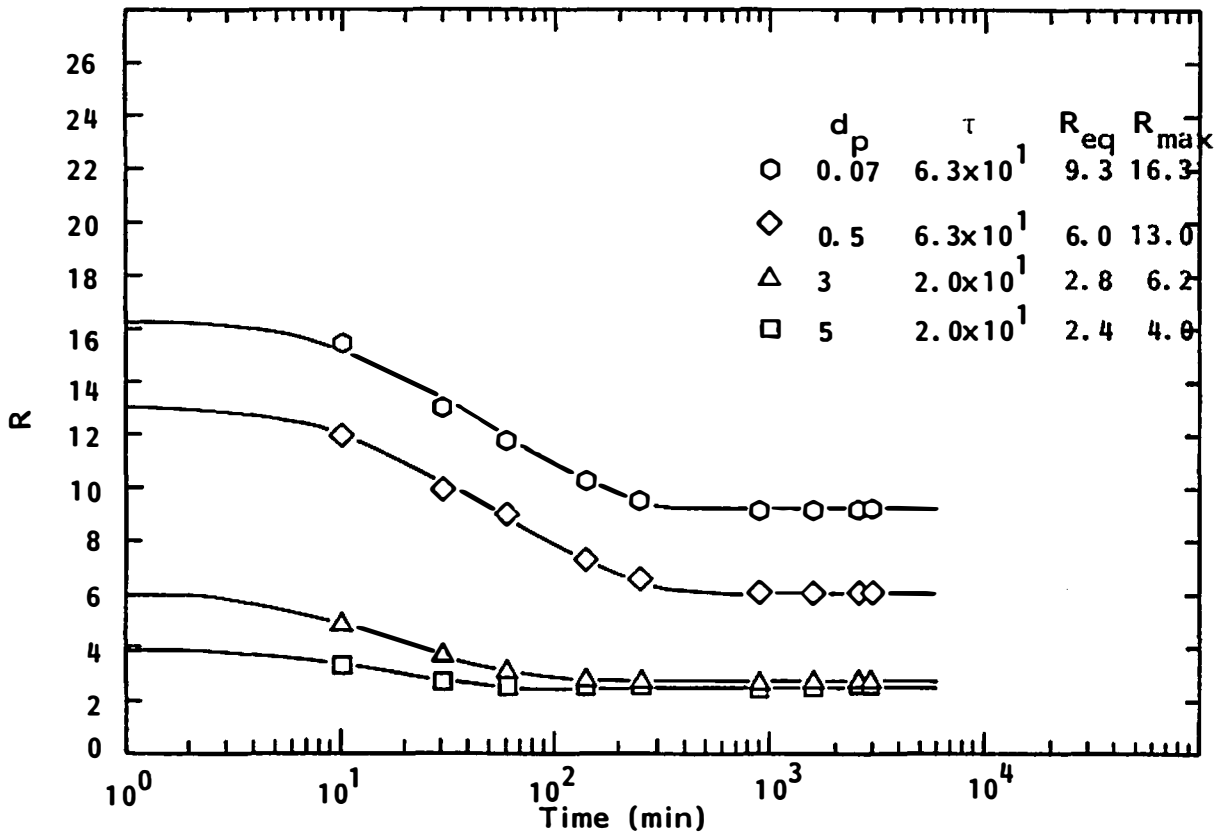

Figure V-11. Comparison between prediction and experimental data for coated $CaCO_3$ in toluene.

Table V-2. Parameters in Equation (V-4) for Toluene/Coated $CaCO_3$

dp (μm)	R_{max} (-)	R_{eq} (-)	τ (min)
0.07	16.3	9.3	63
0.5	13.0	6.0	63
3	6.2	2.8	20
5	4.0	2.4	20

Table V-3. Values of R, ε and t_s for Isotropic Particles

Type	Density (g/cm^3)	DBP Absorption ($cm^2/100g$)	Diameter (μm)	R Toluene	R Hexane	ε Toluene	ε Hexane	t_s (min)
Calcium Carbonate	2.71	-	17	3.02	2.58	66.9	61.2	~30
			3	6.88	7.67	85.5	87.0	~30
			0.4	15.0	16.8	93.3	94.0	~30
			0.07	19.4	20.0	94.8	95.0	~30
Stearic Acid Coated	2.71	-	5	2.42	2.30	58.7	56.5	80
			3	2.76	2.30	63.8	56.5	80
			0.5	5.97	3.64	83.2	72.5	300
			0.07	9.76	11.5	89.8	91.3	300
Carbon Black	1.8	42	0.32(N990)	6.52	4.58	84.7	78.2	30
		71	0.026(N326)	6.36	5.45	84.3	81.7	<10
		121	0.028(N351)	10.8	7.73	90.7	87.1	30
Glass Bead	2.5	-	60(R)	2.12	2.27	52.8	55.9	<<10
			60(S)	2.12	2.12	52.8	52.8	<<10

Table V-4. Values of R, ε and t_s for Anisotropic Particles

Type	Density (g/cm^3)	Size (μm)	R Toluene	R Hexane	ε Toluene	ε Hexane	t_s (min)
Talc	2.75	1.9	15.9	16.5	93.7	93.9	70
Silane Coated Talc	2.75	1.5	16.4	16.2	93.9	93.8	150
Mica	2.84	10	11.5	12.0	91.3	91.7	30
Wollastonite	2.9	20	4.80	4.71	79.2	78.8	<10
		11	4.76	4.71	79.0	80.1	<10
		6	5.87	6.27	83.0	84.1	<10

structure ε. The termination period of sedimentation process is short ($\sim$30 minutes). These suggest that the structure does not collapse and particle-particle interaction forces are strong. Coated calcium carbonates show small R and ε, and long termination periods. The structure collapses easily due to the weak interparticle forces. Glass beads show extremely small values of R, ε and t_s. This is due to the large size of particles.

The results for anisotropic particles (Table V-4) are difficult to interpret due to shape effects.

D.2. Equilibrium

Some particulates possess extremely large porosities ε. These include uncoated calcium carbonates (dp = 0.07 μm, 0.4 μm), talc and coated talc.

It seems reasonable to assume that these particulates form a three-dimensional network structure in liquids. High porosity can be easily obtained in such a structure.

Figure V-12 shows models of loose-packed network structure and close-packed structure.

Uncoated calcium carbonates may have permanent electric dipoles Ca^{2+} and CO_3^{2-} on their surface. These possess electric dipole-dipole interaction forces in addition to the van der Waals interaction forces between particulates. Uncoated calcium carbonates possess strong interaction forces between particles. These may form three-dimensional network structures.

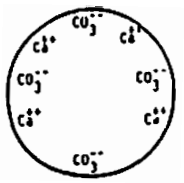

Uncoated $CaCO_3$

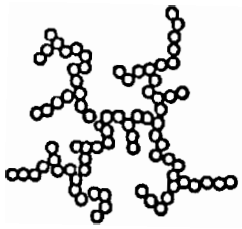

Strong Interaction Forces between Particles (loose-packed structure)

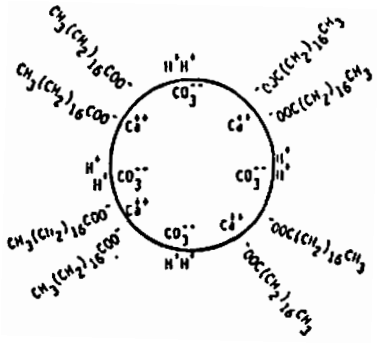

Stearic Acid Coated $CaCO_3$

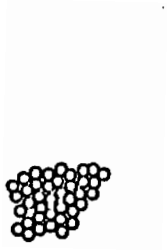

Weak Interaction Forces between Particles (close-packed structure)

Stearic Acid
$CH_3 (CH_2)_{16} COOH$

Figure V-12. Uncoated and stearic acid coated calcium carbonates and their structures in solvent.

Stearic acid, $CH_3(CH_2)_{16}COOH$, on the surface of calcium carbonates, reduces permanent electric dipoles as shown in Figure V-12. These may have weak particle-particle interaction forces and form close-packed structures.

Freundlich and Juliusburger (F-6) and Freundlich and Jones (F-5) measured sedimentation volumes for a wide range of particulates in various vehicles. Their results were converted into the relative sedimentation volume R and summarized in Tables V-5 and V-6. Freundlich and Jones (F-5) reported that the particles have sizes of 1 to 10 μm (Table V-6).

R values of their calcium carbonates varies 3 to 7 depending upon the vehicle. These values are in good agreement with our results at comparable sizes. R values of calcium carbonates in the present work are 2.5 to 3 for 17 μm and 7 to 8 for 3 μm.

D.3. Sedimentation Volume and Rheological Properties

We now compare the rheological properties of small particle filled polymer melts and sedimentation volumes.

It is well known that small particle filled polymer melts possess yield values (or yield stresses) (C-1,L-6,M-18,M-19,S-11,T-2, T-8,V-3,Z-1), and thixotropic time dependent properties (M-18,S-11, T-2,V-3). Yield stresses and thixotropic properties of melt compounds are more prominent with decreasing particle size (S-11). Stearic acid surface coating of calcium carbonates reduced these rheological properties (S-11). These peculiar rheological properties

Table V-5. R and ε Values Obtained from a Work by Freundlich and Juliusburger

Type	Density (g/cm^3)	Size (μm)	R Water	R Seawater	ε Water	ε Seawater	Reference
Quartz	2.65	1-15	1.89	2.75	47.2	63.7	F-6
Solnhofen (95-96% $CaCO_3$)	2.71	10	5.42	4.93	81.6	79.7	F-6

Table V-6. R Values for Various Vehicles Obtained from a Work by Freundlich and Jones

Substance	Chemical Composition	Crystalline Structure	Water	HCl	NaOH	NaCl
Diamond	C	Cubic	3.63 (4)	2.83 (4)		
Graphite	C	Hexagonal	5.80 (1)	5.58 (1)	6.28 (1)	5.84 (1)
Jet	(C)	Amorphous	3.54 (5)	4.07 (5)	9.20 (1)	4.07 (5)
Corundum	Al_2O_3	Hexagonal	3.94 (4)	3.32 (5)	3.89 (4)	3.67 (4)
Hematite	Fe_2O_3	Hexagonal	6.46 (1)	5.18 (1)	7.35 (1)	7.35 (1)
Pyrolusite	MnO_2	Rhombic	4.07 (1)	3.89 (1)	3.89 (1)	4.07 (1)
Litharge	PbO	Amorphous				
Quartz	SiO_2	Hexagonal	1.77 (5)	2.39 (5)	3.01 (4)	2.92 (4)
Rutile	TiO_2	Tetragonal				
Titanium dioxide	TiO_2	Tetragonal	8.50 (1)	6.19 (1)	8.93 (1)	8.63 (1)
Vanadium pentoxide	V_2O_5	Rhombic	2.96 (5)	7.61 (1)		
Tin pyrites	$SnS_2 \cdot Cu_2S \cdot FeS$	Tetragonal	6.68 (1)	9.38 (1)	4.78 (1)	6.63 (1)
Galena	PbS	Cubic	7.79 (1)	7.79 (1)	9.64 (2)	5.27 (1)
Mosaic gold	SnS_2	Hexagonal	5.31 (3)	4.60 (3)	4.25 (3)	5.13 (3)
Fluorspar	CaF_2	Cubic	2.74 (5)	1.86 (5)	2.74 (5)	2.83 (5)

Table V-6 (continued)

Substance	Chemical Composition	Crystalline Structure	Water	HCl	NaOH	NaCl
Barytes	$BaSO_4$	Rhombic	2.74 (1)	2.48 (1)	3.01 (1)	2.74 (1)
Gypsum (oven-dried)	$CaSO_4 \cdot xH_2O$	Rhombic	6.64 (2)	6.11 (2)	4.87 (3)	5.62 (3)
Gypsum (air-dried)	$CaSO_4 \cdot 2H_2O$	Monoclinic	4.69 (3)	5.22 (3)	4.16 (3)	4.16 (3)
Selenite	$CaSO_4 \cdot 2H_2O$	Monoclinic	4.87 (1)	4.20 (1)	3.10 (1)	3.81 (1)
Calcium carbonate (pure)	$CaCO_3$	Hexagonal	4.69 (3)		6.24 (2)	4.48 (3)
Aragonite	$CaCO_3$	Rhombic	3.23 (3)		5.09 (3)	3.01 (3)
Iceland spar	$CaCO_3$	Hexagonal	5.93 (2)		7.43 (2)	6.28 (2)
Limestone	$CaCO_3$	Hexagonal	4.69 (3)		5.66 (3)	4.96 (3)
Marble	$CaCO_3$	Hexagonal	3.01 (3)		4.02 (3)	3.72 (3)
Mica (muscovite)	Complex silicate	Monoclinic	7.48 (2)	7.52 (2)	7.28 (2)	7.08 (2)
Monax glass	Complex silicate	Amorphous	1.78 (5)	2.34 (5)	3.10 (4)	3.10 (4)
Porcelain	Complex silicate	Amorphous	1.78 (5)	2.39 (5)	3.23 (5)	3.01 (5)
Kaolin	Complex silicate	Monoclinic	5.58 (1)	5.75 (1)	6.02 (1)	6.55 (1)
Steatite	Complex silicate ($H_2Mg_3Si_4O_{12}$)	Monoclinic				

Table V-6 (continued)

Substance	Chemical Composition	Crystalline Structure	Water	HCl	NaOH	NaCl
Chalk	$CaCO_3$,mixed with clay	Hexagonal	3.94 (1)		8.41 (1)	5.22 (1)
Solnhofen slate	$CaCO_3$,mixed with clay	Hexagonal	5.22 (1)		9.91 (1)	5.22 (1)

(1) Strongly thixotropic and plastic.

(2) Strongly thixotropic, passively dilatant and not plastic.

(3) Thixotropic, passively dilatant and not plastic.

(4) Dilantant and weakly thixotropic.

(5) Not thixotropic.

Particle size 1 to 10 μm.

may be related to the particle-particle interaction forces and sedimentation volumes.

Figure V-13 compares the yield stress Y_f and relative sedimentation volume R for uncoated and coated calcium carbonates.

Values of yield stresses are determined from literature (S-11). Yield stresses in steady shear flow Y_f were obtained for polystyrene/uncoated and stearic acid coated calcium carbonate compounds at volume traction of 0.30. A Rheometrics Mechanical Spectrometer (cone-plate mode) was used in those experiments. The measurement temperature was 180°C.

The relative sedimentation volume R has been obtained for toluene/calcium carbonates systems at a volume fraction of 0.05.

A strong correlation is found between yield stress and relative sedimentation volume. As relative sedimentation volume increases, the yield stress in melt increases.

The yield stress of uncoated calcium carbonate compounds are greater than coated calcium carbonate compounds at a fixed relative sedimentation volume. This may be due to the particle-polymer molecule interaction.

Freundlich and Jones (F-5) determined rheological properties of suspensions in water, HCl, NaOH and NaCl vehicles as well as the sedimentation volumes. Rheological properties of suspensions are classified into five categories: (1) strongly thixotropic and plastic, (2) strongly thixotropic, passively dilatant and not plastic, (3) thixotropic, passively dilatant and not plastic, (4) dilatant

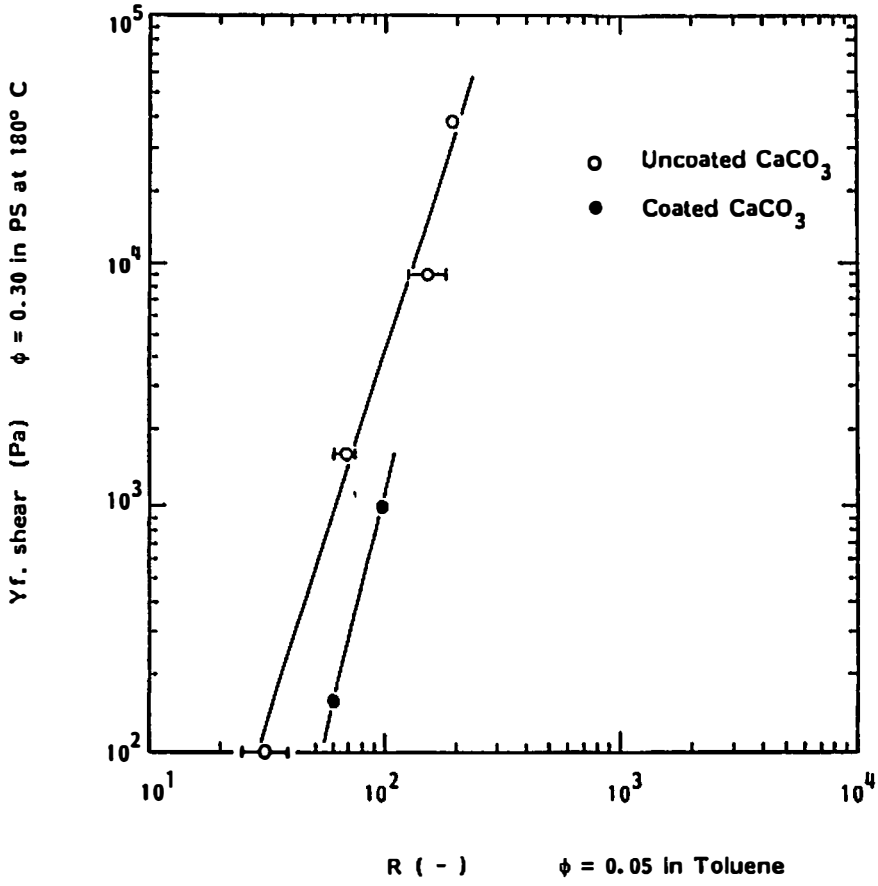

Figure V-13. Shear flow yield stresses of PS/$CaCO_3$ compounds at 180°C as a function of R values in toluene.

and weakly thixotropic, and (5) not thixotropic. These rheological classifications are included in Table V-6.

Figure V-14 shows the correlation between relative sedimentation volume R and rheological properties. This includes the results of earlier work (F-5) and the present research.

We first pay our attention to the results of the present research involving calcium carbonates, coated calcium carbonates and carbon blacks. The particulates which possess yield stress of greater than 1 x 10^3 Pa in polystyrene compounds (ϕ = 0.30) at 180°C were classified into category (1). These include calcium carbonates and carbon blacks. These showed thixotropic viscosity overshoot phenomenon. Stearic acid coated calcium carbonates except the finest one (dp = 0.07 μm) were included under category (5).

Effect of particulate size is distinct. The smaller particulates possess the greater relative sedimentation volumes at each classification.

Results obtained by Freundlich and Jones (F-5) indicates that the relative sedimentation volume R decreases, in general, as thixotropic properties of suspension are enfeebled, and as dilatant properties increase.

A question arises why some of the particulates classified into (1) strong thixotropy and plasticity show very low relative sedimentation volumes. Freundlich and Jones (F-5) reported the sizes of particulates were 1 μm to 10 μm. They fractionated powders by sedimentation in water using Stokes' law (Eq. (V-3)).

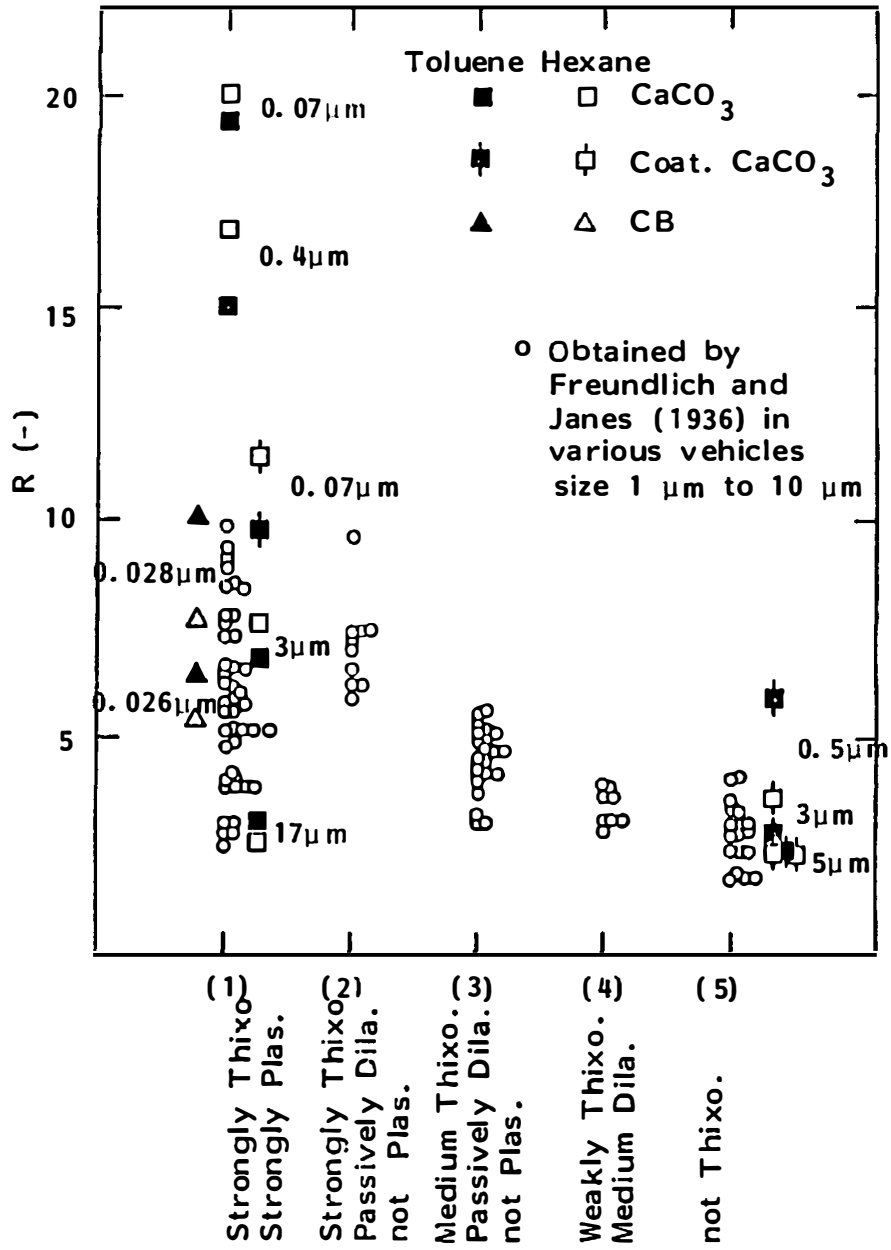

Figure V-14. Relative sedimentation volume R and rheological properties.

As was discussed in the previous section, the particles which have s trong particle-particle interaction may form a loose network structure. If this is formed, the particle size cannot be determined correctly by Stokes' law. The particulates of category (1), strong thixotropy and plasticity, may come under this. Size of some particulates under category (1) may not be correctly determined and presumably greater than the range of 1 μm and 10 μm. These show small relative sedimentation volume due to the effect of particulate size which is clearly shown by the results of the present research.

CHAPTER VI

SOME COMMENTS ON MIXING PROCESSES

A. INTRODUCTION

Dispersion of filler is strongly governed by the conditions of mixing such as the viscosity and stress levels in the compound. It is necessary to understand these to interpret the characteristics of dispersion of compounds.

Here we discuss the shear viscosities and stresses of compounds and the peculiar observation of a thin hard layer of unincorporated filler in an internal mixer.

B. SHEAR VISCOSITY AND STRESS IN MIXING PROCESSES

The viscosity and stress levels of compounds during the mixing process appear to be one of the major factors in controlling the dispersion of filler.

Flows of polymer melts in the mixing devices are complex. We may determine the shear viscosity and stress levels at the nip section of a two roll mill and rotor tip section of an internal mixer. Materials in mixing devices presumably receive the greatest deformation rates in these sections and dispersion of filler seems significant.

The shear viscosity of small particle filled polymer melt is strongly dependent upon the type, size, volume fraction and surface coating of filler as discussed in Chapter IV and in earlier publications (C-1,L-6,M-19,S-10,S-11,T-8).

The compounds prepared for the present research, however, have a volume fraction of 0.05. The effect of small particulates on the viscosity of compound is small at $\phi = 0.05$. In addition, the viscosity of compound is strongly affected by small particles at low shear rate ($\dot{\gamma} < 10^{-1}$ sec^{-1}), but not significantly affected at high shear rates. The viscosity of the compound, accordingly, may be well represented by the viscosity of matrix polymer.

We define the shear rate as

$$\dot{\gamma} = \frac{|V_1 - V_2|}{H} \qquad (sec^{-1}) \qquad \text{(VI-1)}$$

where V_1 and V_2 denote the velocities of rolls and rotors at the surfaces, and H is a gap distance. These are shown for two roll mill and internal mixer in Figure VI-1.

Shear viscosities of unfilled polystyrene and polypropylene were obtained using Monsanto Processability Tester. The shear stresses were determined by

$$\sigma = \eta \cdot \dot{\gamma} \qquad \text{(VI-2)}$$

The literature shows the shear rate at the nip region of the two roll mill when both the front and rear rotors rotate with the

Two Roll Mill

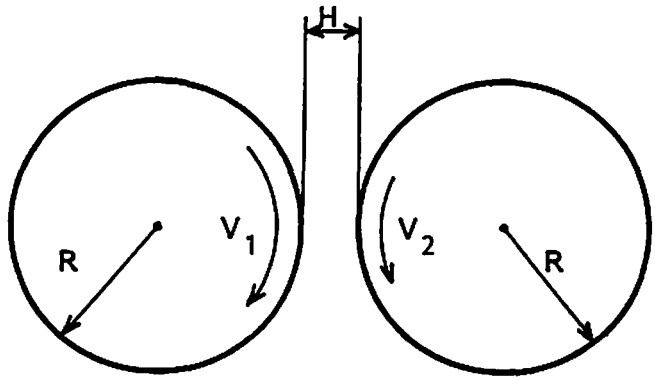

Internal Mixer

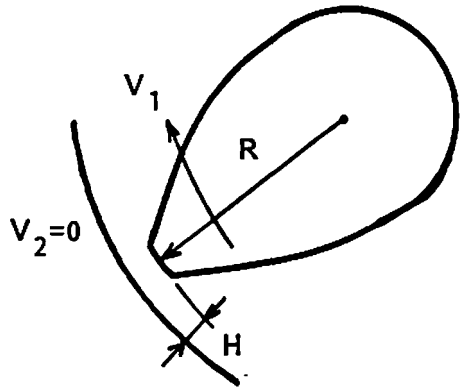

Figure VI-1. Dimensions of mixers.

same speeds. In our case the speeds are very different between the front and rear rotors (front 20 ft/min; rear 7 ft/min).

We must develop the equation of the shear rate distribution for the different rotor speeds. However, the flow rate Q is unknown in our case and we cannot determine the shear rates.

Table VI-1 summarizes the shear rates, shear viscosities and shear stresses in the two roll mill and the internal mixer for polystyrene (at 150°C) and polypropylene (at 175°C). The nip distance in the two roll mill varies depending upon compounds. These were determined for two distances of 5 and 10 mm.

We note that the shear rates in the internal mixer are much greater than those in the two roll mill. Accordingly, the shear stresses are greater in the internal mixer than in the two roll mill. This is namely due to the large nip distances of the two roll mill.

Polystyrene possesses greater shear viscosities and stresses than the polypropylene in the mixing devices.

C. THIN LAYER OF UNINCORPORATED FILLER

A peculiar observation which should be mentioned before the discussion of the level of dispersion is the existence of a hard thin layer formed by unincorporated filler on the chamber wall of the internal mixer. This was found for polystyrene/calcium carbonate systems, especially untreated calcium carbonates.

The chamber wall and rotors were disassembled after mixing. The thin layer of unincorporated filler was observed and weighed. Figure VI-2 shows a schematic drawing of this layer.

Table VI-1. Shear Rates, Shear Viscosities, and Shear Stresses of Matrix Polymers in Mixing Devices

				Polystyrene (150°C		Polypropylene (175°C	
		H (mm)	$\dot{\gamma}$ (sec^{-1})	η (Pa·sec)	σ (Pa)	η (Pa·sec)	σ (Pa)
Two Roll Mill	Front - 20 ft/min Rear - 7 ft/min	5	3.16×10^{0}	2.1×10^{4}	6.6×10^{4}	4.1×10^{3}	1.3×10^{4}
		10	1.58×10^{0}	3.0×10^{4}	5.0×10^{4}	5.0×10^{3}	8.0×10^{3}
Internal Mixer	25 rpm	1.05	4.61×10^{1}	3.4×10^{3}	1.6×10^{5}	1.0×10^{3}	4.6×10^{4}
	50 rpm	1.05	9.23×10^{1}	1.9×10^{3}	1.8×10^{5}	6.4×10^{2}	5.9×10^{4}

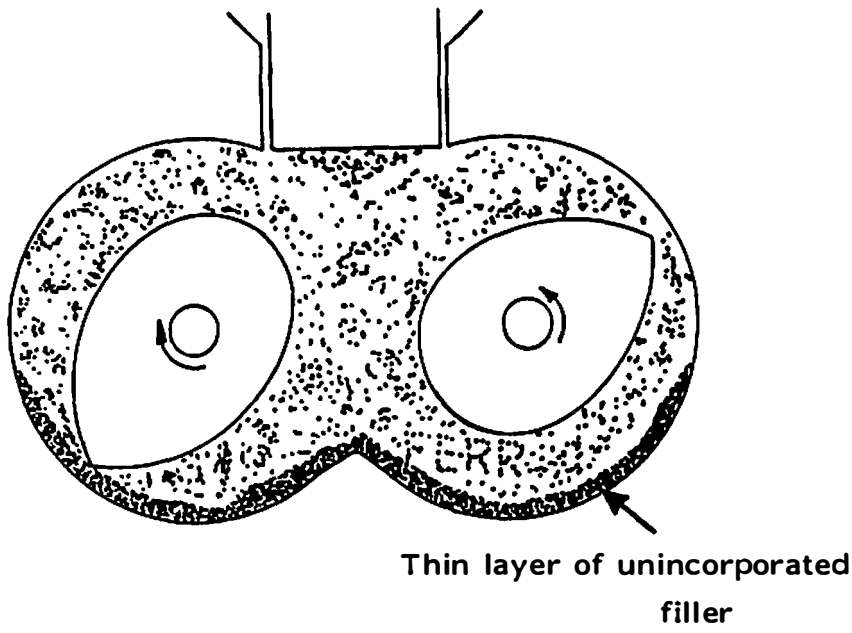

Figure VI-2. Thin layer of unincorporated filler.

Table VI-2 summarizes the amount of unincorporated filler collected from the chamber wall of the internal mixer for the polystyrene/calcium carbonate systems (dp = 0.07 μm, ϕ = 0.05). The rotor speed was 25 rpm. The values shown in Table VI-2 were determined by

$$\frac{\text{Mass of unincorporated filler on the chamber}}{\text{Total mass of the filler added in the chamber}} \times 100 \qquad \text{(VI-3)}$$

The amount of unincorporated filler is significant for polystyrene/uncoated calcium carbonate systems. The layer remains even after 10 minutes of mixing. The layer disappears more rapidly in the coated calcium carbonate compounds.

The amount of the unincorporated filler was not significant in polypropylene compounds.

Table VI-2. Percentage of Unincorporated Filler for PS/$CaCO_3$ Systems (dp = 0.07 μm, ϕ = 0.05)

Mixing Time / System	1 Min	3 Min	5 Min	10 Min
PS/Unc. $CaCO_3$	Not Measured	36%	36%	5%
PS/Coat. $CaCO_3$	14%	11%	5%	~0%

CHAPTER VII

OPTICAL MICROSCOPY

A. INTRODUCTION

A.1. Terminology

We will begin by reviewing and defining the terminology which is often used in this present research. These are a matrix, a particle or a particulate, an ultimate particle or particulate, an aggregate, a dispersion, a structure formed by particles or particulates, an agglomerate, a three-dimensional network structure, etc.

A matrix or a matrix polymer denotes the base polymeric resin which is mixed with filler. This is, in the present research, polystyrene and polypropylene.

A particle or particulate are used in a broad sense. These sometimes mean filler and other times a simple particle or particulate of filler.

When a single particle or particulate is emphasized, the words of an ultimate particle or particulate and individual particle or particulate are commonly used.

Some types of fillers, typically carbon black (C-4), form an aggregate. An aggregate is a fused and a persistent structure. In the case of carbon black, this structure could occur by particle coalescence (fusion) during the formative stage in the furnace (D-12). Aggregate structure can be eliminated by extreme methods, such as ball

milling. In the conventional mixing process, the aggregate is the smallest unit and ultimate form of filler.

Ultimate particles and aggregates often form some type of structure in the matrix commonly due to the particle-particle interactions. We do not distinguish if such a structure is formed in the process of mixing or if it has existed in the filler prior to the mixing process.

In the present research, two distinct types of structures are considered. These are agglomerates and three-dimensional network structures. These structures are distinguished from the aggregate for the reason that the agglomerate and three-dimensional network structures are based on the interparticle interactions but not on a persistent coalescence

The agglomerate is a packed structure of ultimate particulates or aggregates. The three-dimensional network is a continuous structure of particulates and often called an infinite large cluster by the authors of percolation theories. Schematic drawings of these are given in Figure VII-1 in contrast to the aggregate.

Constitution or formation and destruction of these structures may occur in the process of mixing. These are presumably the reversible structures resulting from interparticulate interactions. The destruction of these structures during the mixing process is called dispersion.

ultimate particle

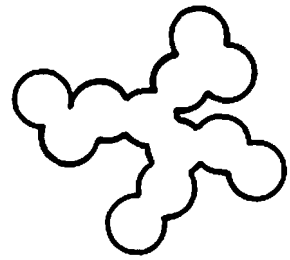

aggregate

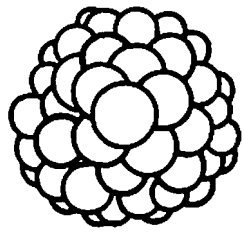

agglomerate

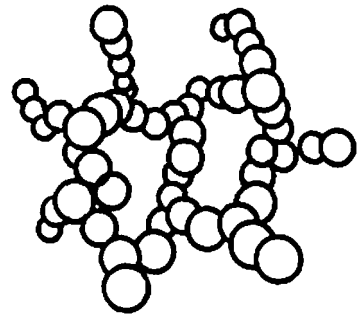

three dimensional
network structure

Figure VII-1. Concepts of ultimate particle, aggregate, agglomerate and three-dimensional network structure.

A.2. Optical Microscopy

Optical microscopy has been commonly used to determine the level of dispersion (B-4,C-3,L-2,M-6,S-9). Methods of dispersion rating were developed for carbon black compounds. These are carefully discussed in Chapter II, Literature Survey.

The smallest object which can be determined under an optical microscope is roughly 20 μm at the magnification of 40 and several microns at the magnification of 400. Ultimate particles and agglomerates which are greater than these sizes may be observed. If the ultimate particles are smaller than 1 μm and well separated from each other, these would not be observed. Only the agglomerates are observed for such particulates.

This method is simple and straightforward to characterize the dispersion based on relatively large agglomerates. Agglomerate size distributions may be determined. Tremendous efforts, however, may be required to acquire reliable results. The application of an image analyzer would help to reduce labor and human error.

Restrictions lie in the loading level of filler as well as the size of the object. If the volume fraction of the filler is high, particulates overlap through the thickness of the specimen and sharp image of agglomerates cannot be procured. This may be solved simply by reducing the thickness of the sample. However, it spontaneously reduces the volume of compound to be observed. The restriction of loading level of filler is less critical for the case of particulates having sizes of less than 1 μm. Ultimate particles are rarely

observed and only agglomerates are focused into the image until the opaqueness of the sample increases due to the reduction of inter-particulate distances at high volume loading level.

A few methods of dispersion rating have been developed by earlier workers. Leigh-Dugmore (L-2) determined the cross sections of carbon black agglomerates and compared these with the total area of coverage. Stump and Railsback (S-9) proposed standard photographs rated 1 to 10 depending upon the level of dispersion (Phillips dispersion rating). Micrographs of compound cross section were compared with them. Medalla (B-4,M-6) was concerned with both amount and average size of the agglomerates and prepared a set of standard micrographs to compare with micrographs of compounds (Cabot dispersion rating).

We will further develop the method of determination of dispersion. In the present research, the number of aggromerates will be determined as a function of the size of agglomerates.

The number of agglomerates in 1 cm^3 of compound N(d) may be defined as

$$N(d) = \left[\frac{N'(d)}{AH}\right] \frac{1}{n} \qquad \text{for } d_i < d < d_{i+1} \qquad \text{(VII-1)}$$

where

N'(d) : number of agglomerates counted on the micrographs;

d : diameter of agglomerate;

A : coverage area of a single micrograph;

H : thickness of the film sample;

n : number of micrographs investigated.

The distribution function is defined as:

$$P(d) = \frac{N(d)}{\Sigma N(d)} \qquad \text{(VII-2)}$$

where N(d) denotes the total number of agglomerates within a certain agglomerate size range as defined in Eq. (VII-1), and $\Sigma N(d)$ denotes the total number of agglomerates observed under the optical microscope.

The volume fraction of agglomerates $\phi(d)$ may be defined as:

$$\phi(d) = V(d)/V_f$$

$$= N(d) \cdot (\frac{\pi}{6} d^3)/\phi \qquad \text{for } d_i < d < d_{i+1} . \qquad \text{(VII-3)}$$

Here

V(d) : total volume of agglomerates within a certain size range;

V_f : total volume of filler;

N(d) : the number of agglomerates within a certain size range in 1 cm^3 compound;

ϕ : volume fraction of compound.

We note that large agglomerates are emphasized by Eq. (VII-3) even when the number is relatively small compared with small agglomerates.

B. EXPERIMENTAL PROCEDURE

Compression molded films of various compounds were observed with a polarized light optical microscope (Leitz, Laborlux 12 pol). The thickness of the compression molded sheets was ~100 μm. The magnifications used were x40 and x400. The agglomerates and ultimate particles were observed through the entire thickness of the film at low magnifications of x40. The depth of sharp focus is greater than 100 μm at the magnification of x40.

Individual ultimate particles and agglomerates were observed under cross polarized light more clearly at high magnification in general. Particulates and agglomerates shine in a dark background of polymer matrix under cross polarized light.

Photographs of microscope image were taken with a Nikon FM-2 camera. Over 30 pictures were taken at the magnification of x40 with Kodak Tri-X film to determine agglomerate size distribution.

The following equation was derived and used to determine the agglomerate size when agglomerates were greater than film thickness.

$$d_a = \left(\frac{3}{2} H d_a'^2\right)^{1/3} \qquad \text{(VII-4)}$$

where d_a denotes diameter of agglomerates, H thickness of film, and d_a' observed diameter of agglomerates which touch film surfaces.

The compounds which were observed under the optical microscope have been summarized in Tables VII-1 and VII-2.

Table VII-1. Compounds Used for Optical Microscopy Study.
Polystyrene Compounds

Filler Type	Ave. Diameter dp (μm)	Volume Fraction (-)	Mixer	Mixing Temp. (°C)	Mixing Time (Minutes)
$CaCO_3$	17.	0.05	Mill	150°C	20
	3.0	0.05	Mill	150°C	20
	0.4	0.05	Mill	150°C	20
	0.07	0.05	Mill	150°C	20
Coated $CaCO_3$	5.0	0.05	Mill	150°C	20
	3.0	0.05	Mill	150°C	20
	0.5	0.05	Mill	150°C	20
	0.07	0.05	Mill	150°C	20
$CaCO_3$	0.07	0.05	IM	150°C	3
					5
					10
Coated $CaCO_3$	0.07	0.05	IM	150°C	1
					3
					5
					10

Table VII-2. Compounds Used for Optical Microscopy Study.
Polypropylene Compounds

Filler Type	Ave. Diameter dp (μm)	Volume Fraction (-)	Mixer	Mixing Temp. (°C)	Mixing Time (Minutes)
$CaCO_3$	17.	0.05	Mill	175°C	20
	3.0	0.05	Mill	175°C	20
	0.4	0.05	Mill	175°C	20
	0.07	0.05	Mill	175°C	20
Coated $CaCO_3$	5.0	0.05	Mill	175°C	20
	3.0	0.05	Mill	175°C	20
	0.5	0.05	Mill	175°C	20
	0.07	0.05	Mill	175°C	20
$CaCO_3$	0.07	0.05	IM	175°C	1
					3
					5
$CaCO_3$	0.07	0.05	IM	175°C	1
					3
					5
					10
$CaCO_3$	3	0.20			
		0.30			
		0.40			
Coated $CaCO_3$	1	0.20			
		0.30			
		0.40	Prepared by Ferro		
Coated $CaCO_3$	3.0	0.05			
		0.10			
Coated $CaCO_3$	0.5	0.05			
		0.10			

C. RESULTS

C.1. General

A wide range of polystyrene and polypropylene compounds were observed with the optical microscope. Compression molded thin films of compound were generally prepared for observation.

The minimum size of agglomerates we could reasonably determine to estimate agglomerate size distribution was 20 μm because it was necessary to use low magnification (x40) to focus through the entire thickness of the film specimens. High magnifications of x400 were used to observe the detailed structure of agglomerates.

C.2. Polystyrene Compounds

Figures VII-2 through VII-5 show some typical optical micrographs of polystyrene compounds processed with a two roll mill or an internal mixer. The volume fractions of these compounds are 0.05. The mixing temperature used was 150°C. The mixing time is 20 minutes for all the two roll mill compounds and varies from 1 minute to 10 minutes for the internal mixer compound.

C.2.a. Two roll mill prepared compounds. Figure VII-2 represents a series of polystyrene/uncoated calcium carbonate compounds prepared on a two roll mill at 150°C. The volume fraction of filler is 0.05. The magnification is x40. The nominal ultimate particle size varies from 17 μm to 0.07 μm. Ultimate particles of 17 μm and 3 μm may be observed. These are well dispersed and

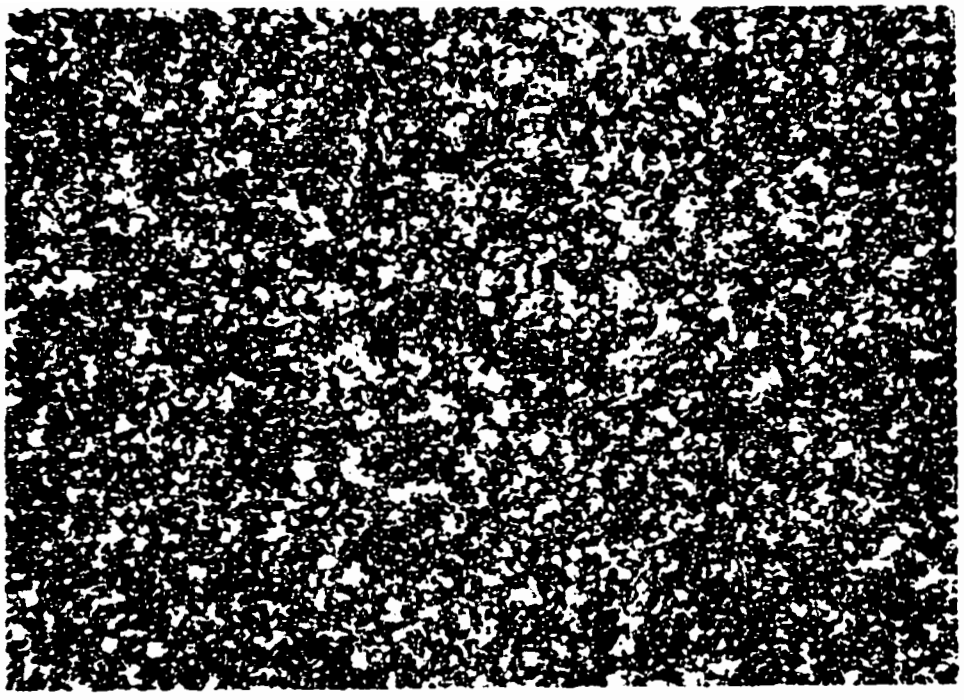

(a) 17μm

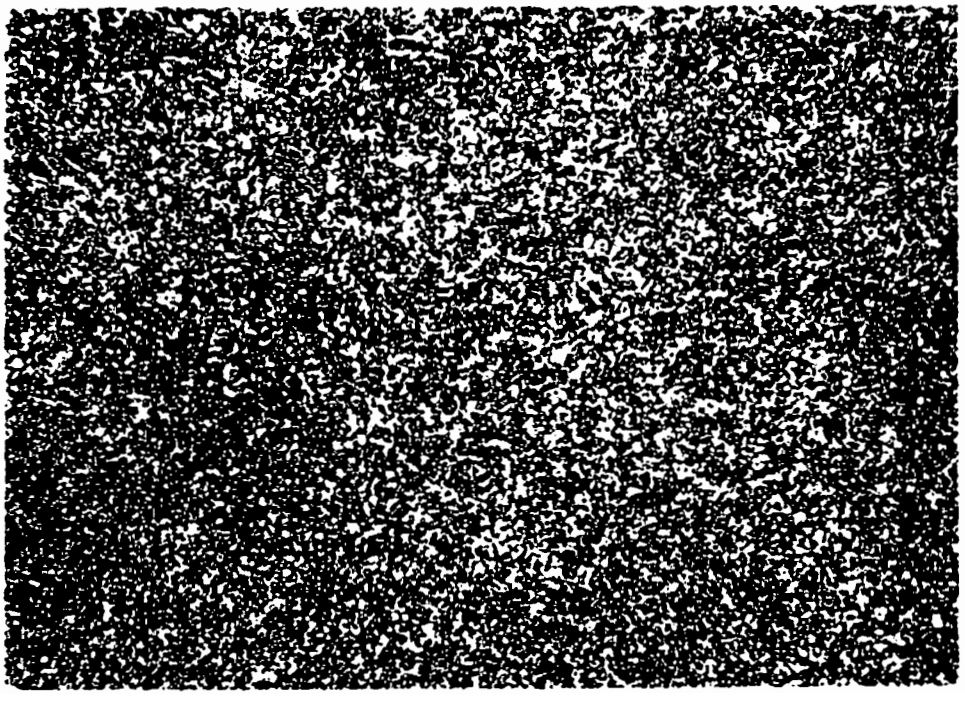

(b) 5μm X 40

Figure VII-2. Optical micrographs of PS/uncoat. $CaCO_3$ compounds (ϕ = 0.05, dp = various) (TRM 150°C, 20 min.).

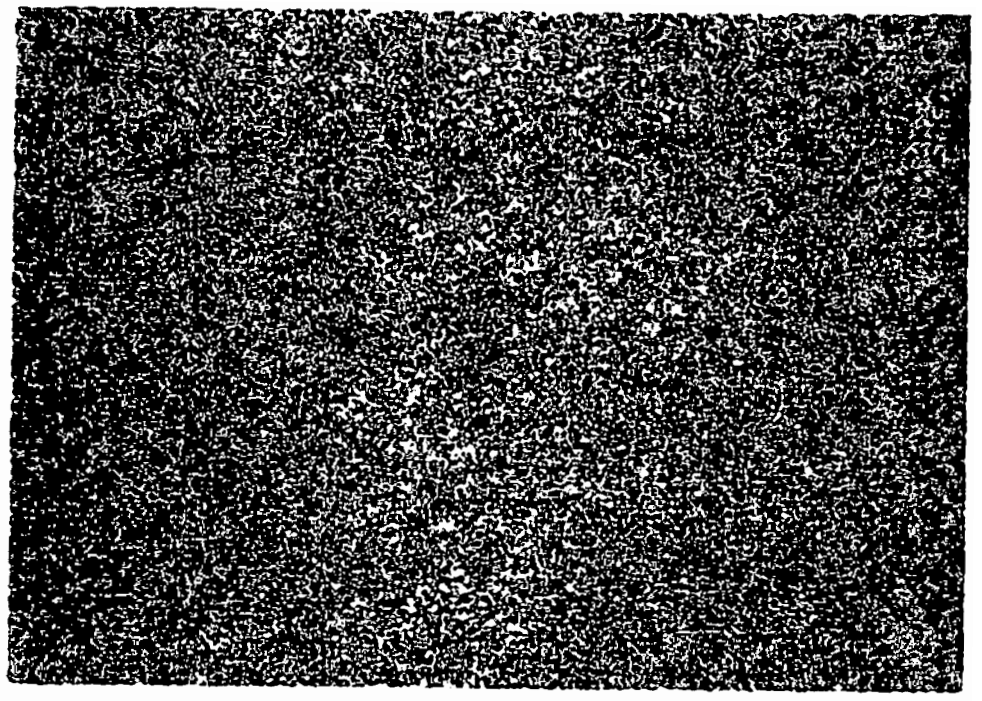

(c) 0.5μm

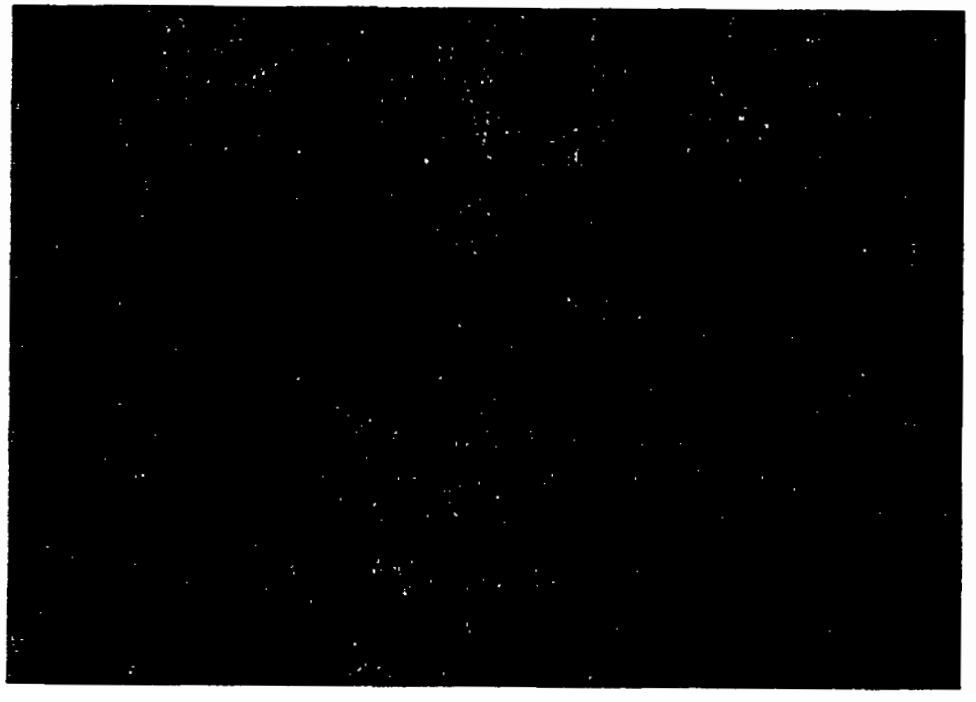

(d) 0.07μm

X 40

Figure VII-2 (continued)

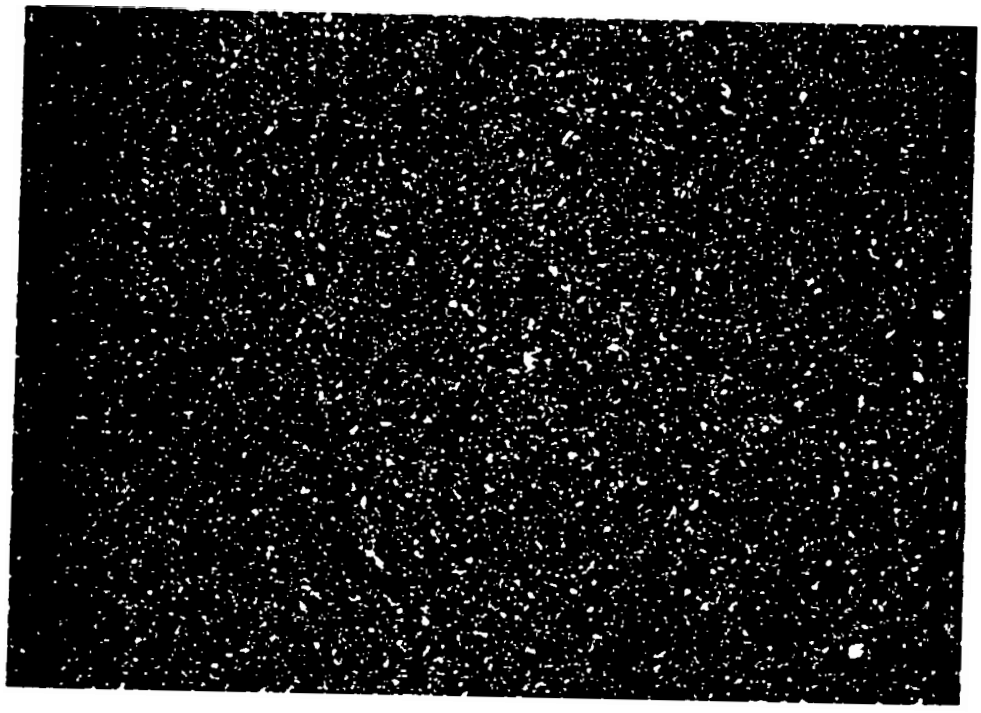

(a) 5μm

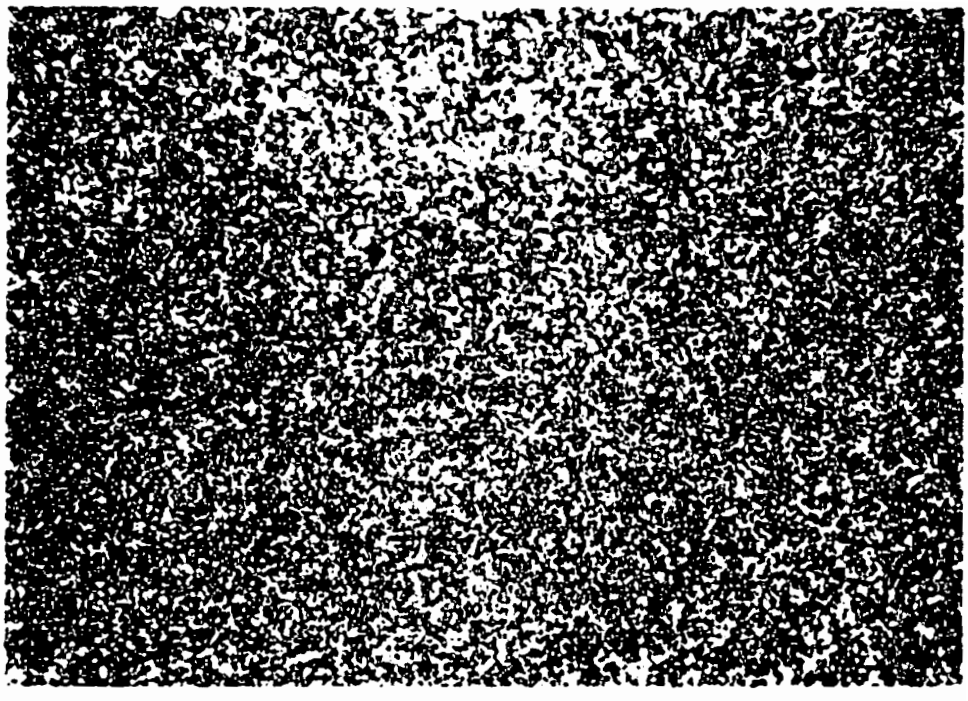

(b) 3μm X 40

Figure VII-3. Optical micrographs of PS/Coat. $CaCO_3$ compounds (ϕ = 0.05, dp = various) (TRM 150°C, 20 min.).

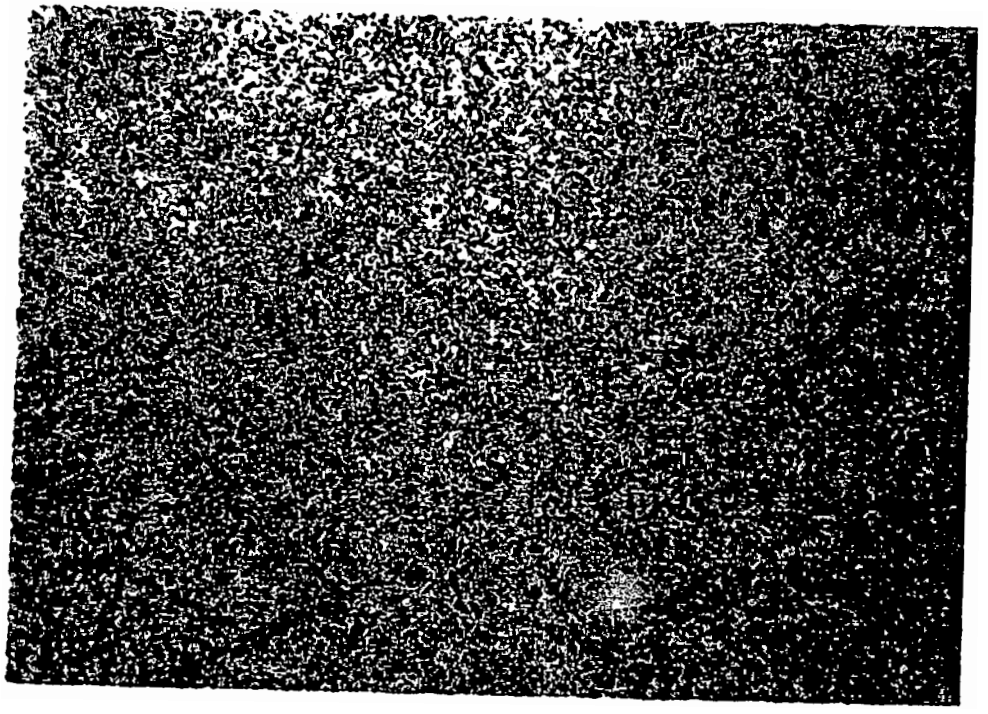

(c) 0.4μm

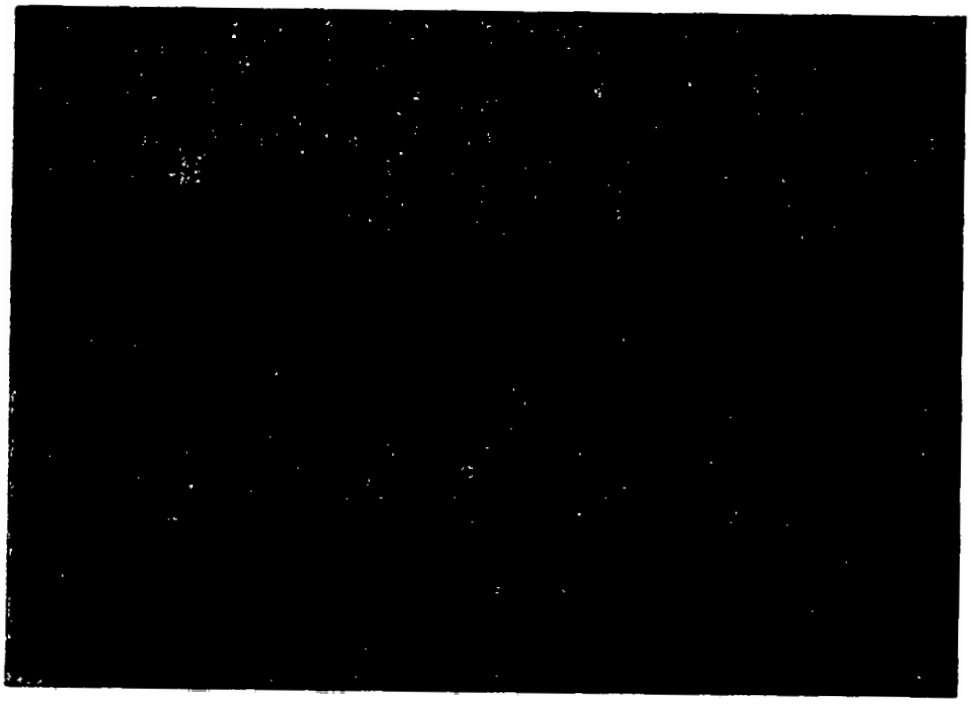

(d) 0.07μm

X 40

Figure VII-3 (continued)

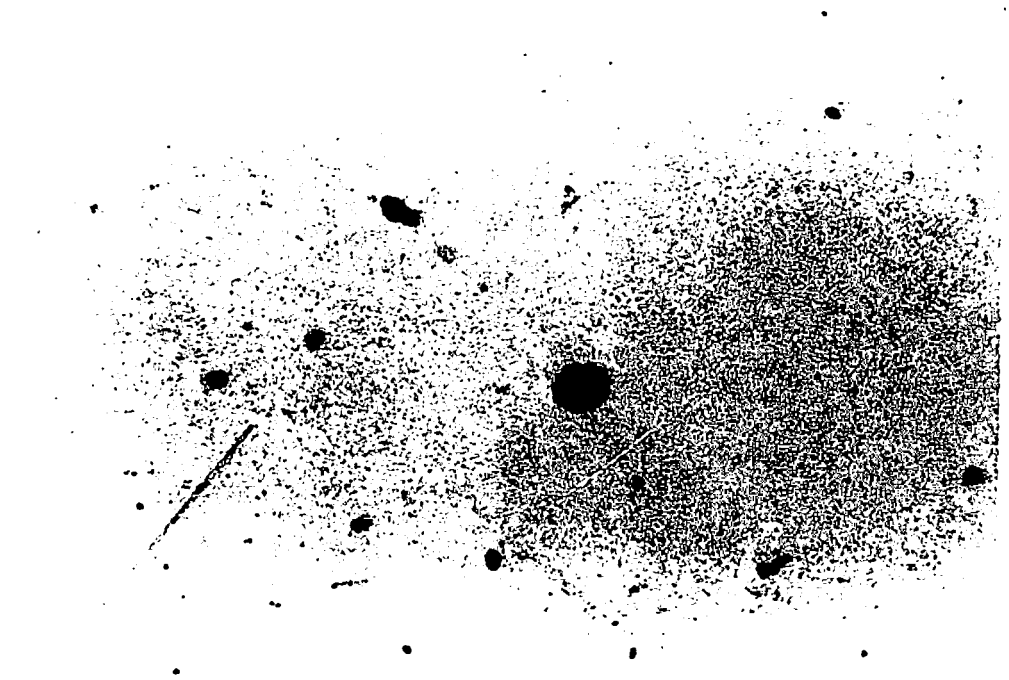

(a) 1 min.

(b) 5 min. X 40

Figure VII-4. Optical micrographs of PS/uncoat. $CaCO_3$ compounds (ϕ = 0.05, dp = 0.07 μm) (IM 150°C, 25 RPM).

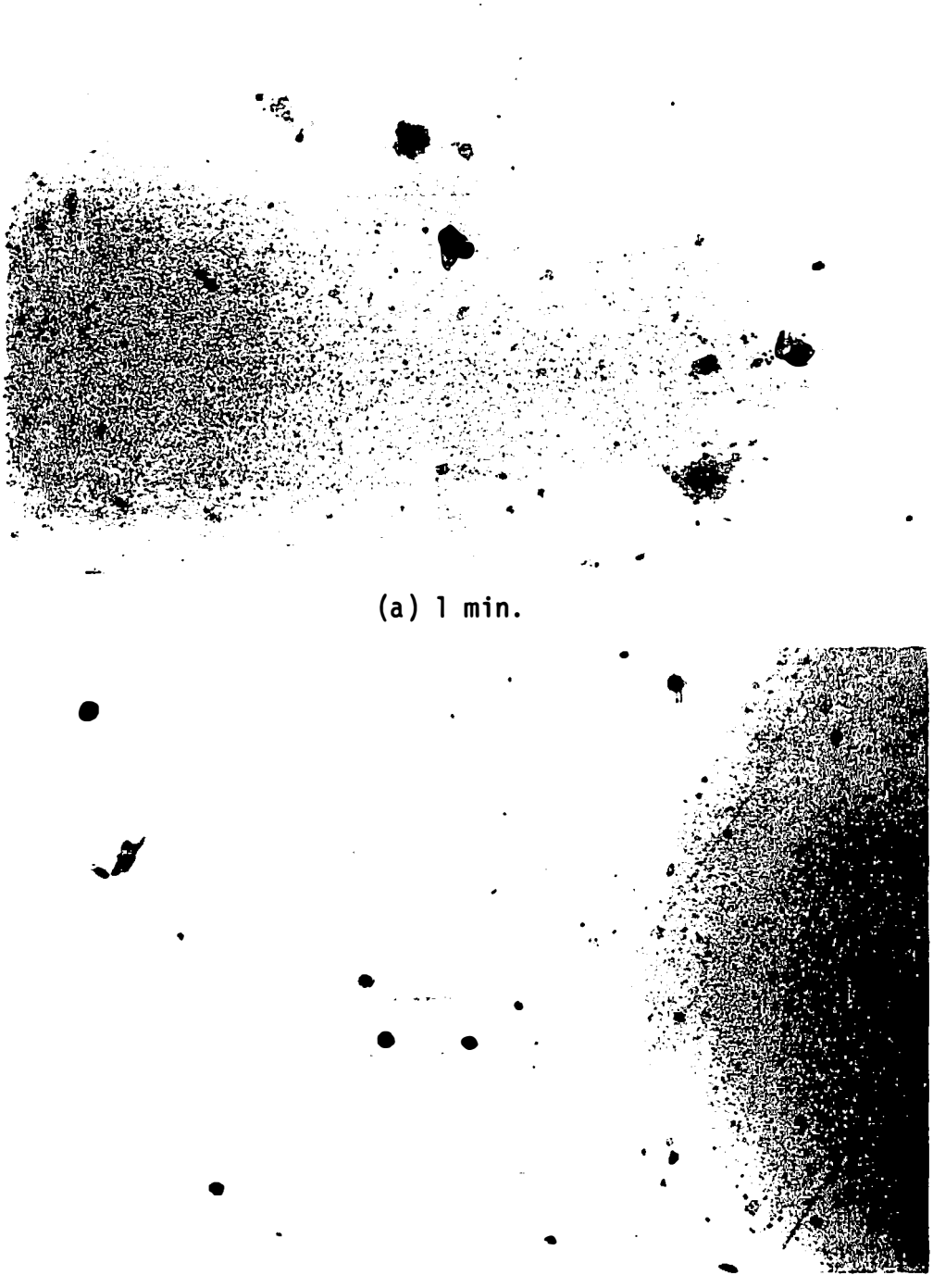

(a) 1 min.

(b) 5 min. X 40

Figure VII-5. Optical micrographs of PS/coat. $CaCO_3$ compounds (ϕ = 0.05, dp = 0.07 μm) (IM 150°C, 25 RPM).

agglomerates are not found. Ultimate particles of 0.4 μm and 0.07 μm calcium carbonates are not visible. Few agglomerates have been observed. These compounds would seem to have fairly good dispersions.

Figure VII-3 presents polystyrene/coated calcium carbonate compounds. Again, we observe fairly good dispersion at any ultimate particle size.

C.2.b. Internal mixer prepared compounds. Figures VII-4 and VII-5 show some typical optical micrographs of internal mixer processed polystyrene/uncoated and coated calcium carbonate compound, respectively. The mixing time varied as indicated in the figures. The ultimate particle size is 0.07 μm for both figures.

The dispersion is clearly different from two roll unit processed compounds. Large agglomerates of particulates are observed in the compounds prepared in an internal mixer for both uncoated and coated calcium carbonates.

C.3. Polypropylene Compounds

We now turn to the polypropylene compounds. Figures VII-6 through VII-10 represent optical micrographs of various polypropylene compounds. Volume fractions are always 0.05. The mixing temperature was 175°C, both for the two roll mill and the internal mixer. The mixing time is again 20 minutes for all two roll mill compounds and varies from 1 minute to 10 minutes for the internal mixer prepared compounds.

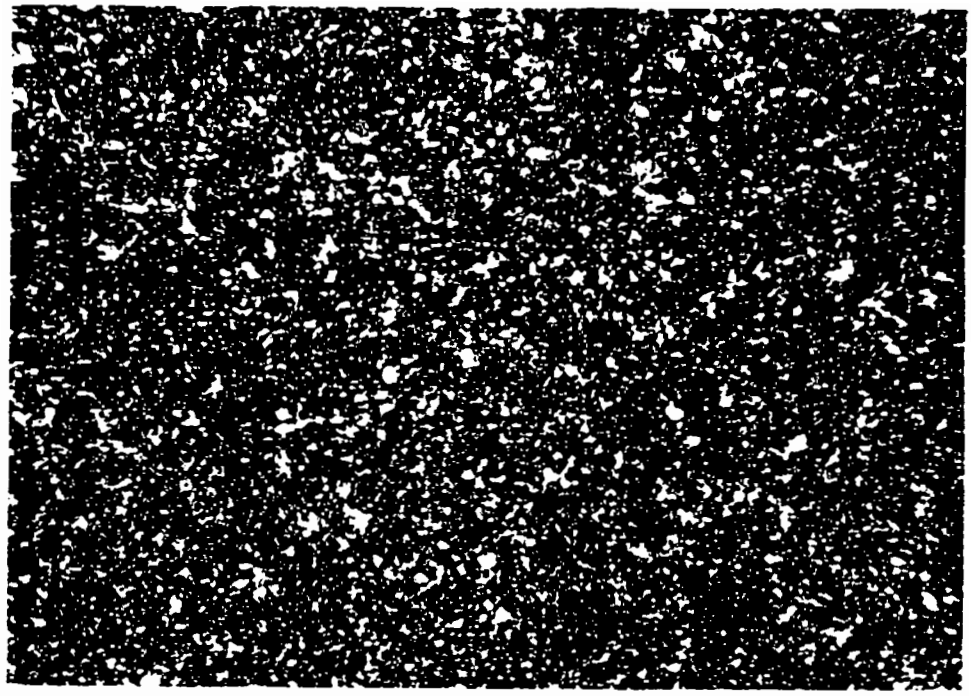

(a) 17 μm

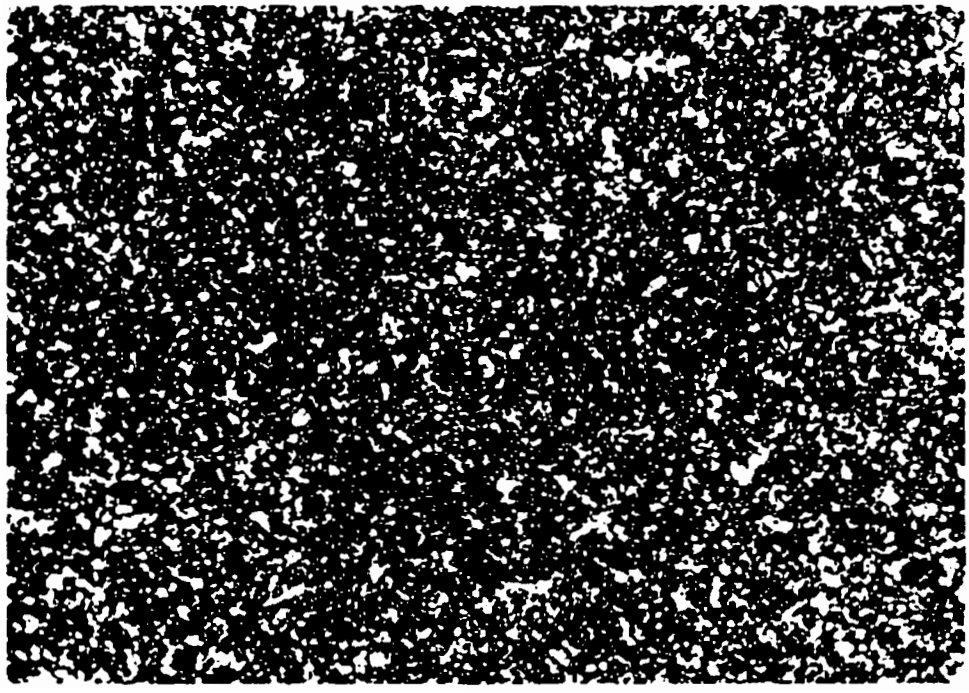

(b) 3 μm

Figure VII-6. Optical micrographs of PP/unc. $CaCO_3$ compounds (TRM 175°C, 20 min.) ϕ = 0.05.

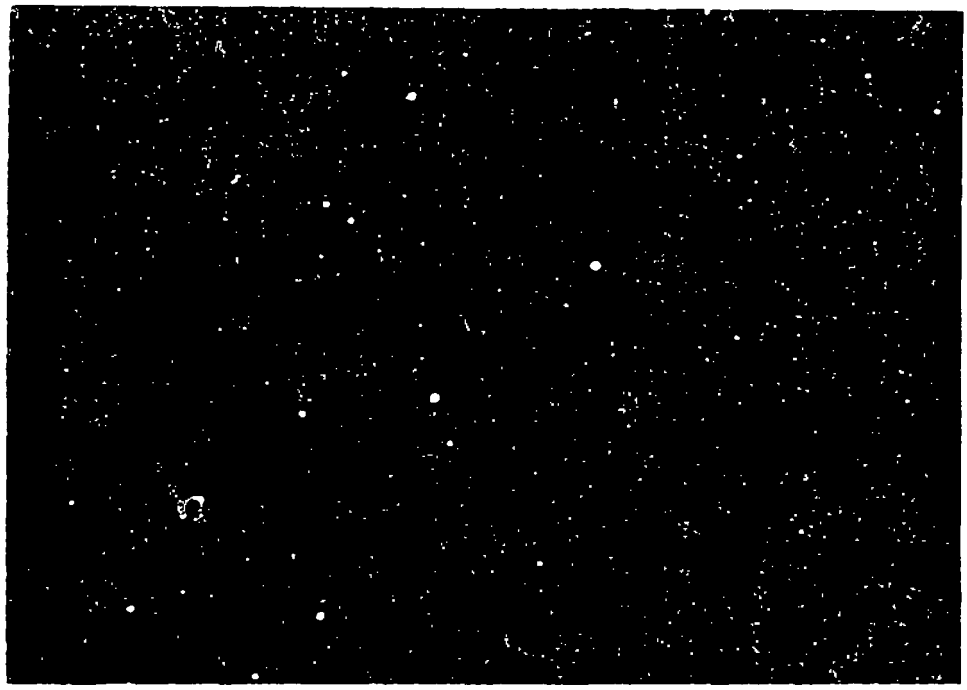

(c) 0.4 μm

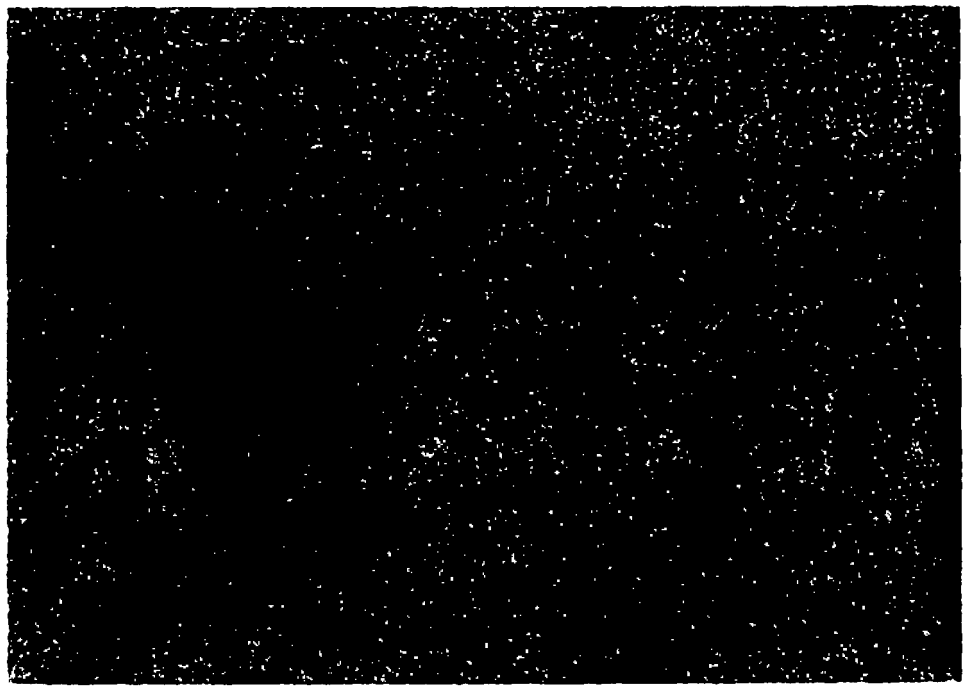

(d) 0.07 μm

Figure VII-6 (continued)

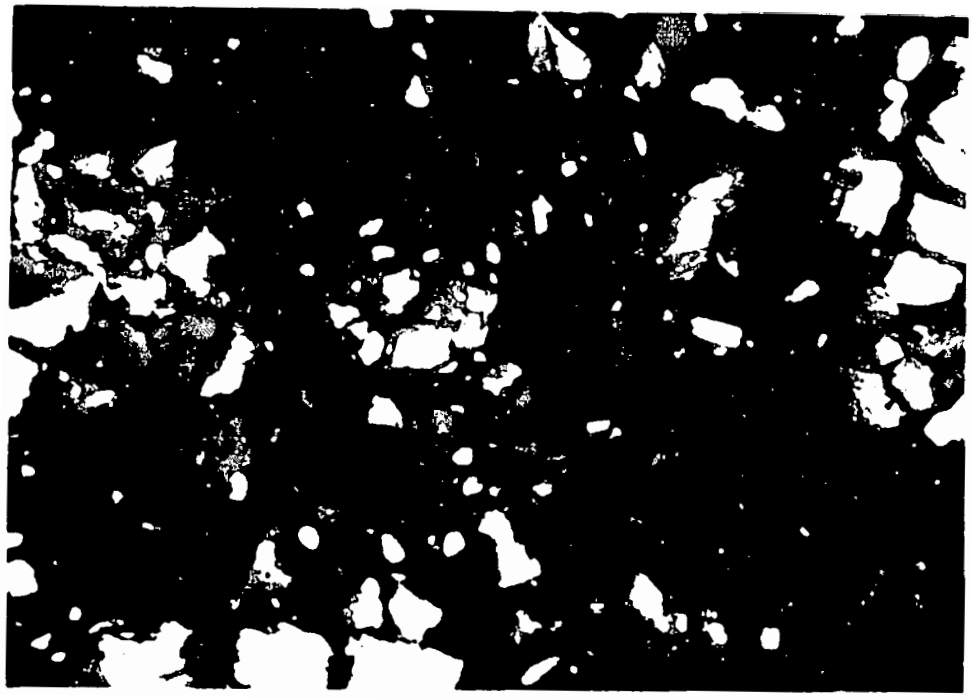

(a) 17μm

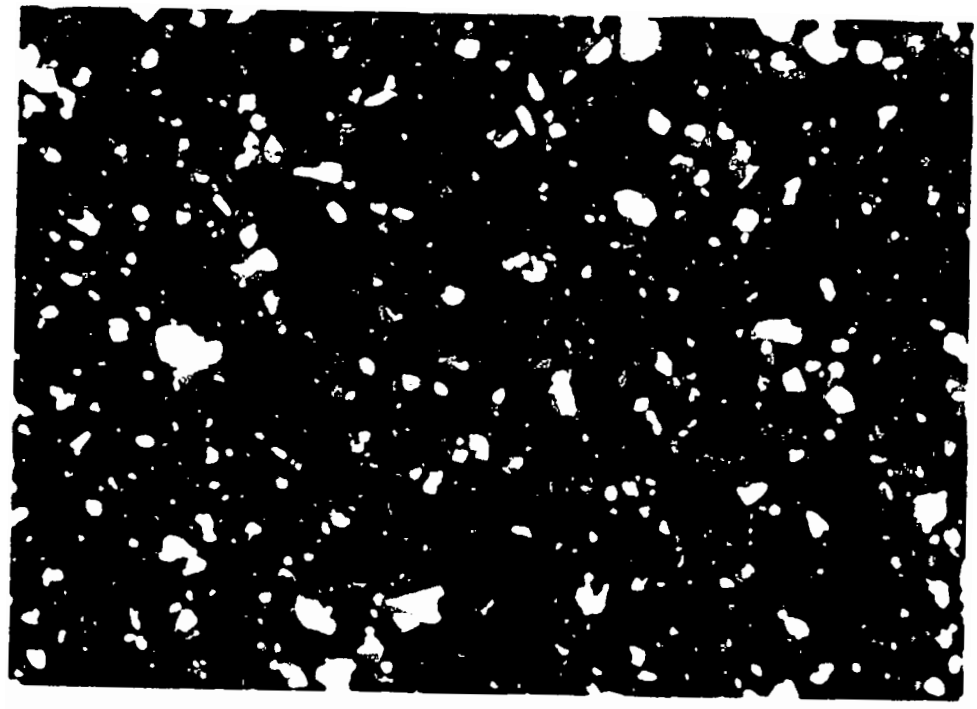

(b) 3μm

Figure VII-7. Optical micrographs of PP/unc. $CaCO_3$ compounds (TRM 175°C, 20 min.) ϕ = 0.05.

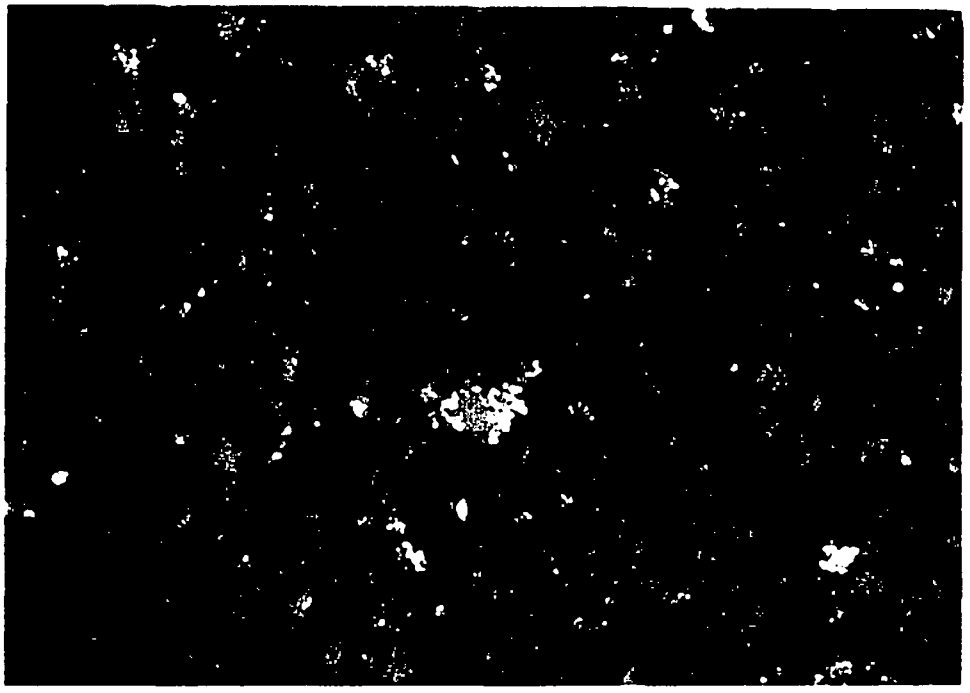

(c) 0.4 μm

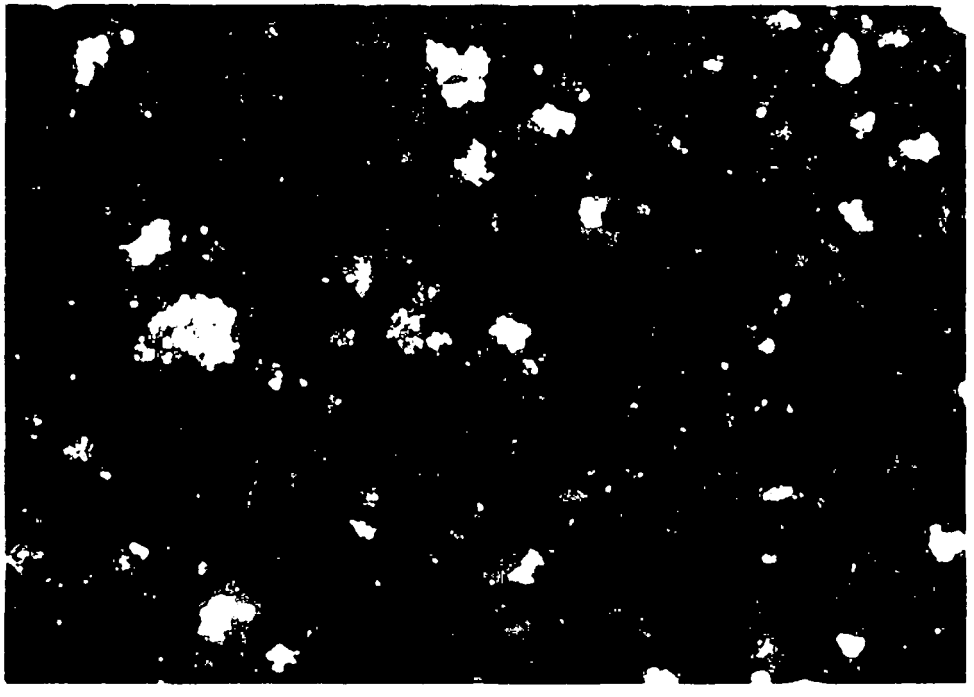

(d) 0.07μm

Figure VII-7 (continued)

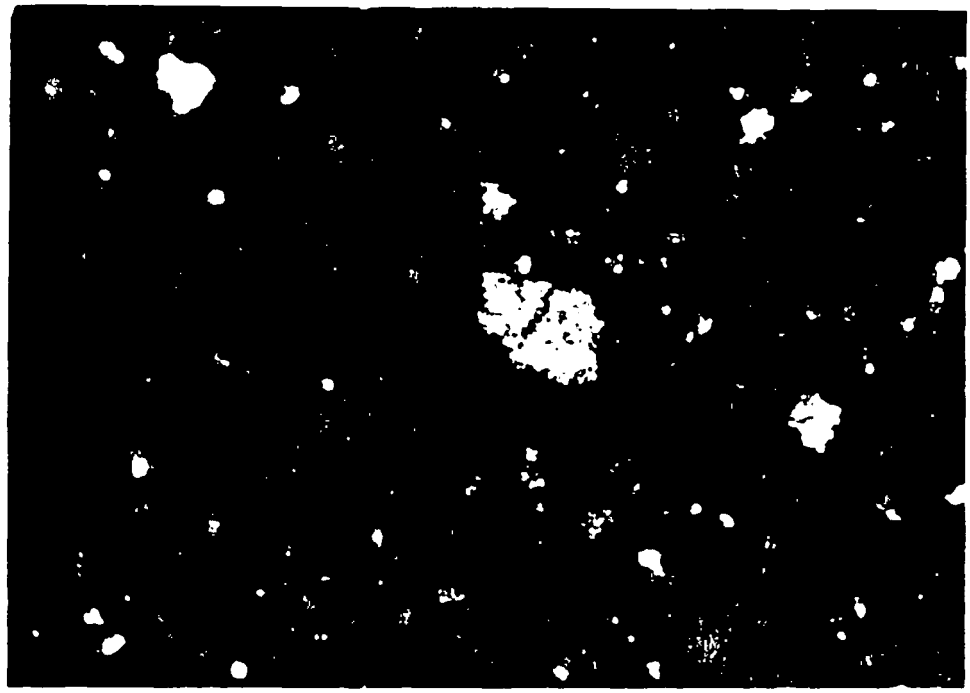

Figure VII-8. Detail structure of agglomerates PP/$CaCO_3$ compounds (TRM 175°C, 20 min.) ϕ = 0.05.

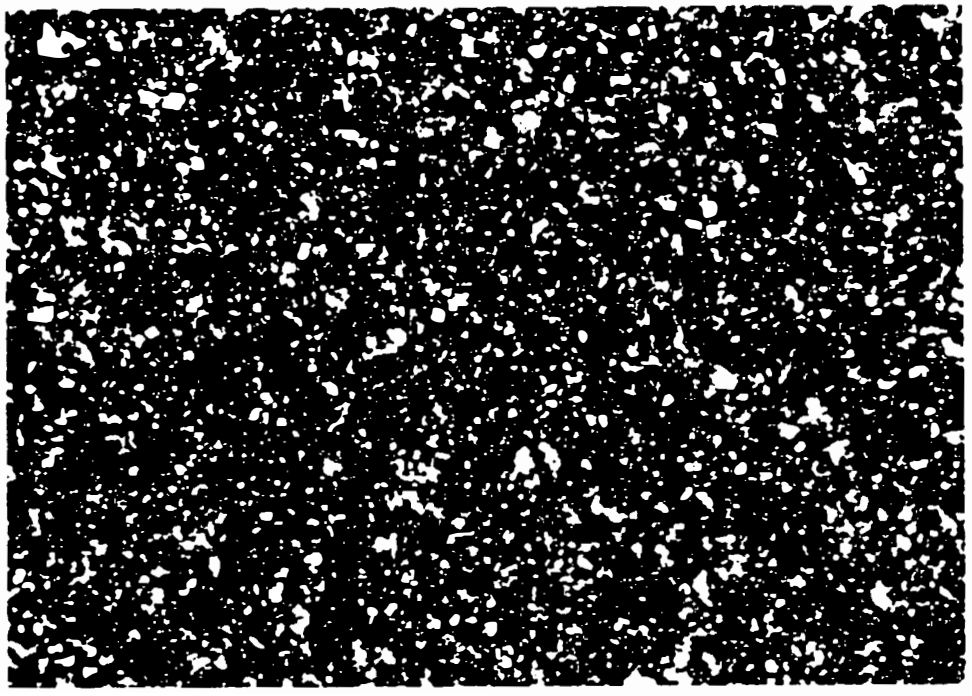

(a) 5 μm

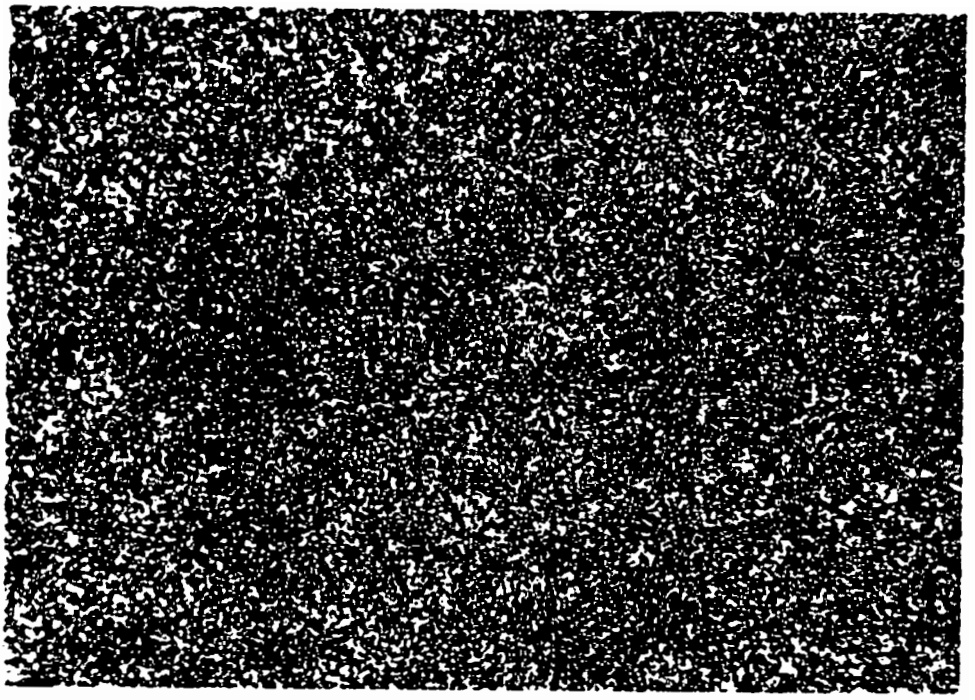

(b) 3μm

Figure VII-9. Optical micrographs of PP/coat. $CaCO_3$ compounds (TRM 175°C, 20 min.) ϕ = 0.05.

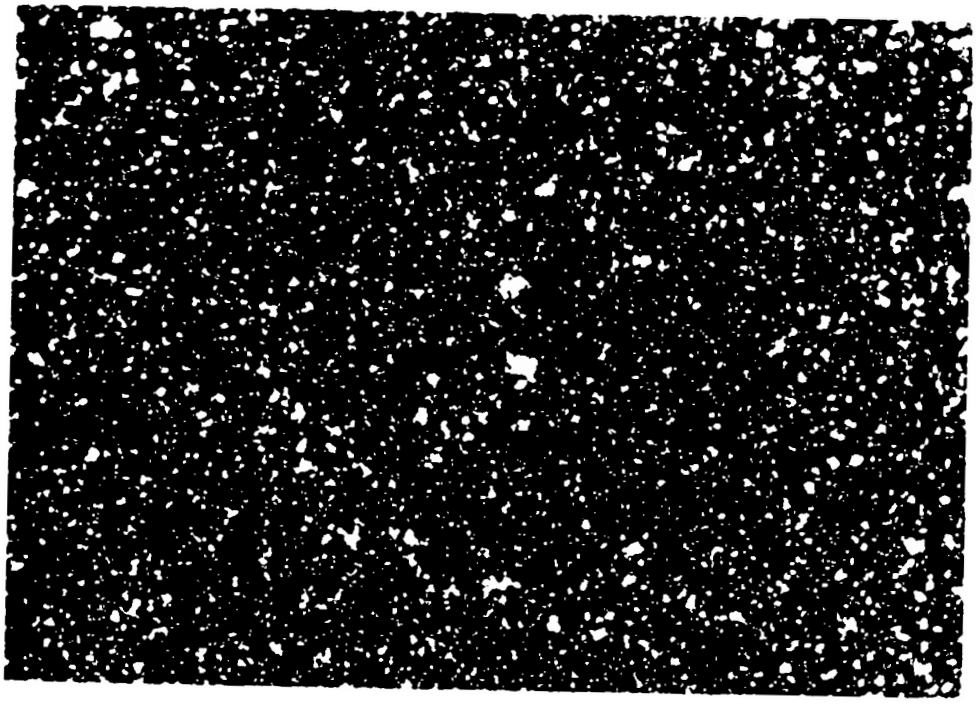

(c) 0.5 μm

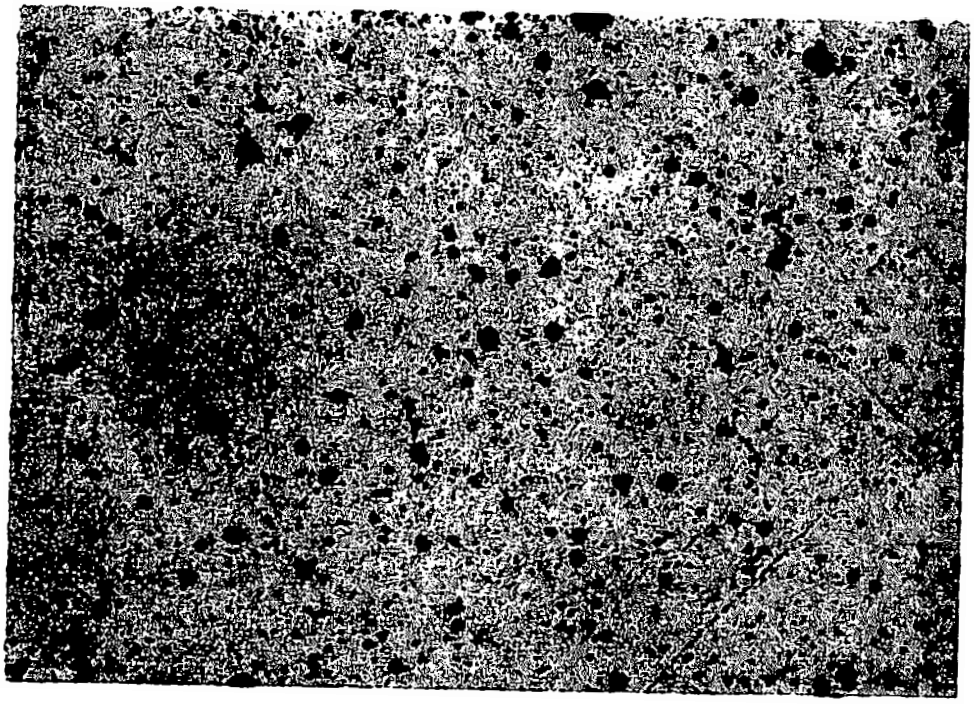

(d) 0.07 μm

Figure VII-9 (continued)

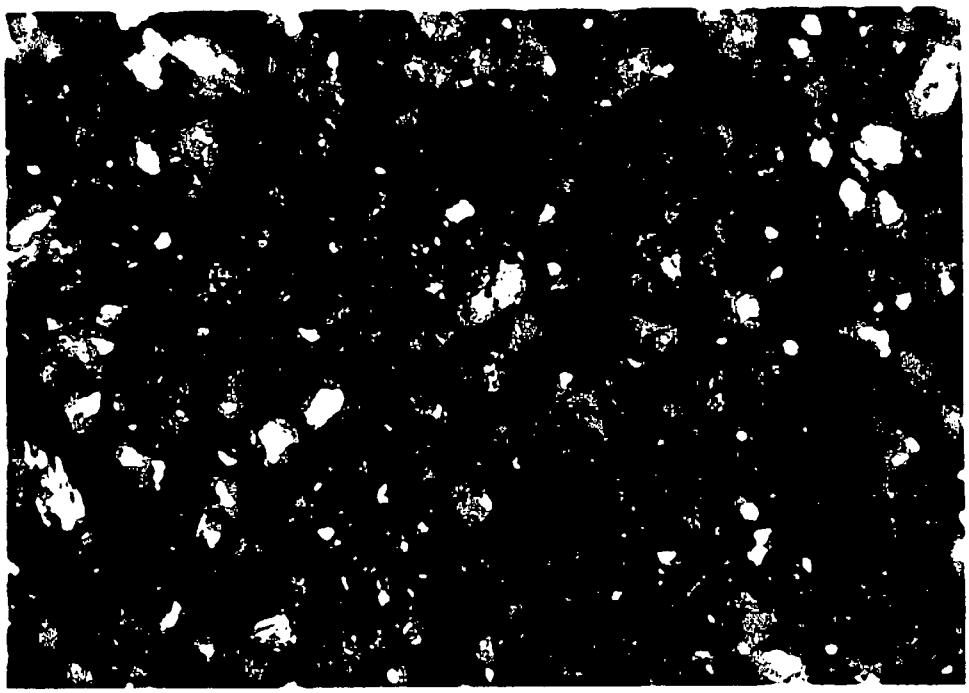

(a) 5 μm

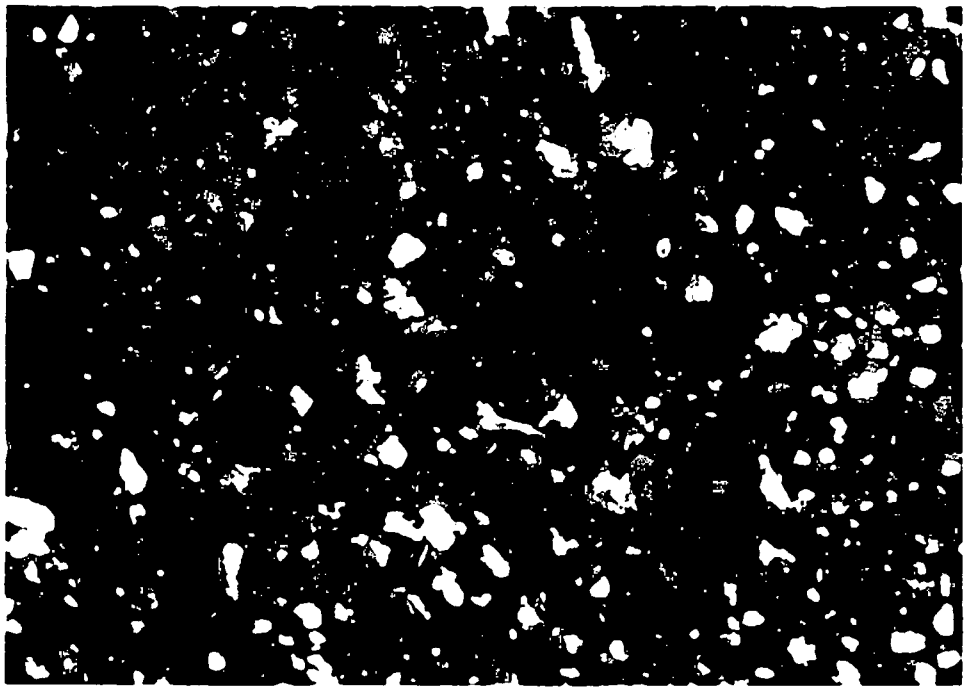

(b) 3 μm

Figure VII-10. Optical micrographs of PP/coat. $CaCO_3$ compounds (TRM 175°C, 20 min.) ϕ = 0.05.

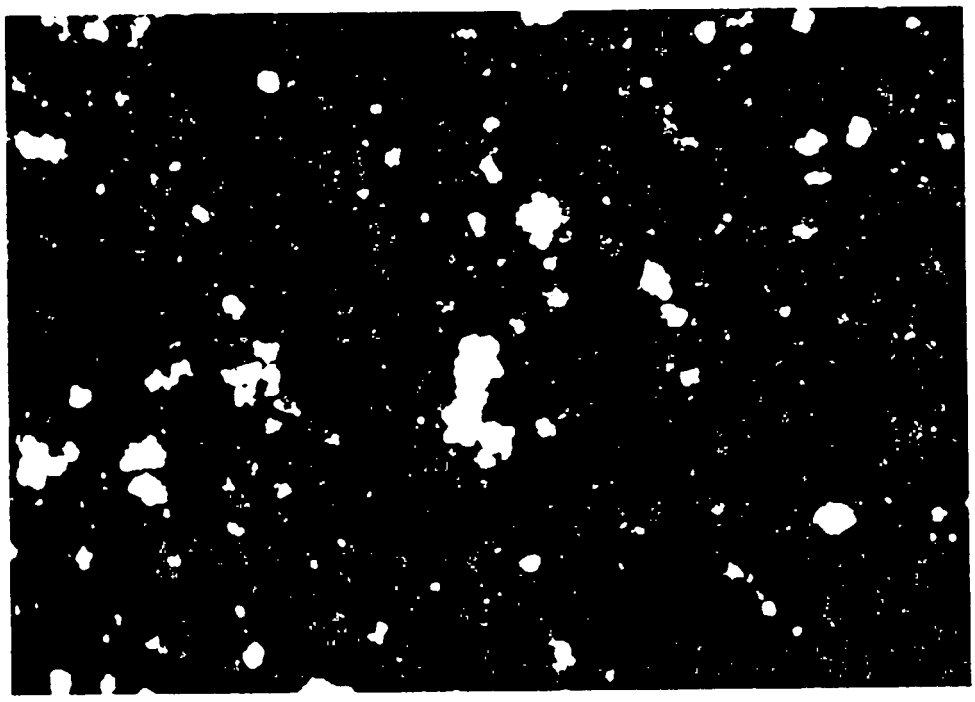

(c) 0.5 μm

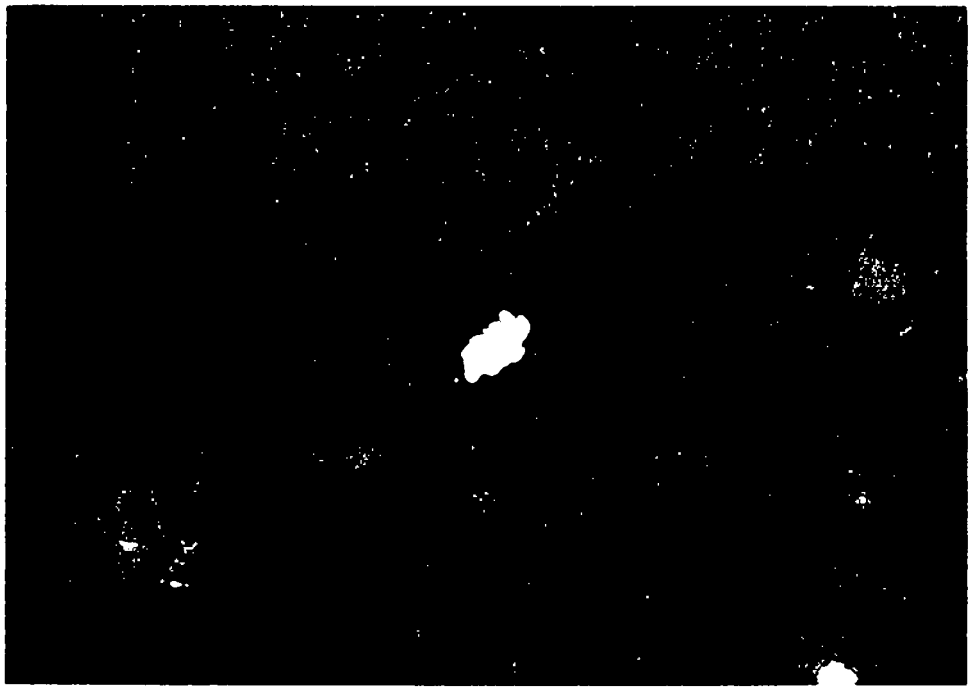

(d) 0.07 μm

Figure VII-10 (continued)

C.3.a. Two roll mill prepared compounds. Figures VII-6 through VII-8 show a series of micrographs of polypropylene/uncoated calcium carbonate compounds prepared by two roll mixing mill. The magnifications are x40 in Figure VII-6 and x400 in Figure VII-7. At low magnifications of x40 (Figure VII-6), it may be seen that the large particulates (larger than 1 μm) form some structures, not found for the case of polystyrene compounds. Smaller particulates (less than 1 μm) form agglomerates obviously. The number of agglomerates in these compounds are much greater than polystyrene compounds.

Details of particulate structure have been presented in Figure VII-7 at a magnification of x400. Some structure may be seen in large size particulates (larger than 1 μm). Many agglomerates may be observed to contain smaller particulates. The ultimate particles are invisible in the micrographs of the two small uncoated calcium carbonates (dp = 0.4 μm and 0.07 μm).

Figure VII-8 presents a close-up view of polypropylene/uncoated calcium carbonate compound (dp = 0.07 μm, ϕ = 0.05) processed on a two roll mixing mill. Agglomerates of calcium carbonate have a broad size distribution. The agglomerate structure is similar to a cauliflower.

Micrographs of polypropylene/stearic acid coated calcium carbonate compounds (again mixed on a two roll mill) are shown in Figures VII-9 and VII-10. Dispersion of large calcium carbonates (larger than 1 μm) with stearic acid surface coating are better than uncoated calcium carbonates for both magnifications (x40 and x400)

(Figures VII-9 and VII-10). Stearic acid surface coating of calcium carbonate improves dispersion. The situation is not clear with smaller particulates whose ultimate diameters are smaller than 1 μm. It is necessary to observe a larger area of compound film for these systems. This will be discussed in a later section.

Figure VII-11 shows some other polypropylene compounds prepared with a two roll mixing mill. These contain micrographs of talc, silane surface coated talc and mica compounds. Large agglomerates are not observed for these particulates. The effect of the surface coating is not clear.

C.3.b. Internal mixer prepared compounds. Optical micrographs of internal mixer compounds have been shown in Figures VII-12 and VII-13. The mixing time varies from 1 minute to 10 minutes. The ultimate particle diameter is 0.07 μm.

Figure VII-12 represents the effect of mixing time for polypropylene/uncoated calcium carbonate compounds. It may be seen that the number and size of agglomerates decrease as mixing progresses. Some very large agglomerates (greater than 100 μm) are observed.

Stearic acid coated calcium carbonate compounds are presented in Figure VII-13. Again, the effect of mixing time is clear. Both number and size of agglomerates decrease with mixing time. It should be noted that the number of agglomerates in the coated calcium carbonate compounds is greater than uncoated calcium carbonate compounds.

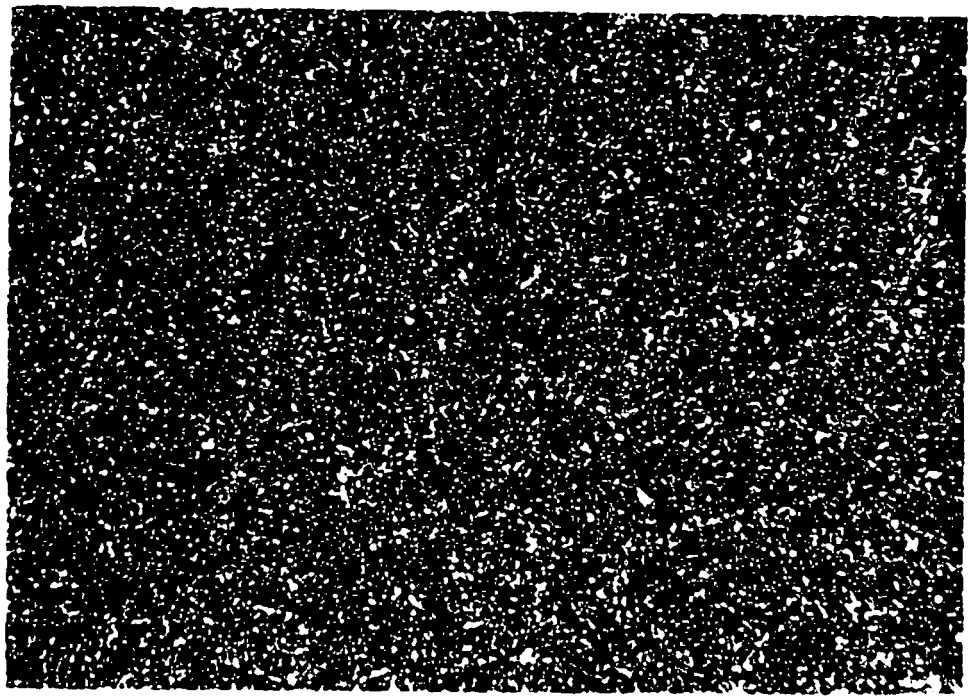

(a) Talc

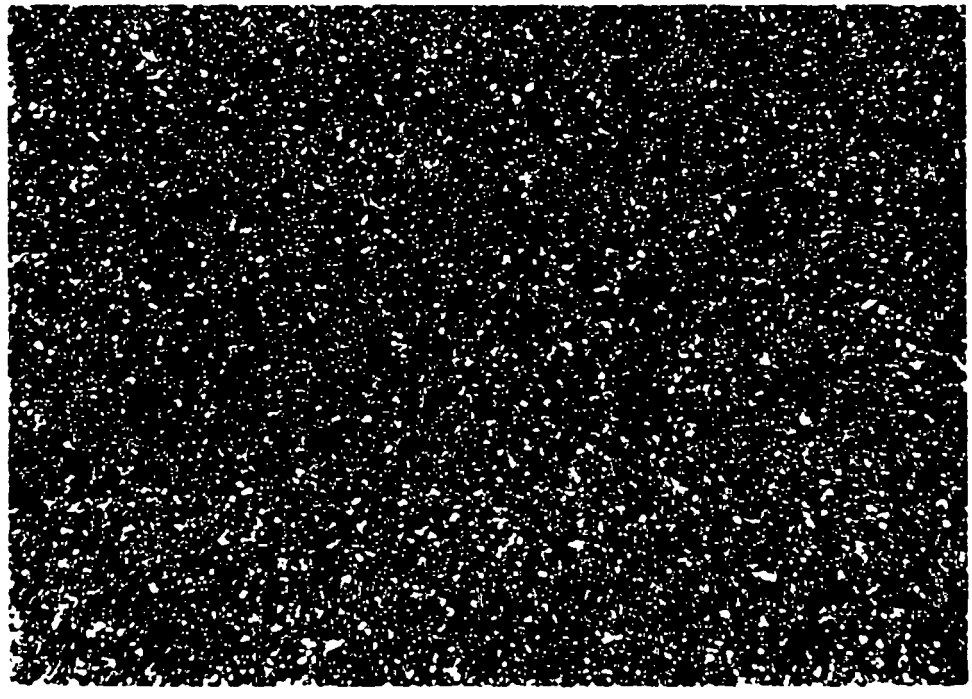

(b) Silane coated Talc

Figure VII-11. Optical micrographs of PP/anisotropic filler compounds (TRM 175°C, 20 min.) ϕ = 0.05.

(c) Mica

Figure VII-11 (continued)

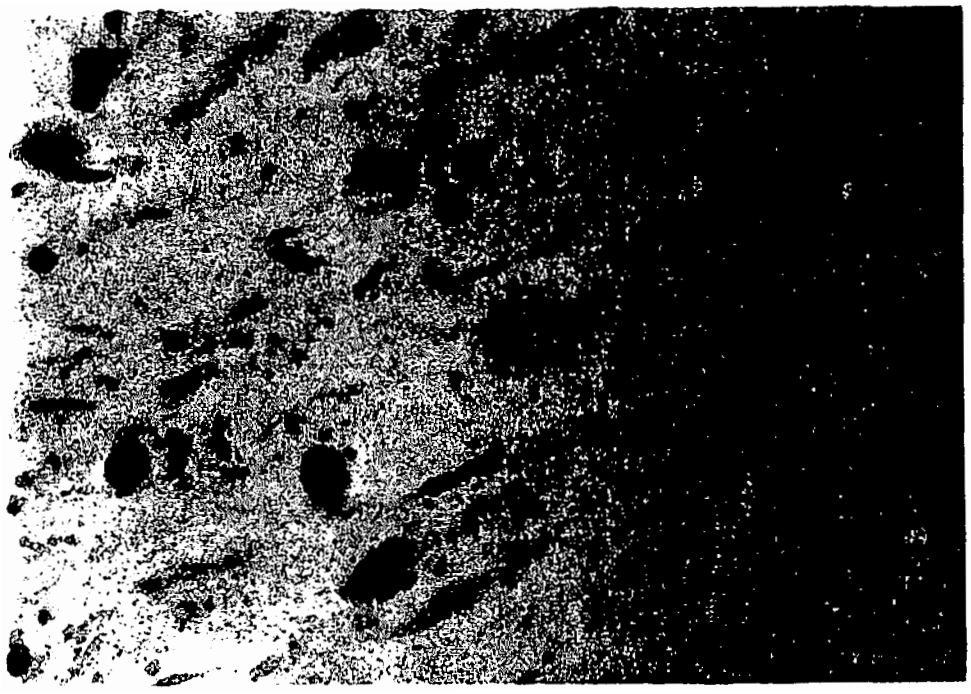

(a) 1 min

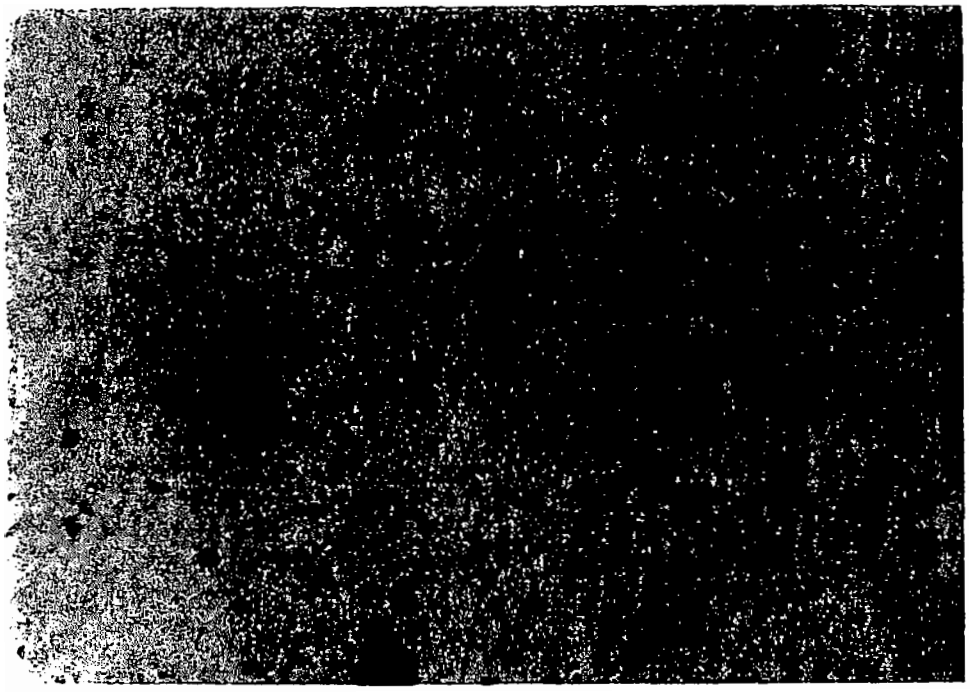

(b) 5 min

Figure VII-12. Optical micrographs of PP/unc. $CaCO_3$ compounds (IM 175°C, 25 RPM).

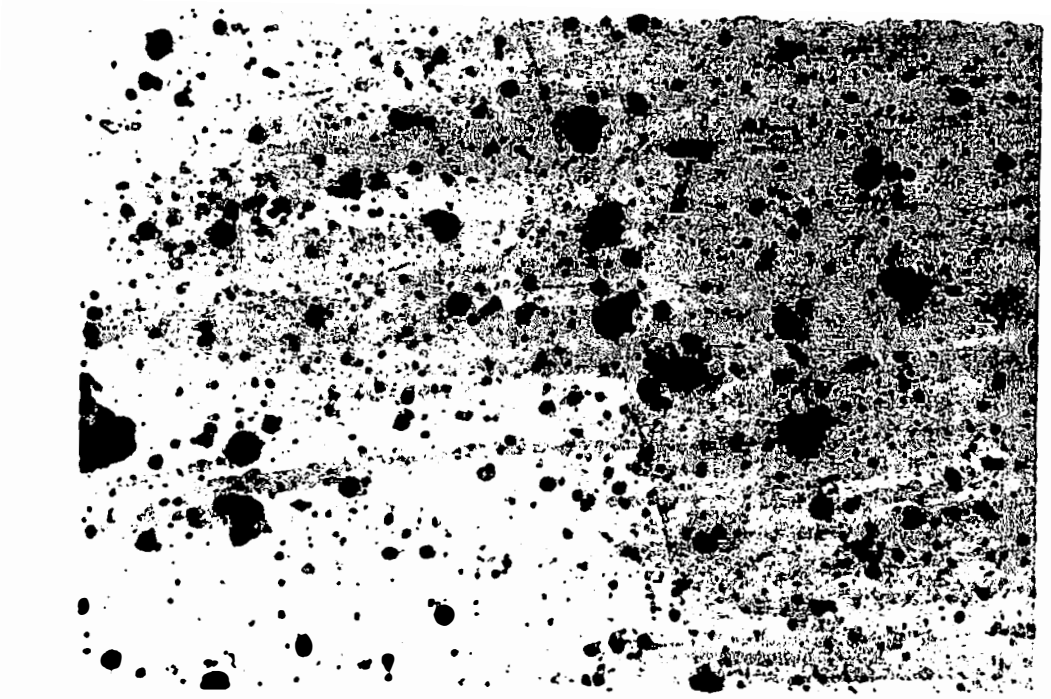

(a) 1 min

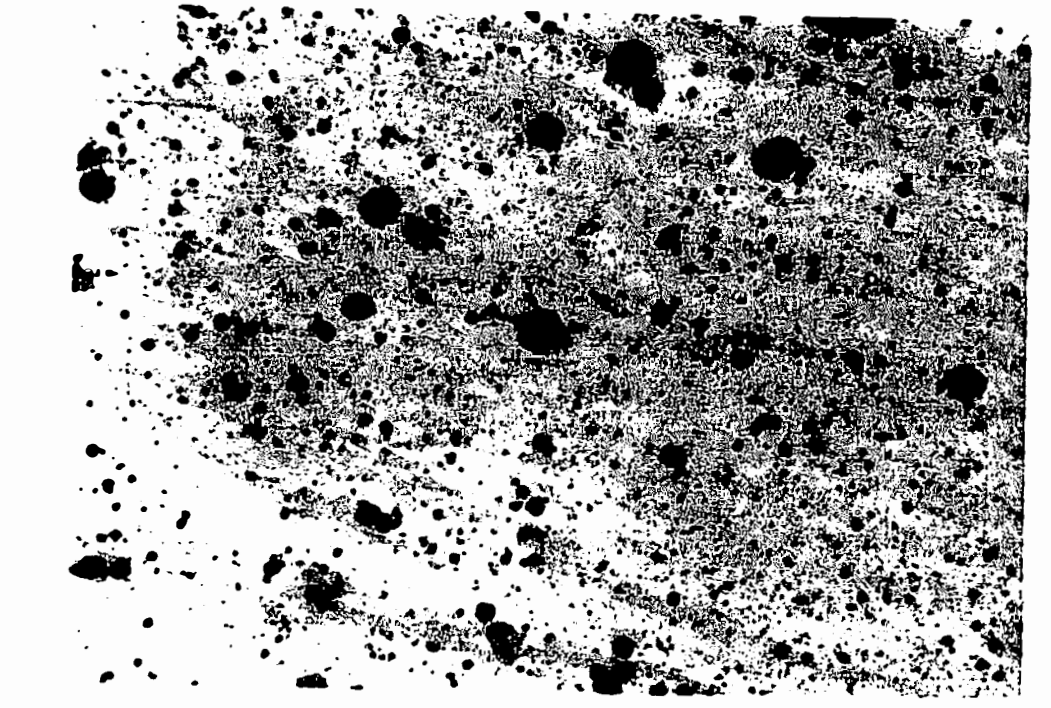

(b) 5 min

Figure VII-13. Optical micrographs of PP/coat. $CaCO_3$ compounds (IM 175°C, 25 RPM).

D. DISCUSSION

D.1. General

We now discuss the dispersion of small particles quantitatively. The number of agglomerates in 1 cm^3 of compound N(d), the distribution function of agglomerates P(d) and volume fraction of agglomerates $\phi(d)$ were defined in Eqs. (VII-1), (VII-2), and (VII-3), respectively. These quantities are determined as a function of the size of agglomerates for various compounds.

D.2. Polystyrene Compounds

Figures VII-14 and VII-15 show the number of agglomerates in 1 cm^3 compound N(d) as a function of diameter of agglomerates d for polystyrene/uncoated and coated calcium carbonate compounds, respectively. The mixing device and mixing time are indicated in the figures. Here IM and TRM are used as abbreviations for internal mixer and two roll mixing mill prepared compounds, respectively. The number of agglomerates decreases drastically with increasing agglomerate size at any mixing time and varies with mixing device.

The number of agglomerates in polystyrene/uncoated calcium carbonate (Figure VII-14) tends to decrease as mixing progresses. One of the peculiar characteristics is that the number of agglomerates decrease is not consistent with increasing mixing time internal mixer prepared compounds, but an intermediate maxima is observed.

It should be pointed out that the number of large agglomerates does not show a rapid decrease with mixing time in internal mixer

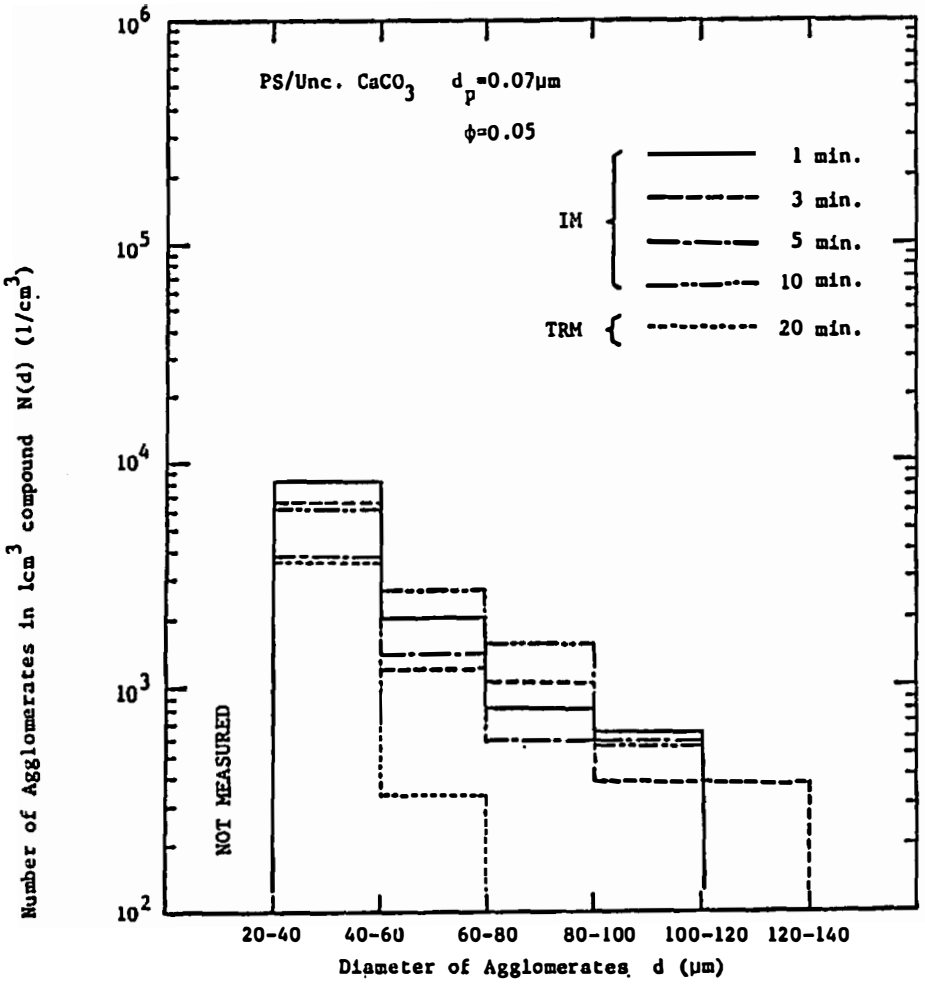

Figure VII-14. N(d) distribution curves for PS/uncoated $CaCO_3$ compounds.

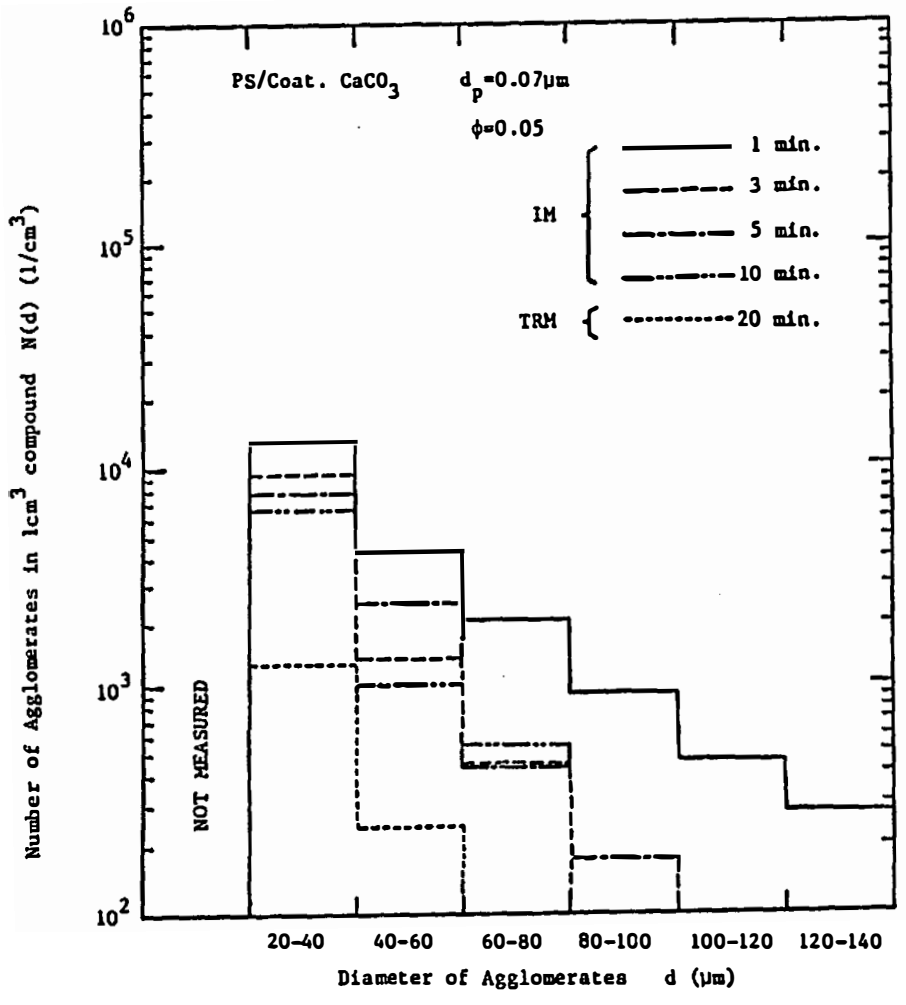

Figure VII-15. N(d) distribution curves for PS/coated $CaCO_3$ compounds.

prepared compounds. The two roll mill prepared compounds have a much smaller number of agglomerates, especially at large agglomerate sizes.

There seem due to be two reasons for the above observations. One is the existence of a thin layer of unincorporated particulates formed on the chamber wall of the internal mixer. This was discussed in the previous chapter. This layer of unincorporated filler could supply the large agglomerates into polymer phase continuously.

Another reason is the viscosity and temperature of the compound during the mixing process. The compound is surrounded by the chamber wall in the internal mixer. The temperature of the compound is generally higher than the set mixing temperature of 150°C due to the viscous heat generation. This was measured during the mixing process by a thermocouple located in a chamber wall. The temperature was 5 to 10°C higher than the set temperature. The compound is exposed to air atmosphere on the two roll mill. It is expected that the actual temperatures of compounds in the internal mixer are substantially higher than on the two roll mill.

The viscosity of polystyrene is strongly dependent upon the temperature as discussed in Chapter IV. Effect of low temperature may overcome the low shear rate in the two roll mill. The viscosity of compound would be much higher in the two roll mill than in the internal mixer. This leads to better dispersion in two roll mill prepared compounds.

Figure VII-15 shows the number of agglomerates N(d) as a function of the diameter of agglomerates d for polystyrene/coated

calcium carbonate compounds. The number of agglomerates decreases drastically with mixing time in the internal mixer, especially in the large agglomerate size region. This may be due to the rapid disappearance of particulate layers on the chamber surface. Large agglomerates were not supplied any more after such layers disappear. The weak particle-particle interaction of stearic acid coated calcium carbonate promotes the disappearance of particle layers and the break-down of large agglomerates. Stearic acid surface treatment may reduce the particle-metal surface interaction as well as interparticle interaction. The two roll mill compound again reduces the number of agglomerates drastically.

Distribution functions P(d) for polystyrene/uncoated and coated calcium carbonate compounds are plotted in Figures VII-16 and VII-17, respectively.

P(d) of the uncoated calcium carbonate compounds (Figure VII-16) tends to scatter. High fraction of large agglomerates (~100 μm) may be observed. They are greater than 2% of the total number of agglomerates. The distribution function of the two roll mill compound shows a sharp decay with agglomerate size.

Coated calcium carbonate compounds (Figure VII-17) are found to possess more consistent appearing distribution functions. The distribution of agglomerates changes after 1 minute of mixing in an internal mixer, and it is unchanged with further mixing. The fraction of large agglomerates (~100 μm) are much smaller than uncoated calcium carbonate compounds. In addition, distribution functions for

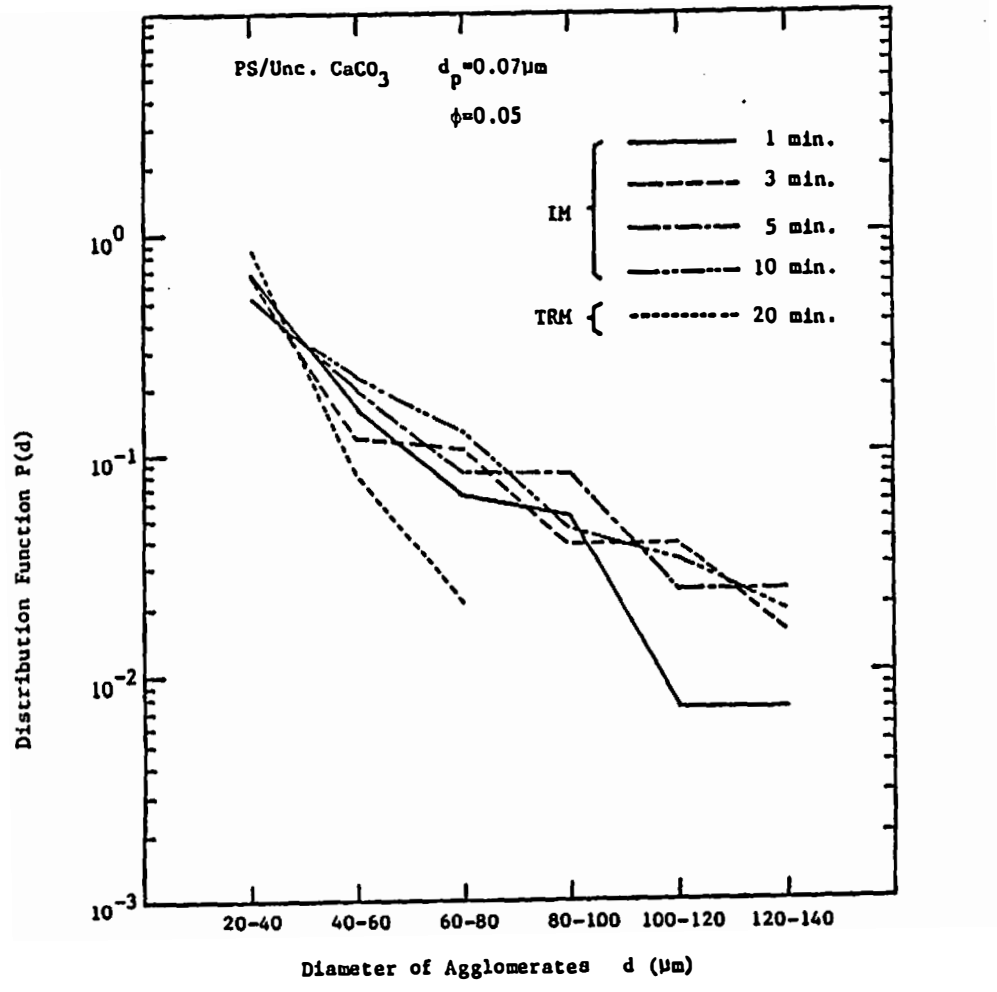

Figure VII-16. P(d) distribution curves for PS/uncoated $CaCO_3$ compounds for various extents of mixing.

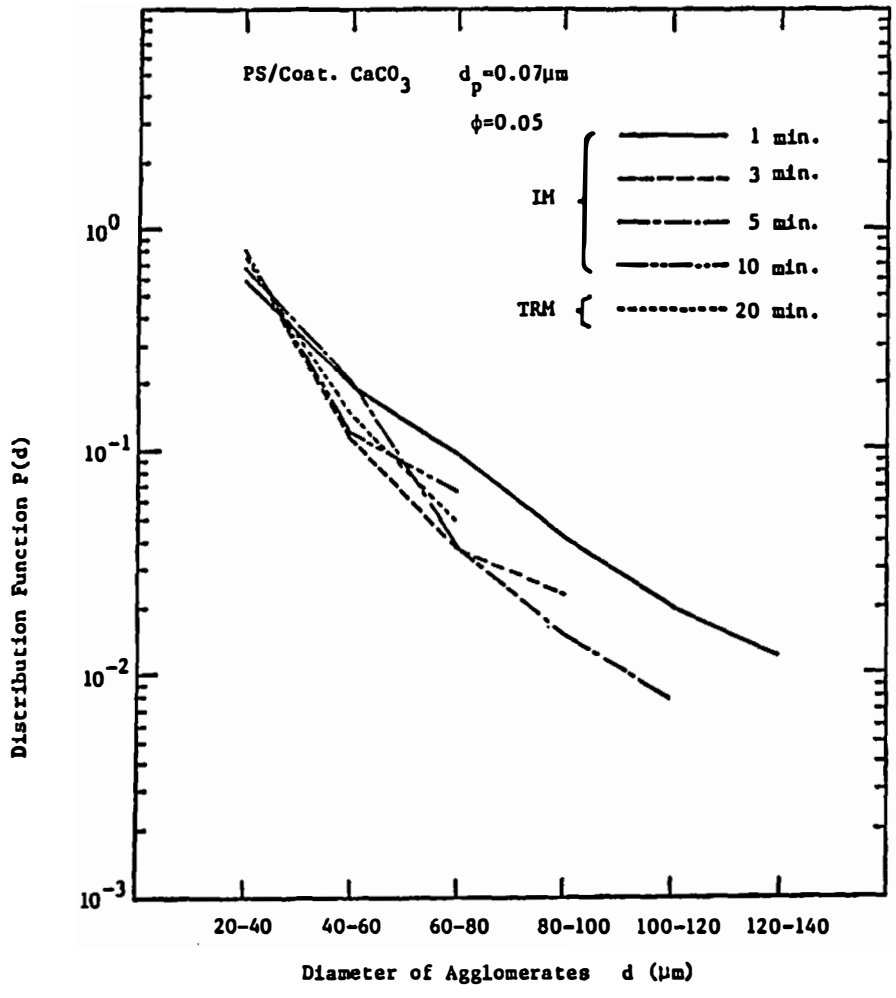

Figure VII-17. P(d) distribution curves for PS/coated $CaCO_3$ compounds for various extents of mixing.

internal mixer prepared compounds after 3 minutes of mixing are quite similar to that of the two roll mill compound.

Figures VII-18 and VII-19 show the volume fraction of agglomerates $\phi(d)$ as a function of agglomerate size range for polystyrene/uncoated and coated calcium carbonate compounds, respectively. Function $\phi(d)$ of uncoated calcium carbonate compounds increases with increasing agglomerate size (Figure VII-18). This suggests the existence of very large agglomerates. Very large agglomerates may be supplied from the unincorporated particle layer on the chamber wall. Such unincorporated particle layers may be regarded as a reservoir of agglomerates of filler. The two roll mill prepared compound is an exception. The $\phi(d)$ function decreases with size of agglomerates.

Figure VII-19 shows the volume fraction of agglomerates for coated calcium carbonates. Functions $\phi(d)$ for all compounds after 3 minutes of mixing tend to decrease slightly with size of agglomerates. The dispersion is better than the case of uncoated calcium carbonate as long as the fraction of large agglomerates are concerned.

D.3. Polypropylene Compounds

Figure VII-20 shows the number of agglomerates N(d) as a function of agglomerate diameter for polypropylene/uncoated calcium carbonate compounds. The function N(d) decreases very rapidly with increasing agglomerate diameter d at any mixing time and device. The function N(d) decreases with mixing time. The reduction of N(d) with mixing time is much more consistent than the case of polystyrene compounds previously discussed.

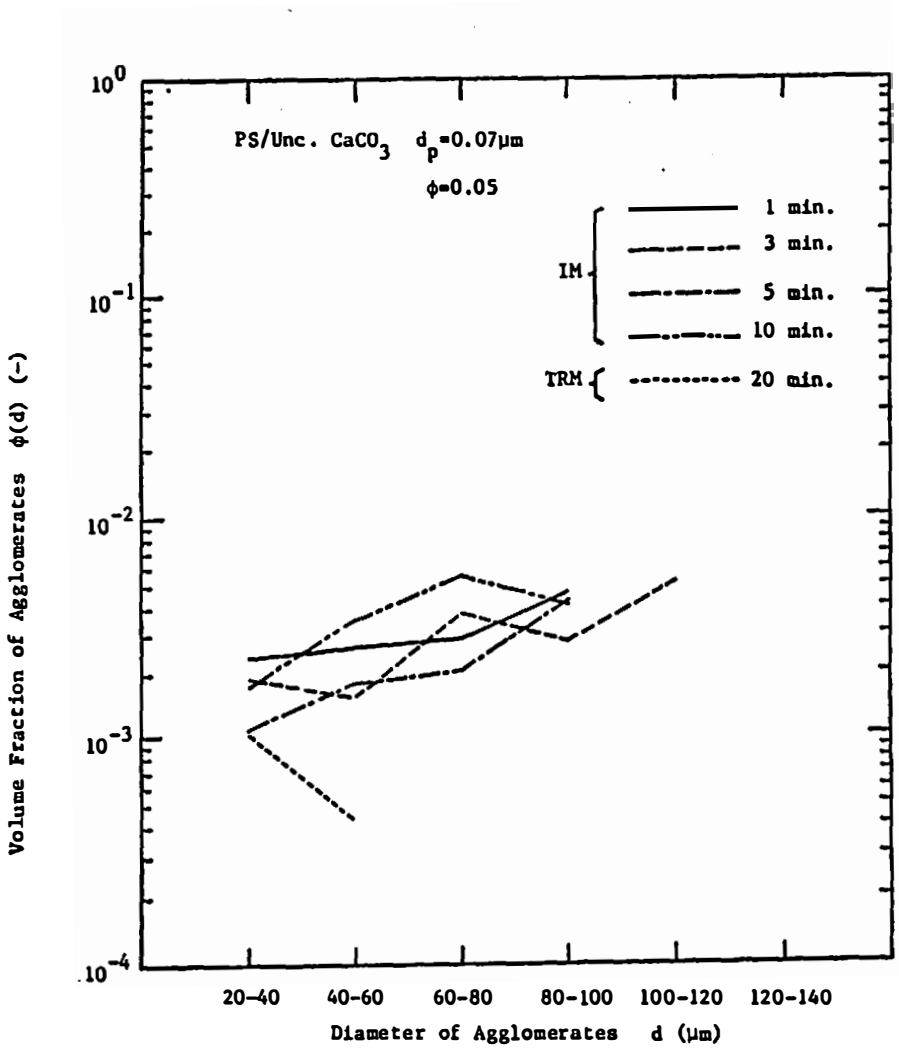

Figure VII-18. $\phi(d)$ distribution curves for PS/uncoated $CaCO_3$ compounds.

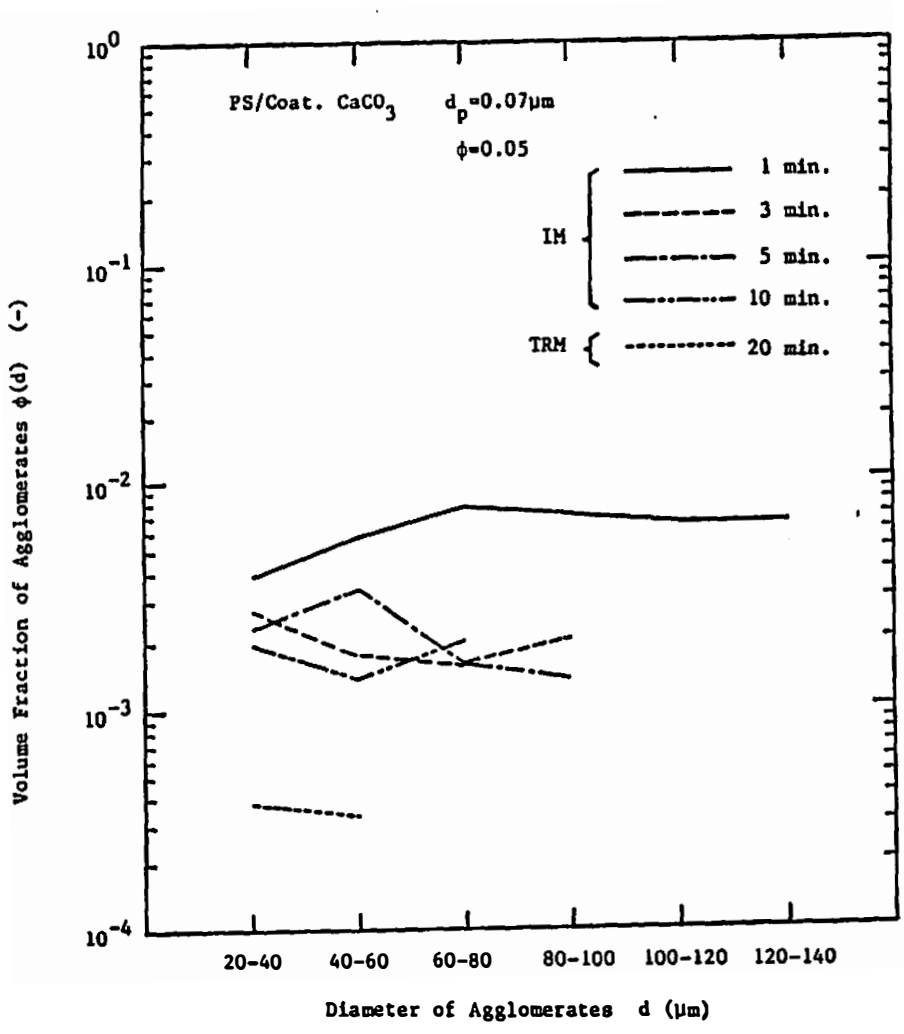

Figure VII-19. $\phi(d)$ distribution curves for PS/coated $CaCO_3$ compounds.

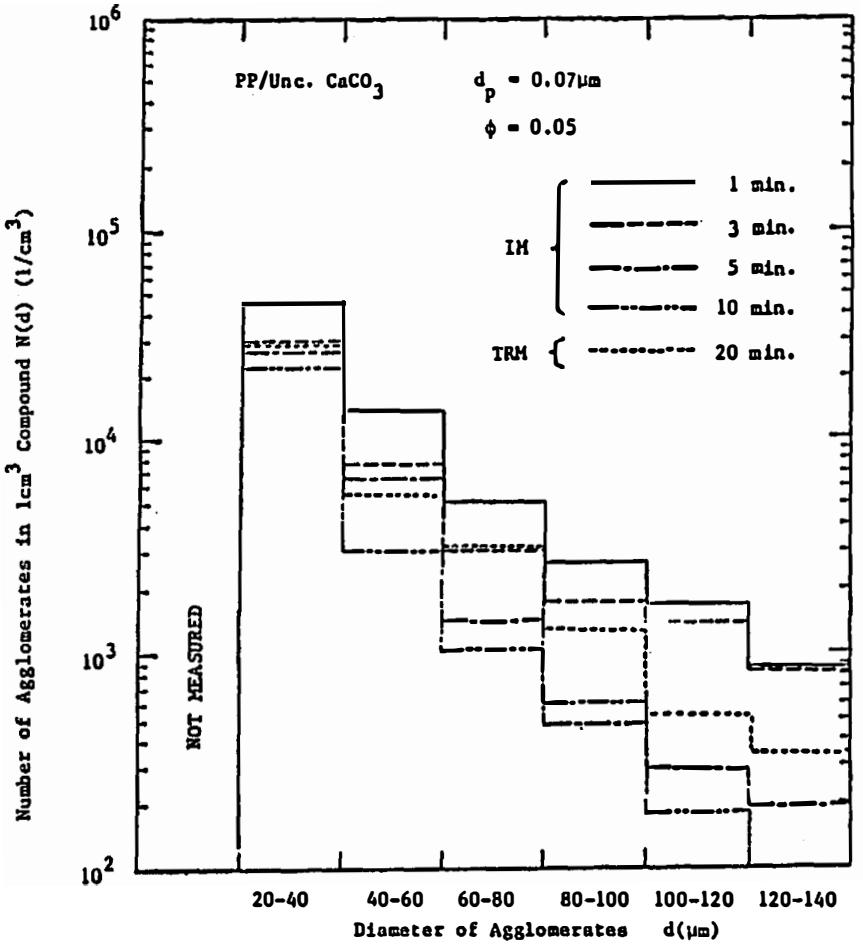

Figure VII-20. N(d) distribution curves for PP/uncoated $CaCO_3$ compounds.

The mixing in a two roll mill is not as effective as the polystyrenes case. A large number of agglomerates still remain after 20 minutes of mixing in a two roll mill, unlike the case of polystyrene compounds.

This significant difference on the amount of large agglomerates between the two roll mill prepared polystyrene and polypropylene compound may result from the marked difference on the activation energies. The activation energies of polystyrene and polypropylene are 25 kcal/mole and 9-10 kcal/mole, respectively (W-7). The viscosity of polypropylene is much less temperature sensitive compared with polystyrene.

It would be expected that the actual temperature of resin during mixing is substantially higher than the set temperature of 175°C in the internal mixer and lower than that in the two roll mill. The change of the viscosity of polypropylene due to the temperature difference in mixing devices is, however, small.

Polypropylene/stearic acid surface coated calcium carbonate compounds possess the greatest number of agglomerates (Figure VII-21) of all. The number of smallest agglomerates (20 μm to 40 μm) is greater than 100,000 per 1 cm^3 of compound. N(d), number of agglomerates, decreases most rapidly with increasing agglomerate diameter and number of large agglomerates (>100 μm) are smaller than that of uncoated calcium carbonate compounds. Stearic acid surface coating of calcium carbonate is effective to reduce the number of large agglomerates both in polystyrene and polypropylene.

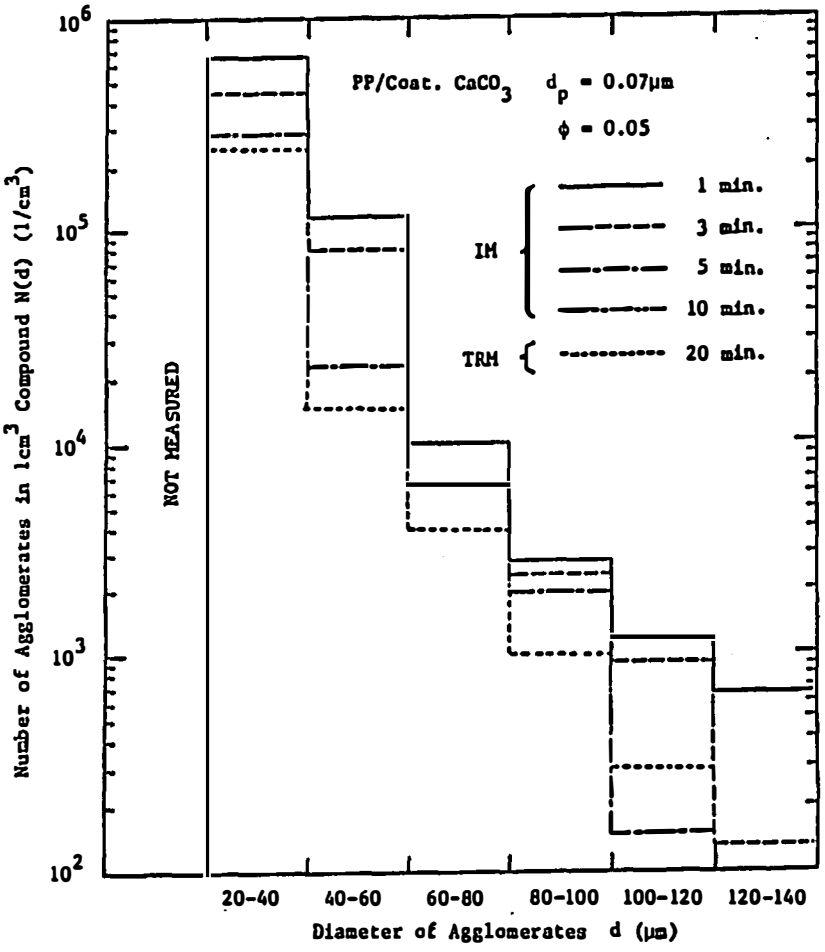

Figure VII-21. N(d) distribution curves for PP/stearic acid coated $CaCO_3$ compounds.

Figure VII-22 and VII-23 show distribution functions for polypropylene/uncoated and coated calcium carbonate compounds, respectively.

It is very clear that the distribution functions of coated calcium carbonate compounds (Figure VII-23) decay much more sharply than uncoated calcium carbonate compounds (Figure VII-22). Fractions of large agglomerates within the size range of 100 μm to 120 μm are 6×10^{-3} to 3×10^{-2} for uncoated calcium carbonate compounds and about 1×10^{-3} for coated calcium carbonate compounds.

The following may be concluded. The stearic acid surface coating of calcium carbonate reduces the fraction of large agglomerates both in polystyrene and polypropylene compounds. The breakdown of agglomerates may be accelerated by surface coating. However, the coated particulate compounds possess greater numbers of small agglomerates.

Figures VII-24 and VII-25 plot the volume fraction of agglomerates $\phi(d)$ as a function of agglomerate size for polypropylene/uncoated and coated calcium carbonate compounds. There is a noticeable difference between these two. The function $\phi(d)$ decreases with increasing agglomerate size much more sharply in coated calcium carbonate compounds (Figure VII-25) than in the uncoated calcium carbonate compounds (Figure VII-24). Stearic acid coating tends to reduce the existence of very large agglomerates.

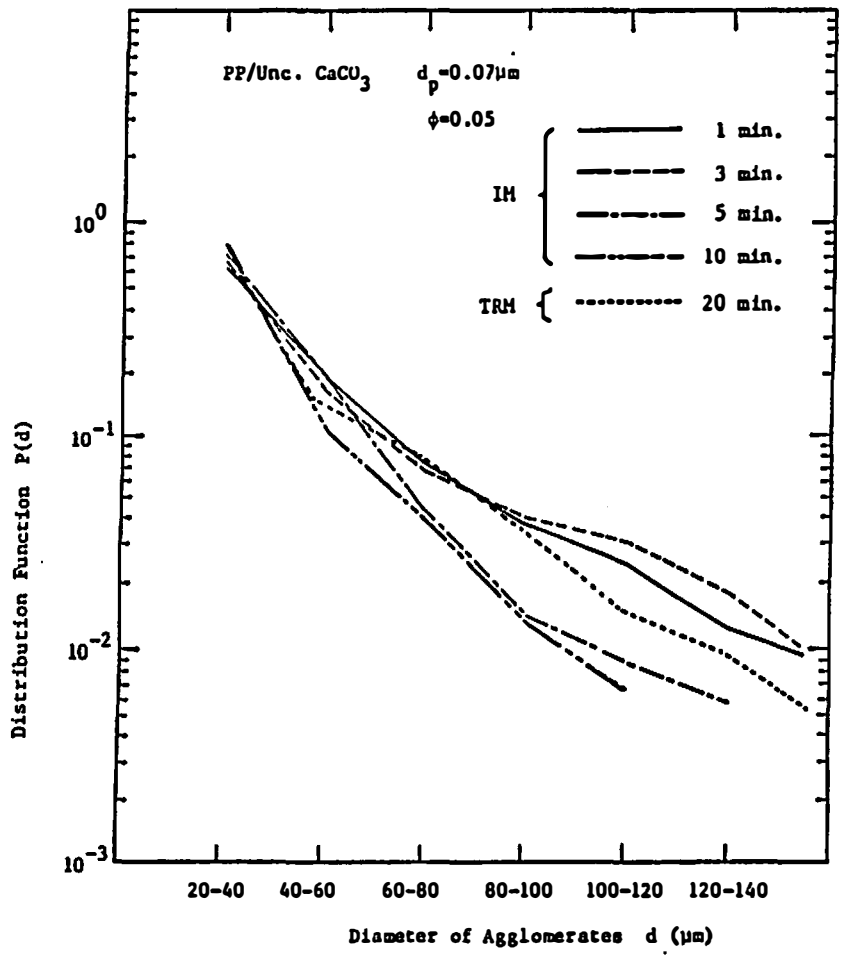

Figure VII-22. P(d) distribution curves for PP/uncoated $CaCO_3$ compounds for various extents of mixing.

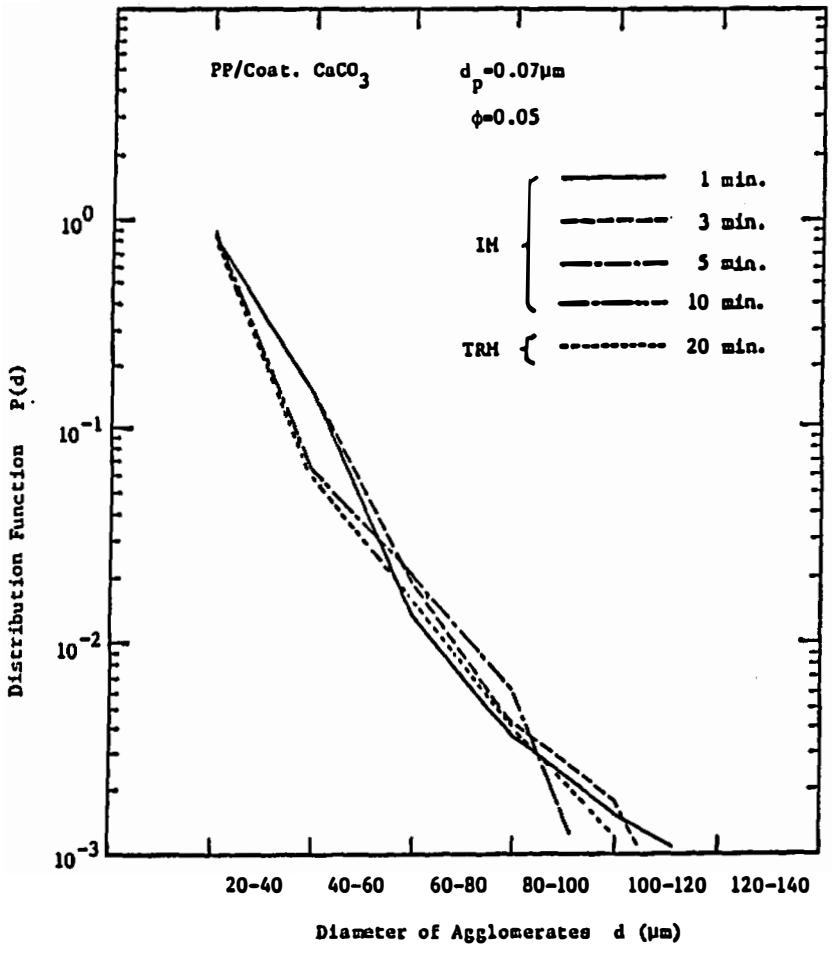

Figure VII-23. P(d) distribution curves for PP/coated $CaCO_3$ compounds for various extents of mixing.

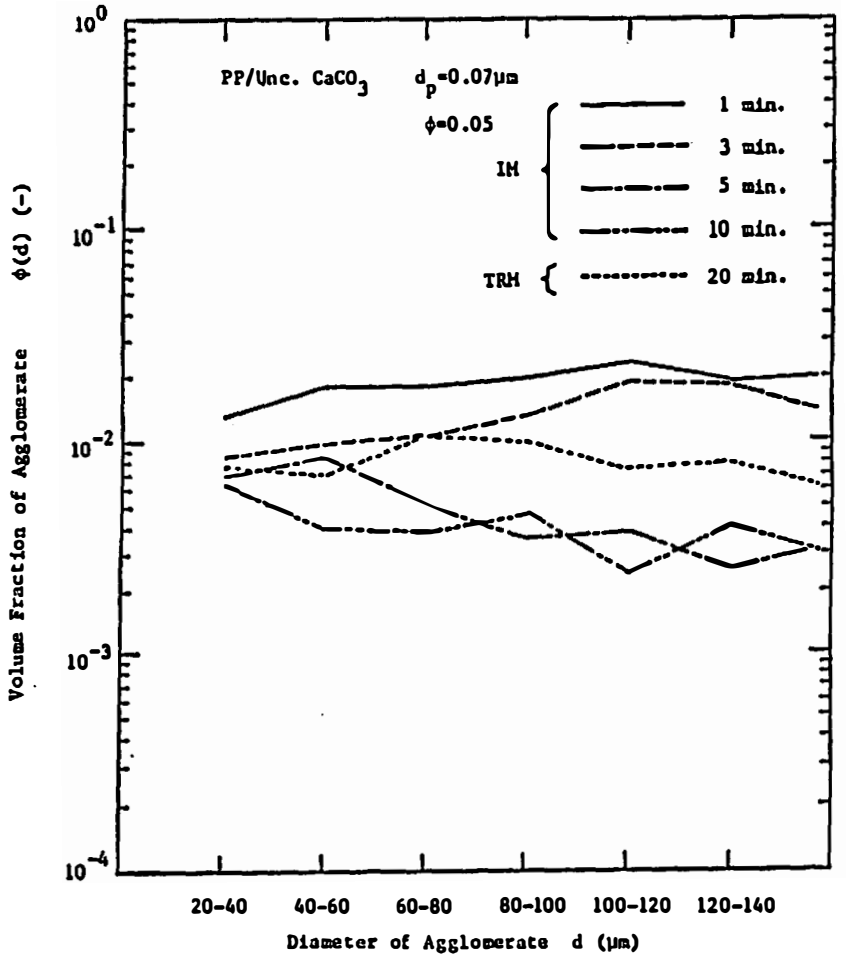

Figure VII-24. $\phi(d)$ distribution curves for PP/uncoated $CaCO_3$ compounds.

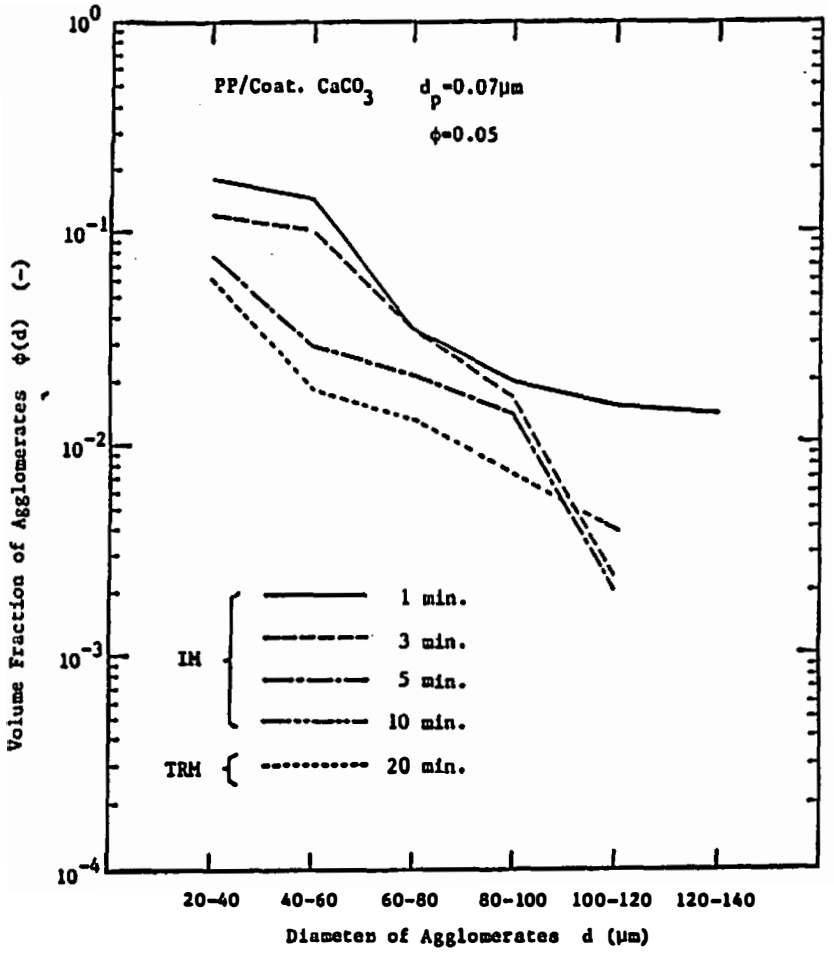

Figure VII-25. $\phi(d)$ distribution curves for PP/coated $CaCO_3$ compounds.

D.4. Representation of Dispersion

Several methods of determination of dispersion are presented in this section. As previously discussed, agglomerates in compounds have been found to possess a wide range of diameter and a sharply decreasing distribution function as agglomerate size increases. Distribution of agglomerate size in stearic acid surface treated calcium carbonate compounds is very different from that with uncoated particles. Coated calcium carbonate compounds possess reduced numbers of large agglomerates compared to uncoated calcium carbonate compounds.

D.4.a. Total number of agglomerates. First we consider the total number of agglomerates in 1 cm^3 of compound $\Sigma N(d)$. This counts the number of agglomerates whose diameter is greater than 20 μm. Figure VII-26 shows $\Sigma N(d)$, total number of agglomerates in 1 cm^3 of compound, as a function of mixing time both in an internal mixer and a two roll mill. Percentage values indicated in this figure for polystyrene compounds show amounts of filler remain on the chamber wall of internal mixer, that is, unincorporated filler. It is clear that dispersion is improved as mixing progresses. Improvement of dispersion occurs first rapidly and approaches steady state. As far as the total number of agglomerates greater than 20 m is concerned, dispersion is the best in polystyrene/coated calcium carbonate system. The order is as follows.

PS/Coat. $CaCO_3$ > PS/Uncoat. $CaCO_3$ > PP/Uncoat. $CaCO_3$ > PP/Coat. $CaCO_3$.

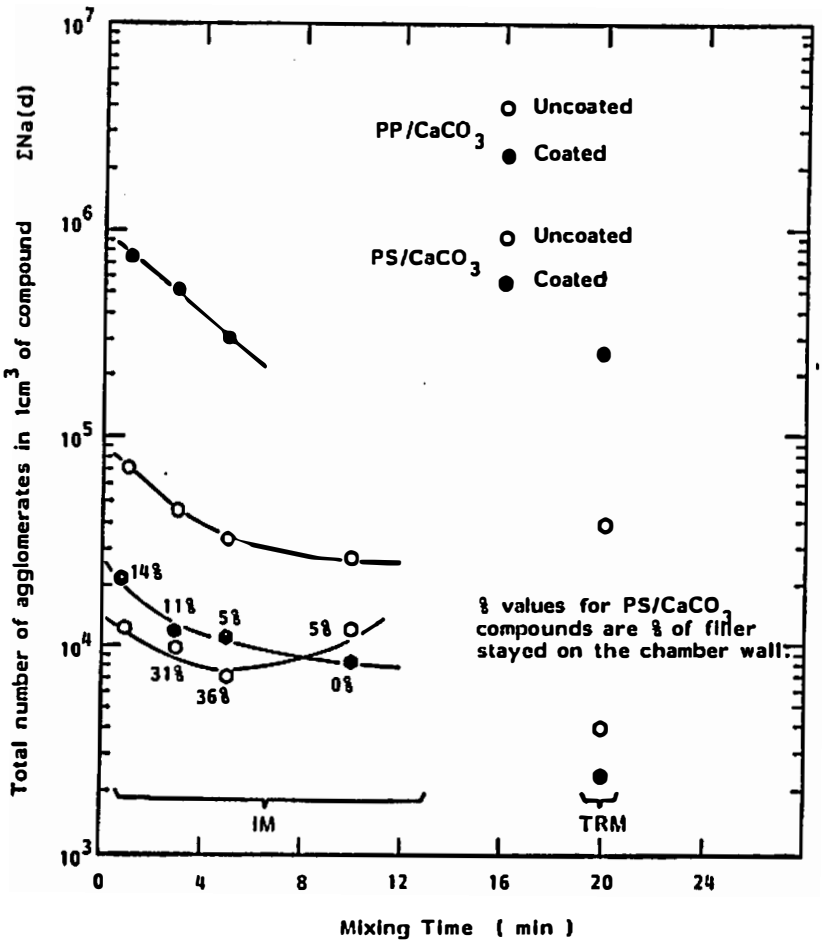

Figure VII-26. Total number of agglomerates in 1 cm^3 of compounds as a function of mixing time.

Good dispersions in polystyrene compounds are due to the high viscosity of matrix polymer during the mixing process.

We note that the dispersion of coated calcium carbonate is worse than uncoated calcium carbonate in polypropylene compounds. This may be due to the weak interaction forces between coated particles and the mechanism of dispersion. Weak interaction forces between particles accelerate the breakdown of agglomerates into the greater number of smaller agglomerates. This may increase the total number of agglomerates in 1 cm^3 of compound. Another reason, the mechanism of dispersion, will be discussed in Chapter XIII, Theory of Mixing.

D.4.b. Total volume fraction of agglomerates. The second method considers the total volume fraction of agglomerates $\Sigma\phi(d)$. Again agglomerates which are greater than 20 μm are counted. Here the function $\phi(d)$ has been defined in Eq. (VII-3). We may plot $1 - \Sigma\phi(d)$ as a function of mixing time (Figure VII-27). In this plot, the best dispersion may be represented as $1 - \Sigma\phi(d)$ equal to 1. Dispersion of filler is improved as mixing time increases.

We address our attention to the large agglomerates. Total volume fraction of agglomerates which are greater than 100 μm, $\sum_{100} \phi(d)$, is considered here. Taking a volume fraction $\phi(d)$ rather than a number of agglomerates N(d) emphasizes the existence of large agglomerates.

The function $\sum_{100} \phi(d)$ for various compounds are shown in Figure VII-28 as a function of mixing time. The function $\sum_{100} \phi(d)$

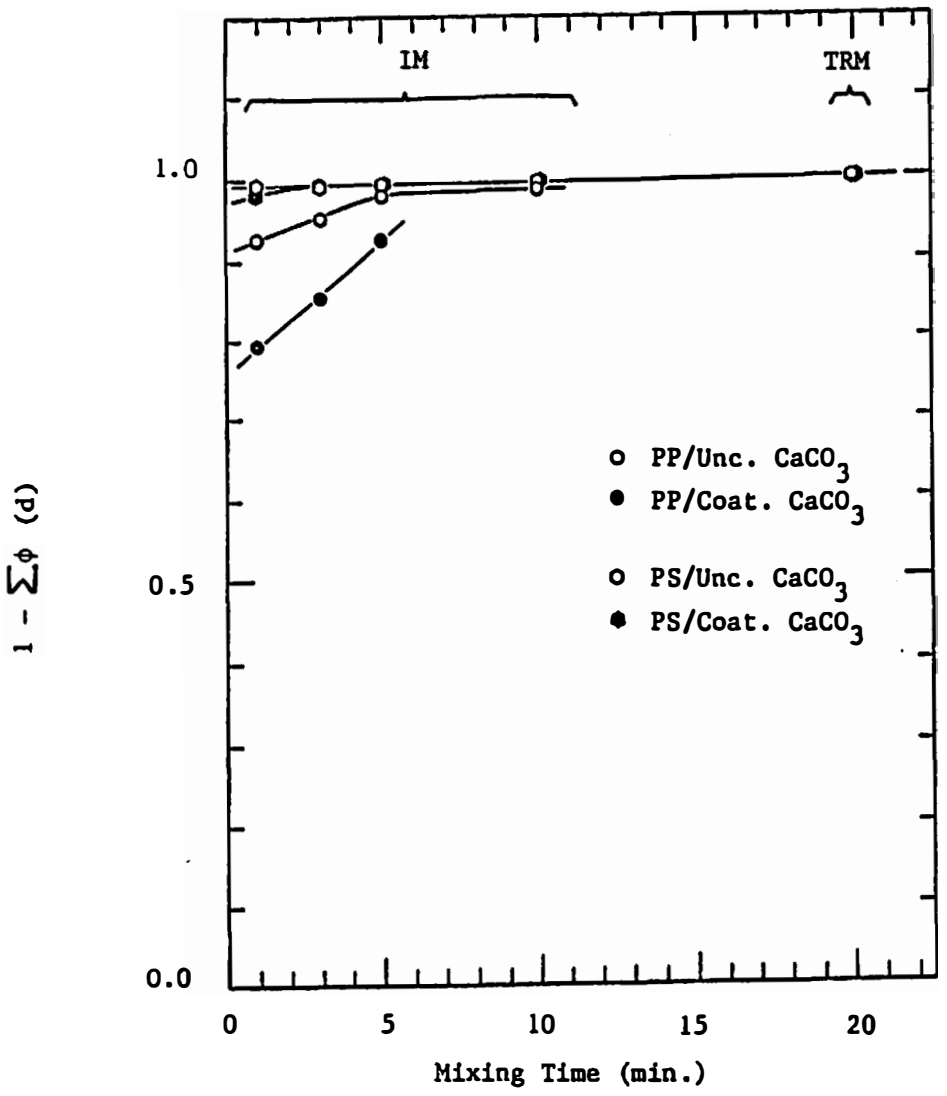

Figure VII-27. 1 - $\Sigma\phi(d)$ as a function of mixing time.

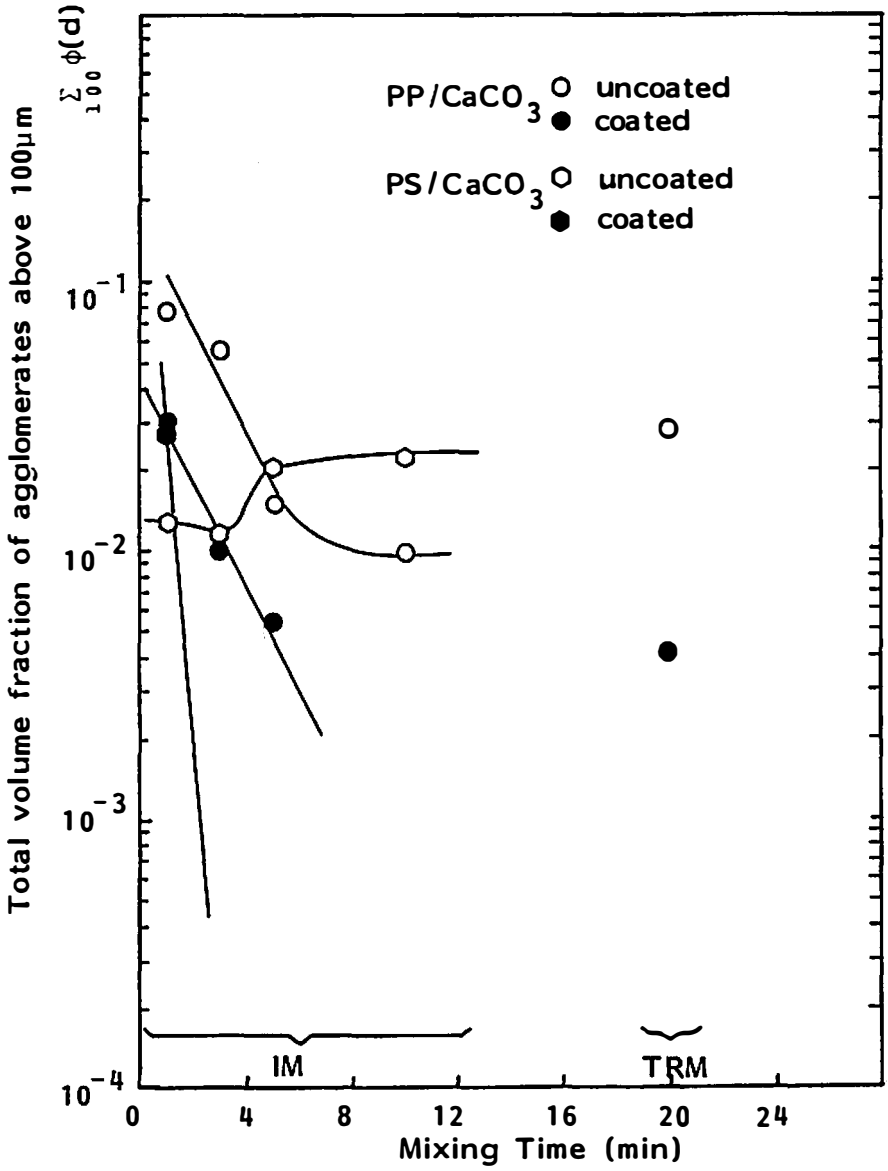

Figure VII-28. Total volume fraction of agglomerates greater than 100 μm as a function of mixing time.

decreases as mixing progresses. Values of $\Sigma_{100} \phi(d)$ are not plotted for the following compounds:

PS/Uncoated $CaCO_3$ TRM mixed

PS/Coated $CaCO_3$ TRM mixed

IM mixed; 3, 5, 10 min.

These compounds have the values of $\Sigma_{100} \phi(d)$ smaller than 1×10^{-3}. The dispersion of these compounds are excellent.

Most compounds improve their dispersion as mixing progresses. The fastest improvement may be seen in polystyrene/coated calcium carbonate compounds. The polystyrene/uncoated calcium carbonate compounds have a peculiar behavior. The dispersion gets worse as mixing time increases in an internal mixer. This is due to the existence of particulate layer. This supplies a number of large agglomerates in matrix phase. Among the internal mixer compounds, order of dispersion is

PS/Coat. $CaCO_3$ > PP/Coat. $CaCO_3$ > PP/Uncoat. $CaCO_3$ > PS/Uncoat. $CaCO_3$.

Stearic acid surface coating contributes the dispersion to reduce the amount of large agglomerates.

We note the order of dispersion level based on the total volume fraction of the large agglomerates $\Sigma_{100} \phi(d)$ is very different from the order of dispersion level determined upon the total number of agglomerates.

D.4.c. Agglomerate number and size relation. We have determined the levels of dispersion for various compounds based on the total number of agglomerates $\Sigma N(d)$, the total volume fraction of

agglomerates $\Sigma\phi(d)$ and the total volume fraction of large agglomerates $\Sigma_{100}\phi(d)$. It was found that the level of dispersion we determined is strongly dependent upon where we address our attention.

An index of dispersion ought to have the characteristics of expressing the complex state of dispersion. Once such an index of dispersion is defined, the grading of the level of dispersion is the matter of where the criterion is set.

A wide range of characteristics of dispersion may be well represented by the number of agglomerates as a function of agglomerate size.

Figures VII-29 through VII-32 present the number of agglomerates in 1 cm^3 N_a as a function of agglomerate size d in logarithmic scales for various compounds. We note that the amounts of agglomerates are well represented by

$$N_a = a \cdot d^{-b} \qquad \text{(VII-5)}$$

where a denotes the number of agglomerates at d = 1 μm and b is the power index. Values of b indicate how rapidly the number of agglomerates decreases with the size of agglomerates. The solid lines in Figures VII-29 through VII-32 are obtained by a least square method.

Tables VII-3 through VII-6 summarize the parameters a, b and the correlation coefficient for various compounds.

The correlation coefficient for the curve fitting with Eq. (VII-5) is greater than 0.97 in general. Total number of

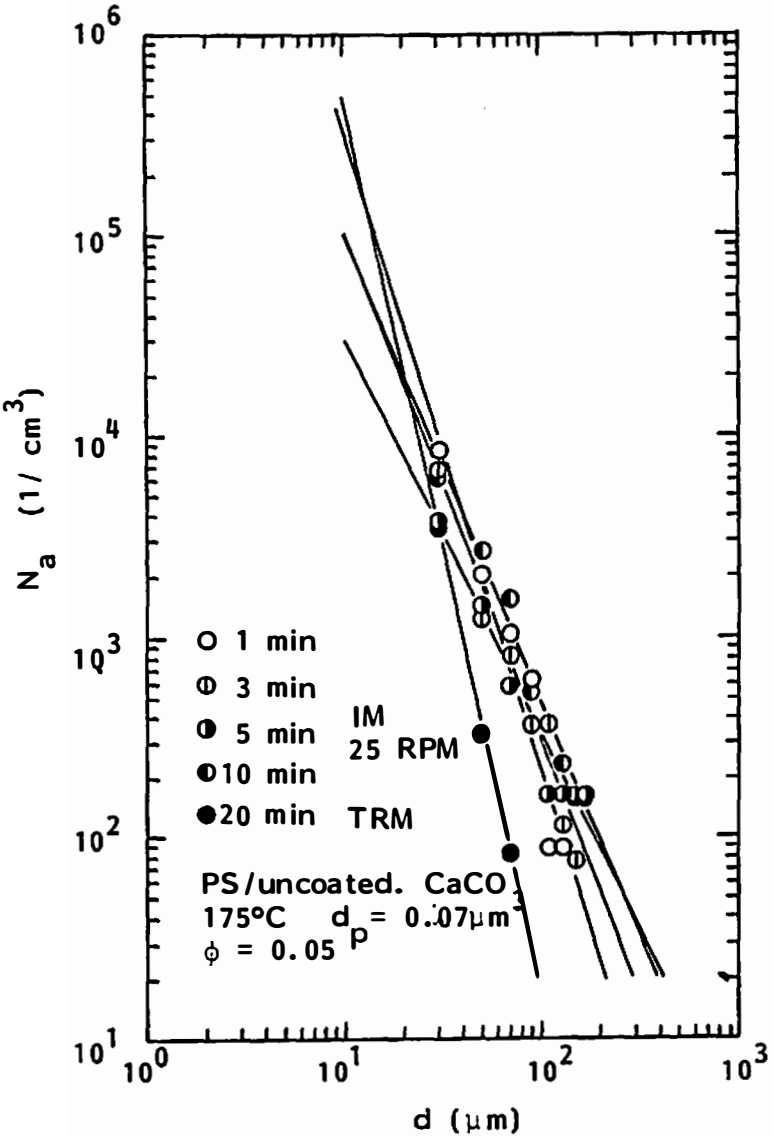

Figure VII-29. Number of agglomerates as a function of agglomerate size for PS/uncoat. $CaCO_3$.

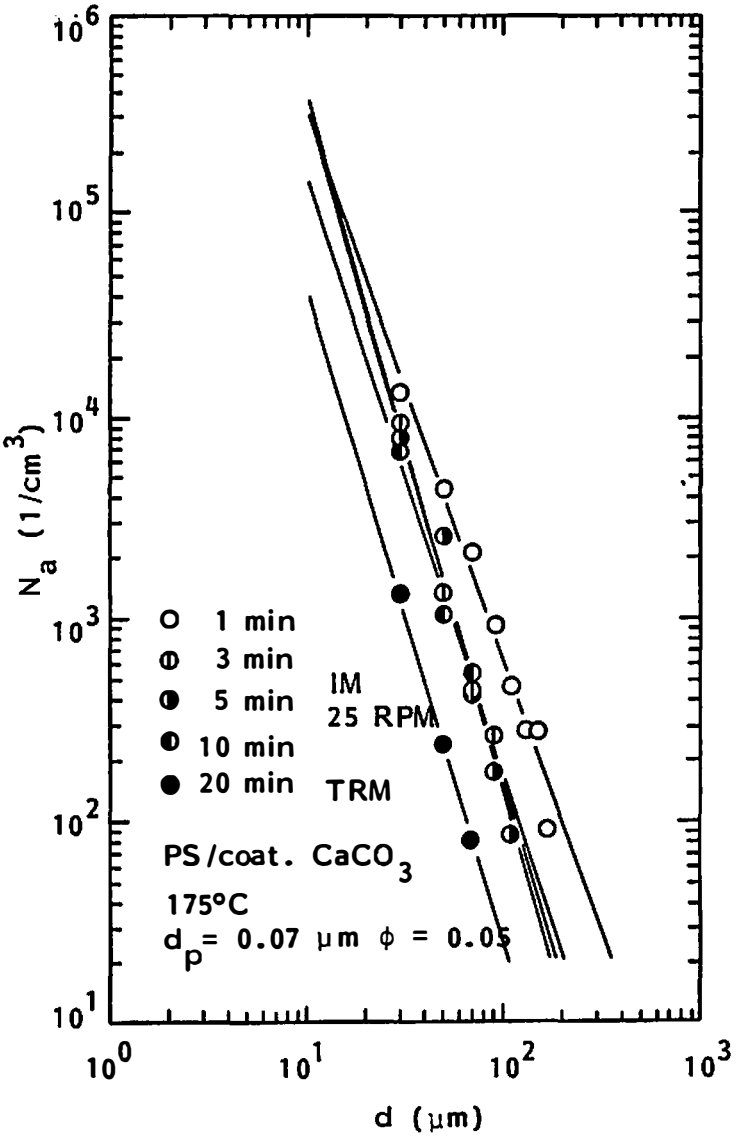

Figure VII-30. Number of agglomerates as a function of agglomerate size for PS/coat. $CaCO_3$.

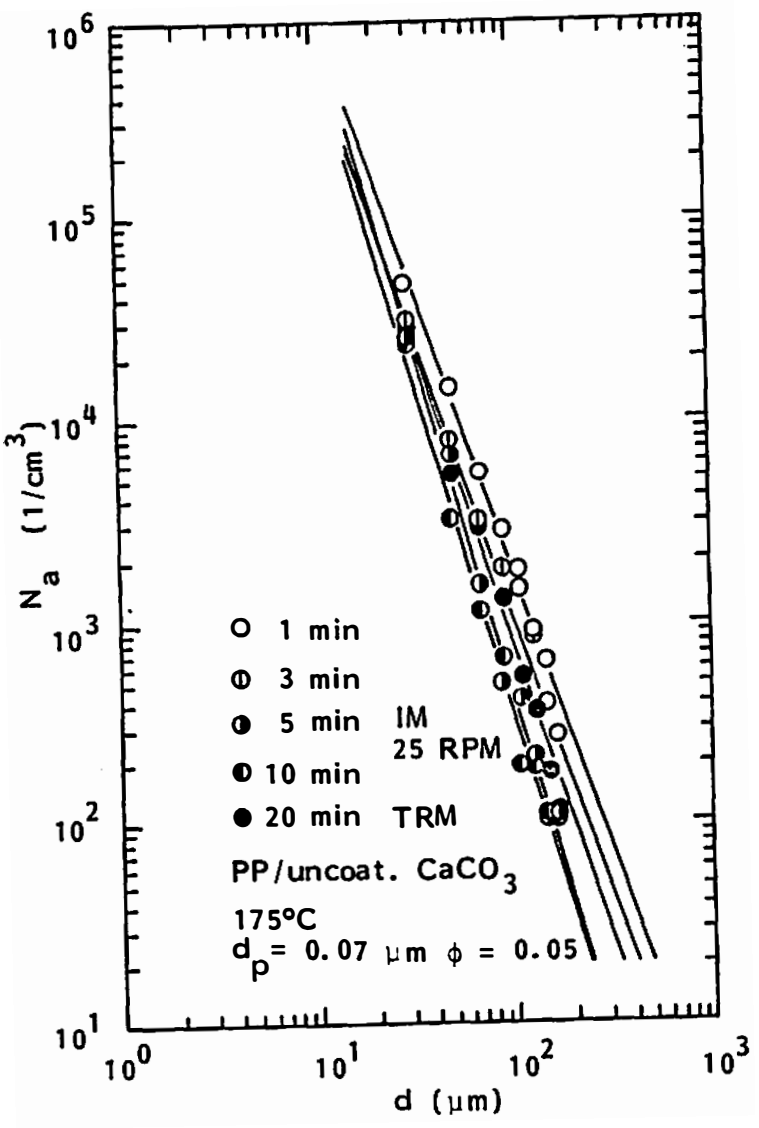

Figure VII-31. Number of agglomerates as a function of agglomerate size for PP/uncoat. $CaCO_3$.

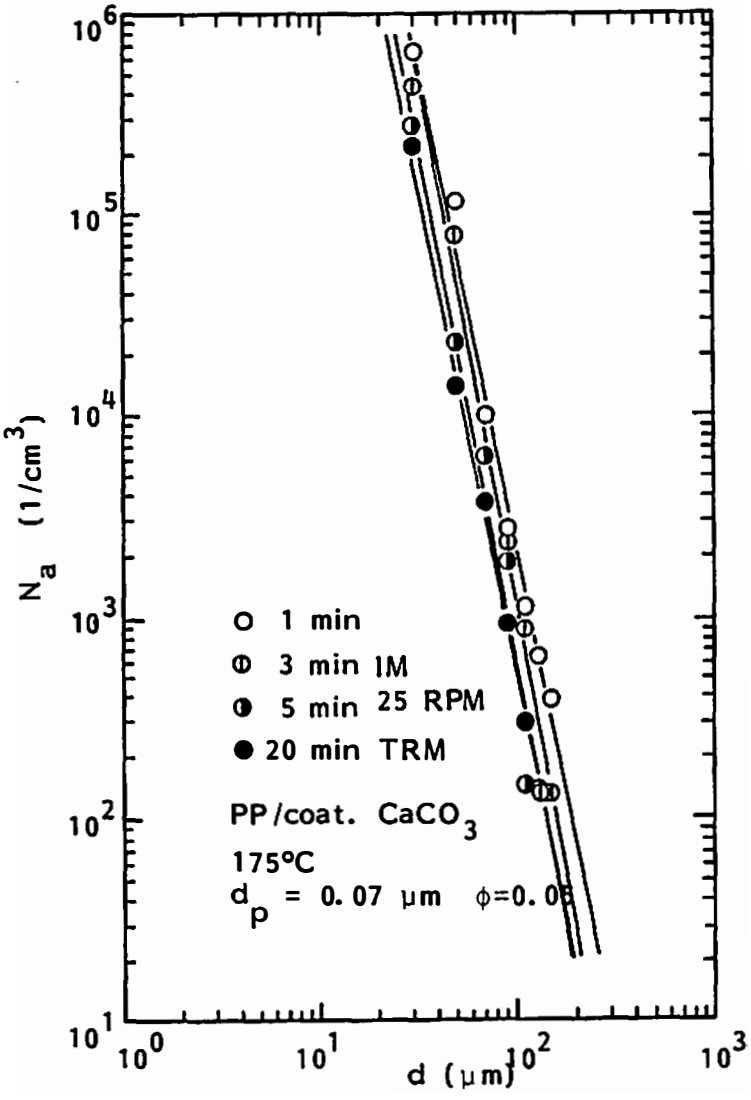

Figure VII-32. Number of agglomerates as a function of agglomerate size for PP/coat. $CaCO_3$.

Table VII-3. Parameter a and b for PS/Unc. $CaCO_3$ (dp = 0.07 μm, ϕ = 0.05)

Device	Time (min)	a ($1/cm^3$)	b (-)	Correlation Coefficient (-)
IM (25 RPM)	1	5.00×10^8	3.18	0.9704
	3	3.72×10^7	2.54	0.9768
	5	2.80×10^6	1.96	0.9708
	10	2.08×10^7	2.32	0.9896
TRM	20	1.35×10^{10}	4.46	0.9995

Table VII-4. Parameter a and b for PS/Coat. $CaCO_3$ (dp = 0.07 μm, ϕ = 0.05)

Device	Time (min)	a ($1/cm^3$)	b (-)	Correlation Coefficient (-)
IM (25 RPM)	1	1.9×10^8	2.75	0.9884
	3	6.90×10^8	3.32	0.9940
	5	2.22×10^9	3.62	0.9896
	10	1.68×10^8	3.01	0.9864
TRM	20	8.81×10^7	3.27	0.9999

Table VII-5. Parameter a and b for PP/Unc. $CaCO_3$ (dp = 0.07 μm, ϕ = 0.05)

Device	Time (min)	a ($1/cm^3$)	b (-)	Correlation Coefficient (-)
IM (25 RPM)	1	9.79×10^8	2.87	0.9930
	3	7.82×10^8	2.93	0.9681
	5	2.92×10^9	3.41	0.9945
	10	1.85×10^9	3.36	0.9940
TRM	20	1.00×10^9	3.05	0.9930

Table VII-6. Parameter a and b for PP/Coat. $CaCO_3$ (dp = 0.07 μm, ϕ = 0.05)

Device	Time (min)	a ($1/cm^3$)	b (-)	Correlation Coefficient (-)
IM (25 RPM)	1	1.20×10^{13}	4.87	0.9936
	3	7.08×10^{13}	5.40	0.9889
	5	2.82×10^{13}	5.34	0.9832
TRM	20	5.25×10^{12}	5.00	0.9984

agglomerates and the size of agglomerates are well represented by a power law relation.

We may define a dispersion index as

$$PL\ ;\ a,\ b,\ c \qquad \text{(VII-6)}$$

where P_L means power law relation of N_a and d, and a, b denote the parameters in power law assumption shown in Eq. (VII-5), and c is a correlation coefficient.

For example, the dispersion index of internal mixer prepared polypropylene/uncoated calcium carbonate compound (mixing temperature, 175°C; rotor speed, 25 rpm; mixing time, 5 minutes) is

$$PL\ ;\ 2.92 \times 10^{9}\ ,\ 3.41\ ,\ 0.9940\ . \qquad \text{(VII-7)}$$

Figures VII-33 and VII-34 plot the values of a and b, respectively. A value represents the number of agglomerates having a diameter of 1 μm. Polypropylene/coated calcium carbonate compounds possess the greatest a values and polystyrene/uncoated calcium carbonate compounds have the smallest (Figure VII-33).

Values of b represent the slopes in log N_a versus log d plots. The greatest slopes are found for polypropylene/coated calcium carbonate compounds. The number of agglomerates decays most rapidly with increasing size in these compounds. The smallest slopes are found for polystyrene/uncoated calcium carbonate compounds.

D.4.d. Relationship between dispersion and mechanical properties. The mechanical properties of polypropylene/calcium

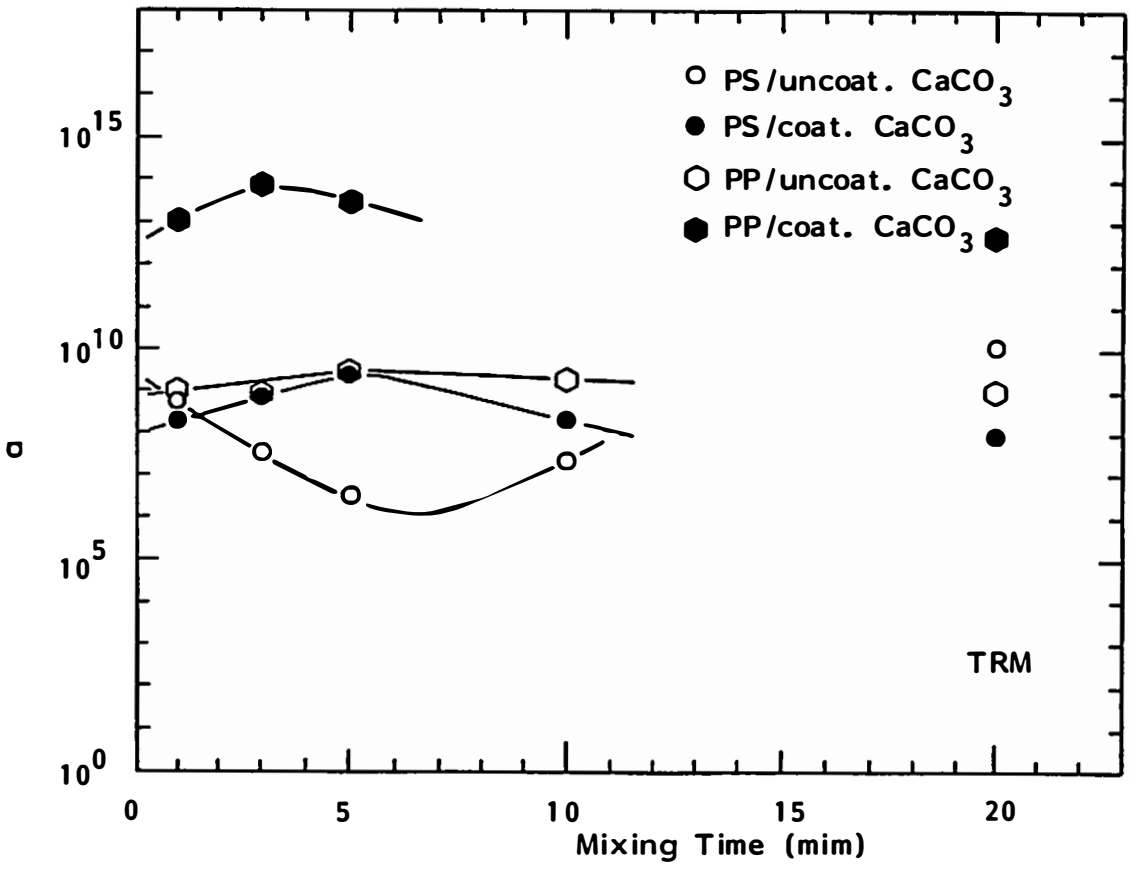

Figure VII-33. a Value as a function of mixing time for various compounds.

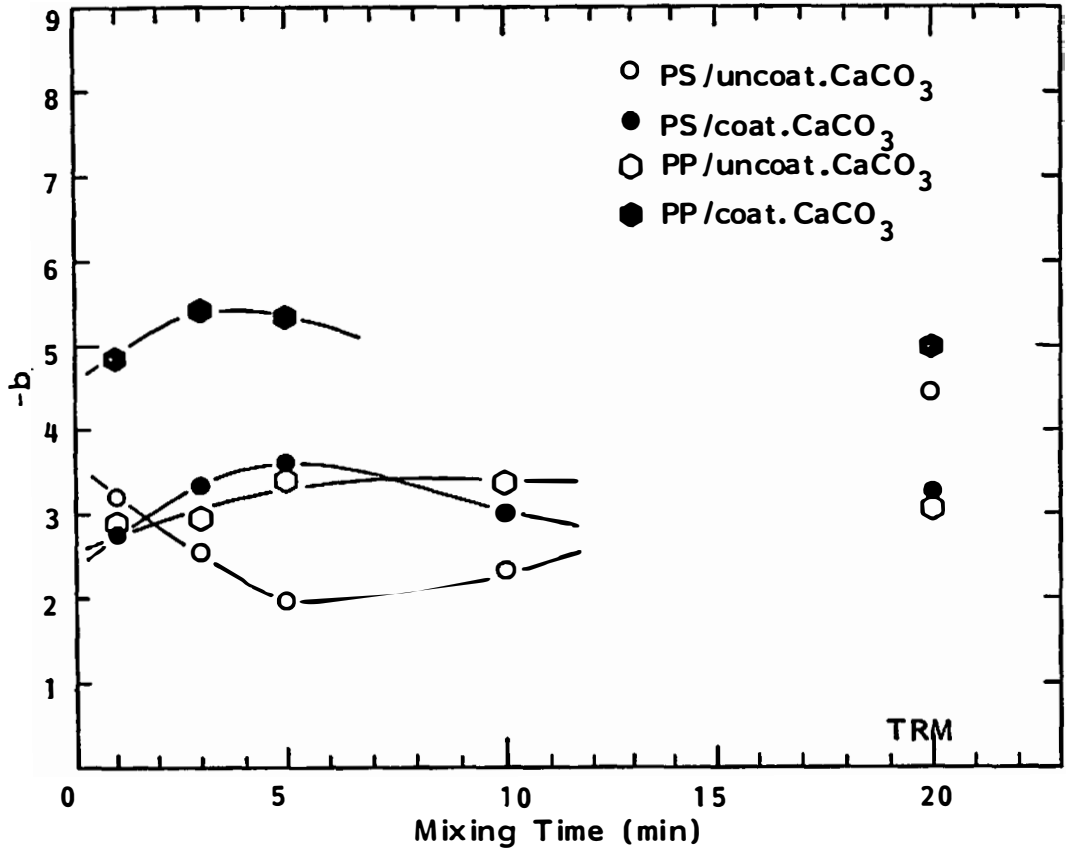

Figure VII-34. -b Values as a function of mixing time for various compounds.

carbonate compounds have been characterized by K. Murali. A Monsanto Tensiometer was used for a tensile test. A series of compounds were compression molded into a thickness of 0.04 cm at 200°C and then quenched in water. Dumbbell shaped specimens were obtained by punching with a dumbbell shape die. The initial sample length was 4 cm. Five to twelve specimens were tested. A strong correlation was found between the function $\sum_{100} \phi(d)$ and elongation at break ε (Figure VII-35). Elongation break ε of series of polypropylene/calcium carbonate compounds is plotted as the function $(\sum_{100} \phi(d))^{-1}$. As the volume fraction of large agglomerates decreases, the elongation at break increases.

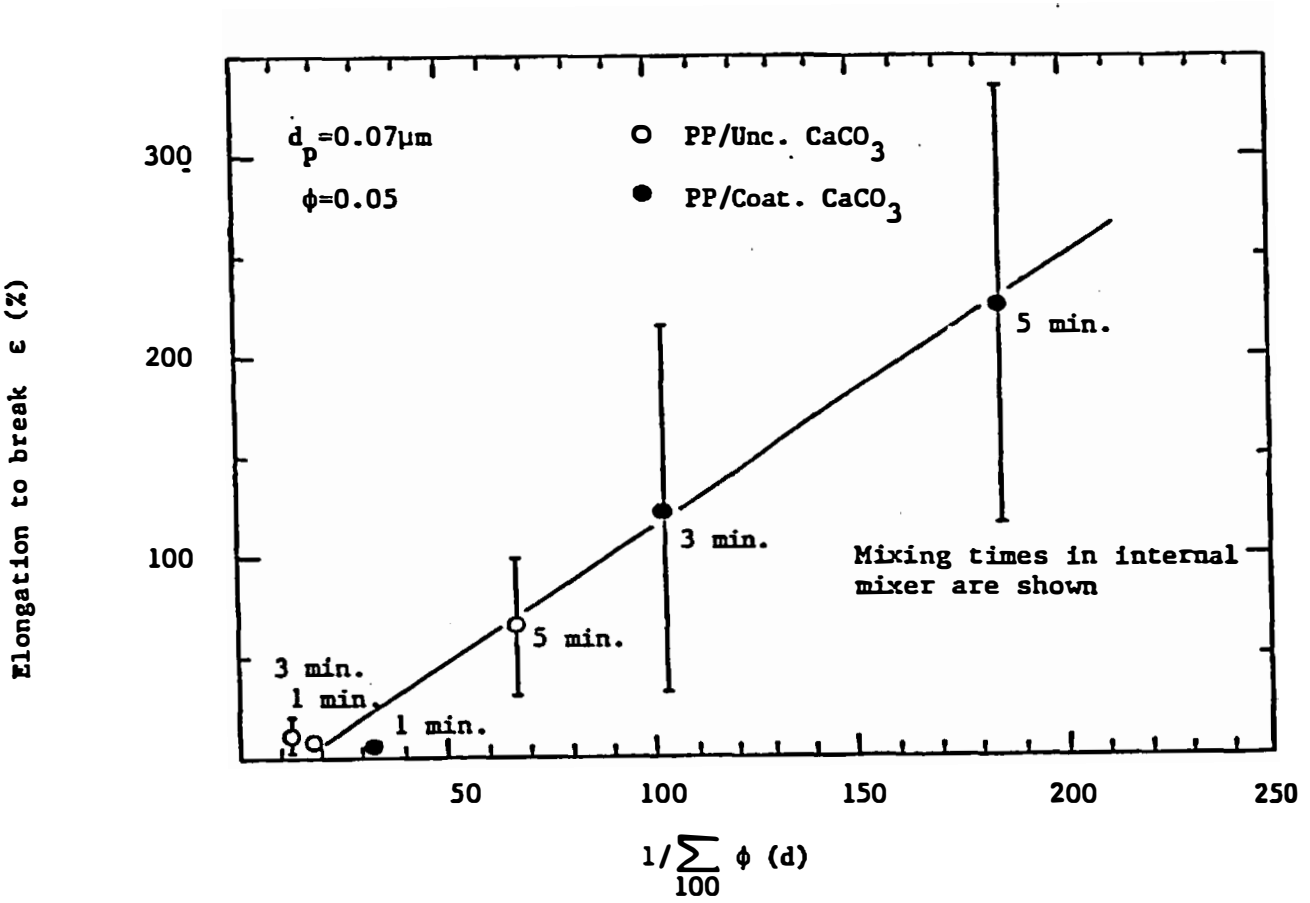

Figure VII-35. Elongation to break as a function of $1/\sum_{100} \phi(d)$ for various compounds.

CHAPTER VIII

SCANNING ELECTRON MICROSCOPY

A. INTRODUCTION

The dispersion of compounds based on large agglomerates (greater than 20 μm) has been characterized by optical microscopy. This was carried out using compression molded thin films of compounds (thickness about 100 μm) and was observed through thickness direction at relatively low magnifications of x40 and x400.

Scanning electron microscopy surveys the surface or fracture surface of compounds at much higher magnification levels. This allows us to make detailed observations of dispersed particulates and agglomerates.

The transmission electron microscope has not been used in the present research. This, in general, requires a very thin specimen ranging from 500 Å to 1000 Å. The thickness of the specimen is generally smaller than the dimensions of many of the ultimate particles employed in the present research.

B. EXPERIMENTAL PROCEDURE

Fracture surfaces of compounds were observed under the scanning electron microscope. Pieces of the mixes prepared were broken into bits with a hammer and compression molded into a thickness of about 1 mm at 200°C and quenched in water. These compound fragments were

broken in a liquid nitrogen. Cross sectional surfaces were observed under a scanning electron microscope.

Some compound sheets were heat treated before fracture in liquid nitrogen. Polystyrene compounds were heated to 190°C for 2 hours. Polypropylene compounds were heated to 180°C and annealed at a cooling rate of -0.33°C/min.

C. RESULTS

C.1. Isotropic Particulates

C.1.a. Calcium carbonate compounds. Figures VIII-1 through VIII-12 present electron micrographs of various polystyrene/calcium carbonate compounds. All compounds were pared on a two roll mill at 150°C. Mixing time is 20 minutes for ϕ = 0.05 and 0.10, 45 minutes for ϕ = 0.30.

Figures VIII-1 through VIII-6 exhibit cross sectional surface of quenched specimen. Figure VIII-1 shows the electron micrographs of polystyrene/uncoated and stearic acid surface coated calcium carbonate compounds (dp = 3 μm, ϕ = 0.05). Both uncoated and coated calcium carbonates appear well dispersed in polystyrene. The particulates are well separated. The volume fraction of filler increases in Figure VIII-2 (ϕ = 0.10), and VIII-3 and VIII-4 (ϕ = 0.30). The particle size is again 3 μm in these micrographs. In the compounds of volume fraction ϕ = 0.10 (Figure VIII-2), particulates are still separated from each other. At the volume fraction of 0.30 (Figures VIII-3 and VIII-4), however, the particulates appear to

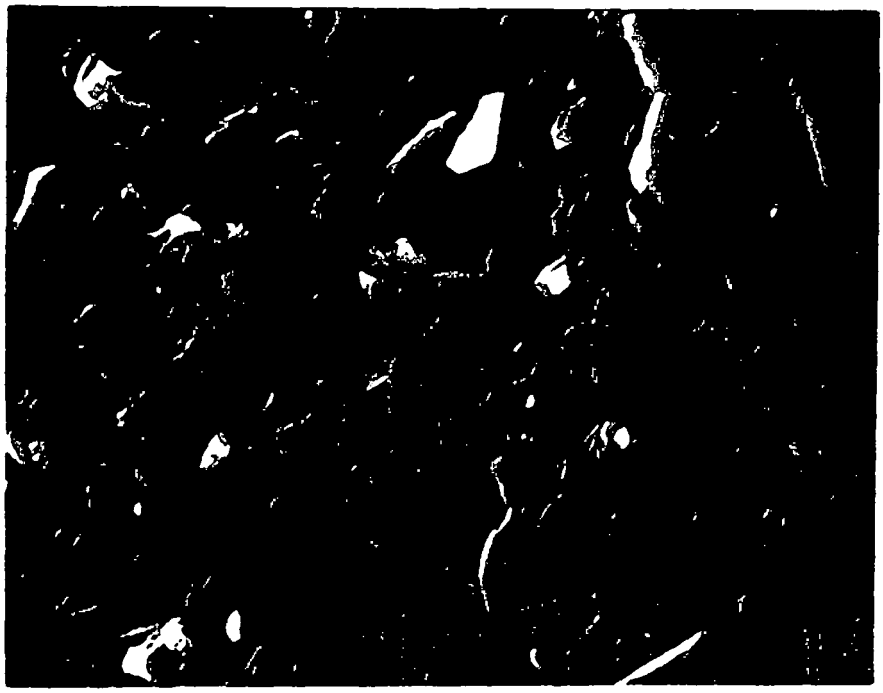

(a) PS/Uncoat. $CaCO_3$ X2000

(b) PS/Coat. $CaCO_3$ X2000

Figure VIII-1. Electron micrographs of PS/$CaCO_3$ compound (ϕ = 0.05, dp = 3 μm) (TRM 150°C 20 min).

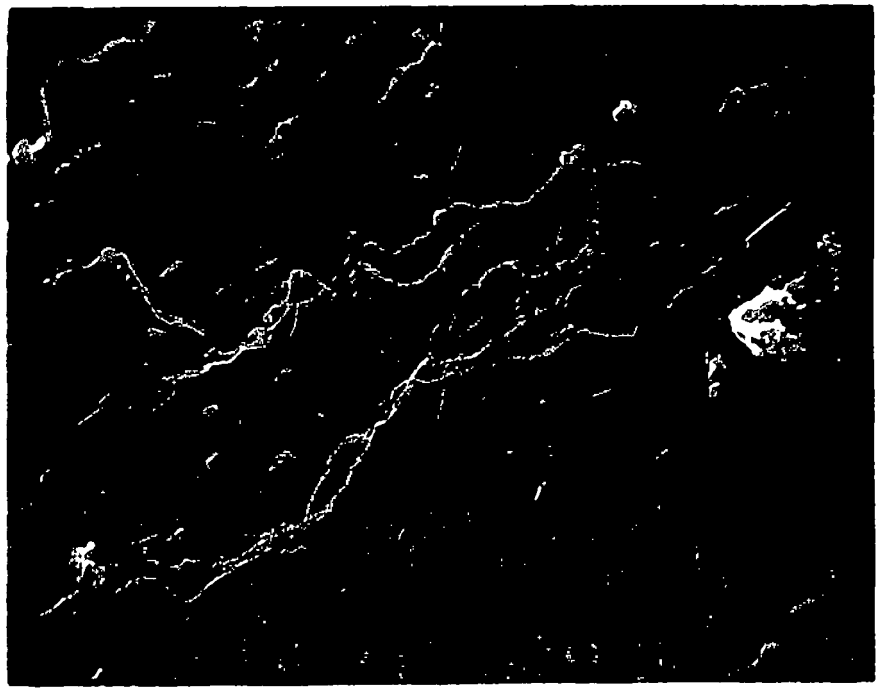

(a) PS/Uncoat. $CaCO_3$ X2000

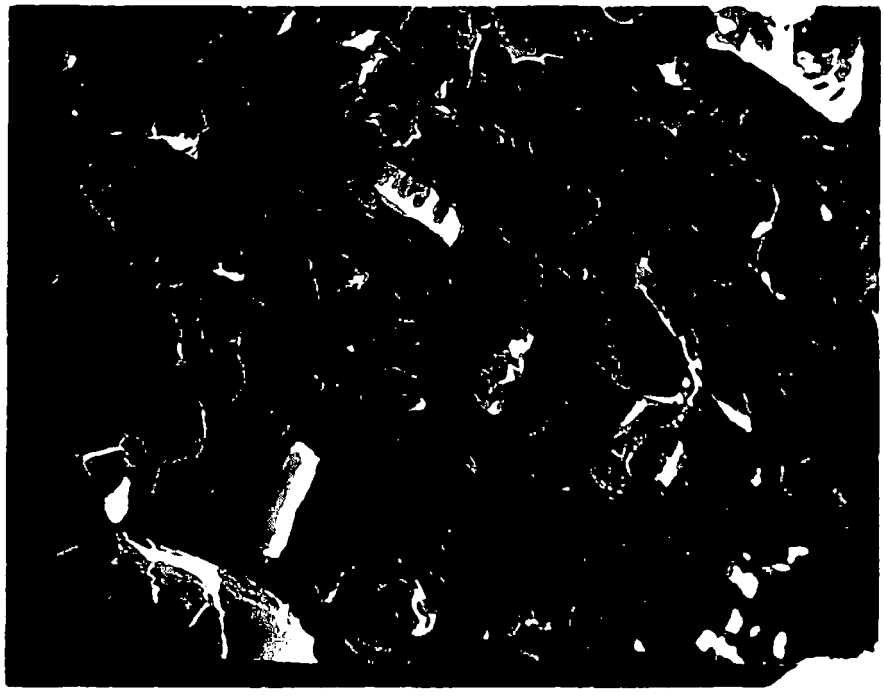

(b) PS/Coat. $CaCO_3$ X2000

Figure VIII-2. Electron micrographs of PS/$CaCO_3$ compound (ϕ = 0.10, dp = 3 μm) (TRM 150°C 20 min).

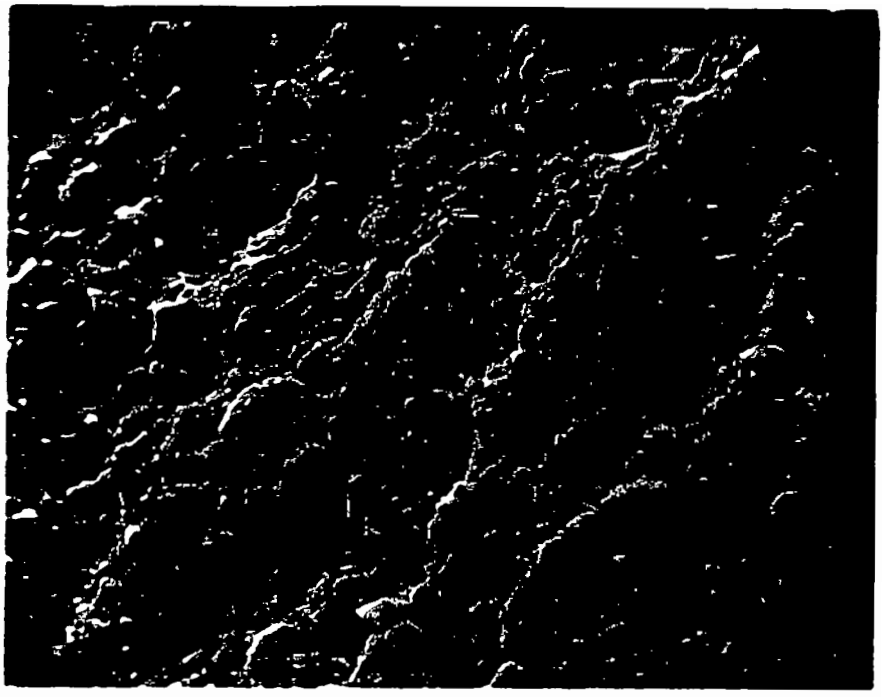

(a) X450

(b) X2000

Figure VIII-3. Electron micrographs of PS/uncoat. $CaCO_3$ (ϕ = 0.30, dp = 3 μm) (TRM 150°C 45 min).

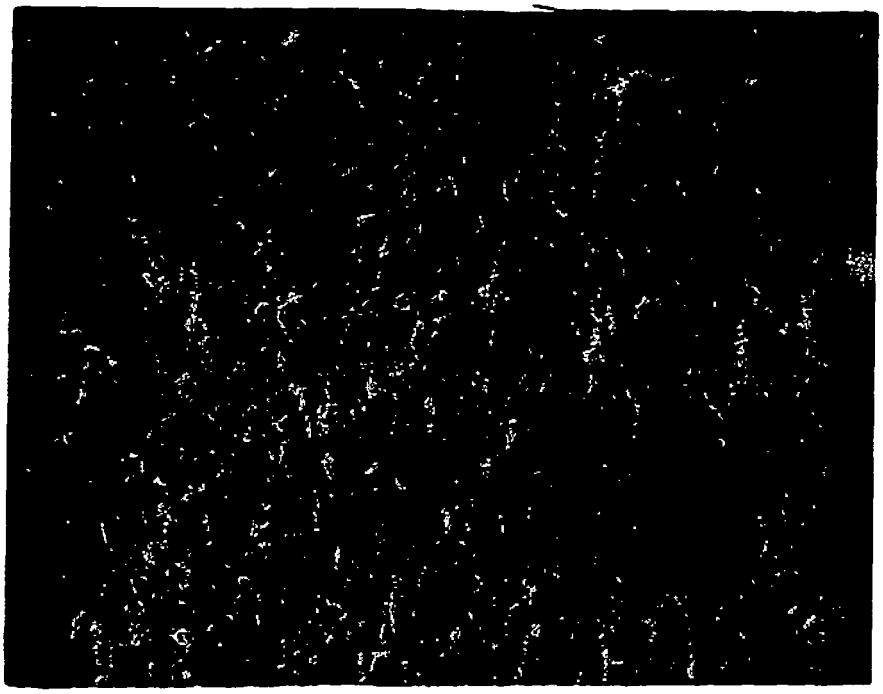

(a) X450

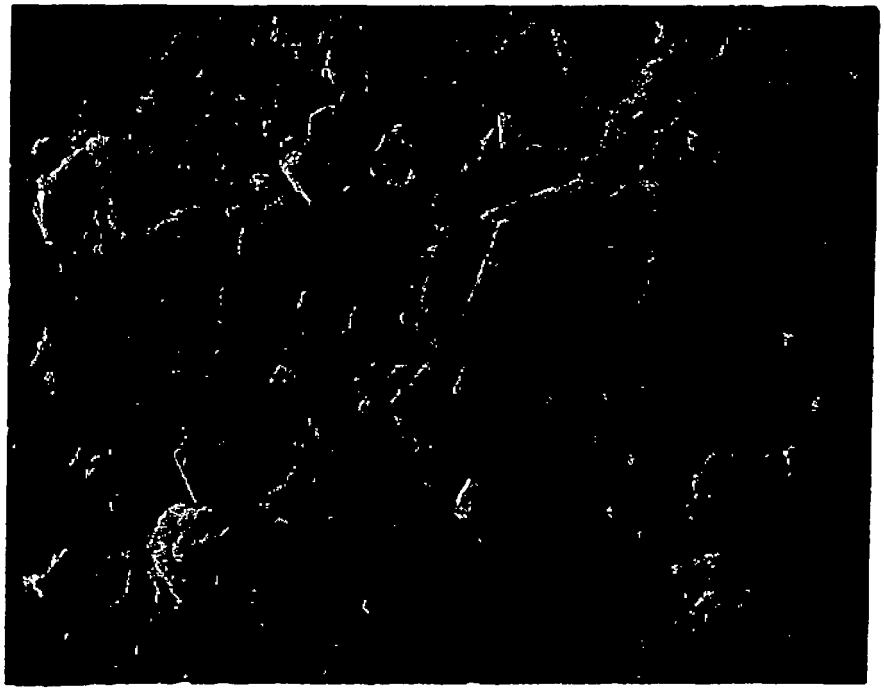

(b) X2000

Figure VIII-4. Electron micrographs of PS/coat. $CaCO_3$ compound (φ = 0.30, dp = 3 μm) (TRM 150°C 45 min).

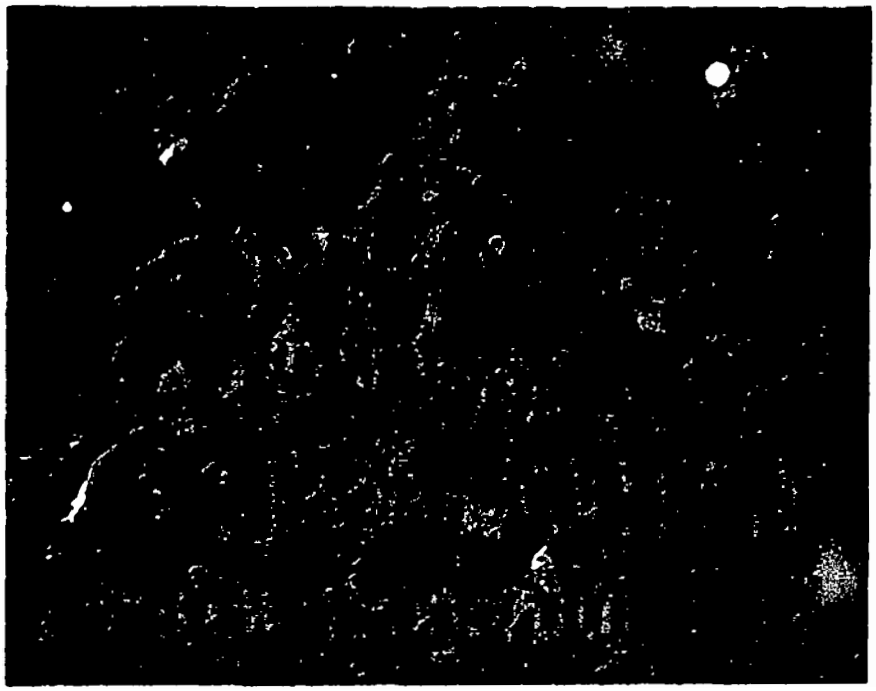

(a) X2000

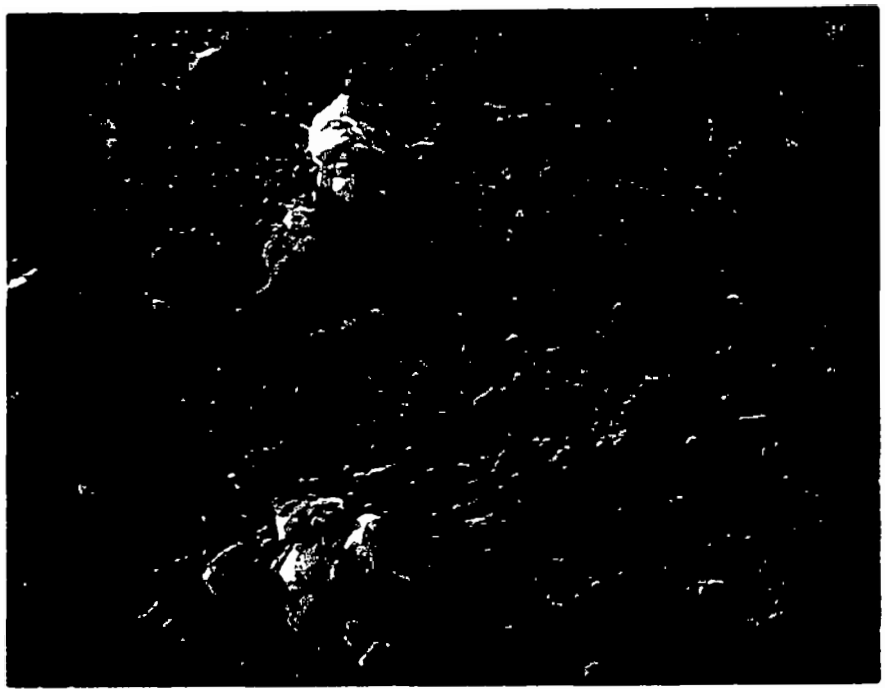

(b) X5000

Figure VIII-5. Electron micrographs of PS/uncoat. $CaCO_3$ compound (ϕ = 0.30, dp = 0.4 μm) (TRM 150°C 45 min).

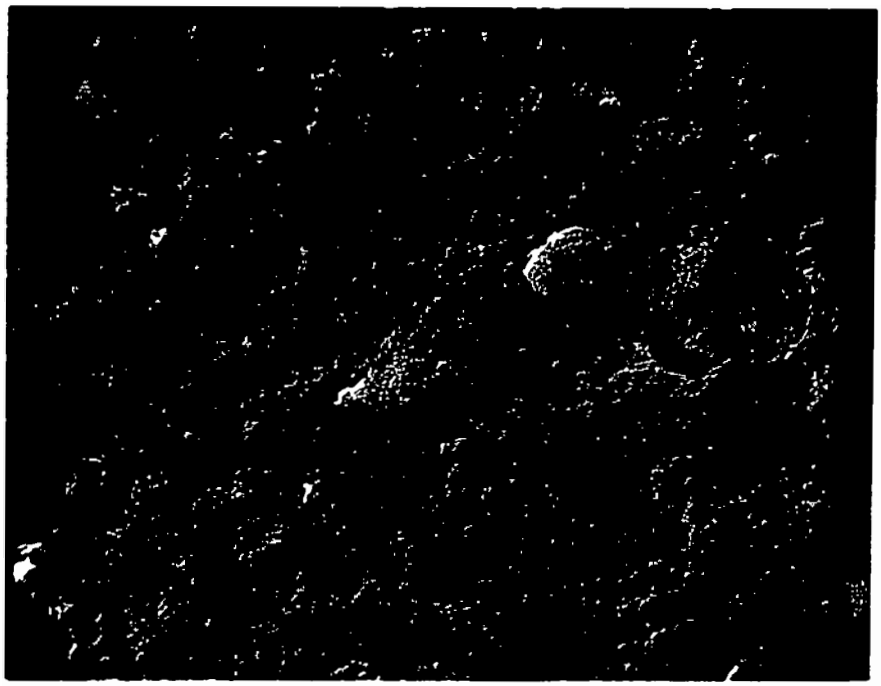

(a) X2000

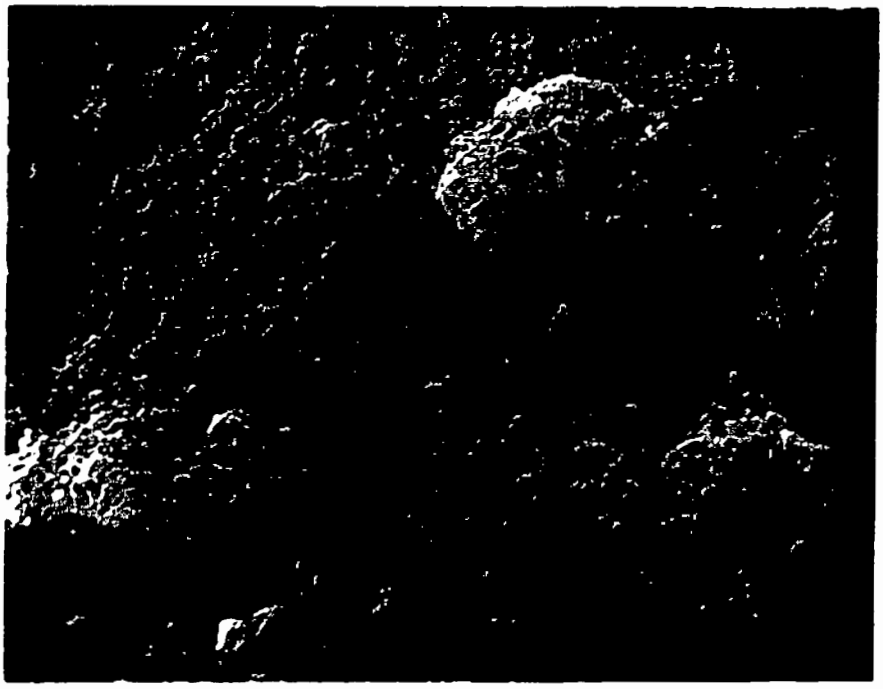

(b) X5000

Figure VIII-6. Electron micrographs of PS/coat. $CaCO_3$ (ϕ = 0.30, dp = 0.5 μm) (TRM 150°C 45 min).

(a) PS/Uncoat. $CaCO_3$ X2000

(b) PS/Coat. $CaCO_3$ X2000

Figure VIII-7. Electron micrographs of heat treated PS/$CaCO_3$ compound (ϕ = 0.05, dp = 3 μm) (TRM 150°C 20 min).

(a) PS/Uncoat. $CaCO_3$ X2000

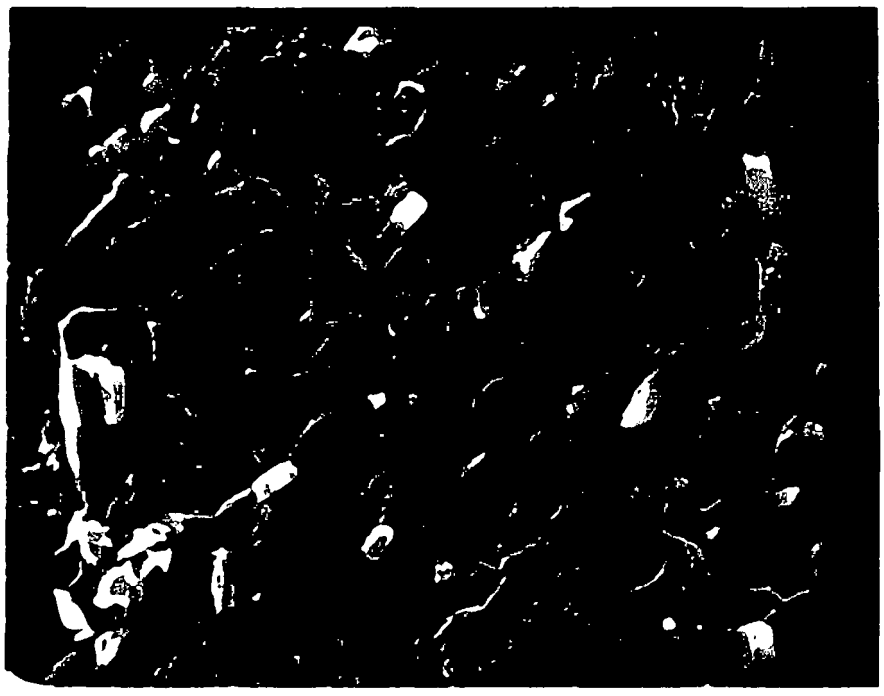

(b) PS/Coat. $CaCO_3$ X2000

Figure VIII-8. Electron micrographs of heat treated PS/$CaCO_3$ compound (ϕ = 0.10, dp = 3 μm) (TRM 150°C 20 min).

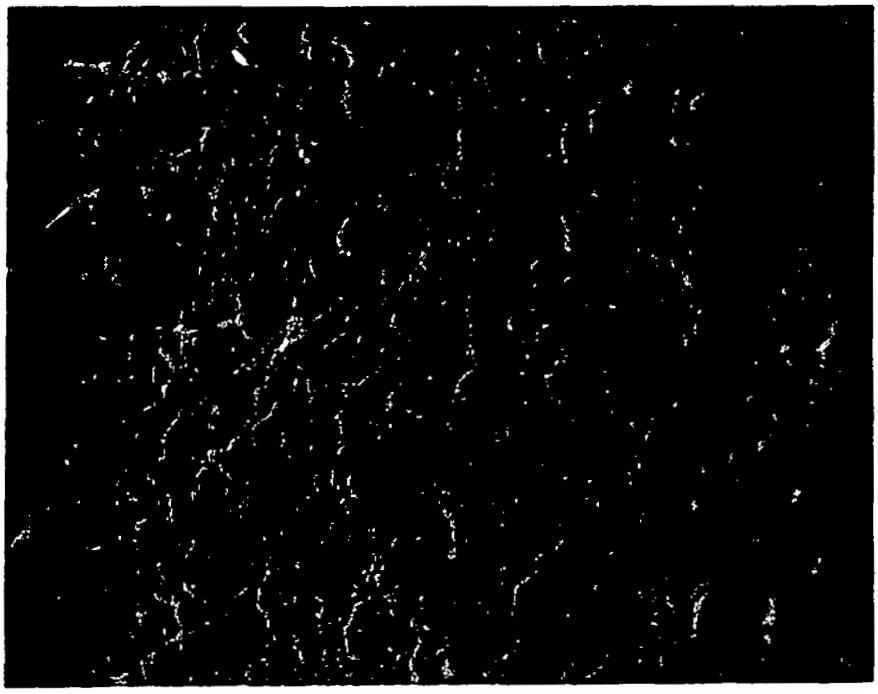

(a) X450

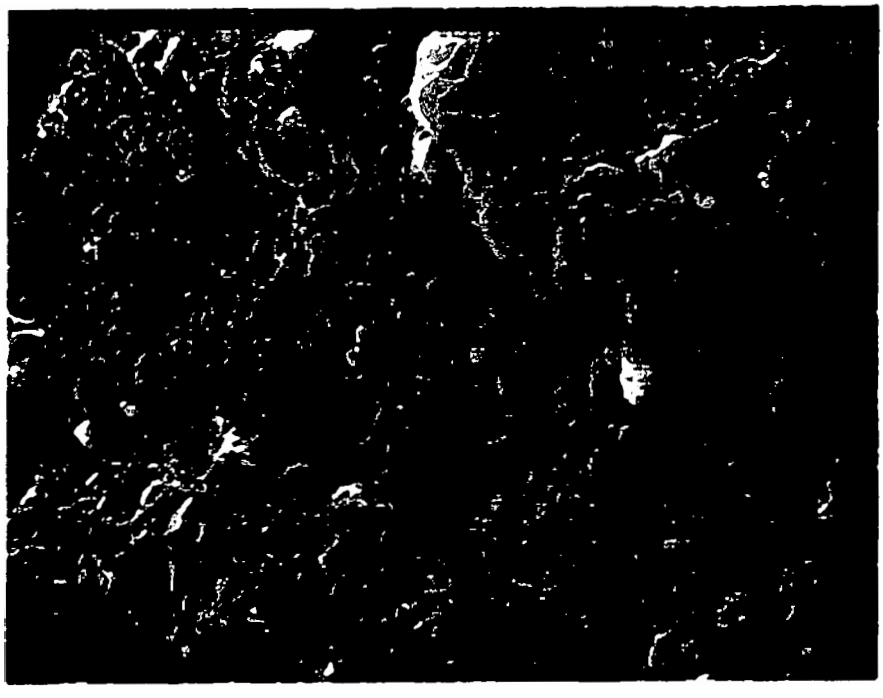

(b) X2000

Figure VIII-9. Electron micrographs of heat treated PS/uncoat. $CaCO_3$ compound (ϕ = 0.10, dp = 3 μm) (TRM 150°C 45 min).

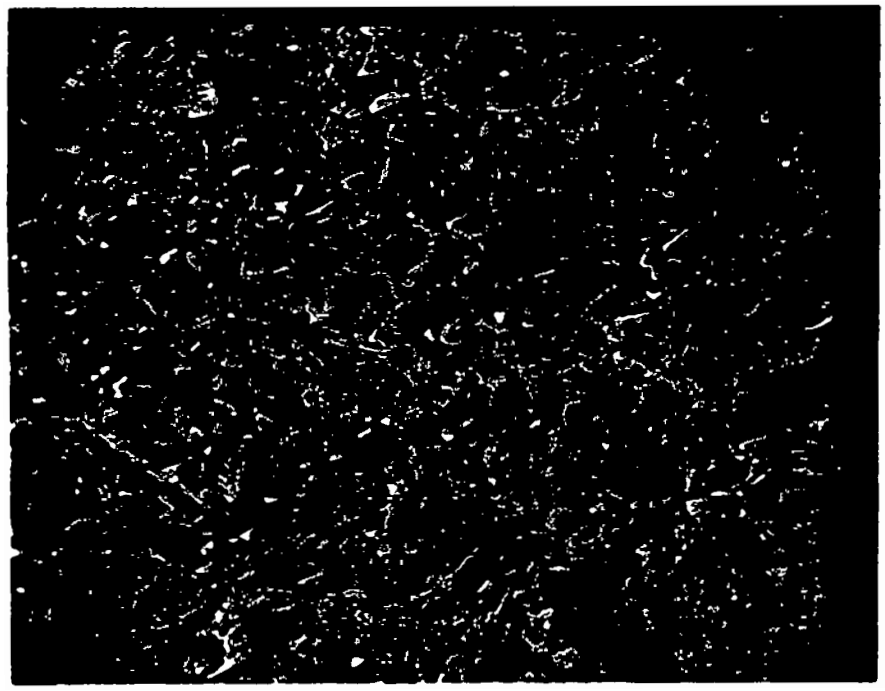

(a) X450

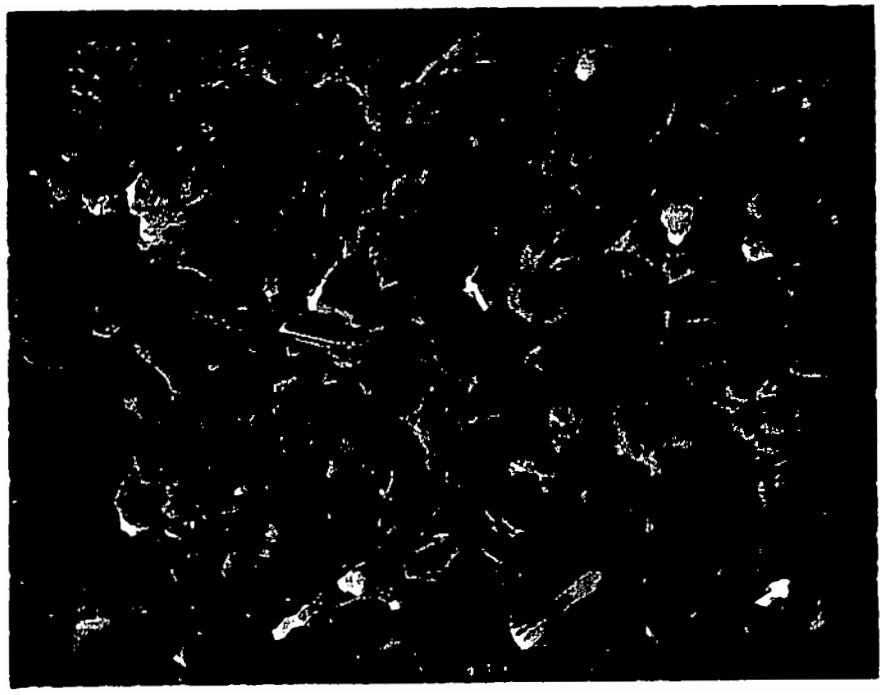

(b) X2000

Figure VIII-10. Electron micrographs of heat treated PS/coat. $CaCO_3$ (ϕ = 0.30, dp = 3 μm) (TRM 150°C 45 min).

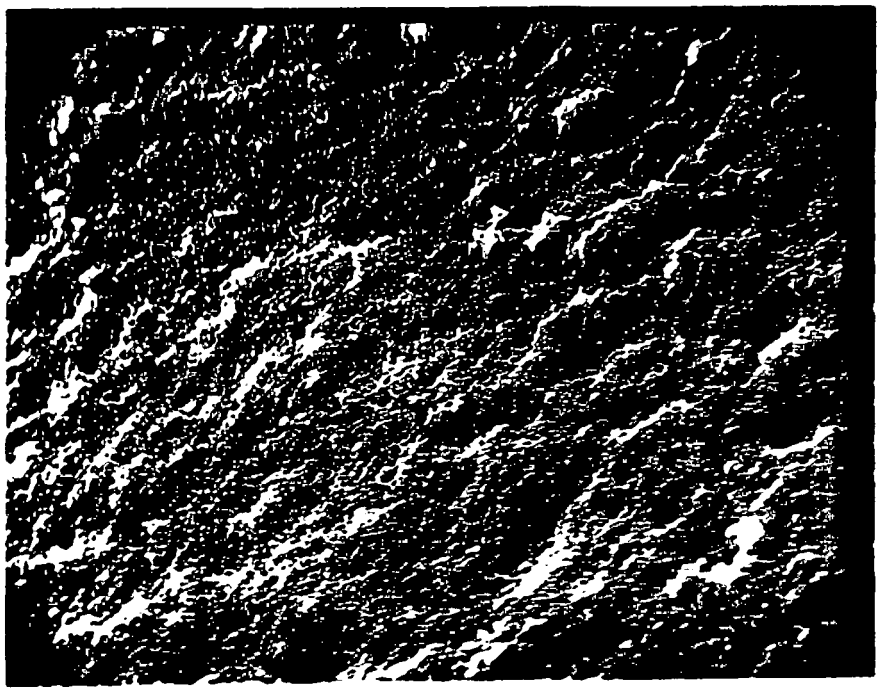

(a) X2000

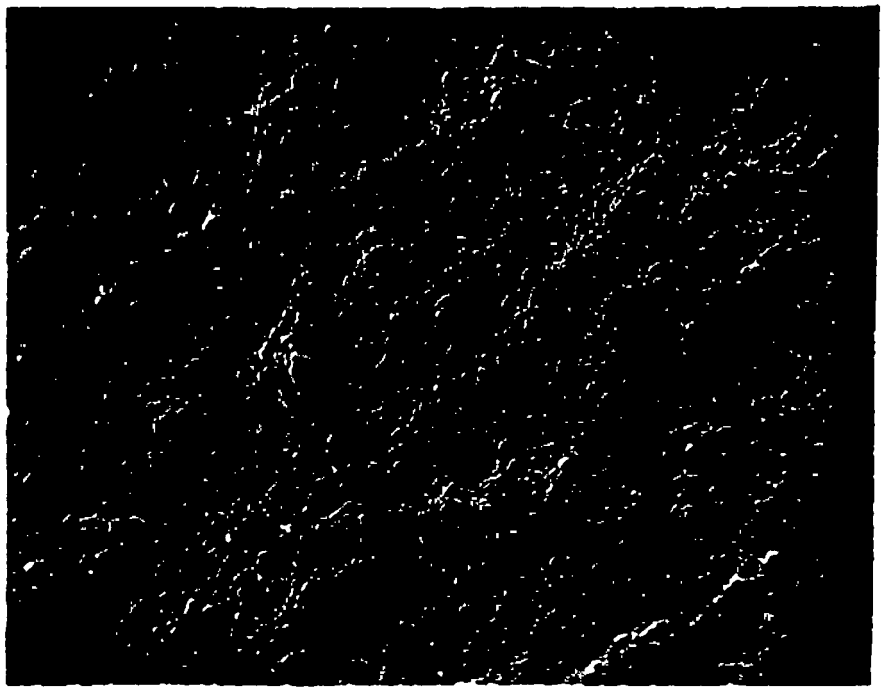

(b) X5000

Figure VIII-11. Electron micrographs of heat treated PS/uncoat. $CaCO_3$ (ϕ = 0.05, dp = 0.4 μm) (TRM 150°C 45 min).

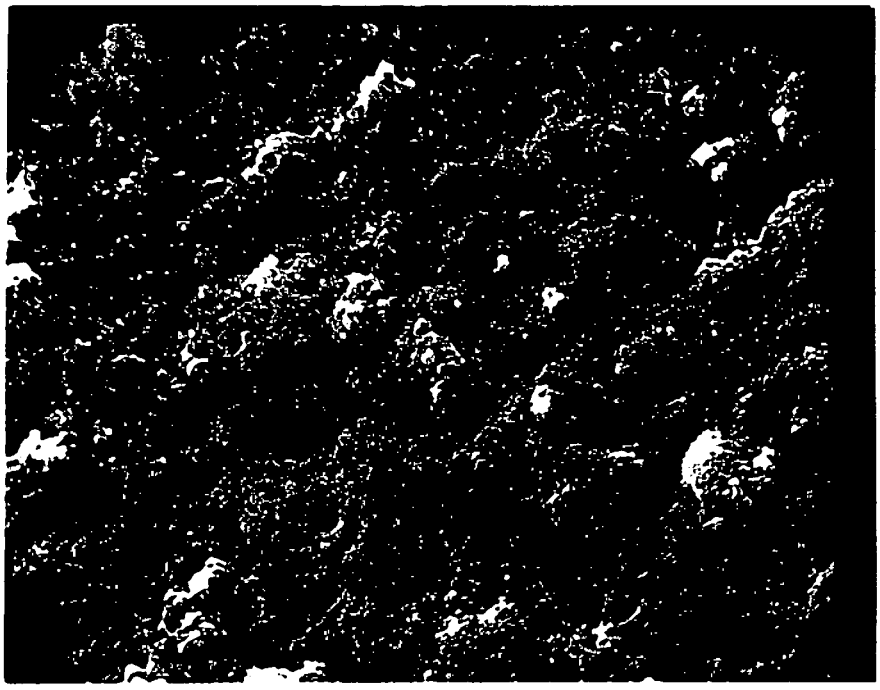

(a) X2000

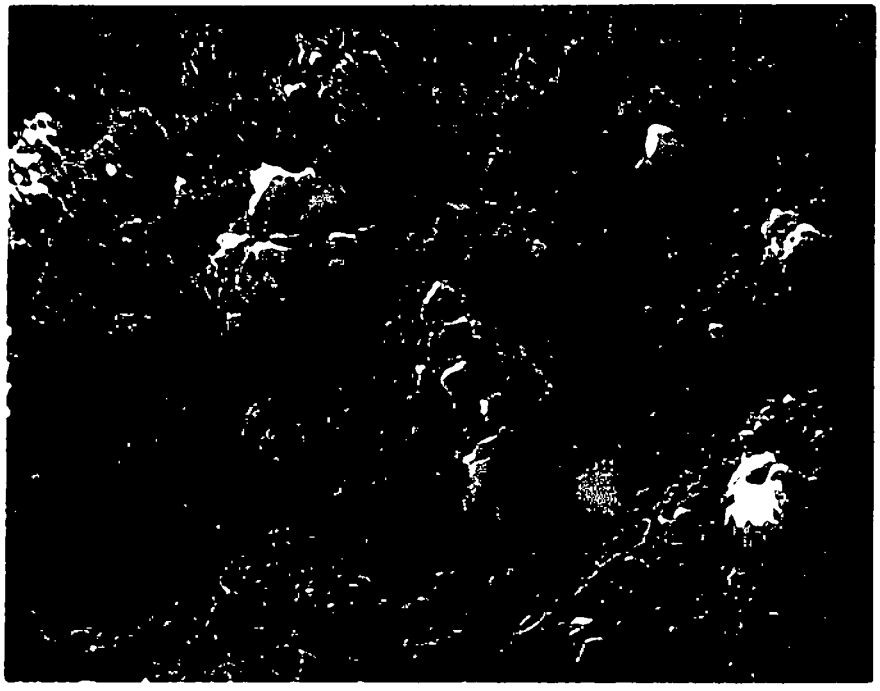

(b) X5000

Figure VIII-12. Electron micrographs of heat treated PS/coat. $CaCO_3$ (ϕ = 0.30, dp = 0.5 μm) (TRM 150°C 45 min).

touch each other. This is more clear in the coated calcium carbonate compound (Figure VIII-4). Coated calcium carbonate particles appear more clearly on the fractured surface than uncoated case. It seems like uncoated particles are covered with polymer. However, the clear existence of agglomerates is not observed in either uncoated and coated samples.

Smaller particulates of calcium carbonate tend to form agglomerates. Figures VIII-5 and VIII-6 exhibit uncoated calcium carbonate (dp = 0.4 μm) and coated calcium carbonate (dp = 0.5 μm) compounds, respectively. The volume fractions are 0.30 in both cases. Some agglomerates may be observed in both uncoated and coated calcium carbonate systems.

Micrographs of heat treated (190°C for 2 hours) polystyrene compounds are given in Figure VIII-7 through VIII-12. It was intended to see if the particulates from some types of structures (typically agglomerates and three-dimensional networks) due to the particle-particle interaction forces during heat treatment at 190°C. Under such conditions polystyrene has a reasonably low viscosity.

Figures VIII-7 and VIII-8 exhibit heat treated low volume fraction compounds (ϕ = 0.05 and ϕ = 0.10, respectively). The particle size is 3 μm. Both uncoated and coated calcium carbonates are well separated and dispersion is unchanged by the heat treatment. Figures VIII-9 and VIII-10 show high volume fraction compounds (ϕ = 0.30). Again, the particle size is 3 μm. Particulates touch each other at this loading level. The particulates appear more

clearly in coated calcium carbonate systems. These two characteristics are the same as the quenched compounds (dp = 3 μm, ϕ = 0.30) shown in Figures VIII-3 and VIII-4. The effect of heat treatment is not clear.

The heat treated compounds containing smaller calcium carbonates (dp = 0.4 μm for uncoated and 0.5 μm for coated) are shown in Figures VIII-11 and VIII-12. Volume loading levels are 0.30. In these micrographs the dispersion of uncoated calcium carbonate seems unchanged (or even improved) by heat treatment (compare Figure VIII-11 and VIII-5), and coated calcium carbonate seems to form agglomerates after heat treatment (compare Figure VIII-12 and VIII-6). In general, the effect of heat treatment is not clear.

C.1.b. Carbon black compounds. The polypropylene/carbon black compound was thermally treated. This was performed in such a way as to melt out and then recrystallize the matrix phase. The compound was heated up to 180°C and cooled down at the cooling rate of -0.33°C/minutes.

Figure VIII-13 shows optical photomicrographs of polypropylene spherulites. Unfilled polypropylene film (thickness of 100 μm) was observed under cross polarized light with a compensator. The size of the spherulites is roughly 100 μm.

Figure VIII-14 represents electron micrographs of heat treated polypropylene/carbon black compounds (dp = 0.32 μm, ϕ = 0.20). Thickness of the compounded sheet is 1 mm. The spherulite structure was observed on fractured cross section surfaces. The size of the spherulite is roughly 50 μm. A rough surface is observed at the

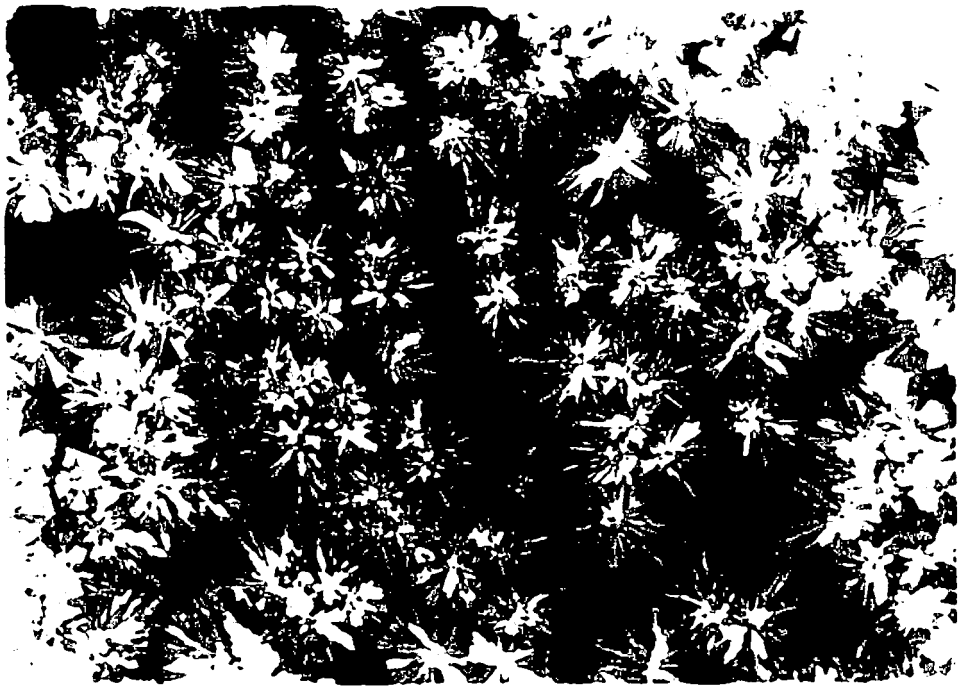

(a) X100

(b) X400

Figure VIII-13. Optical micrographs of heat treated PP. Spherulites under cross polarized light.

(a) X300

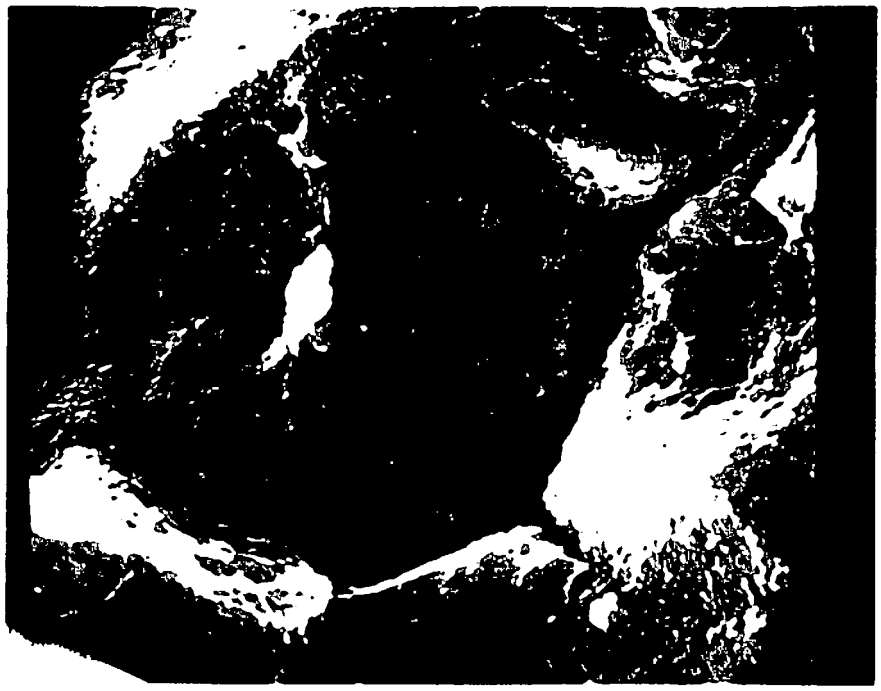

(b) X1000

Figure VIII-14. Electron micrographs of heat treated PP/CB compounds (ϕ = 0.20, dp = 0.32 μm) (TRM 175°C 20 min).

boundary of the spherulites. These may be particulates or aggregates of carbon black. This will be discussed in Chapter XI and Chapter XII in conjunction with the electrical conductivity of heat treated polypropylene/carbon black compounds.

C.2. Anisotropic Particulates

Some anisotropic particles (talc, silane treated talc and mica) compounds have been observed using scanning electron microscopy.

Figures VIII-15 and VIII-16 represent micrographs of the fractured cross section of uncoated and silane coated talc compounds, respectively. No agglomeration is observed. It is significant that the disc shape particulates of talc are oriented in one direction (horizontal direction in micrograph). This presumably occurred in the compression molding process. The direction of compression is vertical in these micrographs. The effect of surface treatment is not clear.

The electron micrograph of the polypropylene/mica compound is given in Figure VIII-17. This again shows a strong orientation of the mica particulates in the perpendicular direction to the compression direction.

D. DISCUSSION

D.1. Isotropic Particulates

Scanning electron microscopy of the isotropic particulate compounds leads us to the following conclusions.

(a) X300

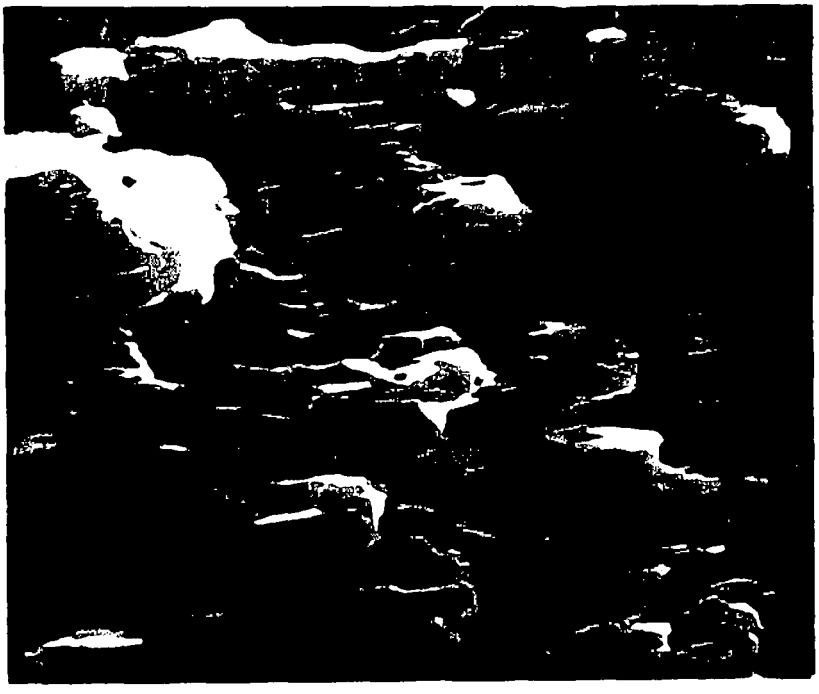

(b) X1000

Figure VIII-15. Electron micrographs of PP/uncoat. talc compound (ϕ = 0.05, dp = 1.9 μm) (TRM 175°C 20 min).

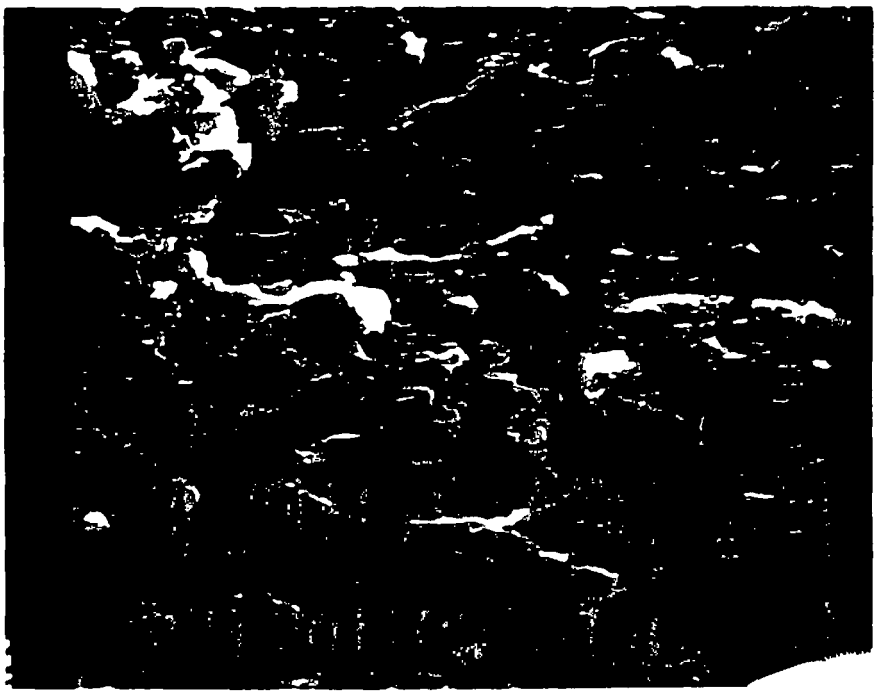

(a) X300

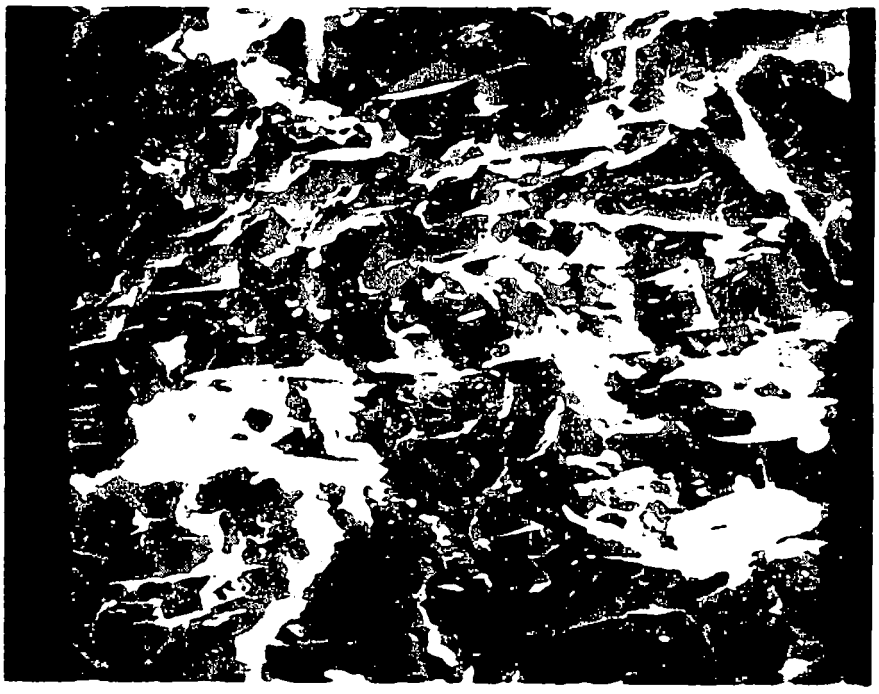

(b) X1000

Figure VIII-16. Electron micrographs of PP/coat. talc (ϕ = 0.05) (TRM 175°C 20 min).

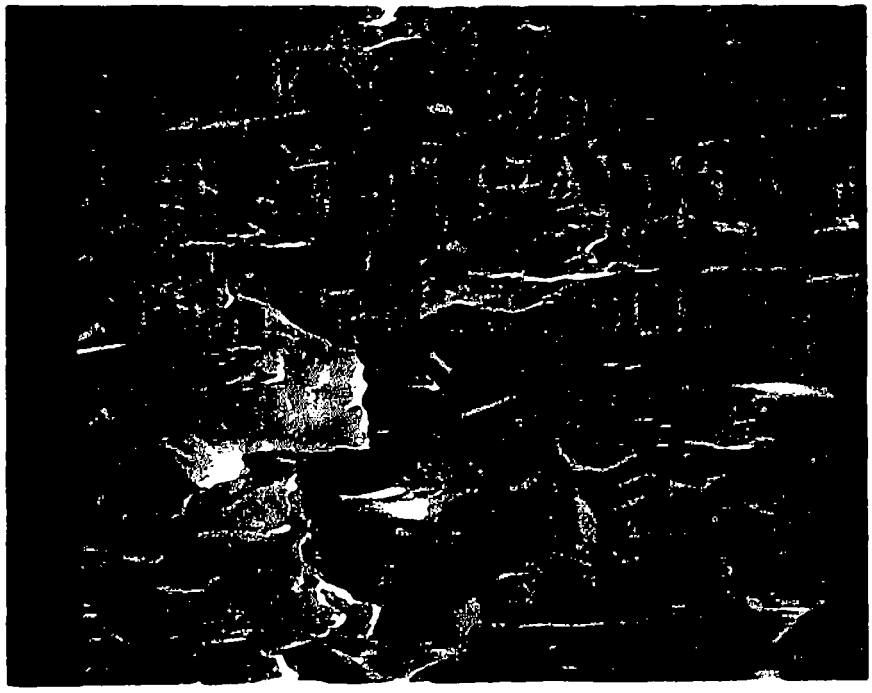

X300

Figure VIII-17. Electron micrograph of PP/mica compound (ϕ = 0.05) (TRM 175°C 20 min).

1. Large particulates (greater than 1 μm) are well separated below the volume fraction of 0.10. These come in contact at a volume fraction of 0.30.

2. Small particulates (less than 1 μm) tend to form agglomerates.

3. Individual particulates appear more clearly in stearic acid coated calcium carbonate.

4. At low volume fractions (less than ϕ = 0.10), particulates do not agglomerate during heat treatment. The effect of heat treatment is not clear at high volume fraction.

Scanning electron microscopy by its character allows us to observe a two-dimensional surface (or cross sectional surface) of the material. The structures which may be formed by particulates are, however, implied to be a three-dimensional. It is often very difficult to distinguish agglomerates in the micrographs. Scanning electron microscopy may be used together with optical microscopy to judge the existence of agglomerates.

Scanning electron microscopy surveys the two-dimensional fracture surface of the compounds. The probability that an agglomerate appears on the surface of the observation is low. A tremendous labor would be required to obtain reliable data since a reasonably large area must be observed. In addition, the sizes of agglomerates which appear on the surface are different from the true diameters of the agglomerates. To overcome this difficulty, one must lean on the statistical formula proposed by Holliday et al. ( ) and Mihira et al ( ).

Quantitative results were not obtained by the method of scanning electron microscopy in the present research.

Stearic acid surface coated calcium carbonates appear more clearly than uncoated ones. Uncoated calcium carbonates are, however, covered with polymer. Debonding of polymer may occur at the surface of coated calcium carbonate when the compound was fractured in liquid nitrogen. Breakage might occur in the polymer phase in uncoated calcium carbonate compound.

It is well known that the small particle filled polymer melts possess thixotropic time dependent rheological properties (M-19, S-10,S-11,S-12,T-8). Suetsugu (S-10) pointed out that the magnitude of stress or viscosity overshoot in steady shear flow is dependent upon the previous aging time and the deformation history. The stress overshoot is greater as the aging time increases. The aging time denotes the period at which compound sample is exposed to an elevated temperature without deformation. It should thus be expected that the filler particulates form or reform some type of structure during the aging process.

It was intended to observe the development of particulate structure after thermal treatment (aging) by electron microscope. However, no clear conclusions were possible.

Heat treatment of polypropylene/carbon black compounds may change the particulate structure or location. Spherulite structures are formed in these compounds and carbon black particulates seem to be squeezed out from the crystalline phase. This cannot be strongly

concluded because of the two-dimensional nature of the scanning electron microscopy method. The formation of the three-dimensional particulate structure such as the network structure during the heat treatment can be observed by electrical conductivity measurement. This will be discussed in Chapter XI, Electrical Conductivity Measurement and Chapter XII, Determination of Dispersion Based on Percolation Theory.

D.2. Anisotropic Particulates

In the compounds of anisotropic fillers which have disc shapes, agglomerates are not found and particulates are separated from each other. This agrees with the observations by optical microscopy. Anisotropic particulates employed in the present research possess relatively large dimensions. Talc and silane coated talc are 1 to 2 μm and mica is 5 to 10 μm in the disc diameters. This may lead to good dispersion. These particulates are found to have high orientation after the compression molding process. This may have a significant effect on the mechanical properties of compounds.

CHAPTER IX

SMALL ANGLE LIGHT SCATTERING

A. INTRODUCTION

We have characterized the dispersion of small particulates by optical microscopy (Chapter VII) and scanning electron microscopy (Chapter VIII).

It has been indicated, in the present research, that it is the particulates which have ultimate particle diameters of less than 1 μm that tend to form agglomerates in compounds. Such agglomerates appear to possess a wide range of sizes. For example, calcium carbonate particulates which possess an average nominal ultimate particle size of 0.07 μm, both in uncoated and in the surface coated mode, form agglomerates of over 100 μm in diameter. Small agglomerates may be expected to have a size approaching the size of ultimate particulates.

Large agglomerates greater than 20 μm have been successfully characterized by the optical microscope at a magnification of 40. Characterization of small agglomerates is, however, more difficult. We have not been able to quantitatively characterize these by optical and electron microscopy methods. At high magnifications in an optical microscope the depth of good forcus is narrow and the coverage area is low.

The small angle light scattering (SALS) technique is a unique method to characterize small agglomerates. This characterizes scatterers (ultimate particles or agglomerates) from sub-micron range to roughly 20 μm or above in diameter. The theoretical background of this technique has been developed in the past several years in conjunction with x-ray scattering. The small angle light scattering method allows us to obtain fast and easy characterization of small particulate filled compounds.

Figure IX-1 compares the small angle light scattering technique and optical microscopy in the size range of characterizing objects. This is done for an example of an internal mixer prepared polypropylene/ uncoated calcium carbonate compound (dp = 0.07 μm, ϕ = 0.05). It ought to be noted that the number of agglomerates increases drastically with decreasing size. The number of the agglomerates in the characterization range of small angle light scattering technique is quite significant.

B. EXPERIMENTAL APPARATUS AND PROCEDURE

The compounds were prepared on a two roll mixing mill and in an internal mixer. Conditions of mixing have been discussed in Chapter III, Materials and Sample Processing.

The mixes were broken into small pieces, and compression molded slowly at the temperature of 200°C into the thickness of 100 μm. Slow compression and high temperatures were used to prevent the further breakdown of agglomerates. Ferrotype stainless

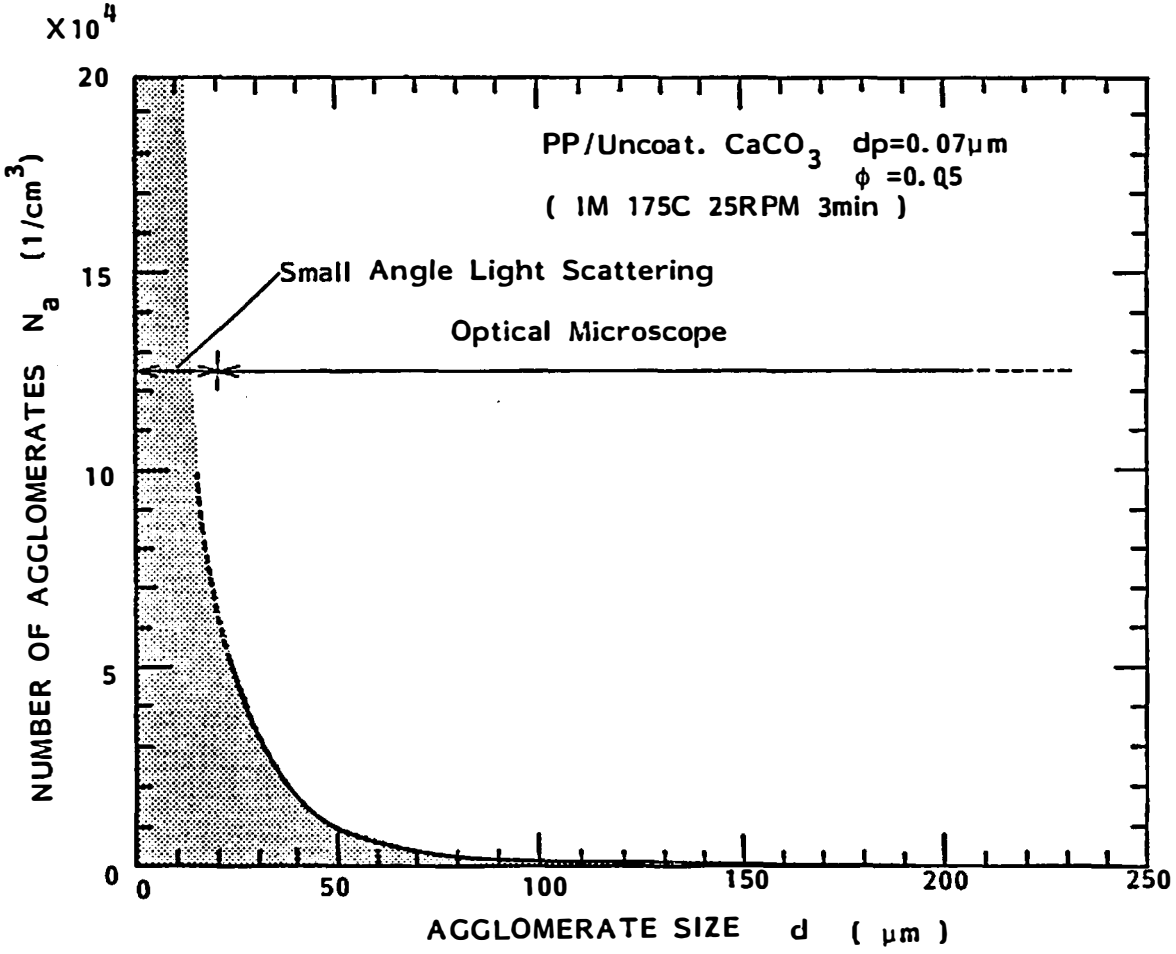

Figure IX-1. Number of agglomerates in unit volume of compound as a function of agglomerate size (comparison of SALS and optical microscope ranges).

steel plates were used for compression molding process to obtain smooth surfaces.

A small angle light scattering apparatus has been constructed by the author in our laboratory. A schematic drawing and photograph of the apparatus are shown in Figures IX-2 and IX-3, respectively.

The apparatus is composed of a dark box, a controller (EG & G Princeton Applied Research; Model 1216 Multichannel Detector Controller), a monitor (Textronix; 605 Storage Monitor), a computer (EG & G Princeton Applied Research; OMA-III System), a printer (EPSON; Dot Matrix Printer, Model FX-80) and a plotter (Bausch & Lomb Houston Instrument; DMP-40 Series Digital Plotter.

The dark box contains (i) a low profile optical bench (Oriel), (ii) a laser light source (Spectra Physics; helium-neon randomly polarized laser, 4 mW, Model 102-4), (iii) a shutter (ILEX), (iv) neutral density filters (Oriel), (v) a polarizer (Oriel), (vi) sample chamber having heaters connected to a temperature controller (OMEGA; programmable controller), (vii) an analyzer (Oriel), (viii) a screen, (ix) camera lens (Nikon; Micro Nikkor 55 mm 1:2.8) and (x) vidicon detector head (EG & G Princeton Applied Research; Silicon Target Detector Head Model 1252B).

This apparatus allows two types of detecting methods. One is a photographic method. A second is a vidicon-computer digital method.

In the photographic method, the screen in the dark box was simply replaced by polaroid film (Kodak; Type-55).

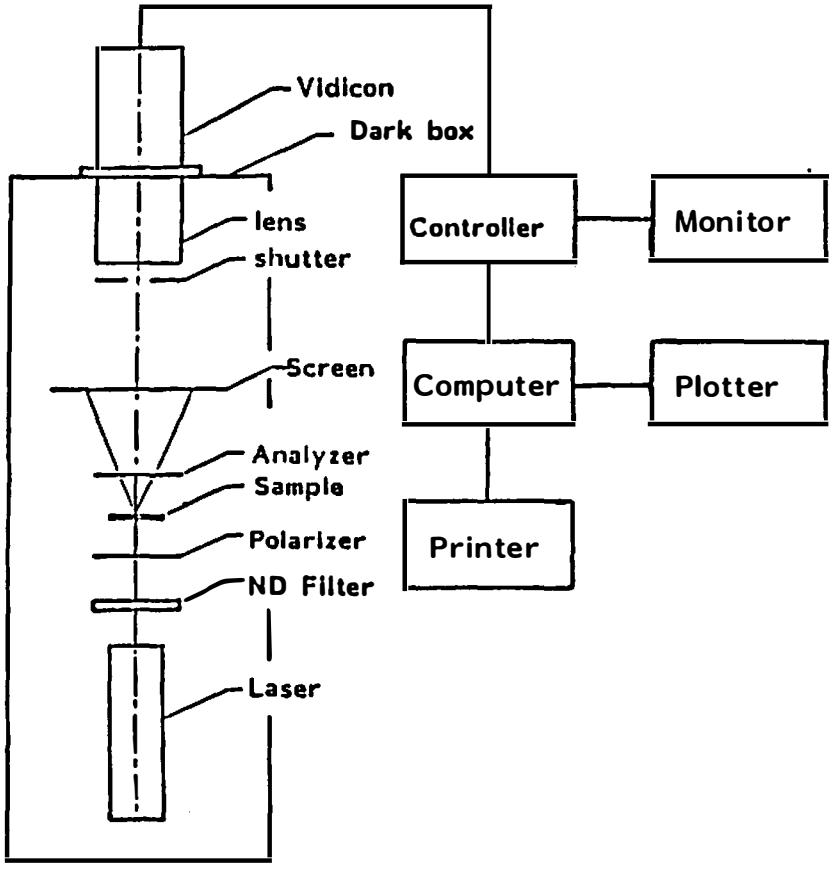

Figure IX-2. Diagram of small angle light scattering apparatus.

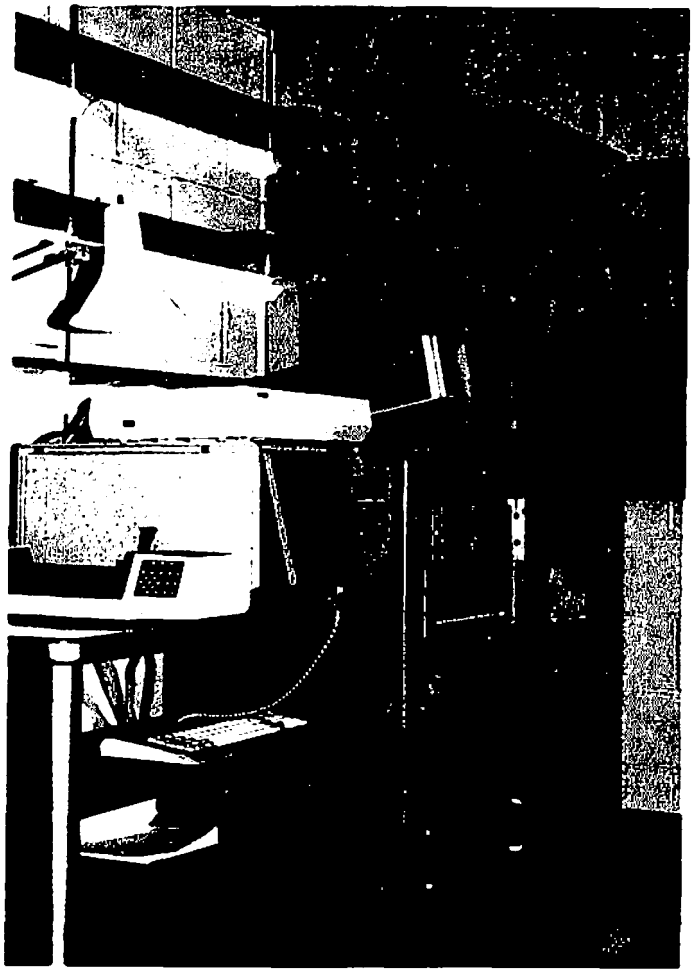

Figure IX-3. Photograph of small angle light scattering apparatus.

The procedure of the vidicon-computer method is as follows. The intensity of the incident beam from the laser light source was reduced with a neutral density filter to a proper intensity level, and polarized with a polarizer. This incident beam impinges on a film specimen of compound in the constant temperature sample chamber. The scattered light passes through the analyzer and projects an image on a screen. This is detected by the vidicon camera unit.

The iris of the camera lens is set to 5.6. The focus of the image was checked by a monitor. The sample-screen distance can vary from 15 cm to 45 cm. The polarizer and analyzer were usually set to a parallel (V_v) position.

The center beam stop was located at the center of the screen when the beam was too strong. The scattering angle 2 was determined by a diffraction grating (Oriel).

The detector was programmed to scan a narrow area including the center beam position. The number of scans for the scattered light image was programmed to 100. Intensities of scattered light were accumulated as a function of position. Five different film samples were examined and the intensity profiles were averaged. Background corrections were carried out.

Average scattered intensity profiles were stored in a floppy disk and used for further treatment. The Debye-Bueche and Guinier theories of scattering were employed to interpret the data. Programs for different theories of scattering and their graphical representations were developed. These include a linear least square curve fitting.

The various compounds which have been characterized by small angle light scattering (vidicon-computer method) are summarized in Tablex IX-1 and IX-2.

C. THEORETICAL BACKGROUND

The pertinent theoretical background of small angle scattering phenomenon is introduced in this section.

C.1. Reciprocal Phenomenon

The scattered intensity profile is governed by (D-4)

$$I(q) = I_e |F(\underset{\sim}{q})|^2 \tag{IX-1}$$

where I_e is the Thomson scattered intensity and the structural amplitude F(q) is

$$|F(\underset{\sim}{q})|^2 = \rho^2 \int_0^\infty \overline{V}(r) \frac{\sin qr}{qr} 4\pi r^2 \, dr \tag{IX-2}$$

or

$$|F(\underset{\sim}{q})|^2 = V \rho^2 \int_0^\infty \gamma(r) \frac{\sin qr}{qr} 4\pi r^2 \, dr \tag{IX-3}$$

where ρ is the electron density, V is volume of scatterer, and $\gamma(\underset{\sim}{r})$ is the correlation function.

Scattering intensity and scatterer size are related mathematically through Fourier inversion. The intensity varies inversely proportional to the characteristic size of the scatterer or the particle. If the size of particles gets larger, the scattering

Table IX-1. Compounds Used for Small Angle Light Scattering Experiment (Polystyrene Compounds)

Filler Type	Avg. Diameter dp (μm)	Volume Fraction ϕ(-)	Mixer	Mixing Temp. (°C)	Mixing Time (Minutes)
$CaCO_3$	17.	0.05	Mill	150°C	20
	3.0	0.05	Mill	150°C	20
	0.4	0.05	Mill	150°C	20
		0.10			
	0.07	0.05	Mill	150°C	20
Coated $CaCO_3$	5.0	0.05	Mill	150°C	20
	3.0	0.05	Mill	150°C	20
	0.5	0.05	Mill	150°C	20
		0.10			
	0.07	0.05	Mill	150°C	20
$CaCO_3$	0.4	0.04	IM	150°C	2
					20
	0.07	0.05	IM	150°C	3
					5
					10
Coated $CaCO_3$	0.5	0.05	IM	150°C	2
					20
	0.07	0.05	IM	150°C	1
					3
					5
					10

Table IX-2. Compounds Used for Small Angle Light Scattering Experiment (Polypropylene Compounds)

Filler Type	Avg. Diameter dp (μm)	Volume Fraction ϕ(-)	Mixer	Mixing Temp. (°C)	Mixing Time (Minutes)
$CaCO_3$	17.	0.05	Mill	175°C	20
	3.0	0.05	Mill	175°C	20
	0.4	0.05	Mill	175°C	20
	0.07	0.05	Mill	175°C	20
Coat. $CaCO_3$	5.0	0.05	Mill	175°C	20
	3.0	0.05	Mill	175°C	20
	0.5	0.05	Mill	175°C	20
	0.07	0.05	Mill	175°C	20
$CaCO_3$	0.4	0.05	IM	175°C	2
					20
	0.07	0.05	IM	175°C	1
					3
					4
Coat. $CaCO_3$	0.5	0.05	IM	175°C	2
					20
	0.07	0.05	IM	175°C	1
					3
					5
					10
$CaCO_3$	3	0.20	Prepared by Ferro		
		0.30			
		0.40			
Coat. $CaCO_3$	1	0.20			
		0.30			
		0.40			
Coat. $CaCO_3$	1.0	0.05			
		0.10			
Coat. $CaCO_3$	0.5	0.05			
		0.10			

intensity curve moves to smaller scattering angles. This is due to the fact that when the scatterer is large, the path difference becomes larger. Hence the intensity decays faster leading to the shift of the scattered intensity toward smaller scattering angle. A sharp decay of the scattered intensity suggests the existence of large scatterers.

C.2. Scattering Angle and Other Scales

We define the q angle as

$$q = \frac{4\pi}{\lambda} \cdot \sin\theta \qquad \text{(IX-4)}$$

where λ is the wavelength of light in air and 2θ is the scattering angle.

The simplest of scattering theories is that of diffraction by an organized array in lattice. This yields a series of discrete peaks governed by

$$n\lambda = 2d_{hkl} \sin\theta \qquad \text{(IX-5)}$$

where d_{hkl} is an interplanar spacing.

Another is the size of isolated domains. This can be estimated by the maxima of the scattered light intensity profile. When domains possess equal diameter and are isolated from each other (H-5),

$$(2\pi d_a/\lambda)\sin\theta = 5.765 \qquad \text{(IX-6)}$$

where d_a is a diameter of domain, that is, diameter of agglomerate

or ultimate particle and 2θ is the scattering angle at first order maxima. Equations (IX-4) and (IX-5) may be rewritten as

$$q = 2n\pi \frac{1}{d_{hkl}} \qquad \text{(IX-7)}$$

and

$$q = 2 \times 5.765/d_a \qquad \text{(IX-8)}$$

respectively.

The interplanar spacing d_{hkl} and domain size d_a are included in the figures of intensity profiles. These scales give us an idea what magnitude of spacing or domain size make major contributions to the intensity profile.

C.3. Guinier's Approximation

Guinier (G-4,G-5) obtained approximated expression of the scattered intensity profile from the consideration of the radius of gyration.

$$\begin{aligned} \frac{I_s(q)}{I_s(0)} &= 1 - \frac{q^2\langle r^2\rangle}{6} + \frac{q^4\langle r^4\rangle}{120} - \cdots \\ &\simeq 1 - \frac{q^2\langle r^2\rangle}{6} \\ &\simeq 1 - \frac{R_g^2 q^2}{3} \\ &\simeq K_1 e^{-R_g^2 q^2/3} \end{aligned} \qquad \text{(IX-9)}$$

where

$$R_g^2 = \frac{1}{2}\langle r^2 \rangle$$

$$= \frac{\int_0^\infty r^2 (r) 2\, r^2 dr}{2\int_0^\infty \gamma(r) 2\pi r^2 dr} \qquad \text{(IX-10)}$$

Here

R_g: radius of gyration of scatterer,

K_1: constant,

$\gamma(r)$: correlation function.

Equation (IX-9) is valid when $R_g q$ is small.

Equation (IX-9) leads to

$$\ln I_s(q) = \ln K_2 - \frac{G_g^2 q^2}{3} \qquad \text{(IX-11)}$$

where K_2 is a constant.

Expressions for the intensity profile may be obtained assuming the correlation function is of the Gaussian form (M-20).

$$\gamma(r) = e^{-r^2/a_2^2} \qquad \text{(IX-12)}$$

where a_2 is called correlation distance. This yields

$$\ln I_s(q) = \ln K_3 - \frac{a_2^2 q^2}{4} \qquad \text{(IX-13)}$$

The radius of gyration R_g and the correlation distance are related by

$$R_g = \left(\frac{3}{4}\right)^{1/2} a_2 \simeq 0.87\, a_2 \qquad \text{(IX-14)}$$

This relation can be obtained by substituting the Gaussian form correlation function (Eq. (IX-12) into Eq. (IX-10)).

We can determine the correlation distance a_2 and the radius of gyration R_g from the slope of the straight line in the ln $I_s(g)$ versus q^2 plot (Guinier plot) near zero angle. Deviations may occur at greater angles. The intensity profile in the Guinier plot is not straight. This is due to the existence of the smaller scatterers. The small q angle region where Guinier's approximated formula is satisfied may be called the Guinier region.

C.4. Debye-Bueche's Statistical Theory

Debye and Bueche (D-6) have investigated the inhomogeneity of Lucite by small angle light scattering. The fluctuation of the refractive index leads to the scattering of light.

They (D-6) proposed a correlation function of

$$\gamma(r) = e^{-r/a_1} \qquad \text{(IX-15)}$$

where a_1 is a correlation distance.

The physical meaning of the correlation function is that the probability of a point at a distance r in an arbitrary direction from a given point in the scatterer will itself also be in the scatterer.

Debye-Bueches correlation function (Eq. (IX-15)) may be derived from the presumption that the inhomogenous phases are of random shape and size (D-6).

They obtained the scattered intensity profile of the form

$$I_s(q) = K_4 \frac{a_1^3}{(1 + a_1^2 q^2)^2} \qquad \text{(IX-16)}$$

where K_4 is a constant. Debye-Bueche's formula (Eq. (IX-16)) was obtained without making restrictions on the magnitude of $q \cdot r$. Their formula is more general than the Guinier approximation (Eq. (IX-9)) in the sense it is not limited to small q but it is based on a random statistic.

Equation (IX-16) may be rewritten

$$I_s^{-1/2}(q) = K_s^{-1/2}(a_1^{-3/2} + a_1^{1/2} q^2) \qquad \text{(IX-17)}$$

The correlation distance a_1 may be obtained from an intercept and a slope of the straight line in the $I^{-1/2}(q)$ versus q^2 plot (Debye-Bueche plot).

Deviation from a straight line may be found in the small angle region. This is due to the existence of the scatterers of greater sizes.

The range of q angle where the intensity profile in the Debye-Bueche plot is well satisfied may be called the Debye-Bueche region.

We can obtain relation between Debye-Bueche type correlation distance a_1 and the radius of gyration R_g by substituting Eq. (IX-15) into Eq. (IX-10). We obtain

$$R_g = 6^{1/2} a_1 \qquad \text{(IX-18)}$$
$$\simeq 2.4\, a_1$$

C.5. Correlation Functions and Distances

Figures IX-4 and IX-5 show the characteristics of Debye-Bueche and Guinier type correlation functions. Both correlation functions decay rapidly at small correlation distances. When the matrix phase is homogeneous and the volume fraction of scatterers is low, the distance r corresponds to the size of the scatterer and the correlation function (r) corresponds to a distribution of the scatterers. Small correlation distances, hence, denote the presence of only small scatterers.

C.6. Radius of Gyration for a Group of Scatterers

Guinier and Debye-Bueche type correlation distances a_2 and a_1 were related to the radius of gyration R_g through Eq. (IX-14) and Eq. (IX-18), respectively.

In the system which contains scatterers of the various shapes and sizes, the experimentally determined radius of gyration R_g is an average value. We consider this problem here.

In the discussion of radius of gyration of a particle, Guinier (G-5) obtained

$$I_s(q) = I_e|F(0)|^2 \left(1 - \frac{q^2\langle r^2\rangle}{6} + \frac{q^4\langle r^4\rangle}{120} - \ldots\right) \qquad \text{(IX-19)}$$

where

$$|F(0)|^2 = n^2 \qquad \text{(IX-20)}$$

and

$$\langle r^2\rangle = 2\,R_g^2 \qquad \text{(IX-21)}$$

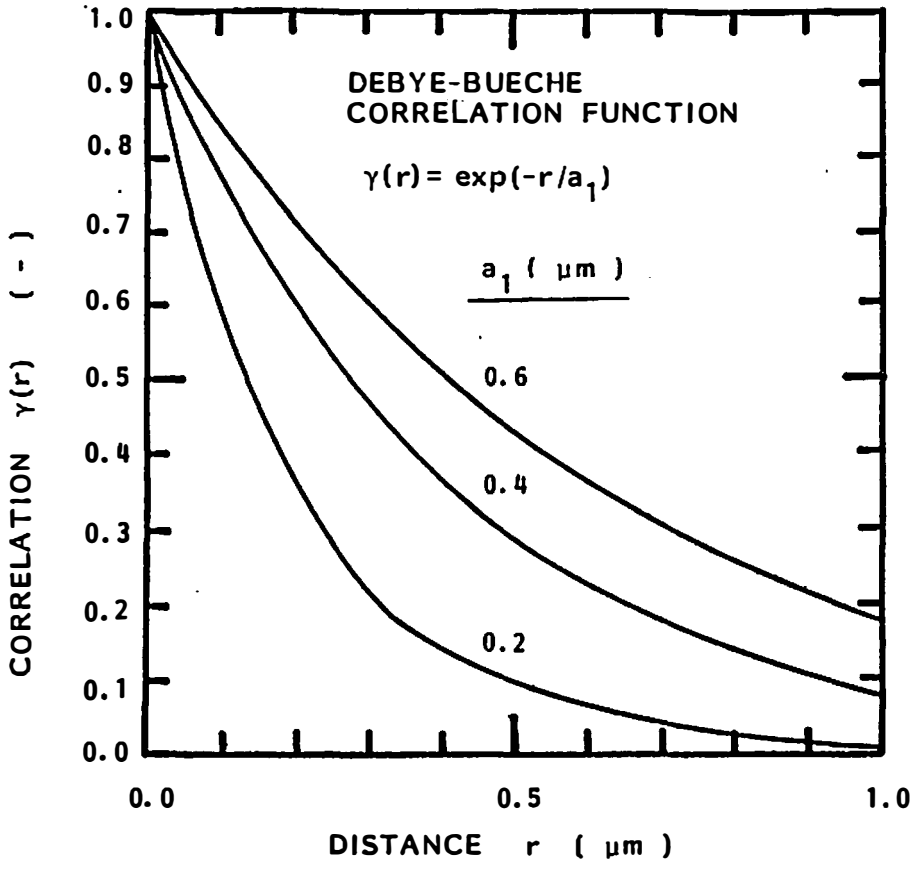

Figure IX-4. Debye-Bueche correlation function for various correlation distances, a_1.

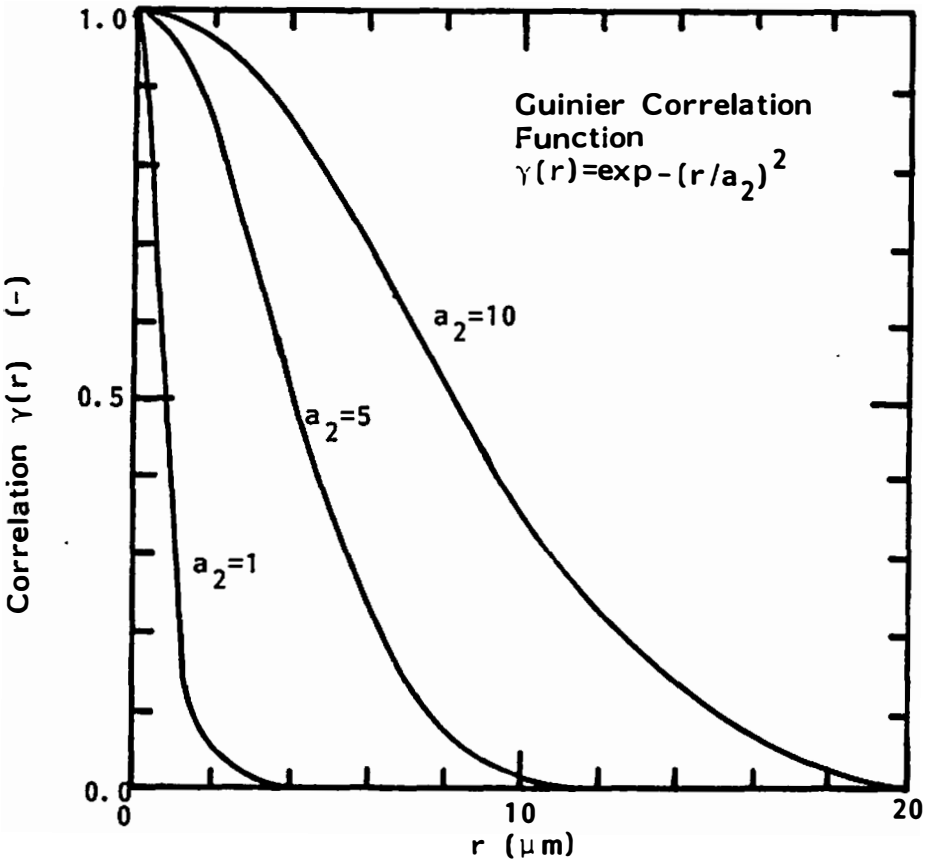

Figure IX-5. Guinier correlation function for various correlation distance a_2.

Here

I_e: Thomson scattered intensity,

R_g: radius of gyration of a particle,

n: number of electrons in a particle.

We may rewrite this for a group of the scatterers:

$$\overline{I_s(q)} = I_e \sum_i P_i n^2 \left(1 - \frac{q^2 R_{g,i}^2}{3} + \ldots\right) \qquad \text{(IX-22)}$$

where i denotes the type of the scatterer, P_i the probability of the type i scatterers, n_i the number of electrons in the type i scatterer, and $R_{g,i}$ is the radius of gyration of type i scatterer. Equation (IX-22) leads to

$$\overline{I_s(q)} = I_e\left(\sum_i P_i n_i^2\right)\left(1 - \frac{q^2}{3}\frac{\sum_i P_i n_i^2 R_{g,i}^2}{\sum_i P_i n_i^2} + \ldots\right) \qquad \text{(IX-23)}$$

Comparing this with Eq. (IX-22) we obtain the characteristic radius of gyration for a group of scatterers.

$$\overline{R_g^2} = \frac{\sum_i P_i n_i^2 R_{g,i}^2}{\sum_i P_i n_i^2} \qquad \text{(IX-24)}$$

We note

$$n_i^2 \propto V_i^2 \propto R_{g,i}^6 \qquad \text{(IX-25)}$$

where V_i denotes the volume of type i scatterer. Equation (IX-24) is then

$$\overline{R_g^2} = \frac{\sum_i P_i R_{g,i}^8}{\sum_i P_i R_{g,i}^6} \qquad \text{(IX-26)}$$

changing into the integration form.

$$\overline{R_g^2} = \frac{\int P(R_g)\, R_g^8\, dR_g}{\int P(R_g)\, R_g^6\, dR_g} \qquad \text{(IX-27)}$$

where $P(R_g)$ is a probability density function.

When the scatterers are spherical, the characteristic diameter of spheres is

$$\overline{d} = 2\left(\frac{5}{3}\right)^{1/2} \overline{R}_g \qquad \text{(IX-28)}$$

C.7. Guinier and Debye-Bueche Regions

Rayleigh (R-3), in 1914, proposed a formula for the scattered intensity profile from a sphere of radius R.

$$I_s(q) = I_e \left(\frac{4\pi}{3}\right)^2 R^6\, \Phi \qquad \text{(IX-29)}$$

where

$$\Phi = \left\{\frac{1}{(qR)^3} (\sin qR - qR \cdot \cos qR)\right\}^2 \qquad \text{(IX-30)}$$

Guinier (G-4,G-5), in the derivation of his approximated formula, assumed $qR < 1$. Under this condition

$$\sin qR \simeq qR - \frac{q^3 R^3}{6} \qquad \text{(IX-31)}$$

and

$$\cos qR \simeq 1 - \frac{q^2 R^2}{2} \qquad \text{(IX-32)}$$

Then Eq. (IX-29) reduces

$$I_s(q) = I_e \rho(\frac{4\pi}{3})^2 R^6 \frac{1}{a} \qquad \text{(IX-33)}$$

The scattered intensity is proportional to R^6 at small angle region (z-average). The important conclusion is that the spheres of large radius R strongly contribute the intensity profile in the Guinier region, when the spheres have distribution in size.

We now consider the Debye-Bueche region. Debye and Bueche (D-6) made no restriction in the angle q when they derived the scattered intensity profile.

At greater qR values the function oscillates. Equation (IX-29) becomes

$$I_s(q) = I_e \rho(\frac{4\pi}{3})^2 \frac{1}{q^6} (\sin qR - qR \cos qR)^2 \qquad \text{(IX-34)}$$

In this region, the contributions from the large scatterer are relatively weak compared with Eq. (IX-33) for the Guinier region.

When the scatterer has the distribution in size, Guinier region at small angle measures the scattered light from the larger scatterer preferably. At larger angles this is no longer the case.

D. PHOTOGRAPHIC METHOD

D.1. Polystyrene Compounds

D.1.a. Results. Typical scattered light intensity profiles of polystyrene compounds are presented in this section. All compounds

described in this section were prepared on a two roll mixing mill. The mixing temperature was 150°C and mixing period is 20 minutes for all compounds.

Polarizer and analyzer were set to V_v position (parallel). The center beam stop was not used in the photographic method.

Figures IX-6 and IX-7 present the scattered light intensities of uncoated and stearic acid coated calcium carbonate compounds, respectively. The volume loading level is 0.05 for both cases. The nominal ultimate particle size varies from 17 μm to 0.07 μm for uncoated calcium carbonates and 5 μm to 0.07 μm for coated calcium carbonates.

All compounds possess a maximum intensity near the center (center is the position of the laser beam), and the intensity decreases as the scattering angle 2θ increases. The intensity of scattered light is independent of the azimuthal angle μ. The scattered light intensity and intensity profile along the scattering angle is dependent upon the compounds.

The smallest particulates (dp = 0.07 μm), both uncoated and coated, show the lowest scattered intensity. The largest calcium carbonate (dp = 17 μm) and the smallest (dp = 0.07 μm) present the sharpest decay of the scattered light intensity along the scattering angle.

D.1.b. Discussion. The characteristics of the scattered light intensity profile reflect the morphological or the structural features of the particulates and their agglomerates in the specimen.

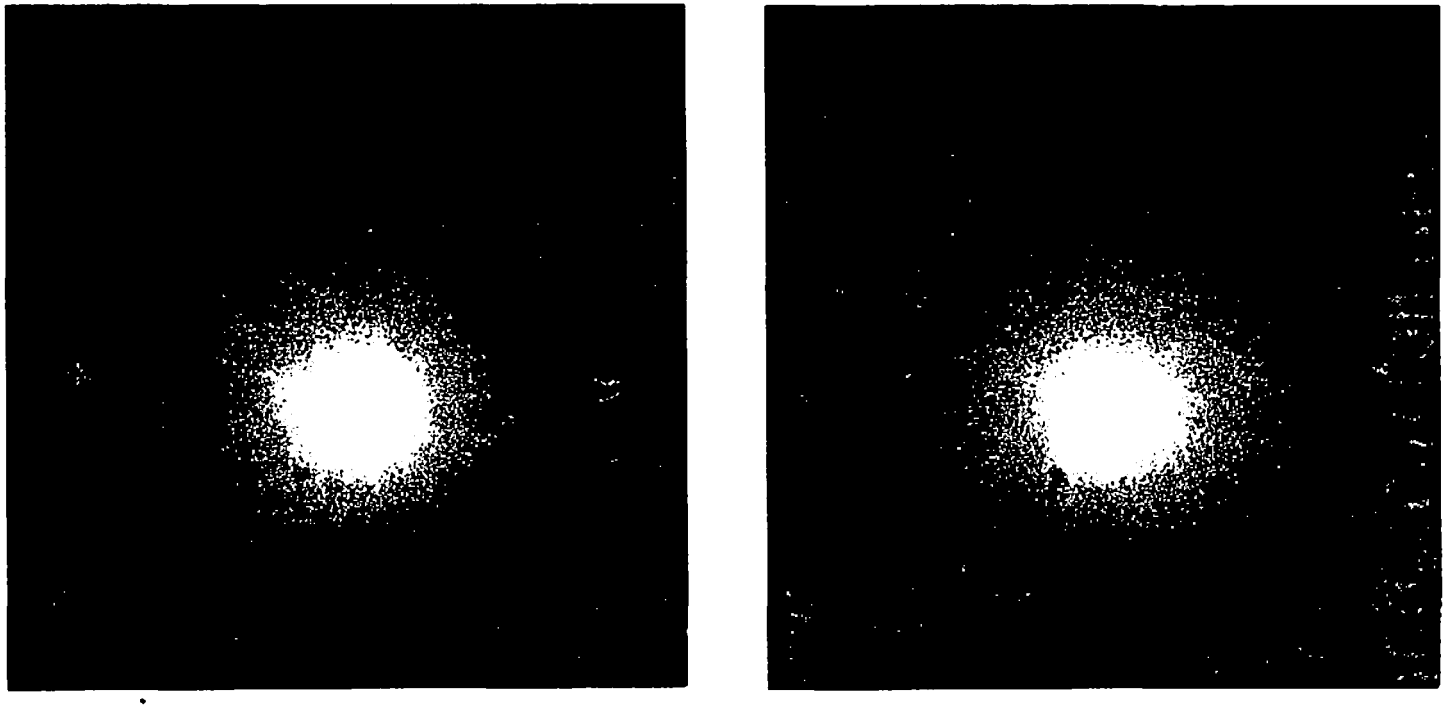

(a) 17 μm (b) 3 μm

Figure IX-6. SALS patterns from PS/unc. $CaCO_3$ compounds (ϕ = 0.05): V_v, NDF = 1.0, 0.5 sec., sample-film = 13 cm.

(c) 0.4 μm

(d) 0.07 μm

Figure IX-6 (continued)

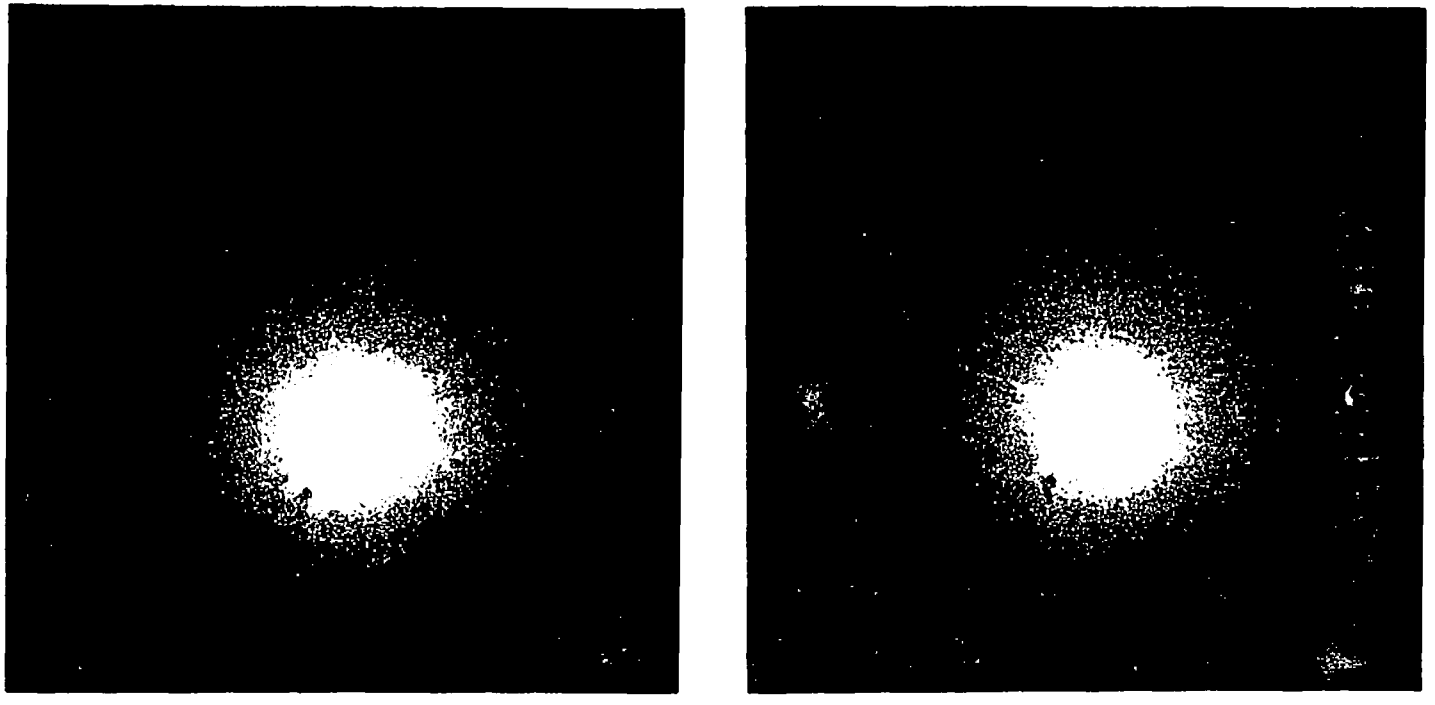

(a) 5 μm (b) 3 μm

Figure IX-7. SALS patterns from PS/coat. $CaCO_3$ compounds (ϕ = 0.05): V_v, NDF = 1.0, 0.5 sec., sample-film = 13 cm.

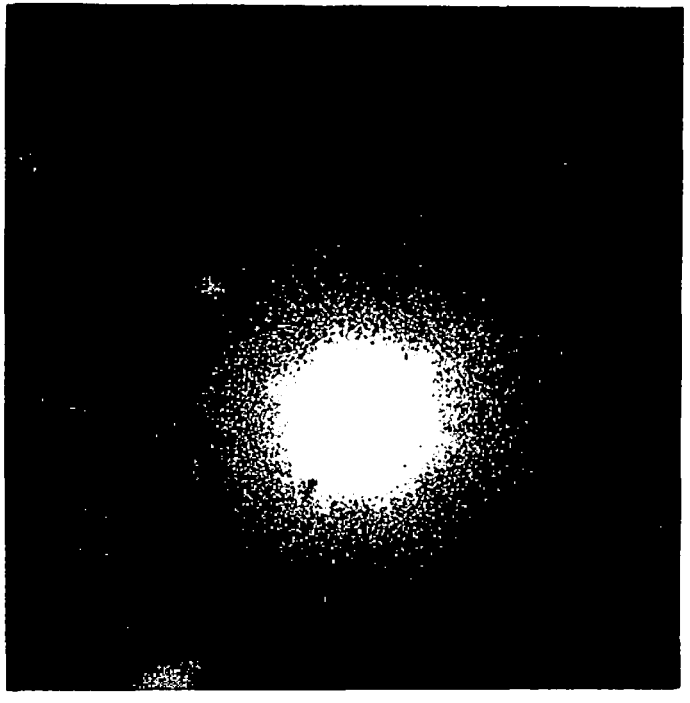

(c) 0.5 μm

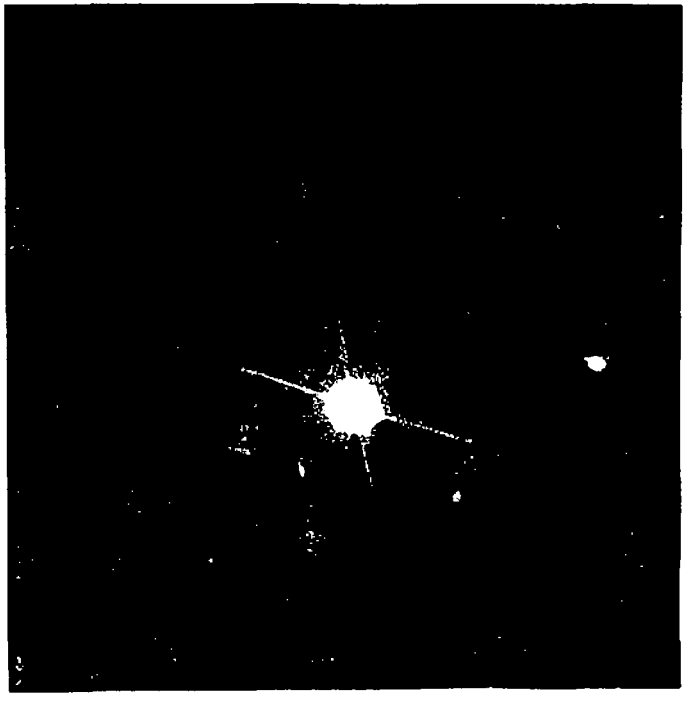

(d) 0.07 μm

Figure IX-7 (continued)

The continuous decay of the scattered light along the scattering angle suggests that the size of scatterer (most likely the ultimate particles or the agglomerates) has a distribution and are not a monodispersed. The distribution of the original particles is not sharp and the occurrence of agglomerates broadens the distribution. Thus sharp peaks should not be expected.

The scattered light intensity is independent of azimuthal angle . This suggests that the shape of the scatterer is isotropic, and any anisotropic structure randomly oriented. Calcium carbonate particulates possess rhombic shapes. Electron micrographs of calcium carbonate compounds in Chapter VIII show random orientations of particulates. Another form of scatterer is the agglomerate. The optical micrographs of the agglomerates in Chapter VII show that the shape of the agglomerates is irregular but may be roughly regarded as spherical.

Intensity and intensity profile of the scattered light reflect the amount of the scatterer and the size distribution of the scatterer, respectively. The lowest intensity is for the smallest calcium carbonate (dp = 0.07 m).

D.2. Polypropylene Compounds

D.2.a. Results. Figure IX-8 shows the H_v pattern and V_v pattern of the unfilled polypropylene film obtained at room temperature. Polypropylene film was quenched in water after compression

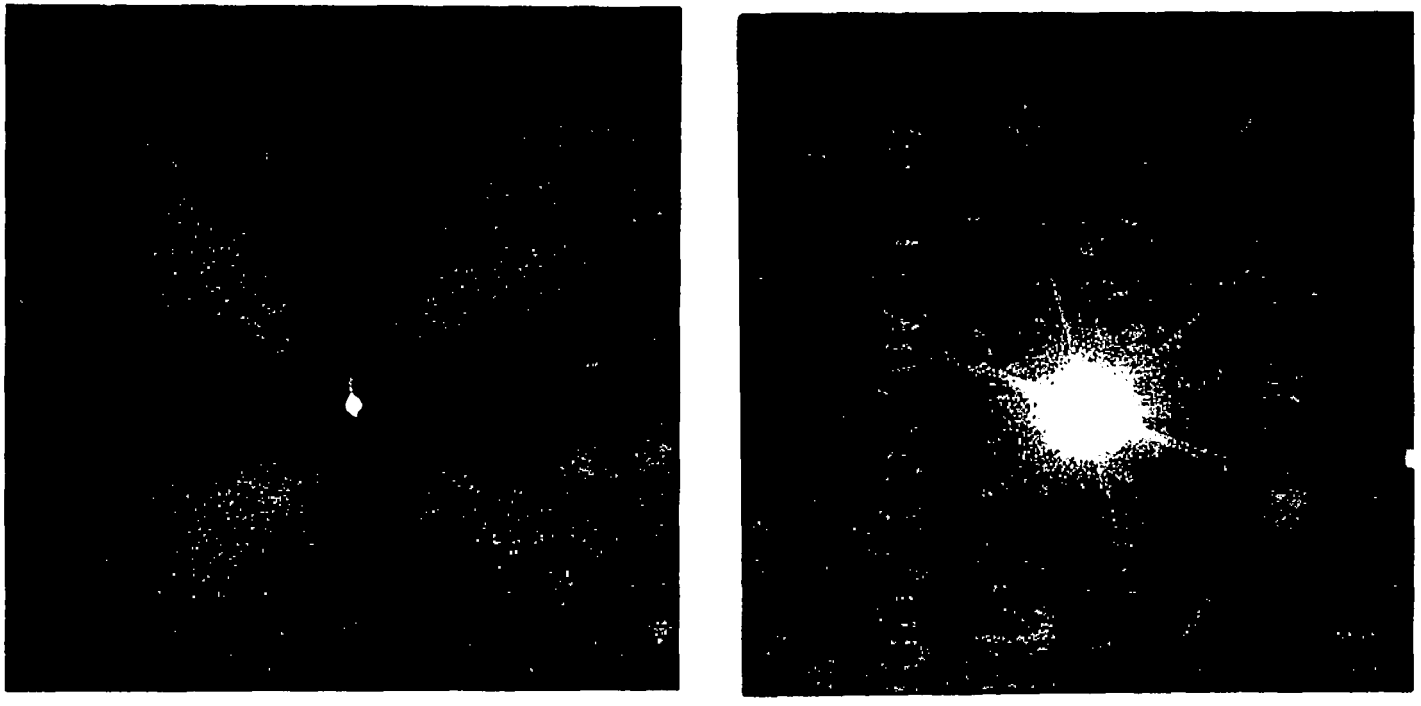

(a) H_v, NDF=0.0, 2sec. (b) V_v, NDF=1.0, 2sec.

Figure IX-8. SALS patterns from unfilled PP: sample-film = 13 cm.

molding. It is clear that the polypropylene film contains a crystalline spherulite phase.

Figures IX-9 through IX-12 represent scattered light intensity profiles for various polypropylene compounds. These include uncoated and coated calcium carbonate, talc and mica compounds. Intensity profiles in Figures IX-9 and IX-10 present H_v and V_v patterns, respectively. These were obtained at room temperature. Intensity profiles in Figures IX-11 and IX-12 were obtained at the elevated temperatures of 185°C with H_v and V_v position, respectively.

It should be noted that the H_v patterns obtained at room temperature (Figure IX-9) seem to be the superposition of two types of intensity patterns. One is the four petal pattern resulting from spherulites of matrix phase or cross (X) pattern from a sheaf structure which is a premature state of spherulite. The other pattern which possesses a maxima at the center is due to the filler particulates. Scattering from the spherulites is dependent upon the azimuthal angle. Scattering from the particulates is independent of the azimuthal angle.

The existence of two types of scattered intensity patterns is less clear in the V_v position (Figure IX-10). We must, however, expect the V_v patterns also result from two distinguishable scatterers, the crystalline phase of polypropylene and filler particulates.

The scattering of light from the crystalline phase of the polypropylene matrix must be eliminated to characterize the dispersion

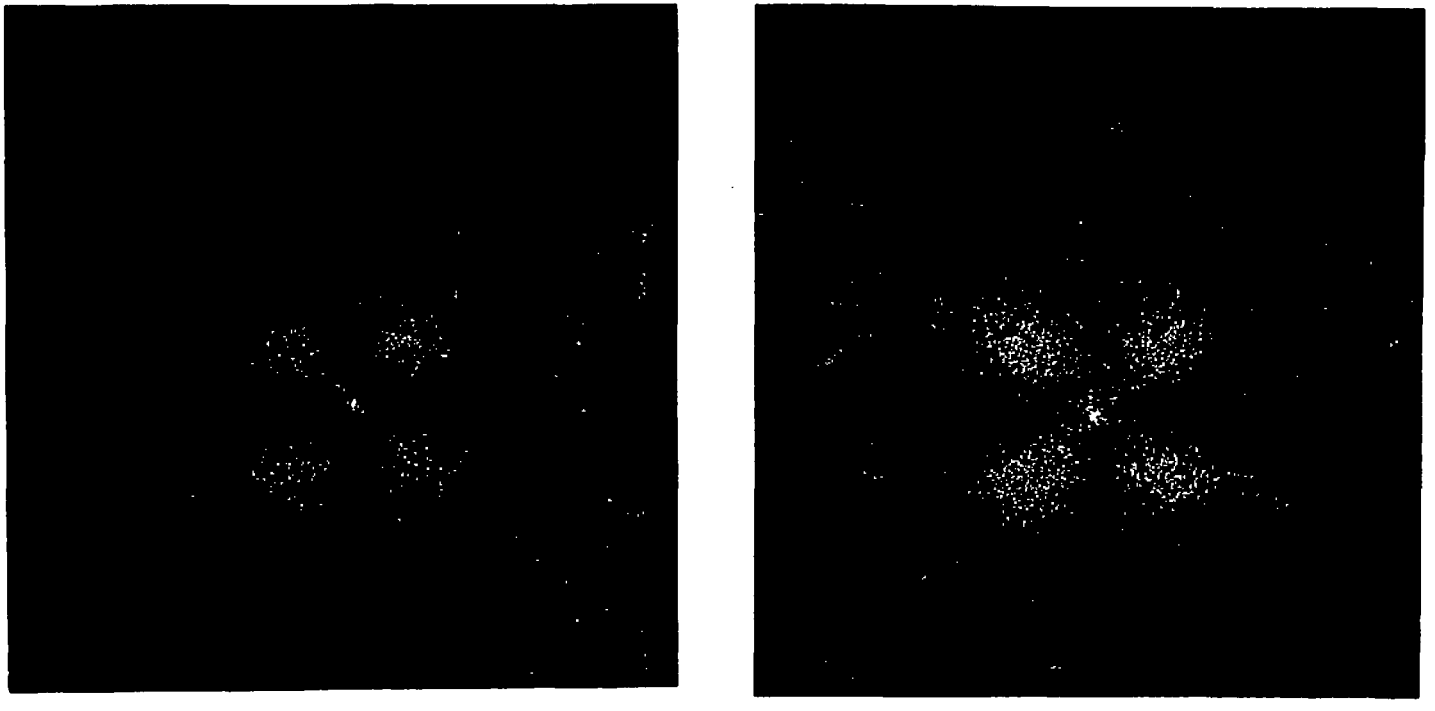

(a) PP/Unc.$CaCO_3$ dp=0.07μm (b) PP/Coat.$CaCO_3$ dp=0.07μm

Figure IX-9. SALS patterns from various PP compounds (ϕ = 0.05): H_v, NDF = 0.0, 2 sec., sample-film = 13 cm.

(c) PP/Mica

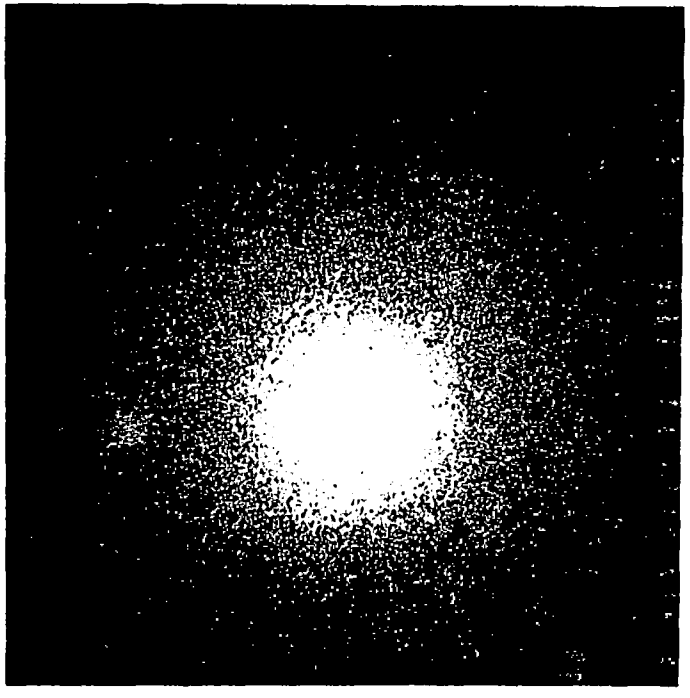

(d) PP/Talc

Figure IX-9 (continued)

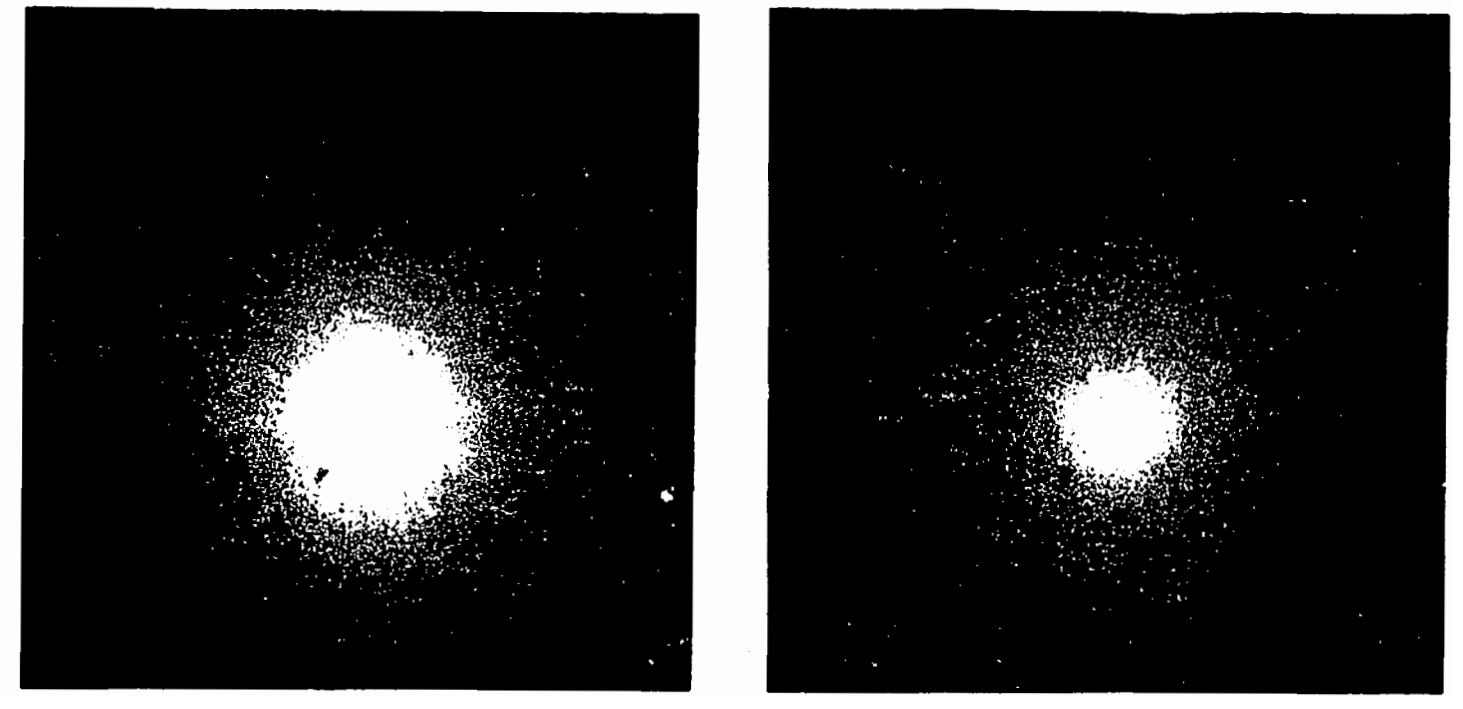

(a) PP/Unc.$CaCO_3$ (b) PP/Coat.$CaCO_3$

Figure IX-10. SALS patterns from various PP compounds (ϕ = 0.05): V_v, NDF = 1.0, 2 sec., sample-film = 13 cm.

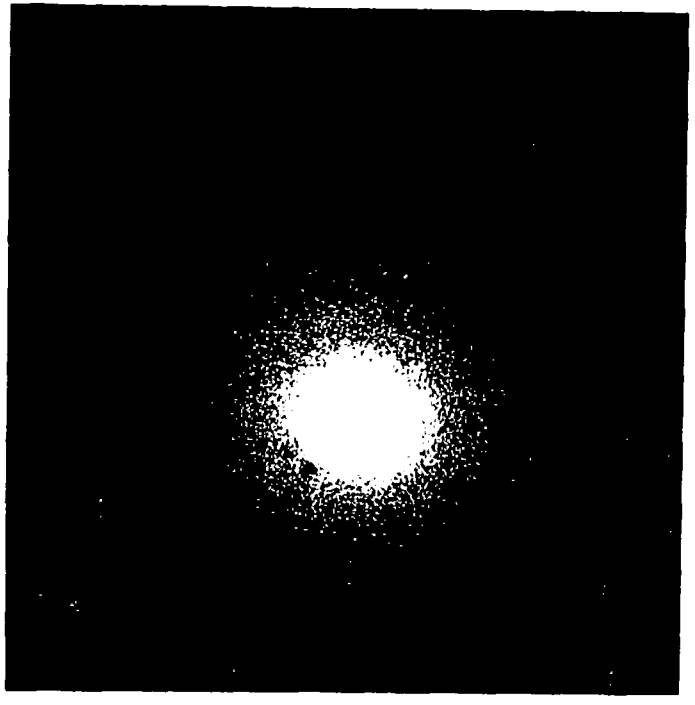

(c) PP/Mica

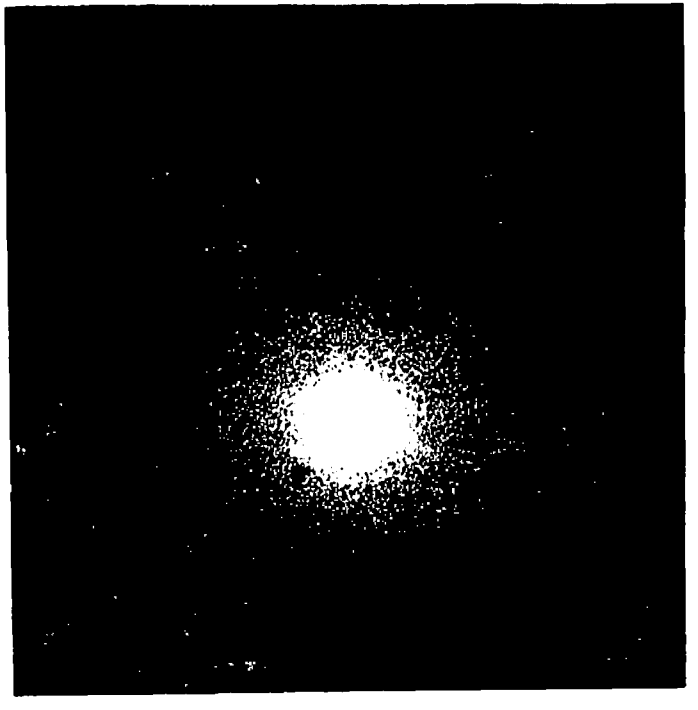

(d) PP/Talc

Figure IX-10 (continued)

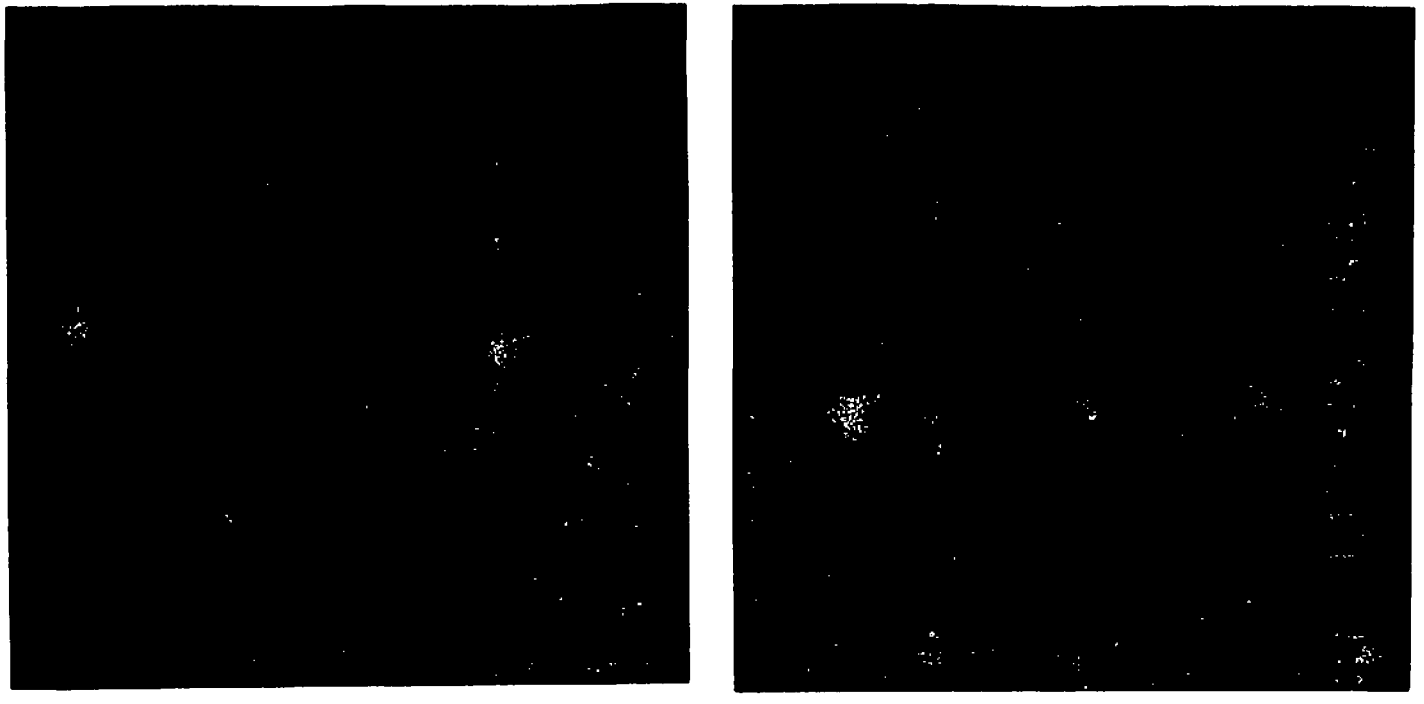

(a) PP/Unc.$CaCO_3$ dp=0.07μm (b) PP/Coat.$CaCO_3$ dp=0.07μm

Figure IX-11. SALS patterns from various PP compounds (ϕ = 0.05) at 185°C: H_v, NDF = 0.0, 2 sec., sample-film = 13 cm.

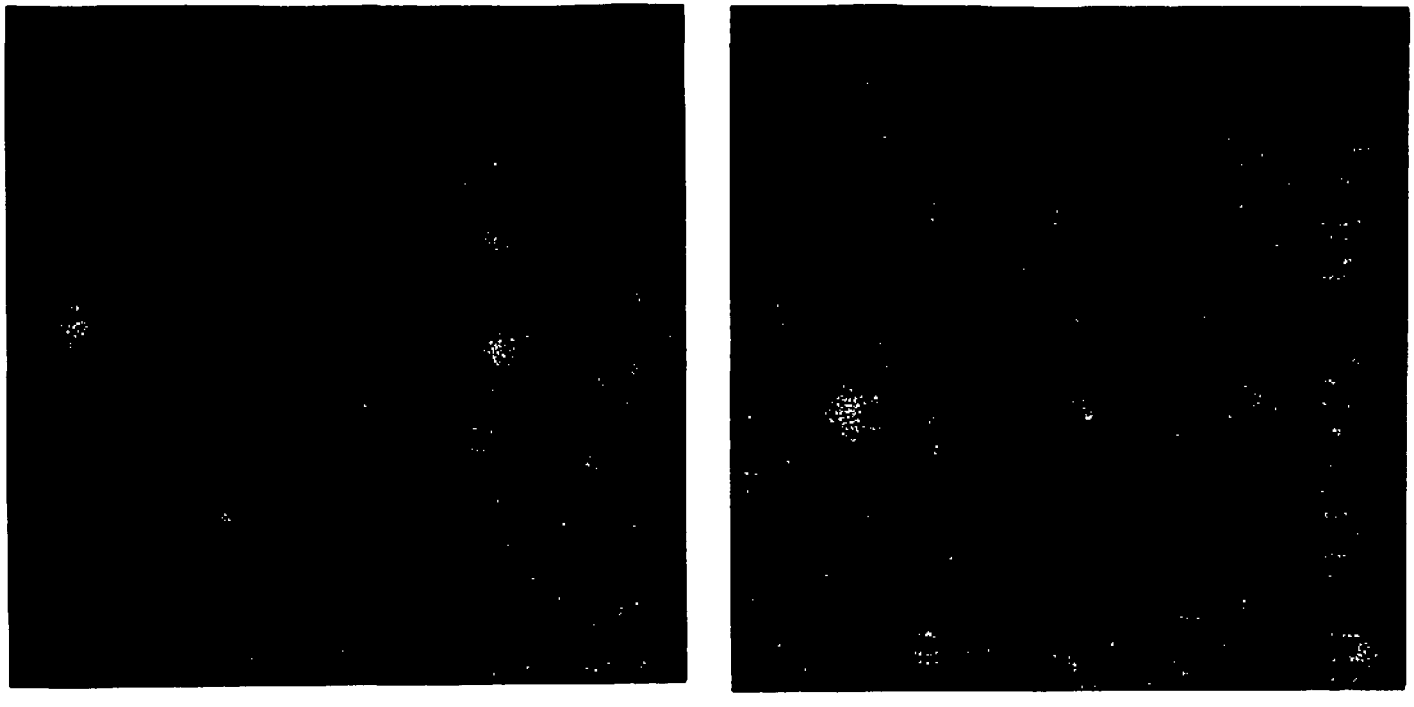

(a) PP/Unc.$CaCO_3$ dp=0.07μm (b) PP/Coat.$CaCO_3$ dp=0.07μm

Figure IX-11. SALS patterns from various PP compounds (ϕ = 0.05) at 185°C: H_v, NDF = 0.0, 2 sec., sample-film = 13 cm.

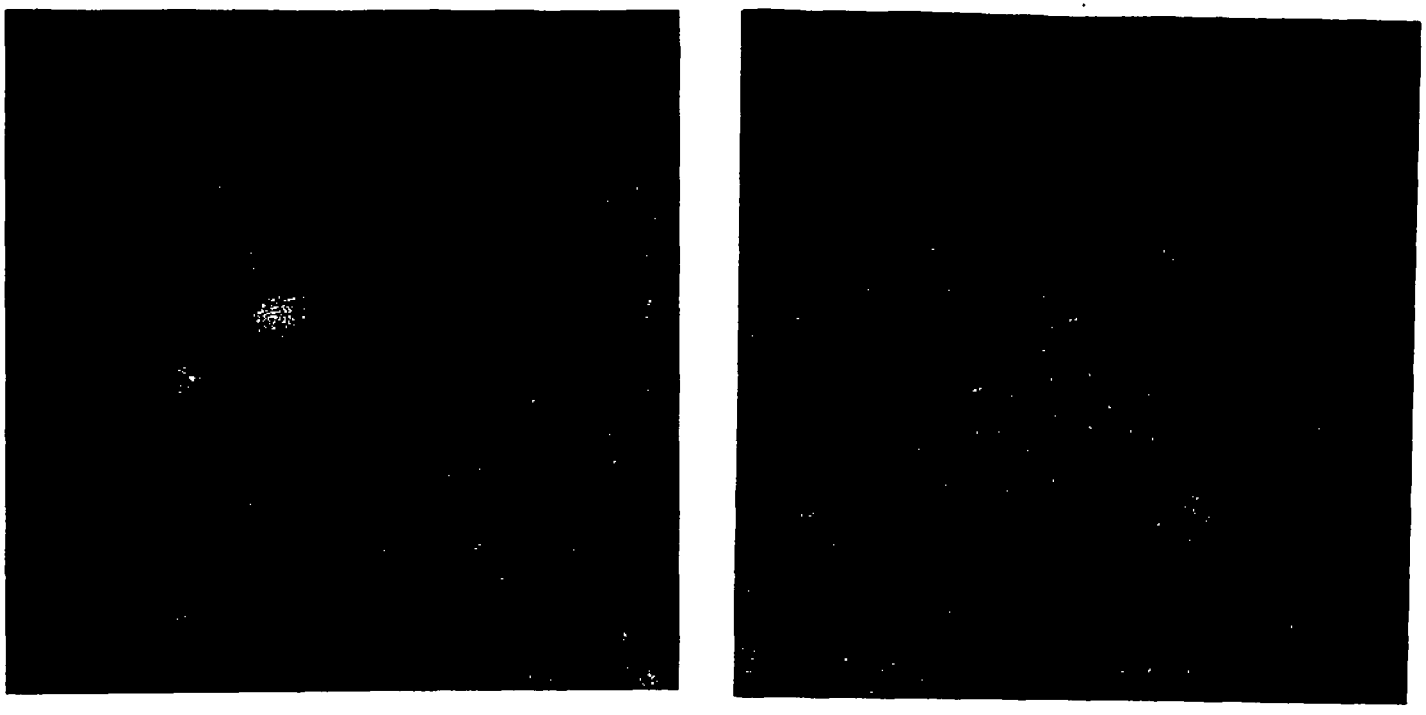

(a) PP/Mica

(b) PP/Talc

Figure IX-11 (continued)

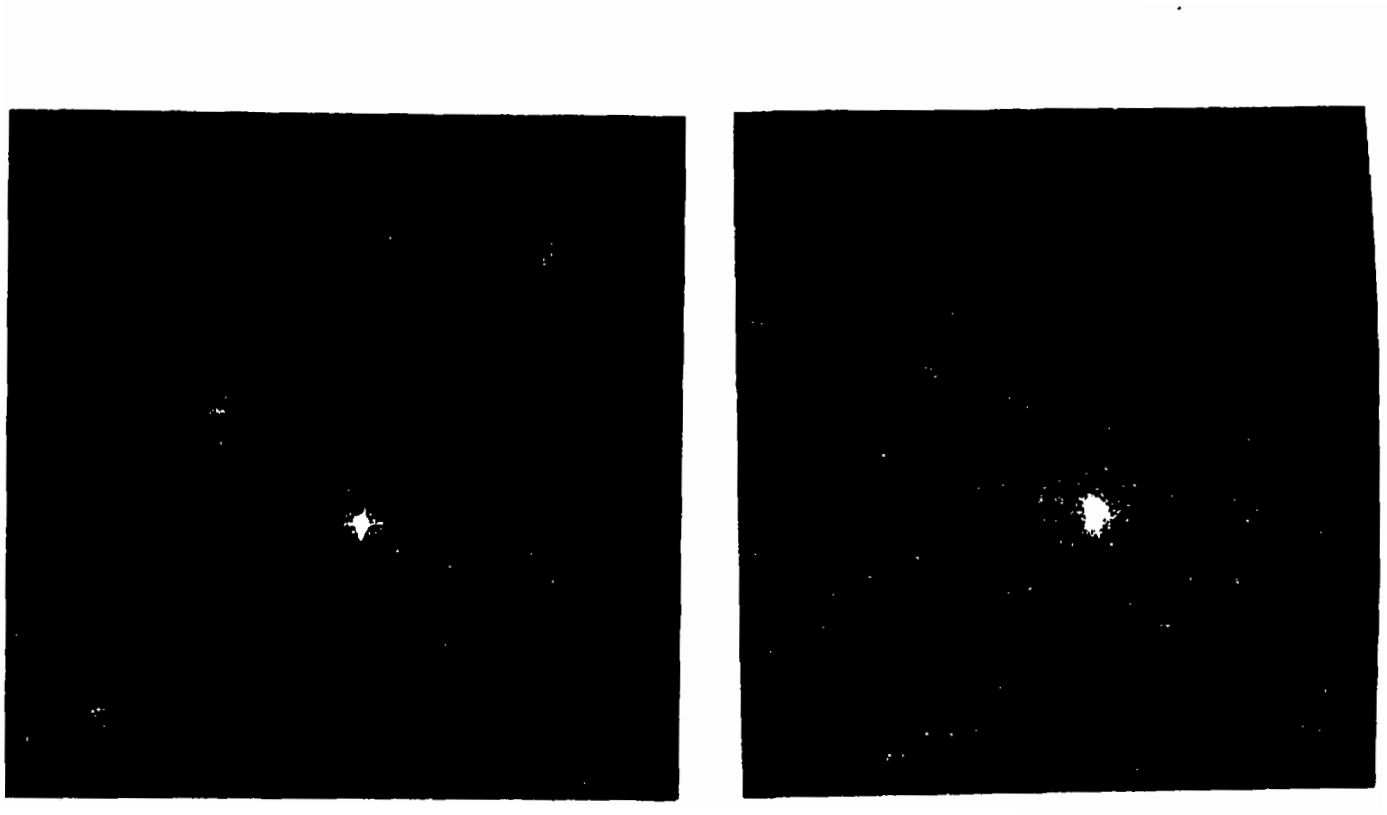

(a) PP/Unc.$CaCO_3$ dp=0.07μm (b) PP/Coat.$CaCO_3$ dp=0.07μm

Figure IX-12. SALS patterns from various PP compounds (ϕ = 0.05) at 185°C: V_V, NDF = 1.0, 2 sec., sample-film = 13 cm.

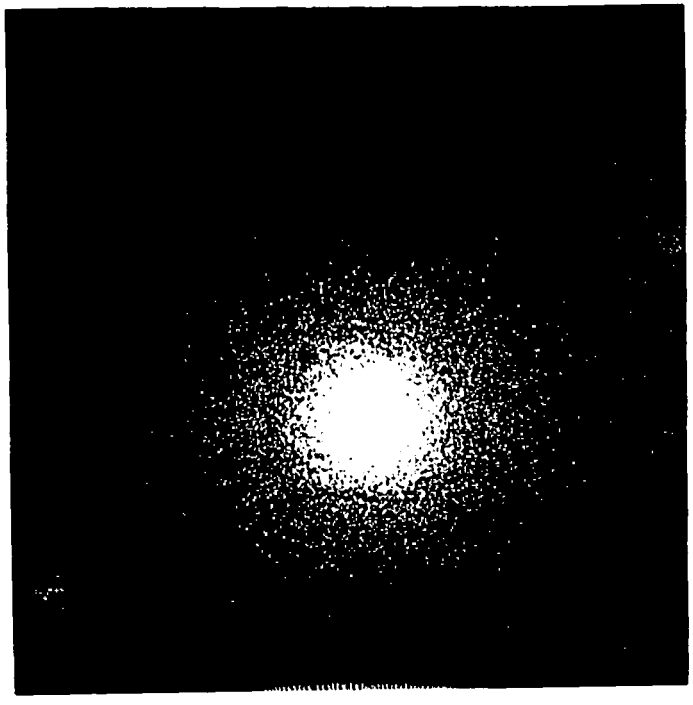

(c) PP/Mica

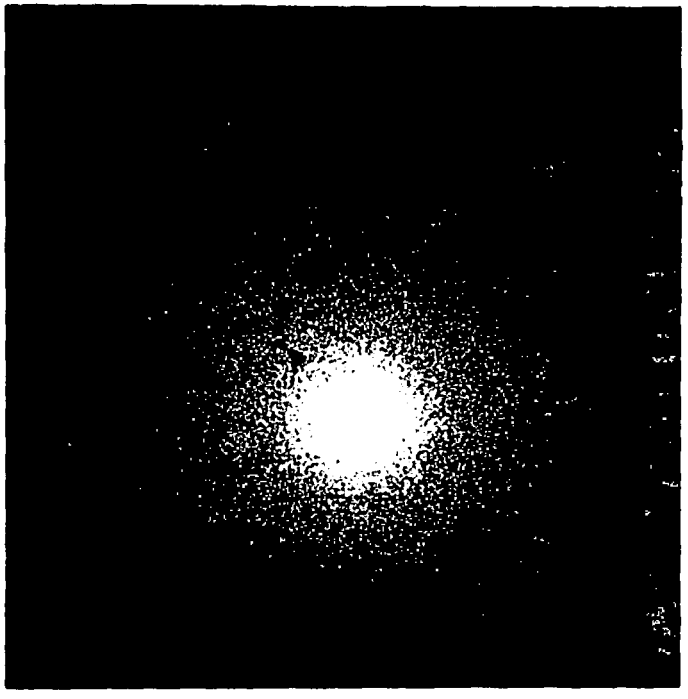

(b) PP/Talc

Figure IX-12 (continued)

f filler particulates. The temperature of the film specimen was elevated to 185°C to melt the polypropylene.

Both H_v and V_v intensity patterns at 185°C given in Figures IX-11 and IX-12 do not show the existence of the spherulite structure. These originate in the filler particulates and their agglomerates alone. The characteristics of the scattered light intensity profiles at the elevated temperature are the same as the polystyrene compounds.

D.2.b. Discussion. Application of small angle light scattering techniques for crystalline polymer compounds requires the use of elevated temperature above the melting temperature of matrix polymer. The intensity of the scattered light, as a result, drastically decreases.

The type of crystalline shape (spherulite or sheaf) is not clear because of the strong intensity near the center of the beam position due to the particulates.

Other characteristics of scattered intensity profiles are quite similar to polystyrene compounds.

E. QUANTITATIVE METHOD (VIDICON-COMPUTER METHOD)

A small angle light scattering apparatus with a two-dimensional position sensitive detector has been used to obtain quantitative data. The apparatus was explained in detail in Section B, Experimental Procedure.

E.1. Polystyrene Compounds

E.1.a. Results. Figures IX-13 and IX-14 represent the relative intensity profiles of polystyrene compounds. These are plotted as a function of q angle. Two other scales, interplanar spacing d_{hkl} and domain size d_a, defined in Eqs. (IX-2) and (IX-3), respectively, were included. These scales give us an idea what magnitude of spacing and domain size which make major contributions to the intensity profile.

Figure IX-13 shows the relative intensity profiles of uncoated calcium carbonate filled polystyrene compounds of volume fraction 0.05. Nominal particle sizes are indicated in the figure. These were prepared in a two roll mixing mill. Particulates having a nominal size of 3 μm exhibit the slowest decay of intensity with q angle. Seventeen μm particulates whow a sharper decay. This indicates the existence of large particulates. We may expect that the decay of scattered light intensity is slower as the size of the scatterer decreases. The relative intensities of the smaller particulates (dp = 0.4 μm and 0.07 μm) decays, however, more rapidly than those of the larger particles. The smallest particulates (dp = 0.07 μm) show the most abrupt decay. This suggests the existence of large scatterers. Optical microscopy (Chapter VII) and electron microscopy (Chapter VIII) of polystyrene compounds indicate the existence of such agglomerates when the particle size is smaller than 1 μm. It is reasonable to regard the more abrupt

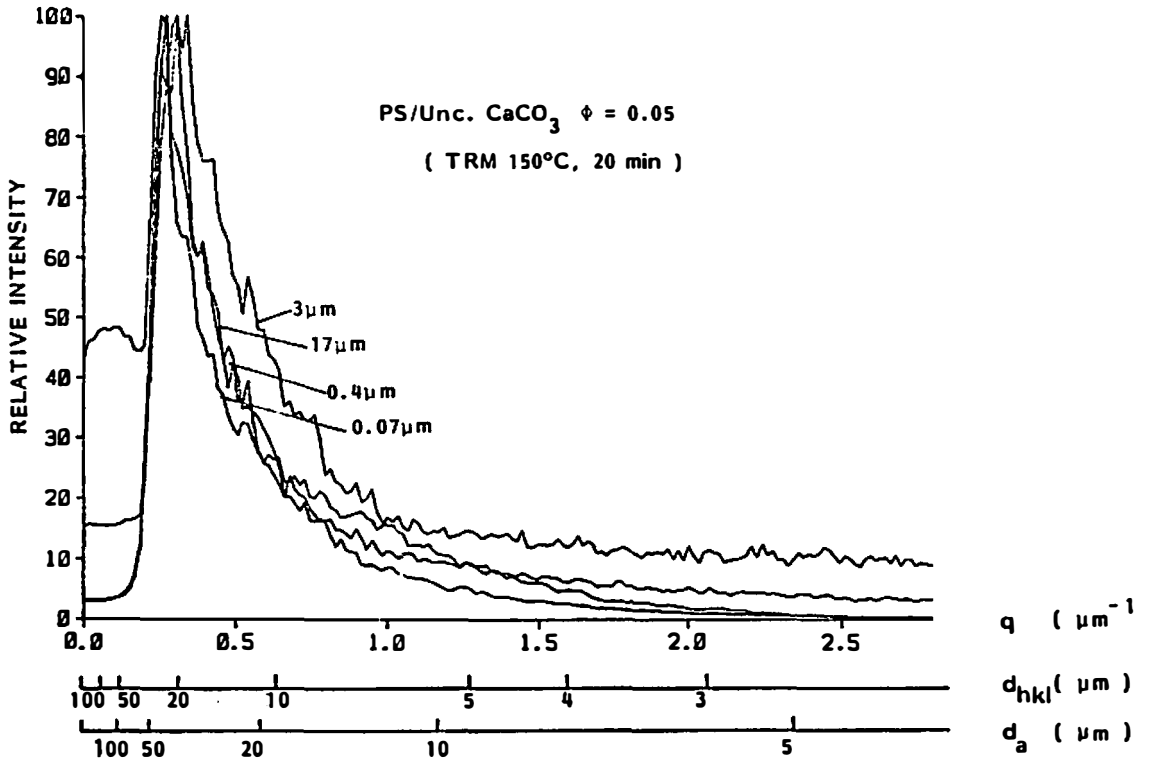

Figure IX-13. Relative intensity profiles of PS/unc. $CaCO_3$ (dp = various, ϕ = 0.05).

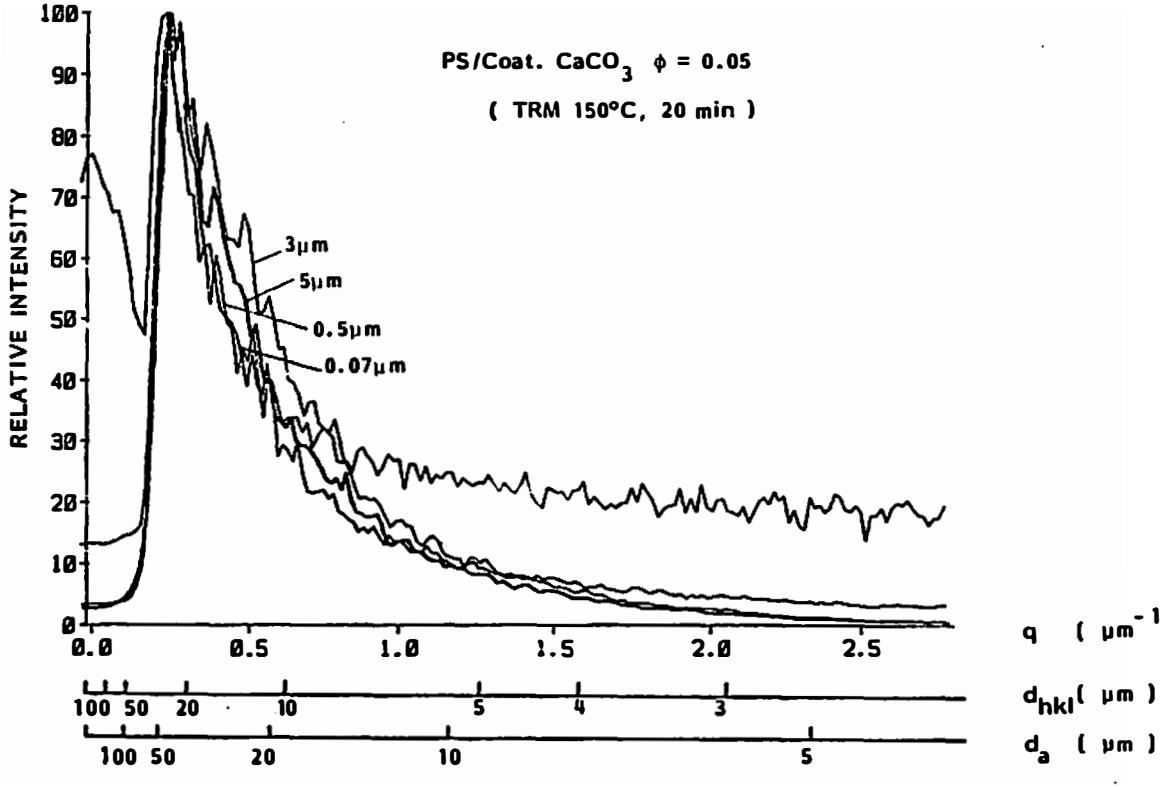

Figure IX-14. Relative intensity profiles for PS/coat. $CaCO_3$ (dp = various, ϕ = 0.05).

decay of intensity profiles for small particulates (dp = 0.4 μm and 0.07 μm) is due to the agglomerates.

The relative intensity profiles of stearic acid calcium carbonate compounds (Figure IX-14) are very similar to the cases of uncoated calcium carbonate compounds. The compounds which contain particulates smaller than 1 μm show an abrupt decay of their intensity profile. Agglomerates have been confirmed for those compounds using optical and electron microscopes.

Figures IX-15 and IX-16 show the behavior of relative intensities for the same series of compounds. The maximum intensities of the 17 m calcium carbonate compounds near zero angle (q = 0) were taken as 100 in constructing the plots. Intensity profiles of other compounds were compared. The scattered intensity drastically decreases with decreasing particle size. This may suggest the number of large scatterers are fewer in the compounds containing the small particulates. In large particulate compounds, the ultimate particles are the large scatterers. The number of large scatterers (ultimate particles) in the compounds of large particulates can be much greater than the number of large scatters (agglomerates) in small particulate compounds.

The effect of the volume fraction of particulates is shown in Figures IX-17 and IX-18 for uncoated and coated calcium carbonate compounds, respectively. Volume fractions of 0.05 and 0.10 are compared. The decay of relative intensity profiles at the higher loading is slightly slower than in the lower loading compound. This may be

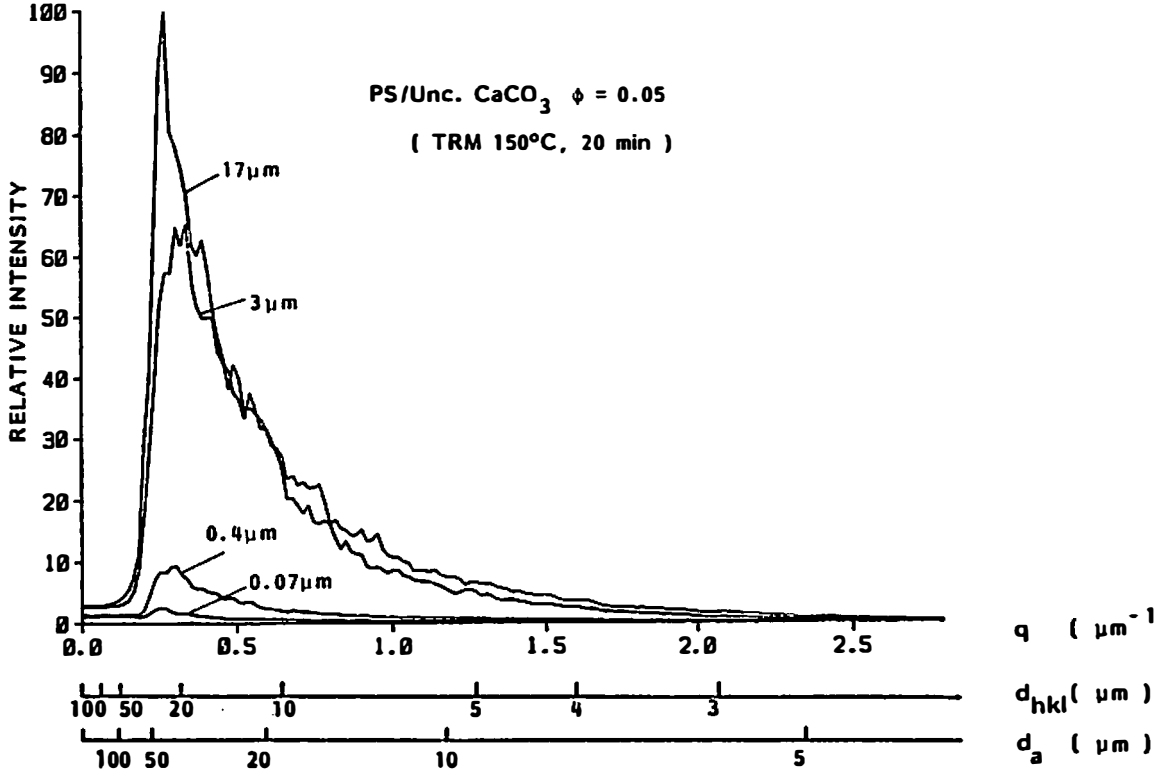

Figure IX-15. Comparison of relative intensity profiles for PS/unc. $CaCO_3$ (dp = various, ϕ = 0.05).

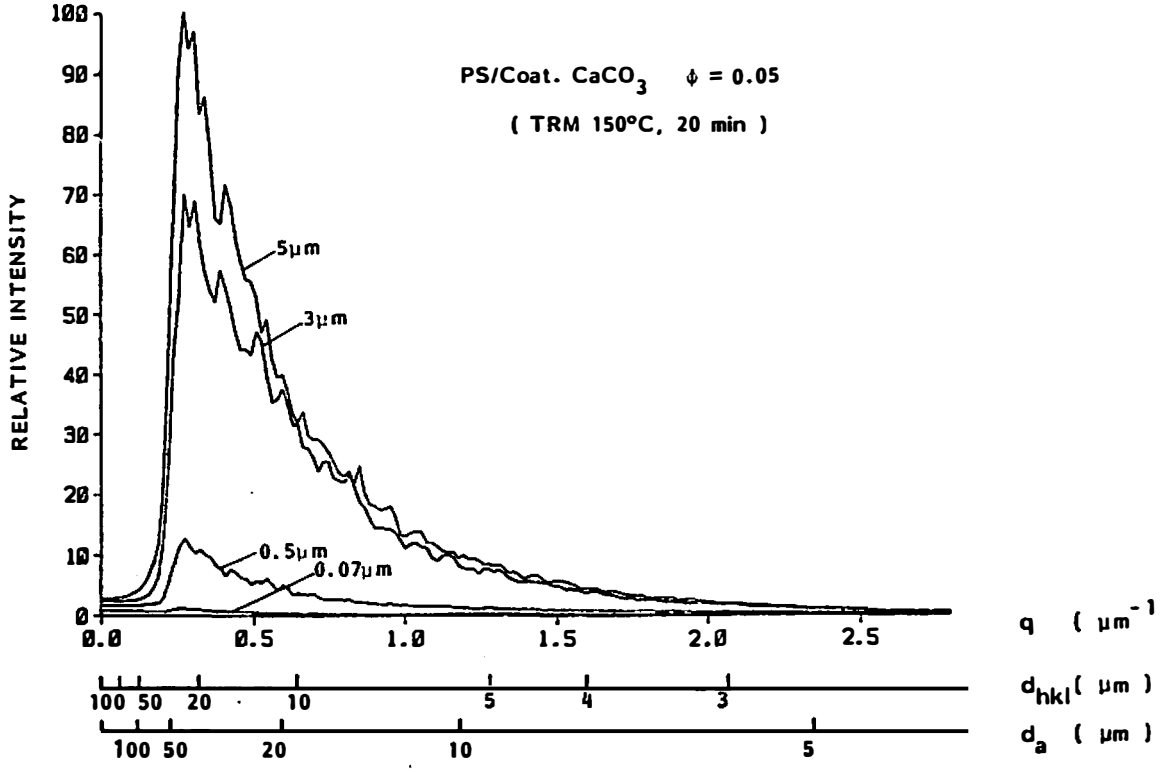

Figure IX-16. Comparison of relative intensity profiles for PS/coat. $CaCO_3$ (dp = various, ϕ = 0.05).

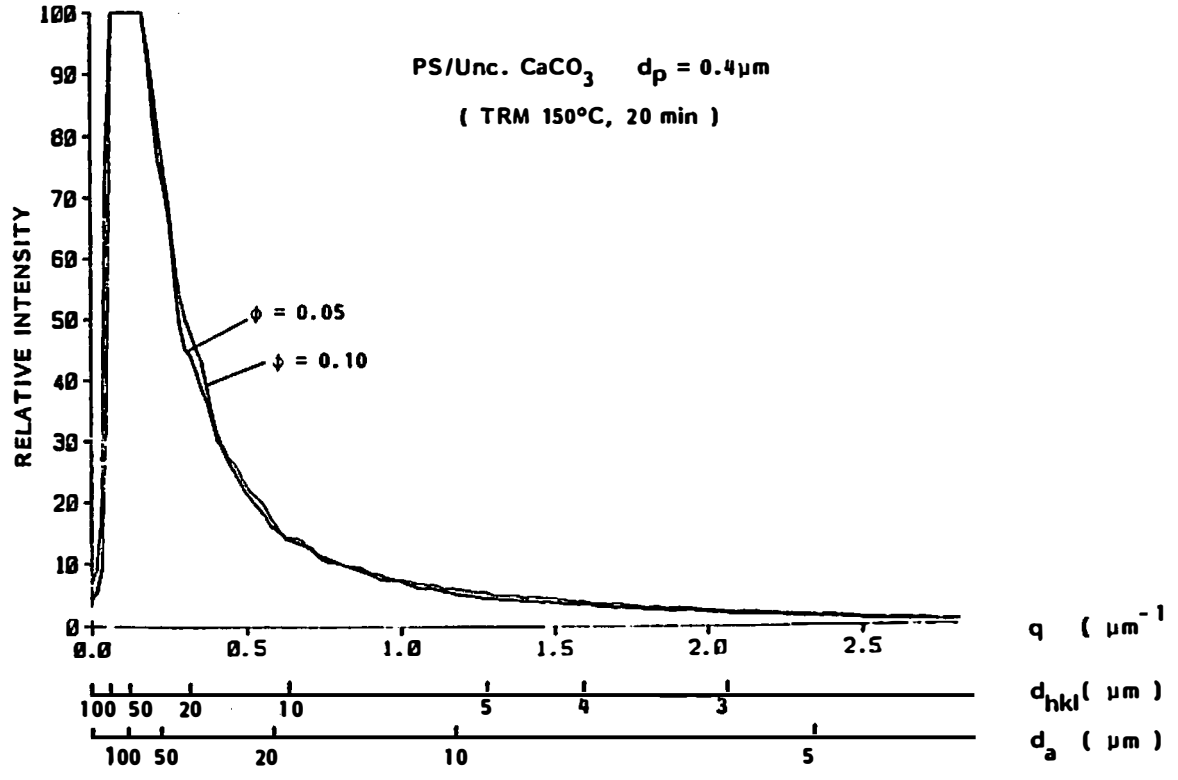

Figure IX-17. Relative intensity profiles for PS/unc. $CaCO_3$ (dp = 0.4 μm, ϕ = 0.05 and 0.10).

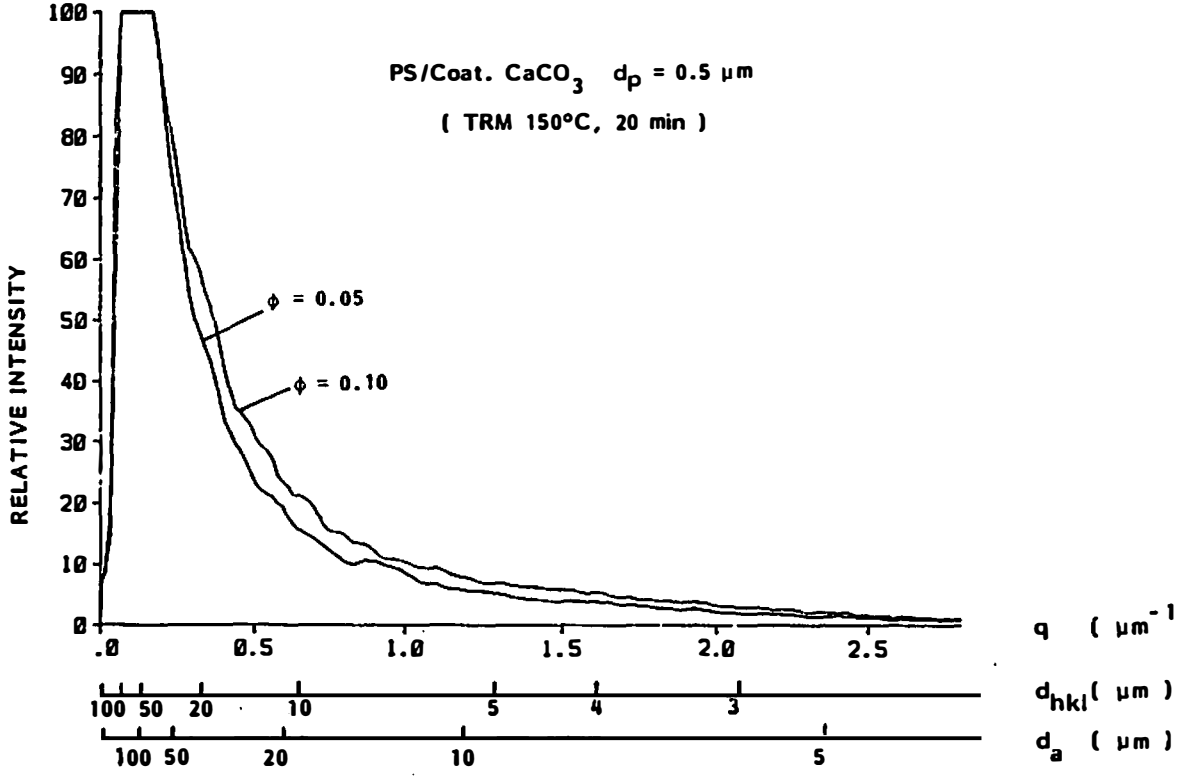

Figure IX-18. Relative intensity profiles for PS/coat. $CaCO_3$ (dp = 0.5 µm, ϕ = 0.05 and 0.10).

an effect of interparticulate distances. As loading level increases, interparticle distance decreases. It can make the decay of the intensity profile slower. This is more significant in coated calcium carbonate compounds.

Compounds were prepared in an internal mixer. Periods of mixing were varied from 1 minute to 20 minutes. All the compounds have a volume fraction of 0.05.

Figures IX-19 and IX-20 show the relative intensity profiles for uncoated calcium carbonate (dp = 0.4 μm) and coated calcium carbonate (dp = 0.5 μm) compounds. The decay of the relative intensity is slow after long periods of mixing for both cases. It suggests the disappearance of agglomerates.

Figures IX-21 and IX-22 represent the behavior of the relative intensities for the smallest particulates (dp = 0.07 m) compounds. Determination of the decay tendency is more difficult here because of the extremely sharp decay in the small angle region and the low magnitude of relative intensities in the large angle region.

E.1.b. Discussion. In this section, we discuss the dispersion of small particulates in plastics in conjunction with the Guinier (G-5) and Debye-Bueche (D-6) theories of small angle light scattering. These theories were introduced in Section A, Theoretical Background.

The Debye-Bueche correlation distance a_1 and Guinier correlation distance a_2 are obtained. These were defined in Eqs. (IX-15) and (IX-12)), respectively.

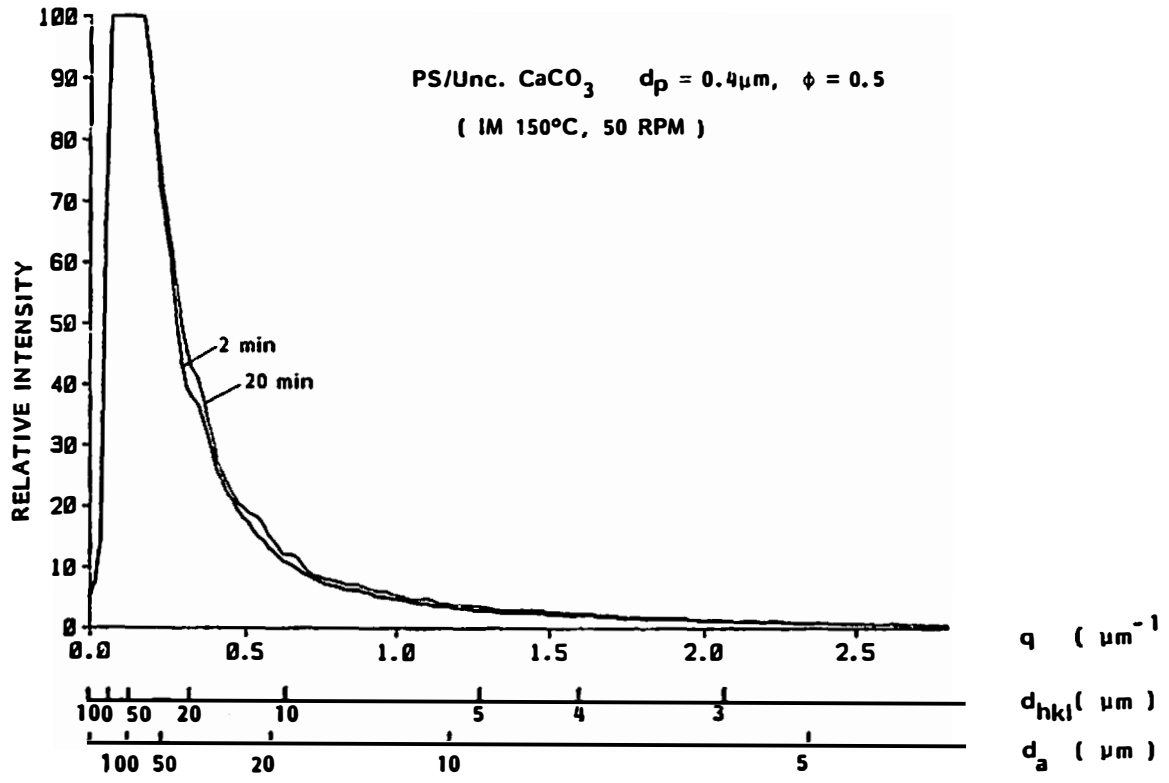

Figure IX-19. Relative intensity profiles for internal mixer prepared PS/unc. $CaCO_3$ (dp = 0.4 μm, ϕ = 0.05).

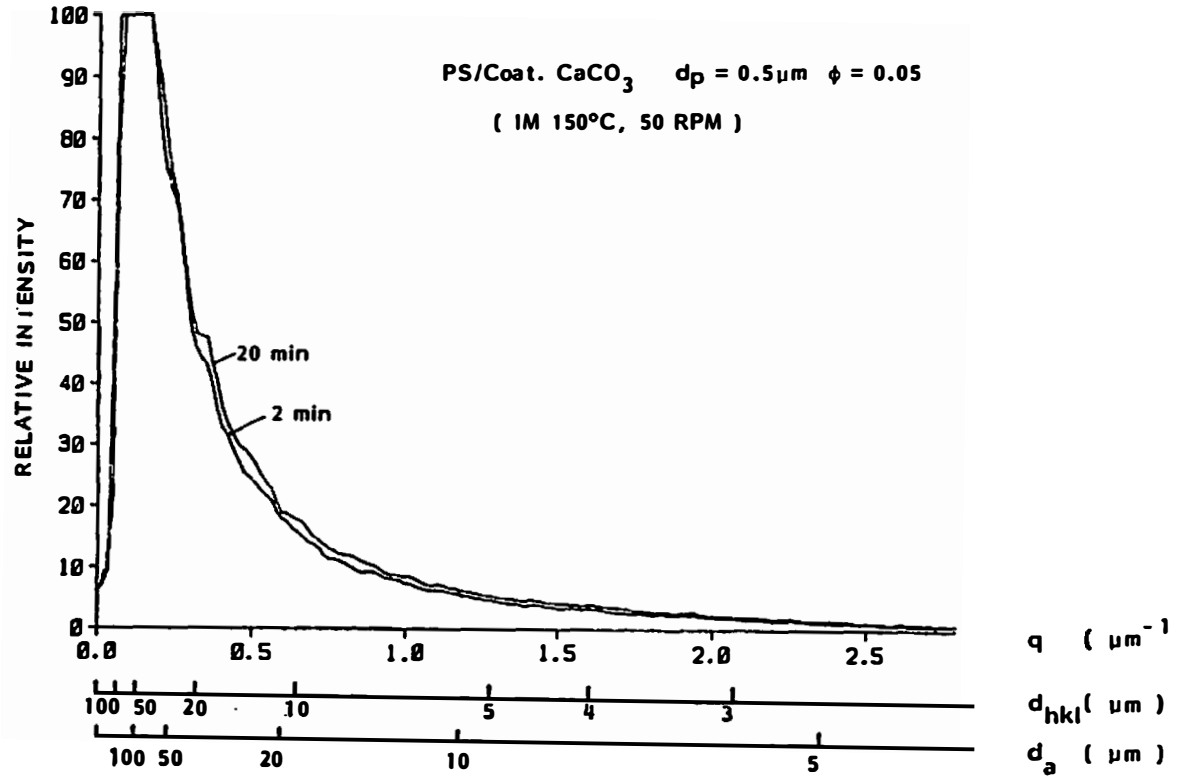

Figure IX-20. Relative intensity profiles for internal mixer prepared PS/coat. $CaCO_3$ (dp = 0.5 μm, ϕ = 0.05).

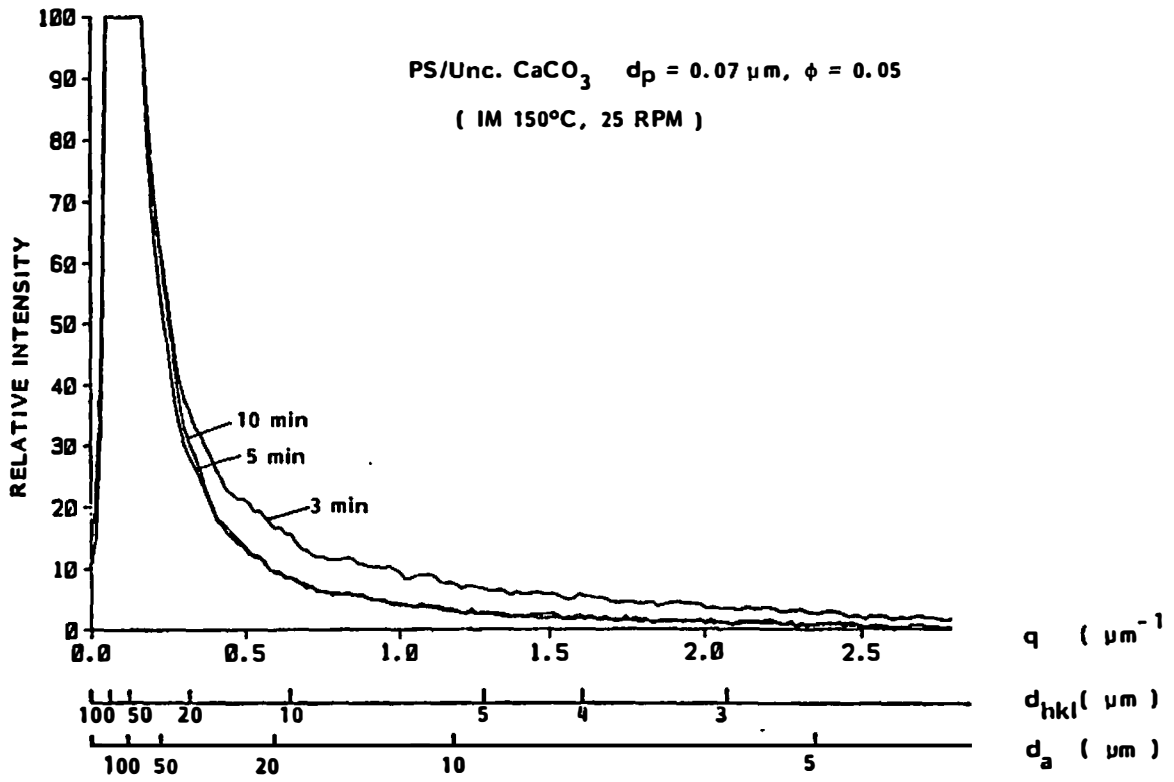

Figure IX-21. Relative intensity profiles for internal mixer prepared PS/unc. $CaCO_3$ (dp = 0.07 µm, ϕ = 0.05).

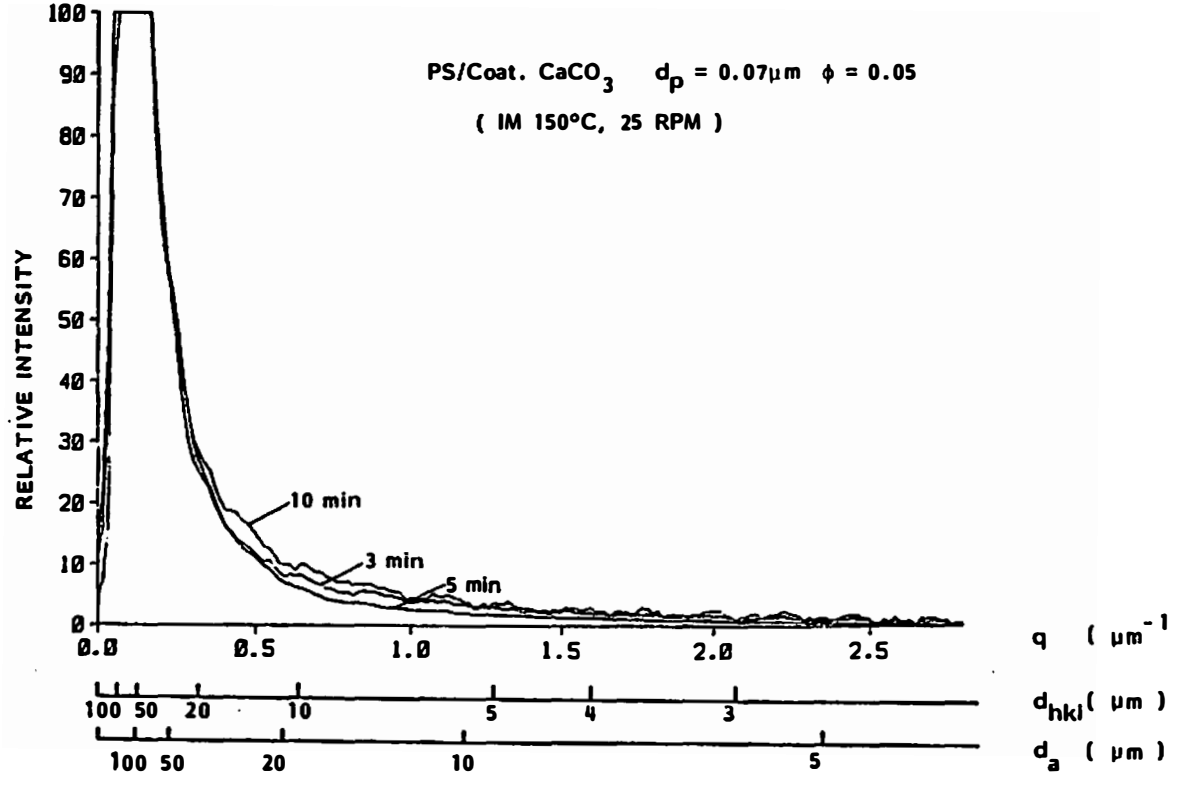

Figure IX-22. Relative intensity profiles for internal mixer prepared PS/coat. $CaCO_3$ (dp = 0.07 μm, ϕ = 0.05).

A Guinier plot (ln I/I_0 vs. q^2) of two roll mill mixed polystyrene/uncoated calcium carbonate compounds is given in Figure IX-23. Straight lines are obtained by least square curve fitting. Particle sizes determined vary from 17 μm to 0.07 μm. The volume fraction is 0.05 for all compounds. The existence of agglomerates has been confirmed for the 0.07 μm and 0.4 μm compounds by optical and electron microscopy.

We note that 0.07 μm particulate compounds exhibit the sharpest decay of ln I/I_0 with q^2 angle. This indicates the existence of large scatterers, i.e., the agglomerates. The occurrence of agglomerates of various sizes was found in optical studies. The correlation distance a_2 of this compound is 11.5 μm and thus much greater than the ultimate particle size of 0.07 μm. The sharp decay of the 17 μm particulate compound is probably due to the large ultimate particles. This calcium carbonate possesses a fairly broad size distribution due to natural grinding manufacturing process. A correlation distance of 10.6 μm is obtained.

The 3 μm and 0.4 μm particulate compounds possess correlation distances of 17.03 μm and 3.75 μm, respectively. The correlation distance of the 0.4 m particulate compound is nearly 10 times greater than the average particle size. This seems again to be due to the formation of agglomerates.

The correlation distance, the radius of gyration and the characteristic diameter are summarized in Table IX-3 for these compounds.

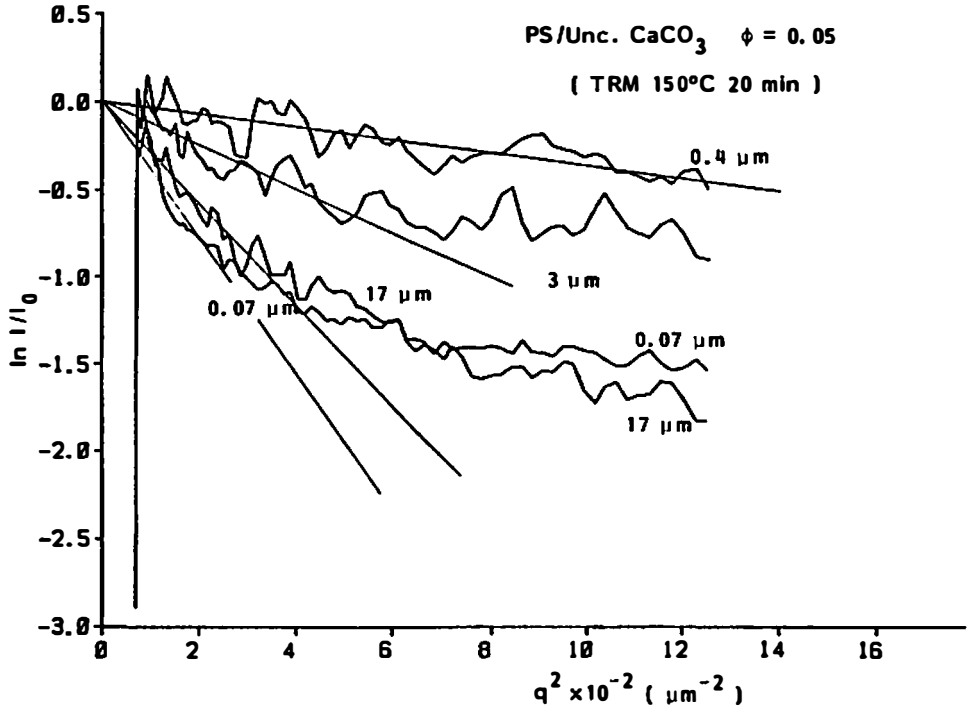

Figure IX-23. Guinier plots for PS/unc. $CaCO_3$ (dp = various, ϕ = 0.05).

Table IX-3. Parameters Obtained from Guinier and Debye-Bueche Plots for Two Roll Mill Prepared PS/Unc. $CaCO_3$ with Various Particle Size

Surface Coating	Nominal Particle Size dp (μm)	Volume Fraction ϕ (-)	Mixing Time (Min.)	Guinier q (μm^{-1})	Guinier a_2 (μm)	$\bar{R}_g$ (μm)	$\bar{d}$ (μm)
No	17.	0.05	20	0.089-0.20	10.6	9.18	23.7
No	3.	0.05	20	0.089-0.23	7.01	6.09	15.7
No	0.4	0.05	20	0.089-0.36	3.75	3.25	8.39
No	0.07	0.05	20	0.089-0.20	11.5	9.96	25.7

We note that the compounds of two fine calcium carbonates (dp = 0.07 μm and 0.4 μm) possess correlation distances which are much greater than the average ultimate particle size. The two coarse calcium carbonates are natural ground grades. These have fairly broad size distributions. Correlation distances are in reasonable agreement with the average ultimate particle sizes.

It is clear that the compounds which contain large agglomerates have much greater correlation distances than the ultimate particle size of the filler.

We now discuss the effect of the volume fraction of filler. Figure IX-24 and Figure IX-25, respectively, represent the Guinier and Debye-Bueche plots for uncoated calcium carbonate compounds. Volume fractions of 0.05 and 0.10 are compared. The nominal particle size is 0.4 μm. The Guinier correlation distances a_2 of Eq. (IX-12) are 7.89 μm for ϕ = 0.05 and 7.00 μm for ϕ = 0.10 are obtained. Large correlation distances compared with nominal particle size are due to agglomerates. The Guinier correlation distances are not significantly affected by the volume fraction of filler.

The Debye-Bueche correlation distance a_1 for these compounds are 0.368 μm (ϕ = 0.05) and 0.551 μm (ϕ = 0.10). These roughly agree with the nominal ultimate particle size of 0.4 μm.

Similar types of plots are obtained for the stearic acid coated calcium carbonate compounds (Figures IX-26 and IX-27). The volume fractions are 0.05 and 0.10 again. Debye-Bueche correlation distances are 0.513 μm for ϕ = 0.05 and 0.600 for ϕ = 0.10. These

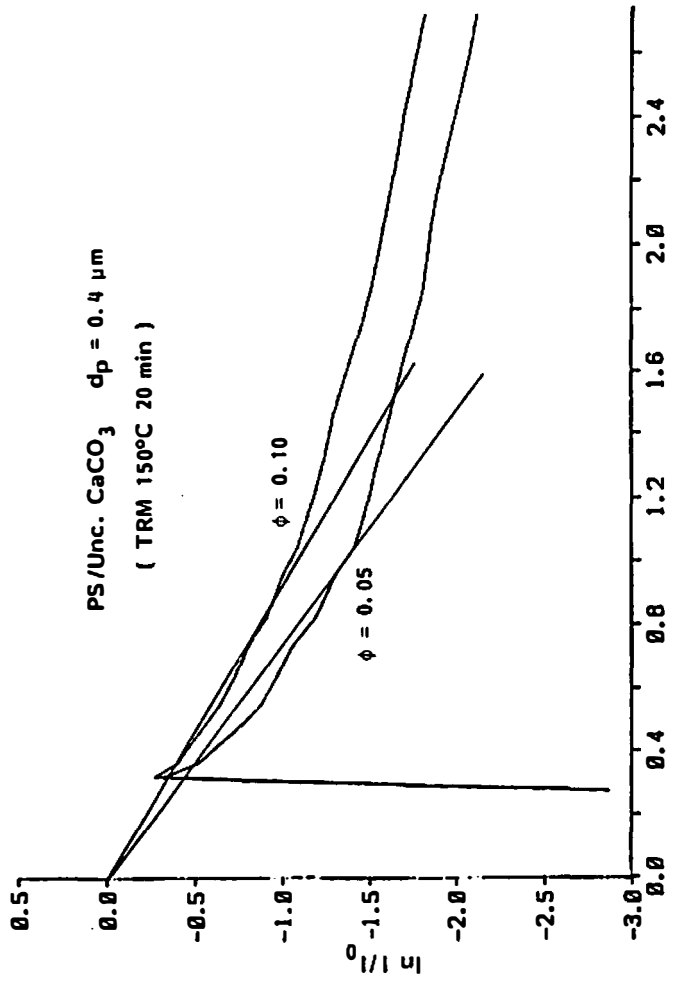

Figure IX-24. Guinier plots for PS/unc. $CaCO_3$ (dp = 0.4 µm, ϕ = 0.05 and 0.10).

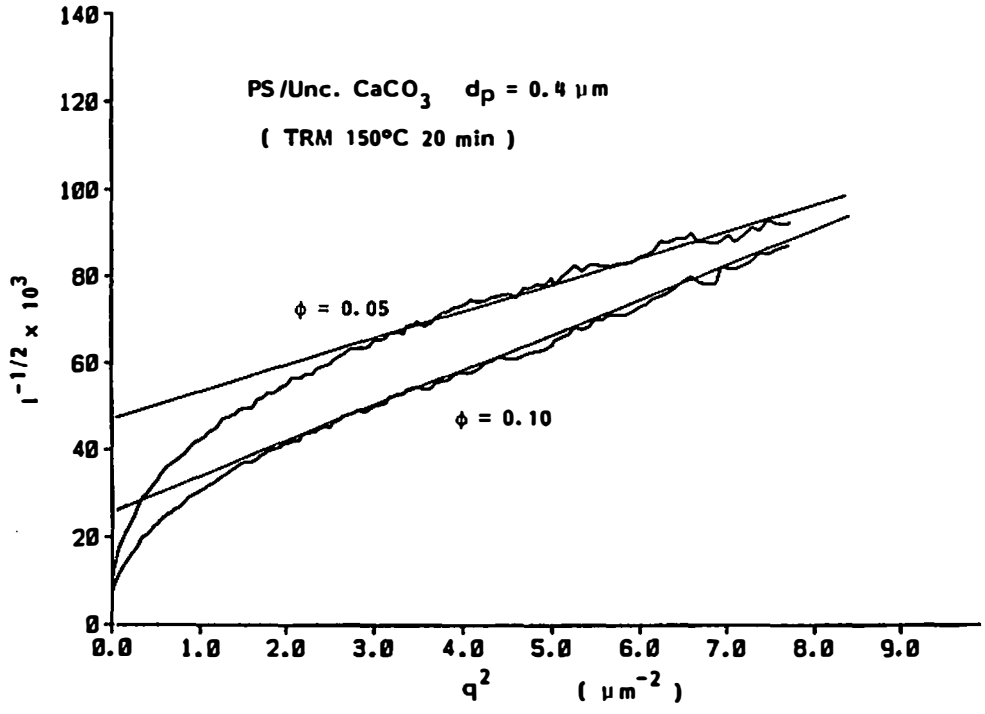

Figure IX-25. Debye-Bueche plots for PS/unc. $CaCO_3$ (dp = 0.4 µm, ϕ = 0.05 and 0.10).

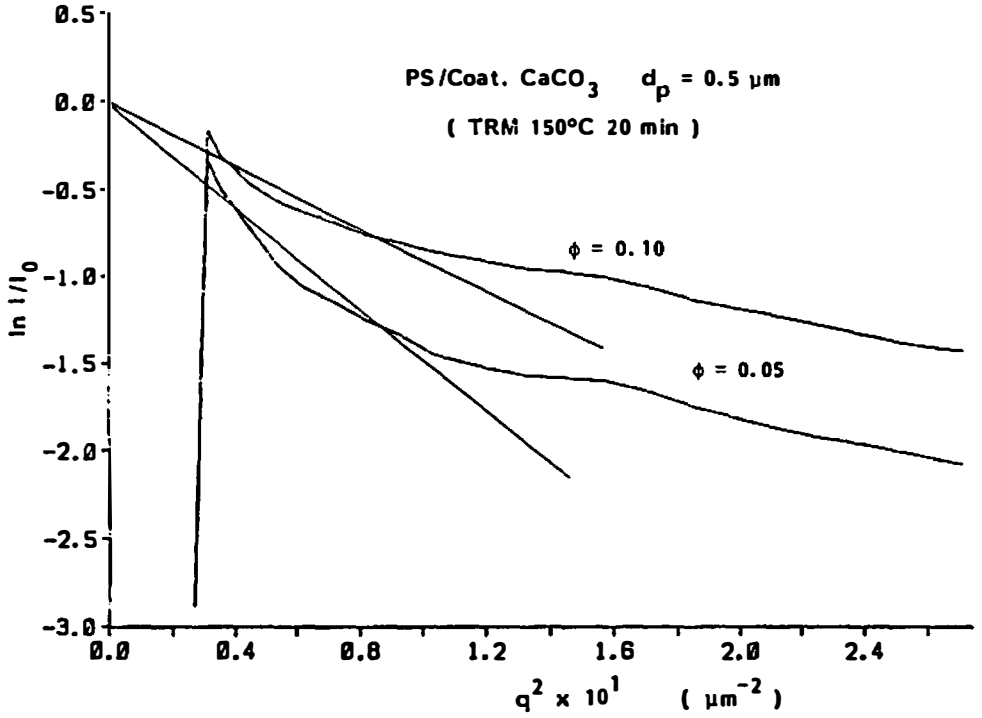

Figure IX-26. Guinier plots for PS/coat. $CaCO_3$ (dp = 0.5 µm, ϕ = 0.05 and 0.10).

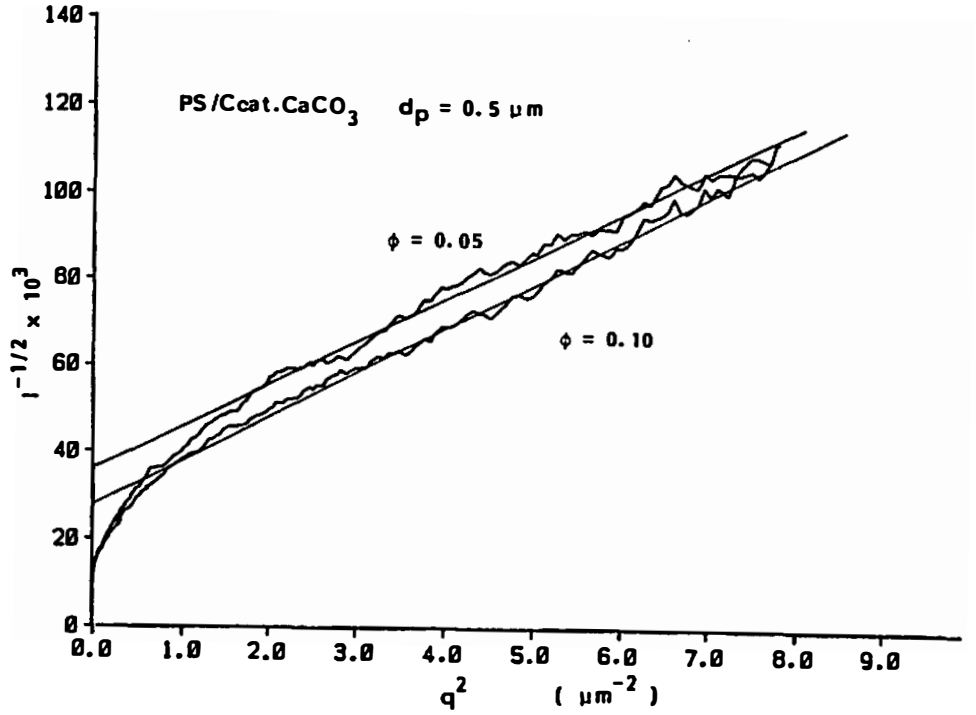

Figure IX-27. Debye-Bueche plots for PS/coat. $CaCO_3$ (dp = 0.5 µm, ϕ = 0.05 and 0.10).

are in good agreement with the nominal particle size of 0.5 μm.

The correlation distances a_2, a_1 obtained from Guinier and Debye-Bueche plots are summarized in Table IX-4. This includes the radius of gyration $\overline{R}_g$ and characteristic diameter of scatterer $\overline{d}$.

These were calculated from the following equations:

		Equation
Guinier	a_2	IX-13
	$\overline{R}_g$	IX-14
	$\overline{d}$	IX-18
Debye-Bueche	a_1	IX-17
	$\overline{R}_g$	IX-18
	$\overline{d}$	IX-28

Characteristic diameters obtained from Debye-Bueche plots are still greater than the nominal particle size.

We now consider the effect of the period of mixing in an internal mixer. The scattered intensity profiles were obtained for five different sections of film specimen and are averaged to determine the correlation distances.

Calcium carbonates which have nominal ultimate particle sizes of less than 1 μm were chosen to study the effect of mixing time. Compounds of these particulates contain agglomerates. It was expected that the improvement of dispersion with mixing time is most pronounced with these particulates due to the breakdown of agglomerates.

Table IX-4. Parameters Obtained from Guinier and Debye-Bueche Plots for Two Roll Mill Prepared $PS/CaCO_3$ Compounds with Different Volume Fractions

Surface Coating	Nominal Particle Size dp (μm)	Volume Fraction ϕ (-)	Mixing Time (Min.)	Guinier				Debye-Bueche			
				q (μm^{-1})	a_2 (μm)	$\bar{R}_g$ (μm)	$\bar{d}$ (μm)	q (μm^{-1})	a_1 (μm)	$\bar{R}_g$ (μm)	$\bar{d}$ (μm)
No	0.4	0.05	20	0.17-0.31	7.98	6.91	17.8	1.53-2.80	0.368	0.901	2.33
Yes	0.5	0.05	20	0.17-0.31	8.16	7.07	18.2	1.53-2.80	0.513	1.26	1.24
No	0.4	0.10	20	0.17-0.31	7.00	6.06	15.7	1.53-2.80	0.551	1.35	3.48
Yes	0.5	0.10	20	0.17-0.31	6.33	5.48	14.15	1.53-2.80	0.600	1.47	3.79

First we determine the effect of the mixing time for uncoated and coated calcium carbonate compounds which have nominal particle sizes of 0.4 μm and 0.5 μm, respectively. Periods of mixing are 2 minutes and 20 minutes in an internal mixer. The rotor speed is 50 rpm and volume fraction is 0.05.

Figures IX-28 and IX-29 give Guinier and Debye-Bueche plots for polystyrene/uncoated calcium carbonate compounds (dp = 0.4 μm, ϕ = 0.05). It is clear that the slopes of both the Guinier and Debye-Bueche plots decrease as mixing progresses. The correlation distances decrease with mixing time.

As discussed in Section C, Theoretical Background, when correlation distances are small, the specimen contains greater amounts of small scatterers. The decrease of correlation distances both in Guinier and Debye regions indicates the disappearance of large agglomerates and the relative increase of small agglomerates.

The effect of mixing time on coated calcium carbonate compounds is not as strong as on uncoated compounds. The distribution of the scatterer size is almost constant after 2 minutes of mixing in the Guinier region (Figure IX-30). In the Debye-Bueche region (Figure IX-31), the effect of mixing is more clear. This indicates that the agglomerate size distribution changed in the direction of producing small agglomerates.

Table IX-5 summarizes correlation distances and other quantities of polystyrene/calcium carbonate compounds (dp = 0.4 μm and 0.5 μm). The quantities computed from both Guinier and

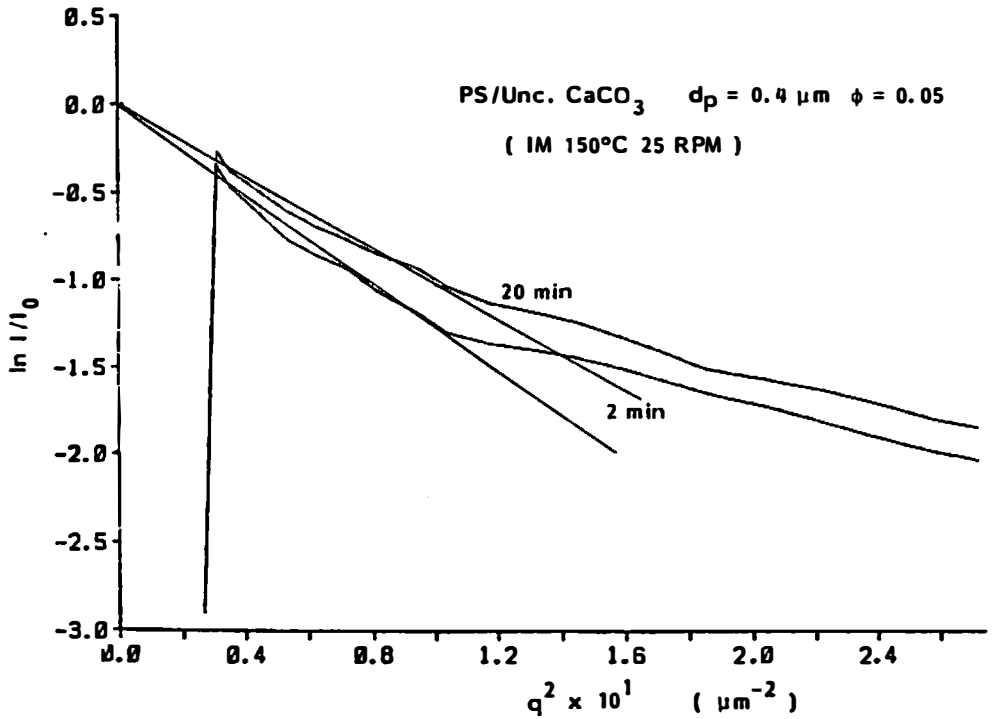

Figure IX-28. Guinier plots for internal mixer prepared PS/unc. $CaCO_3$ (dp = 0.4 µm, ϕ = 0.05).

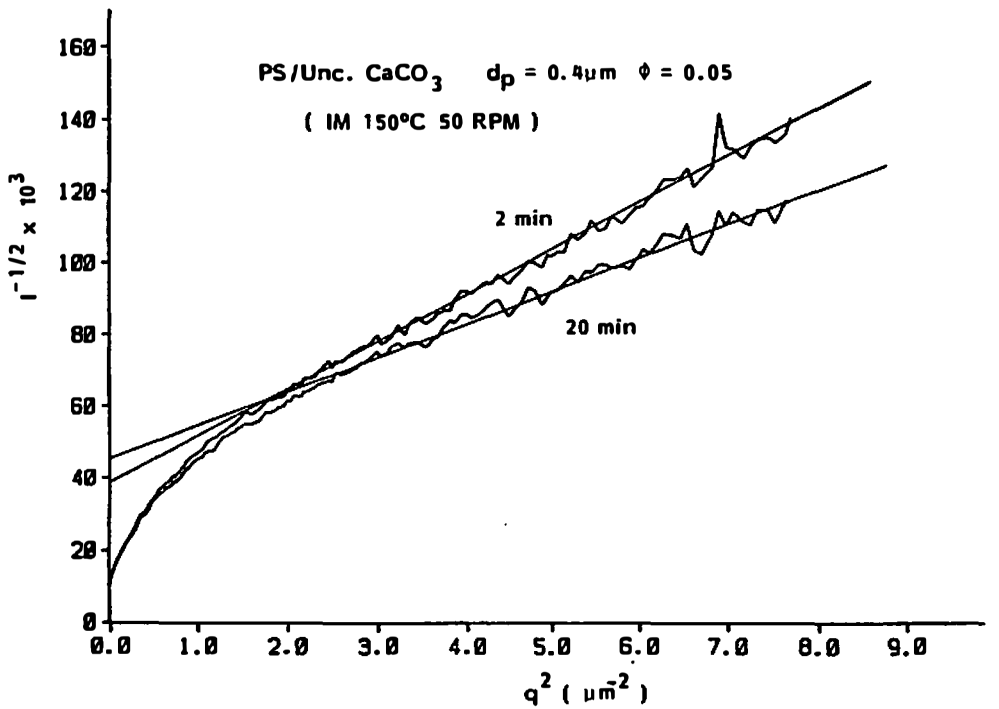

Figure IX-29. Debye-Bueche plots for internal mixer prepared PS/unc. $CaCO_3$ (dp = 0.4 μm, ϕ = 0.05).

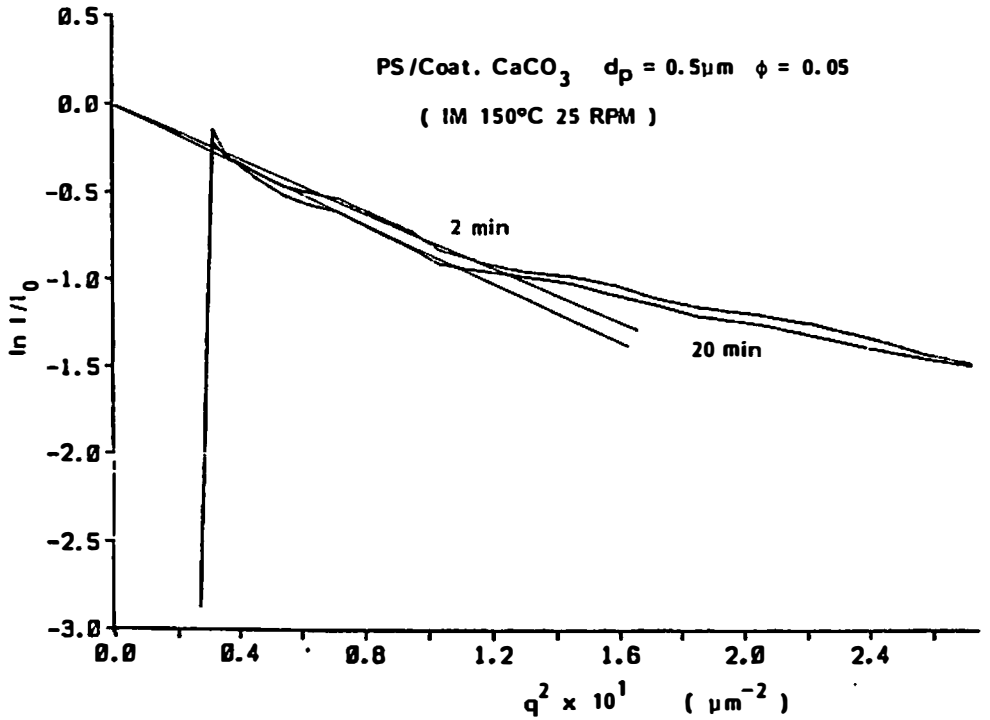

Figure IX-30. Guinier plots for internal mixer prepared PS/coat. $CaCO_3$ (dp = 0.5 µm, ϕ = 0.05).

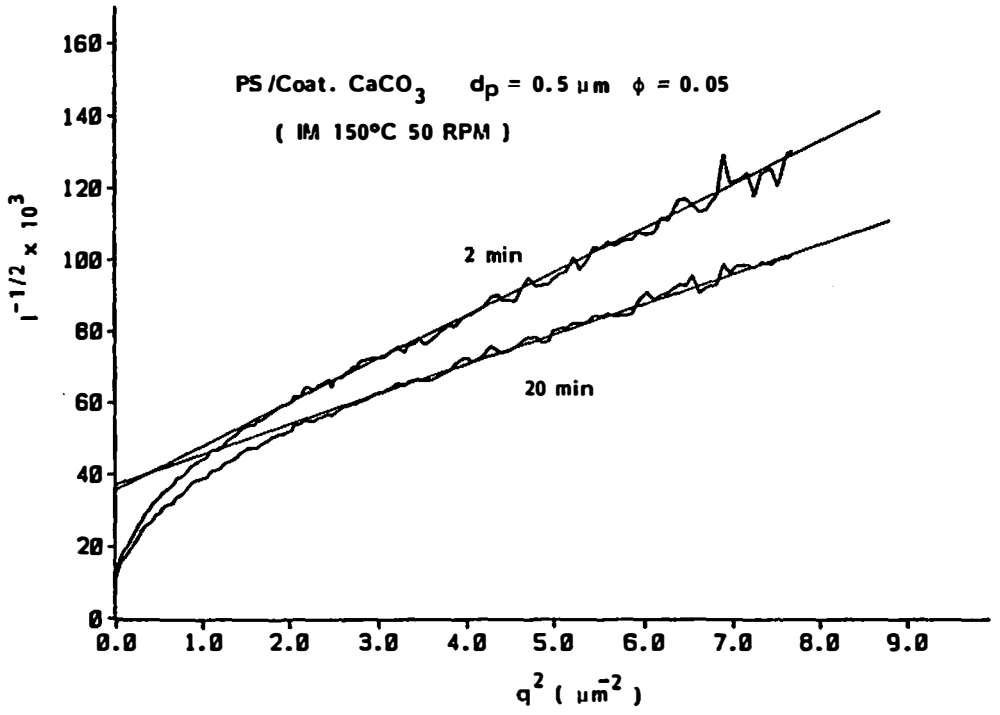

Figure IX-31. Debye-Bueche plots for internal mixer prepared PS/coat. $CaCO_3$ (d_p = 0.4 µm, ϕ = 0.05).

Table IX-5. Parameters Obtained from Guinier and Debye-Bueche Plots for Internal Mixer Prepared $PS/CaCO_3$ Compounds (RPM = 50)

Surface Coating	Nominal Particle Size dp (μm)	Volume Fraction ϕ (-)	Mixing Time (Min.)	Guinier q (μm^{-1})	Guinier a_2 (μm)	Guinier $\bar{R}_g$ (μm)	Guinier $\bar{d}$ (μm)	Debye-Bueche q (μm^{-1})	Debye-Bueche a_1 (μm)	Debye-Bueche $\bar{R}_g$ (μm)	Debye-Bueche $\bar{d}$ (μm)
No	0.4	0.05	2	0.15-0.31	7.63	6.61	17.1	1.53-2.80	0.578	1.42	3.66
No	0.4	0.05	20	0.17-0.31	6.84	5.92	15.3	1.53-2.80	0.450	1.10	2.85
Yes	0.5	0.05	2	0.17-0.31	5.98	5.18	13.4	1.53-2.80	0.577	1.41	3.65
Yes	0.5	0.05	20	0.17-0.31	6.32	5.47	14.1	1.53-2.80	0.482	1.18	3.05

Debye-Bueche plots shows the disappearance of large agglomerates as mixing progresses.

Correlation distances of these compounds obtained from Guinier plots and Debye-Bueche plots are given in Figures IX-32 and IX-33, respectively, as a function of mixing time.

Guinier correlation distances of uncoated calcium carbonate compounds decrease from 7.63 μm to 6.84 μm as mixing progresses. Large agglomerates disappear. Coated calcium carbonate compounds maintain a correlation distance of about 6 μm. This is smaller than the uncoated calcium carbonate compounds. It should be expected that the distribution of agglomerates is rich in small agglomerates in coated clacium carbonate compounds. The small agglomerates changed their size distribution more rapidly during mixing.

We now determine the effect of mixing time for the finest calcium carbonate (dp = 0.07 μm). The volume fraction is again 0.05. Compounds were prepared in an internal mixer at 150°C at the rotor speed of 25 rpm.

Figures IX-34 and IX-35 show Guinier and Debye-Bueche plots for uncoated calcium carbonate compounds. The mixing time varies from 3 minutes to 10 minutes. Guinier plots of these compounds are not well represented by straight lines, but always decay exponentially with angle q^2. We obtain larger correlation distances at smaller angles. Debye-Bueche plots (Figure IX-35) for these compounds are well represented by the straight lines in the large angle region.

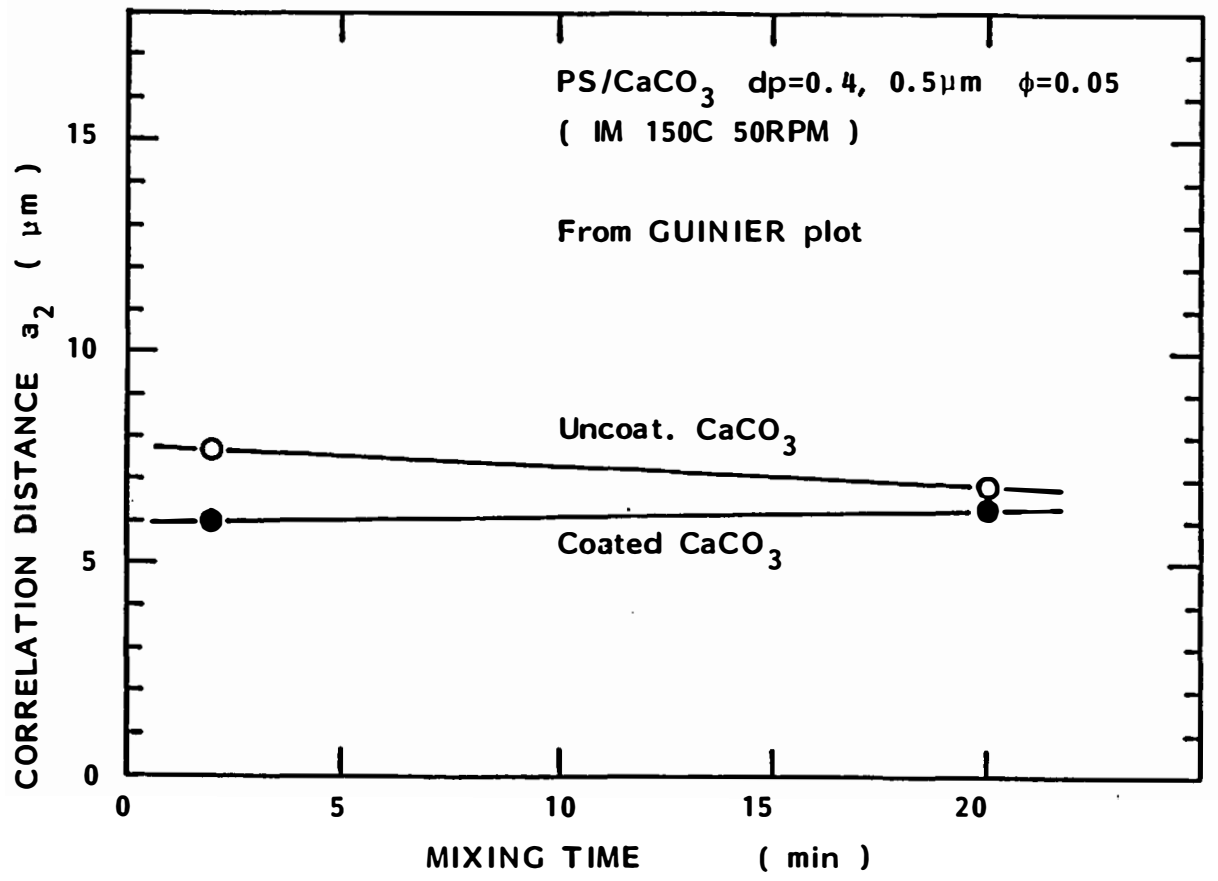

Figure IX-32. Correlation distance a_2 as a function of mixing time for $PS/CaCO_3$ (dp = 0.4, 0.5 μm).

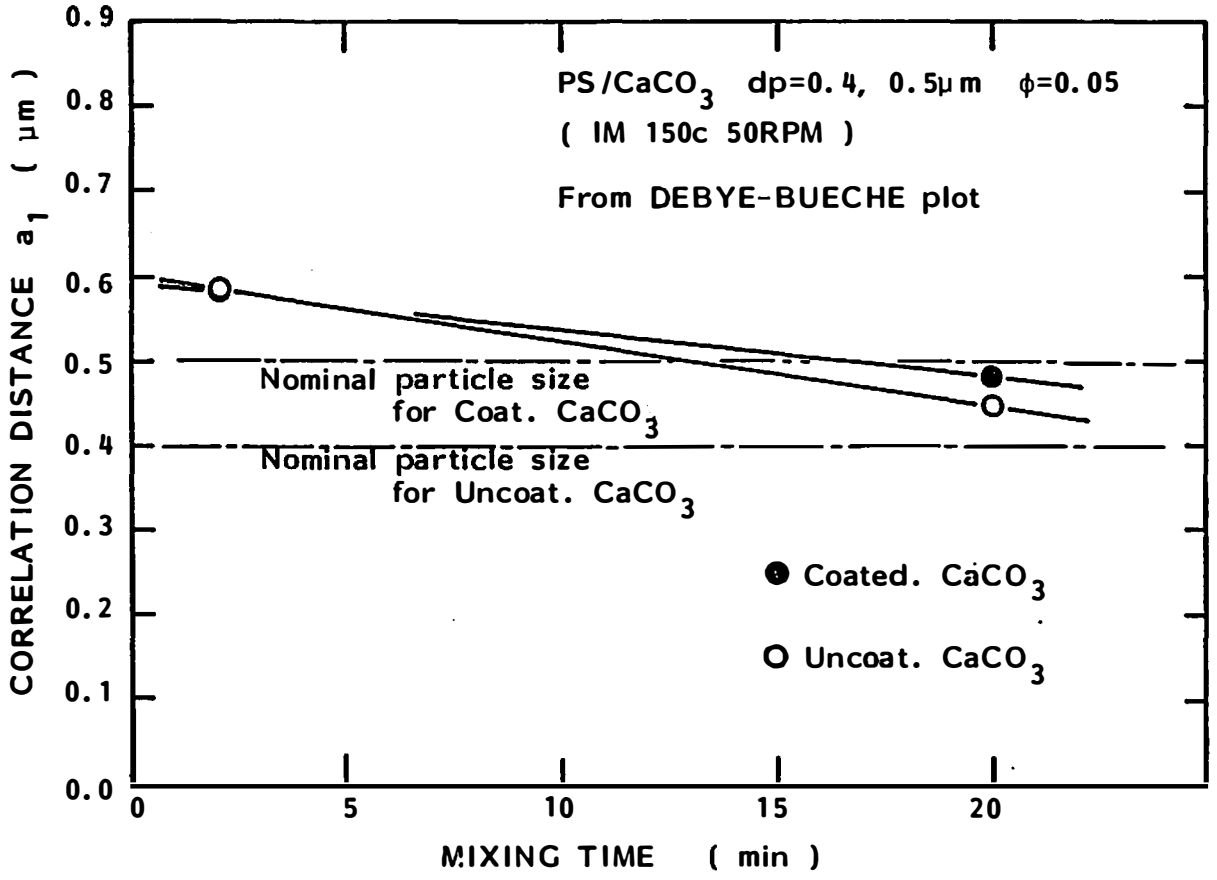

Figure IX-33. Correlation distance a_1 as a function of mixing time for $PS/CaCO_3$ (dp = 0.4, 0.5 μm).

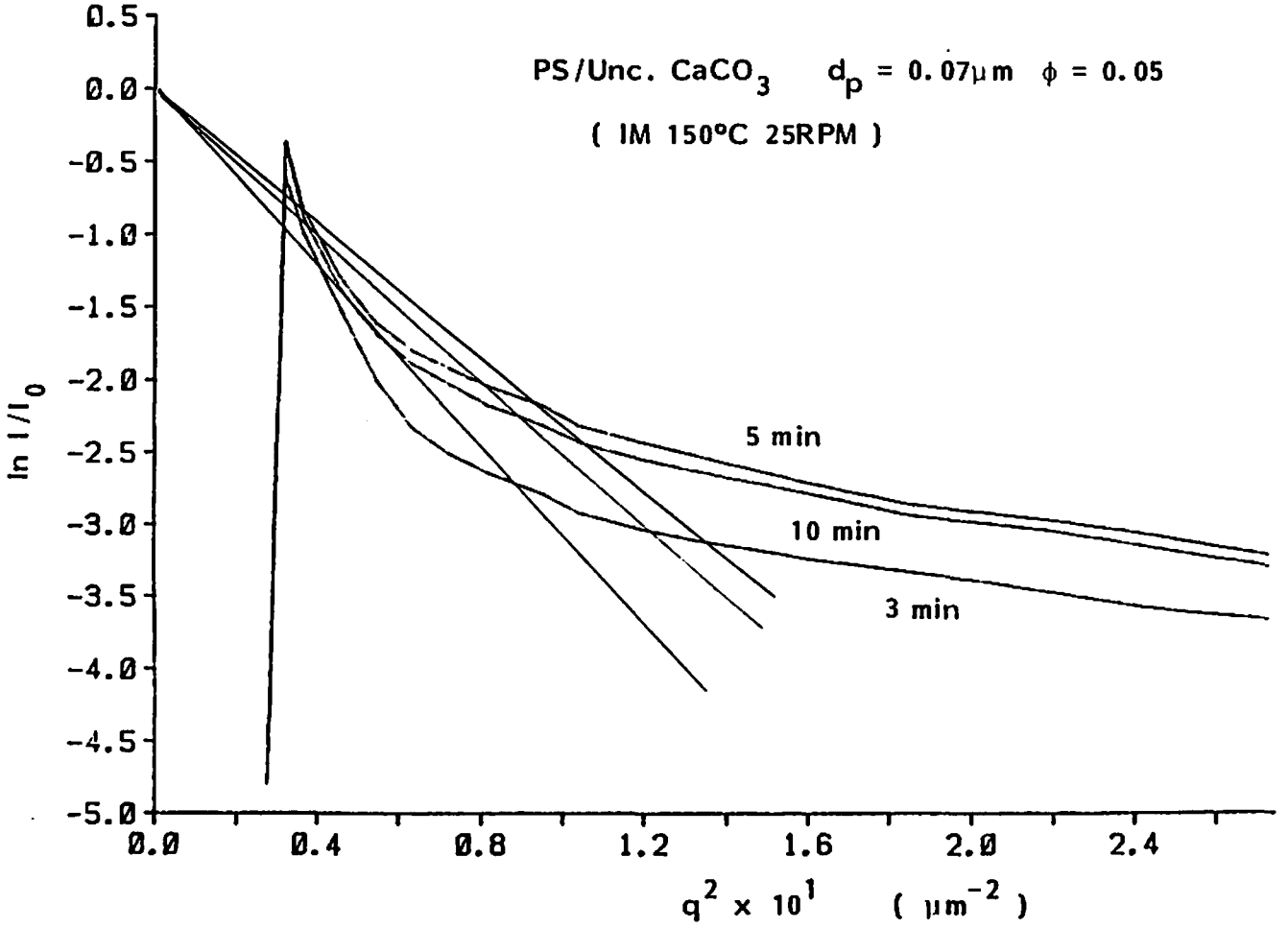

Figure IX-34. Guinier plots for internal mixer prepared PS/unc. $CaCO_3$ (dp = 0.07 μm, ϕ = 0.05).

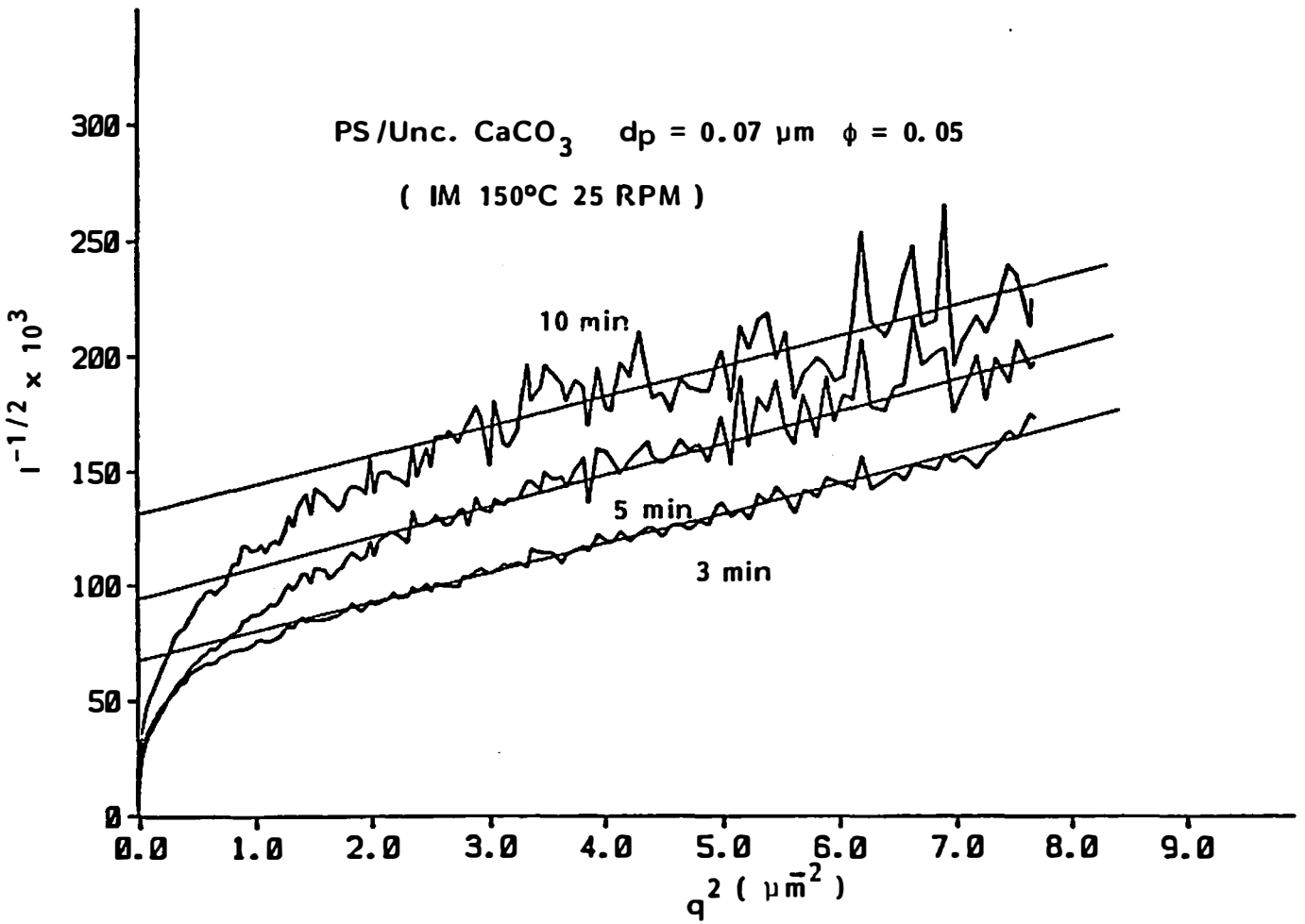

Figure IX-35. Debye-Bueche plots for internal mixer prepared PS/unc. $CaCO_3$ (dp = 0.07 μm, ϕ = 0.05).

Similar plots are obtained for coated calcium carbonate compounds with the same ultimate particle size. These are shown in Figures IX-36 and IX-37.

We summarize the Debye-Bueche and Guinier correlation distances and other quantities in Table IX-6. Correlation distance, in general, decreases as mixing progresses, indicating the disappearance of the large agglomerates.

Guinier and Debye-Bueche correlation distances are plotted as a function of the mixing period in Figures IX-38 and IX-39, respectively. Improvement of dispersion is clear. As the mixing progresses, distribution of agglomerates shifts to the smaller size. Likewise 0.4 m and 0.5 m particulate compounds, smaller correlation distances were determined for coated calcium carbonate compound with 0.07 m particulates. The agglomerate size distribution in the small size range (Debye-Bueche region) shows a drastic change with increasing mixing time. The drastic change of Debye-Bueche correlation distances a_1 suggests that the increasing number of small agglomerates.

E.2. Polypropylene Compounds

E.2.a. Results. The crystalline structure of the polypropylene matrix affects the scattered intensity profile. This was discussed in Section D while considering the Photographic Method. We first discuss the effect of measurement temperature.

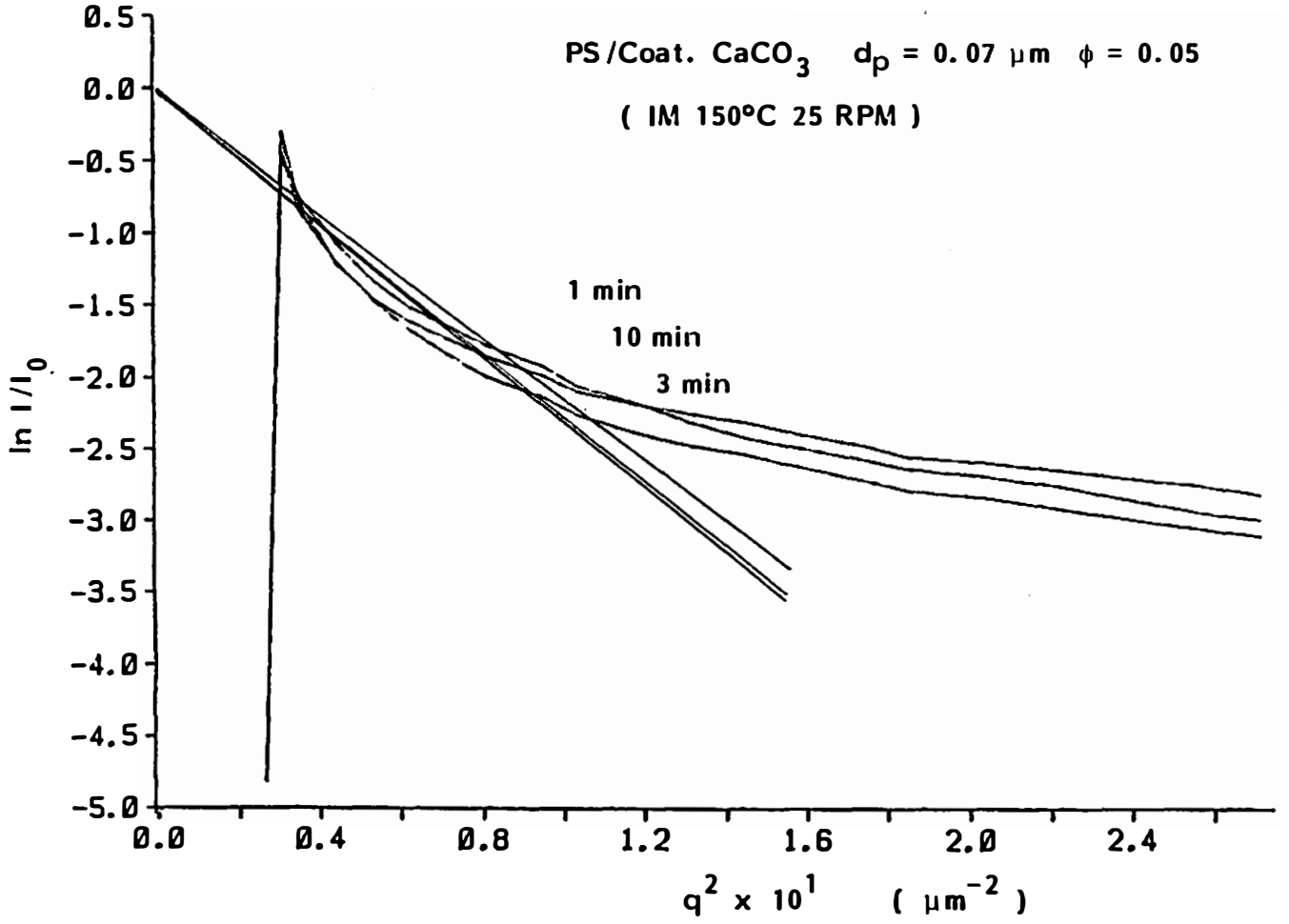

Figure IX-36. Guinier plots for internal mixer prepared PS/coat. $CaCO_3$ (dp = 0.07 μm, ϕ = 0.05).

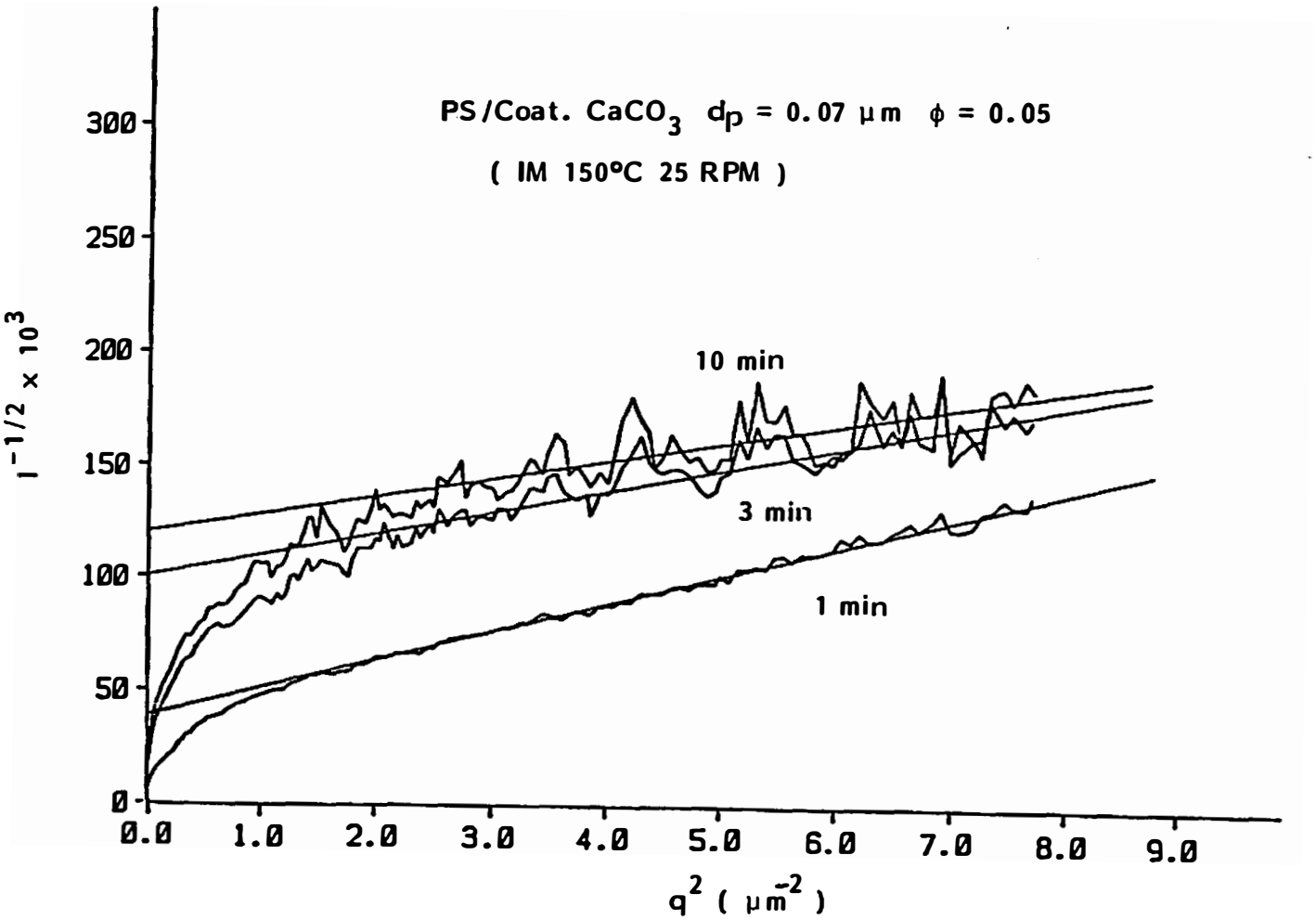

Figure IX-37. Debye-Bueche plots for internal mixer prepared PS/coat. $CaCO_3$ (dp = 0.07 µm, ϕ = 0.05).

Table IX-6. Parameters Obtained from Guinier and Debye-Bueche Plots for Internal Mixer Prepared $PS/CaCO_3$ Compounds (RPM = 25)

Surface Coating	Nominal Particle Size dp (μm)	Volume Fraction ϕ (-)	Mixing Time (Min.)	Guinier				Debye-Bueche			
				q (μm^{-1})	a_2 (μm)	$\bar{R}_g$ (μm)	$\bar{d}$ (μm)	q (μm^{-1})	a_1 (μm)	$\bar{R}_g$ (μm)	$\bar{d}$ (μm)
No	0.07	0.05	3	0.17-0.31	11.8	10.2	26.4	1.53-2.80	0.426	1.04	2.69
No	0.07	0.05	5	0.17-0.31	10.5	9.09	23.5	1.53-2.80	0.387	0.948	2.45
No	0.07	0.05	10	0.17-0.31	10.7	9.27	23.9	1.53-2.80	0.315	0.772	1.99
Yes	0.07	0.05	1	0.17-0.31	9.79	8.48	21.9	1.53-2.80	0.582	1.43	3.68
Yes	0.07	0.05	3	0.17-0.31	10.3	8.92	23.0	1.53-2.80	0.302	0.740	1.91
Yes	0.07	0.05	10	0.17-0.31	10.0	8.66	22.4	1.53-2.80	0.255	0.625	1.61

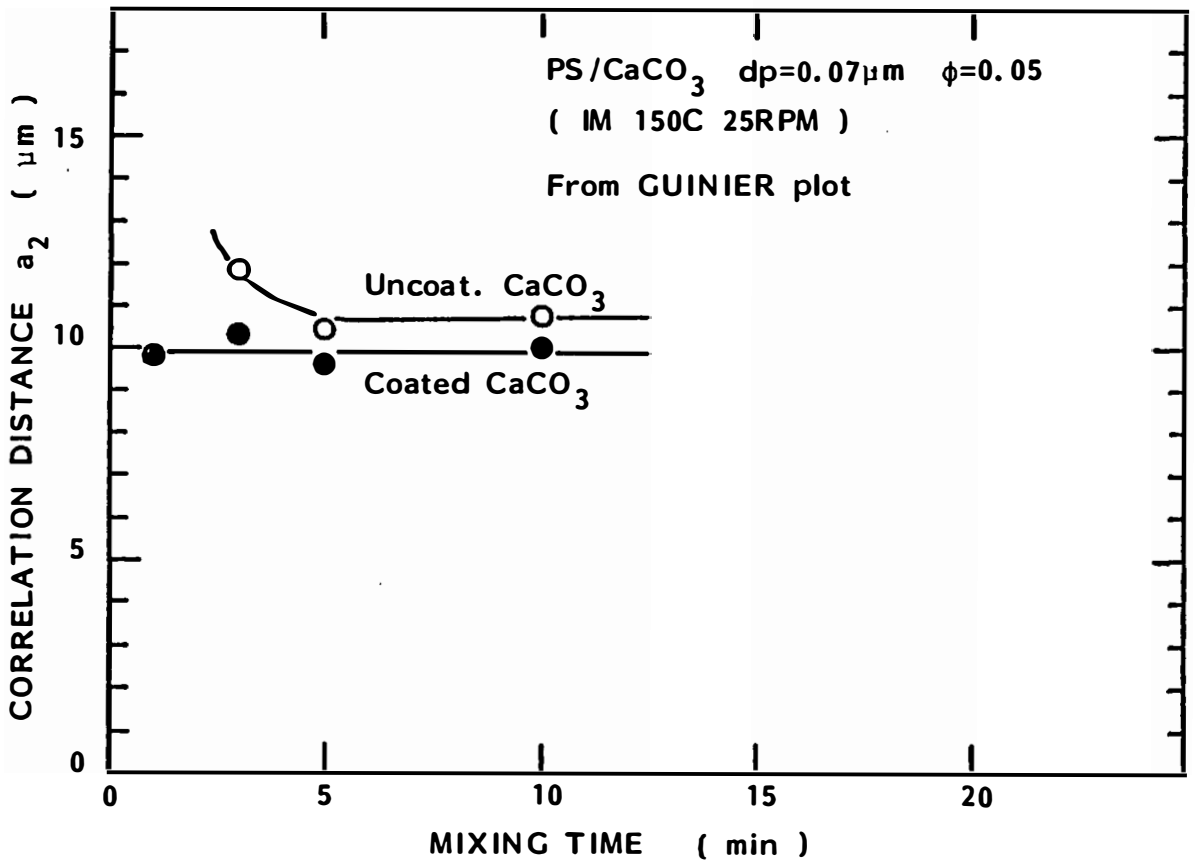

Figure IX-38. Correlation distance a_2 as a function of mixing time for $PS/CaCO_3$ (dp = 0.07 μm).

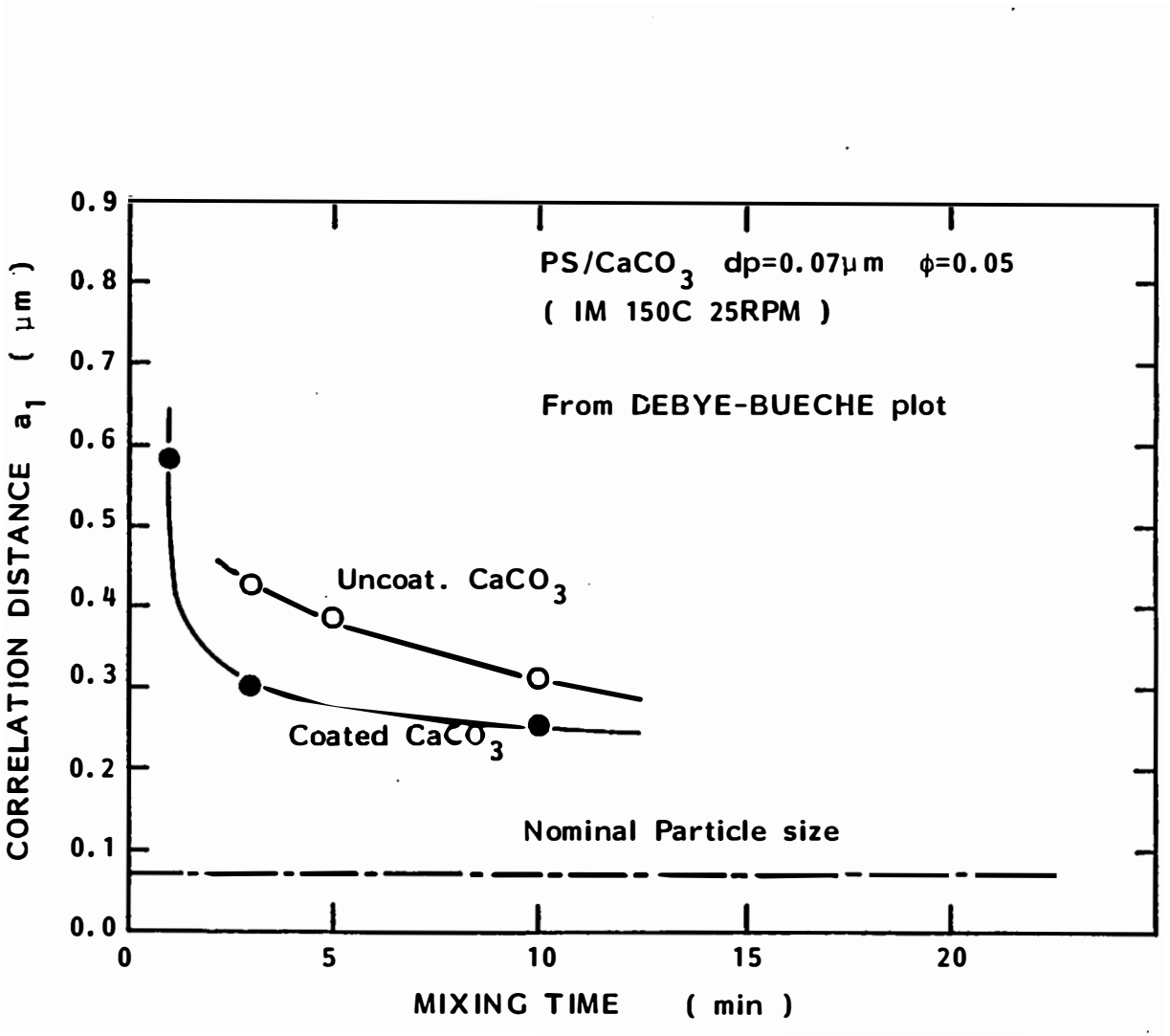

Figure IX-39. Correlation distance a_1 as a function of mixing time for $PS/CaCO_3$ (dp = 0.07 μm).

Figures IX-40 through IX-42 show the effect of temperature increase on the intensity profile of various polypropylene/calcium carbonate compounds prepared both by Ferro Corporation and in our laboratory.

The intensity was measured at room temperature and 185°C where polypropylene is in a molten state. We note maxima in the intensity profile at room temperature. This was taken as 100 in these figures. The intensity at 185°C was compared.

Figures IX-40 and IX-41 show relative intensity profiles of polypropylene/calcium carbonate compounds (prepared by Ferro Corporation) with volume fractions of 0.136 and 0.196, respectively. We observe a remarkable decrease of scattered intensity in the melt stage in both cases. Melt compounds have only 10 percent (ϕ = 0.136) and 50 percent (ϕ = 0.196) of the scattered intensity of the solid state compound. This is due to the disappearance of the crystalline phase of polypropylene at elevated temperatures. This reduction is smaller at high volume fraction.

Figure IX-42 shows relative intensity profiles of polypropylene/calcium carbonate compounds (dp = 0.4 μm, ϕ = 0.05) prepared in our laboratory. Again we observe drastic reductions of scattered intensity at the elevated temperature.

Reductions of intensity of this sort were observed for all polypropylene compounds.

We now discuss intensity profiles of polypropylene compounds at 185°C.

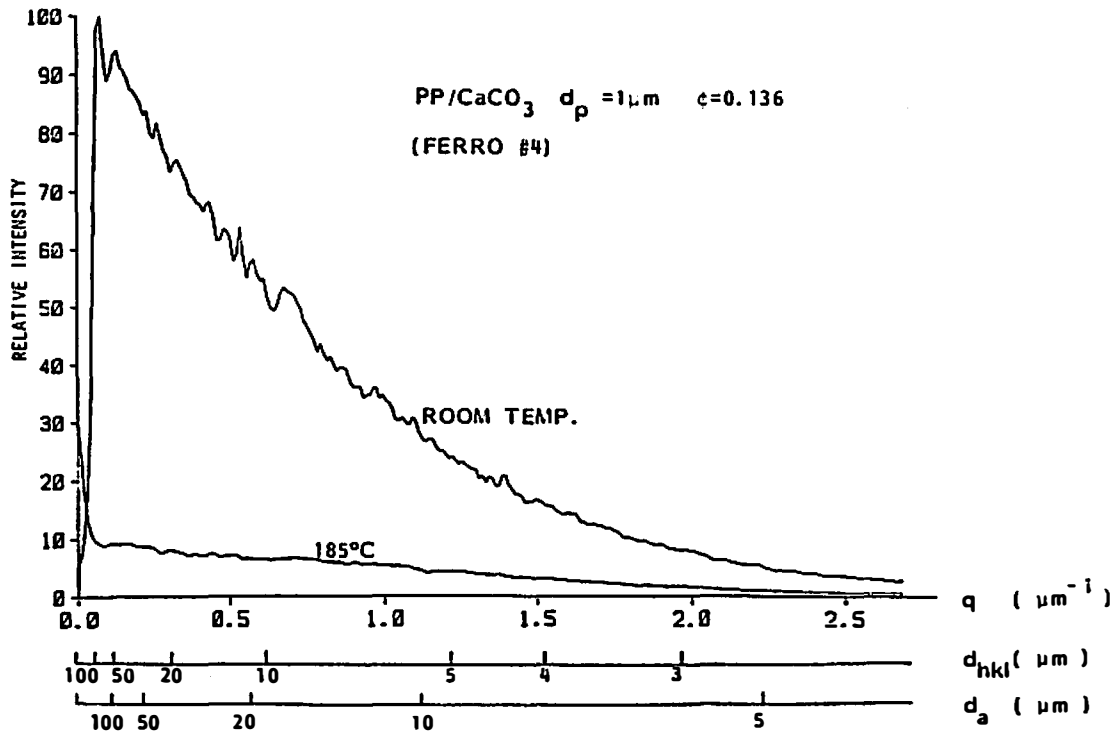

Figure IX-40. Relative intensity profiles for PP/unc. $CaCO_3$ (dp = 1 μm, ϕ = 0.20) at different temperatures.

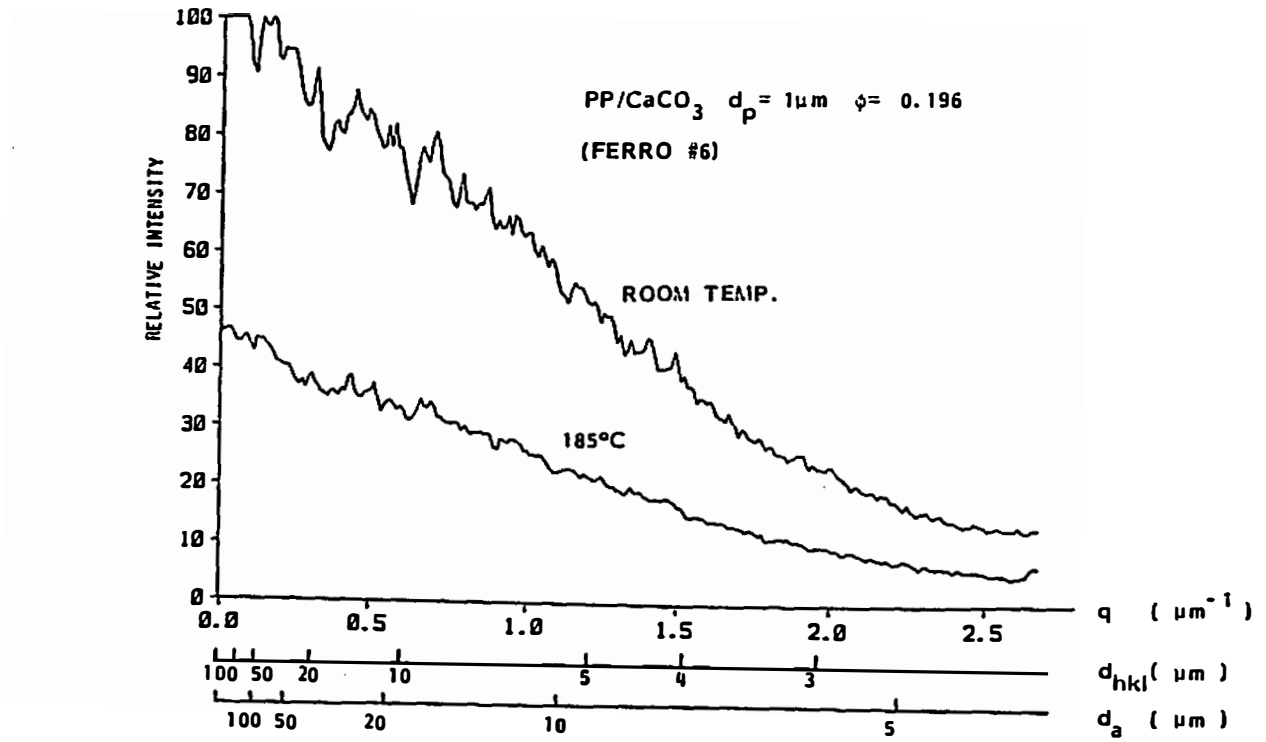

Figure IX-41. Relative intensity profiles for PP/unc. (dp = 1 µm, ϕ = 0.40) at different temperatures.

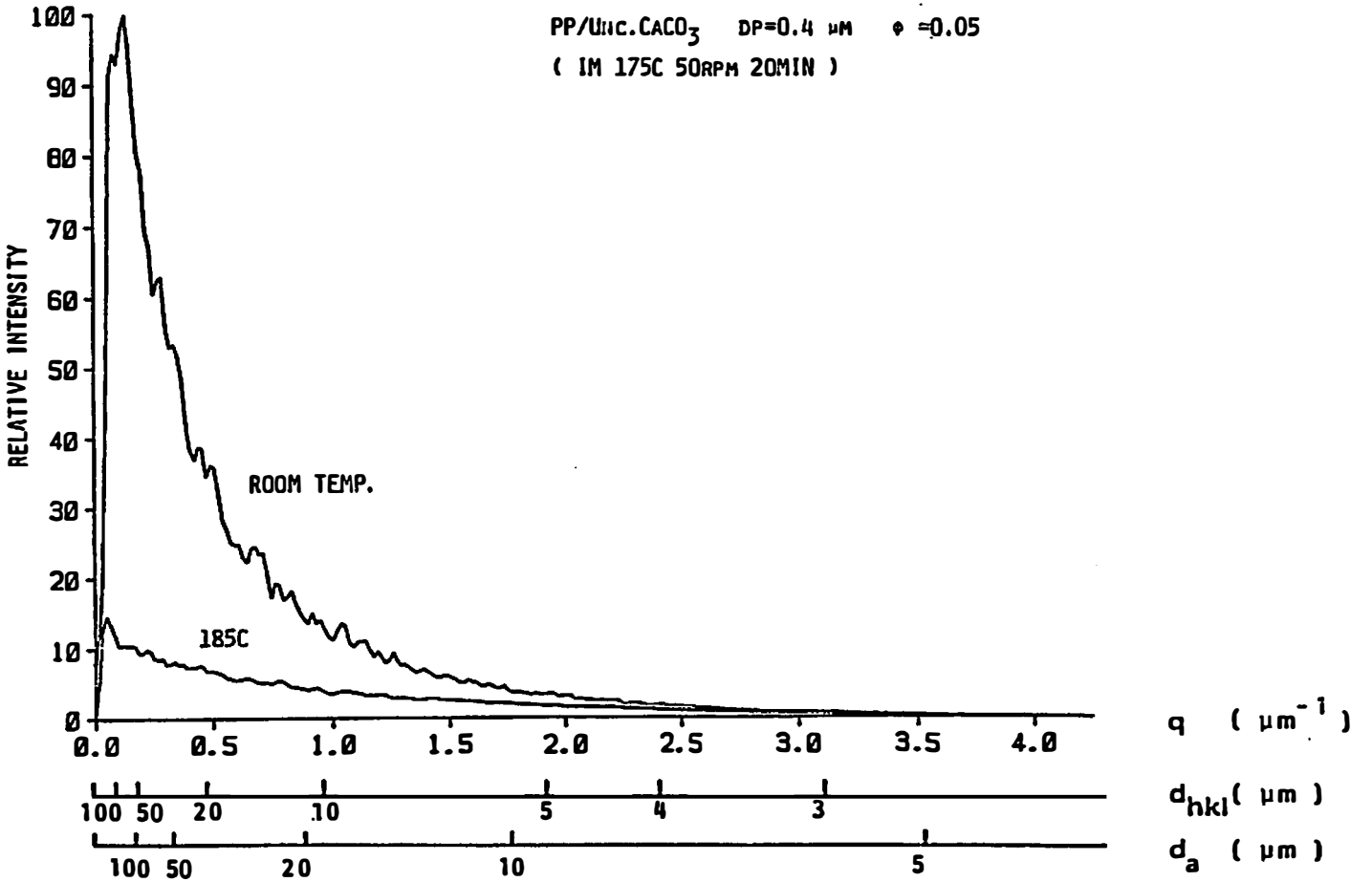

Figure IX-42. Relative intensity profiles for PP/unc. $CaCO_3$ (dp = 0.4 μm, ϕ = 0.05) at different temperatures.

Figure IX-43 gives the effect of particulate size on the relative intensity profiles. Compounds were prepared on a two roll mill. The scattered intensity profile is strongly dependent upon particle size. The sharpness of the decay increases with increasing particulate size which is mentioned in the figure. The smallest particulate size (dp = 0.07 μm) is the exception. Compounds of this particle exhibit abrupt decay-like 17 μm particulate, suggesting the existence of large agglomerates. In the polypropylene matrix, the 0.4 μm calcium carbonate does not show the rapid decay of relative intensity profile. This is different from the behavior of the intensity profiles for the same particles in the polystyrene matrix.

The effect of the volume fraction of filler may be seen in Figures IX-44 and IX-45. The compounds were prepared by Ferro Corporation. The volume fraction varies from 0.084 to 0.196 both in the 3 μm particulate compounds (Figure IX-44) and in the 1 μm particulate compounds (Figure IX-45). The 3 μm uncoated calcium carbonate compounds show a clear effect of volume loading level. As loading level increases, the intensity profile decays more gently. In Figure IX-45 (dp = 1 μm) the effect of the loading level is not clear.

We now turn to the effect of mixing time in an internal mixer. Figures IX-46 and IX-47 show plots for polypropylene/uncoated and coated calcium carbonate compounds, respectively. The nominal particle size is 0.4 μm for uncoated calcium carbonate and 0.5 μm for coated calcium carbonate. The mixing times are 2 minutes and 20 minutes

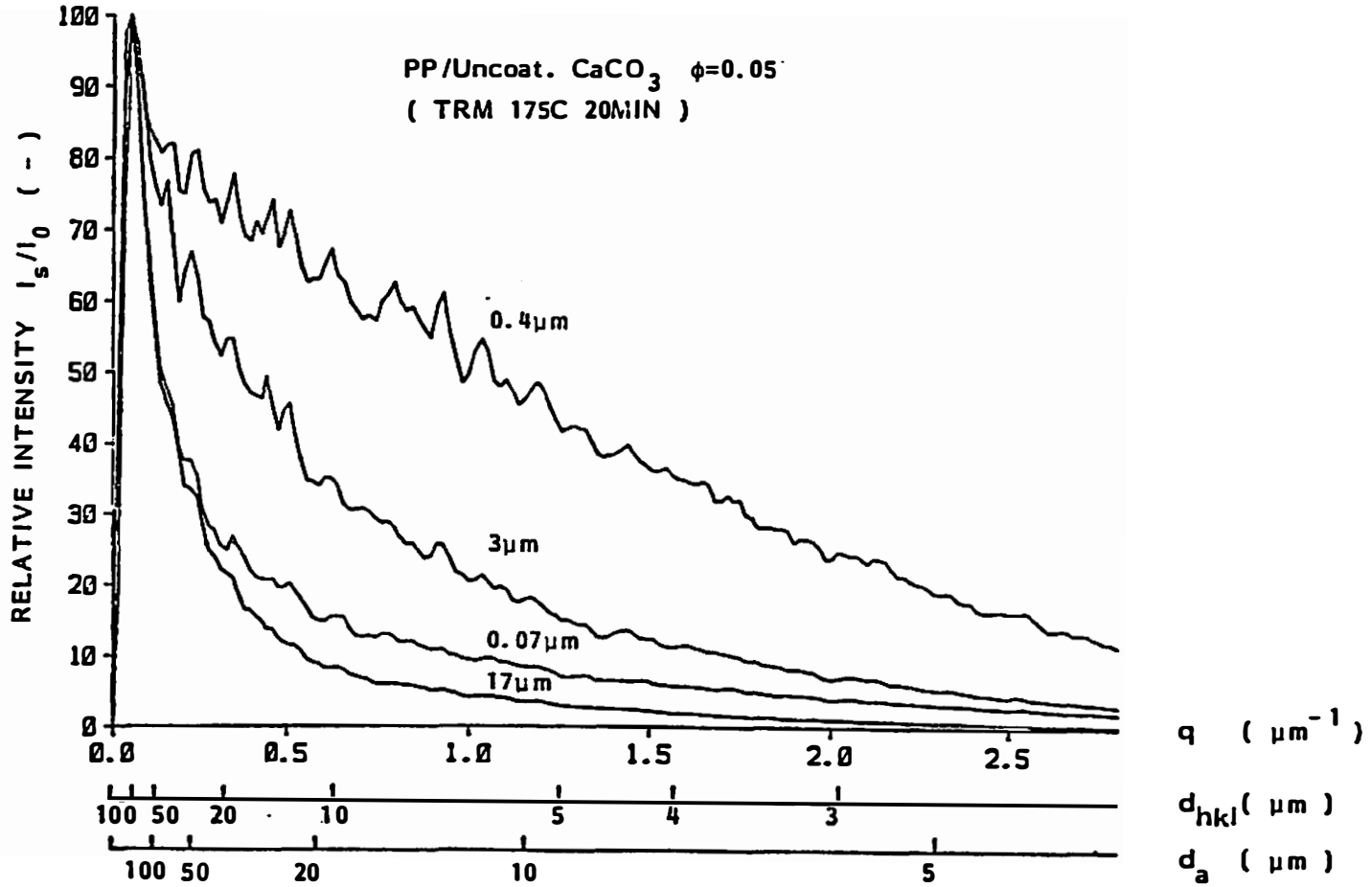

Figure IX-43. Relative intensity profiles for PP/uncoat. $CaCO_3$ (dp = various, ϕ = 0.05).

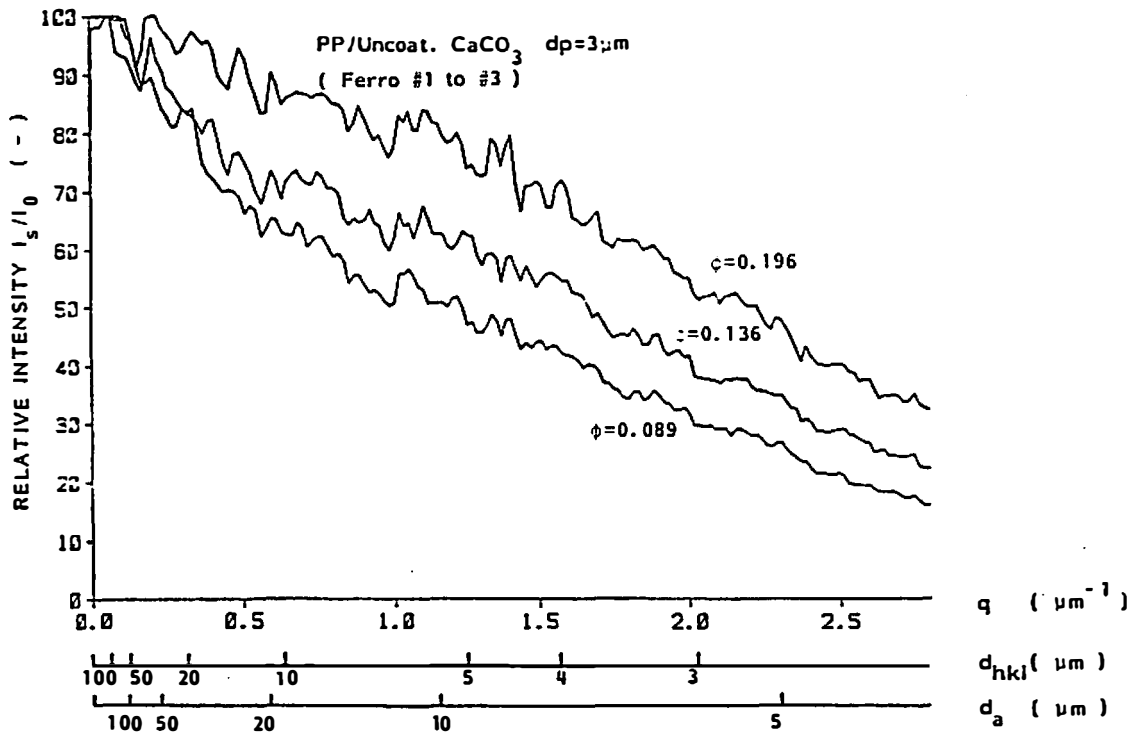

Figure IX-44. Relative intensity profiles for PP/uncoat. $CaCO_3$ (dp = 3 μm, ϕ = various).

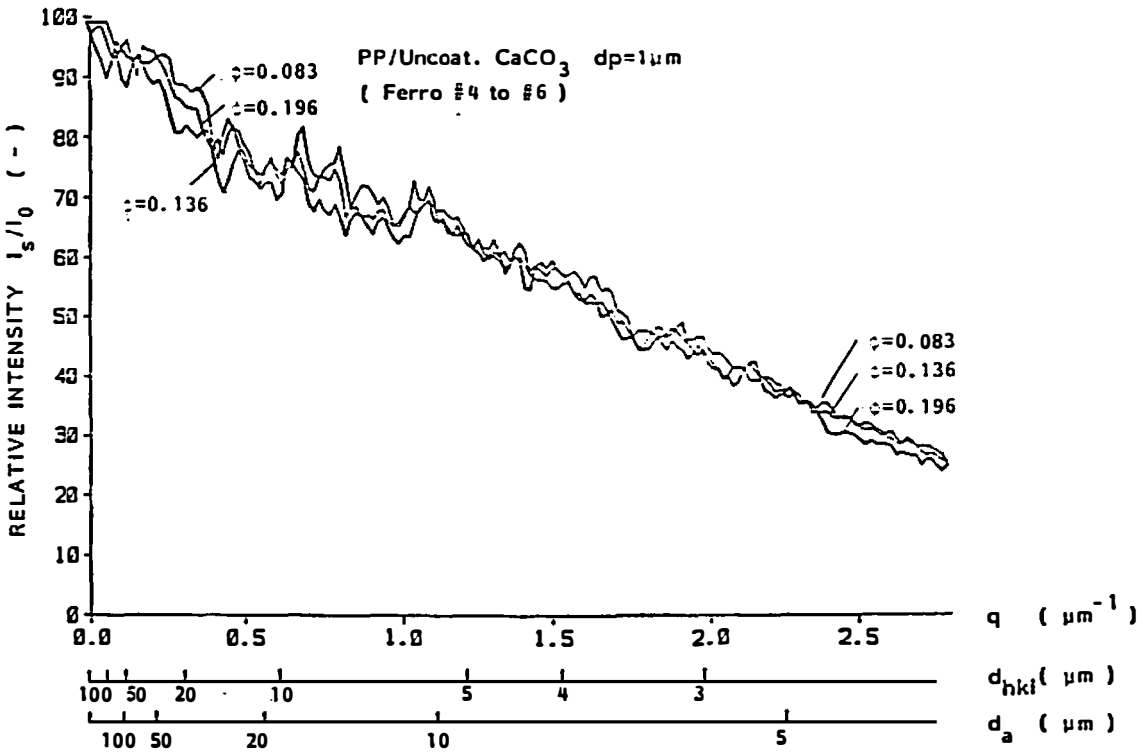

Figure IX-45. Relative intensity profiles for PP/uncoat. $CaCO_3$ (dp = 1 μm, ϕ = various).

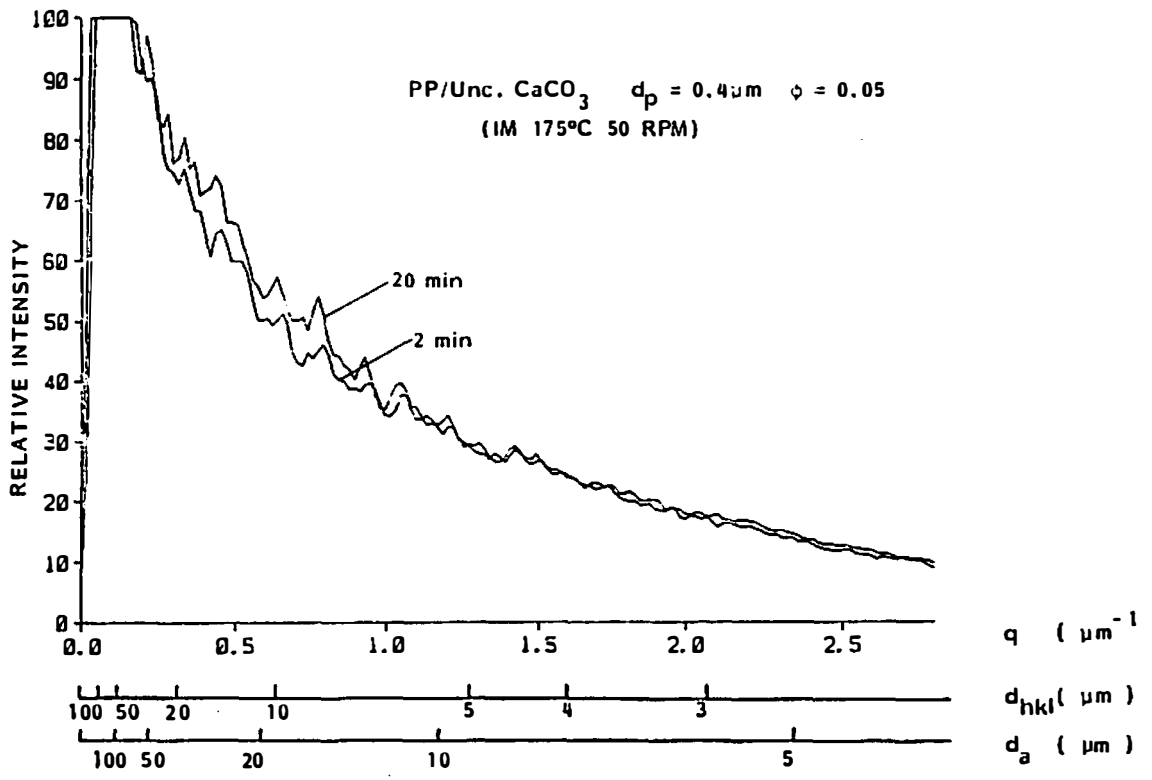

Figure IX-46. Relative intensity profiles for internal mixer prepared PP/unc. $CaCO_3$ (dp = 0.4 µm, ϕ = 0.05).

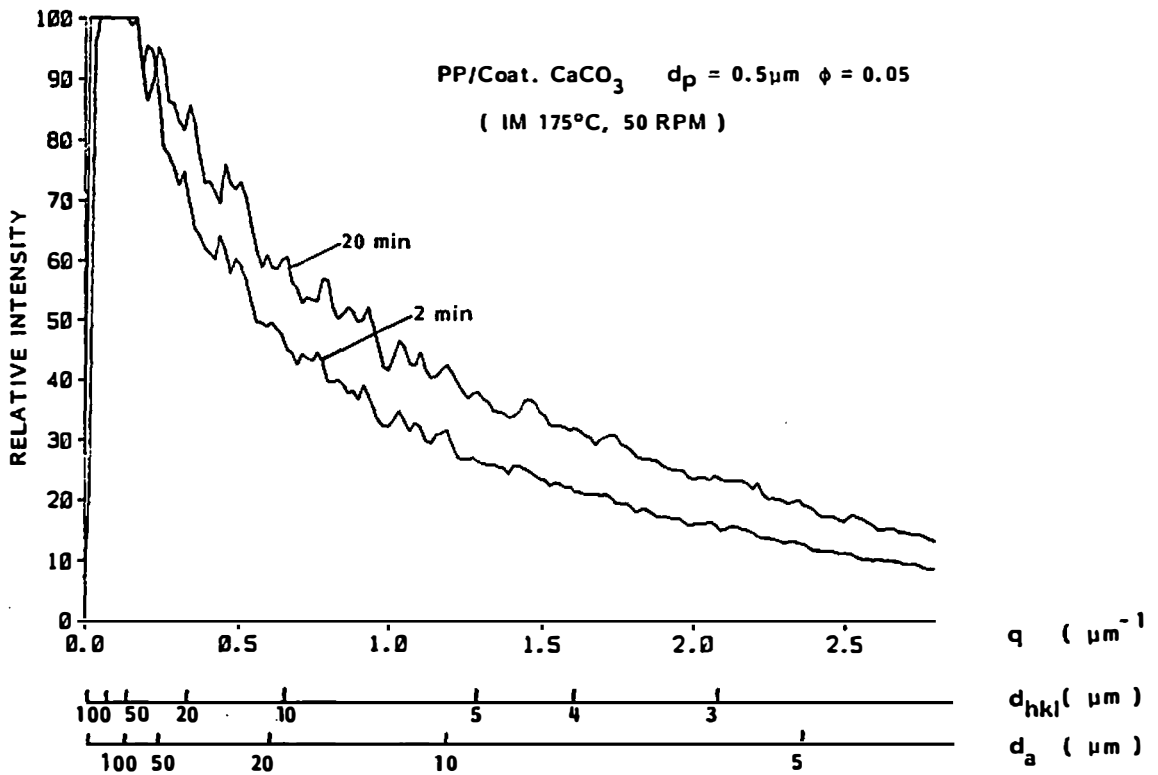

Figure IX-47. Relative intensity profiles for internal mixer prepared PP/coat. $CaCO_3$ (dp = 0.5 μm, ϕ = 0.05).

for both cases. We may observe that the scattering intensity profile becomes broader after long periods of mixing. This suggests the disappearance of large agglomerates as mixing progresses. This is more pronounced for uncoated calcium carbonate compounds.

The relative intensity profiles of the smallest calcium carbonate (dp = 0.07 μm) compounds are given in Figures IX-48 and IX-49. We may observe that the uncoated calcium carbonate compounds (Figure IX-48) exhibit broader intensity profiles than the coated calcium carbonate compounds (Figure IX-49). This indicates that coated calcium carbonate compounds have a greater probability of large agglomerates. The effect of mixing time is not clear in the uncoated clacium carbonate compounds. The intensity profiles of the scattered light get broader after longer periods of mixing in the coated calcium carbonate compounds. This shows that the coated calcium carbonate compounds possess greater numbers of agglomerates after short mixing times. However, the improvement of dispersion is more pronounced than uncoated calcium carbonate compounds.

E.2.b. Discussion. Intensity profiles of the scattered light for various polypropylene/calcium carbonate compounds are replotted as Guinier plots at low angle and Debye-Bueche plots at the greater angle region. The correlation distances were determined. The level of the dispersion is discussed in terms of the correlation distances.

Figures IX-50 and IX-51 present Guinier and Debye-Bueche plots for various polypropylene/uncoated calcium carbonate compounds prepared by a two roll mill. These cover a wide range of particle

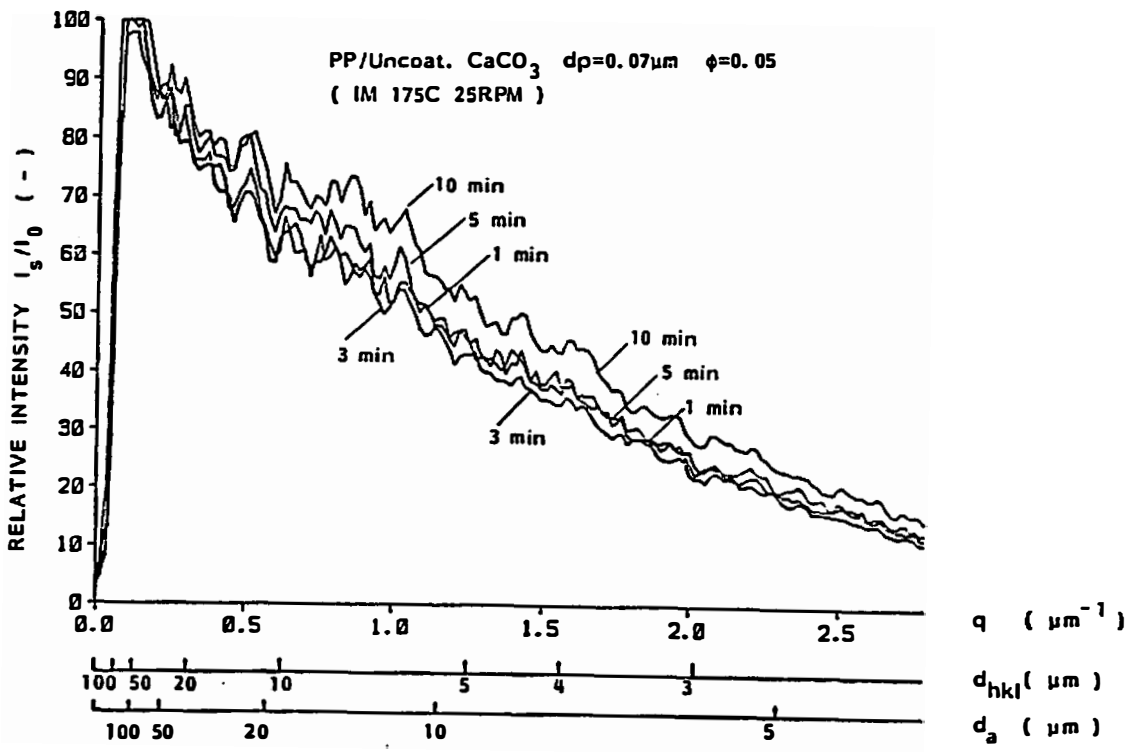

Figure IX-48. Relative intensity profiles for internal mixer prepared PP/uncoat. $CaCO_3$ (dp = 0.07 μm, ϕ = 0.05).

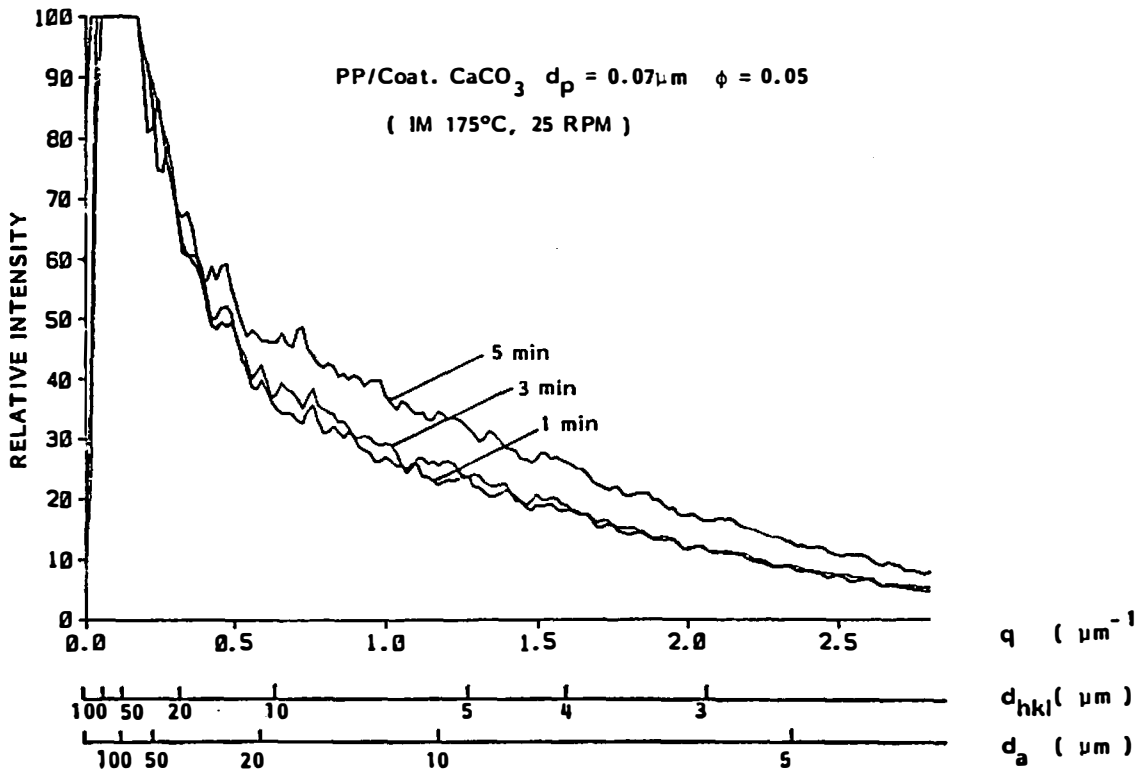

Figure IX-49. Relative intensity profiles for internal mixer prepared PP/coat. $CaCO_3$ (dp = 0.07 μm, ϕ = 0.05).

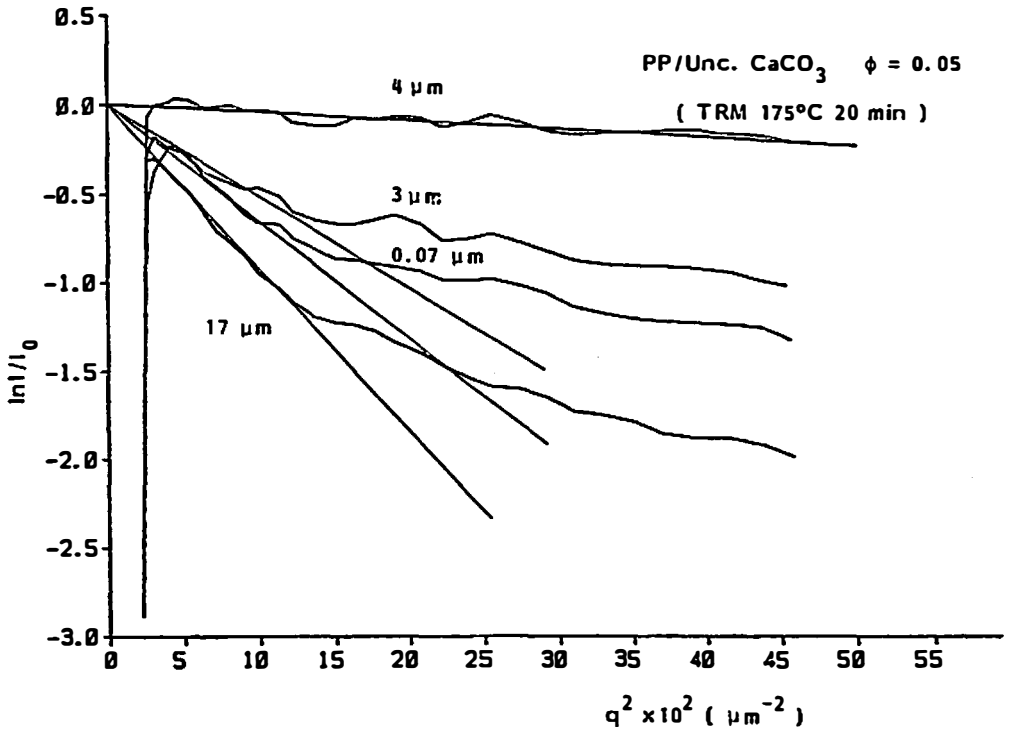

Figure IX-50. Guinier plots for PP/uncoat. $CaCO_3$ (dp = various, ϕ = 0.05).

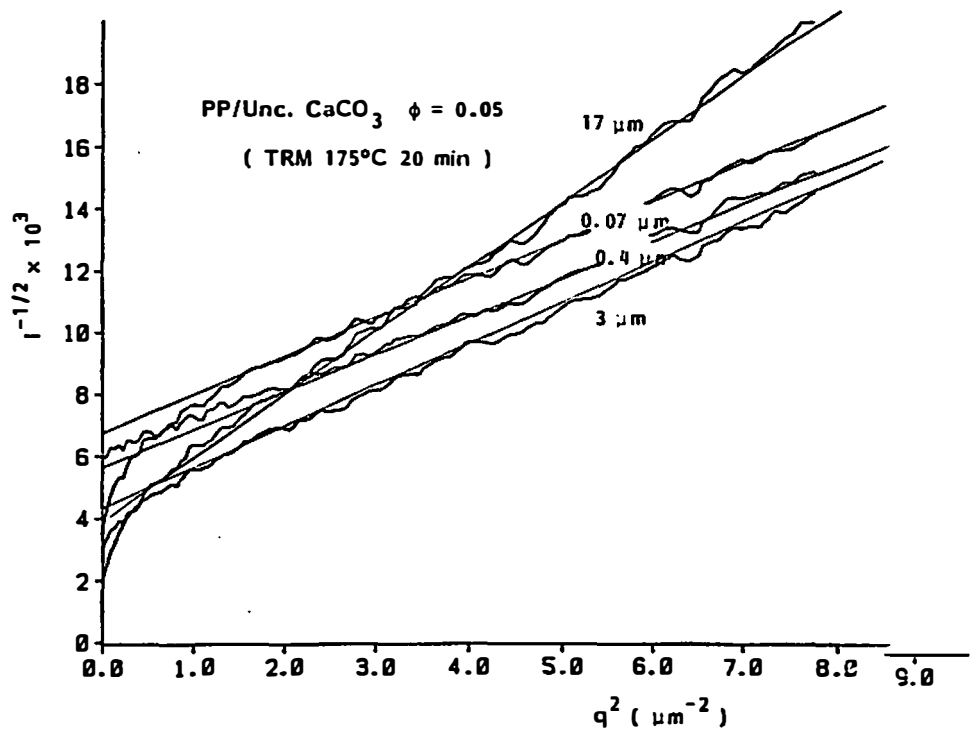

Figure IX-51. Debye-Bueche plots for PP/uncoat. $CaCO_3$ (dp = various, ϕ = 0.05).

sizes, that is, from 0.07 μm to 17 μm. The volume fraction of filler is 0.05 for all compounds. The effect of the size of particulate is clear especially in the Guinier plot (Figure IX-50). The slopes of Guinier plots decrease as the nominal particulate size decreases except for the finest particulate which has a size of 0.07 μm. The smallest particulate has the strongest tendency to form agglomerates in compounds.

The correlation distances determined by the least square method and other quantities are summarized in Table IX-7.

We now determine the effect of the period of mixing for the compounds prepared in an internal mixer. Fine particulates which have nominal average diameters of less than 1 μm were chosen for this study since the existence of agglomerates has been confirmed under optical microscope for such particulates.

First we compare uncoated calcium carbonate compounds which have a nominal particle size of 0.4 μm. Two compounds which have mixing times of 2 minutes and 20 minutes are compared. Figures IX-52 and IX-53 represent Guinier and Debye-Bueche plots. The effect of mixing is clearly seen in a Guinier plot. The slope at low angles decreases as mixing progresses.

Similar plots are obtained for coated calcium carbonate compounds (d_p = 0.5 μm, ϕ = 0.05). Again the effect of the period of mixing is more pronounced in the Guinier region which represents the intensity of the scattered light from large agglomerates (Figure IX-54). The Debye-Bueche plot (Figure IX-55) which

Table IX-7. Parameters Obtained from Guinier and Debye-Bueche Plots for Two Roll Mill Prepared PP/Unc. $CaCO_3$ Compounds with Various Particle Size

Surface Coating	Nominal Particle Size dp (μm)	Volume Fraction ϕ (-)	Mixing Time (Min.)	Guinier				Debye-Bueche			
				q (μm^{-1})	a_2 (μm)	$\overline{R}_g$ (μm)	$\overline{d}$ (μm)	q (μm^{-1})	a_1 (μm)	$\overline{R}_g$ (μm)	$\overline{d}$ (μm)
No	17	0.05	20	0.17-0.31	6.09	5.27	13.6	1.53-2.80	0.733	1.80	4.64
No	3	0.05	20	0.17-0.31	4.63	4.01	10.4	1.53-2.80	0.558	1.44	3.72
No	0.4	0.05	20	0.17-0.31	1.37	1.19	3.06	1.53-2.80	0.464	1.14	2.93
No	0.07	0.05	20	0.17-0.31	4.99	4.32	11.2	1.53-2.80	0.432	1.06	2.73

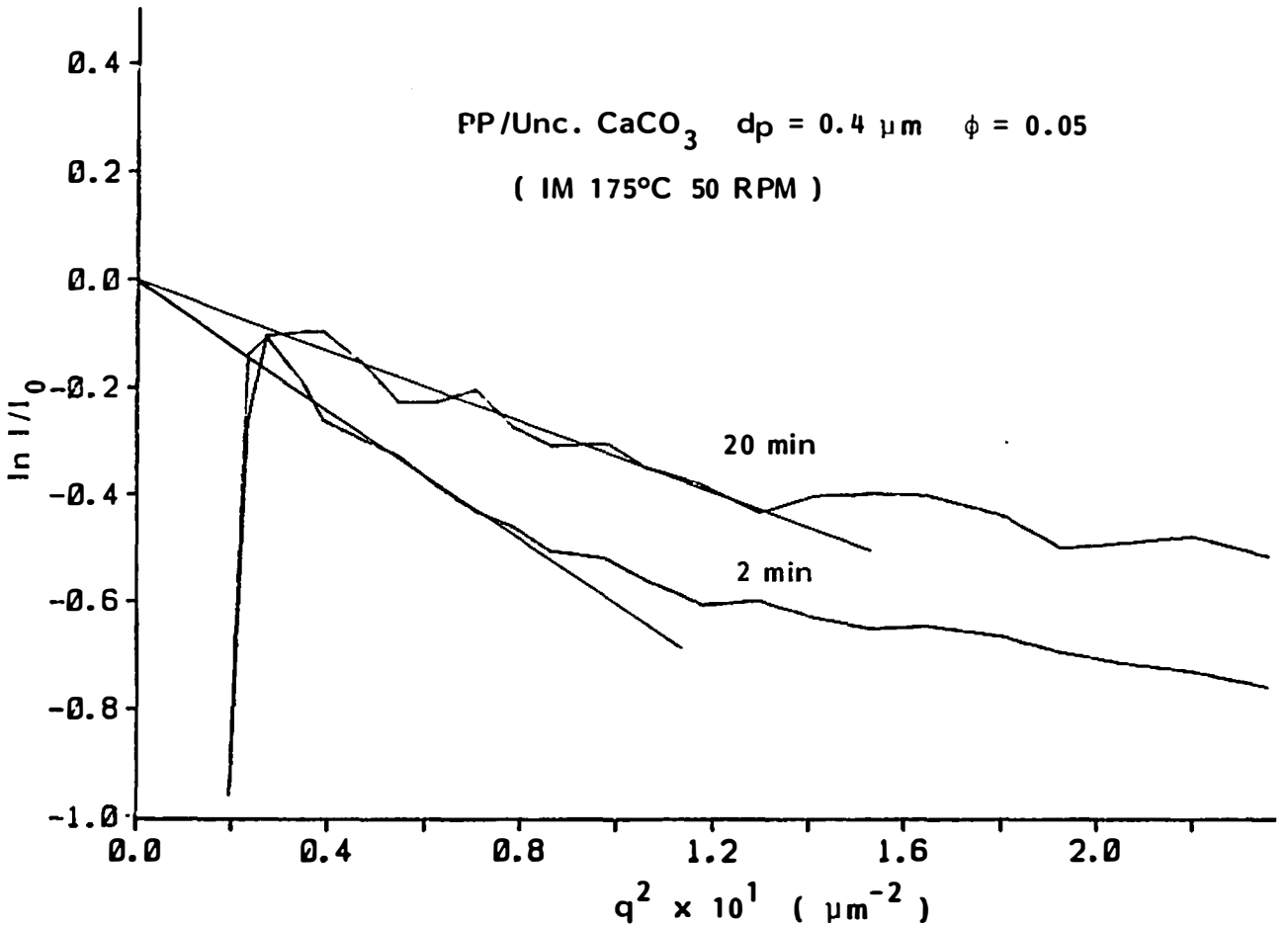

Figure IX-52. Guinier Plots for internal mixer prepared PP/unc. $CaCO_3$ (dp = 0.4 µm, ϕ = 0.05).

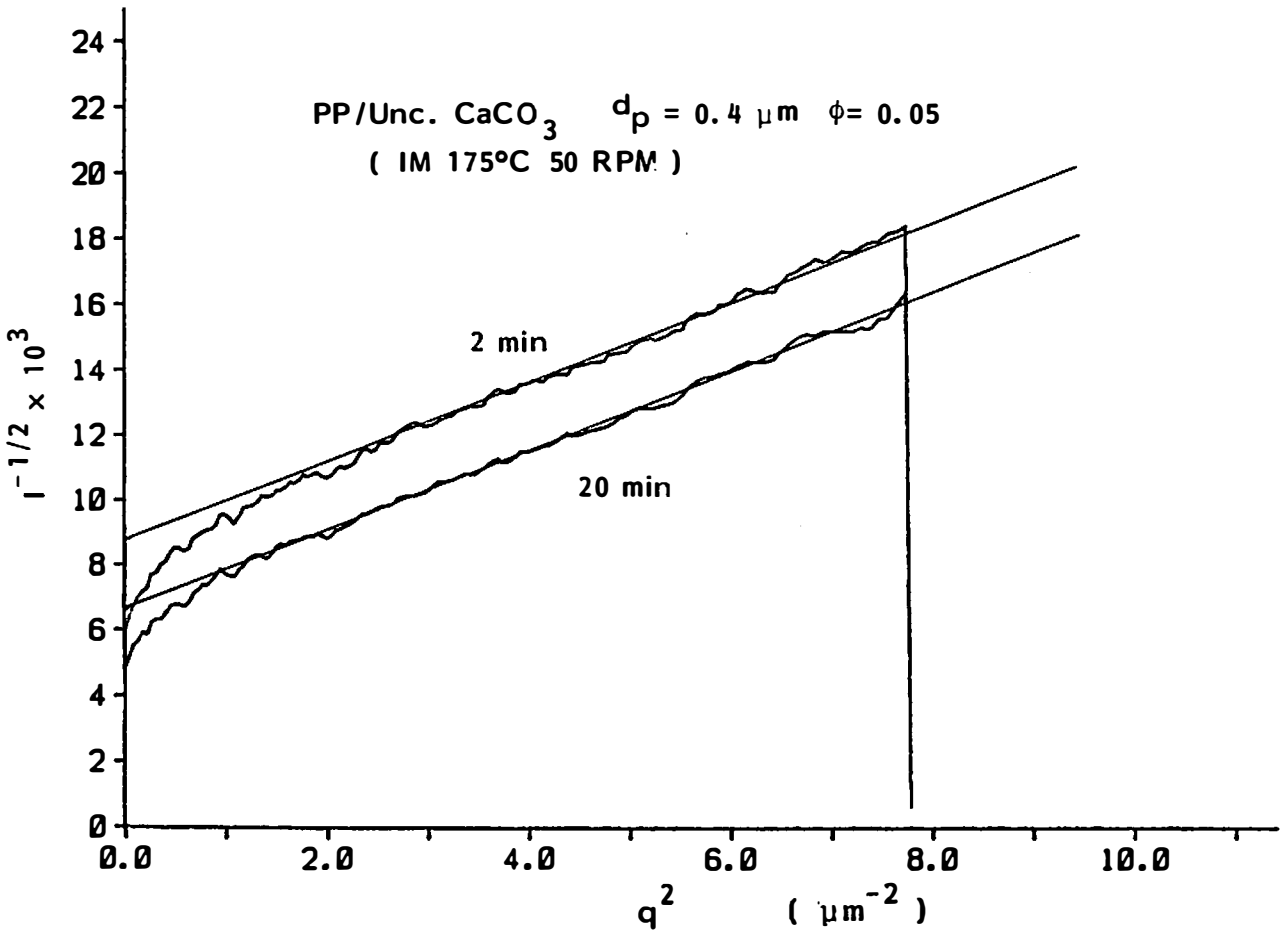

Figure IX-53. Debye-Bueche plots for internal mixer prepared PP/unc. $CaCO_3$ (dp = 0.4 µm, ϕ = 0.05).

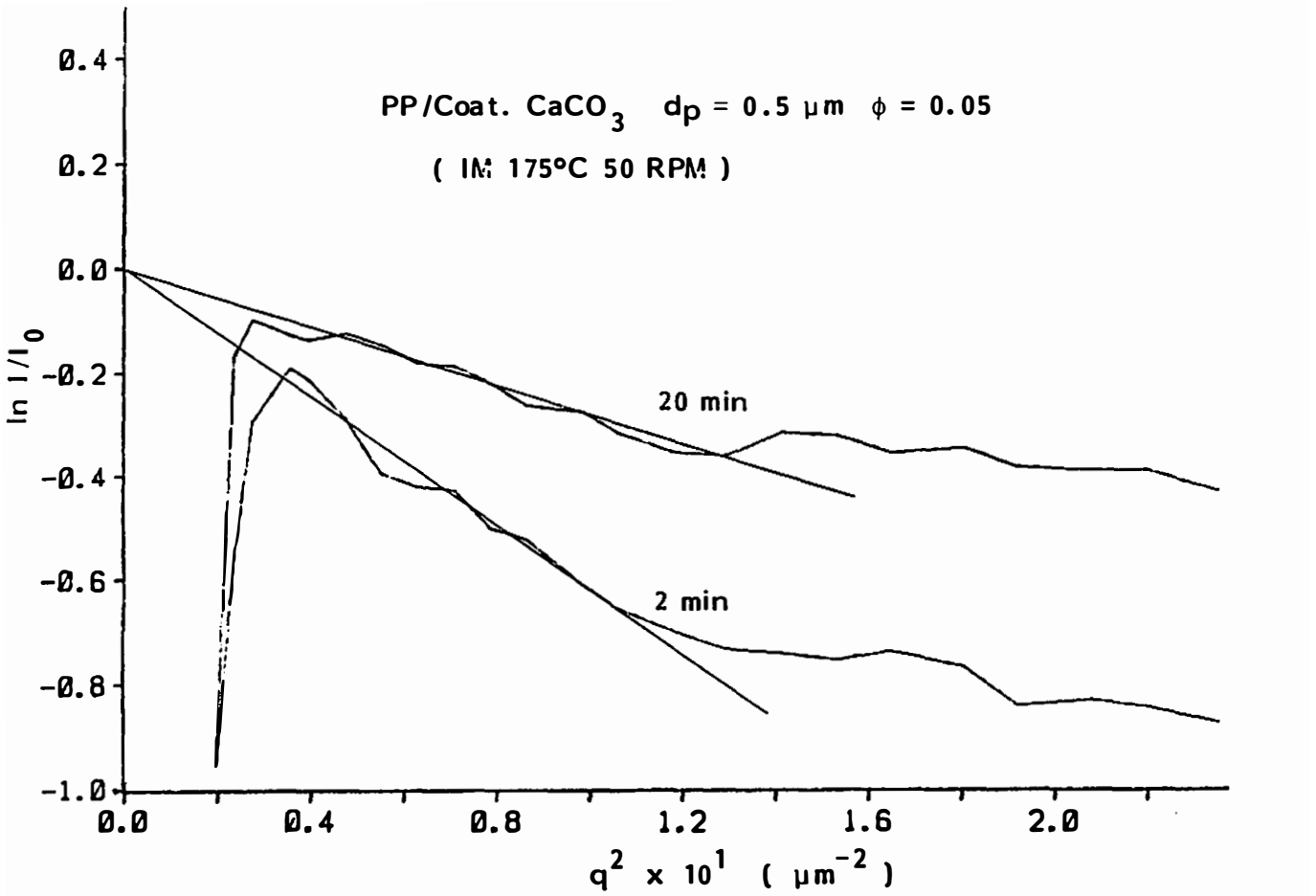

Figure IX-54. Guinier Plots for internal mixer prepared PP/coat. $CaCO_3$ (dp = 0.5 µm, ϕ = 0.05).

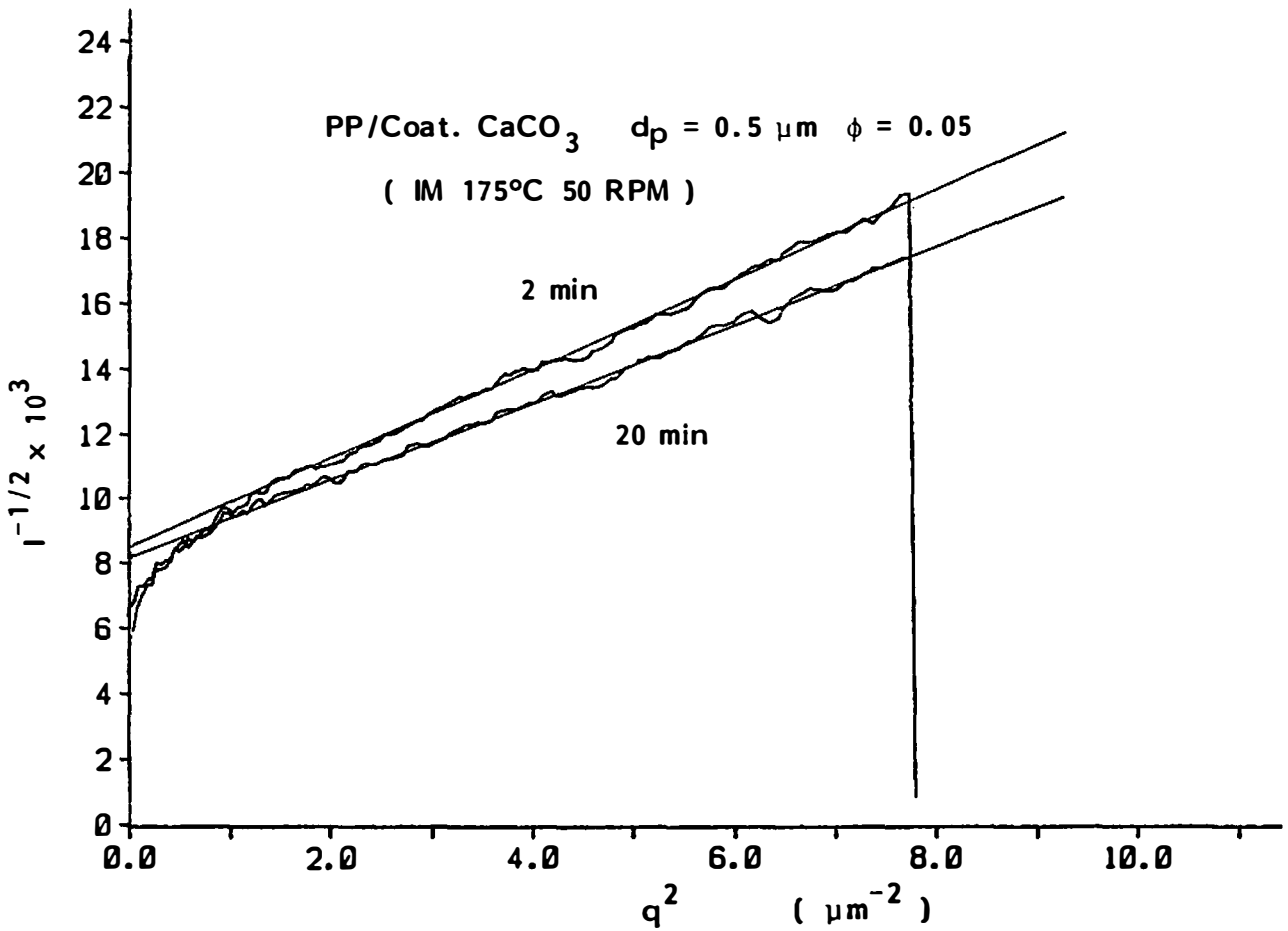

Figure IX-55. Debye-Bueche plots for internal mixer prepared PP/coat. $CaCO_3$ (dp = 0.5 μm, φ = 0.05).

represent greater angle region does not show a clear effect of mixing period.

Correlation distances and other quantities obtained from Guinier and Debye-Bueche plots for these compounds are summarized in Table IX-8. Guinier correlation distances decrease with mixing time. A marked decrease is observed in coated calcium carbonate compounds. We note that the number of agglomerates (or scatterers) decreases more rapidly with increasing size; in other words, distribution of agglomerate size decay more rapidly as the size increases, when the correlation distance is small. Correlation distances in the Debye-Bueche plots are very close to the nominal particulate sizes and improvement of dispersion is not clear in this region.

Correlation distances are plotted as a function of the period of mixing in Figures IX-56 and IX-57.

The effect of mixing period has also been determined for the finest particulate compounds (dp = 0.07 μm). Guinier and Debye-Bueche plots were prepared for the uncoated (Figures IX-58 and IX-59) and coated (Figures IX-60 and IX-61) particles.

Table IX-9 summarizes the Debye-Bueche and Guinier correlation distances for these compounds.

Figures IX-58 and IX-59 plot Debye-Bueche and Guinier correlation distances as a function of mixing time. The change of agglomerate size distribution is clear in the surface treated calcium carbonate compounds during mixing.

Table IX-8. Parameters Obtained from Guinier and Debye-Bueche Plots for Internal Mixer Prepared $PP/CaCO_3$ Compounds (RPM = 50)

Surface Coating	Nominal Particle Size dp (μm)	Volume Fraction ϕ (-)	Mixing Time (Min.)	Guinier q (μm^{-1})	Guinier a_2 (μm)	Guinier $\bar{R}_g$ (μm)	Guinier $\bar{d}$ (μm)	Debye-Bueche q (μm^{-1})	Debye-Bueche a_1 (μm)	Debye-Bueche $\bar{R}_g$ (μm)	Debye-Bueche $\bar{d}$ (μm)
No	0.4	0.05	2	0.17-0.31	4.62	4.00	10.3	1.53-2.80	0.383	0.938	2.42
No	0.4	0.05	20	0.17-0.31	3.33	2.86	7.38	1.53-2.80	0.421	1.03	2.66
Yes	0.5	0.05	2	0.17-0.31	4.60	3.98	10.3	1.53-2.80	0.404	0.990	2.56
Yes	0.5	0.05	20	0.17-0.31	3.07	2.66	6.87	1.53-2.80	0.379	0.928	2.40

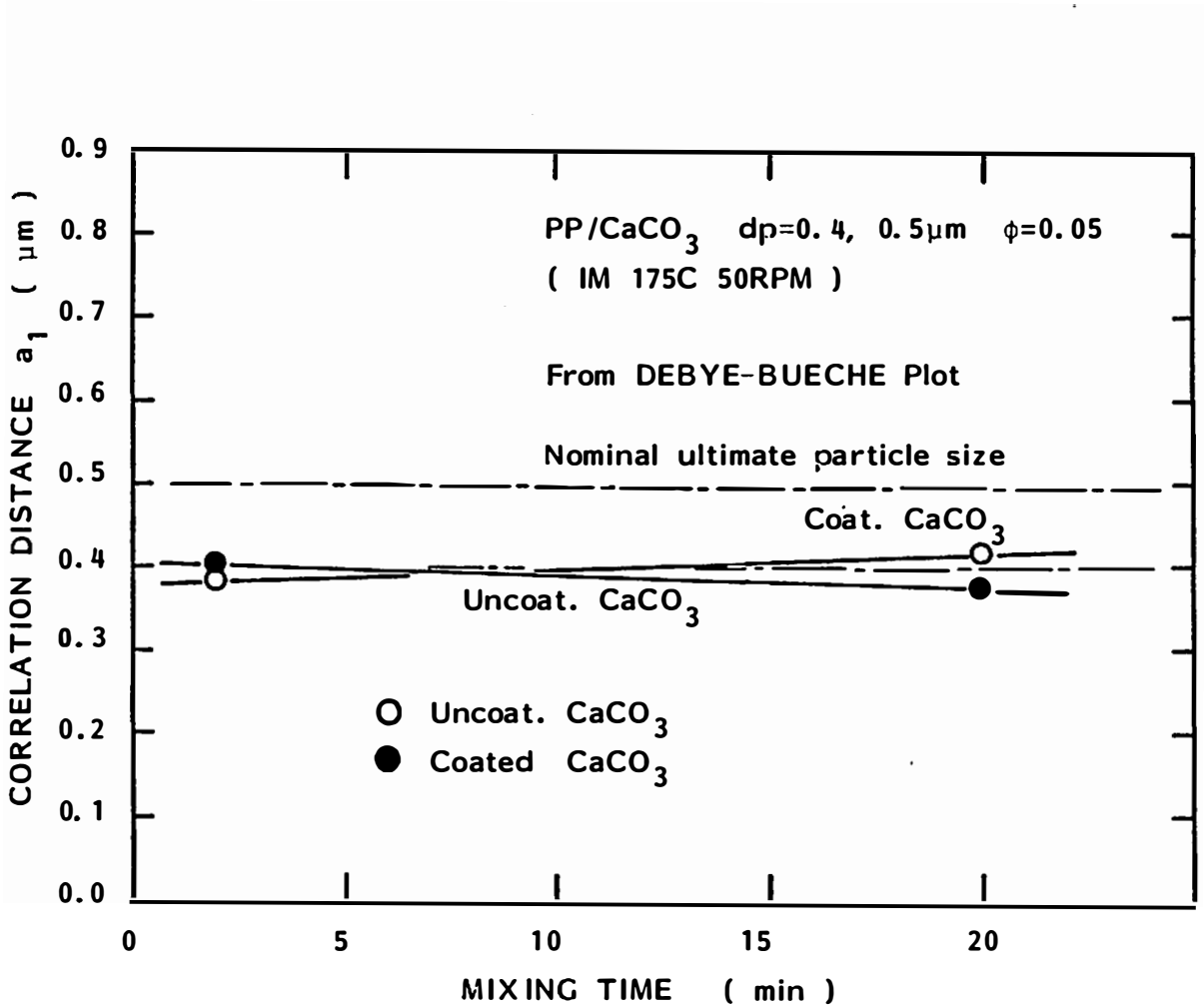

Figure IX-56. Correlation distances a_1 as a function of mixing time for PP/$CaCO_3$ (dp = 0.4, 0.5 μm).

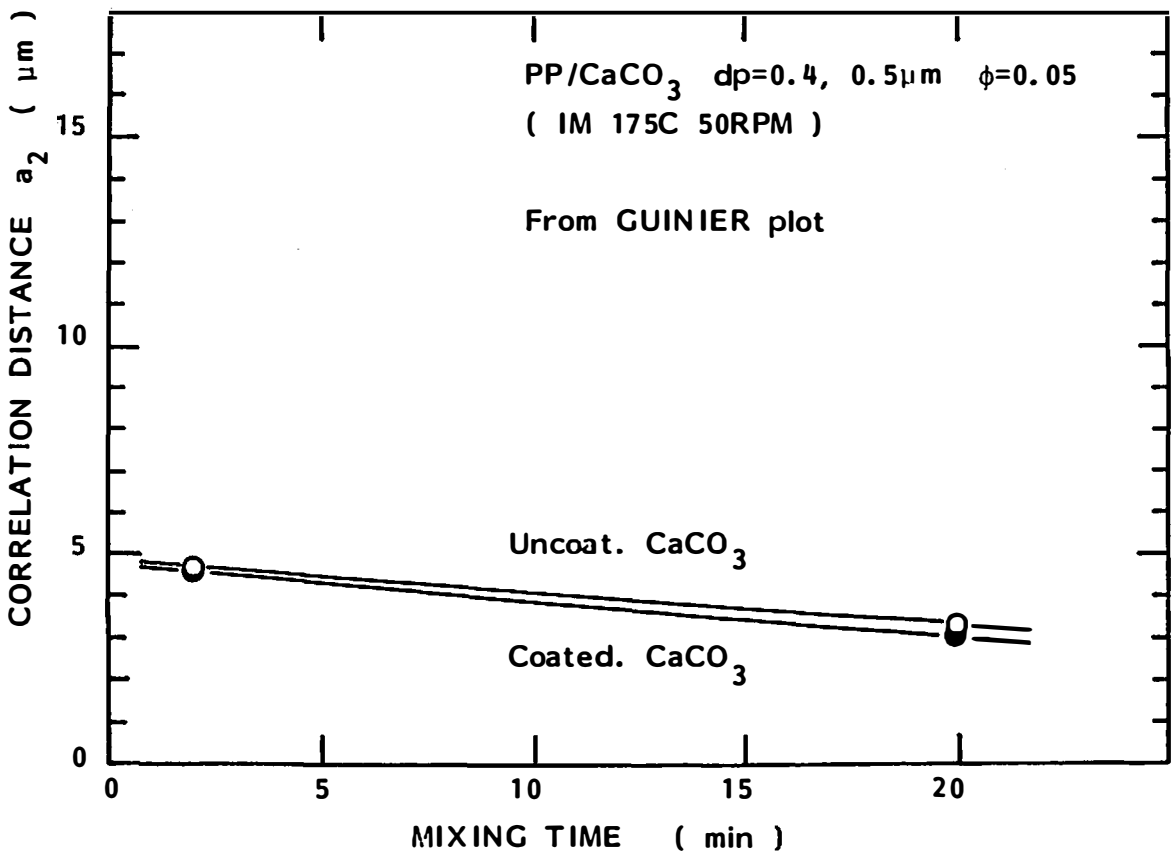

Figure IX-57. Correlation distances a_2 as a function of mixing time for $PP/CaCO_3$ (dp = 0.4, 0.5 μm).

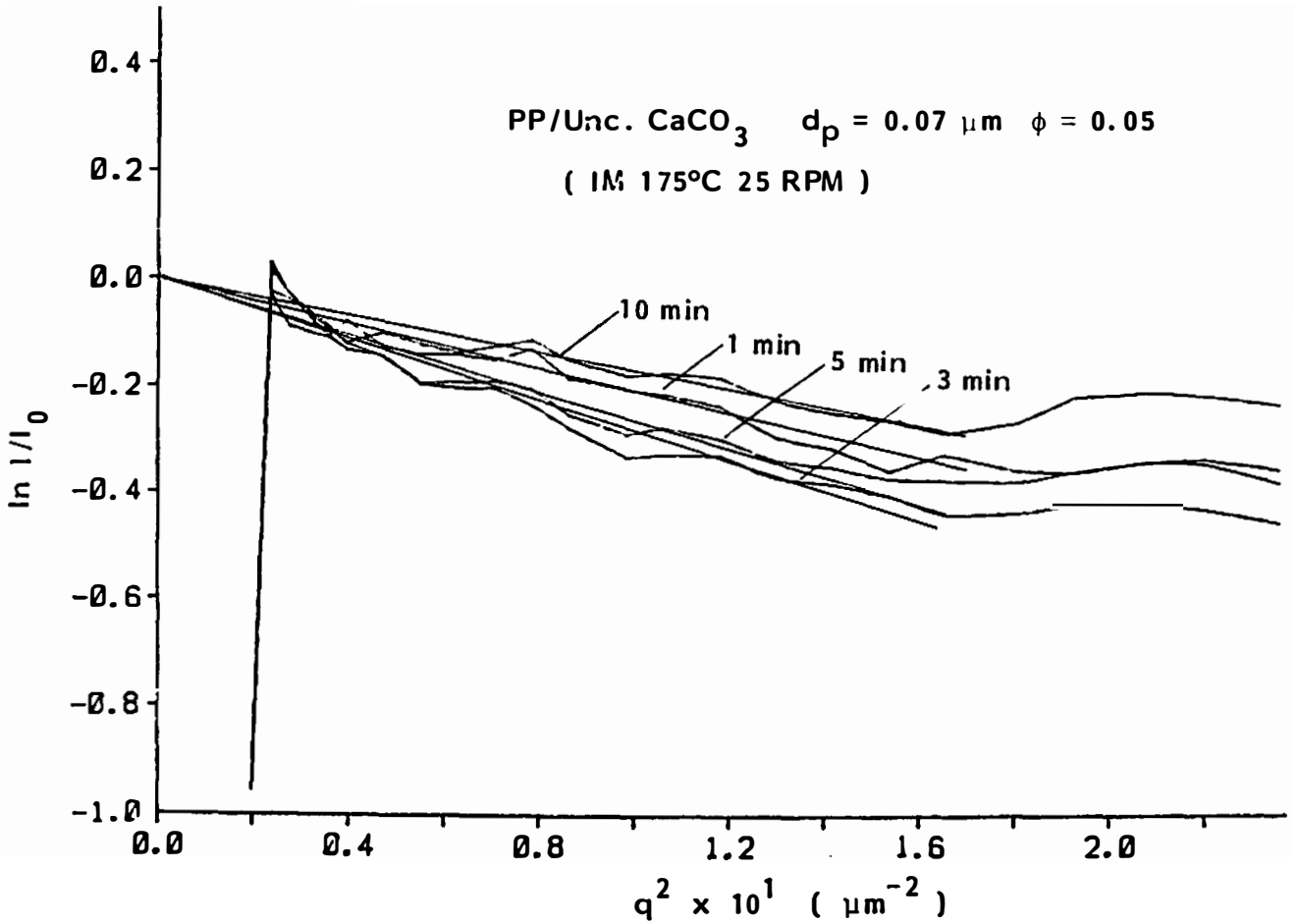

Figure IX-58. Guinier plots for internal mixer prepared PP/unc. $CaCO_3$ (dp = 0.07 µm, ϕ = 0.05).

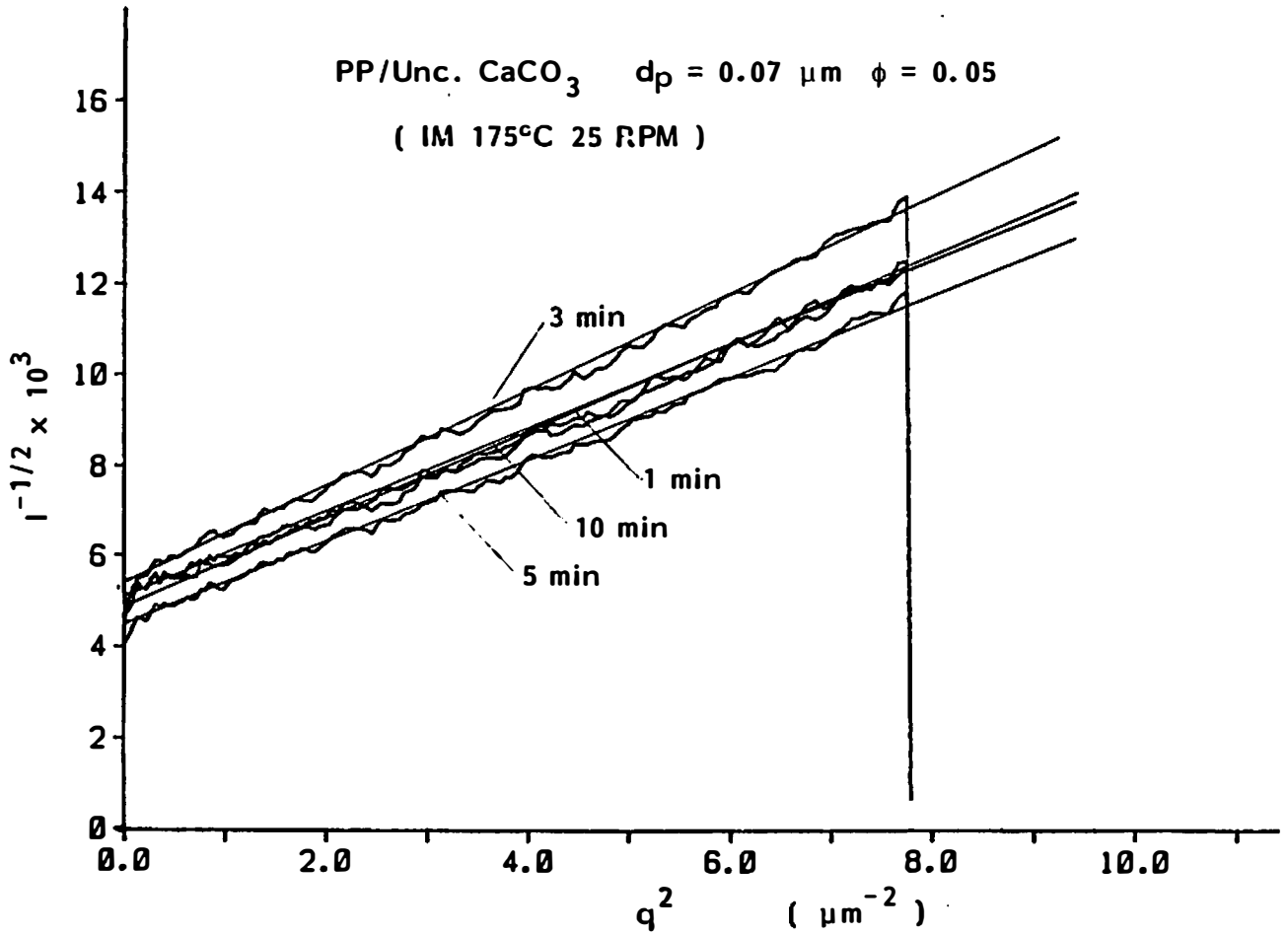

Figure IX-59. Debye-Bueche plots for internal mixer prepared PP/unc. $CaCO_3$ (dp = 0.07 µm, ϕ = 0.05).

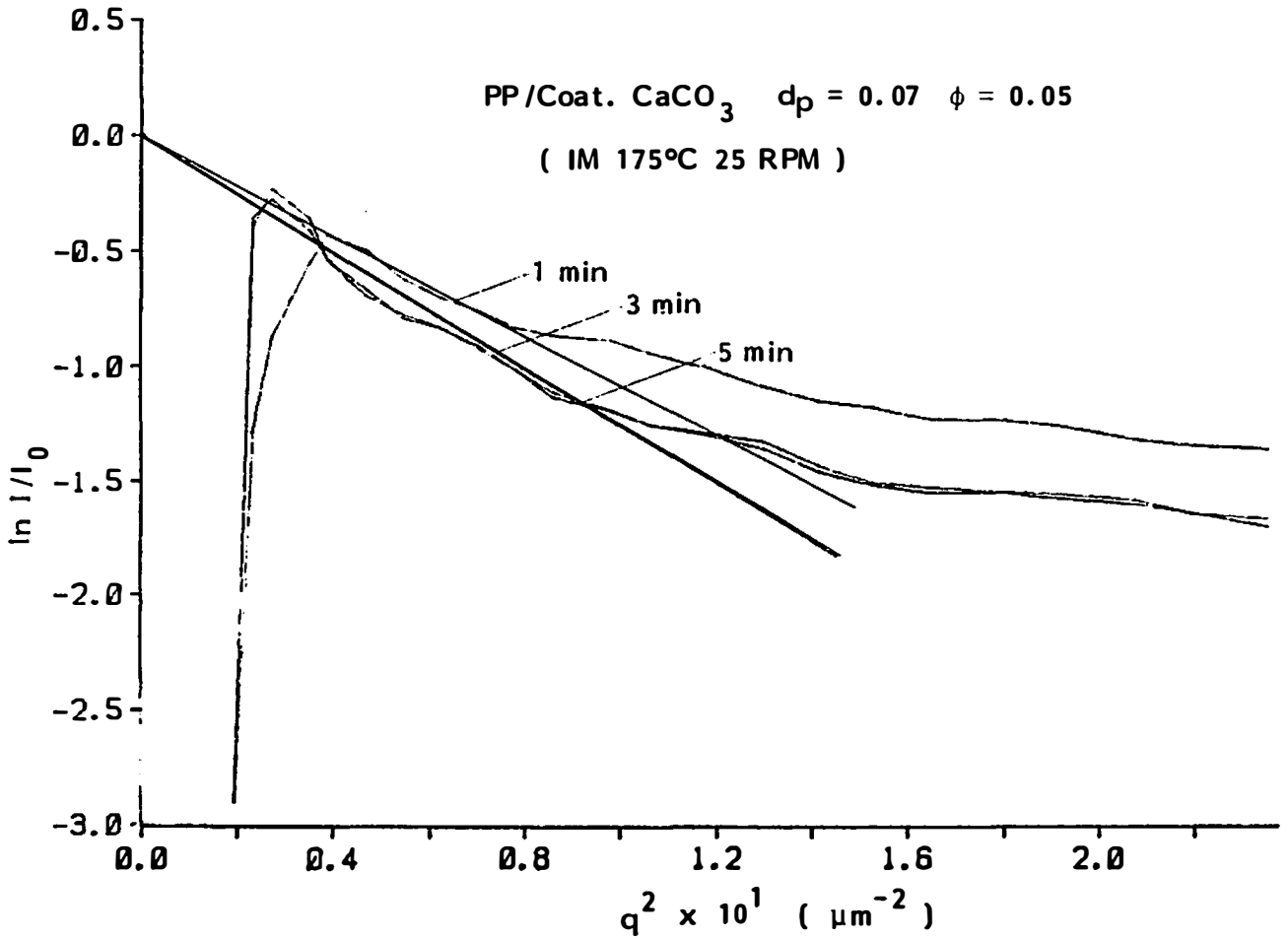

Figure IX-60. Guinier plots for internal mixer prepared PP/coat. $CaCO_3$ (dp = 0.07 μm, ϕ = 0.05).

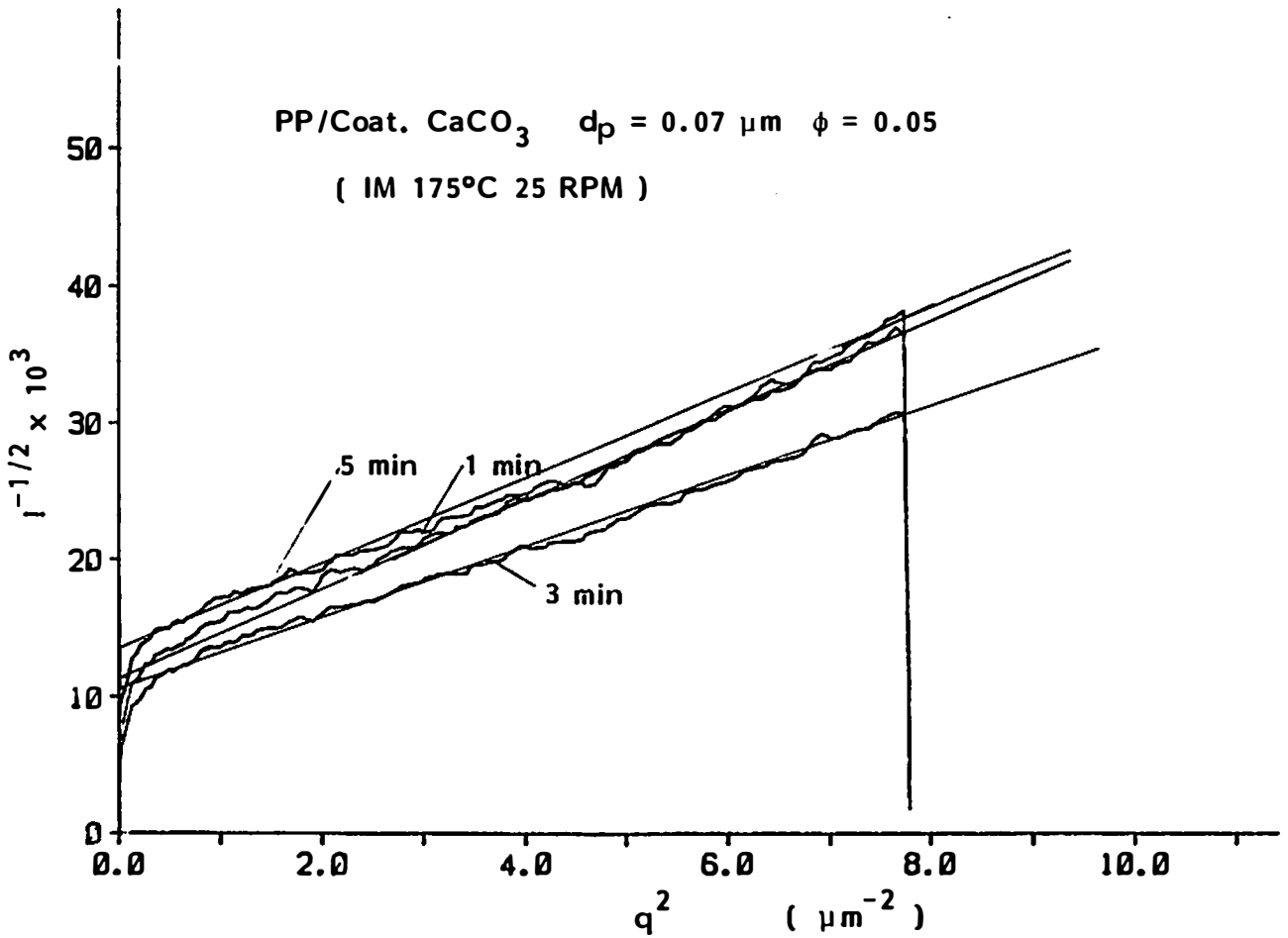

Figure IX-61. Debye=Bueche plots for internal mixer prepared PP/coat. $CaCO_3$ (dp = 0.07 µm, ϕ = 0.05).

Table IX-9. Parameters Obtained from Guinier and Debye-Bueche Plots for Internal Mixer Prepared $PP/CaCO_3$ Compounds (RPM = 25)

Surface Coating	Nominal Particle Size dp (μm)	Volume Fraction ϕ (-)	Mixing Time (Min.)	Guinier q (μm^{-1})	Guinier a_2 (μm)	Guinier $\bar{R}_g$ (μm)	Guinier $\bar{d}$ (μm)	Debye-Bueche q (μm^{-1})	Debye-Bueche a_1 (μm)	Debye-Bueche $\bar{R}_g$ (μm)	Debye-Bueche $\bar{d}$ (μm)
No	0.07	0.05	1	0.17-0.43	2.71	2.35	6.06	0.68-2.80	0.429	1.05	2.71
No	0.07	0.05	3	0.17-0.43	3.15	2.73	7.04	0.68-2.80	0.444	1.09	2.81
No	0.07	0.05	5	0.17-0.43	2.99	2.59	6.69	0.68-2.80	0.453	1.11	2.87
No	0.07	0.05	10	0.17-0.43	2.43	2.10	5.43	0.68-2.80	0.436	1.07	2.76
Yes	0.07	0.05	1	0.17-0.34	6.59	5.71	14.8	1.53-2.80	0.549	1.34	3.47
Yes	0.07	0.07	3	0.17-0.34	6.58	5.70	14.7	1.53-2.80	0.495	1.21	3.13
Yes	0.07	0.07	5	0.17-0.34	6.04	5.23	13.7	1.53-2.80	0.472	1.17	2.99

We may compare correlation distances of polypropylene compounds (Figures IX-62 and IX-63) with polystyrene compounds (Figures IX-37 and IX-38, pp. 291, 293). Decreases of the correlation distances are more significant in the polystyrene compounds. The Debye-Bueche correlation distance of polystyrene compounds (Figure IX-38) approach the nominal average particle size of 0.07 μm more rapidly than polypropylene compounds (Figure IX-63). These may be due to the high viscosity of the polystyrene matrix during the mixing.

The correlation distances were determined by the same methods for some high loading level compounds. Volume fraction varies from 0.084 to 0.196. These correspond to 20 Wt % to 40 Wt %. These were prepared by Ferro Corporation.

Table IX-10 summarizes the correlation distances of high loading level compounds. These are plotted as a function of the volume fraction of filler in Figures IX-64 and IX-65.

Both Guinier and Debye-Bueche correlation distances tend to decrease with increasing volume fraction of filler. This is due to the decreasing inter-particulate distance at high loading level. Abnormal behavior if found for a compound of 1 μm particulate at a volume fraction of 0.196 (closed triangle symbol). The correlation distances are too large compared to the others both in Debye-Bueche and Guiniere region. Agglomerates have been found only for this compound under the optical microscope. The existence of large agglomerates is detected by unusually large correlation distances. This is found in the Guinier correlation distance (Figure IX-63).

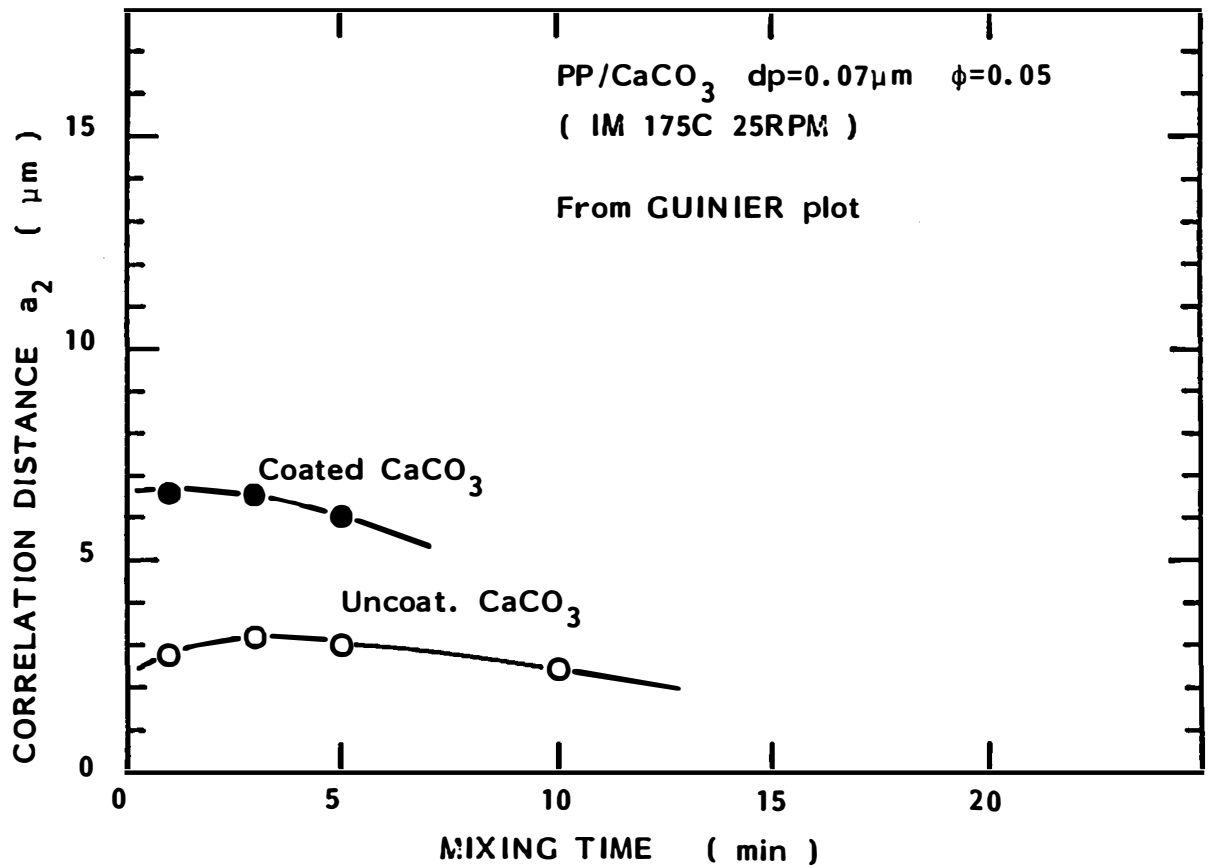

Figure IX-62. Correlation distance a_2 as a function of mixing time for $PP/CaCO_3$ (dp = 0.07 μm).

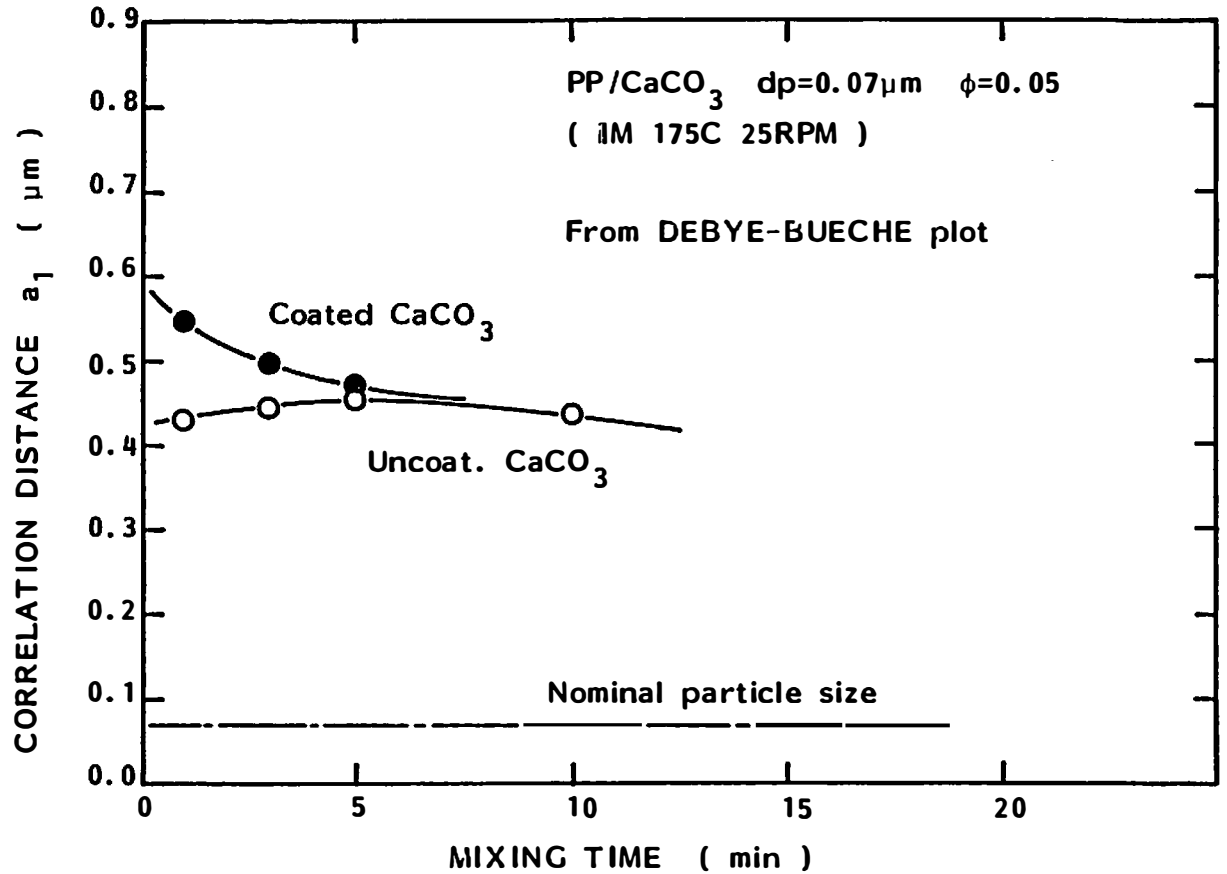

Figure IX-63. Correlation distance a_1 as a function of mixing time for $PP/CaCO_3$ (dp = 0.07 μm).

Table IX-10. Parameters Obtained from Guinier and Debye-Bueche Plots for PP/$CaCO_3$ Compounds with High Volume Fractions of Filler . (Prepared by Ferro.)

Surface Coated	Nominal Particle Size dp (μm)	Volume Fraction ϕ (-)	Mixing Time (Min.)	Guinier				Debye-Bueche			
				q (μm^{-1})	a_2 (μm)	$\bar{R}_g$ (μm)	$\bar{d}$ (μm)	q (μm^{-1})	a_1 (μm)	$\bar{R}_g$ (μm)	$\bar{d}$ (μm)
No	3	0.084	-	0.17-0.68	1.61	1.39	3.58	1.53-2.80	0.385	0.943	2.43
No	3	0.136	-	0.17-0.68	1.30	1.13	2.91	1.53-2.80	0.359	0.879	2.27
No	3	0.196	-	0.17-0.68	0.838	0.726	1.87	1.53-2.80	0.320	0.784	2.02
Yes	1	0.084	-	0.17-0.68	1.36	1.18	3.04	1.53-2.80	0.341	0.835	2.16
Yes	1	0.136	-	0.17-0.68	1.24	1.07	2.77	1.53-2.80	0.325	0.796	2.06
Yes	1	0.196	-	0.17-0.68	1.26	1.09	2.82	1.53-2.80	0.318	0.779	2.01

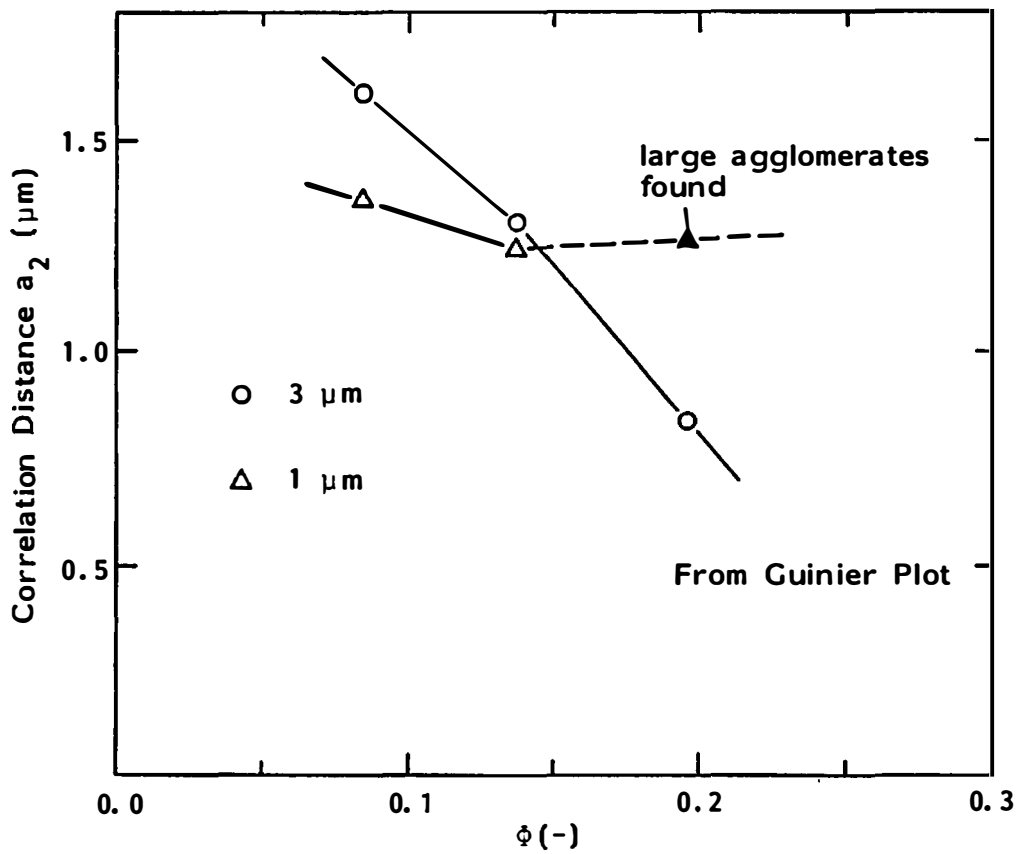

Figure IX-64. Guinier correlation distance a_2 as a function of volume fraction of filler.

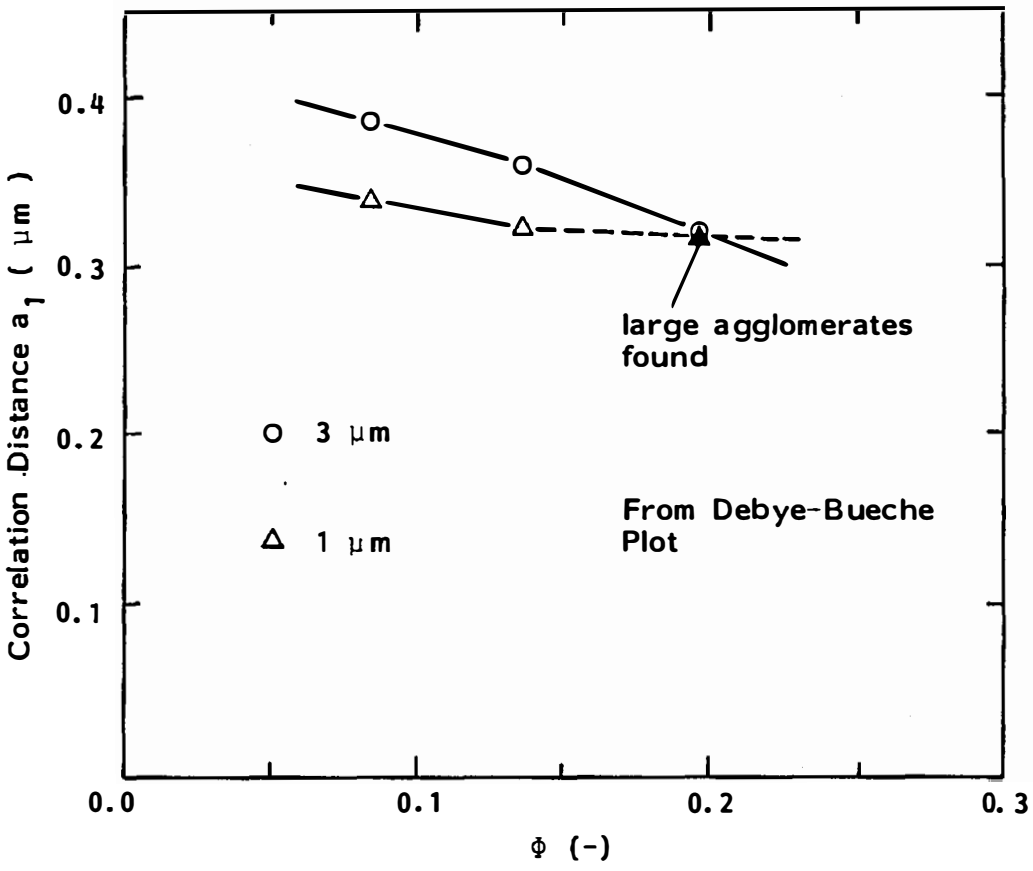

Figure IX-65. Debye-Bueche correlation distance a_1 as a function of volume fraction of filler.

CHAPTER X

ELECTRICAL CONDUCTIVITY MEASUREMENT

A. INTRODUCTION

In the present chapter, electrical conductivities of various carbon black compounds are reported. These include two roll mill and internal mixer prepared polypropylene/carbon black compounds.

Three types of carbon blacks were employed. Those are N990, N326, and N351 (supplied by Huber Corporation). N990 has the largest diameter (dp = 0.32 μm) and the lowest structure among all. N326 and N351 possess almost identical diameters (dp = 0.026 μm and 0.028 μm, respectively), but N351 has a higher structure than N326. Here the term structure concerns the characterization of the black aggregates.

The polystyrene/carbon black compounds usually possessed much lower electrical conductivities than the polypropylene/carbon black compounds. The electrical conductivities of the polystyrene/carbon black compounds ($<10^{-10}\ \Omega^{-1}\ cm^{-1}$) were then no longer measurable using the apparatus developed in our laboratory. The conductivities of such compounds were measured using the apparatus of Prof. R. W. Roberts (Department of Chemical Engineering, University of Akron) with the help of Mr. K. Murali.

B. EXPERIMENTAL PROCEDURE

Samples for electrical conductivity measurement require special preparation, namely to minimize contact resistance. An apparatus has been developed in our laboratory.

Compounds were prepared on the two roll mill and in the internal mixer. Methods of compounding have been discussed in detail in Chapter III, Materials and Sample Processing.

Mixes were compression molded at 200°C into a thickness of 0.36 mm. Carbon blacks, in general, exist in the form of pellets before compounding. The thickness of the compound sheet (0.36 mm) was chosen to be greater than the size of the carbon black pellets (roughly 0.1 mm). Then carbon black pellets, if those exist in the compounds, do not reach from one surface to the other surface of the sheet sample. This avoids measuring the conductivity of carbon black itself if dispersion is poor.

Compression molded mixes were quenched in water. Some mixes were annealed from 200°C to 90°C at the cooling rate of -1.34°C/min. Ferro type stainless steel plates were used to obtain the smooth surfaces. The surfaces of the sheet samples were scrubbed with fine steel wool to remove the polymer film which may cover the carbon black aggregates or agglomerates.

Silver paint (DuPont Electronic Materials Inc. Conductor Composition) was applied on both surfaces of the sheet sample to minimize the contact resistance between sample and electrodes.

Samples were vacuum dried at 60°C for the period of 24 hours before the measurements.

The compounds used for electrical conductivity measurement are summarized in Table X-1.

An electrical conductivity measurement apparatus has been constructed in our laboratory. A schematic drawing and photographs of the apparatus are given in Figures X-1 and X-2, respectively.

The apparatus is composed of a regulated power supply (Lambda; Regulated Power Supply), a voltage readout (Keithley; 192 Programmable Digital Multimeter), an electric current readout (Fluke; 8050 A Digital Multimeter), a buffer unit and a test specimen. The test section has two electrodes and two guard rings. Both the electrodes and the guard rings are copper. The guard rings prevent the surface current of the conductive test specimen. Weight of 100 gr. was used to obtain a good contact between the electrodes, the guard rings and the sheet sample. The copper electrodes and the guard rings were polished with steel wool before the measurements.

The voltage and the electric current through the thickness direction of the sheet specimen were measured. The area of measurement is 10 cm^2 (2.5 cm x 4 cm).

C. RESULTS AND DISCUSSION

The electrical conductivity was calculated with the following equation.

Table X-1. Compounds Used for Electrical Conductivity Measurements

Polymer	Grade	Volume Fraction (-)	Mixer†	Mixing Time (min)
Polystyrene (mix. temp. = 150°C)	N990	0.30	TRM	20
Polypropylene (mix. temp. = 175°C)	N990	0.30	TRM	20*
		0.25	TRM	20
		0.20	TRM	20*
		0.15	TRM	20
	N351	0.30	TRM	20
		0.20	TRM	20
		0.10	TRM	20
		0.05	TRM	20
	N326	0.30	TRM	20
		0.20	TRM	20
		0.10	TRM	20
		0.05	TRM	20
	N990	0.20	IM	0
		0.20	IM	3
		0.20	IM	5
		0.20	IM	10
		0.20	IM	20
	N351	0.20	IM	0
		0.20	IM	3
		0.20	IM	5
		0.20	IM	10
		0.20	IM	20
		0.05	IM	0
		0.05	IM	3
		0.05	IM	5
		0.05	IM	10
		0.05	IM	20
	N326	0.20	IM	0
		0.20	IM	3
		0.20	IM	5
		0.20	IM	10
		0.20	IM	20

†TRM = two roll mill; IM = internal mixer.

*Includes annealed sample.

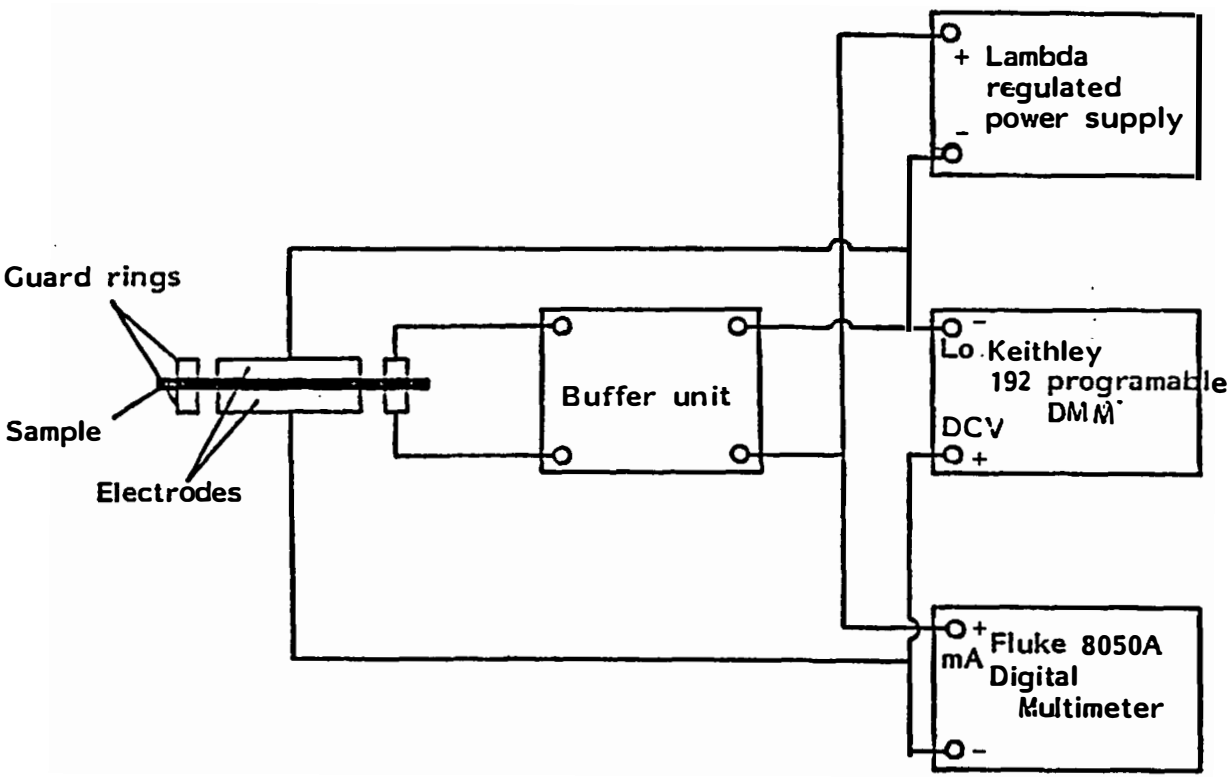

Figure X-1. Electrical conductivity measurement apparatus.

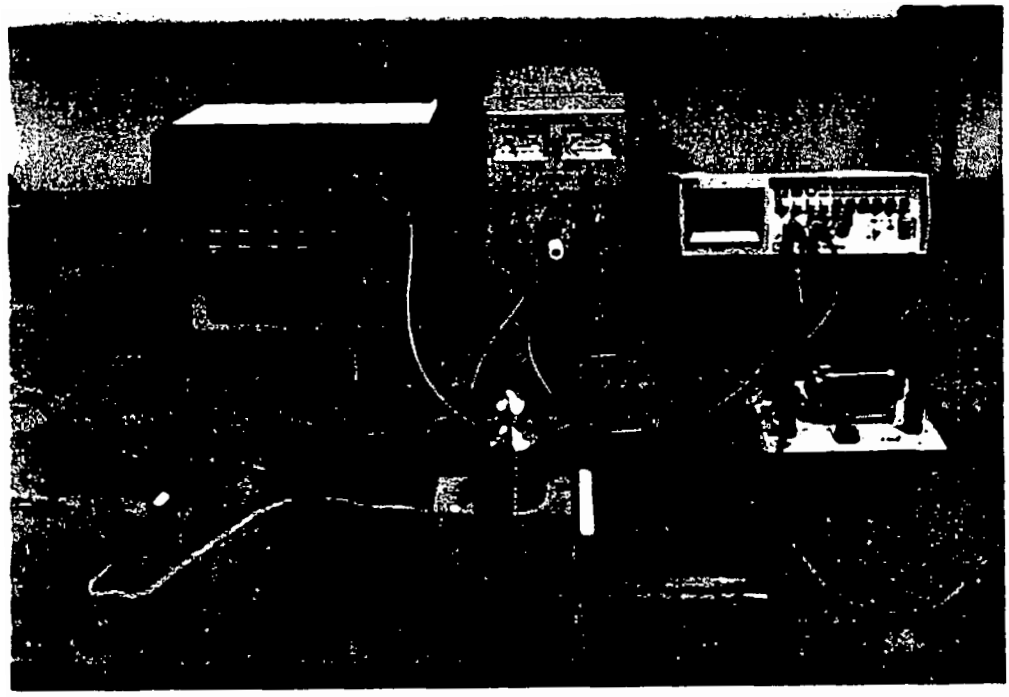

(a) Overall View

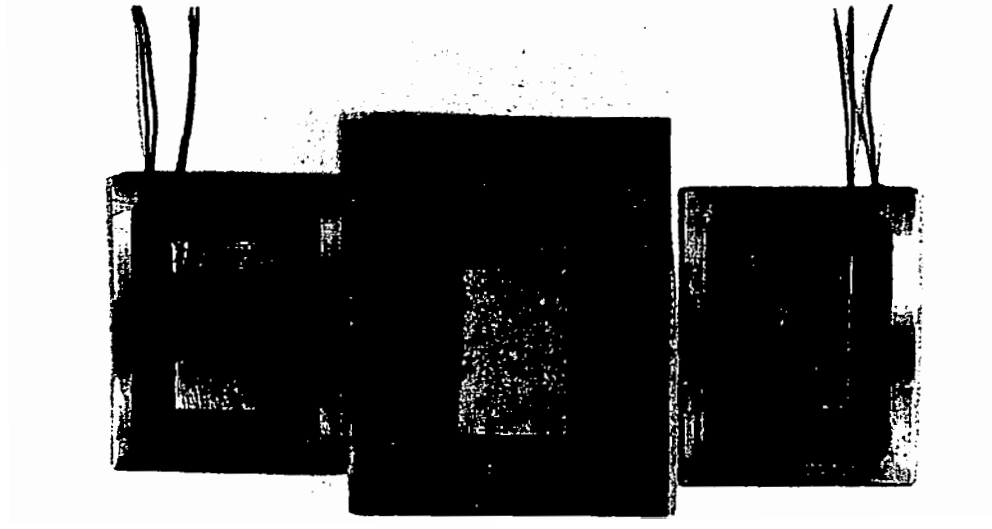

(b) Electrodes and Sample

Figure X-2. Photographs of electrical conductivity measurement apparatus.

$$\sigma = \frac{I}{V}\frac{H}{A} \ (\Omega^{-1} \cdot cm^{-1}) \qquad (X\text{-}1)$$

where σ denotes electrical conductivity, I the electric current through the specimen, V the applied voltage through the specimen, H the thickness of the specimen, and A is the measurement area.

C.1. Effect of Applied Voltage

Electrical conductivities of carbon black compounds have been determined for a wide range of applied voltages.

Polystyrene/carbon black compounds (dp = 0.32 μm, ϕ = 0.30) were prepared in a two roll mixing mill. Electrical conductivities of this compound are exhibited as a function of applied voltage in Figure X-3. The applied voltage was changed from 1 volt to above 200 volts. The electrical conductivity of compounds appears to be an exponentially increasing function with applied voltage.

The behavior of the electrical conductivity σ in the low voltage region is given in Figures X-4 through X-6.

Figure X-4 shows the electrical conductivity behavior of polypropylene/carbon black compounds (N351, dp = 0.028 μm). The volume fraction of carbon black ϕ varies from 0.10 to 0.30. These compounds were prepared in a two roll mill. The applied voltage covers 10^{-4} volt to 1 volt. In the low voltage region (below 1 volt), electric conductivities σ of compounds are constant at any volume fraction. It is found that the electrical conductivity increases with increasing volume fraction of filler.

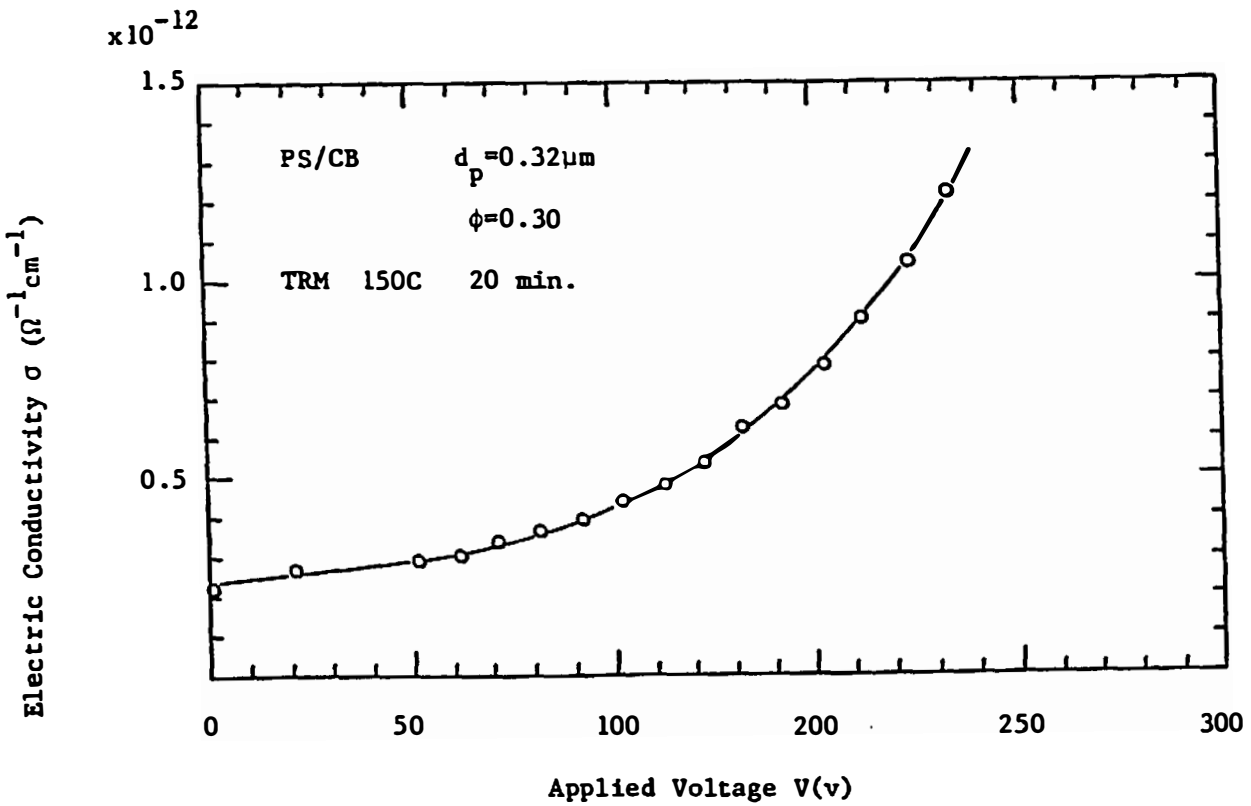

Figure X-3. Electrical conductivity as a function of applied voltage for PS/CB.

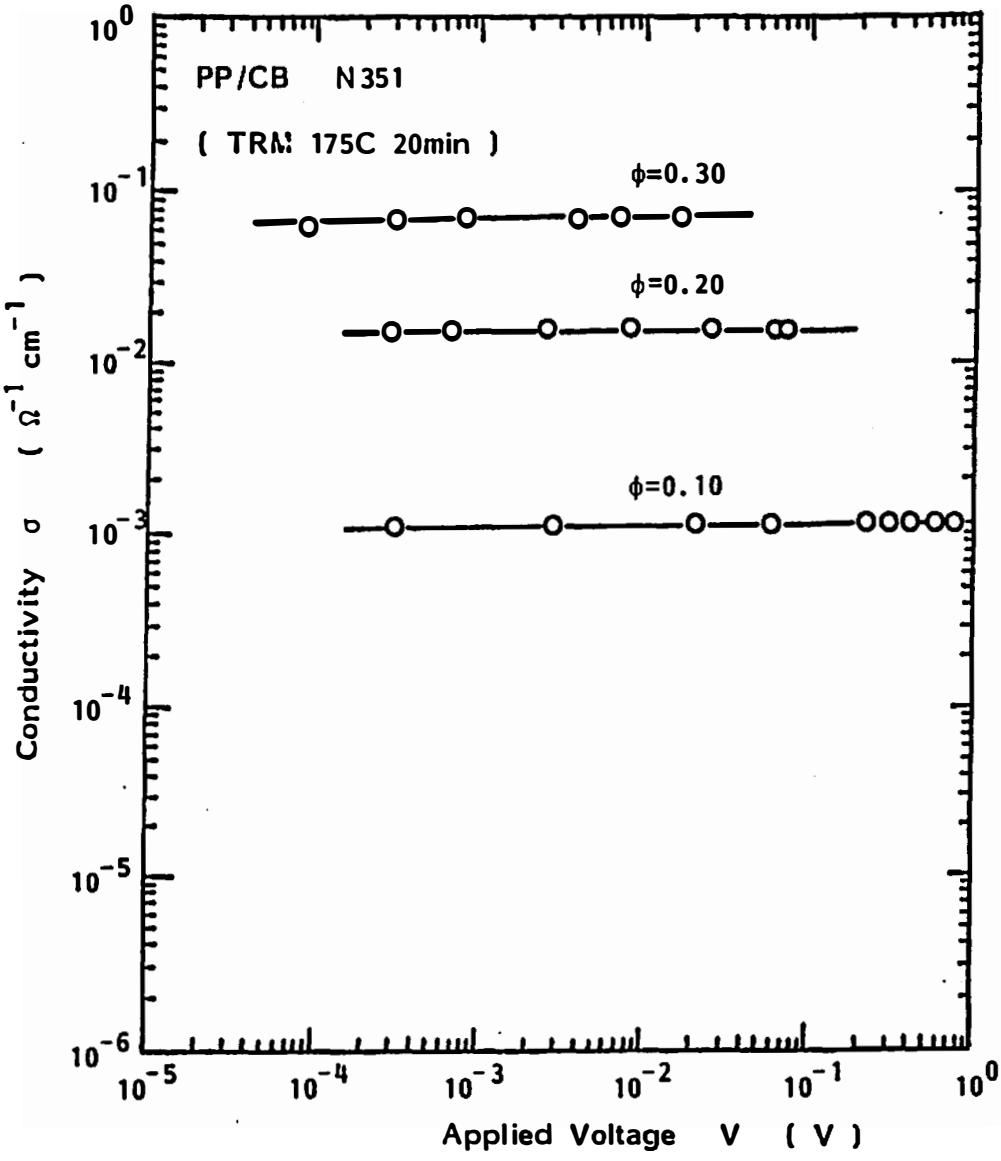

Figure X-4. Electrical conductivity as a function of applied voltage for PP/CB with various volume fractions.

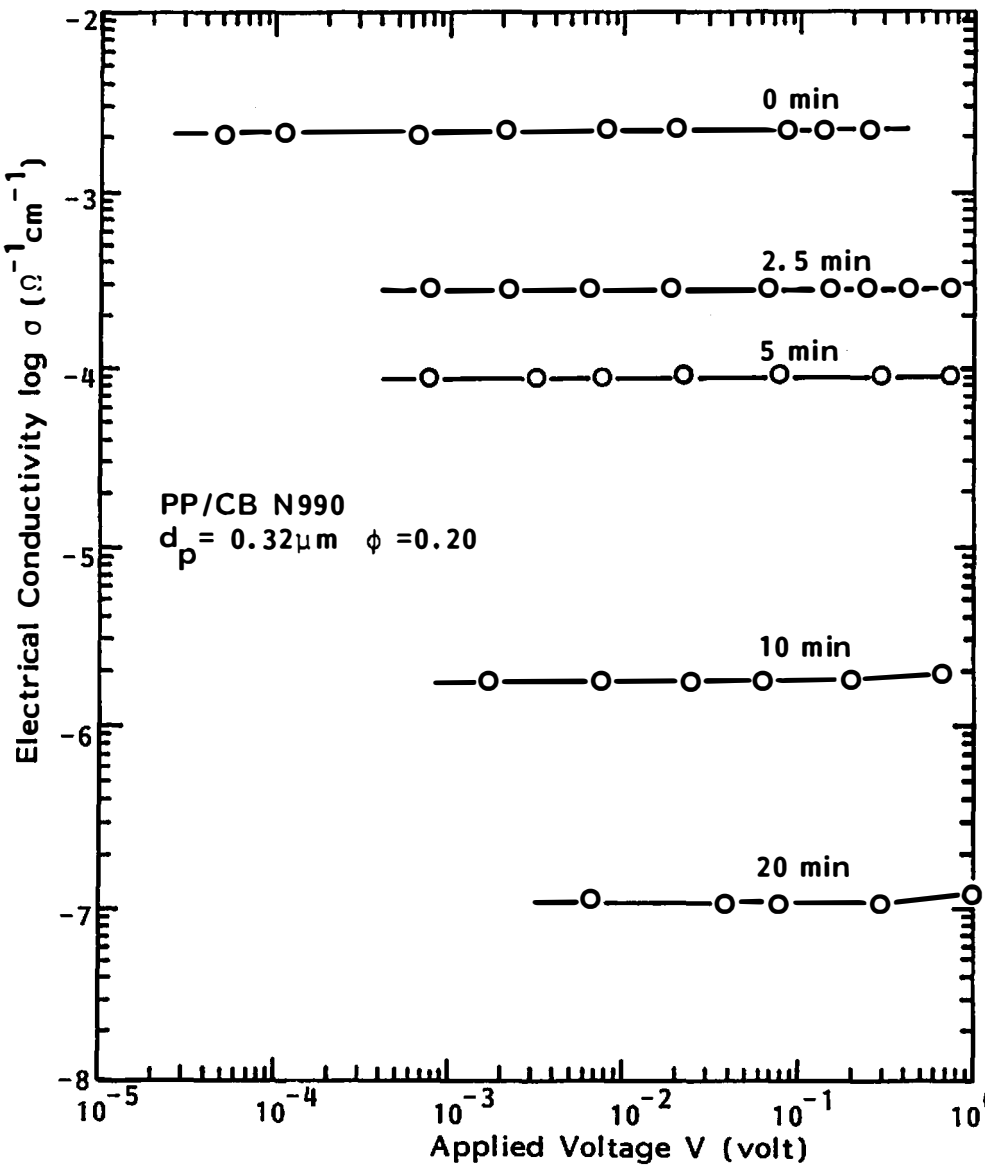

Figure X-5. Electrical conductivity as a function of applied voltage for PP/CB N990 with various mixing times.

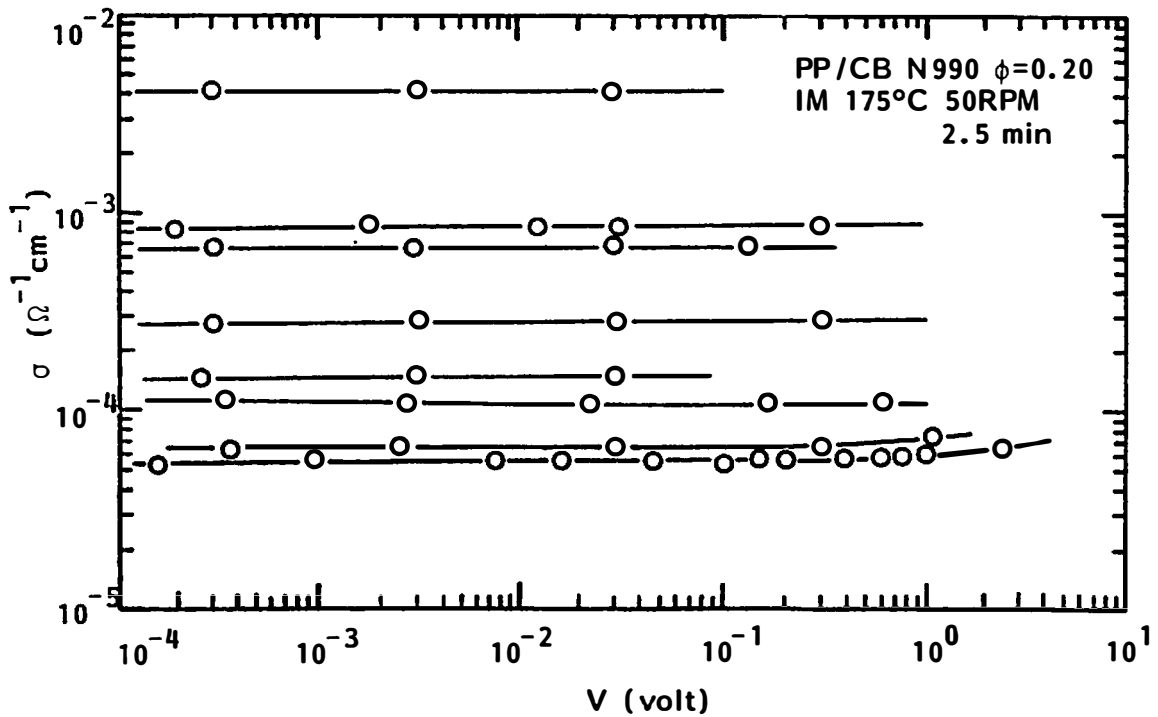

Figure X-6. Fluctuation of electrical conductivity of internal mixer prepared compounds.

Electrical conductivities in the low voltage region for the internal mixer prepared polypropylene/carbon black compounds (N990, dp = 0.32 μm, ϕ = 0.20) were given in Figure X-5. Mixing time varies from 0 minute (immediately after the filler disappeared near entrance of internal mixer) to 20 minutes. The applied voltage again covers 10^{-4} volt to 1 volt. Electrical conductivities of the lower conductivity compounds were no longer measurable at the very low voltage region because of the extremely low values of the electric current reading (see Eq. (X-1)).

It is found that the electric conductivities of N990 black compounds are constant in the low applied voltage region with any mixing time. The electrical conductivity of internal mixer compound decreases drastically as mixing progresses.

Electrical conductivity was measured for eight sheet samples of the internal mixer compounds and four sheet samples of the two roll mill prepared compounds. The electrical conductivity of these sheet samples varies. An example is given in Figure X-6. Polypropylene/carbon black compounds (dp = 0.32 μm, ϕ = 0.20) were prepared in an internal mixer. The mixing time is 2.5 minutes. Eight different sheet samples covers conductivity from 5.3×10^{-5} to 4.1×10^{-3} Ω^{-1} cm^{-1}. One of the reasons for this fluctuation may be nonuniform mixing in the internal mixer. Similar fluctuations are observed for the two roll mill prepared compounds. The fluctuation is, in general, greater for the low conductivity compounds.

C.2. Effect of Volume Fraction and Type of Carbon Black

Electrical conductivities of various compounds were represented as a function of volume fraction of carbon black in Figure X-7. Both two roll mill mixed compounds and internal mixer prepared compounds were mixed for a period of 20 minutes. Conductivities were averaged over four samples for the two roll mill compounds and eight samples for the internal mixer compounds. The maximum and minimum values of conductivities were indicated. Conductivities of two roll mill compounds were plotted with closed symbols and internal mixer compounds with open symbols. We note that the N990 black (dp = 0.32 μm) compounds possess the lowest electrical conductivities at any volume fraction. N351 (dp = 0.028 μm) and N326 (dp = 0.026 μm) black compounds show similar conductive behavior. N326 black compounds, however, possess slightly higher conductivity than N351 black compounds at any volume fraction. The order of electrical conductivity is the same as the inverse order of black particle diameter.

Conductivity: N326 $\geqslant$ N351 $\gg$ N990

Black Diameter: 0.026 $\leqslant$ 0.028 $\ll$ 0.32 (m)

The conductivity behavior of compounds appears to be governed by black diameter. As the diameter of the carbon black increases, electrical conductivity decreases. Dibutyl phthalate (DBP) structure index does not have a strong correlation with conductivity.

Conductivity: N326 $\geqslant$ N351 $\gg$ N990

DBP Index: 71 121 42

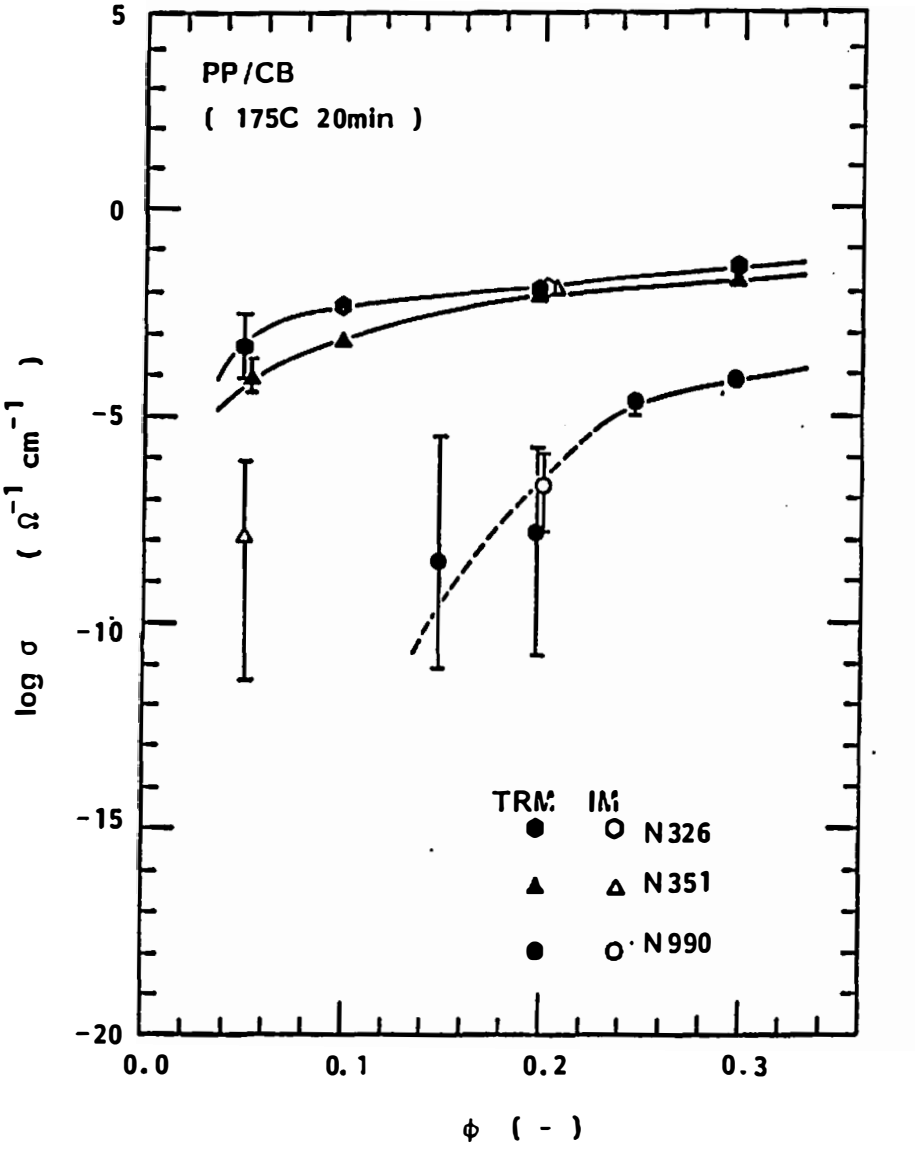

Figure X-7. Electrical conductivity as a function of volume fraction of CB for PP/CB.

Electrical conductivity decreases with decreasing volume fraction of carbon black. This is most conspicuous in N990 black compounds. Electrical conductivities of internal mixer compounds are found to be approximately the same as two roll mill compounds at high volume fractions (ϕ = 0.20). At low volume fraction (ϕ = 0.05), the internal mixer compounds have lower conductivity than two roll mill compounds.

C.3. Effect of Annealing and Matrix Polymer

A few polypropylene/carbon black (N990) compounds which were mixed on a two roll mill at 175°C for 20 minutes were annealed in a compression molding process. These are compression molded at 200°C and annealed with a cooling rate of -1.34°C/min. Figure X-8 compares the electrical conductivities of quenched polypropylene compounds (closed symbols) and annealed compounds (open symbols). These are averaged over four samples. Heat treatment has a notable effect on electrical conductivity of compounds. The conductivity of polypropylene/carbon black compounds increased 16 times at the volume fraction of 0.30 and 500 times at the volume fraction of 0.20.

The electrical conductivity of polystyrene/carbon black compound is added in Figure X-8. Mixing temperature is 150°C. The polystyrene compound possesses much lower conductivity in contrast to polypropylene compounds. This is probably due to the higher viscosity of the polystyrene matrix during mixing. A continuous network structure of carbon black may be induced by annealing. The

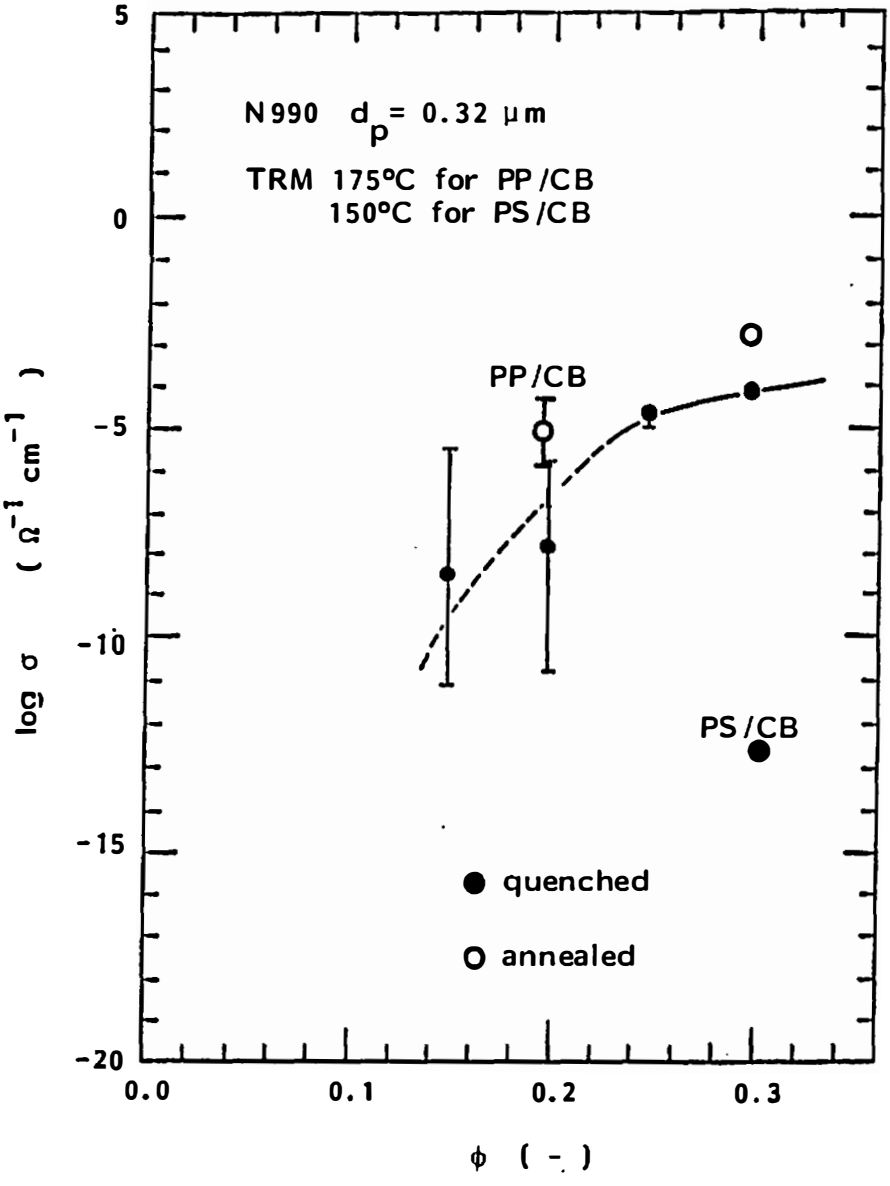

Figure X-8. Effect of heat treatment on electrical conductivity.

formation of crystalline phase during the annealing may promote network formation in the case of polypropylene.

C.4. Effect of Mixing Time

The electrical conductivity of compounds changes with mixing time. The effect of mixing time was determined for the internal mixer compounds.

Figure X-9 shows electrical conductivity as a function of mixing time for three types of polypropylene/carbon black compounds. The mixing time varies from 0 minute to 20 minutes. The volume fraction of black is the same for all compounds, that is, 0.20. N990 black compounds show an abrupt decay of conductivity in the first 10 minutes and maintain a constant value. The other two types of blacks (N326 and N351) show only minor decreases of conductivities with mixing time.

A similar plot is obtained for two different volume fractions of N351 black (ϕ = 0.20 and 0.05) in polypropylene in Figure X-10. The conductivity of low volume fraction compounds (ϕ = 0.05) decreases in the first 2.5 minutes of mixing then decreases slowly.

C.5. Qualitative Correlation with the Level of Dispersion

The results of the electrical conductivity measurement obtained in the present research indicate correlations with the level of dispersion of carbon black. Low conductivity corresponds to good dispersion. We may compare the trends with those we have seen in the calcium carbonate compounds via optical microscopy.

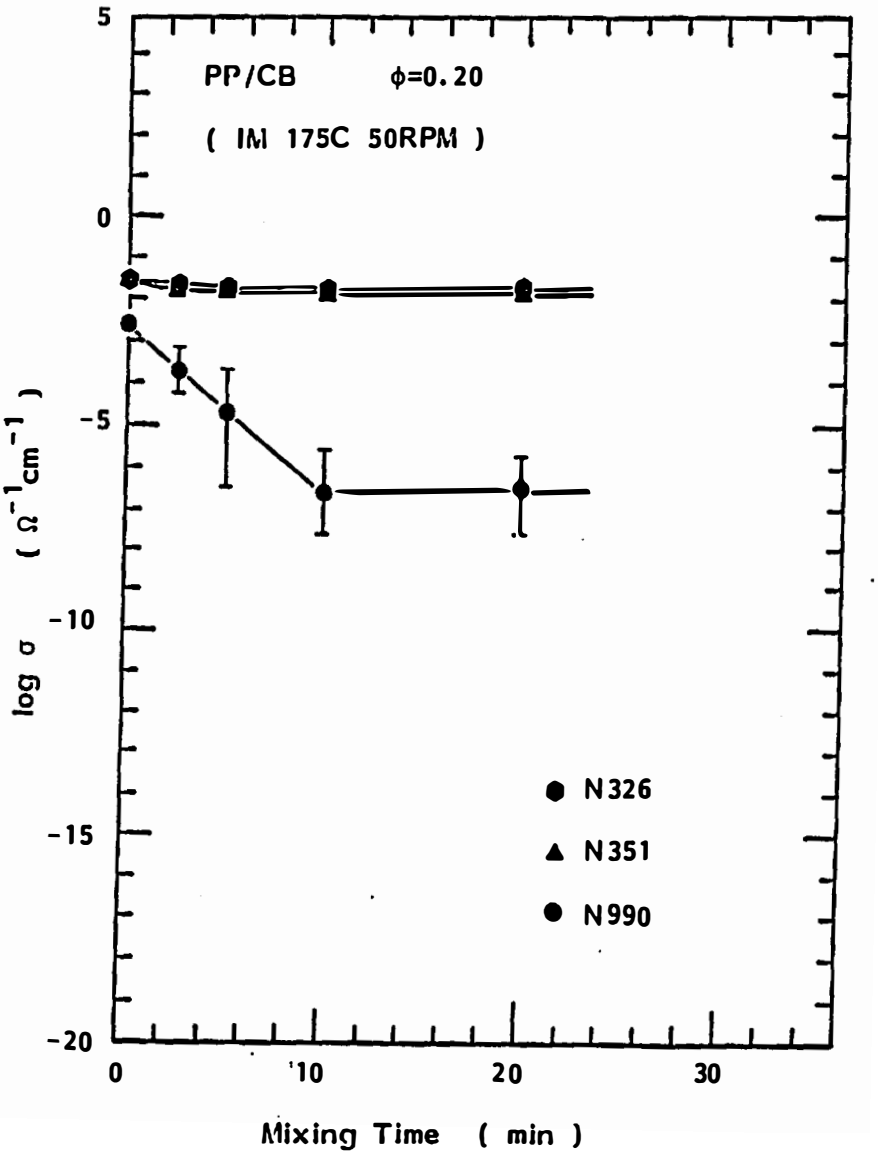

Figure X-9. Electrical conductivity as a function of mixing time for PP/CB (ϕ = 0.20).

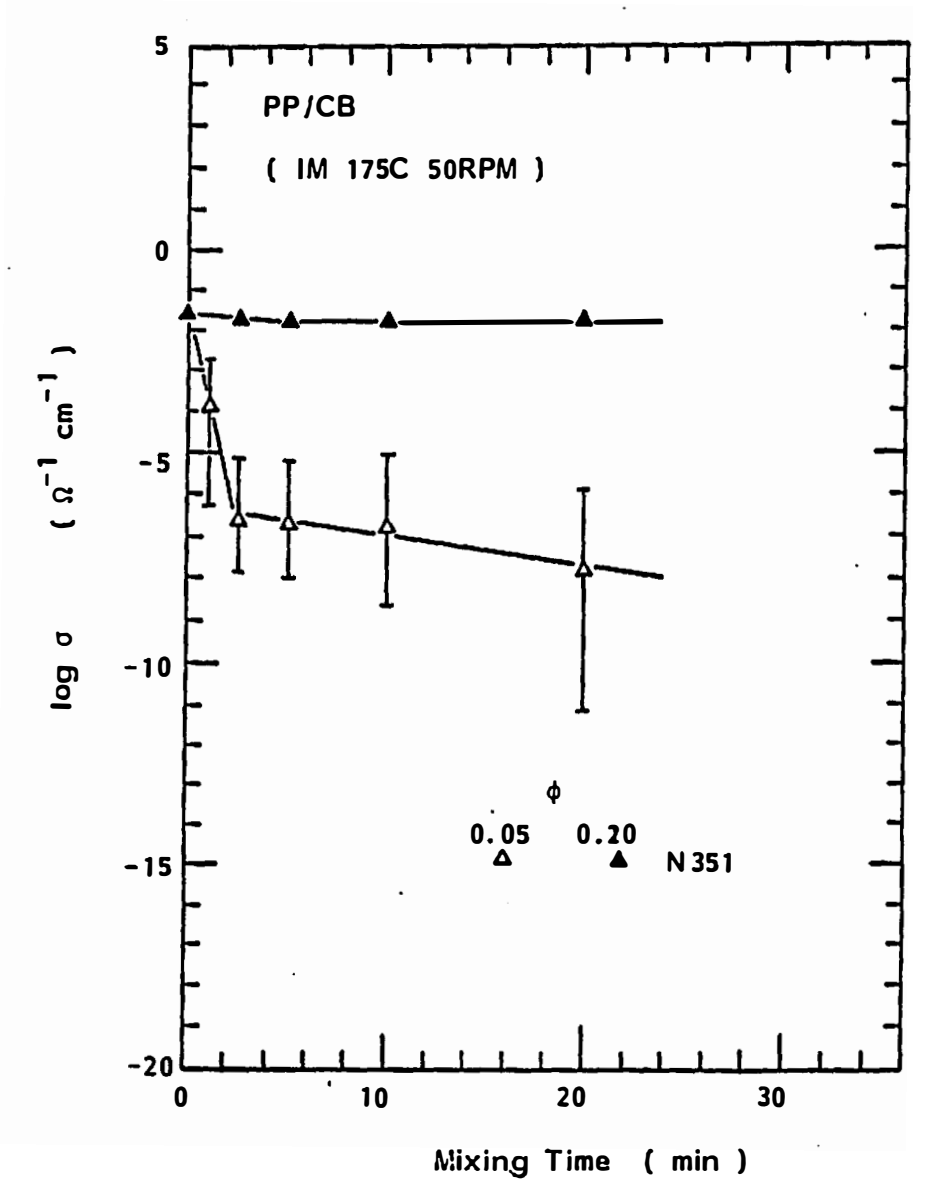

Figure X-10. Electrical conductivity as a function of mixing time for PP/CB (ϕ = 0.05, 0.20).

1. Polypropylene/carbon black compounds conductivities are greater than the conductivities of the polystyrene/carbon black compounds. This is similar to the calcium carbonate compounds and may be attributed to polypropylene possessing much lower viscosity than polystyrene. This presumably leads to the lower level of dispersion.

2. The compounds of the finer carbon blacks possess greater electrical conductivity than the coarse black. The stronger particle-particle (or aggregate-aggregate) interaction has been indicated for the finer blacks and calcium carbonates by the sedimentation volume experiment (Chapter V). This strong particle-particle interaction leads to lower levels of dispersion.

3. Electrical conductivities of black compounds decreases as mixing progresses.

All of the above shows that compounds which presumably have low levels of dispersion show high electrical conductivities.

Several authors (B-5,C-3,D-1,H-9) have reported a correlation between the electrical conductivity and the mixing conditions for various elastomer/carbon black compounds. As mixing progresses, the electrical conductivities of compounds decreases. They compared their results of electrical conductivity measurement with electron photomicrographs (D-1), optical photomicrographs (B-5,C-3) and surface roughness measurements (C-3). It was generally found that the electrical conductivity is high when the level of dispersion of black is low.

No qualitative explanation for the relationship between the conductivity of compound and the level of dispersion has been presented. We will qualitatively interpret the results of electrical conductivity measurement with percolation theory, and formulate its relation to the dispersion level in the following chapter.

CHAPTER XI

DETERMINATION OF DISPERSION FROM ELECTRICAL CONDUCTIVITY MEASUREMENTS

In this chapter, we use percolation theory to develop a representation of dispersion based on electrical conductivity measurements. Levels of dispersion have been determined for a series of polypropylene and polystyrene/carbon black compounds using the newly proposed concepts. Finally, the degree of dispersion is compared with mechanical property of compounds.

A. ELECTRICAL CONDUCTIVITY AND PERCOLATION THEORY

It is of our interest to determine the internal structure and dispersion of conductive filler from the electrical conductivity of compounds. Since the 1950's, various authors (B-5,C-3,C-1,H-9,M-6, P-5,V-2,V-4,V-5,V-6,V-7) have measured electrical conductivity of carbon black filled systems to characterize the level of dispersion. It is generally believed that a sequential structure formed by carbon black in a matrix increases conductivity of a compound. No quantitative theory which interprets electrical conductivity of compounds to characterize the level of dispersion has been proposed to the present.

A.1. Simple Register Model

The simplest model which explains the conductivity-structure relationship is illustrated in Figure XI-1(a) and (b).

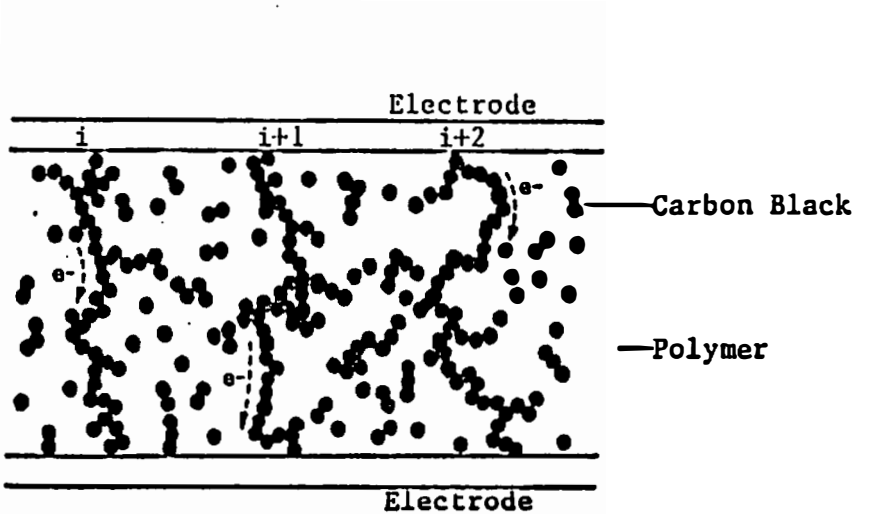

(a) Schematic representation of sequential carbon black structure in polymer.

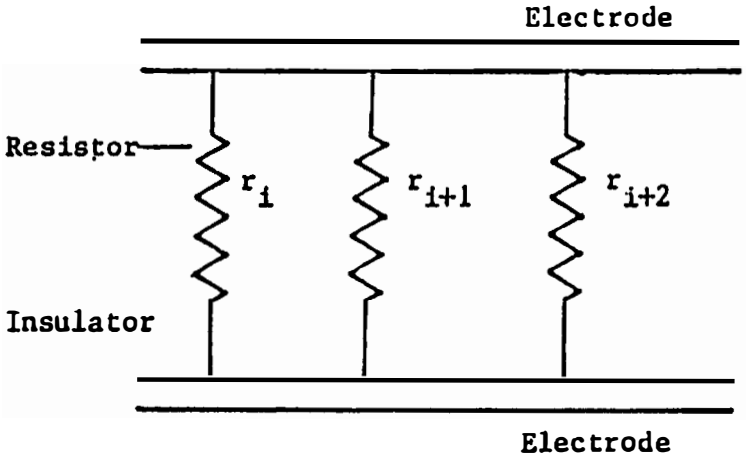

(b) Replacement of sequential structure with electric register in insulator.

Figure XI-1. Possible mechanism of conductivity in particle filled compounds.

Figure XI-1(a) shows the segmental structure of carbon black in compounds. The carbon black structure connects an electrode to another electrode. Electrons transfer along the segmental structure (pathway) and conduction occurs. We may replace long chains of particles reaching from one electrode to another electrode with electric registers (Figure XI-1(b). It suggests that the conductivity is

$$\sigma = \sum_{i=1}^{n} \frac{1}{r_i} = \frac{n}{r} \qquad \text{(XI-1)}$$

where n is the number of long bridges per unit area, r is the resistance of a single long chain of carbon black. The high conductivity of compounds is associated with the number of long chains.

However, it seems more reasonable to assume a three-dimensional network structure where chains are connected by shunts in a very complex manner. It requires a more sophisticated method of characterizing the conductivity of such systems.

A.2. Percolation Model

We now assume that carbon black forms a three-dimensional network structure in matrix. A schematic drawing of a three-dimensional network structure is given in Figure XI-2.

A.2.a. Contact resistance and conductivity. Before turning to a discussion of quantitative characterization of dispersion, we shall discuss the contact resistance of two spheres.

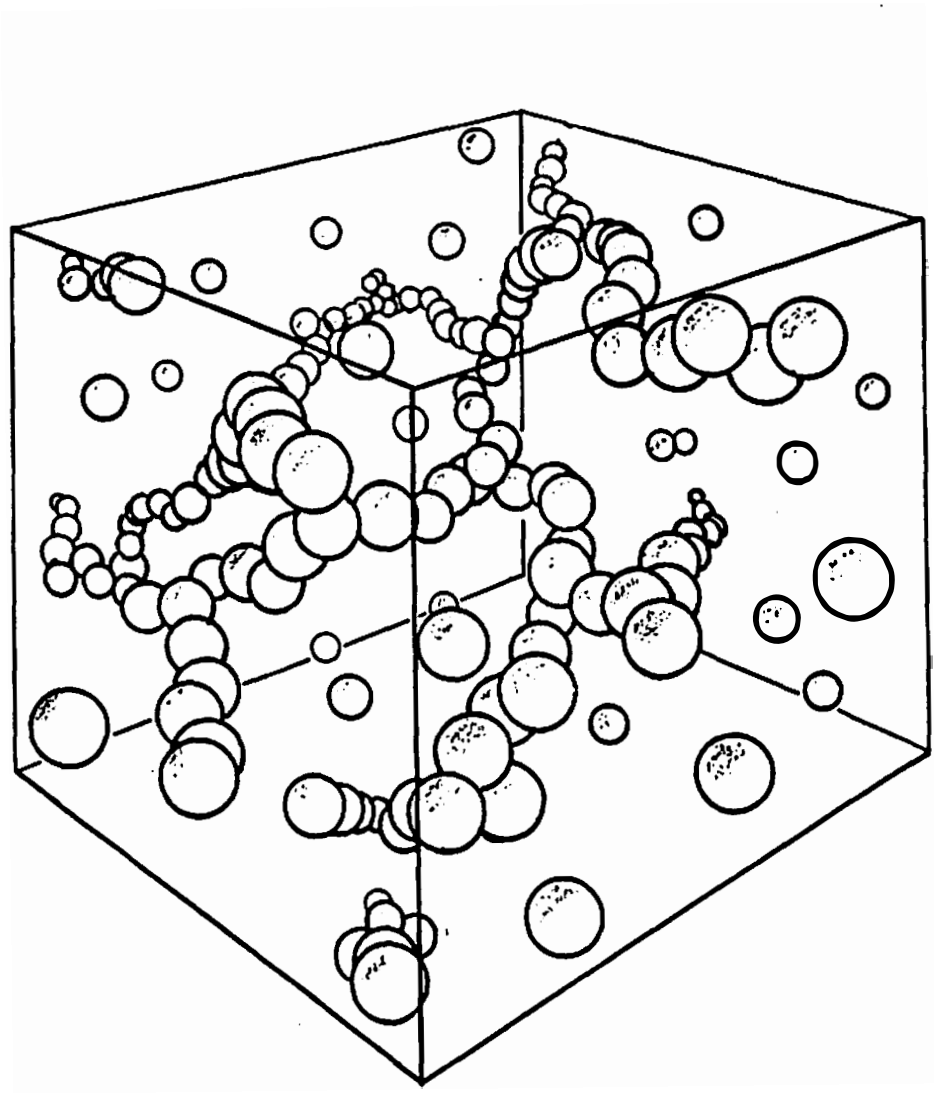

Figure XI-2. Concept of three-dimensional network structure (or infinitely large cluster).

When the contacting area between two substances is large enough, the resistance is inversely proportional to the area. However, if the area is small then constriction of the current tends to make resistance inversely proportional to the diameter of the contact area (B-6).

$$r_{cont} = \frac{1}{2a\sigma} \tag{XI-2}$$

where r_{cont} denotes contact resistance between two substances, a diameter of contact area, and σ conductivity of contacting substance. We may assume

$$a \propto d_p \tag{XI-3}$$

where d_p is the diameter of contacting particles.

Here we shall consider the resistance of one pathway. It is clear that

$$R_{path} = R_{cont} + R_{body} \tag{XI-4}$$

where R_{path} is a resistance of one pathway, R_{cont} and R_{body} are the total contact and body resistance (the resistance due to the particles) in one pathway. Assuming the average number of particles which form a pathway through a unit length is inversely proportional to the diameter of particles, in the network formation, we obtain

$$R_{cont} = \overline{N} \cdot r_{cont} \propto \frac{1}{2d_p^2\sigma} \tag{XI-5}$$

$$R_{body} = \frac{L}{A\sigma} \propto \bar{N} \cdot d_p/\sigma \cdot d_p^2 \propto \frac{1}{d_p^2\sigma} \tag{XI-6}$$

where L is the extended length of path, A is the cross sectional area of pathway, and $\bar{N}$ is the number of particles in a pathway.

$$\bar{N} \propto \frac{1}{d_p} \tag{XI-7}$$

Then we obtain

$$R_{path} \propto \frac{1}{d_p^2} \cdot \tag{XI-8}$$

The resistance of a pathway is inversely proportional to the square of particle size.

Now we shall consider the resistivity ρ by taking into account the number of pathways per unit surface area n.

$$\begin{aligned} n &\propto (\text{size of a lattice site})^2 \\ &\propto d_p^2 \end{aligned} \tag{XI-9}$$

Finally we obtain

$$\begin{aligned} R_{path} &= n \cdot R_{path} \\ &\propto (d_p^2) \cdot \frac{1}{(d_p^2)} \end{aligned} \tag{XI-10}$$

It is noteworthy that resistivity and conductivity of an entire system consisting of contacting spheres are independent of size of spheres, though contact resistance is a function of size of spheres.

A.2.b. Electrical conductivity-volume fraction relationship. Electrical conductivity-volume fraction relationship may be obtained for two distinguished mix conditions, that is, a "random mix" and "separate mix."

First, we consider the percolation theory (K-4,K-5,K-6,R-5) for a "random mix." Rudd and Frisch (R-5) proposed the following equation for percolation probability above a critical probability:

$$P_{(p)} = k(p - p_c)^{\beta} \qquad \text{for } p > p_c \tag{XI-11}$$

where $P_{(p)}$ denotes percolation probability, k proportional constant, p probability of occupied sites in lattice and p_c critical probability above which percolation occurs.

Kirkpatrick (K-5,K-6) proposed an equation which relates percolation probability P to the electrical conductivity.

$$G(p) = \frac{\sigma(p)}{\sigma(1)} = P_{(p)} \cdot \frac{D(p)}{D(1)} \tag{XI-12}$$

and

$$\frac{D(p)}{D(1)} = (p - p_c)^{1.1} \tag{XI-13}$$

where

G(p): normalized conductivity;

$\sigma(p)$: conductivity at probability of occupancy p;

$\sigma(1)$: conductivity at probability of occupancy 1 (completely occupied lattice).

Substituting Eqs. (XI-11) and (XI-13) into Eq. (XI-12), we obtain

$$G(p) = \frac{\sigma(p)}{\sigma(1)} = k(p - p_c)^{1.1+\beta} \qquad \text{(XI-14)}$$

We may rewrite this equation with volume fraction of occupied site in lattice

$$G(\phi) = \frac{\sigma(\phi)}{\sigma(\phi_{max})} = k(\frac{\phi}{f} - \frac{\phi_c}{f})^{1.1+\beta} \qquad \text{(XI-15)}$$

because

$$\phi = p \cdot f \qquad \text{(XI-16)}$$

where

ϕ: volume fraction of filler;

ϕ_{max}: maximum attainable volume fraction of filler;

ϕ_c: critical volume fraction of filler above which percolation occurs;

f: fill factor.

ϕ_{max}, ϕ_c, f and β are the known quantities and are summarized in Table XI-1.

We should determine the proportionality constant k in Eq. (XII-15) to obtain a complete conductivity-volume fraction relationship. The percolation probability obtained by Kirkpatrick (K-5,K-6) and Dean et al. (D-2,D-3) is shown in Figure XI-3.

Table XI-1. Constants for Equation (XI-15)

Lattice	Filling Factor f	Critical Volume Fraction ϕ_c	Constant β	Constant k
s.c.	0.5236	0.16	0.35-0.40	0.976
b.c.c.	0.6802	0.16	0.30-0.40	0.850
f.c.c	0.7405	0.16	0.33-0.40	0.827
References		D-11,F-8,F-9, H-1,R-6,S-2, S-17	K-6	Present Work

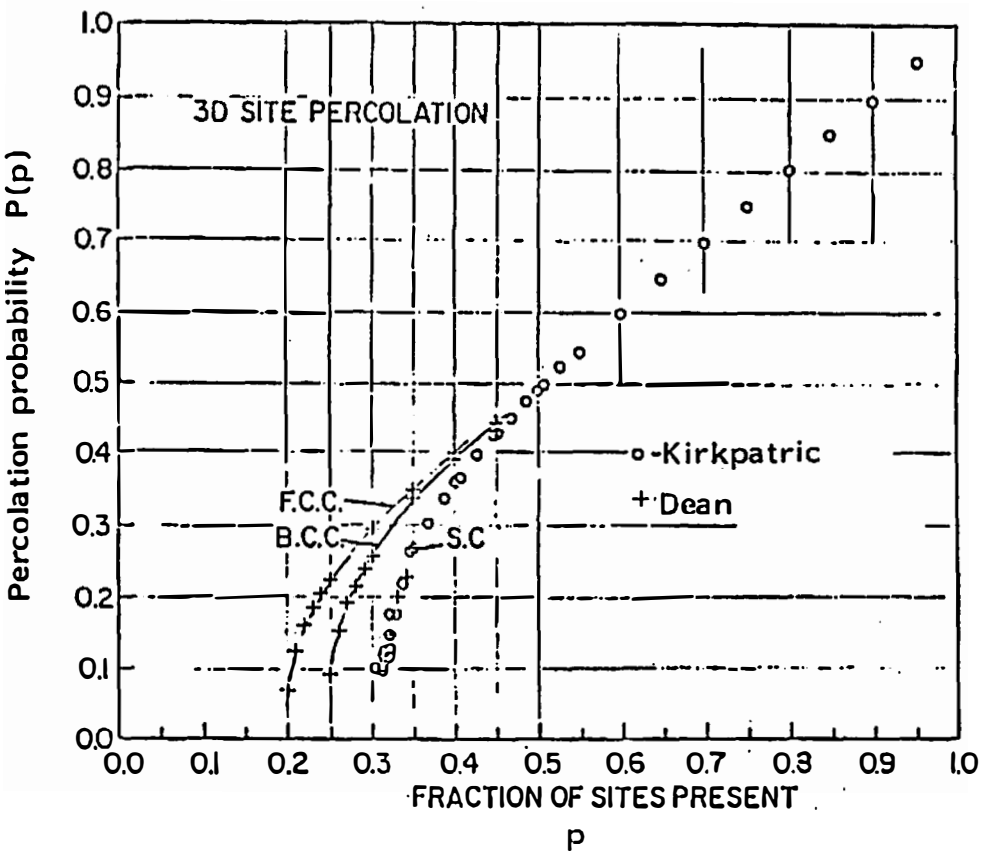

Figure XI-3. Percolation probability for various three-dimensional lattices by numerical simulation by Kirkpatrick and Dean et al.

We note that the percolation probabilities of all lattices (simple cubic, body centered cubic, face centered cubic) are close to 0.50 at p = 0.50. We use the following equations to estimate k.

$$\lim_{p \to 0.50} P_{(p)} = \lim_{p \to 0.50} k(p - p_c)^{\beta} = 0.50 \qquad \text{(XI-17)}$$

or

$$\lim_{\phi \to 0.50f} P_{(\phi)} = \lim_{\phi \to 0.50f} k(\frac{\phi}{f} - \frac{\phi_c}{f})^{\beta} = 0.50 \qquad \text{(XI-18)}$$

k values obtained for each lattice are shown in Table XI-1.

The percolation probability calculated from Eq. (XI-11) is compared with the results of numerical simulation by Kirkpatrick (K-5,K-6) and Dean et al. (D-2,D-3) as a function of volume fraction of particle ϕ in Figure XI-4. A good fit was obtained for any lattice. The constants used in calculation are summarized in Table XI-2.

Equation (XI-15) with the constants in Table XI-2 represent a conductivity-volume fraction relationship for a complete "random mix."

We now define a "separate mix" where particles are separated from each other and evenly dispersed. Conductivity-volume fraction relationship for a "separate mix" has been proposed by Maxwell (M-4) for dilute systems.

$$\sigma(\phi) = \left\{\frac{2r_1 + r_2 + \phi(r_1 - r_2}{2r_1 + r_2 - 2\phi(r_1 - r_2} \cdot r_2\right\}^{-1} . \qquad \text{(XI-19)}$$

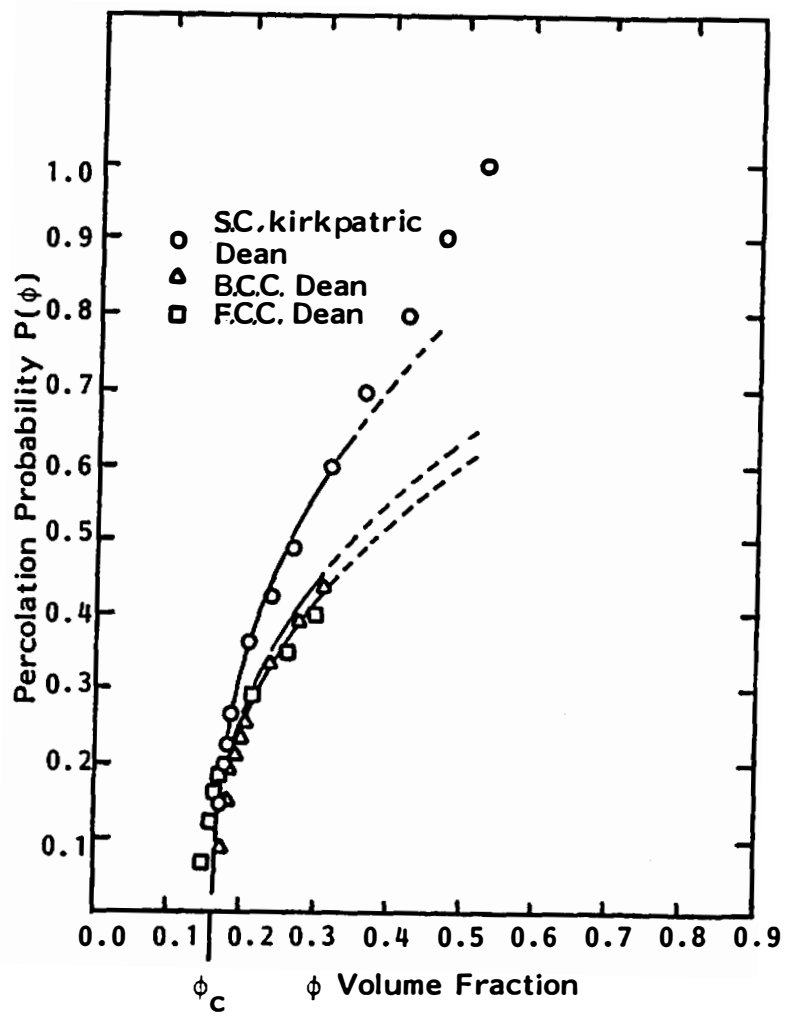

Figure XI-4. Percolation probability for various three-dimensional lattices. Solid and broken lines are calculated results.

Table XI-2. Constants Used for Equations (XI-11) and (XI-15)

Lattice	Filling Factor f	Critical Volume Fraction ϕ_c	Constant β	Constant k
s.c.	0.5236	0.16	0.40	0.976
b.c.c.	0.6802	0.16	0.40	0.850
f.c.c.	0.7405	0.16	0.40	0.827

We may rewrite this

$$\sigma(\phi) \simeq \left(\frac{r_2 - \phi r_2}{r_2 + 2\phi r_2} \cdot r_2\right)^{-1} \qquad \text{(XI-20)}$$

for $r_1 << r_2$. Here r_1 and r_2 are resistivities of conductive particles and matrix, respectively.

Random Mix Limit and Separate Mix Limit

We may plot the electrical conductivities obtained by Eqs. (XI-15) and (XI-20) for "random mix" and "separate mix," respectively, as a function of volume fraction of filler (Figure XI-5). We assumed

$$\sigma(\phi_{max}) = f\sigma_{CB} \qquad \text{(XI-21)}$$

where $\sigma(\phi_{max})$ denotes the conductivity at the maximum attainable volume fraction, and σ_{CB} is the conductivity of carbon black which is approximately $1 \times 10^{3}\ \Omega^{-1} \cdot cm^{-1}$. The conductivity of polymer matrix is assumed to be $1 \times 10^{-17}\ \Omega^{-1} \cdot cm^{-1}$.

The "separate mix limit" and "random mix limit" are defined in Figure XI-5. Topological schematic views for separate mix and random mix are added. It is pointed out that the increase in electrical conductivity with volume fraction for separate mix is very small. The electrical conductivity for the random mix, in contrast, shows a marked increase at the critical volume fraction of 0.16, and then approaches a constant value at high volume fraction. The type of lattices (simple cubic, body centered cubic and face centered cubic

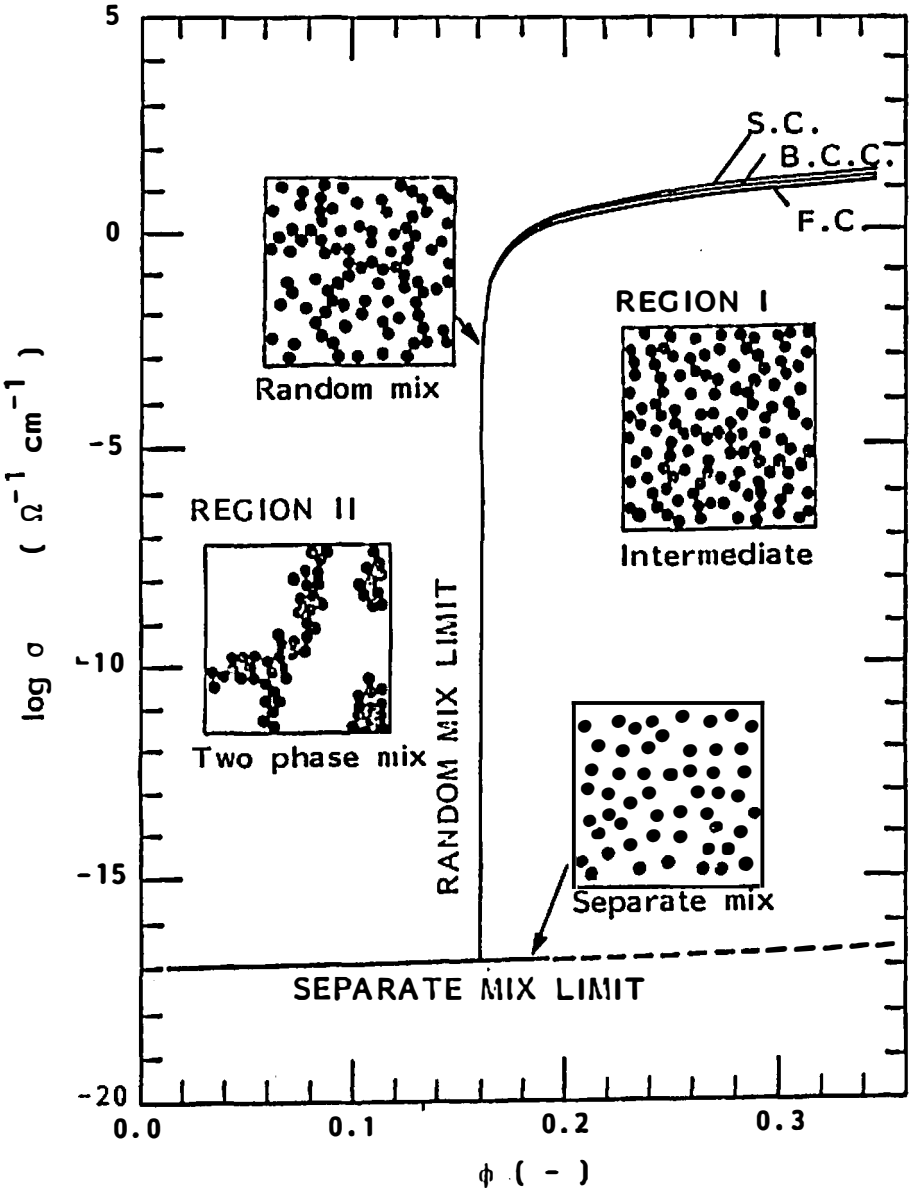

Figure XI-5. Calculated electric conductivity as a function of volume fraction of filler.

lattice) does not show a significant difference with conductivity behavior.

Region I and Region II may be defined. Region I covers the area above the critical volume fraction ϕ = 0.16 and between the random mix limit and separate mix limit. In Region I, the sequence of particles are intermediate between random and separate. Region II covers from below critical volume fraction and above the separate mix limit. In Region II, the compound possesses conductivity which is greater than the separate mix limit at low volume fraction. A two phase mix where a large portion of particles form sequential structure may be realistic in this region.

A.2.c. Degree of dispersion. The separate mix limit and random mix limit have been defined and given in Figure XI-5. The electrical conductivity of actual compounds, however, does not necessarily follow these limits since dispersion of particles does not always realize an ideal separate mix and ideal random mix.

We shall discuss the conductivity behavior of the model compounds. Figure XI-6 shows the topological schematic views of three model compounds in reference to theoretical conductivity behavior. We assume three model compounds possess identical electric conductivities of $10^{-5}\ \Omega^{-1} \cdot cm^{-1}$. When the volume fraction of compound is the same as the volume fraction of the random mix limit (center), the fraction of particulates which are a part of an infinitely large cluster (three-dimensional sequential network structure) is given by

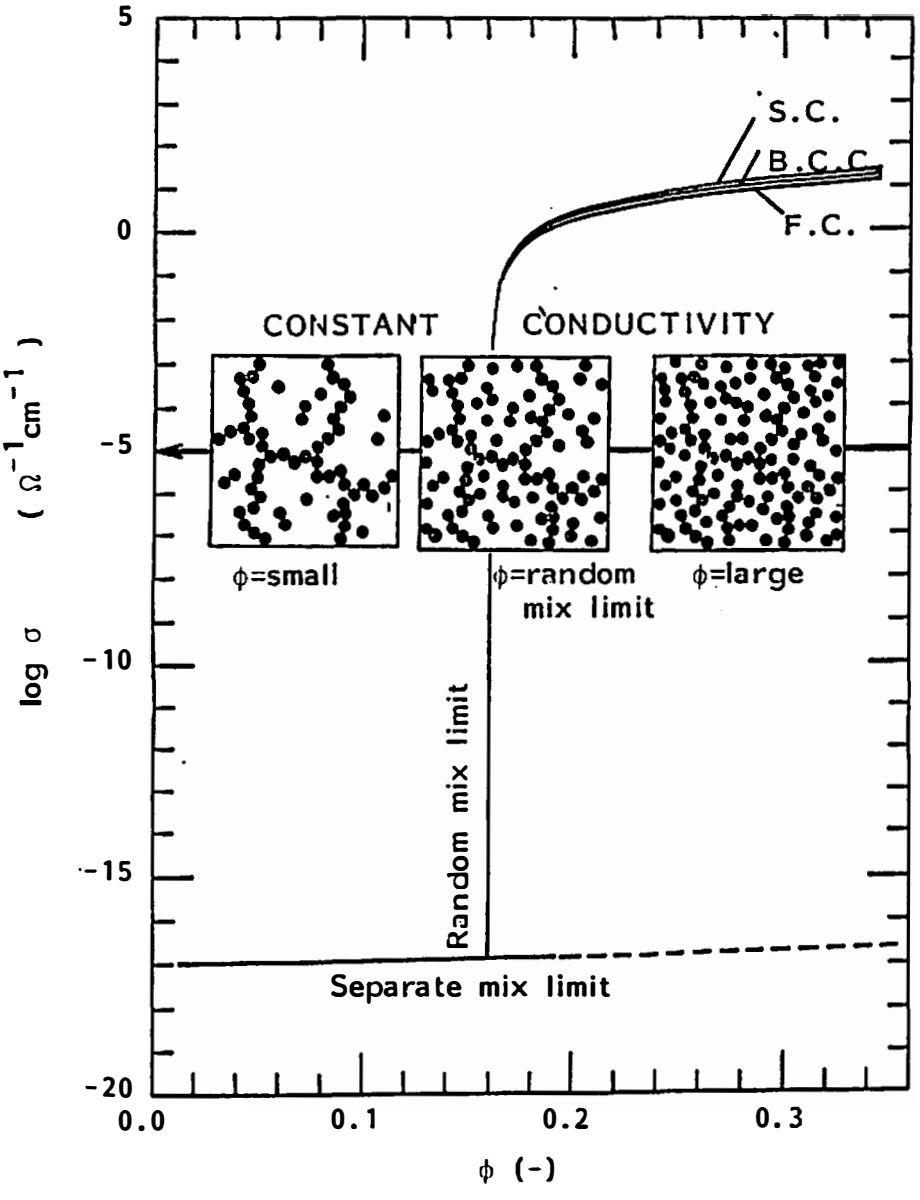

Figure XI-6. Interpretation of conductive behavior for model compounds.

a percolation probability P( ) for a random mix. Rewriting Eq. (XI-12), we obtain

$$P_{(p)} = \frac{\sigma(p)}{\sigma(1)} \cdot \left[\frac{D(p)}{D(1)}\right]^{-1}$$

$$= \frac{\sigma(p)}{\sigma(1)} \cdot (p - p_c)^{-1.1} \qquad \text{(XI-22)}$$

Substituting Eq. (XI-11) into Eq. (XI-22) to eliminate p and p_c

$$P_{(p)} = \left[\frac{\sigma(p)}{\sigma(1)} \cdot k^{1.1/\beta}\right]^{\beta/(\beta+1.1)} \qquad \text{(XI-23)}$$

With volume fraction ϕ, this leads to

$$P_{(\phi)} = \left[\frac{\sigma(\phi)}{\sigma(\phi_{max})} \cdot k^{1.1/\beta}\right]^{\beta/(\beta+1.1)} . \qquad \text{(XI-24)}$$

We now remove some particulates which are not a part of the three-dimensional network structure from the model compound in Figure XI-6. It is represented by the left side of the drawing (ϕ = small). The sequential network structure has not been touched to retain constant conductivity. Inversely, we may add some particulates, again, without touching the particulates which form a network structure. This is represented by the right side of the drawing (ϕ = large).

It is noteworthy that the number of particulates which form a network structure is identical; however, the fraction of particles which form the network structure differs from each other among the three model compounds as shown. We rewrite Eq. (XI-24) for these model compounds:

$$P(\phi) = \left[\frac{\sigma(\phi)}{\sigma(\phi_{max})} \cdot k^{1.1/\beta}\right]^{\beta(1.1+\beta)} \cdot \frac{\phi_{rl}}{\phi} \qquad \text{(XI-25)}$$

where ϕ_{rl} denotes the volume fraction at the random mix limit.

We define dispersion index (D.I.) as the fraction of particulates being a part of an infinitely large cluster (or three-dimensional network structure). Therefore

D.I. = Fraction of particles which are part of a three-dimensional network structure

$$= P(\ )$$

$$= \left[\frac{\sigma(\phi)}{\sigma(\phi_{max})} \cdot k^{1.1/\beta}\right]^{\beta/1.1+\beta)} \cdot \frac{\phi_{rl}}{\phi} . \qquad \text{(XI-26)}$$

Here

$\sigma(\phi)$: experimentally obtained electrical conductivity;

$\sigma(\phi_{max})$: electrical conductivity at maximum attainable volume fraction (given in Eq. (XII-21));

ϕ: volume fraction of filler in compound;

ϕ_{rl}: volume fraction of filler at random mix limit;

k, β: constants given in Table XI-2.

We may define an average network distance assuming the network is formed in a three-dimensional simple cubic lattice. The average network distance is:

$$\overline{D_{net}} = \left(\frac{\pi}{2} \cdot \frac{1}{(D.I.)\phi}\right)^{1/2} \cdot dp \qquad \text{(XI-27)}$$

where D.I. is the dispersion index defined by Eq. (XI-26), and dp denotes diameter of particulates. The concept of average network distance is summarized in Figure XI-7.

We note that the dispersion index, D.I., proposed here is independent of partizle size and average network distance, $\overline{D_{net}}$, is a function of particle size.

It is clear that values of dispersion index and average network separation distance change as shown in Table XI-3. Dispersion index changes from 0 to 1 and average network distance from infinity to $(\pi/2\phi)^{1/2} \cdot dp$.

A.2.d. Effect of agglomerates. A compound, in practice, may contain agglomerates as well as a continuous three-dimensional network structure. We consider the effect of the agglomerates on the electrical conductivity.

We may assume that the agglomerates are separated from each other in the matrix which contains a three-dimensional network sequence of conductive filler. This is schematically shown in Figure XI-8. Maxwell's expression for a separate mix can simply be rewritten.

$$\sigma'(\phi_a) = \left(\frac{2r_a + r_m + \phi_a(r_a - r_m)}{2r_a + r_m - 2\phi_a(r_a - r_m)} \cdot r_m\right)^{-1} \qquad \text{(XI-28)}$$

where

$\sigma'(\phi_a)$: conductivity of compound which contains agglomerates;

ϕ_a: volume fraczion of agglomerates;

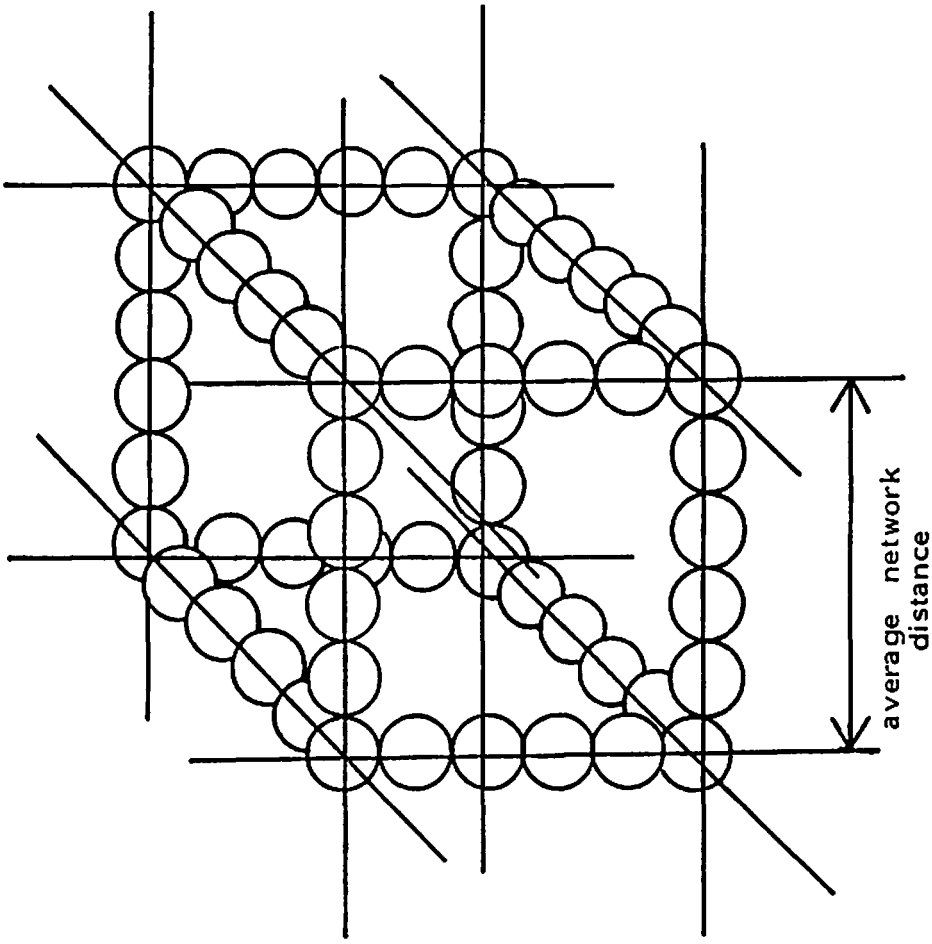

Figure XI-7. Concept of average network distance.

Table XI-3. Characteristics of Dispersion Index and Average Network Distance

	Best Dispersion (Not Infinitely Large Network)	Worst Dispersion (Complete Two Phase)
Dispersion Index D.I.	0	1
Average Network Distance $\overline{D}_{net}$	∞	$(\pi/2\phi)^{1/2} \cdot dp$

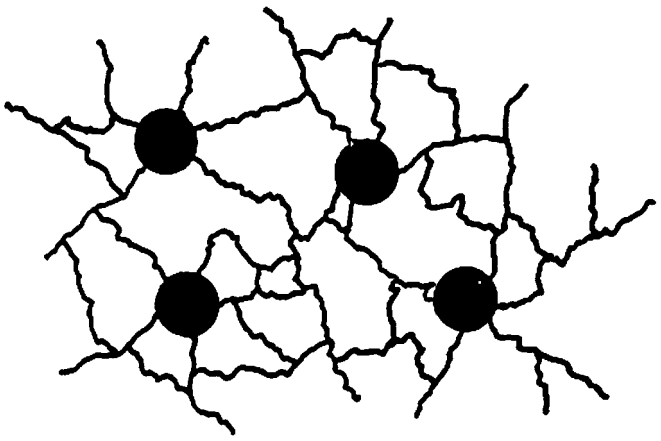

Figure XI-8. Schematic representation of a compound which has both agglomerates and network structure.

r_a: resistivity of agglomerates;

r_m: resistivity of matrix which contains three-dimensional network structure.

We may assume that the resistivity of agglomerates is much smaller than that of matrix, that is, $r_a << r_m$. Equation (XI-28) reduces to

$$\sigma'(\phi_a) \simeq \left(\frac{r_m - \phi_a r_m}{r_m + 2\phi_a r_m} \cdot r_m\right)^{-1}$$

$$\simeq F(\phi_a) \cdot (r_m)^{-1} \qquad \text{(XI-29)}$$

and

$$F(\phi_a) = \frac{1 + 2\phi_a}{1 - \phi_a} \qquad \text{(XI-30)}$$

where $(r_m)^{-1}$ is the conductivity of the matrix which contains a network of particulates. When the system contains no agglomerate $\phi_a = 0$, the function $F(\phi_a) = 1$, then the conductivity of the system is identical to that of a matrix containing a network. The function $F(\phi_a)$ is plotted as a function of ϕ_a in Figure XI-9. The electrical conductivity of compound $\sigma'(\phi_a)$ is two times greater than that of the matrix when the volume fraction of agglomerates ϕ_a is 0.25. The increase of the electrical conductivity of compound due to the existence of agglomerates is trivial in comparison with the conductivity of compound which varies exponentially from 10^{-17} to 10^{0} depending upon the network szructure of the conductive filler. The electric conductivity is relatively insensitive to the existence of agglomerates.

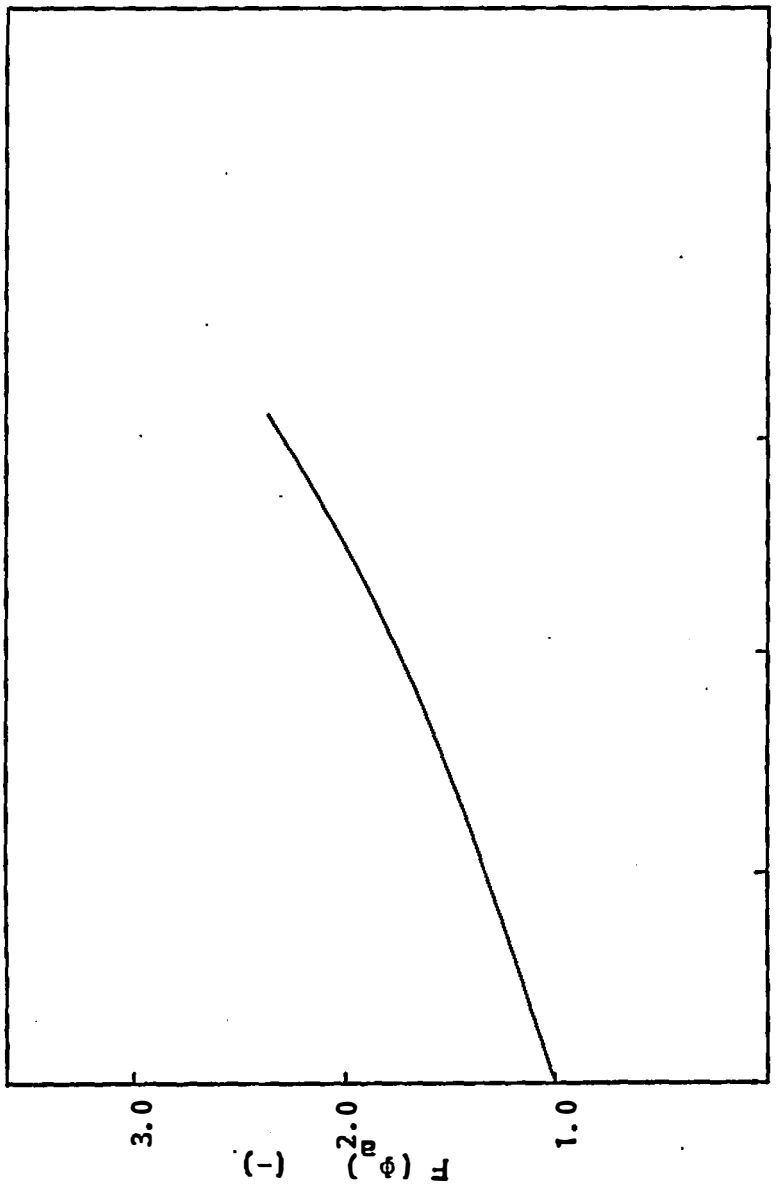

Figure XI-9. Function $F(\phi_a)$ as a function of ϕ_a.

B. DISCUSSION

B.1. Dispersion Indices and Average Network Distances of Carbon Black Compounds

Dispersion indices and average network separation distances have been determined for polypropylene and polystyrene/carbon black compounds.

Figure XI-10 gives the dispersion indices of various polypropylene/carbon black compounds as a function of the volume fraction of carbon black. All compounds were prepared in a two roll mixing mill and internal mixer having a mixing time of 20 minutes. We note that the physical significance of the dispersion index defined in Eq. (XI-26) is the fraction of particles being part of a three-dimensional network structure. The dispersion is best at D.I. = 0 and worst at D.I. = 1. N326 and N351 black carbon compounds possess large dispersion indices at any volume fraction. Six percent to 13% of carbon black forms a segmental network structure. N326 black (dp = 0.026 μm) always shows a slightly greater dispersion index than the N351 black (dp = 0.028 μm). N990 black (dp = 0.32 μm) compounds show the best dispersion. The dispersion index falls from 1.3×10^{-2} to 1.5×10^{-3} with decreasing volume fraction. The percentage of black forming a network structure changes from 1.3% to 0.15%.

The particle size of carbon black may be a significant parameter in determining the levels of dispersion. Dispersion is improved as average particle size increases. The correlation between dispersion

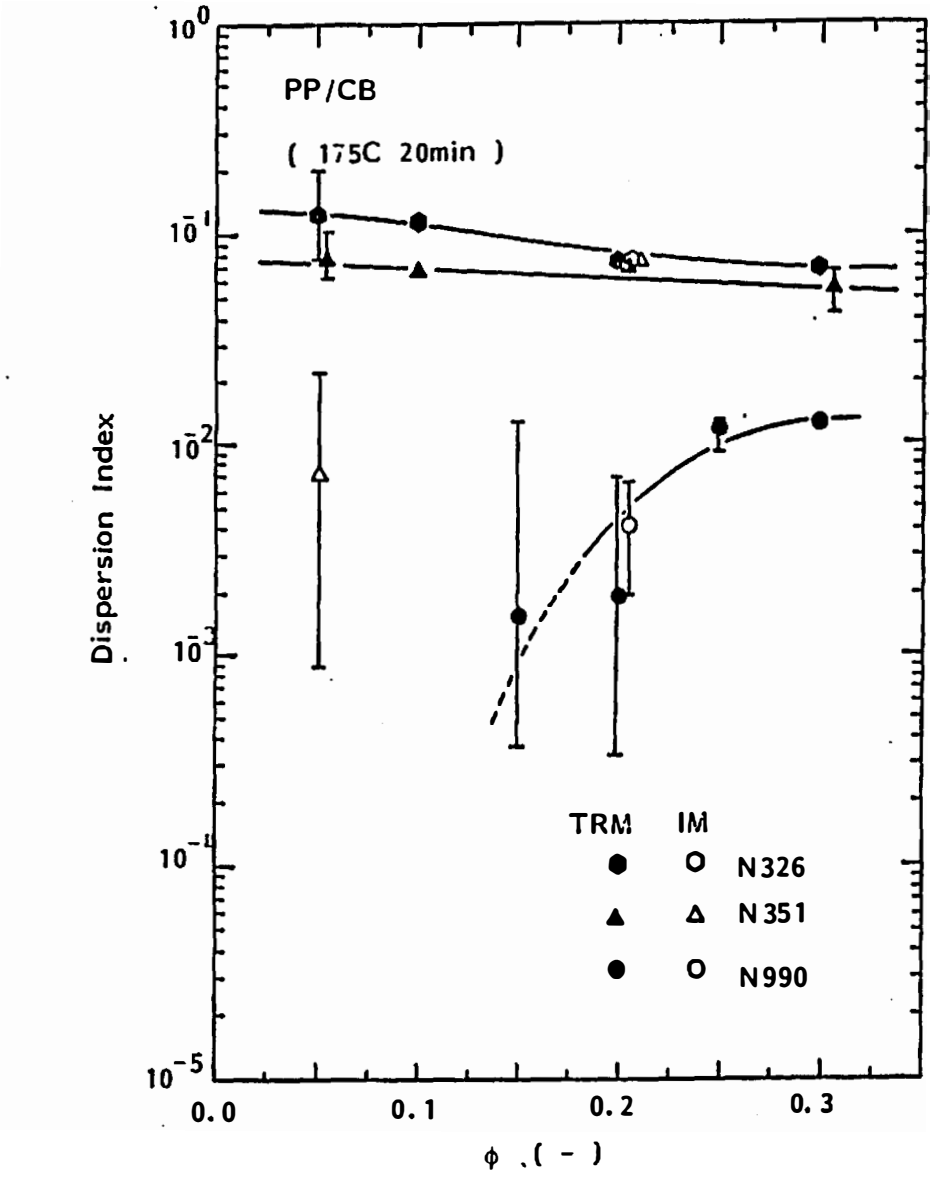

Figure XI-10. Dispersion index of various PP/CB compounds as a function of volume fraction.

and structure of carbon black aggregates is not clear. This is summarized in Table XI-4.

Two roll mill processed N321 and N351 compounds (closed hexagonal and triangular symbols) tend to increase dispersion index slightly as volume fraction decreases. This may be related to the mixing process in the two roll mill. The weight of the compounds was set constant (300 gr.) regardless of volume fraction of filler in the two roll mill mixing process. The total volume of compound is greater at low volume fractions since carbon black possesses greater density than polypropylene. The nip distance between the two rolls was considerably greater at low volume fraction compound to maintain appropriate mixing conditions. It is important to note that the low volume fraction compounds, as a result, were mixed with substantially lower shear rate and stress than high volume fraction compounds. In the internal mixer, the distance between rotor tip and chamber wall is always constant regardless of volume fraction. Low volume fraction compounds (ϕ = 0.05) appear to have better dispersion than high volume fraction compounds (ϕ = 0.20) in the internal mixer (open triangular symbol).

The average network distance of the same series of polypropylene/carbon black compounds is given in Figure XI-11 as a function of volume fraction. We note that the greater average network distance denotes good dispersion. The average network distance of all compounds decreases with increasing volume fraction. N990 black compounds possess the largest network distances. This ranges

Table XI-4. Dispersion Index, Network Distance, Particle Size and DBP Index for Carbon Black Compounds

	Type of Carbon Black					
	N990		N351		N326	
Dispersion Index D.I.	1.5×10^{-3}-1.3×10^{-2}	<<	5.8×10^{-2}-8.0×10^{-2}	<	7.0×10^{-2}-1.3×10^{-1}	
$\overline{D_{net}}$ (μm)	6.4×10^{0}-2.7×10^{1}	>>	2.7×10^{-1}-5.5×10^{-1}	>	2.2×10^{-1}-4.0×10^{-1}	
dp (μm)	0.32	>>	0.028	>	0.026	

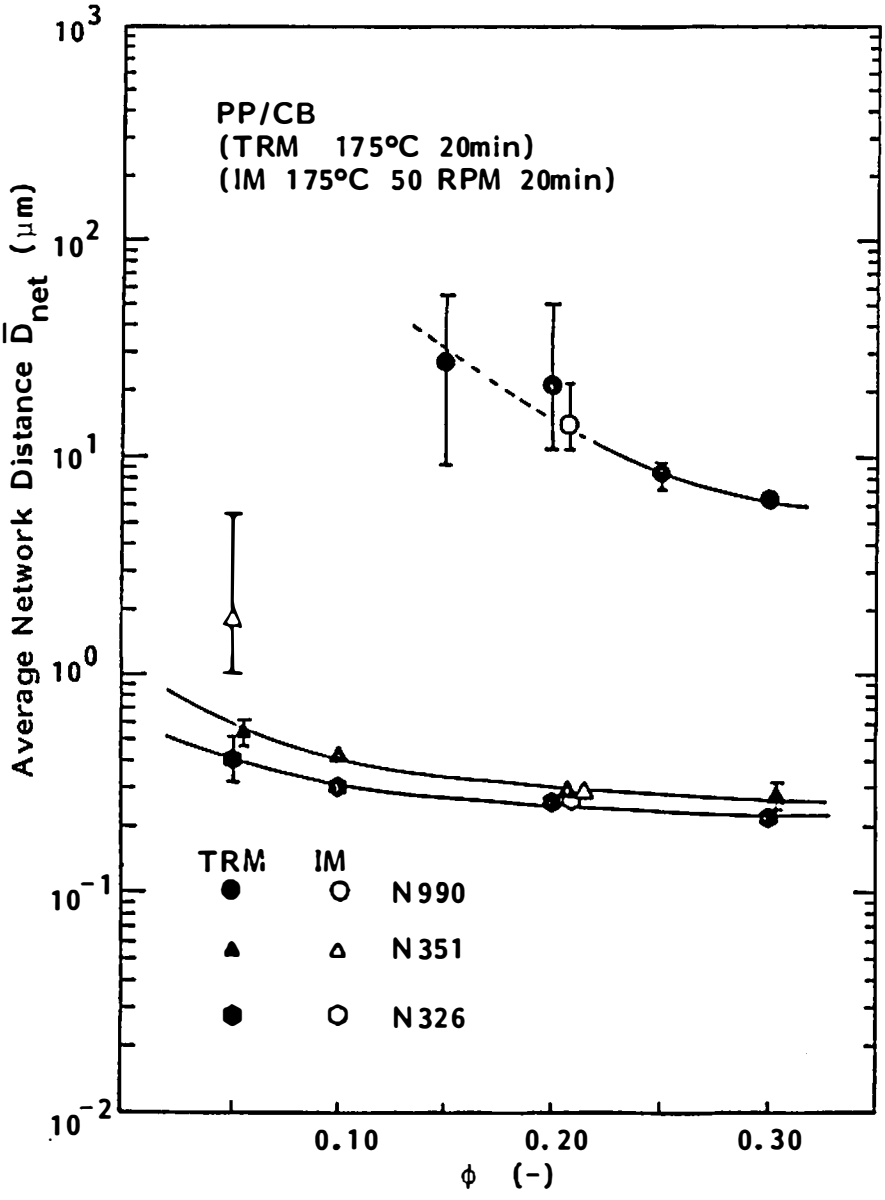

Figure XI-11. Average network distance of various PP/CB compounds as a function of volume fraction.

from 6.4×10^{0} μm to 2.7×10^{1} μm. The average network distance of N990 compound is about 20 to 85 times greater than the ultimate particle size of low structure N990 black. N326 and N351 black compounds possess much smaller network distances than N990 black. These ranges are 2.2×10^{-1} μm to 5.5×10^{-1} μm for two roll mill prepared compounds. Correlations among dispersion index, average network distance, particle diameter and DBP structure index are summarized in Table XI-4.

The effect of annealing is shown in Figures XI-12 and XI-13 for N990 black compounds prepared in a two roll mill. Two types of compounds were annealed from 200°C to 90°C at a cooling rate of -1.34°C/min. The dispersion index increases and average network distance decreases with heat treatment.

The formation of the three-dimensional network is promoted by heat treatment. This may be due to the formation of crystalline phase in matrix polypropylene. Carbon black particles might be pushed out from a crystalline phase as an impurity during the formation of spherulites. This mechanism concentrates the carbon black in the amorphous phase. An increasing fraction of black may form network structures at high concentrations.

The dispersion indices of internal mixer compounds are summarized in Figures XI-14 and XI-15. The mixing time varies from 0 to 20 minutes. The volume fractions of all compounds are 0.20 in Figure XI-14. N326 and N351 black compounds maintain large dispersion indices regardless of mixing time. Seven to 8% of carbon

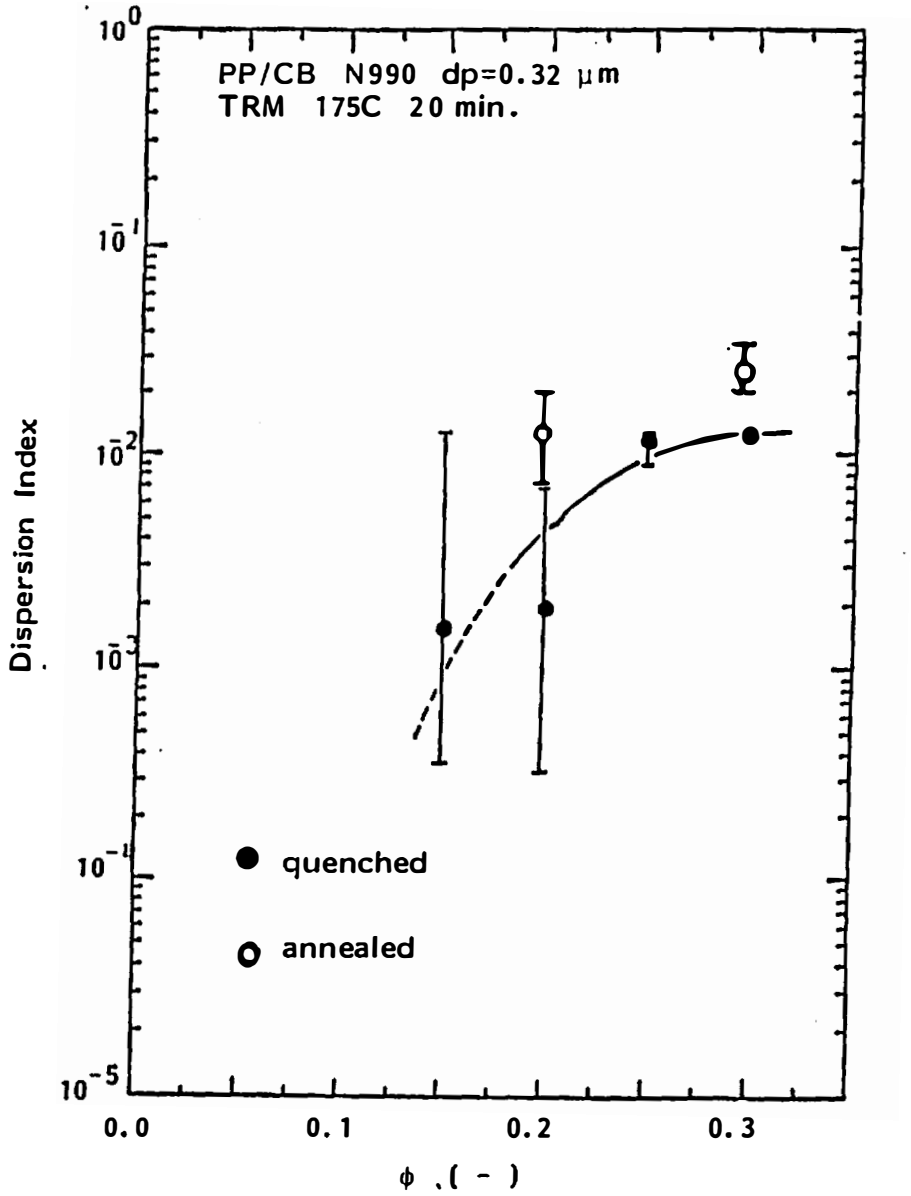

Figure XI-12. Dispersion index of various PP/CB compounds as a function of volume fraction.

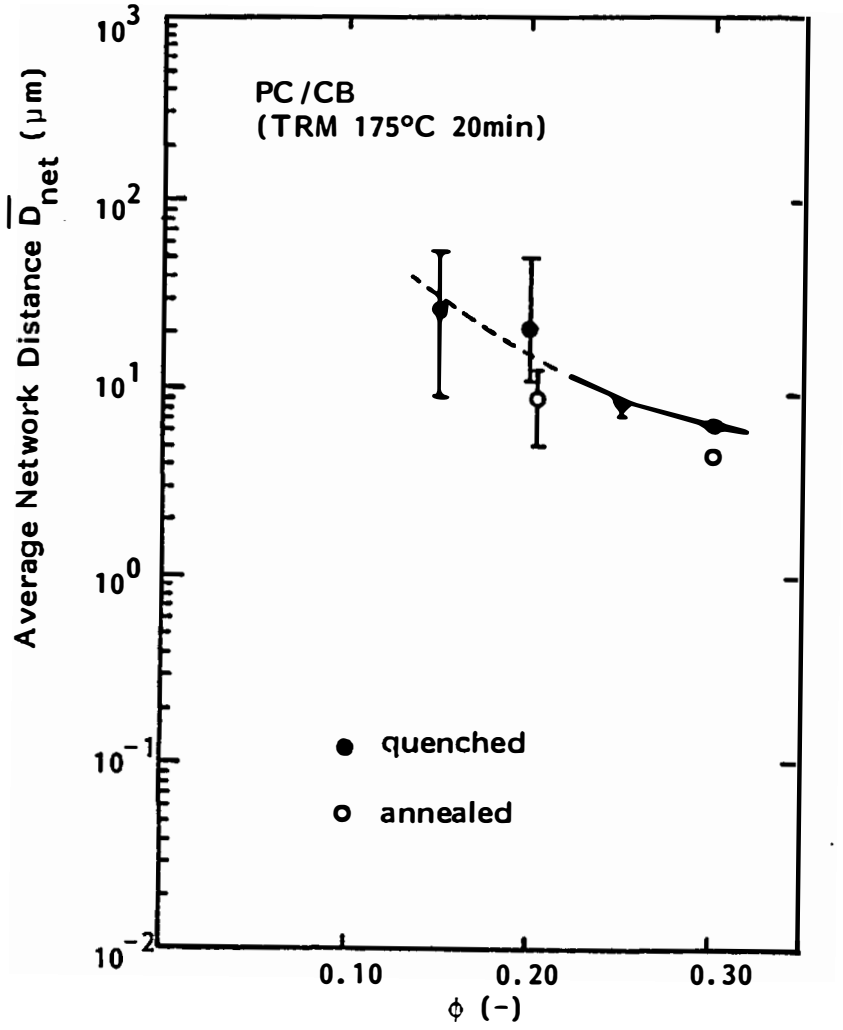

Figure XI-13. Average network distance of various N990 carbon black compounds as a function of volume fraction.

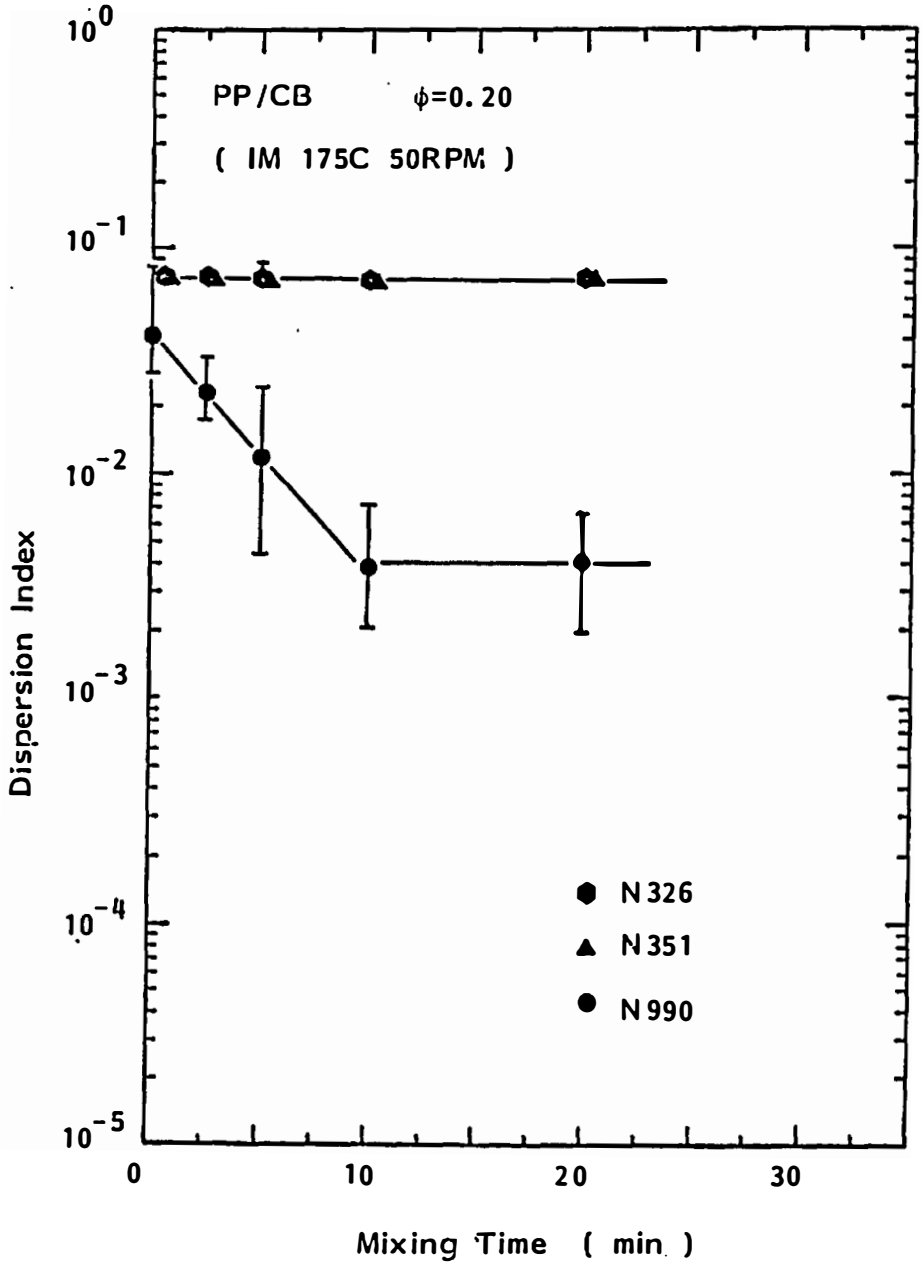

Figure XI-14. Dispersion index of internal mixer compounds as a function of mixing time.

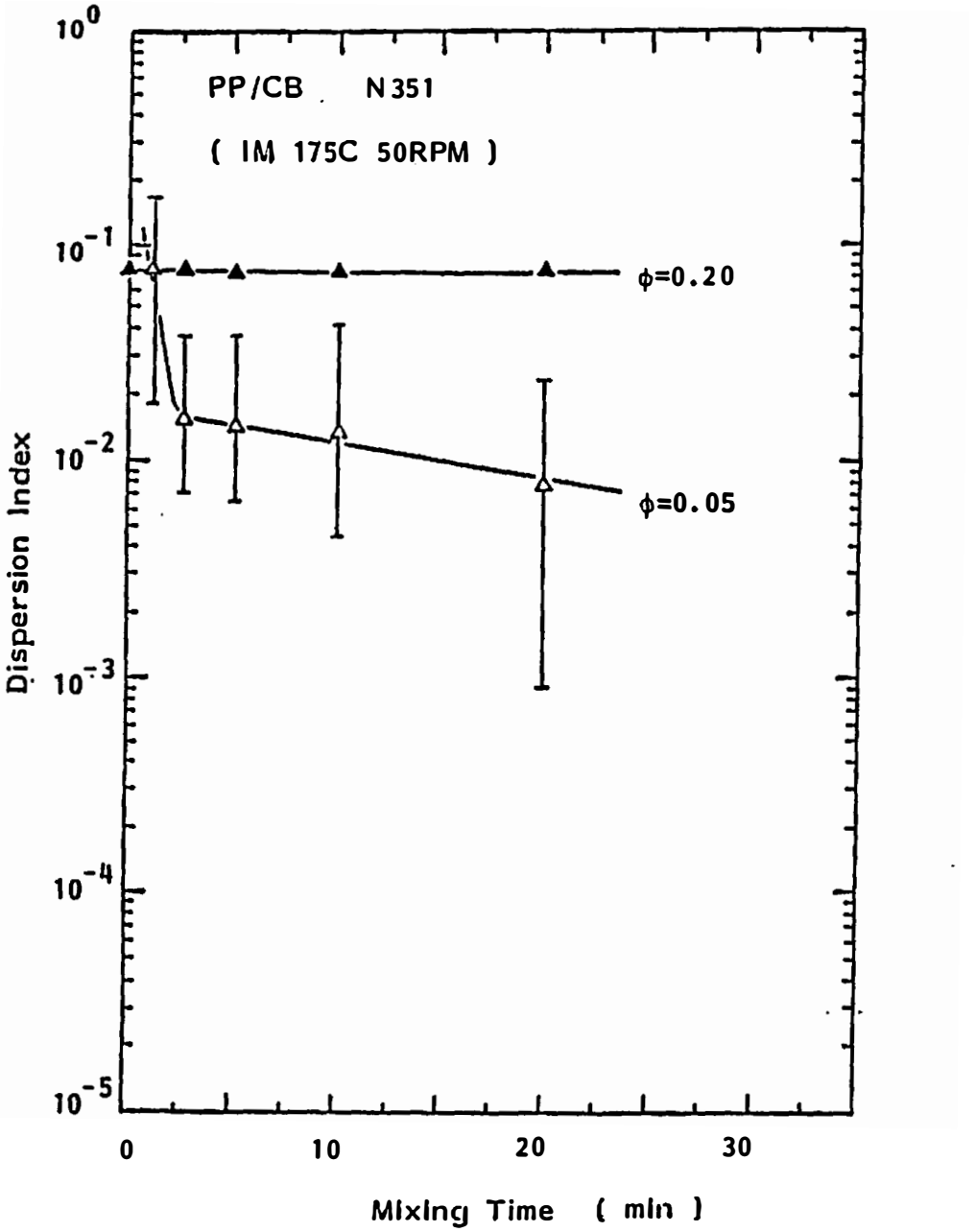

Figure XI-15. Dispersion index of internal mixer compounds as a function of mixing time.

black can form three-dimensional structures. In contrast, N990 black compounds exhibit improved dispersion with mixing time. The black constituting structure sharply drops from 4.4% to 0.38% in the first 10 minutes, then maintains constant values.

Low volume fraction compounds of N351 black show improvement of dispersion during mixing processes (Figure XI-15). The dispersion index suddenly decreases in the first 2.5 minutes and decays gradually over the mixing period of 20 minutes.

The average network distance of the same series of polypropylene/carbon black compounds is given as a function of mixing time in an internal mixer (Figure XI-16). It is clear that N990 compounds and N351 black compounds (ϕ = 0.05) indicate progress of dispersion with mixing time. N326 and N351 compounds (ϕ = 0.20) show no improvement.

The dispersion indices and average network distances of all the polypropylene/carbon black compounds and polystyrene/carbon black compound have been summarized in Tables XI-5 through XI-7 and Table XI-8.

B.2. Mechanical Properties and Level of Dispersion

The tensile stress-strain characteristics of various PP/CB compounds mixed in the internal mixer (IM) and two roll mill (TRM) have been measured using a Monsanto tensometer. The samples were compression molded at 200°C and quenched. Dumbbell shaped specimens were obtained by punching with a dumbbell shaped die. The test specimen of very brittle samples was cut using a sharp razor blade.

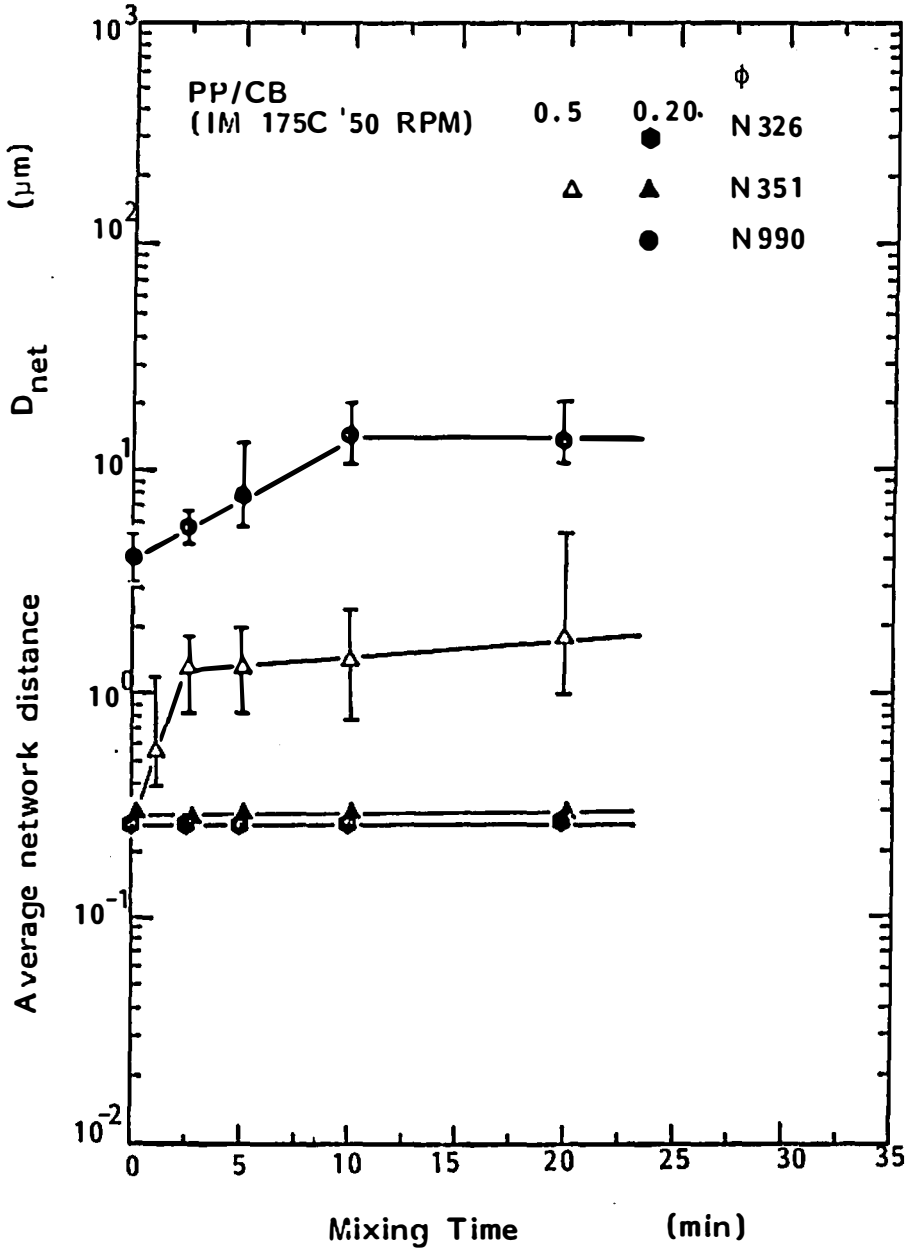

Figure XI-16. Average network distance of various internal mixer compounds as a function of mixing time.

Table XI-5. Dispersion Index and Average Network Distance for Two Roll Mill Processed PP/CB Com ounds

PP/CB TRM 175C 50 RPM						
CB	ϕ (-)	T_{mix} (min)	Number of Samples (-)	$\log\sigma_{min} < \overline{\log\sigma} < \log\sigma_{max}$ (Ω^{-1} cm^{-1})	$D.I._{min} < \overline{D.I.} < D.I._{max}$ (-)	$\bar{D}_{net\ max} > \bar{D}_{net} > \bar{D}_{net\ min}$ (μm)
N990	0.15	20	4	-11 < -8.4 < -5.3	$3.4\times10^{-4} < 1.5\times10^{-3} < 1.3\times10^{-2}$	$5.6\times10^{1} < 2.67\times10^{1} < 9.1\times10^{0}$
	0.20	20	4	-10.7 < -7.7 < -5.6	$3.1\times10^{-4} < 1.9\times10^{-3} < 7.0\times10^{-3}$	$5.1\times10^{1} < 2.1\times10^{1} < 1.1\times10^{1}$
	0.25	20	4	-4.8 < -4.4 < -4.3	$9.2\times10^{-3} < 1.2\times10^{-2} < 1.3\times10^{-2}$	$8.4\times10^{0} < 7.3\times10^{0} < 7.0\times10^{0}$
	0.30	20	4	-4.1 < -3.9 < -3.9	$1.2\times10^{-2} < 1.3\times10^{-2} < 1.3\times10^{-2}$	$6.7\times10^{0} < 6.4\times10^{0} < 6.4\times10^{0}$
N326	0.05	20	4	-3.9 < -3.1 < -2.3	$8.0\times10^{-2} < 1.3\times10^{-1} < 2.1\times10^{-1}$	$5.2\times10^{-1} < 4.0\times10^{-1} < 3.2\times10^{-1}$
	0.10	20	4	-2.1 < -2.1 < -2.0	$1.2\times10^{-1} < 1.2\times10^{-1} < 1.3\times10^{-1}$	$3.0\times10^{-1} < 3.0\times10^{-1} < 2.0\times10^{-1}$
	0.20	20	4	-1.7 < -1.7 < -1.7	$7.7\times10^{-2} < 7.7\times10^{-2} < 7.7\times10^{-2}$	$2.6\times10^{-1} < 2.6\times10^{-1} < 2.6\times10^{-1}$
	0.30	20	4	-1.3 < -1.2 < -1.2	$6.6\times10^{-2} < 7.0\times10^{-2} < 7.0\times10^{-2}$	$2.3\times10^{-1} < 2.2\times10^{-1} < 2.2\times10^{-1}$
N351	0.05	20	4	-4.2 < -3.9 < -3.4	$6.7\times10^{-2} < 8.0\times10^{-2} < 1.1\times10^{-1}$	$6.1\times10^{-1} < 5.5\times10^{-1} < 4.7\times10^{-1}$
	0.10	20	4	-3.0 < -3.0 < -2.9	$6.9\times10^{-2} < 6.9\times10^{-2} < 7.4\times10^{-2}$	$4.2\times10^{-1} < 4.2\times10^{-1} < 4.1\times10^{-1}$
	0.20	20	4	-1.9 < -1.8 < -1.8	$6.8\times10^{-2} < 7.3\times10^{-2} < 7.3\times10^{-2}$	$3.0\times10^{-1} < 2.9\times10^{-1} < 2.9\times10^{-1}$
	0.30	20	4	-2.0 < -1.5 < -1.2	$4.3\times10^{-2} < 5.8\times10^{-2} < 7.0\times10^{-2}$	$3.1\times10^{-1} < 2.7\times10^{-1} < 2.4\times10^{-1}$

Table XI-6. Dispersion Index and Average Network Distance for Two Roll Mill Processed PP/CB Compounds (after Heat Treatment)

PP/CB TRM 175C 20 MIN Annealed in HP -1.34°C/min						
CB	ϕ (-)	T_{mix} (min)	Number of Samples (-)	$\log\sigma_{min} < \overline{\log\sigma} < \log\sigma_{max}$ (Ω^{-1} cm^{-1})	$D.I._{min} < \overline{D.I.} < D.I._{max}$	$\overline{D}_{net\ max} > \overline{D}_{net} > \overline{D}_{net\ min}$ (μm)
N990	0.20	20	4	$-5.9 < -5.0 < -4.1$	$5.9\times10^{-3} < 1.0\times10^{-2} < 1.8\times10^{-2}$	$1.2\times10^{1} < 9.0\times10^{0} < 6.7\times10^{0}$
	0.30	20	4	$-2.8 < -2.7 < -2.6$	$2.6\times10^{-2} < 2.8\times10^{-2} < 3.0\times10^{-2}$	$4.5\times10^{0} < 4.4\times10^{0} < 4.2\times10^{0}$

Table XI-7. Dispersion Index and Average Network Distance for Internal Mixer Processed PP/C8 Compounds

PP/C8 IM 175C 50 RPM						
C8	ϕ (-)	T_{mix} (min)	Number of Samples (-)	$\log\sigma_{min} < \overline{\log\sigma} < \log\sigma_{max}$ (Ω^{-1} cm^{-1})	$D.I._{min} < \overline{D.I.} < D.I._{max}$	$\overline{D}_{net\ max} > \overline{\overline{D}}_{net} > \overline{D}_{net\ min}$ (μm)
N990	0.20	0	8	-3.4 < -2.6 < -1.6	$2.7\times10^{-2} < 4.4\times10^{-2} < 8.2\times10^{-2}$	$5.5\times10^{0} < 4.3\times10^{0} < 3.1\times10^{0}$
		2.5	8	-4.2 < -3.7 < -3.1	$1.7\times10^{-2} < 2.3\times10^{-2} < 3.3\times10^{-2}$	$6.9\times10^{0} < 5.9\times10^{0} < 4.9\times10^{0}$
		5	8	-6.5 < -4.7 < -3.6	$4.1\times10^{-3} < 1.2\times10^{-3} < 2.4\times10^{-2}$	$1.4\times10^{1} < 8.2\times10^{0} < 5.1\times10^{0}$
		10	8	-7.7 < -6.6 < -5.6	$1.9\times10^{-3} < 3.8\times10^{-3} < 7.0\times10^{-3}$	$2.1\times10^{1} < 1.5\times10^{1} < 1.1\times10^{1}$
		20	8	-7.7 < -6.5 < -5.7	$1.9\times10^{-3} < 4.1\times10^{-3} < 6.6\times10^{-3}$	$2.1\times10^{1} < 1.4\times10^{1} < 1.1\times10^{1}$
N326	0.20	0	8	-1.8 < -1.7 < -1.6	$7.3\times10^{-2} < 7.7\times10^{-2} < 8.2\times10^{-2}$	$2.7\times10^{-1} < 2.6\times10^{-1} < 2.5\times10^{-1}$
		2.5	8	-1.8 < -1.7 < -1.7	$7.3\times10^{-2} < 7.7\times10^{-2} < 7.7\times10^{-2}$	$2.7\times10^{-1} < 2.6\times10^{-1} < 2.6\times10^{-1}$
		5	8	-1.8 < -1.7 < -1.5	$7.3\times10^{-2} < 7.7\times10^{-2} < 8.7\times10^{-2}$	$2.7\times10^{-1} < 2.6\times10^{-1} < 2.5\times10^{-1}$
		10	8	-1.8 < -1.7 < -1.6	$7.3\times10^{-2} < 7.7\times10^{-2} < 8.2\times10^{-2}$	$2.7\times10^{-1} < 2.6\times10^{-1} < 2.5\times10^{-2}$
		20	8	-1.8 < -1.7 < -1.7	$7.3\times10^{-2} < 7.7\times10^{-2} < 7.7\times10^{-2}$	$2.7\times10^{-1} < 2.6\times10^{-1} < 2.6\times10^{-2}$
N351	0.20	0	8	-1.8 < -1.7 < -1.5	$7.3\times10^{-2} < 7.1\times10^{-2} < 8.7\times10^{-2}$	$2.9\times10^{-1} < 2.8\times10^{-1} < 2.7\times10^{-1}$
		2.5	8	-1.8 < -1.7 < -1.6	$7.3\times10^{-2} < 7.7\times10^{-2} < 8.2\times10^{-2}$	$2.9\times10^{-1} < 2.8\times10^{-1} < 2.7\times10^{-1}$
		5	8	-1.8 < -1.8 < -1.7	$7.3\times10^{-2} < 7.3\times10^{-2} < 7.7\times10^{-2}$	$2.9\times10^{-1} < 2.0\times10^{-2} < 2.8\times10^{-1}$
		10	8	-1.9 < -1.8 < -1.6	$6.8\times10^{-2} < 7.3\times10^{-2} < 8.2\times10^{-2}$	$3.0\times10^{-1} < 2.9\times10^{-2} < 2.7\times10^{-1}$
		20	8	-1.7 < -1.7 < -1.6	$7.7\times10^{-2} < 7.7\times10^{-2} < 8.2\times10^{-2}$	$2.8\times10^{-1} < 2.8\times10^{-1} < 2.7\times10^{-1}$
N351	0.05	1	8	-6.3 < -3.9 < -2.7	$1.8\times10^{-2} < 8.0\times10^{-2} < 1.7\times10^{-1}$	$1.2\times10^{0} < 5.5\times10^{-1} < 3.8\times10^{-1}$
		2.5	8	-7.9 < -6.6 < -5.2	$6.9\times10^{-3} < 1.5\times10^{-2} < 3.6\times10^{-2}$	$1.9\times10^{0} < 1.3\times10^{0} < 8.3\times10^{-1}$
		5	8	-8.1 < -6.7 < -5.2	$6.1\times10^{-3} < 1.4\times10^{-2} < 3.6\times10^{-2}$	$2.0\times10^{0} < 1.3\times10^{0} < 8.3\times10^{-1}$
		10	8	-8.7 < -6.8 < -5.0	$4.2\times10^{-3} < 1.3\times10^{-2} < 4.1\times10^{-2}$	$2.4\times10^{0} < 1.4\times10^{0} < 7.8\times10^{-1}$
		20	8	-11.3 < -7.8 < -5.9	$8.5\times10^{-4} < 7.3\times10^{-3} < 2.3\times10^{-2}$	$5.4\times10^{0} < 1.8\times10^{0} < 1.0\times10^{0}$

Table XI-8. Dispersion Index and Average Network Distance for Two Roll Mill Processed PS/CB Compound

CB	ϕ (-)	Number of Samples (-)	$\log\sigma$ (Ω^{-1} cm^{-1})	D.I. (-)	$\overline{D}_{net}$ (μm)
N990	0.30	1	-12.7	6.16×10^{-5}	9.33×10^{1}

The initial sample length was 4 cm and about 0.04 cm in thickness. The jaw speed was 0.2 in/min (0.508 cm/min). Ten specimens were used for each test.

The elongation to break of various polypropylene/carbon black compounds is plotted as a function of the dispersion index (D.I.) which was obtained from electric conductivity measurements. Figure XI-17 shows the results for internal mixer compounds (ϕ = 0.05, 0.20) with various mixing times.

The periods of mixing are indicated in the figure for all compounds. We note D.I. = 0.0 and 1.0 which means the best and worst dispersion, respectively. All the compounds which have a large dispersion index (i.e., bad dispersion) have small elongations to break. N351 and N326 compounds (ϕ = 0.20) maintain large dispersion indices at any mixing time. All of these have small elongations to break. In the case of N990 compounds dispersion has improved during mixing and elongation to break has increased. The N351 compound at a volume fraction of 0.05 shows an improvement of dispersion as mixing progresses. These increase elongation to break also.

Figure XI-18 shows the results for two roll mill compounds. Mixing time is always constant but volume fraction varies. N990 compounds have better dispersion at low volume fractions and elongation to break increases with decreasing volume fraction. N351 and N326 compounds, however, have a large dispersion index at lower volume fractions, and elongation to break in this system increases with increasing dispersion index. This suggests that the percolation

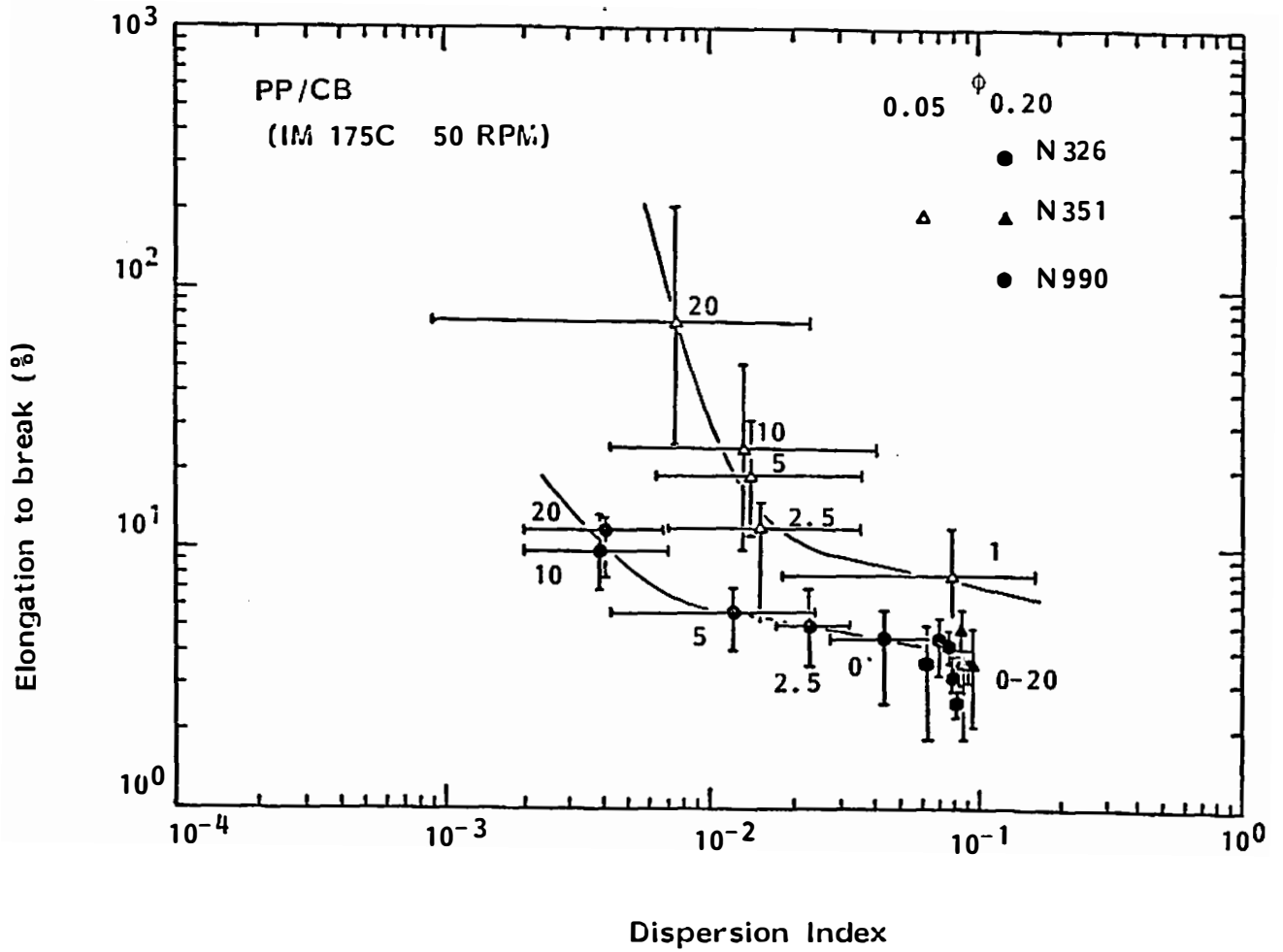

Figure XI-17. Elongation to break for various internal mixer compounds as a function of dispersion index.

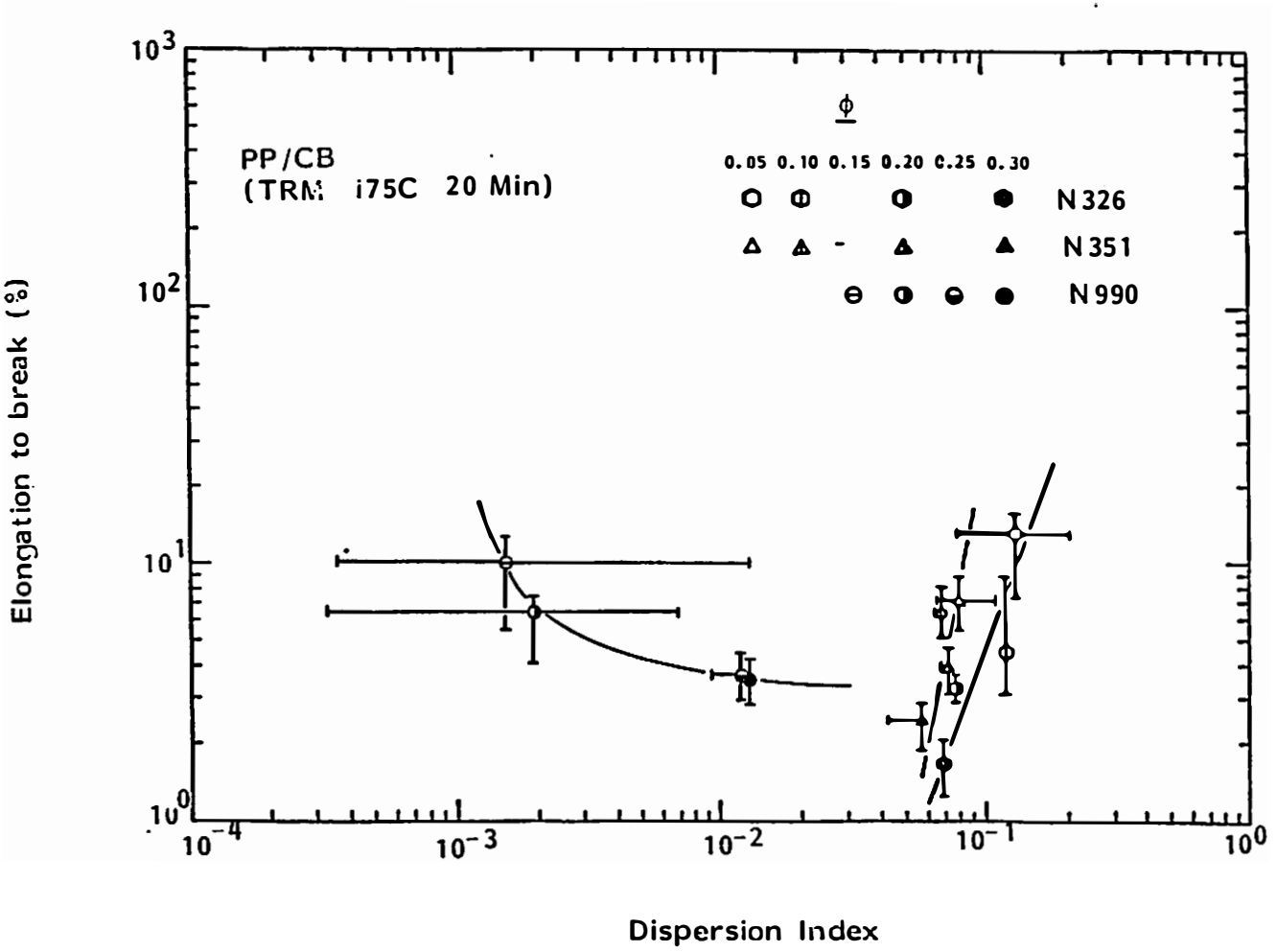

Figure XI-18. Elongation to break for various two roll mix compounds as a function of dispersion index.

probability $P(\phi)$ alone is not the responsible parameter for the failure mechanism.

The average network distance $\overline{D_{net}}$ is another index of dispersion. $\overline{D_{net}}$ is related to the volume fraction of filler which forms network in compounds, (D.I.) $\cdot \phi$. Therefore, $\overline{D_{net}}$ may be a better responsible parameter for the mechanical properties.

Figures XI-19 and XI-20 show the relation between elongation to break and average network distance. We note that a larger network distance means better dispersion. Figure XI-19 shows the results of internal mixer compounds (ϕ = 0.05, 0.20) (mixing time = variable). The elongation to break increases with increasing network distance. All compounds which have a small network distance ($\sim$0.3 μm) have small elongation to break ($\sim$4%). N990 compounds (ϕ = 0.20) and N351 compounds (ϕ = 0.05) increased the network distance with mixing time and elongation to break increases. Compounds with less carbon black have larger elongations to break at fixed network distance.

Figure XI-20 shows the results for two roll mill compounds The mixing time is always 20 minutes, but volume fraction varies from 0.05 to 0.30. All compounds (N990, N351 and N326) have a larger elongation to break at greater network distance. Figure XI-21 shows the relation between elongation to break and network distance for all polypropylene/carbon black compounds. Two roll mill compounds (closed symbols) have various volume fractions and the mixing time is always 20 minutes. The internal mixer prepared compounds (open symbols) have constant volume fraction (ϕ = 0.05, 0.20) and mixing time varying from

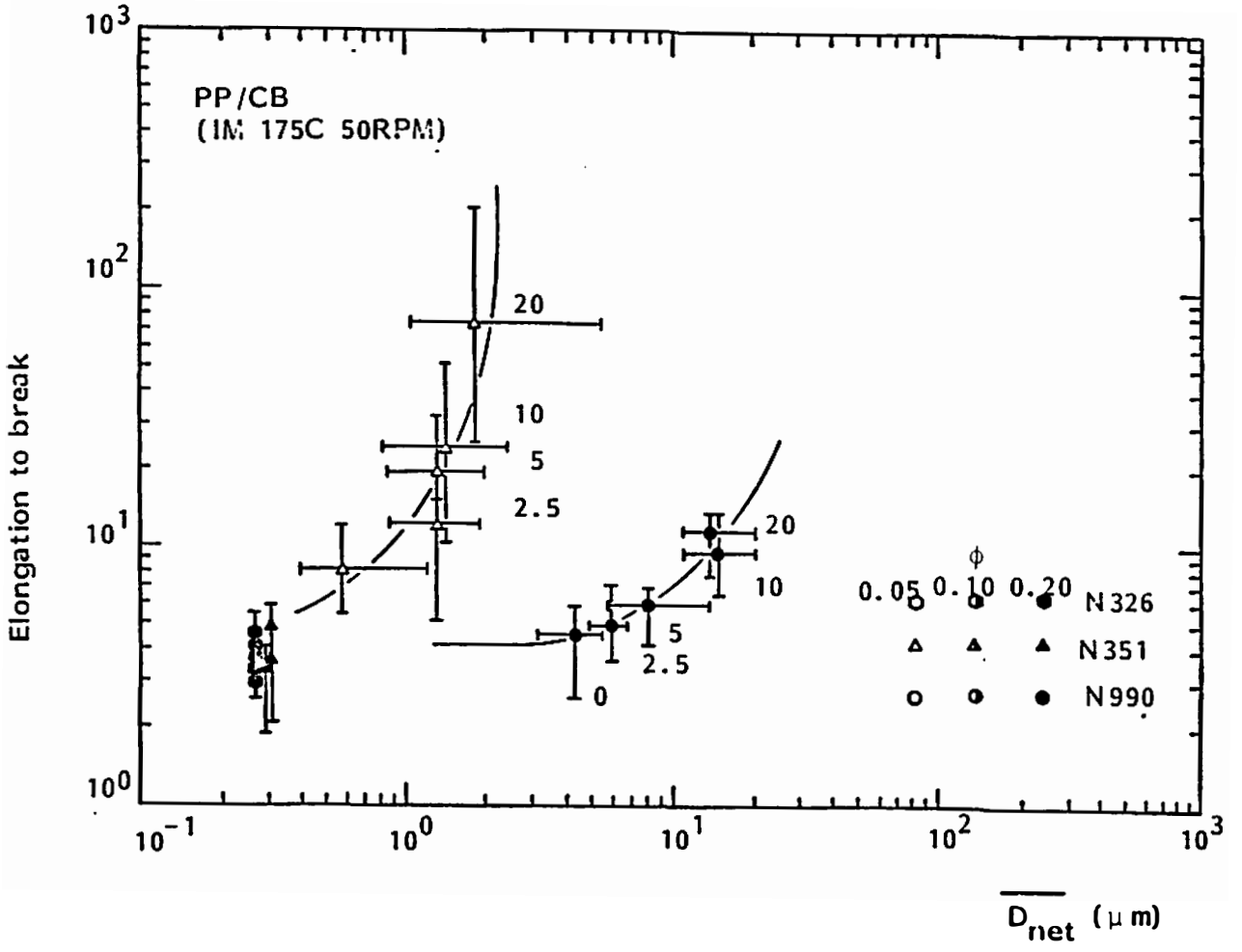

Figure XI-19. Elongation to break for various internal mixer compounds as a function of D_{net}.

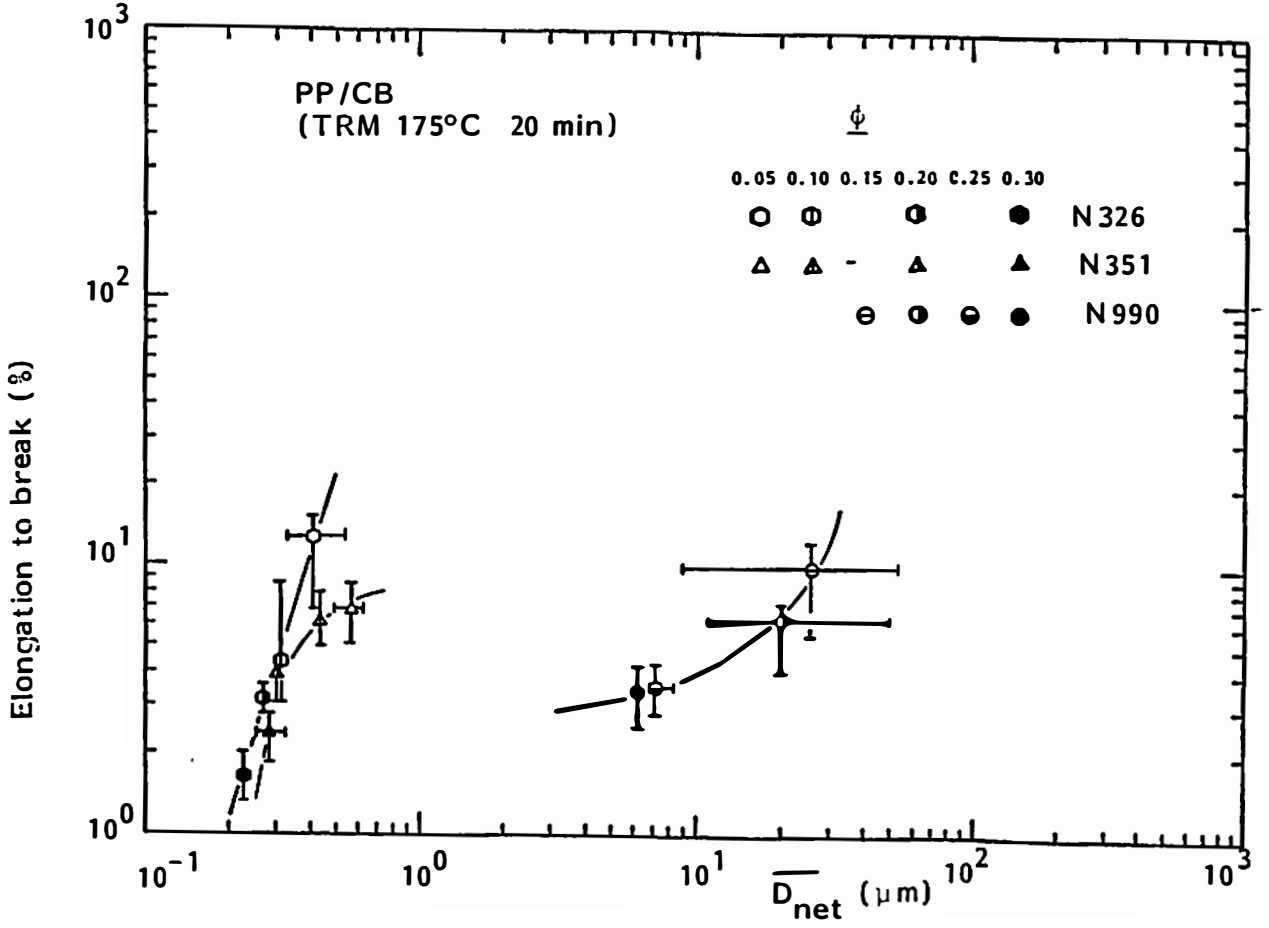

Figure XI-20. Elongation to break for various two roll mill compounds as a function of $\overline{D}_{net}$.

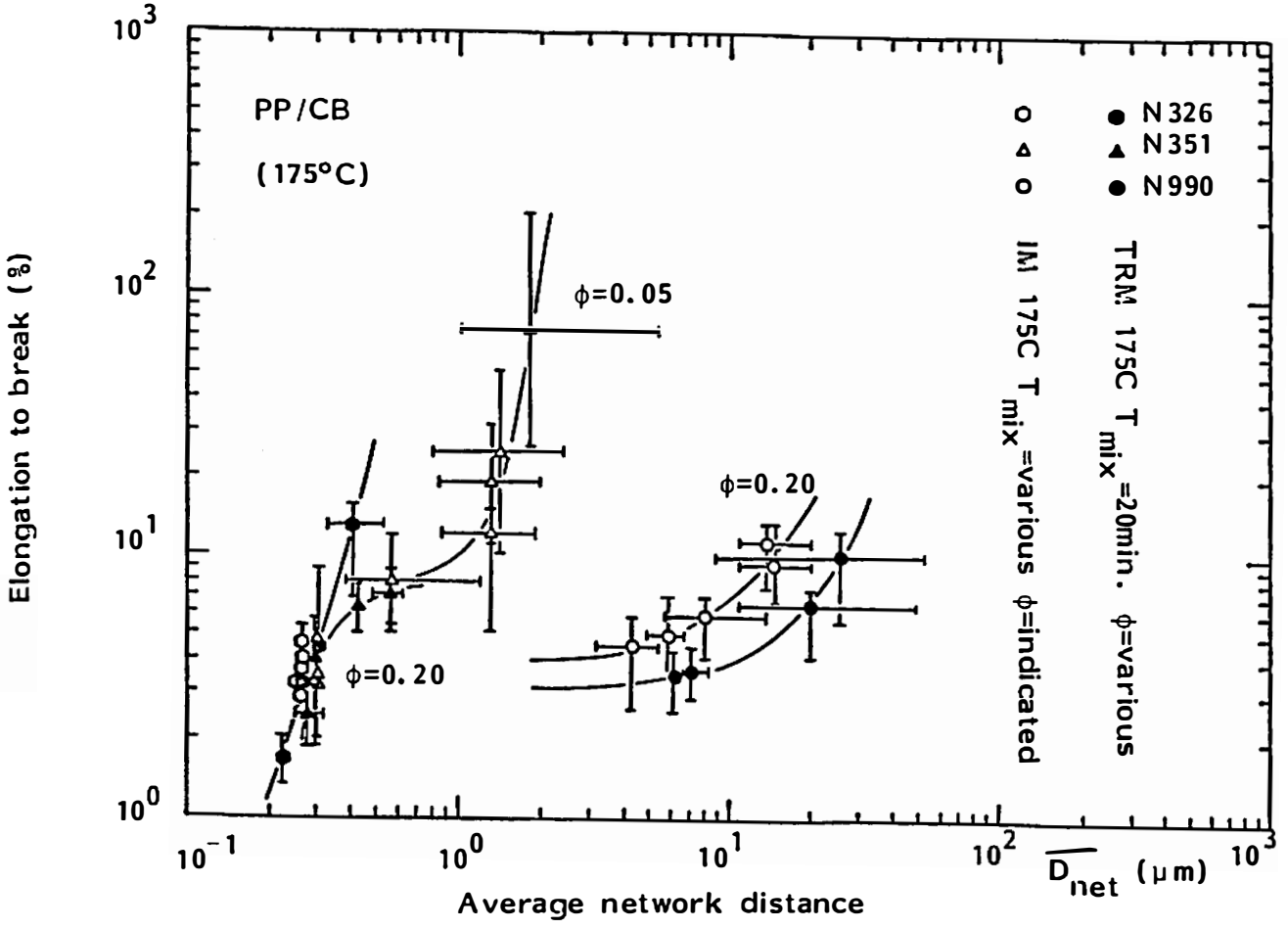

Figure XI-21. Elongation to break for various PP/CB compounds as a function of $\overline{D_{net}}$.

0 minutes to 20 minutes. All compounds tend to have small elongations to break at small network distances. N351 compounds cover a wide range of network distances. The elongation to break of N351 compounds have a plateau (or transient) region at a network distance of 0.4 to 1.0 μm. At larger network distances, the elongation to break increases rapidly. This plateau region may correspond to a yield point. The internal mixer prepared N990 compounds have a larger elongation to break than two roll mill compounds at fixed network distance. The reason is not clear.

The elongation to break of compounds were characterized by an average network distance. The elongation to break increases with increasing network distance. The propagation of a crack may occur more easily when network distance is small.

CHAPTER XII

THEORY OF MIXING

A. INTRODUCTION

A.1. Terminology

We will begin by reviewing and defining the terminology which is used in the present chapter. These are the incorporation process, distributive mixing and a dispersive mixing.

The incorporation process takes place at the beginning of the mixing. One or more types of ingredients (for example, fillers) are added into the mixing device and then these are taken into the matrix phase. The ingredients, when they were surrounded by the matrix phase, can be the states of the ultimate particles, the aggregates or the agglomerates. This step of the mixing is called the incorporation process.

When the ingredients are incorporated with the form of the agglomerates, the agglomerates which have not experienced the breakdown are called the initial agglomerates.

The incorporated substances such as the ultimate particles, the aggregates and the agglomerates may change their relative position, distances and arrangements during the mixing process.

Distributive mixing refers to such relative motions of substances due to the deformation given to the mixture. Spencer and

Wiley (S-7) have referred to this kind of mixing as repetitive mixing McKelvey (M-5) has used the term simple mixing.

The incorporated substances, for instance the agglomerates of filler particulates, initially retain their form. The breakdown of such substances occurs due to the stresses acting on them rather than the deformation. The mixing which promotes the breakdown or the reduction of the sizes of such substances is called dispersive mixing.

A.2. General

In the present chapter, we shall consider the incorporation process, distributive mixing and dispersive mixing.

To deal with these mixing steps explicitly, we must know the mechanism of the incorporation process, the deformation rates and the stress levels at the various locations in the mixer. These, however, are still unknown. We shall simplify these in the following discussion.

The process of incorporation will be expressed with a simple function based on the experimental results. Distributive mixing will be considered assuming simple shear flow in the mixer. The incorporation, distributive mixing and dispersive mixing are not completely independent processes, but are continuing ongoing processes.

Existing theories of dispersion should be modified by taking the incorporation process into consideration.

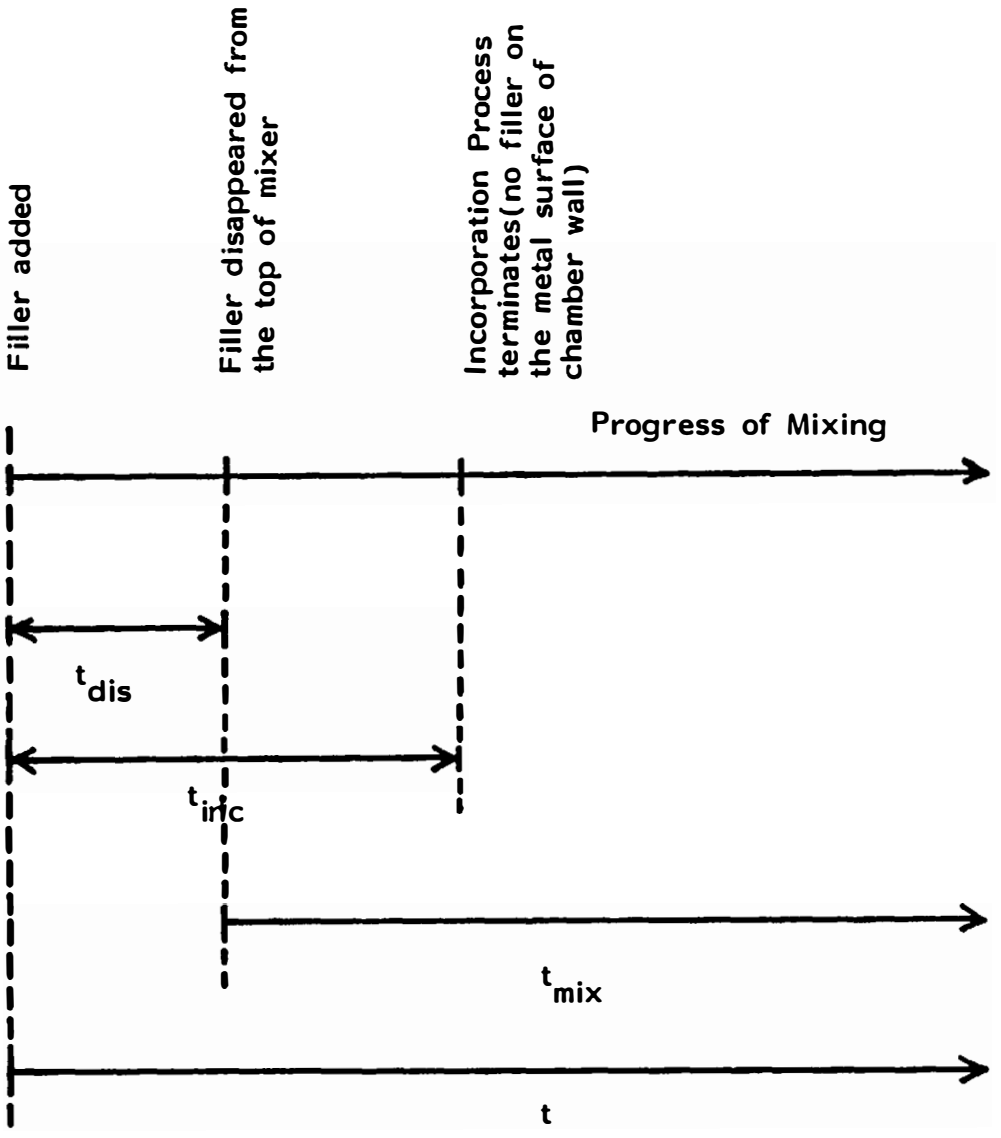

Figure XII-1. Time scales of mixing process.

B. TIME SCALES OF MIXING PROCESS

We define the time scale of the mixing process including incorporation.

In Chapter III, Materials and Sample Processing, the mixing time was defined as the period of mixing after the filler was incorporated into the polymer phase. This was determined by observations from the top of the internal mixer chamber. It should be noted that the mixing time was not counted immediately after the filler was added.

We define the following time scales in addition to the previously defined mixing time t_{mix}.

t : total mixing time measured from the instant that the filler was added

t_{dis} : period in which filler disappears from the top of the internal mixer chamber

t_{inc} : period after which all the filler was incorporated into the matrix phase.

Therefore

$$t = t_{dis} + t_{mix} \qquad \text{(XII-1)}$$

These are summarized in Figure XII-1.

C. INCORPORATION PROCESS

C.1. General

Incorporation of filler into the polymer matrix phase takes place immediately after the addition of filler into the mixer. The process of incorporation has been studied experimentally and an empirical relation is proposed.

The process of incorporation was studied by two methods. One is by observing the unincorporated filler from the top of the mixing chamber until all filler disappears. The period of the disappearance of the filler was measured. The other method is by studying the inside of the mixing chamber. The internal mixer was deassembled after a certain period of mixing and the mix was removed from the chamber and the rotors. Unincorporated filler was collected from the chamber wall and rotor surface and weighed.

C.2. Experimental Results

The periods t_{dis} and t_{inc} are shown in Table XII-1 for various internal mixer prepared calcium carbonate compounds. The ultimate particle size is 0.07 μm and the volume fraction is 0.05. The fill factor is 0.9. The results we cite are the average of four runs.

It appears that the polystyrene compounds have shorter periods of disappearance of filler t_{dis} than polypropylene compounds. The uncoated calcium carbonate requires a greater t_{dis} than coated calcium carbonate both in polystyrene and polypropylene compounds.

Table XII-1. t_{dis} and t_{inc} for Various Calcium Carbonate Compounds (dp = 0.07, ϕ = 0.05)

	t_{dis} (min)	t_{inc} (min)
PS/Unc. $CaCO_3$	0.5	>10
PS/Coat. $CaCO_3$	0.33	∿10
PP/Unc. $CaCO_3$	1.75	∿1.75
PP/Coat. $CaCO_3$	1.33	∿1.33

The period of incorporation t_{inc} is much greater in the polystyrene compounds than in polypropylene compounds. In polystyrene compounds, the unincorporated filler stayed on the chamber wall after the filler disappeared from the top of the chamber. The incorporation process terminates when the filler on the chamber wall disappears in polystyrene compounds.

In polypropylene compounds, most of the filler was incorporated when the filler disappeared from the top of the mixing chamber. The incorporation of filler coincides with the disappearance of filler from the top of the chamber ($t_{dis} \simeq t_{inc}$). Uncoated calcium carbonate takes a greater period to be incorporated than coated calcium carbonate both in the polystyrene and polypropylene compounds.

C.3. Discussion

The periods of incorporation of filler are much greater in the polystyrene compounds than in the polypropylene compounds. This is due to the difference of the incorporation process of the filler. Two types of incorporation mechanism will be discussed. These are called "simultaneous incorporation" and "thin layer incorporation."

C.3.a. Simultaneous Incorporation. In the polypropylene compounds, no filler was found on the metal surface of the mixing chamber. When the filler disappeared from the top of the chamber, all filler was incorporated into the matrix phase. The period of disappearance of filler from the top of the chamber t_{dis} is the same as the period of incorporation t_{inc} ($t_{dis} \approx t_{inc}$) as indicated in Table XII-1. The disappearance of filler and incorporation of filler takes place simultaneously.

The filler may be taken into the polymer phase near the opening of the mixing chamber without forming the layer of unincorporated filler on the metal surface of the chamber.

Flow visualization of the motion of elastomers and mixing in an internal mixer has been carried out by Min and White (M-15,M-16, M-17). They replaced the front panel of the mixing chamber of an internal mixer (HAAKE Reocord Type M) with a glass window. Flow patterns were then videotaped.

For polypropylene/zinc oxide system at 180°C it was found that the rotor tip moves the polymer and a small portion of filler from near the chamber opening (M-17). Filler is incorporated into the polymer phase with every revolution of rotor until it disappears from the top of the chamber. Figure XII-2 gives a schematic drawing of the simultaneous incorporation mechanism.

C.3.b. Thin Layer Incorporation. The second mechanism of incorporation is a "thin layer incorporation." Filler disappears from the top of the chamber and forms a thin layer on the chamber

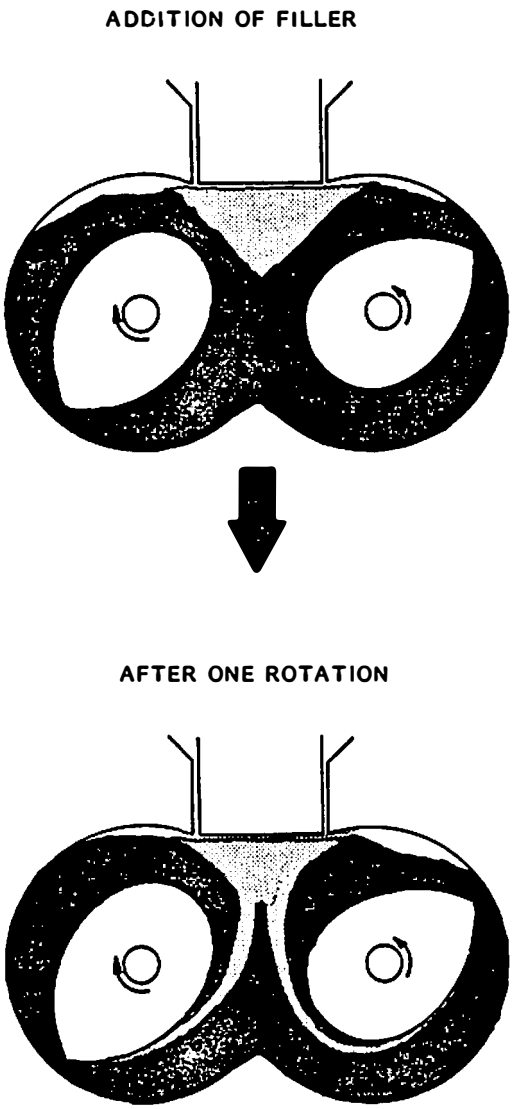

Figure XII-2. Schematic representation of simultaneous incorporation.

wall. Incorporation of filler occurs at the layer structure and the fraction of unincorporated filler decreases gradually as mixing progresses. The period for the incorporation is much greater than the period for the disappearance of filler at the top of the chamber ($t_{dis} < t_{inc}$).

A similar mechanism was observed by Min and White (M-17) for the polystyrene/zinc oxide system at 160°C in Haake reocord mixer.

Figure XII-3 shows a schematic representation of the thin layer formation.

Tight bands were formed around the rotors by polystyrene. These bands seem hardly to touch the chamber wall surface. Filler falls down to the bottom of the chamber through the tight band of polymer melt and forms a thin layer on the chamber metal surface. A major portion of incorporation may occur from the layer of unincorporated filler.

C.3.c. Rate of Incorporation. The fraction of the unincorporated filler is plotted as a function of the total mixing time for various calcium carbonate compounds in Figure XII-4. The fraction of unincorporated filler decreases roughly exponentially as mixing progresses.

A simple exponential formation may be used to express the incorporation process.

$$\phi_{uni} = \exp(-t/\overline{t}_{inc}) \qquad \text{(XII-2)}$$

where ϕ_{inc} denotes the fraction of unincorporated filler, t total

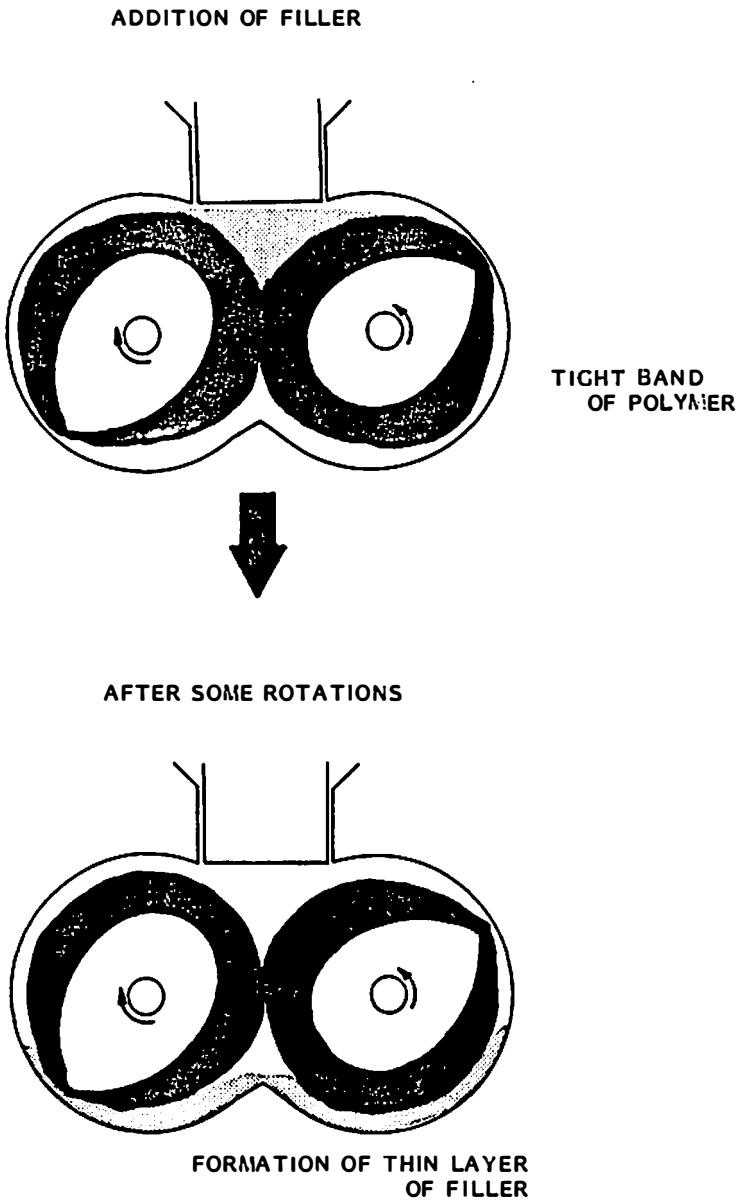

Figure XII-3. Schematic representation of thin layer incorporation.

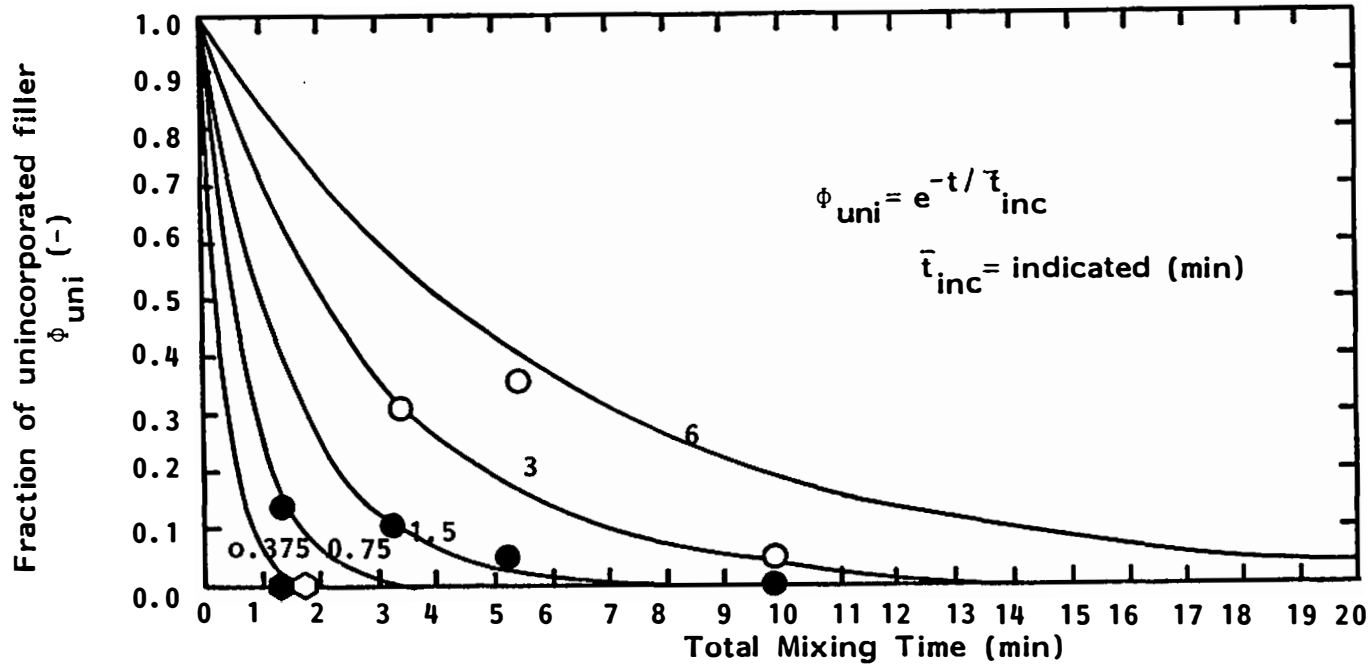

Figure XII-4. Comparison between prediction and experimental data.

mixing time as defined in the previous section and $\bar{t}_{inc}$ is the characteristic time for the incorporation process.

The predictions of Eq. (XII-2) are compared with the experimental results in Figure XII-4. Reasonable agreement was obtained. The approximate values of the characteristic time for incorporation process are summarized in Table XII-2.

Table XII-2. Characteristic Time for Incorporation Process for Various Compounds

	$\bar{t}_{inc}$ (min)
PS/Unc. $CaCO_3$	3 to 6
PS/Coat. $CaCO_3$	0.75 to 1.5
PP/Unc. $CaCO_3$	0.375
PP/Coat. $CaCO_3$	0.375

Polystyrene/calcium carbonate compounds which exhibited the thin layer incorporation mechanism possess large characteristic times. Polystyrene/uncoated calcium carbonate compounds have the largest characteristic time. Uncoated calcium carbonate possesses stronger particle-particle interaction forces than coated calcium carbonate. This may result in a stronger layer, and incorporation occurs slowly.

Polypropylene compounds which showed the "simultaneous" incorporation mechanism possess small characteristic times.

D. DISTRIBUTIVE MIXING

D.1. General

As discussed in Section A.1, Terminology, there are two types of mixing: distributive mixing and dispersive mixing. Distributive mixing refers to the dislocation and the transportation of the fluid elements which contain the agglomerates, aggregates and ultimate particles. The breakdown of the agglomerates is not of concern in this process.

D.2. Representation of Distributive Mixing

Figure XII-5 shows a schematic representation of the motion of the fluid elements. The positions of two fluid elements k and ℓ are given by x_k and x_ℓ, respectively. These are separated from each other by a distance a. After a certain period of time t, the fluid elements k and ℓ change their position to x'_k and x'_ℓ with a separation distance of a'. The motion of these may be represented by r_k and r_ℓ.

We may represent distributive mixing through

$$D = \frac{a'}{a} = \frac{|x'_k - x'_\ell|}{|x_k - x_\ell|}$$

$$= 1 + \frac{|r_k - r_\ell|}{a} \qquad \text{(XII-3)}$$

where D is a distributive mixing index.

We need to consider the following:

1. Distributive mixing D is dependent upon the relative positions of fluid elements in the flow direction.

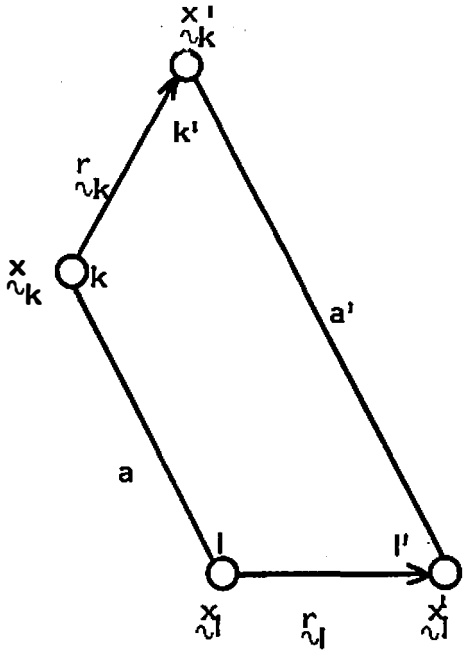

Figure XII-5. Motion of the fluid elements.

2. Distributive mixing D is dependent upon the initial separation distance a.

Figure XII-6 shows two examples of the variation of the relative position of fluid elements in the flow direction in shear flow and elongational flow. It is clear that the combinations of the fluid elements perpendicular to the shear flow direction increases their distances and the combinations of the fluid elements parallel to the shear flow direction maintain their distances constant. In elongational flow, the distances increase for the fluid elements parallel to the flow direction and the distances decrease for the fluid elements perpendicular to the flow direction.

An example of the dependence on the initial separation distance of fluid elements is given in Figure XII-7. Fluid elements 1, 2 and 3 having a constant interelement approach the tip region of an internal mixer moving past a wall. Elements 2 and 3 successfully pass through the gap between the tip and chamber wall but element 1 does not. Their locations after a certain time are indicated as 1', 2' and 3'. We note that the distances between 1' and 2' or 3' are much greater than the distance between 2' and 3'.

It becomes clear that we need to consider the total number of pairs of fluid elements in the mixer. The general form of the index of distributive mixing is then

$$D = \frac{1}{n} \sum_{i=1}^{n} \frac{a_i'}{a_i} \qquad \text{(XII-4)}$$

Shear Flow

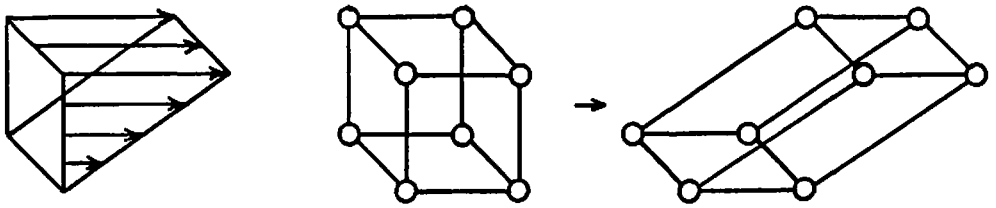

Elongational Flow

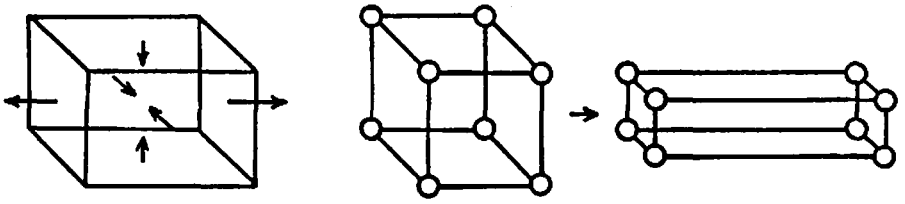

Figure XII-6. Motions of fluid elements in shear and elongational flow.

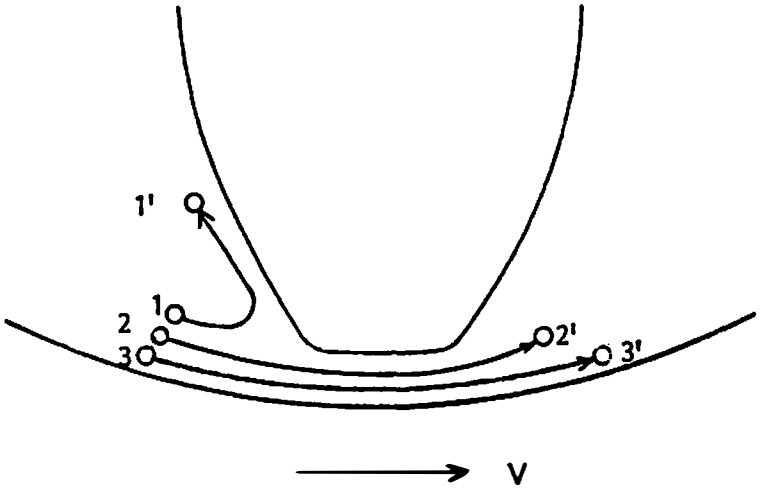

Figure XII-7. Motions of Fluid Elements in a Complex Flow Pattern.

where i is the index for the pair of the two fluid elements, n the total number of the pairs, a_i and a_i' denote the distances of pair i before and after a certain period of time.

D.3. Index of Distributive Mixing For an Internal Mixer

D.3.a. Simplification. A computation of the index of the distributive mixing requires the analysis of the flow pattern in the internal mixer. However, the flow patterns in the internal mixer are not known.

We will proceed by simplifying the flow in the internal mixer and compute the index of distributive mixing D. Figure XII-8 shows the dimensions of the internal mixer used in the present research. We may define three deformation rate zones, a high deformation zone in the rotor tip region, a low deformation zone between the chamber wall and rotor shafts and a stagnant zone between the two rotors. The existence of the stagnant zone was first pointed out by Min and White (M-15,M-16).

We may further simplify the flow in the internal mixer as follows:

1. Only shear flow occurs in the mixer.

2. Mixer possesses three shear rate zones: (i) a high shear rate zone in the rotor tip region, (ii) a low shear rate zone between the chamber wall and rotor shafts, and (iii) a stagnant zone (see Figure XII-8).

R_0= 19.60 mm H_1= 1.05 mm

R_1= 18.55 mm H_2=14.05 mm

R_2= 5.55 mm W = 2.5 mm

θ = 240°

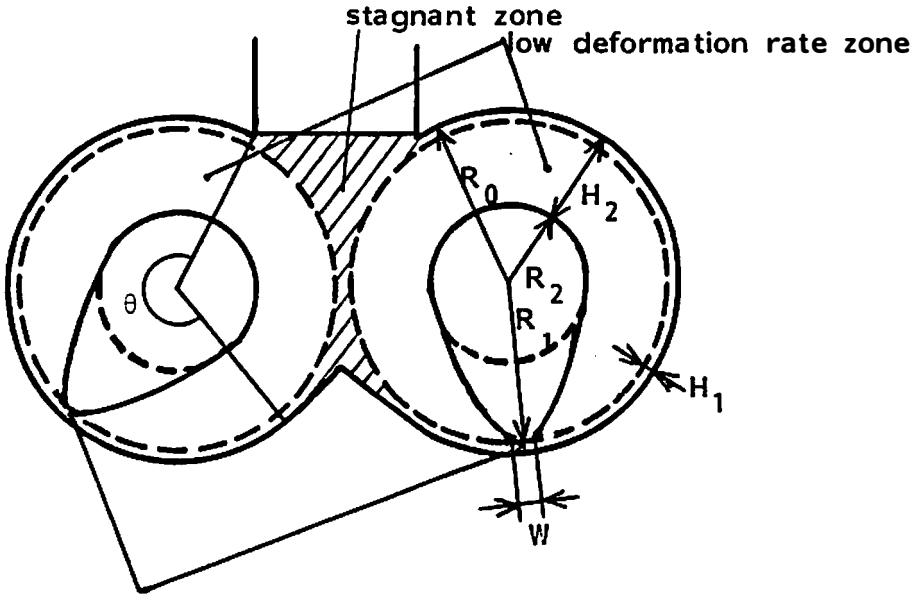

Figure XII-8. Deformation zones and dimension of mixer.

We set only two fluid elements aligned perpendicular to the shear flow direction. The initial separation of the element a is assumed to be smaller than the gap distance in the rotor tip region.

Under these simplifications, Eq. (XII-4) reduces to:

$$D_i = \frac{a + \dot{\gamma}_i \cdot a \cdot t_i}{a} = 1 + \dot{\gamma}_i \cdot t_i \qquad \text{(XII-5)}$$

where i denotes the location in the mixer, $\dot{\gamma}_i$ shear rate and t_i the deformation time at the location i.

D.3.b. Index of Distributive Mixing. We compute the index of the distributive mixing for the internal mixer used in the present research. The rotor speed is set to 50 rpm.

We first fix the two fluid elements near the chamber wall perpendicular to the shear direction to determine the levels of the distributive mixing in high and low shear rate zones. We obtain the deformation time in the high shear zone as

$$t_{high} = W/\frac{\Omega}{60}) \cdot 2\pi R_1 \qquad \text{(XII-6)}$$

where W is the width of tip, Ω the rotor angular velocity and R_1 the radius of rotor. The period of deformation in the low shear rate zone is determined by

$$t_{low} = \Delta t - t_{high} \qquad \text{(XII-7)}$$

where Δt is the period of the one revolution of the rotor.

The shear rates, the deformation time and the index for distributive mixing for one revolution of the rotors in each region are summarized in Table XII-3. We note the same levels of distributive mixing occur in high and low shear rate zones. The low shear rate zone plays an important roll in distributive mixing. The index of dispersive mixing is 0 at the stagnant zone.

Table XII-3. Indices of Distributive Mixing at Each Zone (For a Fixed Pair of Fluid Elements)

	$\dot{\gamma}_i$ (sec^{-1})	t_i (sec)	D_i (-)
High Shear Zone	9.23×10^{1}	2.57×10^{-2}	3.37×10^{0}
Low Shear Zone	2.07×10^{0}	1.17×10^{0}	3.42×10^{0}
Stagnant Zone	0.0	-	0.0

E. DISPERSIVE MIXING

E.1. General

Dispersive mixing refers to the breakdown of agglomerates into the smaller agglomerates or ultimate particles and aggregates. The breakdown of agglomerates is dependent upon the stress levels acting on the agglomerates.

Two mechanisms of development of dispersion have been published. One is the rupture model (M-2) and the other is the onion model (S-4). In Sections E.2 and E.3, we will review and modify these theories for further development. We will improve these theories with an experimental incorporation function in Sections E.6 and E.6.

E.2. Rupture Model of Dispersion

Manas-Zloczower, Nir and Tadmor (M-2), in 1982, proposed a rupture model of dispersion. They assumed that rupture of agglomerates occurs when the hydrodynamic separating forces exceeds the cohesive force of the agglomerates.

They (M-2) assumed that the rupture of agglomerates occurs only in the high shear zone near the tip of the rotors and considered the probability that a fluid passes through the high shear (narrow gap) zone.

$$P(n,k) = \frac{n!}{k!(n-k)!} \left(\frac{v}{V}\right)^k \left(1 - \frac{v}{V}\right)^{n-k} \qquad \text{(XII-8)}$$

Here

- $P(n,k)$: probability that a fluid element passes k times through the high shear zone
- n : number of rotor revolutions
- k : number of passes through the high shear zone
- v : volume of fluid which passes through high shear zone in one revolution of rotors
- V: total volume of fluid in mixer.

This is well approximated by the Poisson distribution.

$$P(t,k) = (t^{*k}/k!)e^{-t^*} \qquad \text{(XII-9)}$$

where

$$t^* = \frac{t}{\bar{t}} = \frac{n \cdot \Delta t}{\bar{t}} = \frac{v}{V} \cdot n \qquad \text{(XII-10)}$$

Here

t^* : dimension less mixing time

t : mixing time

$\bar{t}$: mean residence time in the high shear

Δt : period for one revolution of rotor.

Then

$$\bar{t} = \left(\frac{V}{v}\right) \Delta t \qquad \text{(XII-11)}$$

The size of agglomerate after j times of rupture is given by

$$d_j = 2^{-j/3} d_0 \qquad j = 0,1,2, \ldots , m \qquad \text{(XII-12)}$$

where d_0 is the size of initial agglomerates. m is the number of the rupture after that agglomerate size reaches ultimate particle size or aggregate size. m is an integer which satisfies

$$m \leqslant 3 \log\left(\frac{d_0}{d_p}\right)/\log 2 < m + 1 \qquad \text{(XII-13)}$$

The volume fraction of agglomerates of size d_j which experienced j rupture periods in the fluid element which has passed k times through the high shear zone is given by

$$u_{(d_j)} = \frac{k! \cdot X^j \cdot (1 - X)^{k-j}}{(k - j)!\ j!} \qquad \text{(XII-14)}$$

$j = 0, \ldots , k$ for $m > k$

$j = 0, \ldots , m-1$ for $m \leqslant k$

where X is a fraction of broken agglomerates during one pass through the high shear zone.

The volume fraction of ultimate particles is

$$u(d_m) = 1 - \sum_{j=0}^{m-1} u(d_j) \qquad \text{for } m \leqslant k \tag{XII-15}$$

Finally, the volume fraction of agglomerates of size d_j in the mixer after a total mixing period of t is obtained as

$$Y(t,d_j = \sum_{k=j}^{S} P(t,k) \cdot u(d_j)$$

$$= \frac{(xt^*)^j}{j!} \exp(-xt^*) \tag{XII-16}$$

$$s = n \qquad \text{for } n < m$$

$$= m-1 \qquad \text{for } n \geqslant m$$

$$j = 0,1,2, \ldots , S$$

where n is the number of rotor revolutions during the mixing period t. The fraction of the ultimate particles or aggregate is then

$$Y(t,d_m) = 1 - \sum_{j=0}^{m-1} \frac{(xt^*)^j}{j!} \exp(-xt^*) \qquad \text{for } n \geqslant m \tag{XII-17}$$

E.3. Modification of Rupture Model

We shall upgrade the rupture theory of dispersion with an exponential incorporation function.

The incorporation function has been given by

$$_{uni} = \exp[-t/\bar{t}_{inc}] \qquad \text{(XII-18)}$$

where $_{uni}$ denotes the fraction of unincorporated filler, t is the total mixing time and $\bar{t}_{inc}$ is the characteristic time for incorporation.

We consider the fraction of filler newly incorporated between the i-1 revolution and i revolution of the rotors. This is given by

$$I_i = \exp(-(i-1)\cdot\Delta t/\bar{t}_{inc}) - \exp(-i\cdot\Delta t/\bar{t}_{inc})$$

$$= \exp(-i\cdot\Delta t/\bar{t}_{inc})\cdot[\exp(\Delta t/\bar{t}_{inc}) - 1] \qquad \text{(XII-19)}$$

where Δt is the period for one revolution of the rotors. Function I_i decreases exponentially with the time of mixing.

We now turn to the volume fraction of agglomerates of size d_j in the mix after n rotor revolutions.

The volume fraction of agglomerates of size d_j due to the incorporated filler during the first revolution of rotors is given by

$$Y_1(n,d_j) = I_1 \cdot \frac{(xt^*_{e1})^j}{j!} \cdot \exp(-xt^*_{e1}) \qquad \text{(XII-20)}$$

Here t^*_{e1} denotes the dimensionless effective mixing time

$$t^*_{e1} = n \cdot \frac{\Delta t}{\bar{t}} \qquad \text{(XII-21)}$$

where n is the number of rotor revolutions at the instant that the mixing was terminated and i is the number of rotor revolutions when

the incorporation of filler I_i occurred. The effective dimensionless mixing time decreases for the belatedly incorporated filler. Other symbols are the same as previously defined.

Subsequently, the volume fraction of agglomerates of size d_j in the compound due to the newly incorporated filler during the ith revolution is given by

$$Y_i(n,d_j) = I_i \cdot \frac{(xt^*_{ei})^j}{j!} \cdot \exp(-xt^*_{ei}) \qquad \text{(XII-22)}$$

where

$$t^*_{ei} = (n - i + 1) \cdot \frac{\Delta t}{\bar{t}} \qquad \text{(XII-23)}$$

The fraction of agglomerates $Y_i(n,d_j)$ ought to be summed to count the contribution of the incorporated filler at every instant. The total volume fraction of agglomerates of size d_j in the mix after n times of rotor revolution is then given by

$$\begin{aligned} Y(n,d_j) &= \sum_{i=1}^{n} Y_i(n,d_j) \\ &= \sum_{i=1}^{n} I_i \cdot \frac{(xt^*_{ei})^j}{j!} \exp(-xt^*_{ei}) \qquad \text{(XII-24)} \\ j &= 0,1,2, \ldots , n \qquad \text{for } n < m \\ &= 0,1,2, \ldots , m-1 \qquad \text{for } n \leqslant m \end{aligned}$$

where I_i, d_j, t^*_{ei} and m are defined in Eqs. (XII-19), (XII-12), (XII-23) and (XII-13), respectively.

The fraction of dispersed ultimate particles of the aggregate after mixing, Y_m, is obtained from

$$Y_m = 1 - \sum_{j=0}^{m-1} Y(n,d_j) - \exp(-n \cdot \Delta t/\bar{t}_{inc}) \qquad \text{(XII-25)}$$

where the third term of the equation denotes the fraction of unincorporated filler after n times of revolution.

E.4. Onion Model of Dispersion

Shiga and Furuta (S-4) reported the onion mechanism of dispersion in 1983. They have found the tails of agglomerates in the elastomer/carbon black compounds and assumed that the dispersion of carbon black agglomerate progresses with peeling-off the skin of agglomerates like an onion.

They (S-4) assumed that the ratio of the mass of carbon black peeled off and the mass of black agglomerate is governed by

$$R_j = \frac{M_{j-1} - M_j}{M_{j-1}} \propto \frac{\eta}{\rho d_{j-1}}$$

$$= \frac{\alpha}{d_{j-1}} = 1 - \left(\frac{d_j}{d_{j-1}}\right)^3 \qquad \text{(XII-26)}$$

Here

M : mass of agglomerates

j : number of peel-off that the agglomerate experienced

ρ : density

α : constant

They assumed the probability that a fluid element passes k times through during n times of rotor revolution is given by the binomial distribution as did Tadmor et al. (Eq. XII-8)).

The volume distribution function for agglomerates of size d_j after n rotor revolutions $C_n(d_s)$ was given by

$$C_n(d_s) \prod_{i=1}^{s} K_i = \sum_{j=0}^{s} n P_j \cdot \left(\frac{d_s}{d_{s-j}}\right)^3 C_0(d_{s-j}) \prod_{i=1}^{s-j} \qquad \text{(XII-27)}$$

where

$$K_i = \frac{d_i}{d_{i-1}} + \frac{1}{3} \frac{d_{i-1}}{d_i^2} \qquad \text{(XII-28)}$$

E.5. Modification of Onion Model

We may rewrite the volume fraction of agglomerates of dize d_j for the onion model.

Using Shiga and Furuta's assumption of the rate of peel-off mechanism (Eq. (XII-26)), the diameter of agglomerates which experienced j peel-off times is given by

$$d_j = \left(1 - \frac{R_1 d_0}{d_{j-1}}\right)^{1/3} d_{j-1} \qquad \text{(XII-29)}$$

where R_1 denotes the ratio of the mass of peeled off and the mass of agglomerate for the first peel-off. The onion mechanism of dispersion terminates when $R_1 d_0/d_{j-1}$ is Eq. (XII-29)) reaches 1.

$$\frac{R_1 d_0}{d_{m-1}} \leqslant 1 < \frac{R_1 d_0}{d_m} \qquad \text{(XII-30)}$$

where m is the critical number of peel-offs.

The volume fractions of agglomerates of size d_j which experienced j peel-off times in the fluid element which has passed k times through the high shear zone is given by (see Appendix A):

$$\begin{aligned} u_k(d_j) &= \left(\frac{d_j}{d_0}\right)^3 && \text{for } k = j < m \\ &= 0 && \text{for } k \neq j,m \end{aligned} \qquad \text{(XII-31)}$$

and that of ultimate particles is

$$\begin{aligned} u_k(d_m) &= 1 - \left(\frac{d_k}{d_0}\right)^3 && \text{for } k < m \\ &= 1 && \text{for } k \geqslant m \end{aligned} \qquad \text{(XII-32)}$$

The volume fraction of agglomerates of size d_j in the mixer after the total mixing time of t may be given by (see Appendix B):

$$\begin{aligned} Y(d_j) &= P(t,j) \quad u_j(d_j) \\ &= (t^{*j}/j!)e^{-t^*}\left(\frac{d_j}{d_0}\right)^3 \end{aligned} \qquad \text{(XII-33)}$$

$$j = 0,1,2, \ldots , n \qquad \text{for } n < m$$

$$j = 0,1,2, \ldots , m-1 \qquad \text{for } n \leqslant m$$

Here $P(t,j)$ and $u_j(d_j)$ are given by Eqs. (XII-9) and (XII-31)), respectively.

The fraction of the ultimate particles or aggregates is then,

$$Y(d_m) = 1 - \sum_{j=0}^{m-1} Y(d_j) \qquad \text{for } n > 0 \qquad \text{(XII-34)}$$

We now modify the onion theory of dispersion with the incorporation rate function of Eq. (XII-19). Again, the volume fraction of agglomerate of size d_j in the compound after the n times of rotor revolution $Y(n,d_j)$ is of interest.

Following the same procedure as shown in the previous section, we consider the effect of the newly incorporated filler between each revolution.

During the first revolution of the rotor, fraction I_1 of filler is newly incorporated. The volume fraction of agglomerates of size d_j in the compound after n times of revolution is given by

$$Y_1(n,d_j) = I_1 \quad (t^*_{e1}/j!) \cdot (\frac{d_j}{d_0})^3 \cdot \exp(-t^*_{e1}) \qquad \text{(XII-35)}$$

where

$$t^*_{e1} = n \cdot \frac{\Delta t}{\bar{t}} \qquad \text{(XII-36)}$$

t_{e1} is the effective dimensionless mixing time.

Subsequently, fraction I_i of filler is newly incorporated between i-1 to ith revolutions. $Y_i(n,d_j)$ is given by

$$Y_i(n,d_j) = I_i \cdot (t^{*j}_{ei}/j!) \cdot (\frac{d_j}{d_0})^3 \quad \exp(-t^*_{ei}) \qquad \text{(XII-37)}$$

where

$$t^*_{ei} = (n - i + 1) \cdot \frac{\Delta t}{\bar{t}} \qquad \text{(XII-38)}$$

The compound contains the filler which was incorporated at the various levels of rotor revolutions. This filler, which had the initial agglomerate size d_0 when incorporated, is dispersed and reduces in size due to the rotor revolutions during the effective mixing time. The total volume fraction of agglomerates of size d_j in the compound after n times of rotor revolution is then given by

$$Y(n,d_j) = \sum_{i=1}^{n} Y_i(n,d_j)$$

$$= \sum_{i=1}^{n} I_i \cdot (t^{*j}_{ei}/j!) \cdot (\frac{d_j}{d_0})^3 \cdot \exp(-t^*_{ei}) \qquad \text{(XII-39)}$$

$$j = 0,1,2, \ldots , n \qquad \text{for } n < m$$

$$= 0,1,2, \ldots , m-1 \qquad \text{for } n \geq m$$

where I_i, d_j, t^*_{ei} and m are defined in Eqs. (XII-19), (XII-29), (Xii-38) and (XII-30), respectively.

The fraction of the dispersed ultimate particles or aggregates after mixing, Y_m, may be determined by

$$Y_m = 1 - \sum_{j=0}^{m-1} Y(n,d_j) - \exp(-n \cdot \Delta t/\bar{t}_{inc}) \qquad \text{(XII-40)}$$

where $Y(n,d_j)$ is given in Eq. (XII-39).

F. CHARACTERISTICS OF DISPERSION THEORIES

We discuss the characteristics of the dispersion theories including the rupture model, the modified rupture model, the onion model and the modified onion model.

Computer programs were developed for these models. The programs are given in Appendixes C through F.

F.1. General

We may set two parameters according to the mixing conditions. These are:

volume fraction of filler, ϕ = 0.05

rotational speed of rotor = 50 rpm

The fill factor of the agglomerate is assumed to be 0.5

We discuss the volume fraction of agglomerates as a function of relative agglomerate size. Here we define

$$\text{Volume fraction of agglomerates} = Y/f = \frac{\text{total volume of agglomerates of size } d_j}{\text{total bulk volume of filler}} \qquad \text{(XII-41)}$$

and

$$\text{Relative agglomerate size} = d_j/d_0 = \frac{\text{size of agglomerates after j ruptures}}{\text{size of initial agglomerates}} \qquad \text{(XII-42)}$$

F.2. Rupture Model

We first discuss the characteristics of the original rupture model proposed by Manas-Zloczower et al. (M-2) shown in Eq. (XII-16). In this model, the incorporation process was not considered but the initial agglomerates were assumed to be in the matrix phase when the mixing was initiated.

Figures XII-9 and XII-10 compare the volume fraction of agglomerates for two different X values: X = 0.10 (Figure XII-9) and X = 0.01 (Figure XII-10). As the X value decreases, the agglomerates possess a lower probability of rupture in the high shear zone.

The periods of the mixing are 1, 3, 5 and 10 minutes in both figures. In both figures it is clear that the volume fraction of the smaller agglomerates increases as the mixing progresses. At X = 0.19 (Figure XII-9), the volume fraction of the initial agglomerates (d_j/d_0 = 1.0) decreases rapidly and the fractions of the small agglomerates increase drastically with increasing mixing time. The maxima of the distribution is found at the smaller relative agglomerate size as the mixing progresses. At X = 0.01 (Figure XII-10), the agglomerates break with more difficulty. The distribution curves change less drastically in comparison with Figure XII-9.

The greatest fractions of agglomerates are found near the relative agglomerate size of 1.0.

Figures XII-11 and XII-12 compare the volume fraction of agglomerates for two different $\bar{t}$: $\bar{t}$ = 0.20 (Figure XII-11) and

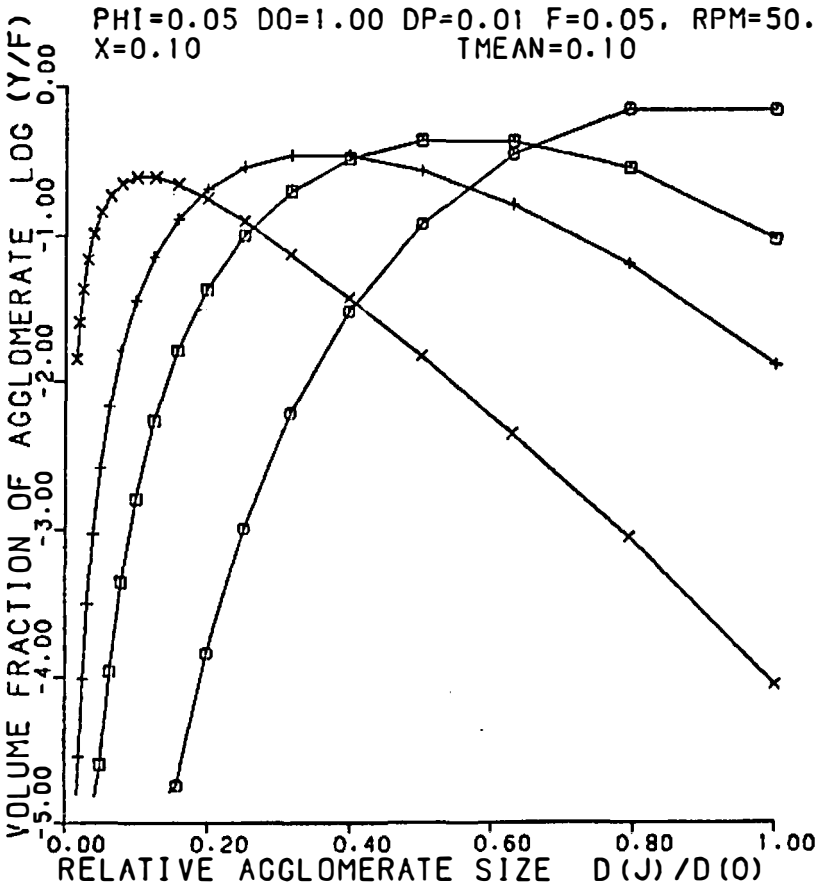

Figure XII-9. Volume fraction of agglomerate as a function of relative agglomerate size (x = 0.10, t = 0.10) with rupture model.

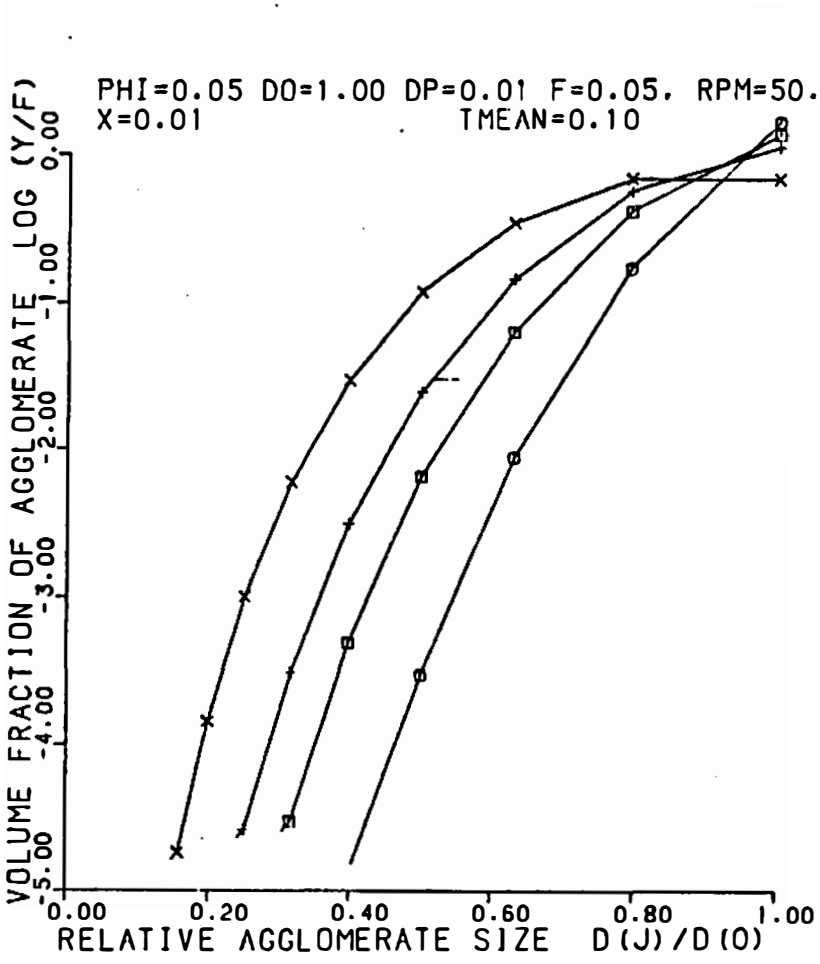

Figure XII-10. Volume fraction of agglomerate as a function of relative agglomerate size (x = 0.01, t = 0.10) with rupture model.

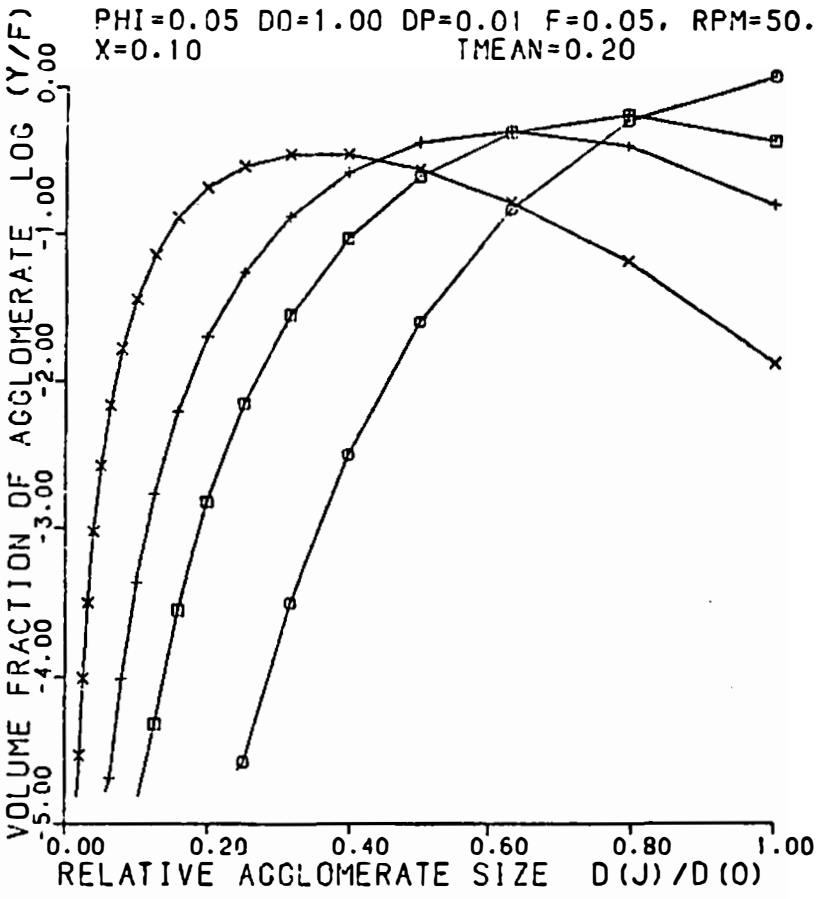

Figure XII-11. Volume fraction of agglomerate as a function of relative agglomerate size (x = 0.10, t = 0.20) with rupture model.

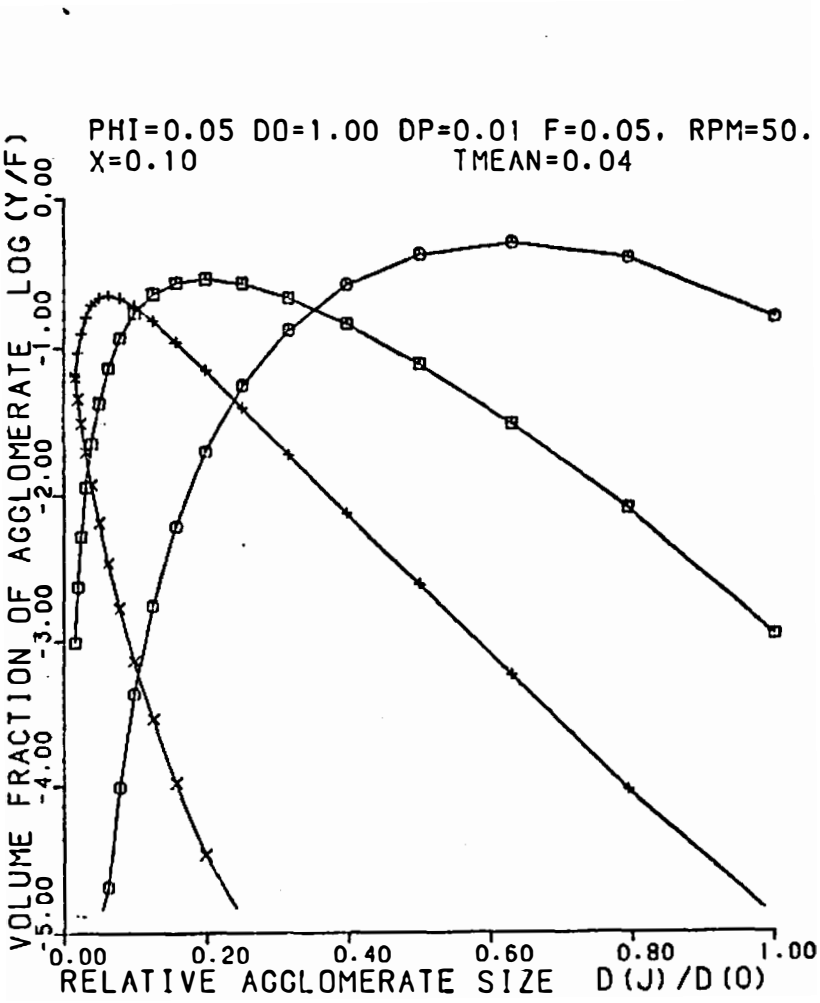

Figure XII-12. Volume fraction of agglomerate as a function of relative agglomerate size (x = 0.10, t = 0.04) with rupture model.

$\bar{t}$ = 0.04 (Figure XII-12). As $\bar{t}$ decreases, the volume of the fluid which can pass through the high shear zone during one revolution of the rotors increases. The change of distribution curves is more drastic at $\bar{t}$ = 0.04 compared with $\bar{t}$ = 0.20. The volume fraction of the large agglomerates decreases extremely rapidly with $\bar{t}$ = 0.04 (Figure XII-12).

The decay of the volume fraction of the large agglomerates occurs rapidly when X is large and $\bar{t}$ is small.

F.3. Modified Rupture Model

The rupture theory of the dispersion was modified earlier in this chapter through introducing an incorporation rate function. This is shown in Eq. (XII-24).

We first discuss the effect of the incorporation process. The incorporation rate function has been given by Eq. (XII-19). The volume fraction of agglomerates is given by Eq. (XII-24).

First we set the function X (fraction of broken agglomerates during one pass through the high shear zone) constant, that is, X = 1.00. The effect of the incorporation process is shown in Figure XII-13 (t_{inc} = 1.00) and Figure XII-14 (t_{inc} = 10.0). The distributions of the volume fractions of the agglomerates have the same characteristic features compared with the distributions predicted from the original rupture model.

The modified rupture model with the incorporation rate function predicts flatter distributions. The volume fractions of agglomerates do not decrease rapidly with increasing relative agglomerate size

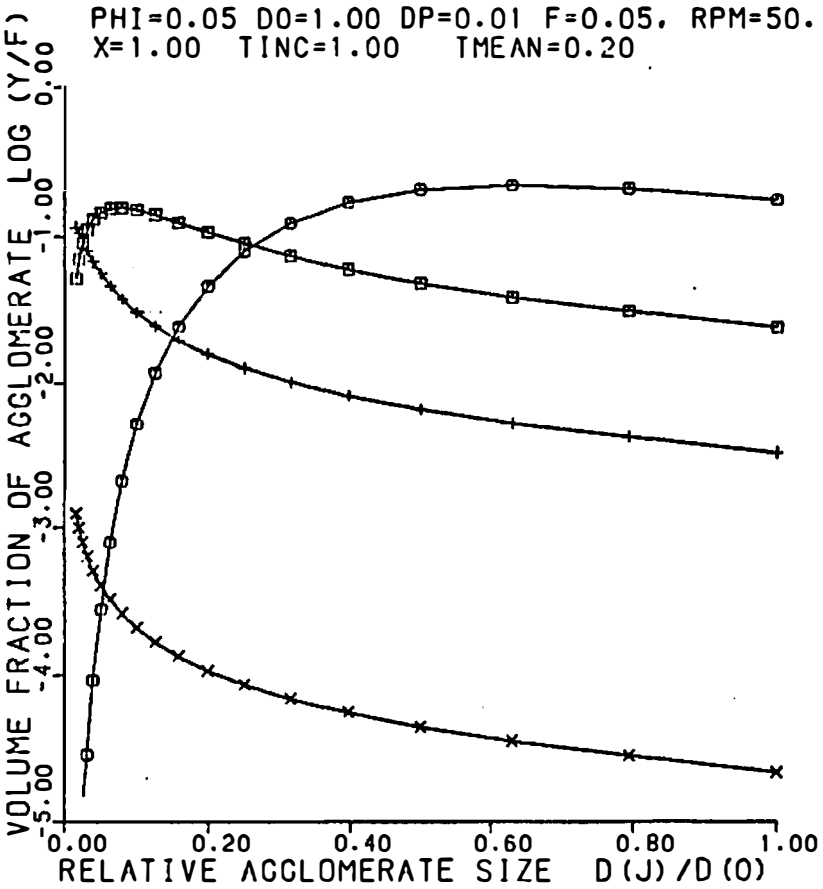

Figure XII-13. Volume fraction of agglomerate as a function of relative agglomerate size (x = 1.00, $t_{inc.}$ = 1.00, t = 0.20) with modified rupture model.

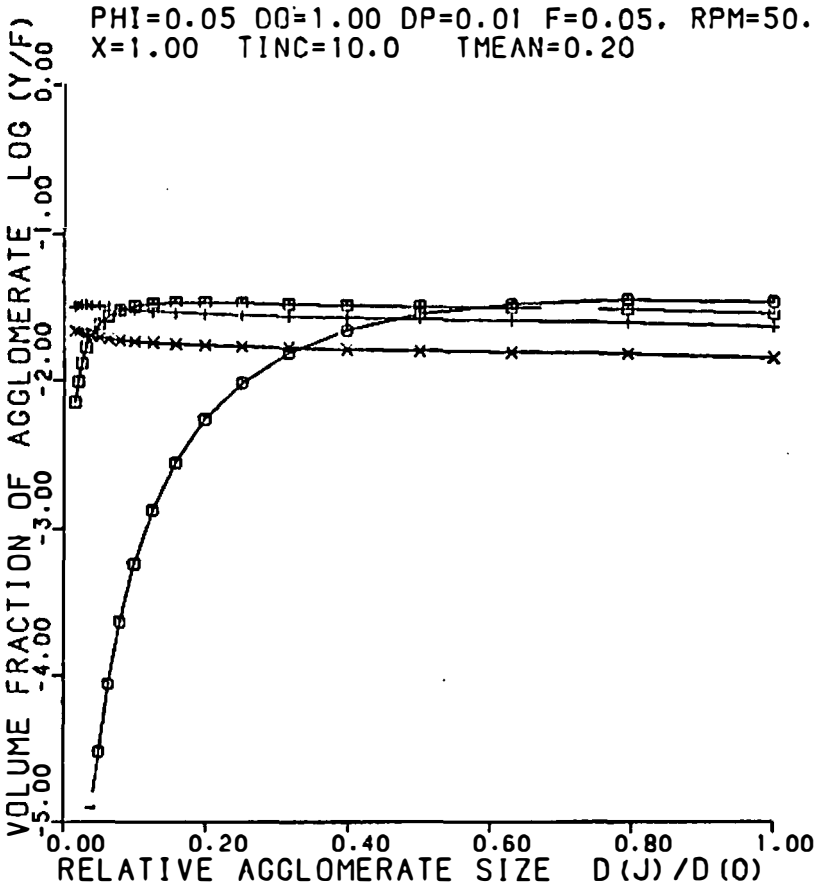

Figure XII-14. Volume fraction of agglomerate as a function of relative agglomerate size (x = 1.00, t_{inc} = 10.0, t = 0.20) with modified rupture model.

since the large agglomerates are continuously incorporated through the mixing process. When the incorporation process is slow (t_{inc} = 10.0) this peculiar characteristic is pronounced as shown in Figure XII-14. The volume fractions of the agglomerates retain large values at any mixing times.

Figures XII-15 and XII-16 show the effect of the incorporation process for smaller X (X = 0.10). The characteristic incorporation times t_{inc} are again 1.00 and 10.0. Plateau regions are observed for the large relative agglomerate sizes for slow incorporation process, t_{inc} = 10, as shown in Figure XII-16. The rapid decay in the small agglomerate sizes are due to the small fraction of broken agglomerates during one pass through the high shear zone X.

F.4. Onion Model

Shiga and Furuta (S-4) proposed Eq. (XII-27) assuming the onion mechanism of dispersion. We shall, however, use Eq. (XII-33) which was rewritten with the Poisson distribution function. Again, we use the set of parameters:

ϕ = 0.05

rpm = 25

f = 0.05.

Other parameters are the variables.

Again, we discuss the volume fraction of the agglomerates as a function of the relative agglomerate size.

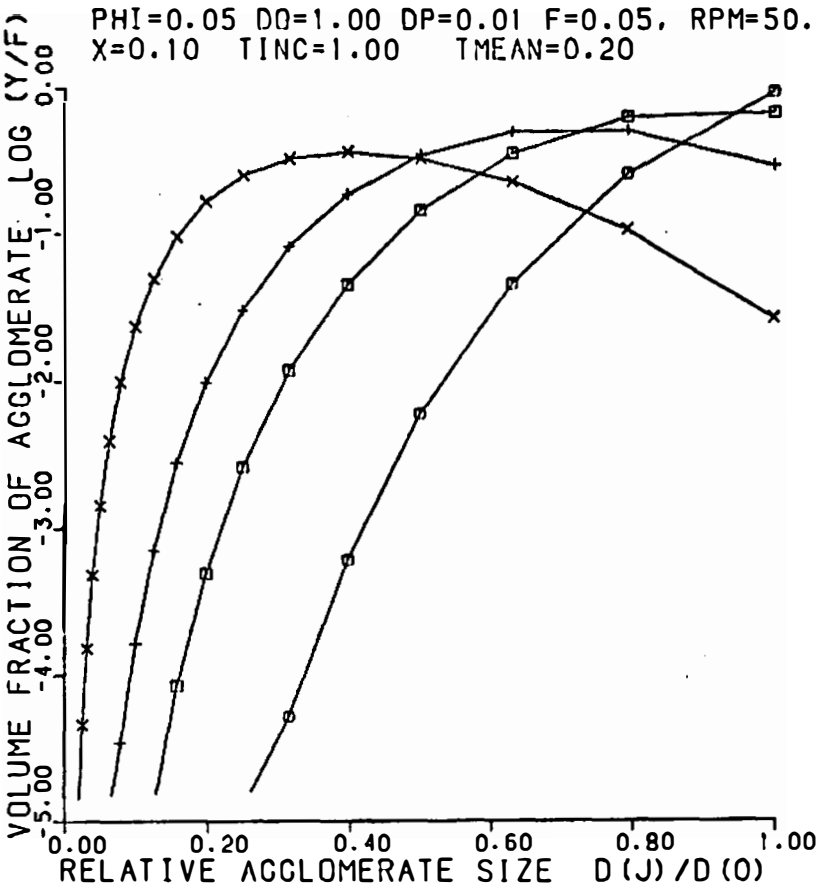

Figure XII-15. Volume fraction of agglomerate as a function of relative agglomerate size (x = 0.10, t_{inc} = 1.00, t = 0.20) with modified rupture model.

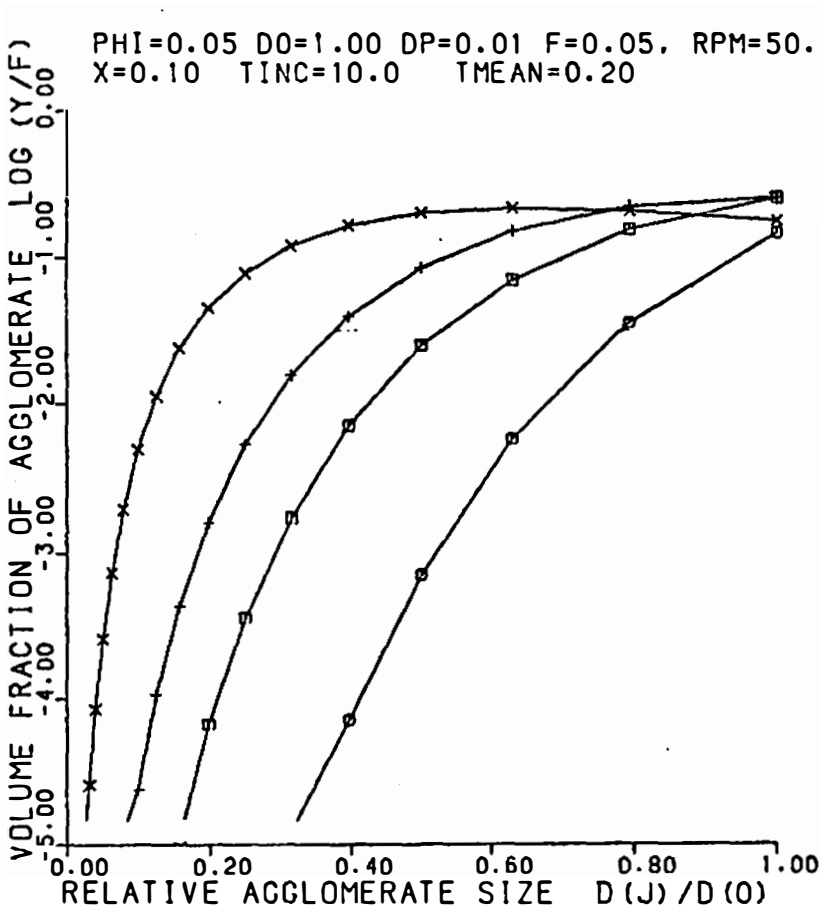

Figure XII-16. Volume fraction of agglomerate as a function of relative agglomerate size (x = 0.10, t_{inc} = 10.0, t = 0.20) with modified rupture model.

Figures XII-17 and XII-18 compare the volume fraction of agglomerates for two different R_1 values: R_1 = 0.10 (Figure XII-17) and R_1 = 0.30 (Figure XII-18). The value of R_1 corresponds to the ratio of the mass of particles peeled off from the surface of the agglomerate to the mass of the agglomerate. The distribution curves predicted by the onion model possess the clear maximas compared with the predictions from the rupture model. The maximum values of the volume fraction of the agglomerates decreases rapidly as mixing progresses. Other characteristics of the onion model is that the reduction of the agglomerates terminates at a certain size.

At a larger R_1 value (Figure XII-18), the volume fractions of agglomerates decrease more rapidly and the breakdown of the agglomerates terminates at the larger size compared with the predictions with the smaller R_1 value (Figure XII-18). The distribution curve with R_1 = 0.30 is always smaller than 10^{-5} at a mixing time of 10 minutes so the curve does not appear in Figure XII-18.

We now compare the distribution of agglomerates for two different $\bar{t}$ values. As the value of $\bar{t}$ decreases, the volume of compound which passes through the high shear zone during one revolution of the rotors increases. The effect of $\bar{t}$ is presented in Figure XII-19 ($\bar{t}$ = 0.50) and Figure XII-20 ($\bar{t}$ = 0.20). The volume fractions of the agglomerates and the relative agglomerate size at the peaks decrease more rapidly with the greater R_1 value. The distribution curve at a mixing period of 10 minutes is always smaller than 10^{-5} for R_1 = 0.30.

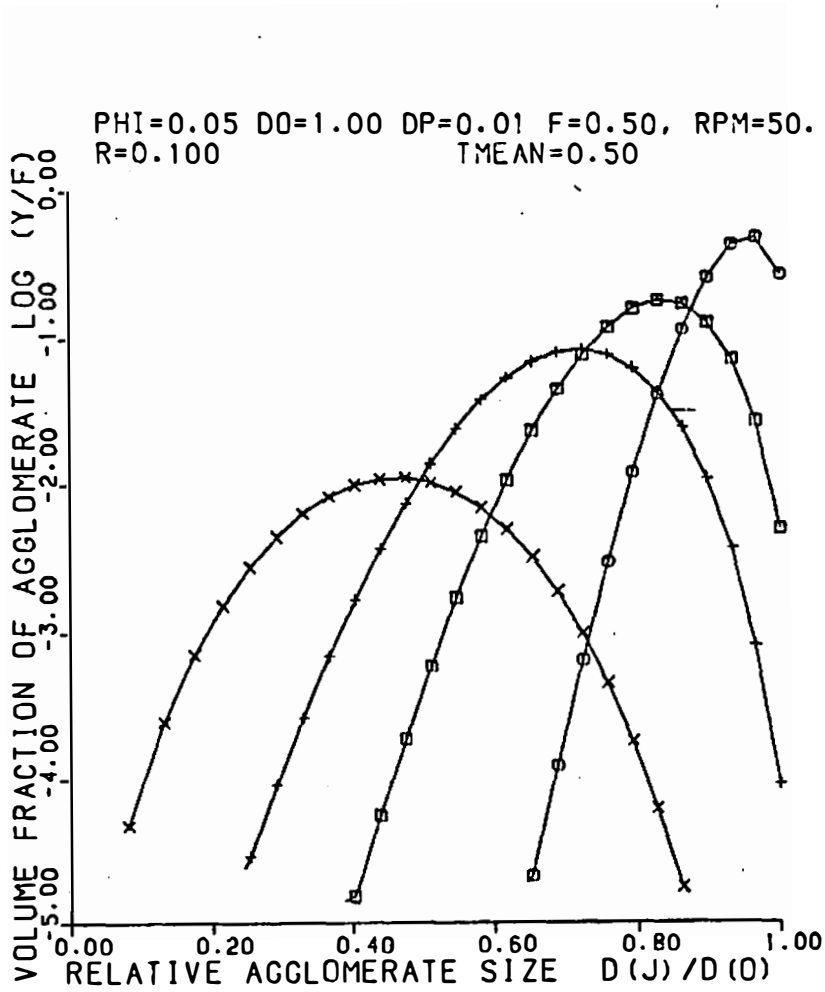

Figure XII-17. Volume fraction of agglomerate as a function of relative agglomerate size (R_1 = 0.10, t = 0.50) with onion model.

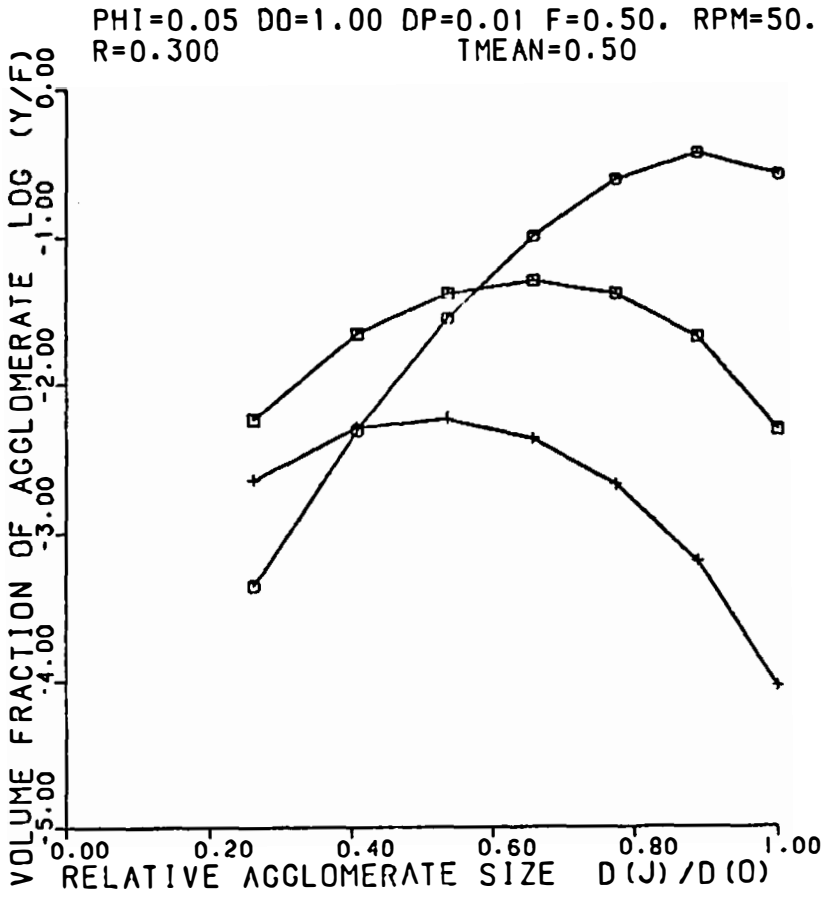

Figure XII-18. Volume fraction of agglomerate as a function of relative agglomerate size (R_1 = 0.30, t = 0.50) with onion model.

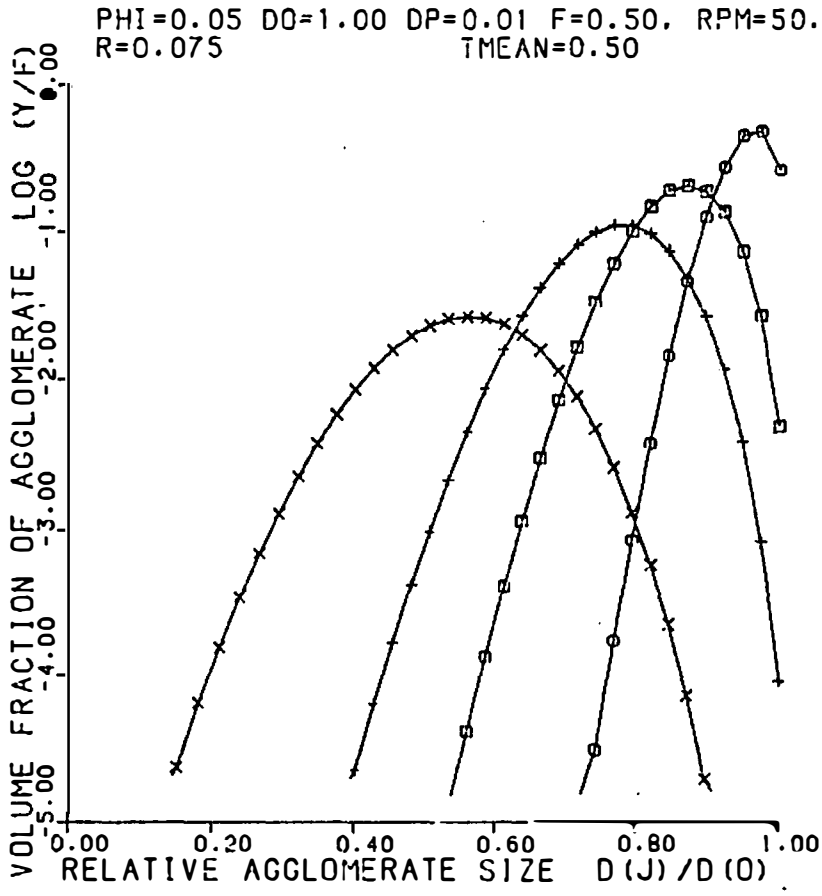

Figure XII-19. Volume fraction of agglomerate as a function of relative agglomerate size (R_1 = 0.075, t = 0.50) with onion model.

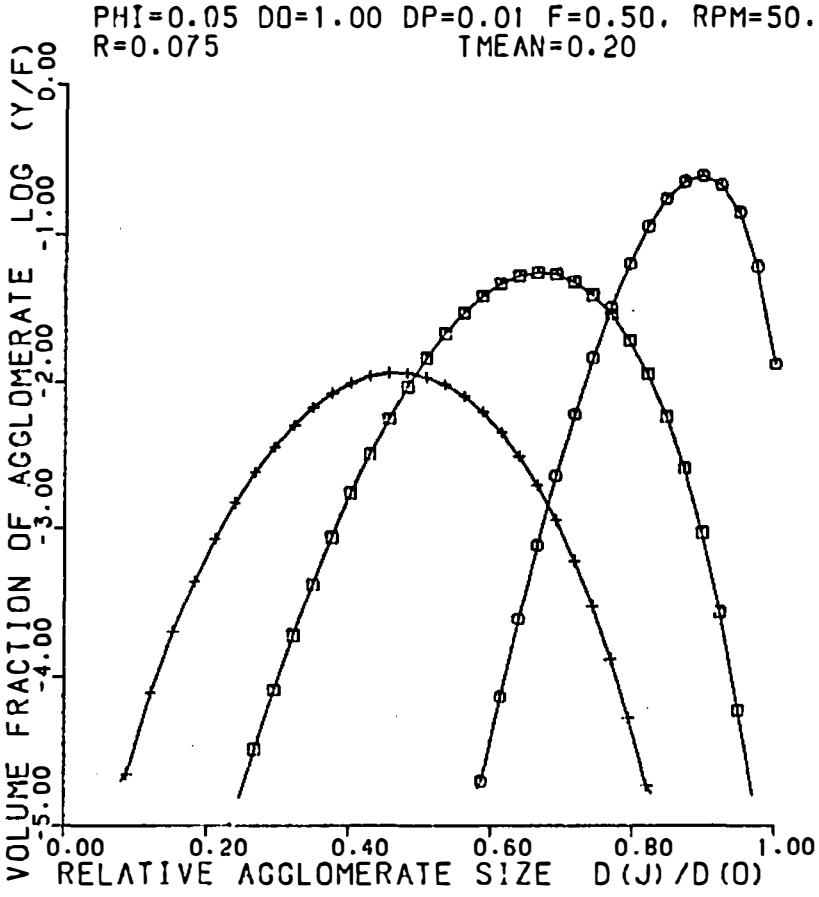

Figure XII-20. Volume fraction of agglomerate as a function of relative agglomerate size (R_1 = 0.075, t = 0.20) with onion model.

F.5. Modified Onion Model

The onion theory of dispersion was modified with the rate of incorporation function. The volume fraction of the agglomerates is given by Eq. (XII-39).

The effect of the characteristic incorporation time t_{inc} is shown in Figures XII-21 and XII-22 for $R_1 = 0.10$ and $\bar{t} = 0.50$. The values of t_{inc} are 1.0 in Figure XII-21 and 10.0 in Figure XII-22. The plateau regions appear in the large relative agglomerate sizes with large t_{inc} value (Figure II-22). The maxima of the distribution curves disappear and the volume fraction of the agglomerates decrease monotonically as the value of t_{inc} increases.

Figures XII-23 and XII-24 compare the volume fraction of the agglomerates for $\bar{t} = 0.10$ and $\bar{t} = 0.04$. The characteristic incorporation period t_{inc} is 10.0 in both figures. The effect of the incorporation process is more pronounced at smaller $\bar{t}$ value. The plateau regions appear clearly in Figure XII-23. In Figure XII-24, the volume fractions of the agglomerates do not show significant changes with mixing time.

G. COMPARISON OF EXPERIMENTAL DATA WITH THEORETICAL PREDICTIONS

G.1. Introduction

In this section, the predictions from the above described theory of dispersion will be compared with experimental data obtained in the present research. The volume fractions of agglomerates have

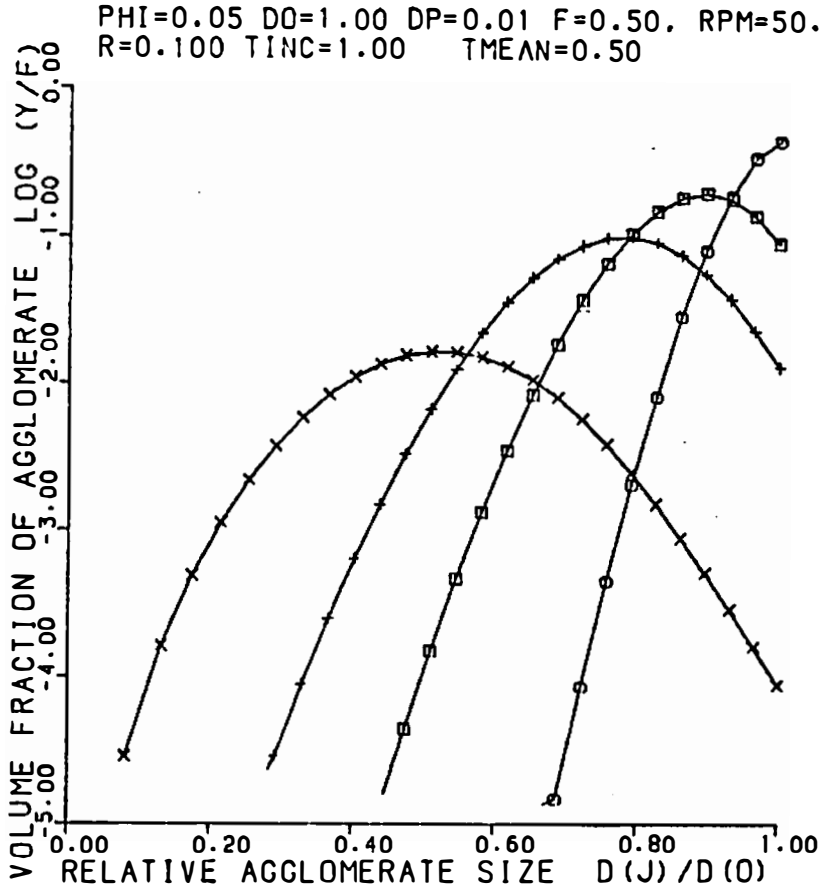

Figure XII-21. Volume fraction of agglomerate as a function of relative agglomerate size (R_1 = 0.10, t_{inc} = 1.00, t = 0.50) with modified onion model.

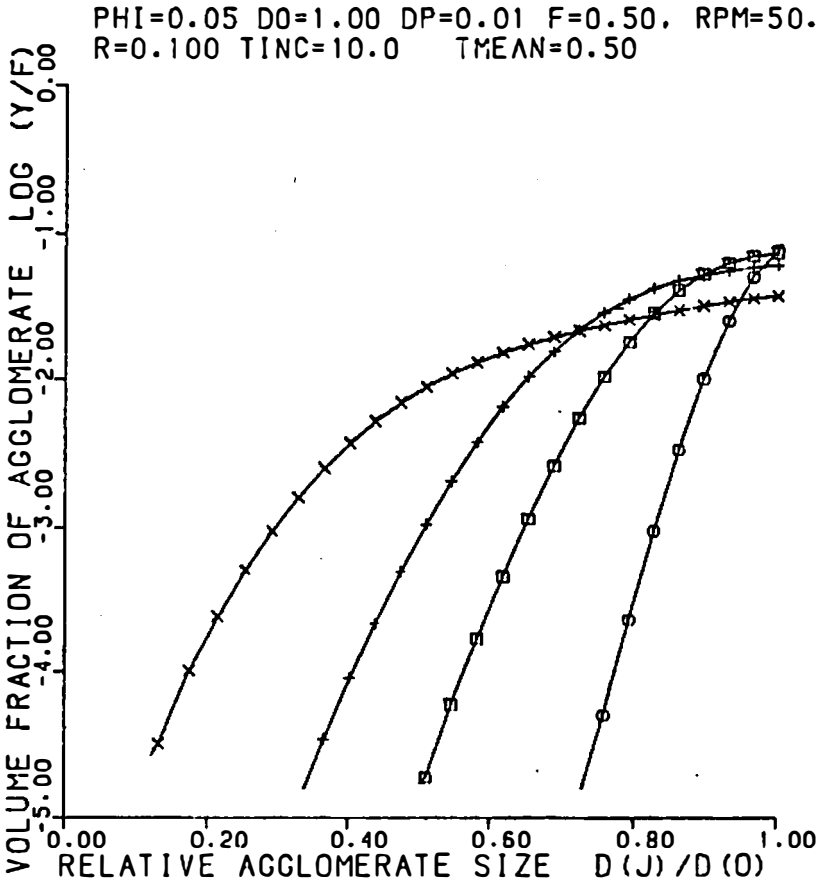

Figure XII-22. Volume fraction of agglomerate as a function of relative agglomerate size (R_1 = 0.10, t_{inc} = 10.0, t = 0.50) with modified onion model.

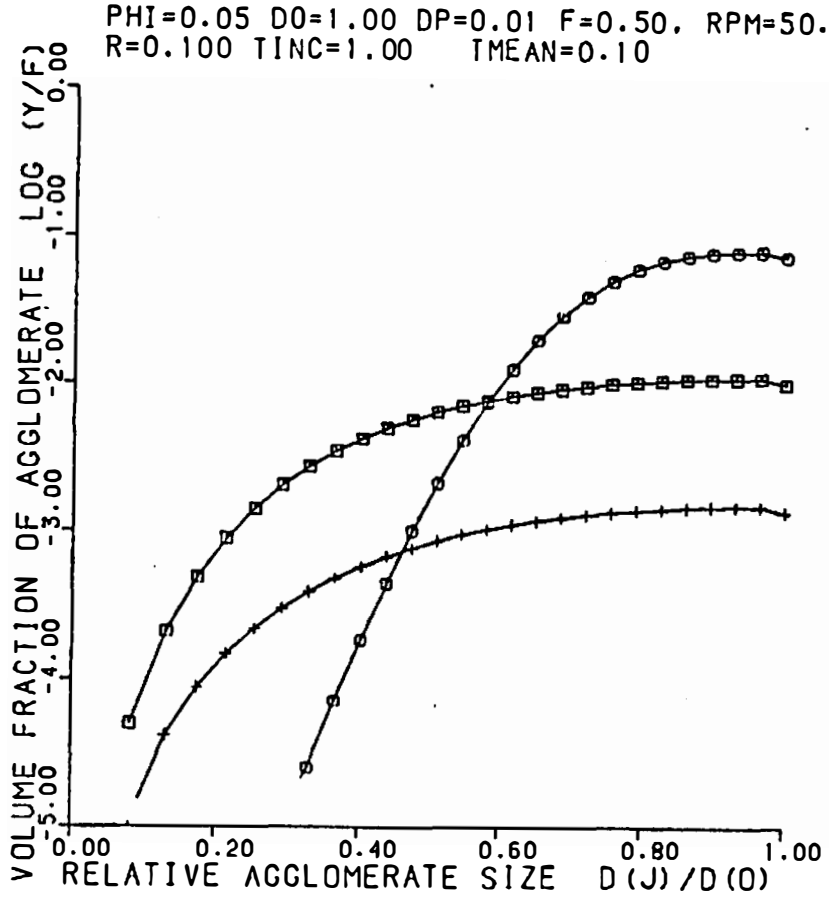

Figure XII-23. Volume fraction of agglomerate as a function of relative agglomerate size (R_1 = 0.10, t_{inc} = 10.0, t = 0.10) with modified onion model.

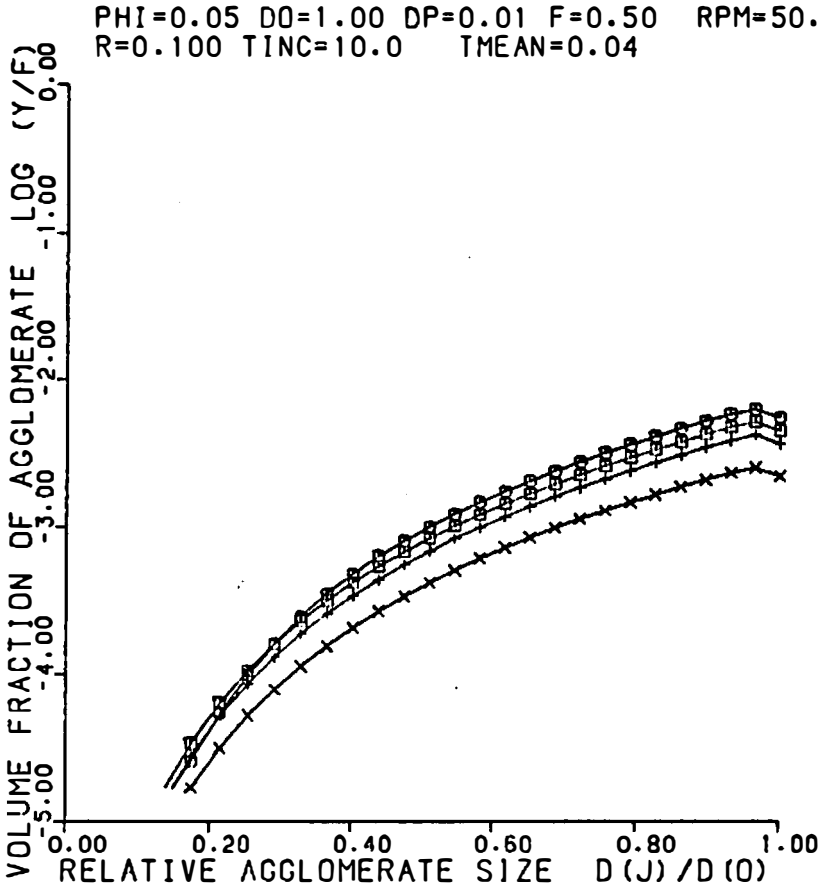

Figure XII-24. Volume fraction of agglomerate as a function of relative agglomerate size (R_1 = 0.10, t_{inc} = 10.0, t = 0.04) with modified onion model.

been obtained as a function of the agglomerate size range by optical microscopy. These will be compared with the theoretical predictions. The theories of dispersion include the rupture theory, rupture theory with the incorporation rate function, the onion theory, and onion theory with the incorporation function.

G.2. Equations and Parameters

The equations used for the theoretical predictions are summarized in Table XII-4. The physical meanings of the parameters have been summarized in Table XII-5.

Some parameters are determined directly from the experimental conditions. These are cited in Table XII-5. The mean residence time $\bar{t}$ may be determined as follows. The mean residence time is

$$\bar{t} = \left(\frac{V}{v}\right) \Delta t \qquad \text{(XII-43)}$$

where V denotes the total volume of compound, v the volume of the compound which passes through the high shear zone during one revolution of rotors and Δt denotes the period of one revolution of the rotors. The value of v is determined as

$$v \leqslant H_1 \cdot (2\pi R_0) \cdot W \cdot n_b \cdot \theta \qquad \text{(XII-44)}$$

Here

H_1 = gap distance (0.105 cm)

R_0 = chamber radius (1.96 cm)

W = chamber width (4.70 cm)

Table XII-4. Equations Used for the Theoretical Predictions

Model	Volume Fraction of Agglomerates (Equation No.)	Agglomerate Size (Equation No.)
Rupture	XII-16	XII-12
Modified Rupture	XII-24	XII-12
Onion	XII-33	XII-29
Modified Onion	XII-39	XII-29

Table XII-5. Parameters Used for the Theoretical Predictions

Parameter	Meaning	Values
ϕ	Volume fraction of filler in compound	0.05
f	Fill factor in agglomerate	0.05
RPM	Rotor speed	25 RPM
d_0	Initial agglomerate size	Variable
d_p	Ultimate particle size	0.07 μm
X	Fraction of broken agglomerate during one pass through the high shear zone (Rupture and Modified Rupture)	Variable
R_1	Initial mass reduction ratio of agglomerate (Onion and Modified Onion)	Variable
$\bar{t}$	Mean residence time in high shear zone	Can be determined
$\bar{t}_{inc}$	Characteristic time for incorporation process	Determined from experiment

n_b = number of blade per unit length (4/3)

θ = total angle of high shear zone (4/3).

We obtain

$$v \leqslant 10.8 \ (cm^3) \qquad \text{(XII-45)}$$

The total volume of the compound V is 63 cm^3. We obtain

$$\bar{t} \geqslant 0.233 \ (min) \qquad \text{(XII-46)}$$

for the rotor speed of 25 rpm.

The fill factor of the agglomerates was assumed to be 0.5. The initial agglomerate size d_0, the fraction of broken agglomerates during one pass through the high shear zone X (rupture model) and the initial mass reduction rate R_1 are the unknown parameters.

The breakdown of the agglomerates is dependent upon the stress levels in the internal mixer. Table XII-6 summarizes the shear stresses of polystyrene and polypropylene in the high shear zone (rotor tip regions) and in the low shear zone (rotor shaft regions).

It should be noted that the polystyrene exhibits much greater shear stresses than polypropylene. It is noteworthy that the stress level of polystyrene in the low shear rate zone is as high as the stress of polypropylene in the high shear rate zone.

G.3. Comparison of Experimentally Obtained Volume Fractions of Agglomerates with Theoretical Predictions

We compare the experimentally measured volume fractions of agglomerates with the theoretical predictions for the internal mixer prepared calcium carbonate compounds.

Table XII-6. Shear Stresses at High and Low Shear Rate Zones for PS and PP

	$\dot{\gamma}$ (sec^{-1})	σ (Pa)	
		PS (150°C)	PP (175°C)
High shear zone	4.61×10^{1}	1.6×10^{5}	4.6×10^{4}
Low shear zone	1.03×10^{0}	$\sim 4 \times 10^{4}$	$\sim 6 \times 10^{3}$

Gap at high shear zone: 1.05 mm
Gap at low shear zone: 14.05 mm
Rotor speed: 25 RPM

The matrix polymers were polystyrene and polypropylene. The standard mixing temperatures were 150°C and 175°C, respectively. Both untreated and the stearic acid surface treated calcium carbonates possess the nominal ultimate particle size of 0.07 μm. The volume fraction of the agglomerates were determined using optical microscopy. The volume fractions were summed within the range of 20 μm to 140 μm. The predicted volume fractions are also summed. The computer programs are presented in Appendixes D and G.

The total mixing times were used for the computation because the dispersion is initiated as soon as the filler was added. In the figures, however, only the mixing times are indicated to keep consistency with other chapters. The total mixing time and the mixing time have been defined in the previous section.

The curve fittings were carried out by changing the variable parameters. Some results are shown in this section.

Experimentally determined volume fractions of agglomerates are not included in these figures when the number of agglomerates observed with the optical microscope are very low. These are not reliable. This often happens in the large agglomerate size ranges. When the theories predict the volume fraction of agglomerates is lower than 10^{-4}, they are not plotted.

G.3.a. Comparison with Rupture Model.

G.3.a.1. PS/Uncoated $CaCO_3$ Compounds. Figures XII-25 through XI-27 show the comparison of the experimental data with the rupture model. The lines show the experimental data and the symbols show the

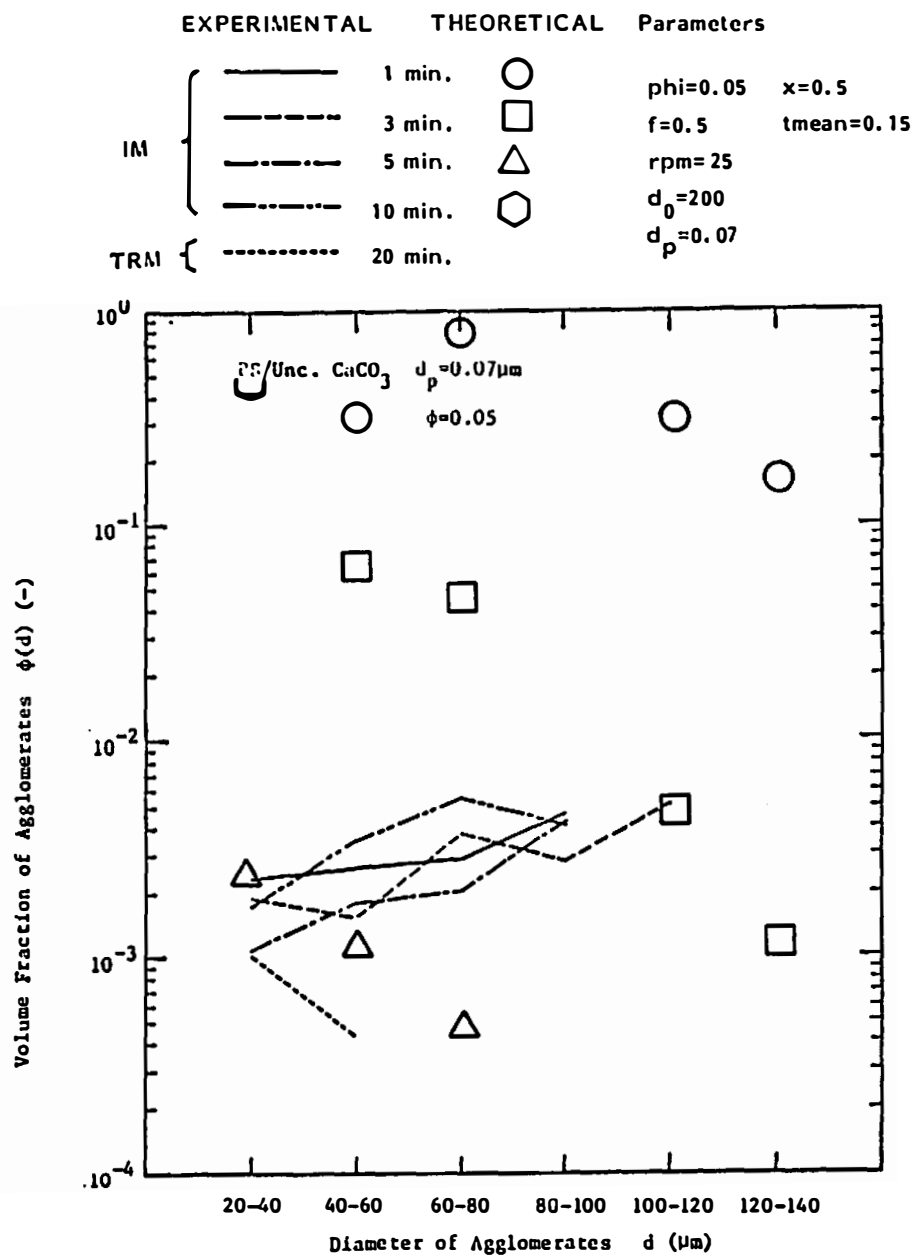

Figure XII-25. Comparison of experimental data with theoretical predictions for PS/unc. $CaCO_3$ (x = 0.5, $\bar{t}$ = 0.15) with rupture model.

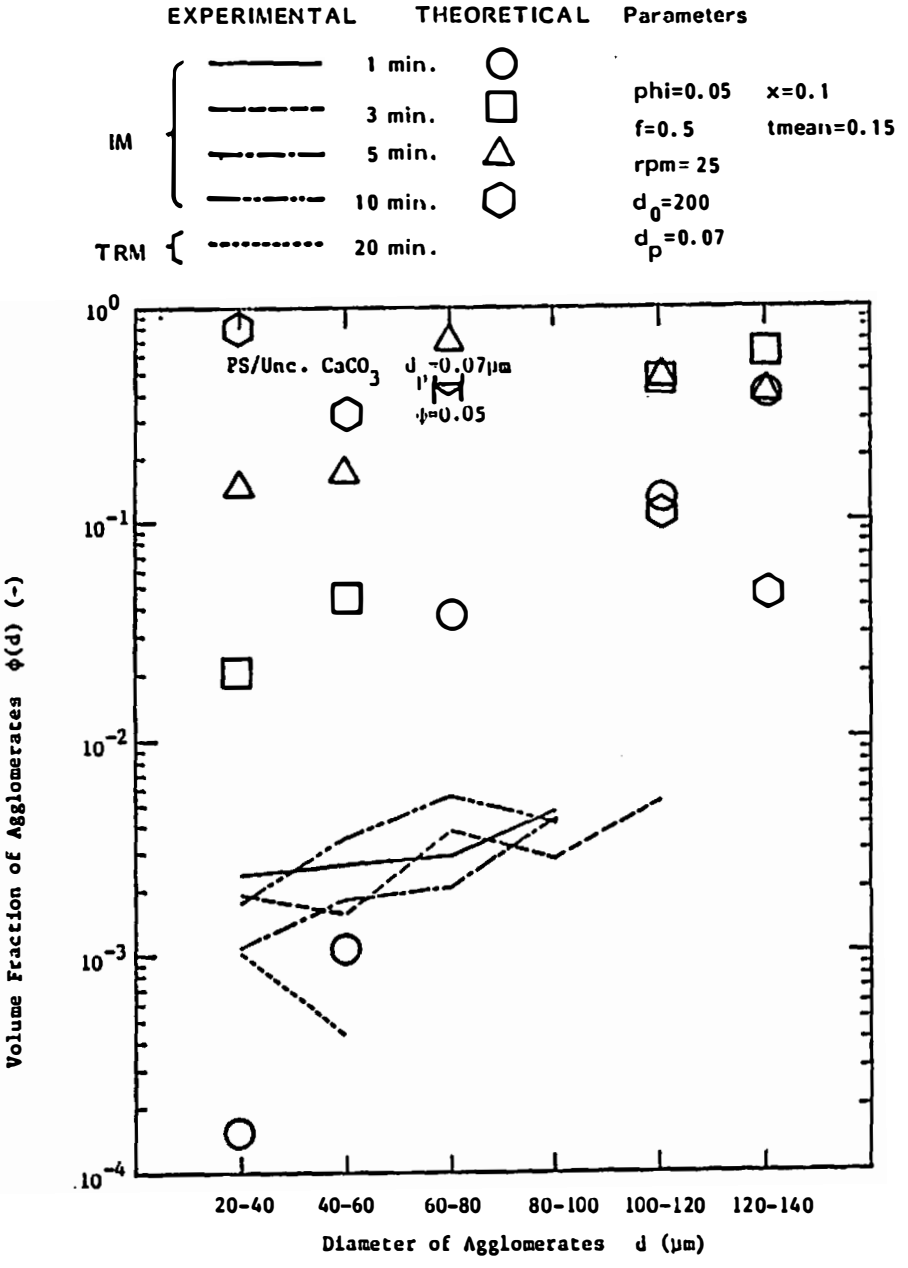

Figure XII-26. Comparison of experimental data with theoretical predictions for PS/unc. $CaCO_3$ (x = 0.1, $\bar{t}$ = 0.15) with rupture model.

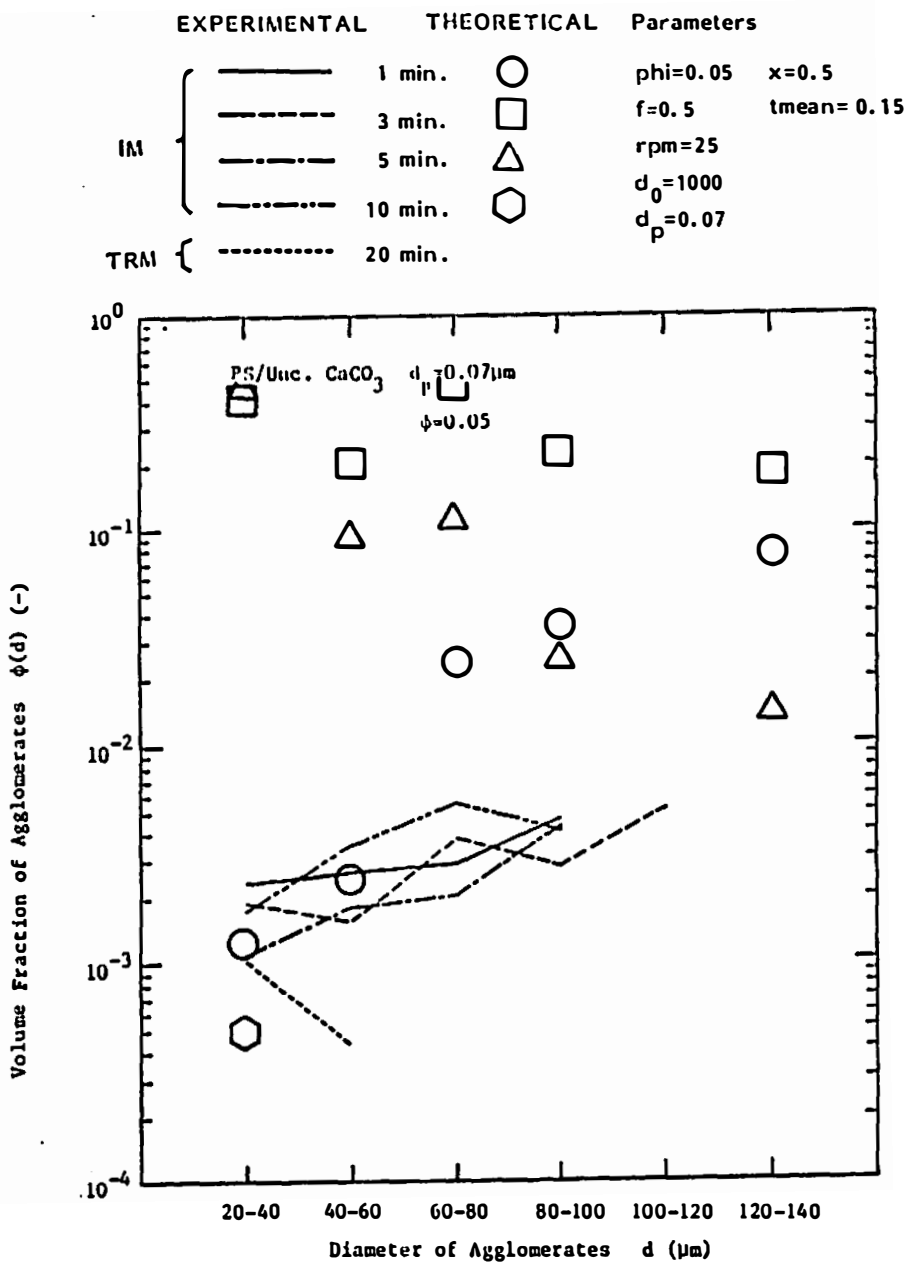

Figure XII-27. Comparison of experimental data with theoretical predictions for PS/unc. $CaCO_3$ ($x = 0.5$, $\bar{t} = 0.15$) with rupture model.

theoretical predictions. The mixing times are 1, 3, 5 and 10 minutes. Curve fitting was attempted with various sets of parameters d_0 and X. In the rupture theory, the dispersion is governed by $X/\overline{t}$. Then $\overline{t}$ was retained constant. Large discrepancies are found. This is presumably due to the slow incorporation process of these compounds. In the rupture model, the incorporation process was neglected and the initial agglomerates were assumed to be in the matrix phase when the mixing initiates.

G.3.a.2. PS/Coated $CaCO_3$ Compounds. Figures XII-28 through XII-30 present the comparison of the experimental data with the predictions for the polystyrene/coated calcium carbonate compounds. Again, the parameters d_0 and X are the variables. Large discrepancies are found. A reasonable fit was not obtained with any set of parameters.

G.3.a.3. PP/Uncoated $CaCO_3$ Compounds. The same type of comparisons are shown in Figures XII-31 through XII-33 for polypropylene/uncoated calcium carbonate compounds. Again, large errors are found between the experimental data and predictions.

G.3.a.4. PP/Coated $CaCO_3$ Compounds. Figures XII-34 through XII-36 give the same types of comparison for the polypropylene/coated calcium carbonate compounds. The distribution of the volume fraction of the agglomerates of these compounds are peculiar. The volume fractions of the agglomerates always increase with decreasing agglomerate size range. Qualitative agreement is found in Figure XII-36. The incorporation processes of these compounds were

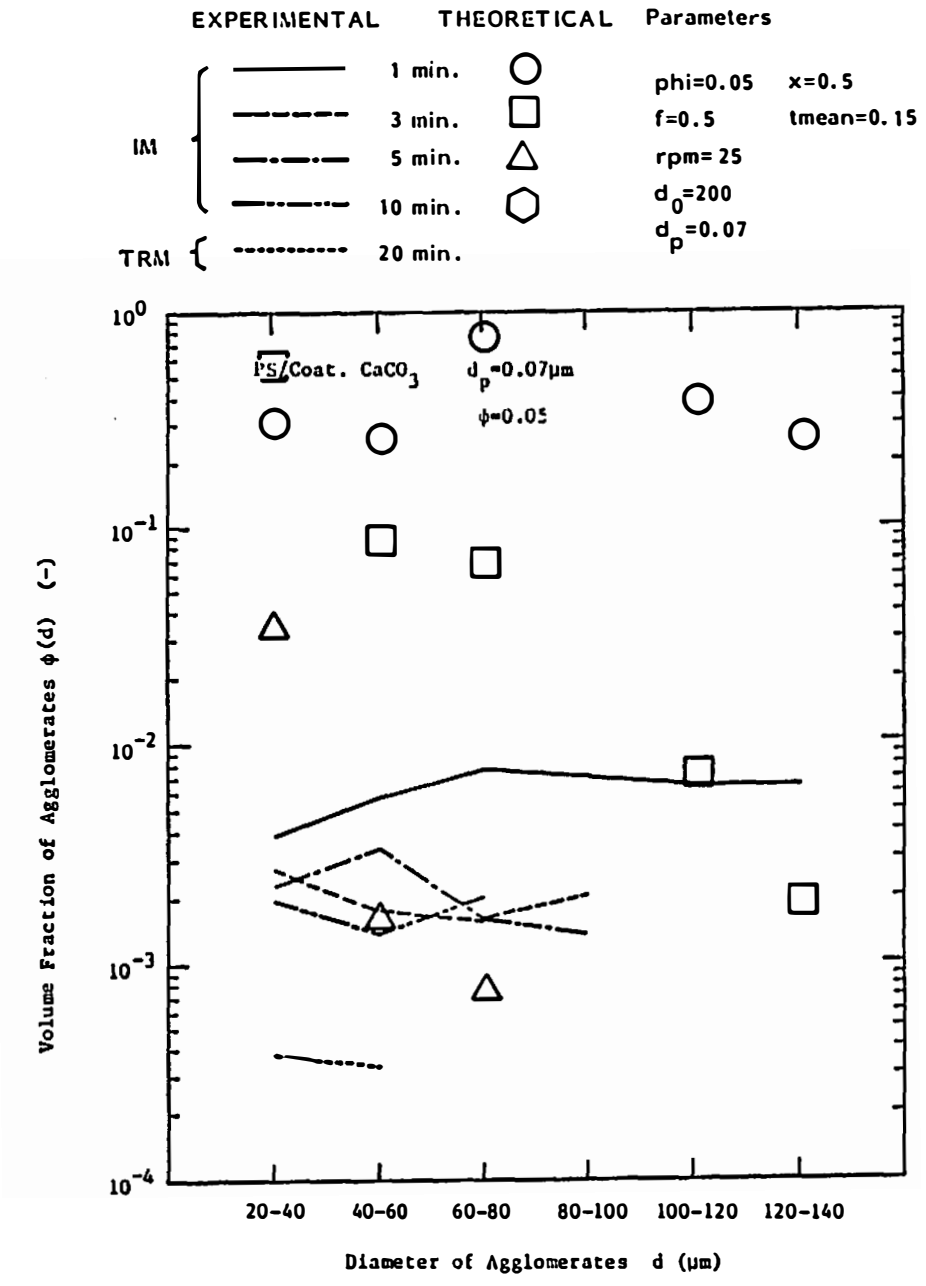

Figure XII-28. Comparison of experimental data with theoretical predictions for PS/coat. $CaCO_3$ (x = 0.5, $\bar{t}$ = 0.15) with rupture model.

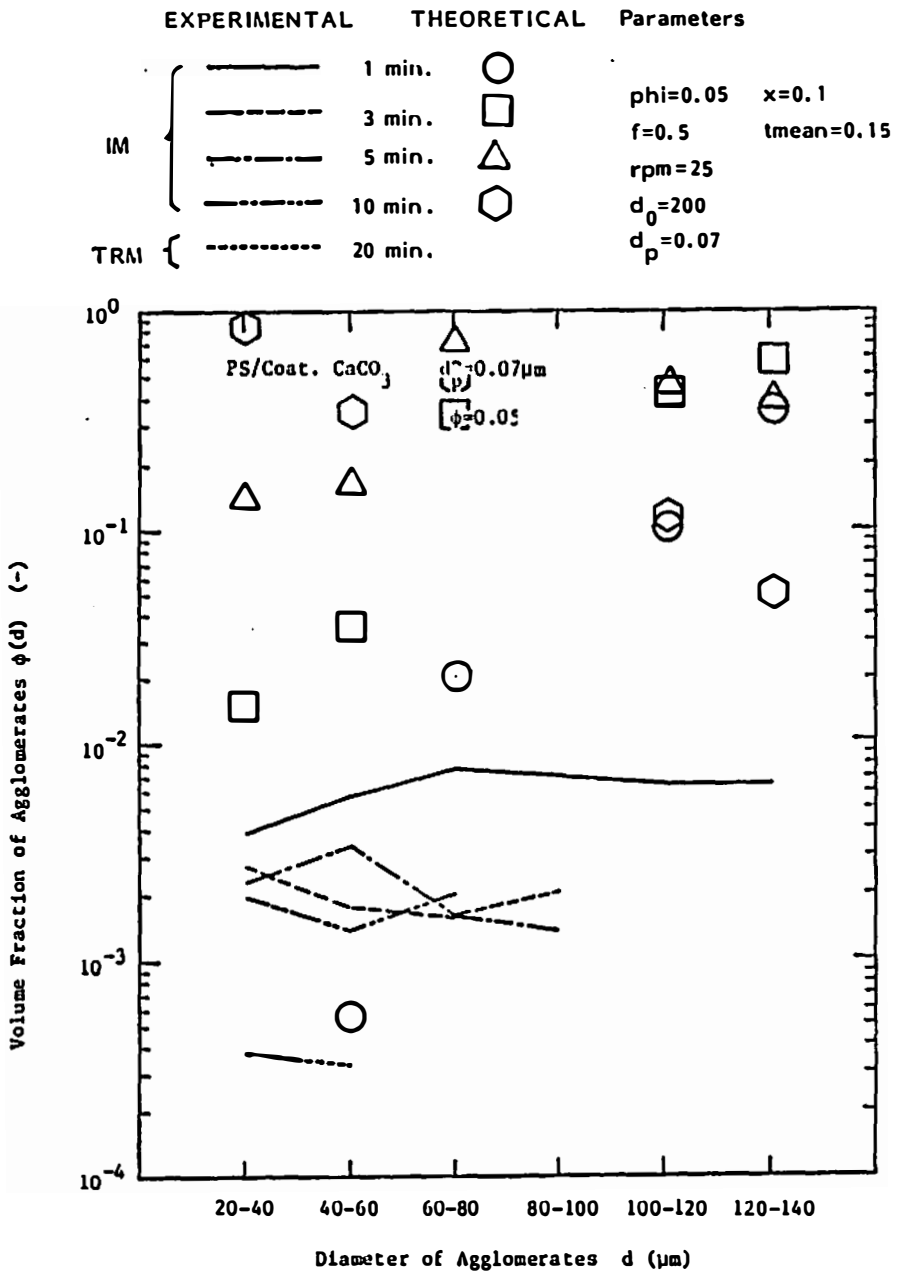

Figure XII-29. Comparison of experimental data with theoretical predictions for PS/coat. $CaCO_3$ (x = 0.1, $\bar{t}$ = 0.15) with rupture model.

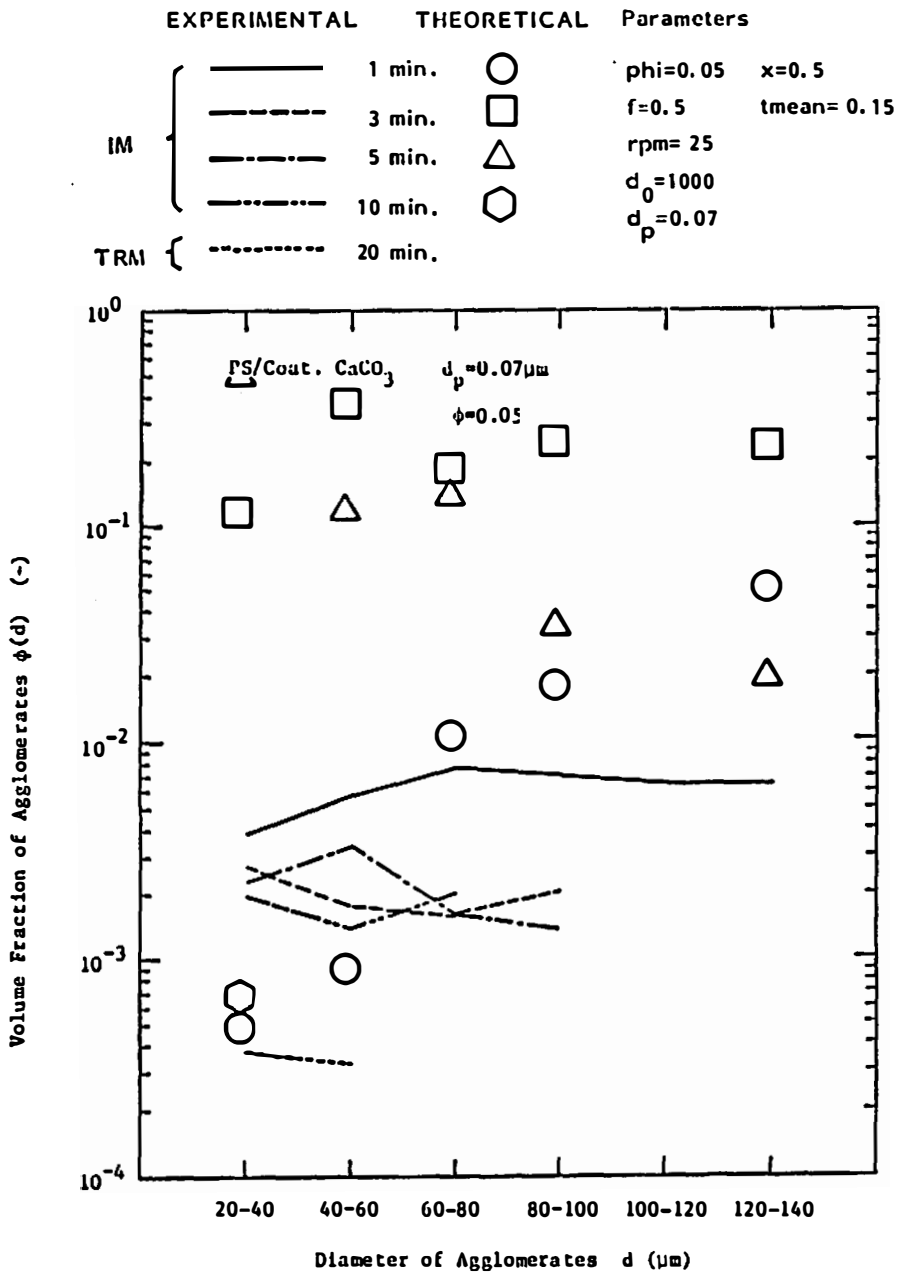

Figure XII-30. Comparison of experimental data with theoretical predictions for PS/coat. $CaCO_3$ ($x = 0.5$, $\bar{t} = 0.15$) with rupture model.

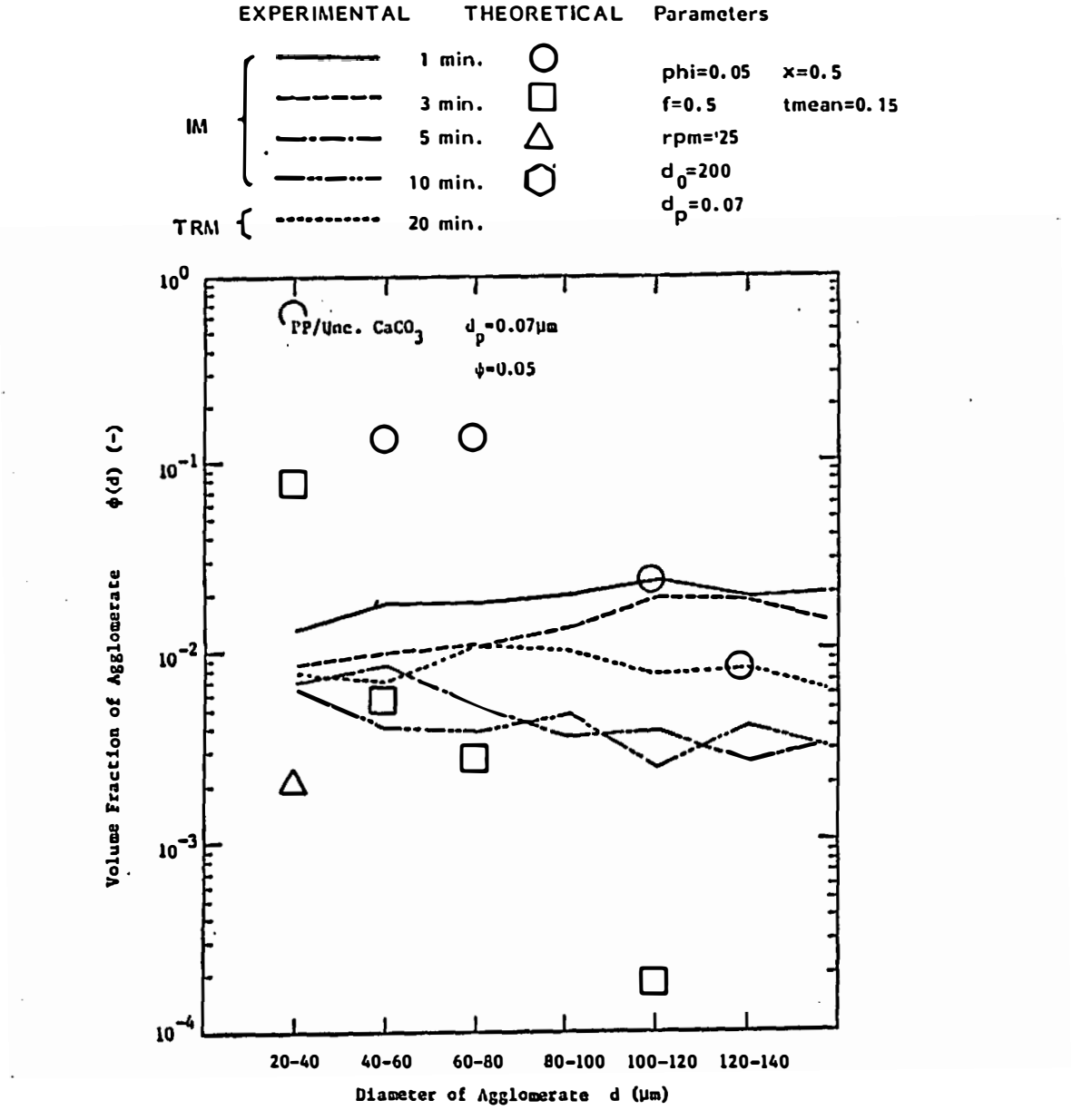

Figure XII-31. Comparison of experimental data with theoretical predictions for PP/unc. $CaCO_3$ ($x = 0.5$, $\bar{t} = 0.15$) with rupture model.

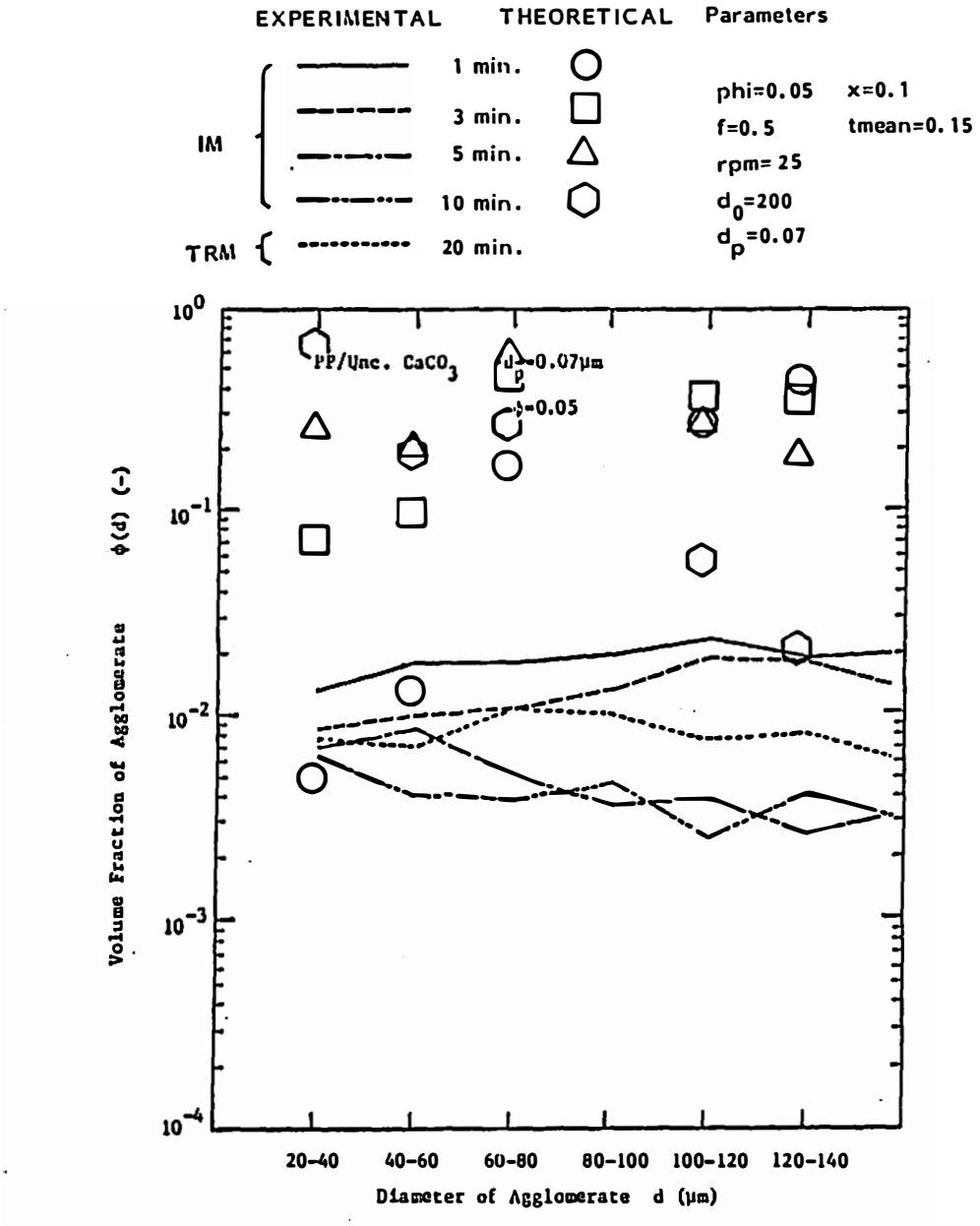

Figure XII-32. Comparison of experimental data with theoretical predictions for PP/unc. $CaCO_3$ ($x = 0.1$, $\bar{t} = 0.15$) with rupture model.

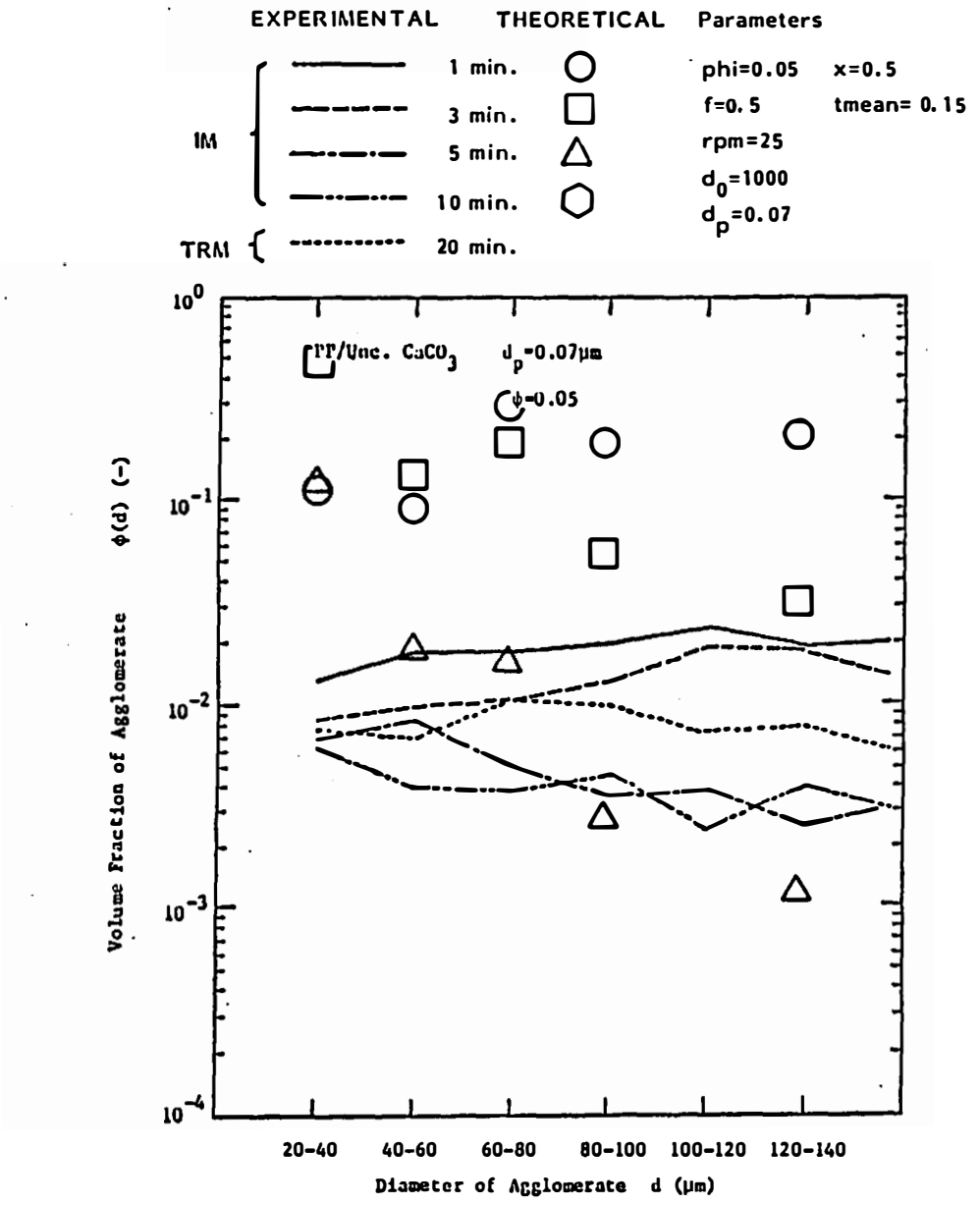

Figure XII-33. Comparison of experimental data with theoretical predictions for PP/unc. $CaCO_3$ ($x = 0.5$, $\bar{t} = 0.15$) with rupture model.

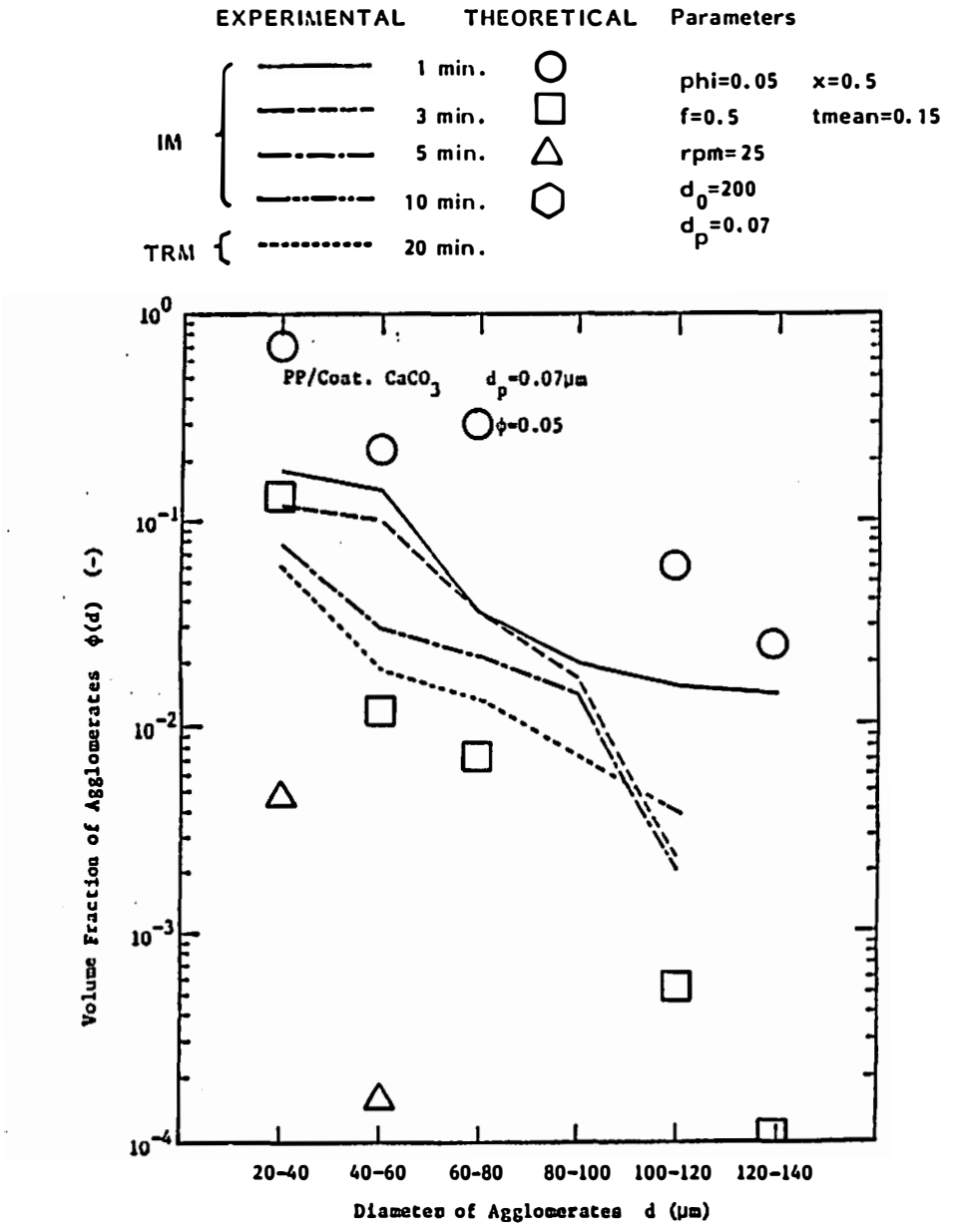

Figure XII-34. Comparison of experimental data with theoretical predictions for PP/coat. $CaCO_3$ (x = 0.5, $\bar{t}$ = 0.15) with rupture model.

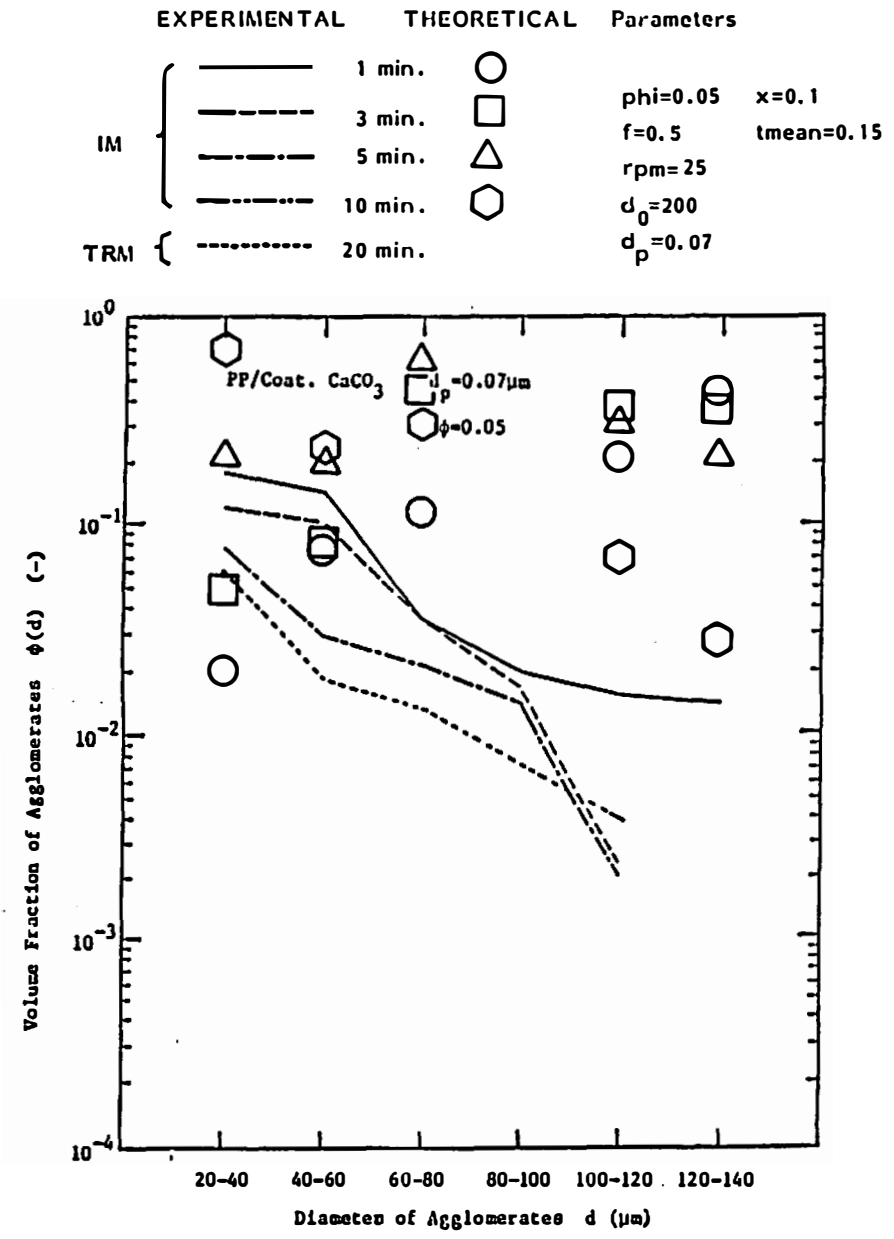

Figure XII-35. Comparison of experimental data with theoretical predictions for PP/coat. $CaCO_3$ (x = 0.1, $\bar{t}$ = 0.15) with rupture model.

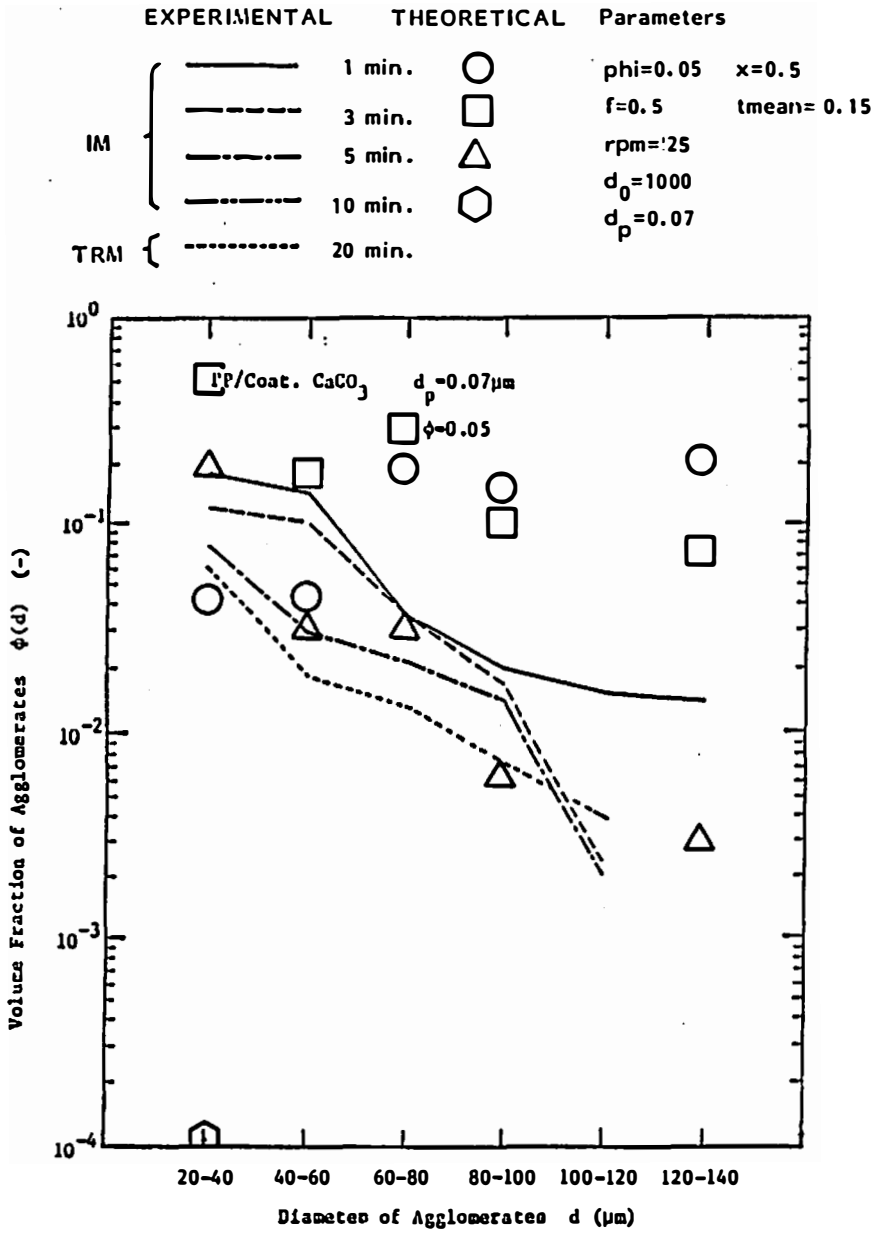

Figure XII-36. Comparison of experimental data with theoretical predictions for PP/coat. $CaCO_3$ (x = 0.5, $\bar{t}$ = 0.15) with rupture model.

experimentally found to terminate in a very short period, roughly 1.33 minutes. This may be a reason for the qualitative agreement with the theory without the consideration of the incorporation process.

G.3.b. Comparison with Modified Rupture Model.

G.3.b.1. PS/Uncoated $CaCO_3$ Compounds. We now use the modified rupture theory with the incorporation rate function.

Figures XII-37 and XII-38 present comparisons of experimental data with the theoretical predictions. We have determined the characteristic time of the incorporation process for these compounds, that is, 3 to 6 minutes.

The parameters used for Figure XII-37 are $X = 1.0$, $\bar{t} = 0.15$ and $\bar{t}_{inc} = 6.0$. It was assumed that all the agglomerates rupture in the high shear zone, that is, $X = 1.0$. The predicted volume fractions of the agglomerates are still greater than the experimental data.

We should recall that the polystyrene exhibits very large stress levels. The shear stress of polystyrene in the low shear stress zone (rotor shaft region) is as high as the stress of the polypropylene at high shear zone. If the rupture of the agglomerates occurs in the high shear zone in the polypropylene compounds, the rupture of the agglomerates should also occur in the low shear zone in the polystyrene compounds.

We may assume that the rupture of agglomerates takes place anywhere in the mixer, that is, v equals V. We obtain $\bar{t}$ to be 0.02. (We note, however, the binomial distribution cannot be approximated by the Poisson distribution under this condition.)

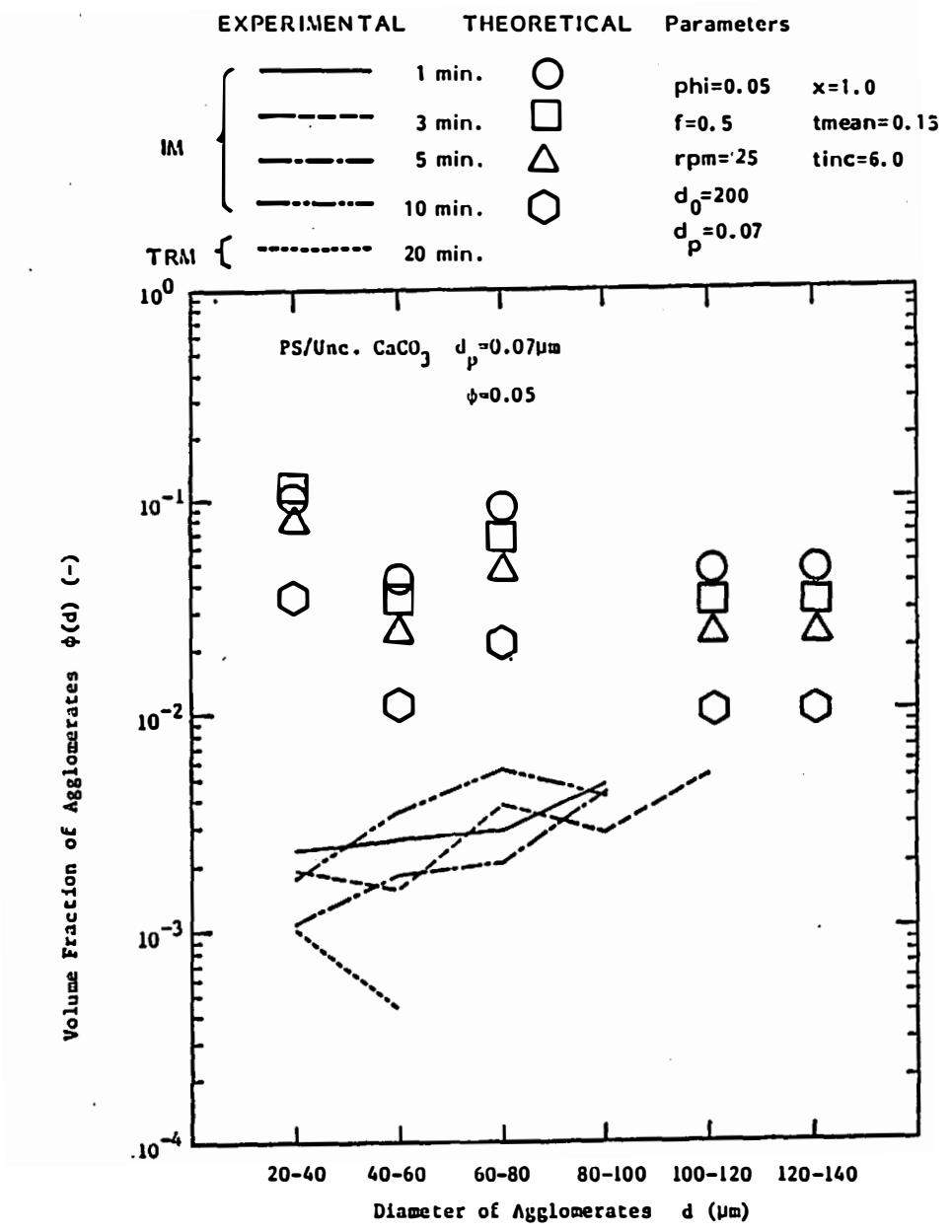

Figure XII-37. Comparison of experimental data with theoretical predictions for PS/unc. $CaCO_3$ (x = 1.0, $\bar{t}$ = 0.15, t_{inc} = 6.0) with modified rupture model.

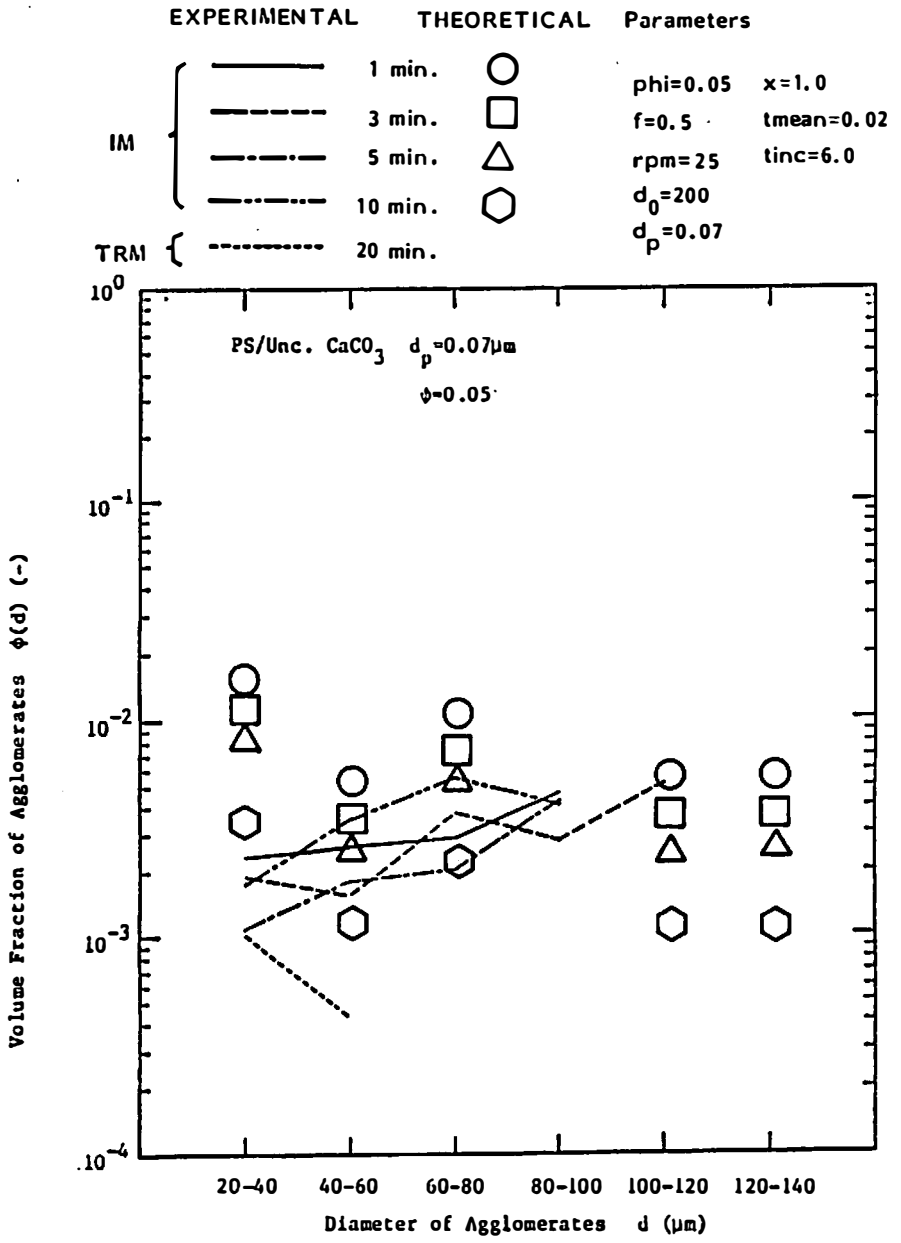

Figure XII-38. Comparison of experimental data with theoretical predictions for PS/unc. $CaCO_3$ (x = 1.0, $\bar{t}$ = 0.02, $\bar{t}_{inc}$ = 6.0) with modified rupture model.

The theoretical predictions with $\bar{t}$ = 0.02 are shown in Figure XII-38. Other parameters were unchanged. Good agreement with experiment is found.

In the polystyrene compounds, the rupture of the agglomerates would appear to occur in the low shear zone as well as high shear zone, and the slow incorporation process governs the dispersion.

G.3.b.2. PS/Coated $CaCO_3$ Compounds. Figures XII-39 and XII-40 compare the predictions and experimental data for the polystyrene/coated calcium carbonate compounds. The characteristic time of incorporation was determined to be 0.75 to 1.5 minutes.

Figure XII-39 shows the predictions with X = 1.0, $\bar{t}$ = 0.02 and $\bar{t}_{inc}$ = 1.0. The predictions are qualitatively correct. Both experimental data and the prediction show very flat distributions.

Better agreements were achieved with greater incorporation time ($\bar{t}_{inc}$ = 6.0) as shown in Figure XII-40.

Again, the rupture of agglomerates takes place in low shear zone as well.

G.3.b.3. PP/Uncoated $CaCO_3$ Compounds. Figures XII-41 through XII-43 show the same types of comparison for the polypropylene/uncoated calcium carbonate compounds.

In Figure XII-41, the predictions are much lower than the experimental values (predicted values below 10^{-4} were not plotted). The value of X is reduced to 0.2 from 1.0 in Figure XII-42. Predictions are greater than the experimental data within the mixing time of 5 minutes and lower than the experimental values after 10 minutes of mixing.

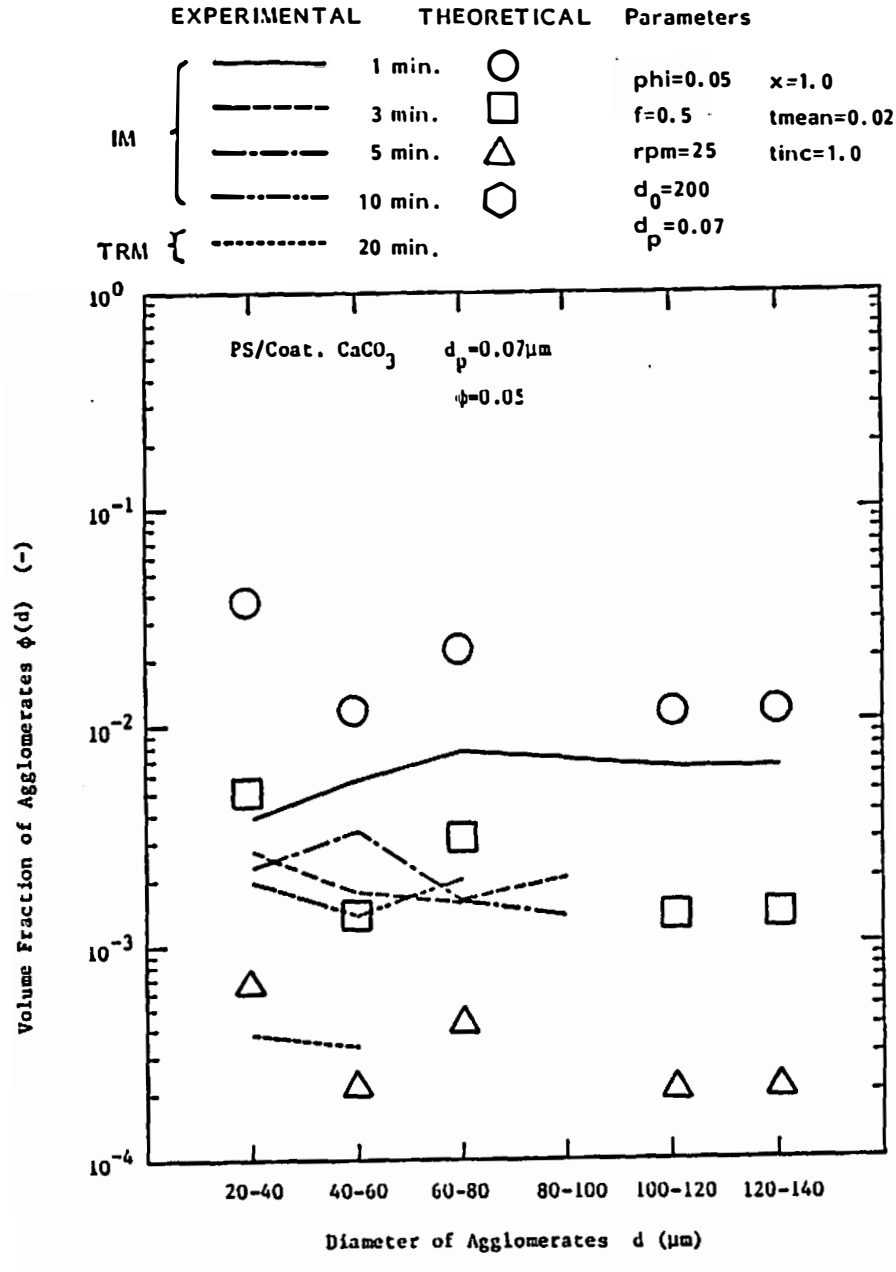

Figure XII-39. Comparison of experimental data with theoretical predictions for PS/coat. $CaCO_3$ ($x = 1.0$, $\bar{t} = 0.02$, $t_{inc} = 1.0$) with modified rupture model.

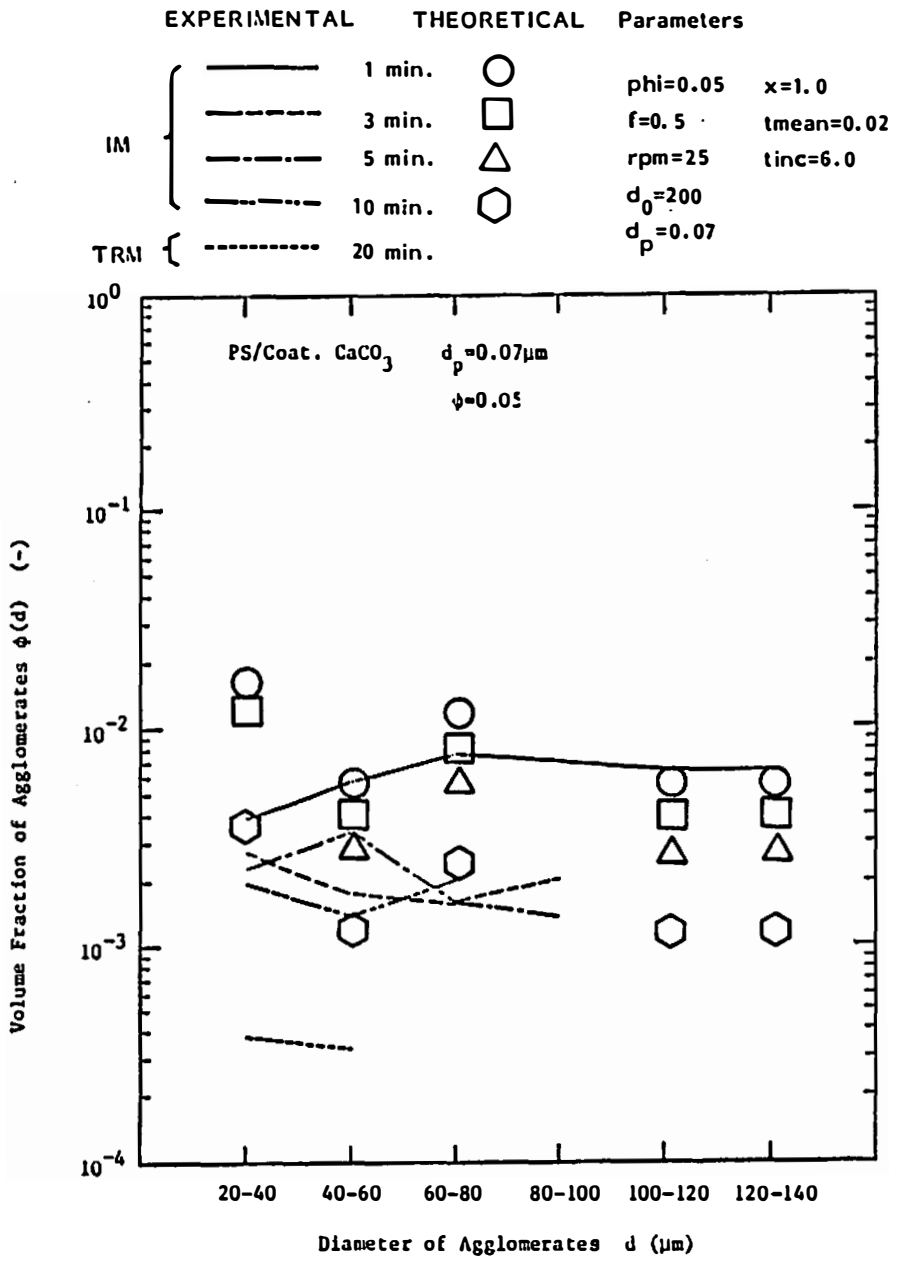

Figure XII-40. Comparison of experimental data with theoretical predictions for PS/coat. $CaCO_3$ (x = 1.0, $\bar{t}$ = 0.02, $\bar{t}_{inc}$ = 6.0) with modified rupture model.

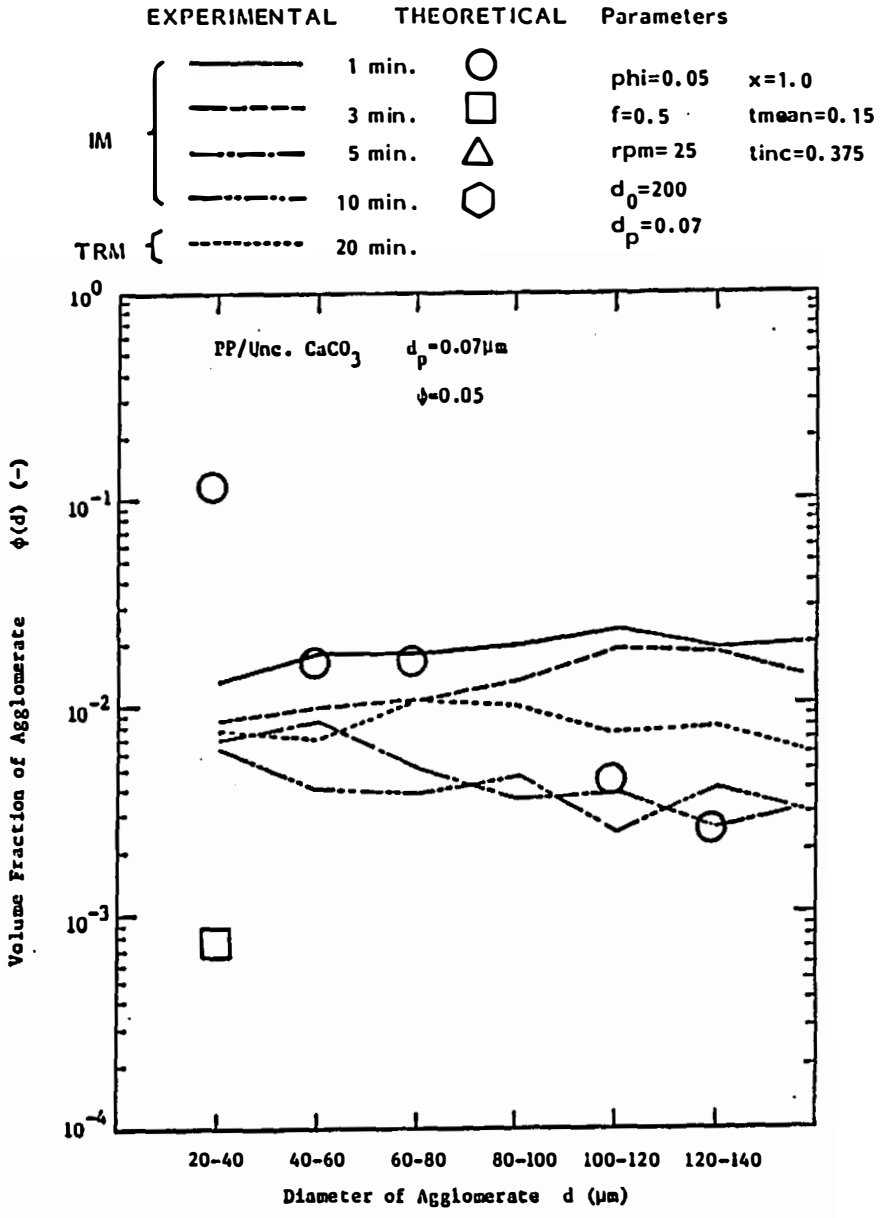

Figure XII-41. Comparison of experimental data with theoretical predictions for PP/unc. $CaCO_3$ (x = 1.0, $\bar{t}$ = 0.15, t_{inc} = 0.375) with modified rupture model.

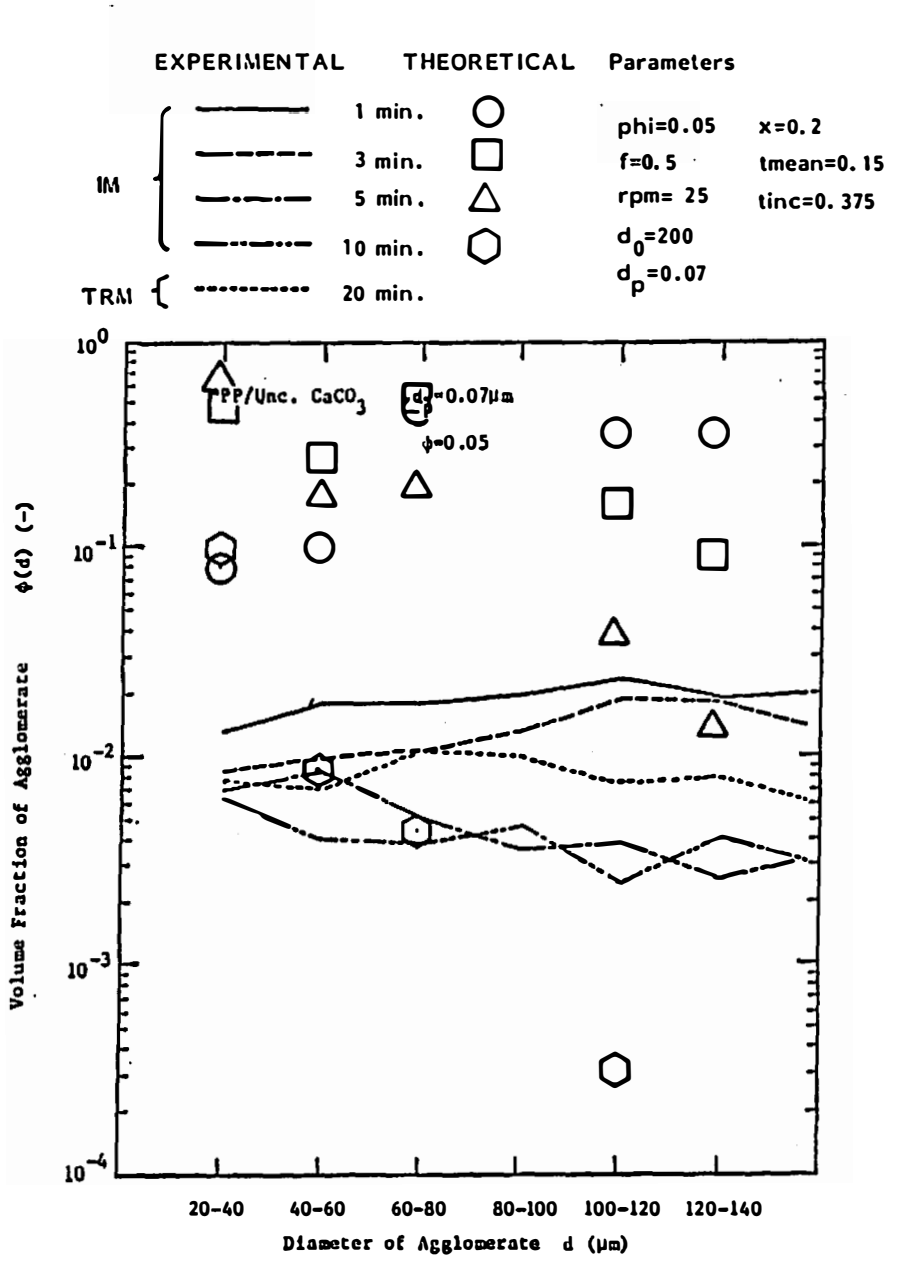

Figure XII-42. Comparison of experimental data with theoretical predictions for PP/unc. $CaCO_3$ (x = 0.2, $\bar{t}$ = 0.15, t_{inc} = 0.375) with modified rupture model.

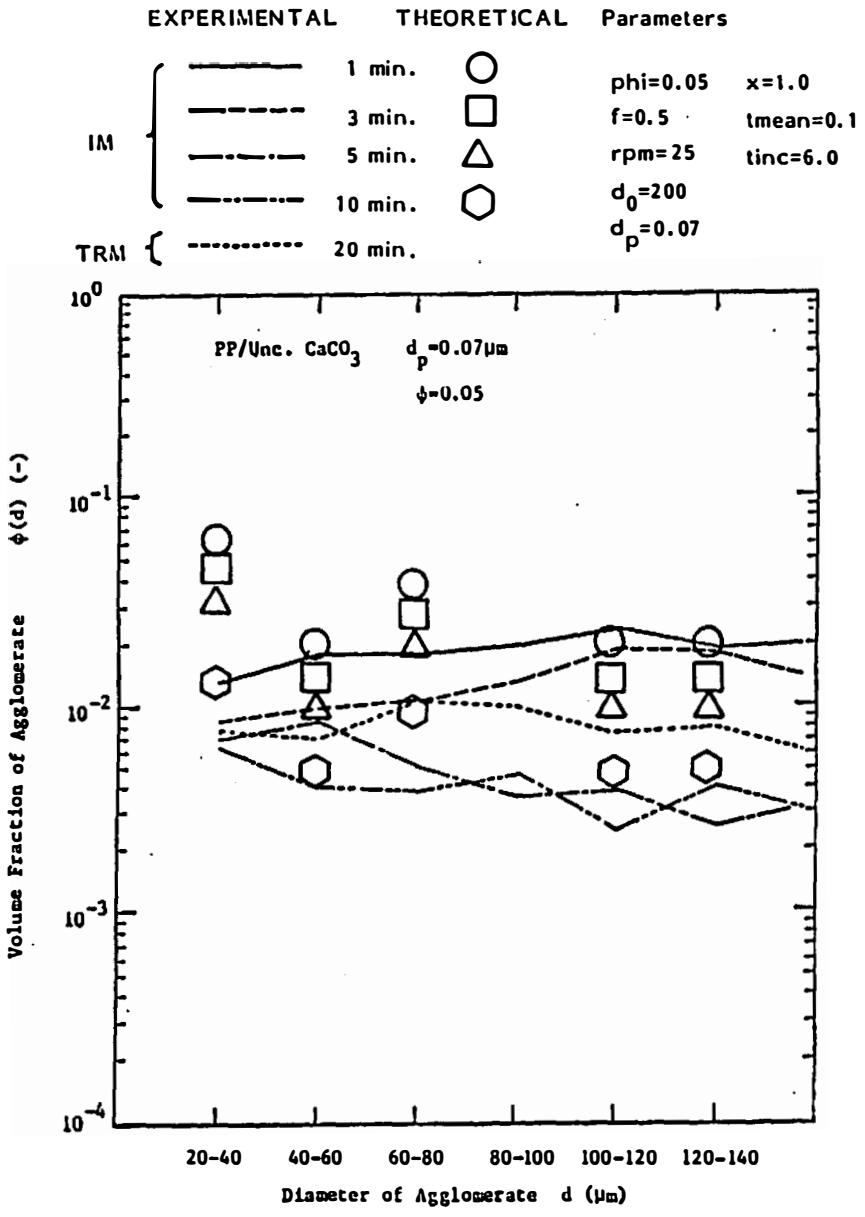

Figure XII-43. Comparison of experimental data with theoretical predictions for PP/unc. $CaCO_3$ ($x = 1.0$, $\bar{t} = 0.1$, $t_{inc} = 6.0$) with modified rupture model.

Reasonable agreement is achieved with X = 1.0, $\bar{t}$ = 0.1 and $\bar{t}_{inc}$ = 6.0 as presented in Figure XII-43. This denotes that the rupture occurs primarily in the high shear zone ($\bar{t} \leqslant 0.223$) and that all agglomerates brought into the high shear zone ruptures (X = 1.0). The characteristic incorporation time is much greater than the experimentally determined value of 0.375.

G.3.b.4. PP/Coated $CaCO_3$ Compounds. The same type of comparisons are made for the polypropylene/coated calcium carbonate compounds in Figures XII-44 and XII-45. The characteristic incorporation time is determined to be 0.375 minute for these compounds. Qualitative agreement is obtained with $\bar{t}_{inc}$ = 0.375 (Figure XII-44). Better agreement was obtained with greater incorporation time ($\bar{t}_{inc}$ = 3.0) using the above parameters as shown in Figure XII-45.

G.3.c. Comparison with Onion Model.

G.3.c.1. PS/Uncoated $CaCO_3$ Compounds. Experimentally determined volume fractions of agglomerates are compared with the onion theory for the polystyrene/uncoated calcium carbonate compounds. Figures XII-46 through XII-49 show the comparisons for the various sets of parameters.

In Figure XII-46, the parameters are d_0 = 200, R_1 = 0.1 and $\bar{t}$ = 0.15. The theory predicts the volume fractions of agglomerates smaller than 10^{-4} after 5 minutes of mixing. These are much smaller than the experimental data.

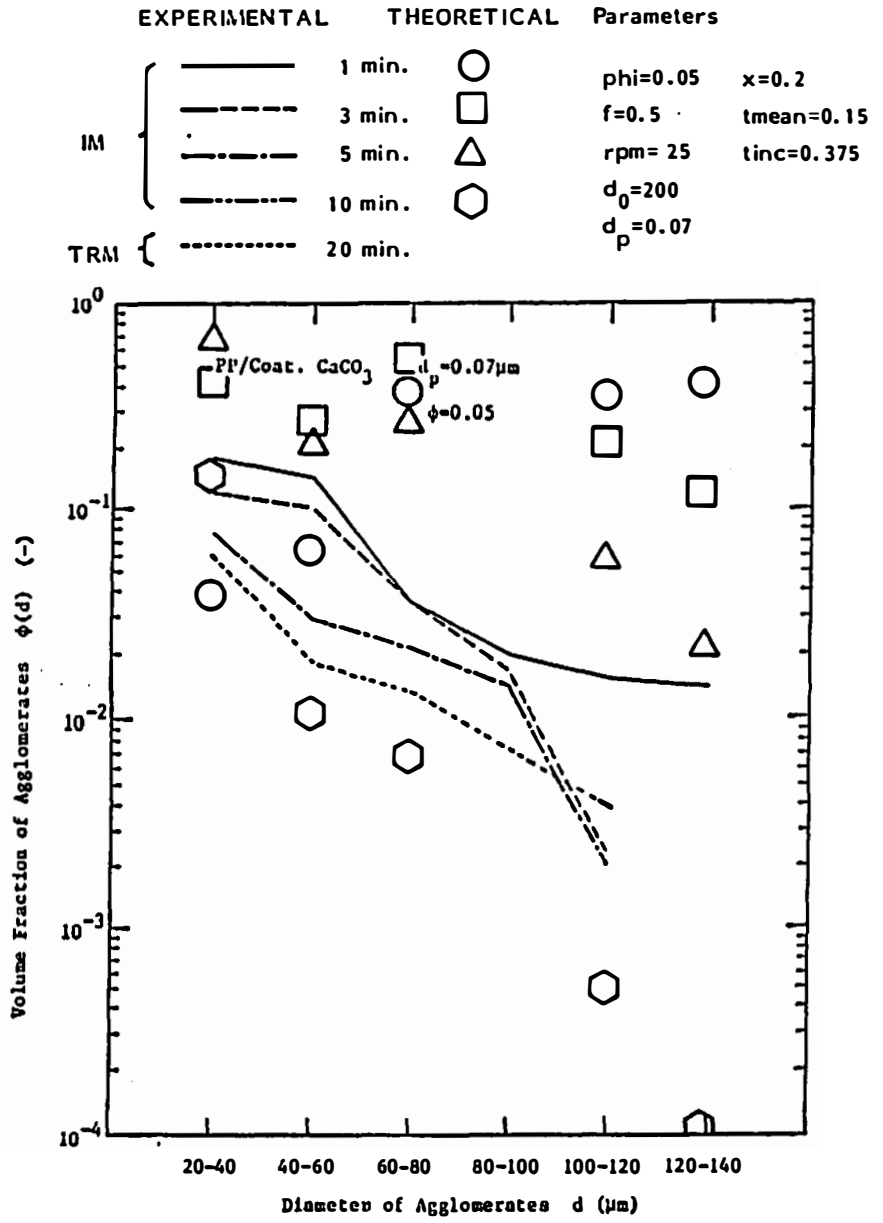

Figure XII-44. Comparison of experimental data with theoretical predictions for PP/coat. $CaCO_3$ (x = 0.2, $\bar{t}$ = 0.15, t_{inc} = 0.375) with modified rupture model.

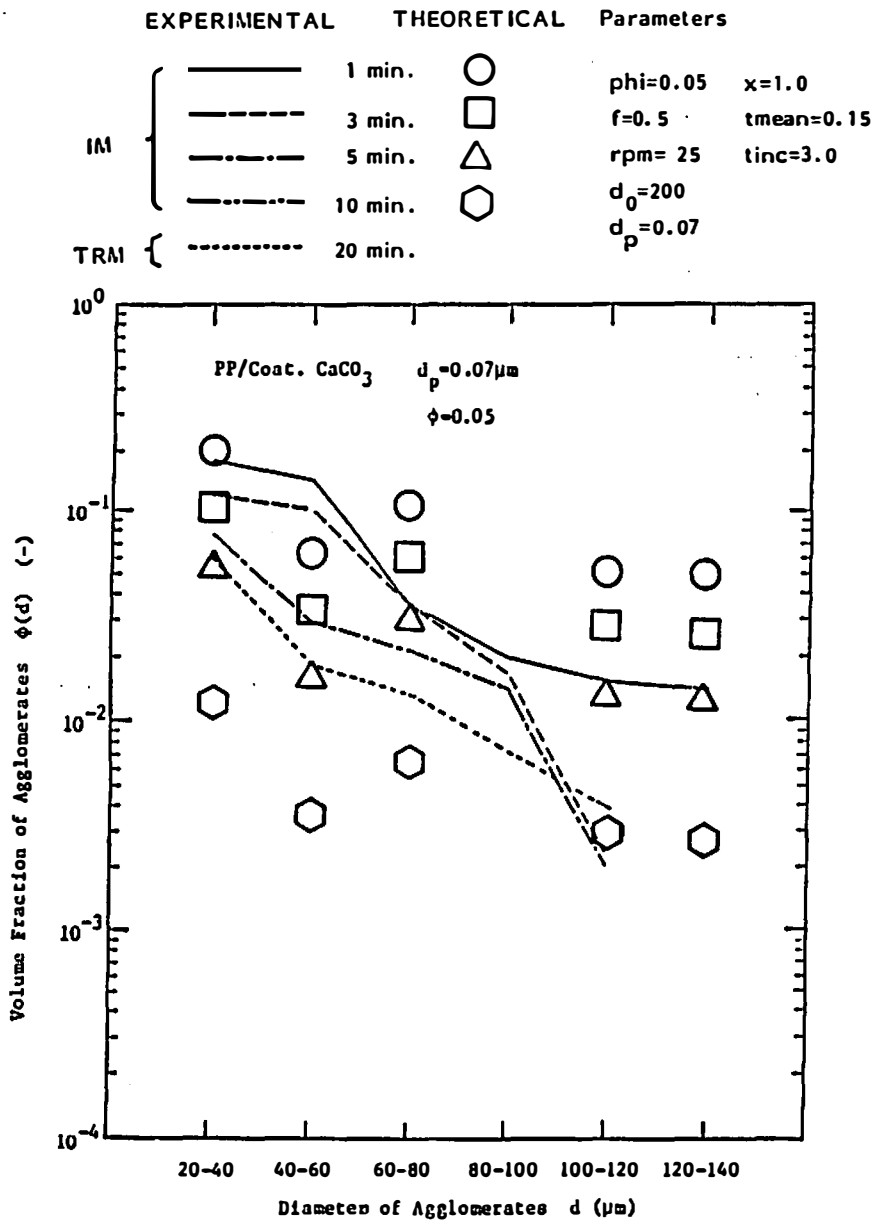

Figure XII-45. Comparison of experimental data with theoretical predictions for PP/coat. $CaCO_3$ (x = 1.0, $\bar{t}$ = 0.15, t_{inc} = 3.0) with modified rupture model.

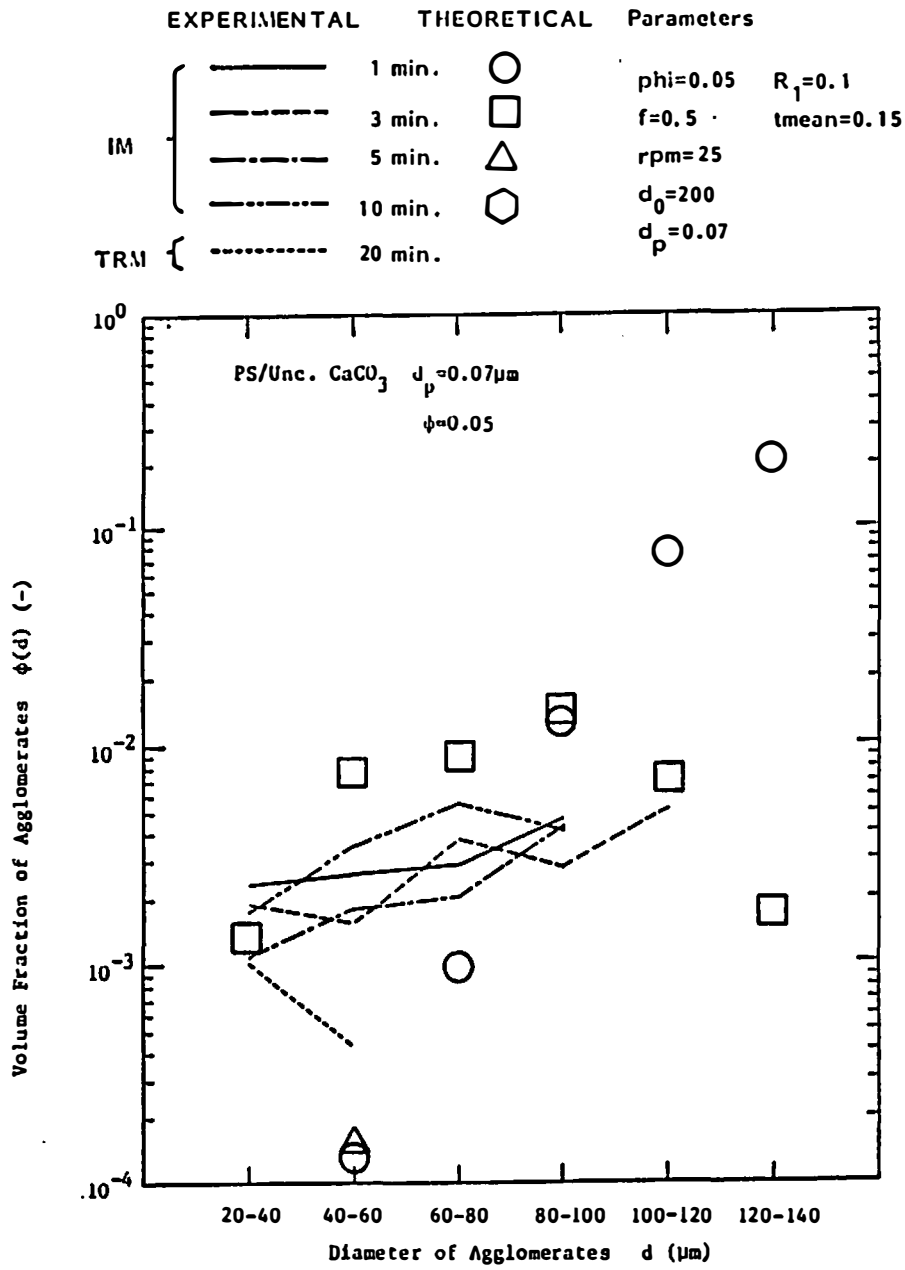

Figure XII-46. Comparison of experimental data with theoretical predictions for PS/unc. $CaCO_3$ (R_1 = 0.1, $\bar{t}$ = 0.15) with onion model.

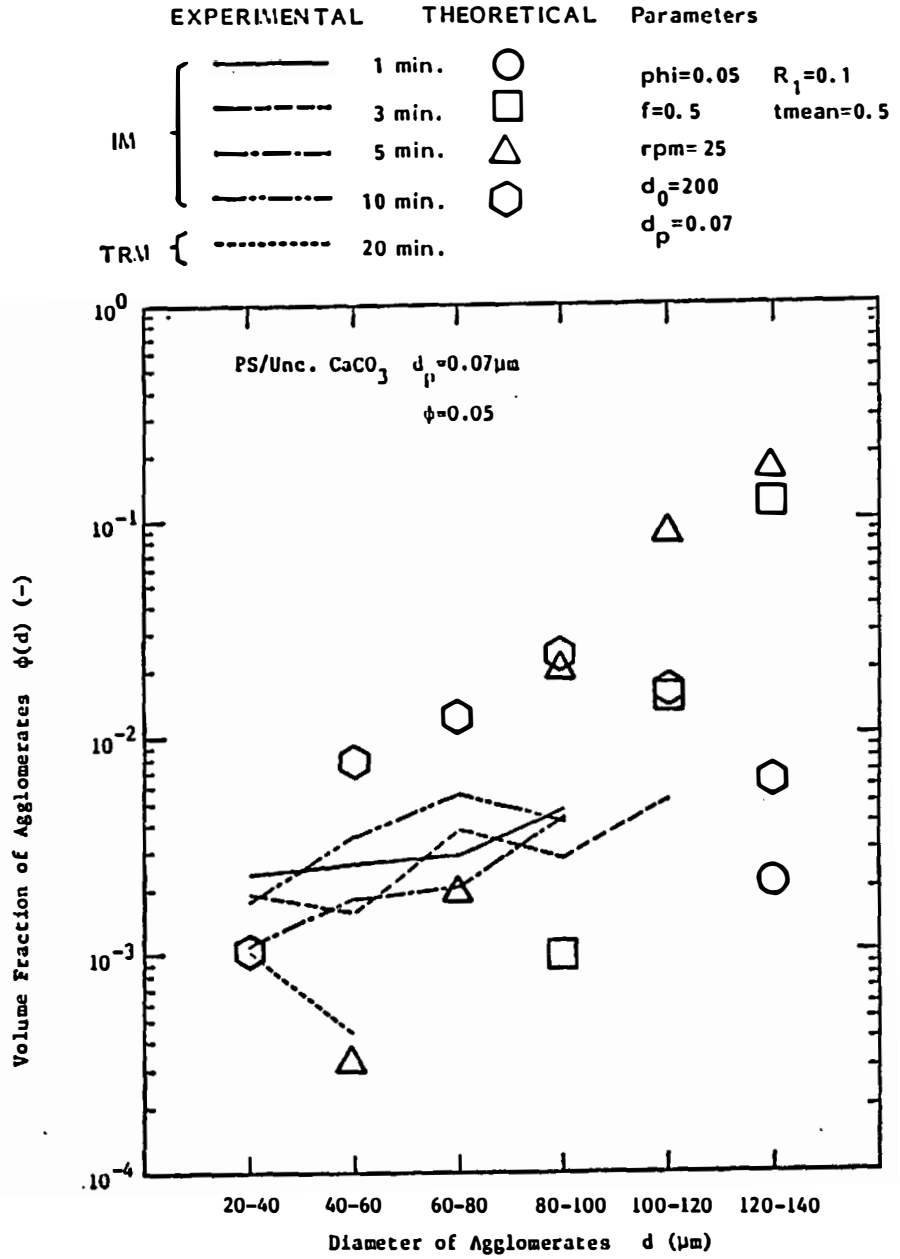

Figure XII-47. Comparison of experimental data with theoretical predictions for PS/unc. $CaCO_3$ (R_1 = 0.1, $\bar{t}$ = 0.5) with onion model.

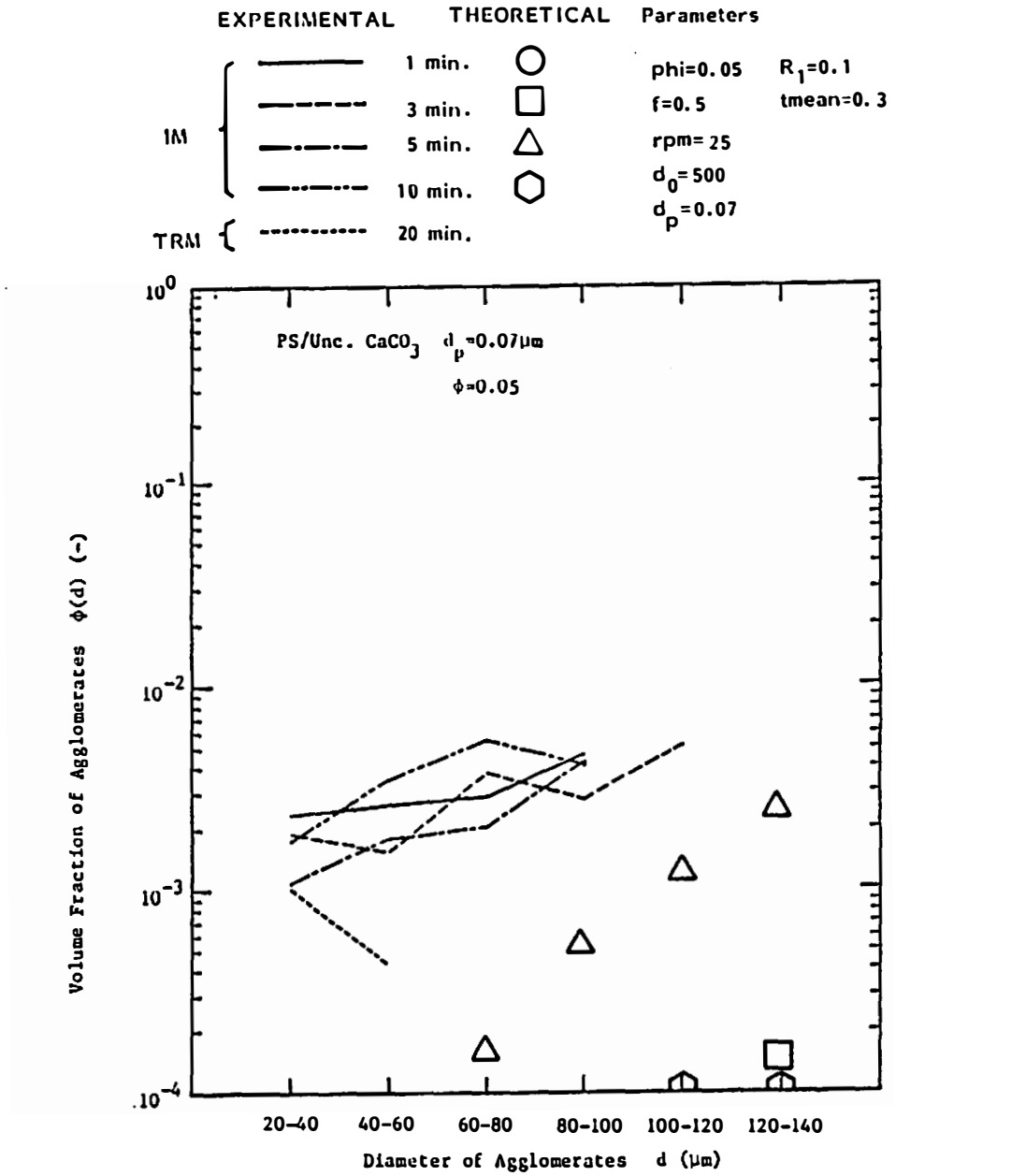

Figure XII-48. Comparison of experimental data with theoretical predictions for PS/unc. $CaCO_3$ (R_1 = 0.1, $\bar{t}$ = 0.3) with onion model.

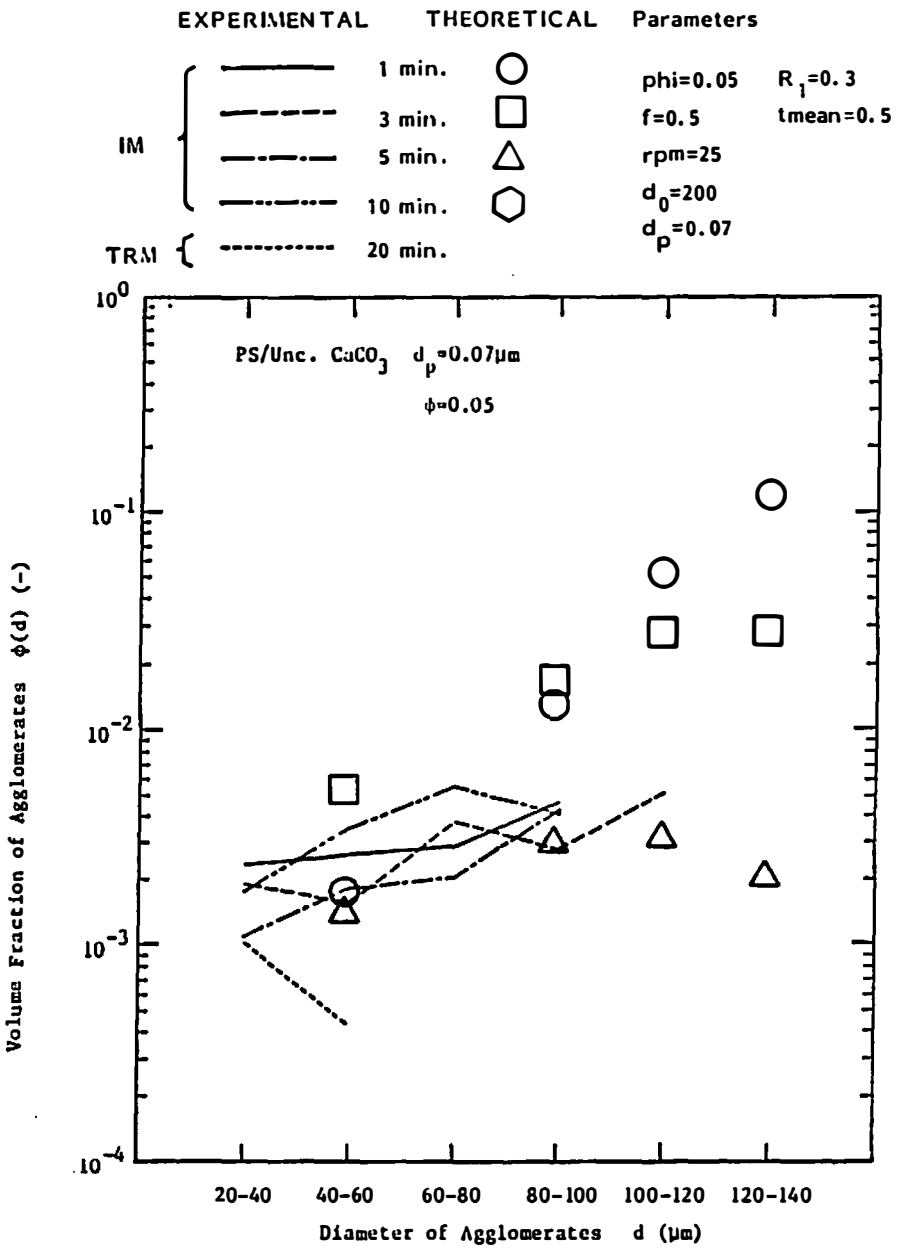

Figure XII-49. Comparison of experimental data with theoretical predictions for PS/unc. $CaCO_3$ (R_1 = 0.3, $\bar{t}$ = 0.5) with onion model.

A large $\bar{t}$ value slows down the breakdown of the agglomerates (Figure XII-47). The predictions for the mixing times of 3 to 10 minutes are reasonable. However, the theory predicts too small a value for 1 minute mixing.

We may change the size of the initial agglomerates from 200 μm to 500 μm (Figure XII-48). The predicted values are much smaller than the experimental data for the numbers of the combinations of R_1 and $\bar{t}$. Figure XII-48 is an example.

The computation was carried out for the different R_1 values. A reasonable fit was obtained with d_0 = 200 and $\bar{t}$ = 0.5 (Figure XII-49). However, the prediction for 10 minutes of mixing is of the order of 10^{-6} which is well below the experimental data. A good fit was not obtained.

G.3.c.2. PS/Coated $CaCO_3$ Compounds. Two examples of comparison are given in Figures XII-50 and XII-51 for the polystyrene/coated calcium carbonate compounds.

The predictions from the onion theory tend to be strongly decreasing functions with decreasing agglomerate size range unlike the rupture theory. In the onion theory, the number of the agglomerates remains constant during mixing and the volume of the agglomerates decreases by a peel-off mechanism. On the other hand, in the rupture theory, the number of the agglomerates increases by rupture mechanism and the total volume of the agglomerates is retained constant until these become ultimate particles. A good fit was not found.

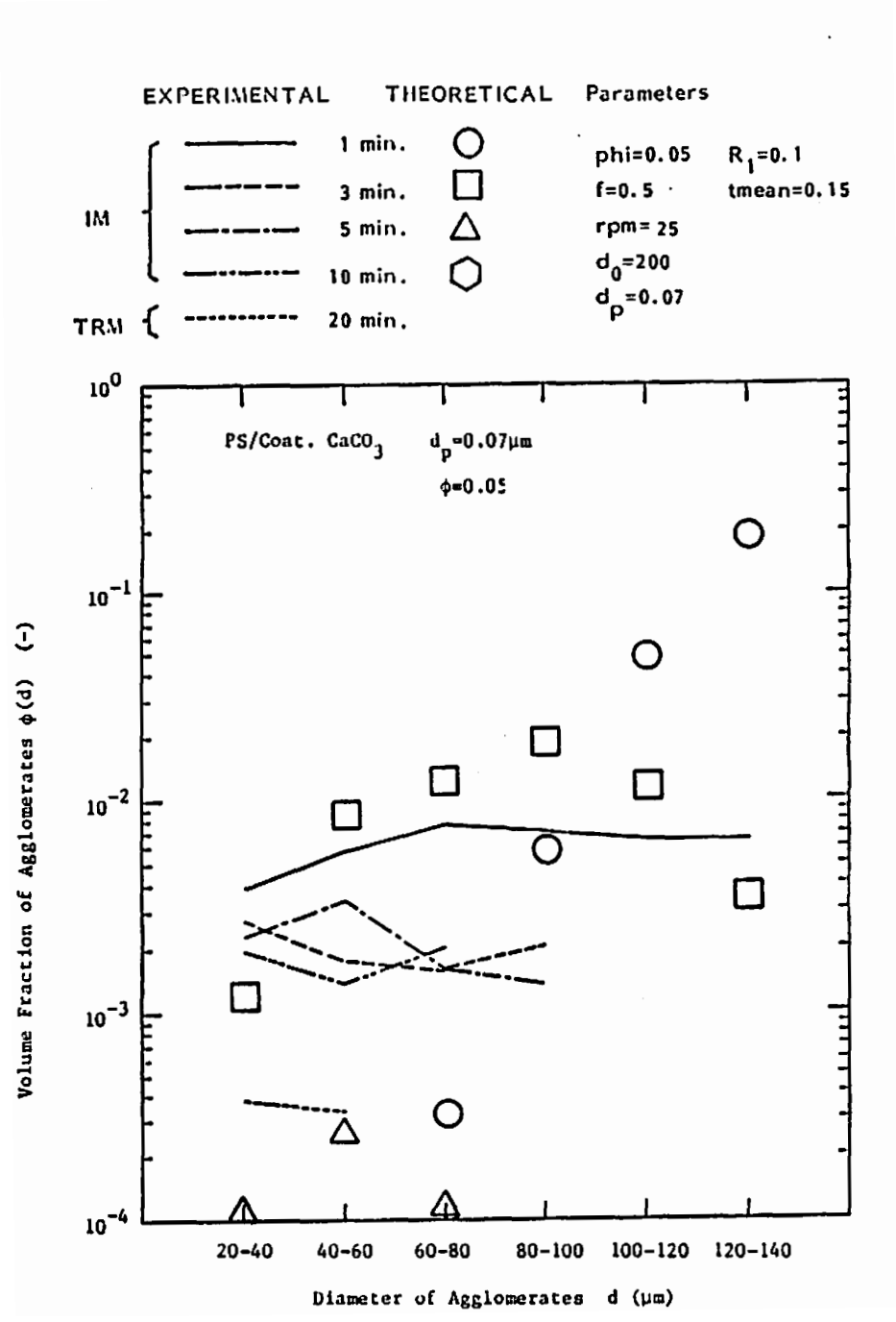

Figure XII-50. Comparison of experimental data with theoretical predictions for PS/coat. $CaCO_3$ (R_1 = 0.1, $\bar{t}$ = 0.15) with onion model.

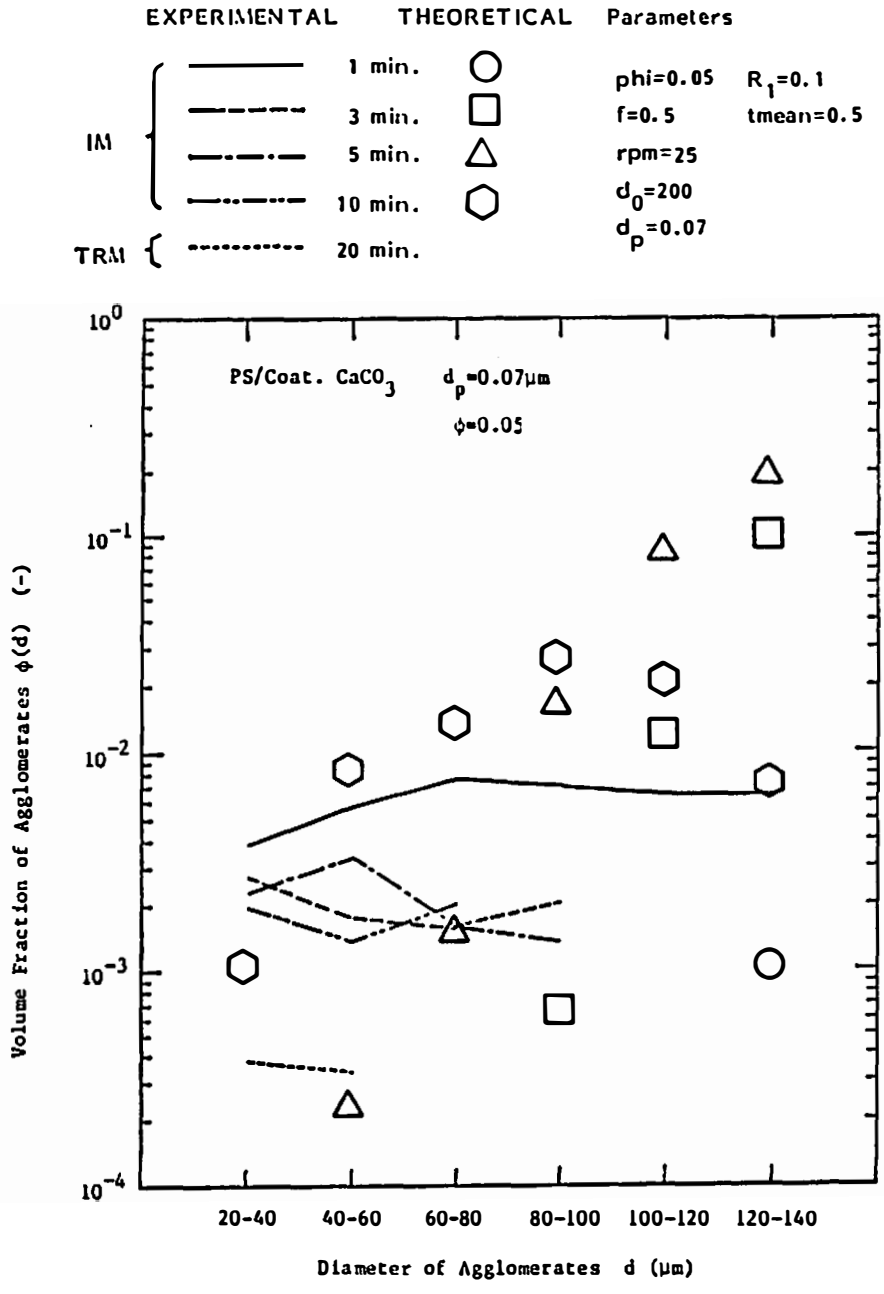

Figure XII-51. Comparison of experimental data with theoretical predictions for PS/coat. $CaCO_3$ (R_1 = 0.1, $\bar{t}$ = 0.5) with onion model.

G.3.c.3. PP/Uncoated $CaCO_3$ Compounds. Figures XII-52 and XII-53 present the same type of comparison. The onion model does not predict the flat distributions of the volume fractions of the agglomerates. Large discrepancies are found.

G.3.c.4. PP/Coated $CaCO_3$ Compounds. The volume fractions of the agglomerates of the polypropylene/coated calcium carbonate compounds are strongly increasing functions with decreasing agglomerate size range. Such a distribution was not predicted by the onion theory. Examples are shown in Figures XII-54 and XII-55.

G.3.d. Comparison with Modified Onion Model. The onion model has been modified with the incorporation rate function. We now employ the modified onion model to compare its prediction with the experimental values.

G.3.d.1. PS/Uncoated $CaCO_3$ Compounds. The characteristic time of the incorporation process for the polystyrene/uncoated calcium carbonate compounds is obtained to be 3.0 to 6.0.

Figures XII-56 and XII-57 present a comparison of the experimental values with the predictions from modified onion model. The values of $\overline{t}_{inc}$ are 6.0 in Figure XII-56 and 3.0 in Figure XII-57. The other variables are $d_0 = 200$, $R_1 = 0.1$ and $\overline{t} = 0.15$ in both figures. Fairly good agreement was obtained. Both predictions and the experimental values are the increasing functions with the agglomerate size range.

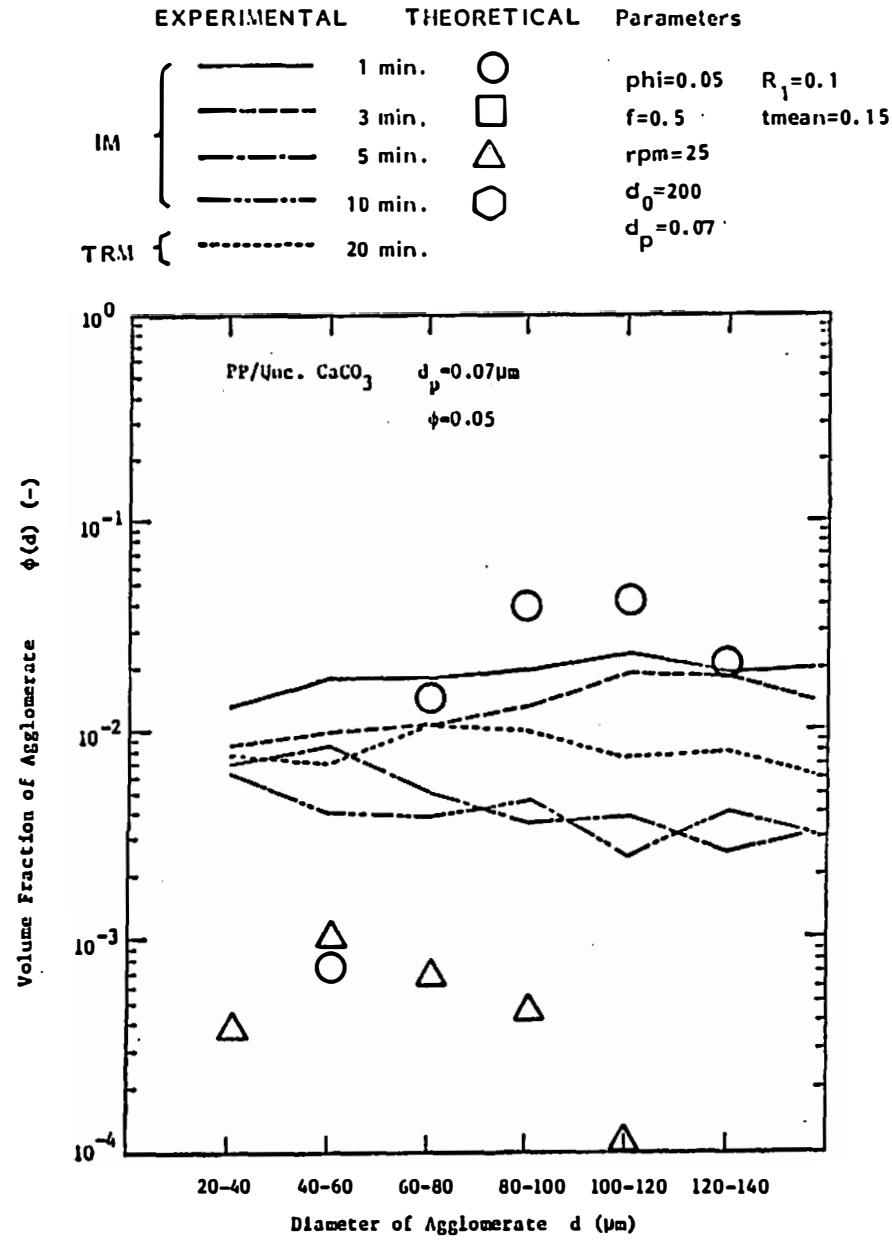

Figure XII-52. Comparison of experimental data with theoretical predictions for PP/unc. $CaCO_3$ (R_1 = 0.1, $\bar{t}$ = 0.15) with onion model.

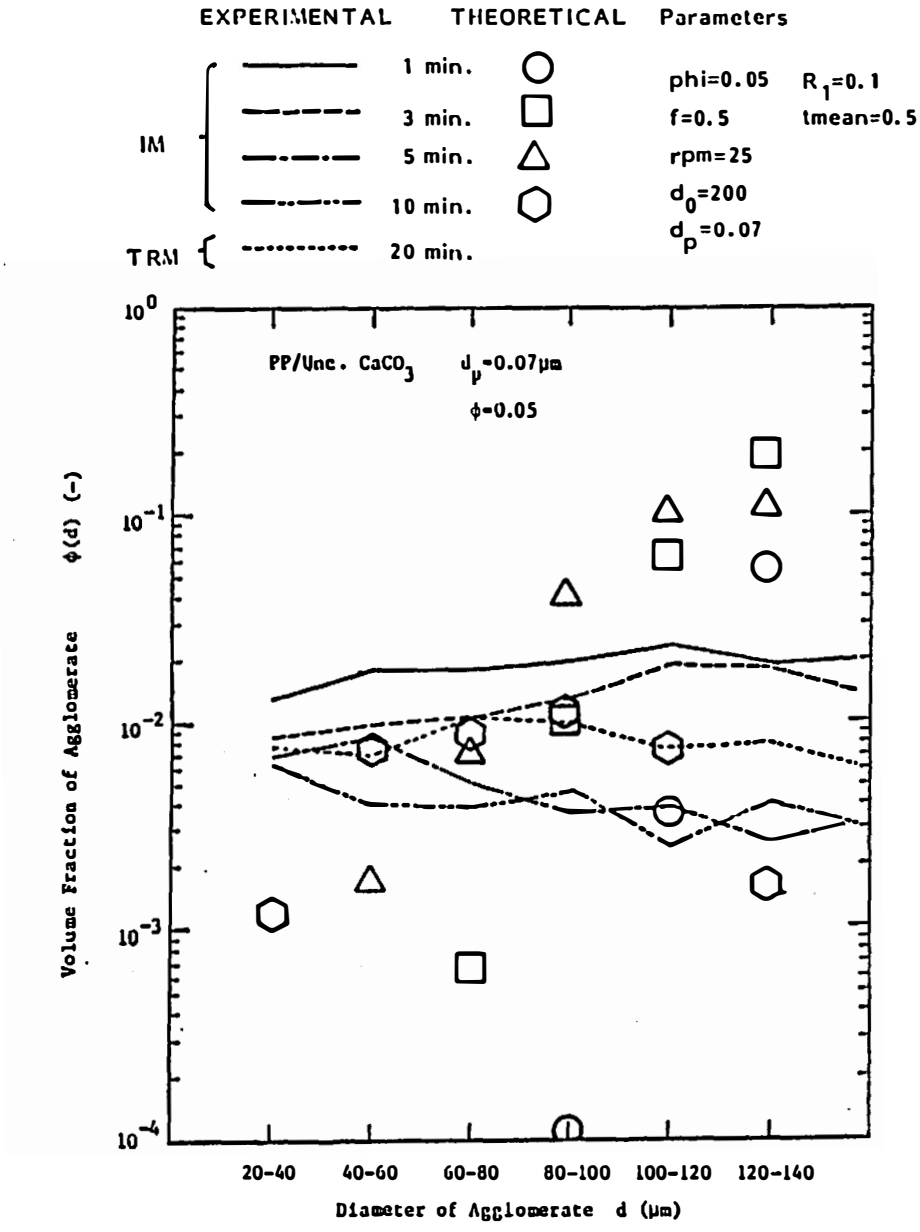

Figure XII-53. Comparison of experimental data with theoretical predictions for PP/unc. $CaCO_3$ (R_1 = 0.1, $\bar{t}$ = 0.5) with onion model.

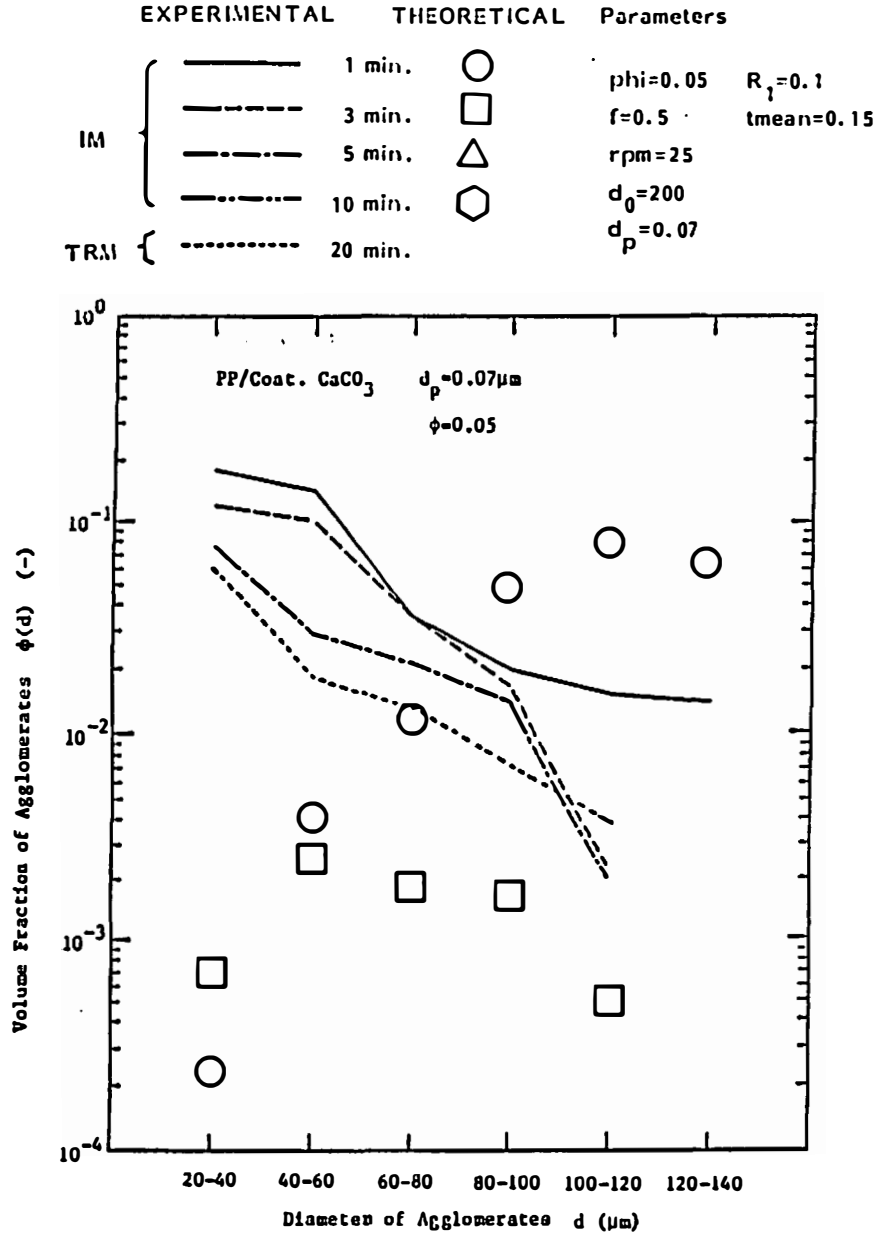

Figure XII-54. Comparison of experimental data with theoretical predictions for PP/coat. $CaCO_3$ (R_1 = 0.1, $\bar{t}$ = 0.15) with onion model.

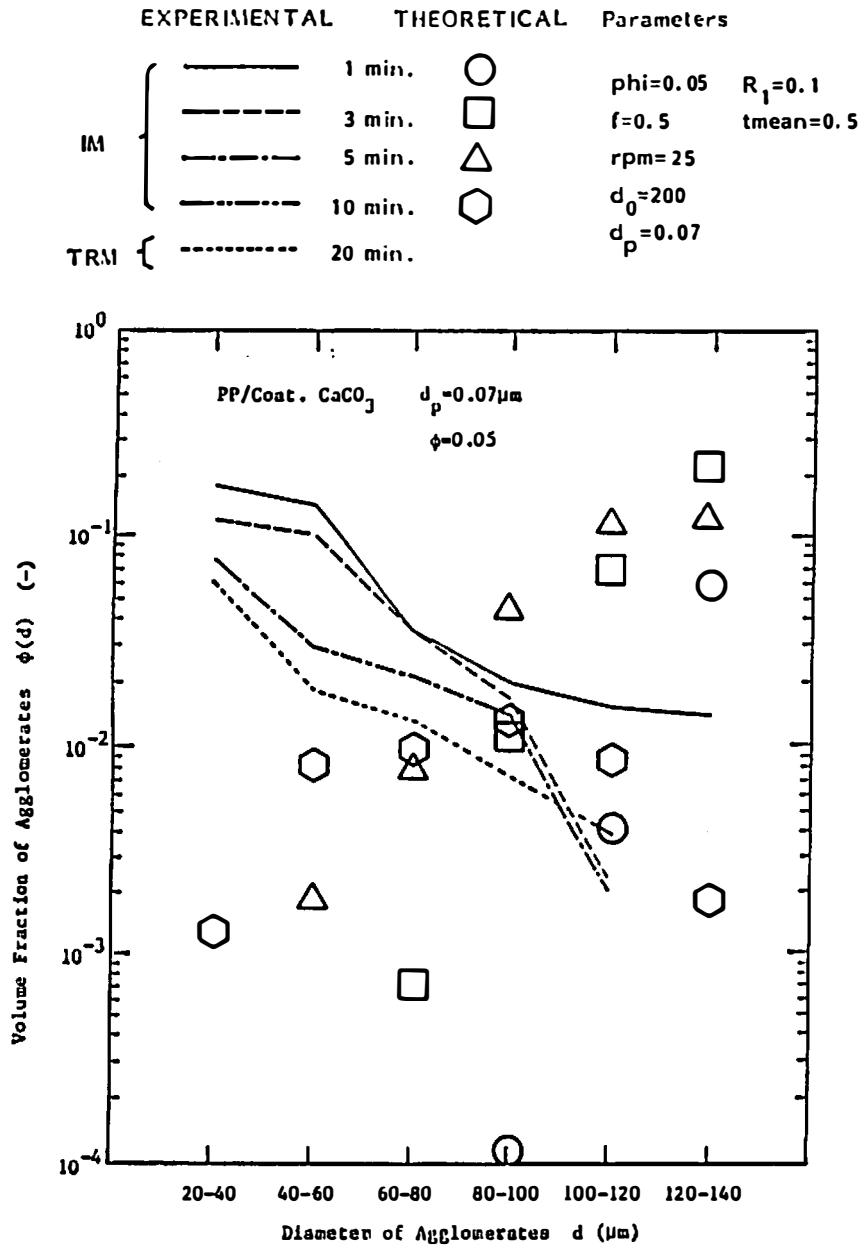

Figure XII-55. Comparison of experimental data with theoretical predictions for PP/coat. $CaCO_3$ (R_1 = 0.1. $\bar{t}$ = 0.5) with onion model.

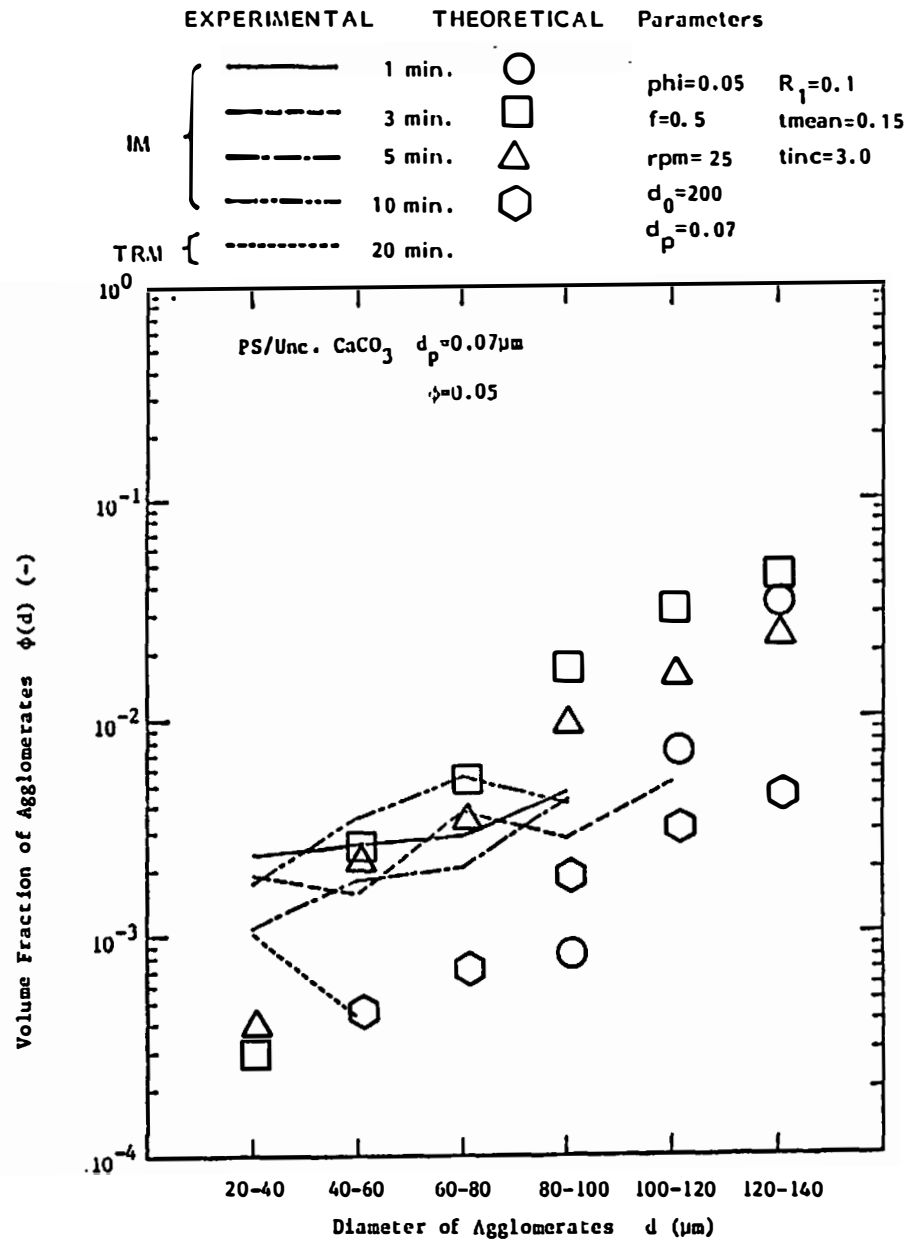

Figure XII-56. Comparison of experimental data with theoretical predictions for PS/unc. $CaCO_3$ (R_1 = 0.1, $\bar{t}$ = 0.15, t_{inc} = 3.0) with modified onion model.

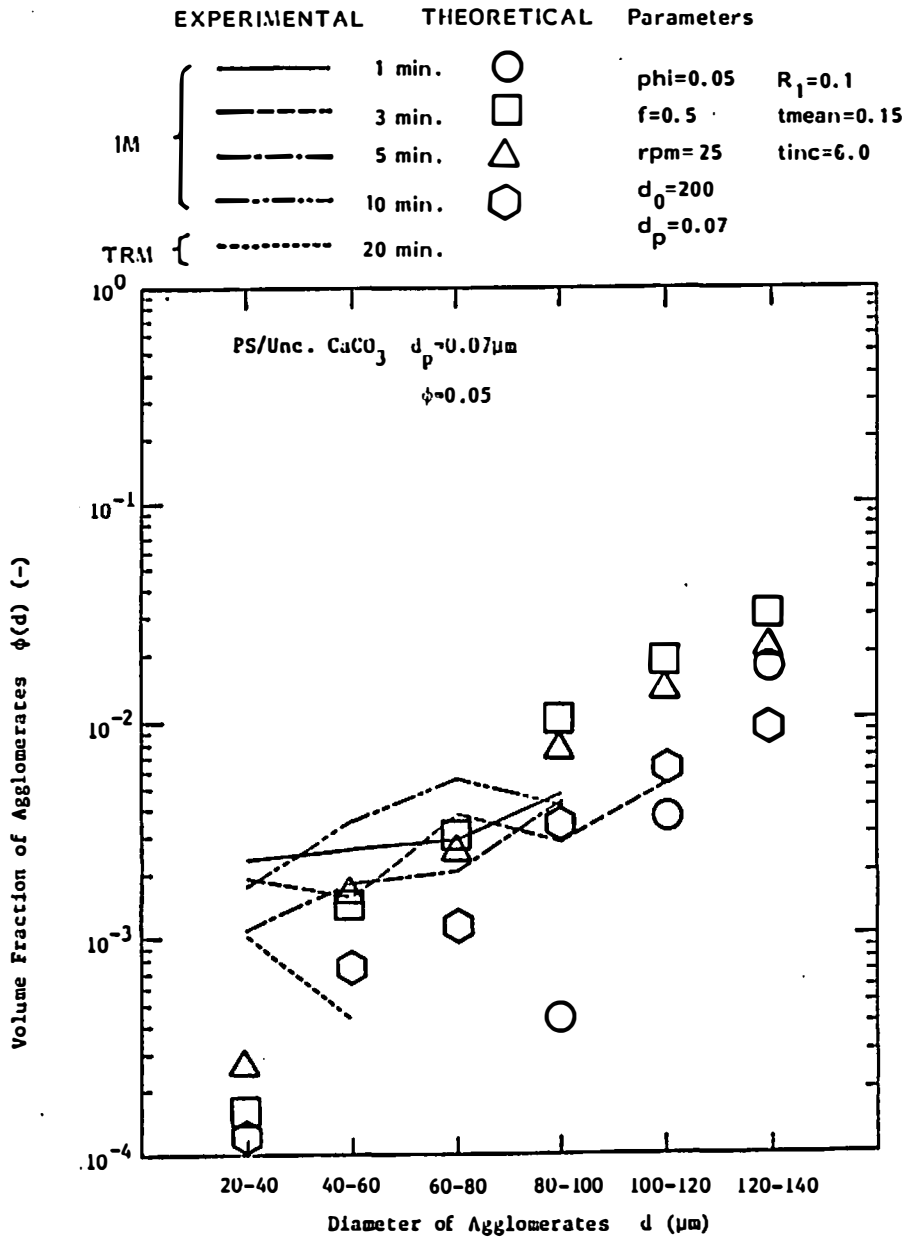

Figure XII-57. Comparison of experimental data with theoretical predictions for PS/unc. $CaCO_3$ (R_1 = 0.1, $\bar{t}$ = 0.15, t_{inc} = 6.0) with modified onion model.

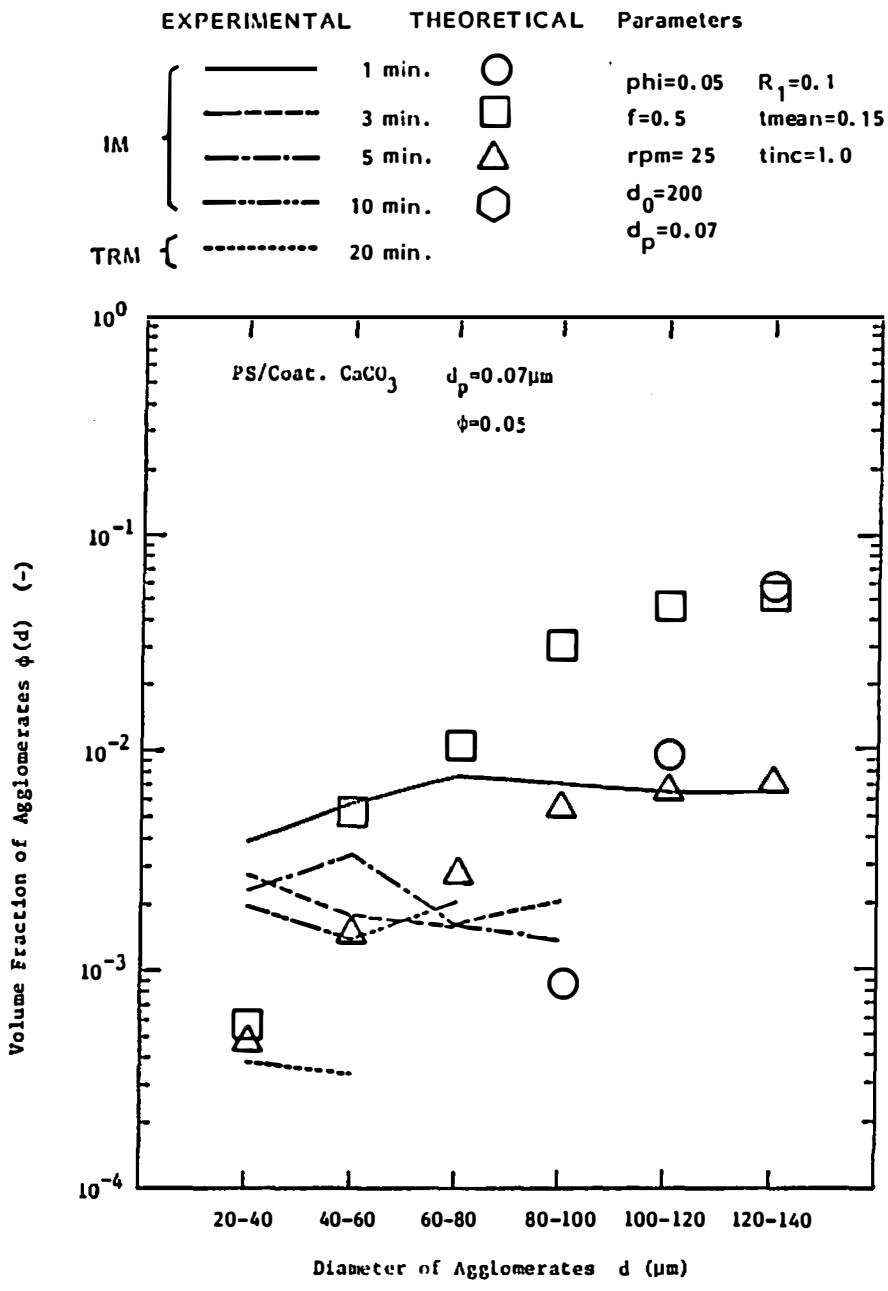

Figure XII-58. Comparison of experimental data with theoretical predictions for PS/coat. $CaCO_3$ (R_1 = 0.1, $\bar{t}$ = 0.15, t_{inc} = 1.0) with modified onion model.

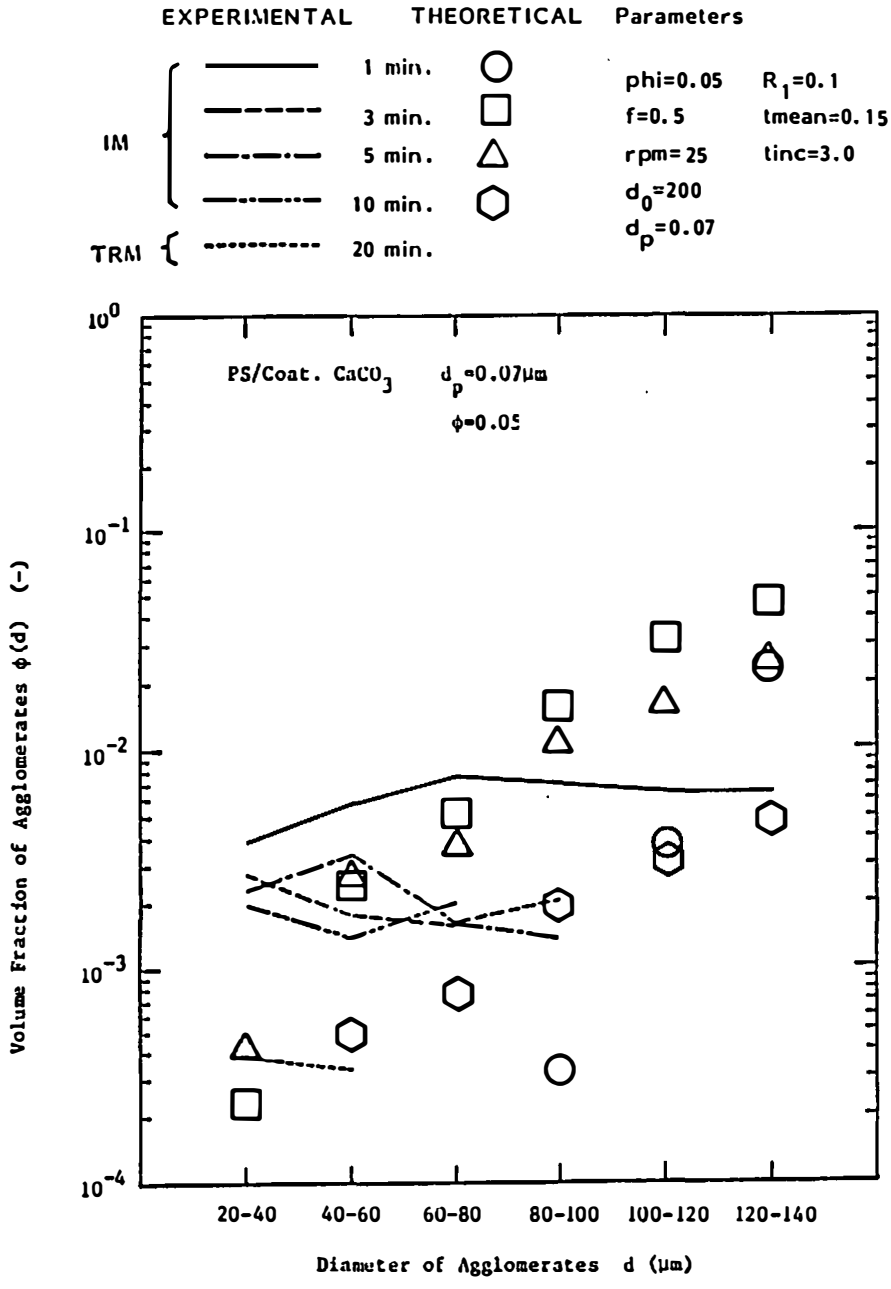

Figure XII-59. Comparison of experimental data with theoretical predictions for PS/unc. $CaCO_3$ (R_1 = 0.1, $\bar{t}$ = 0.15, t_{inc} = 3.0) with modified onion model.

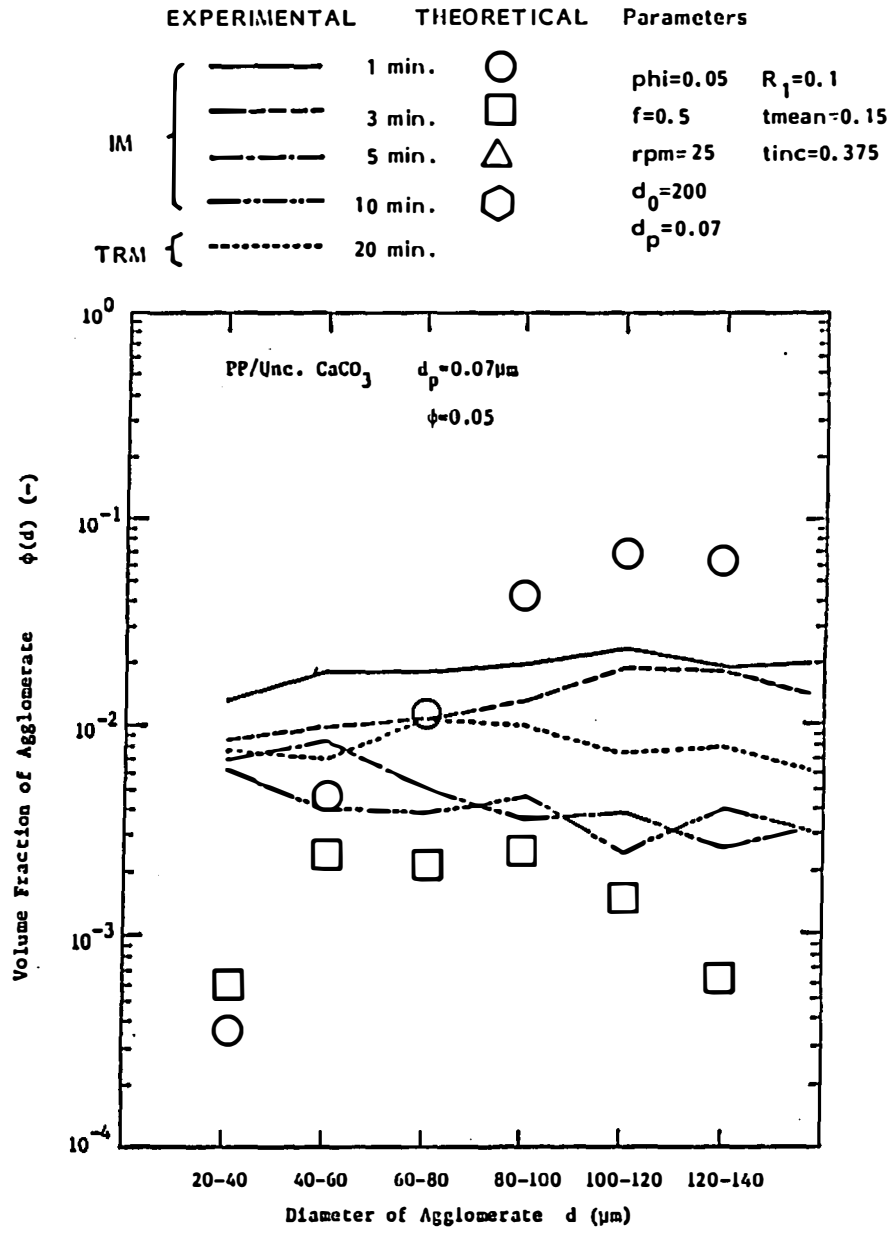

Figure XII-60. Comparison of experimental data with theoretical predictions for PP/unc. $CaCO_3$ (R_1 = 0.1, $\bar{t}$ = 0.15, t_{inc} = 0.375) with modified onion model.

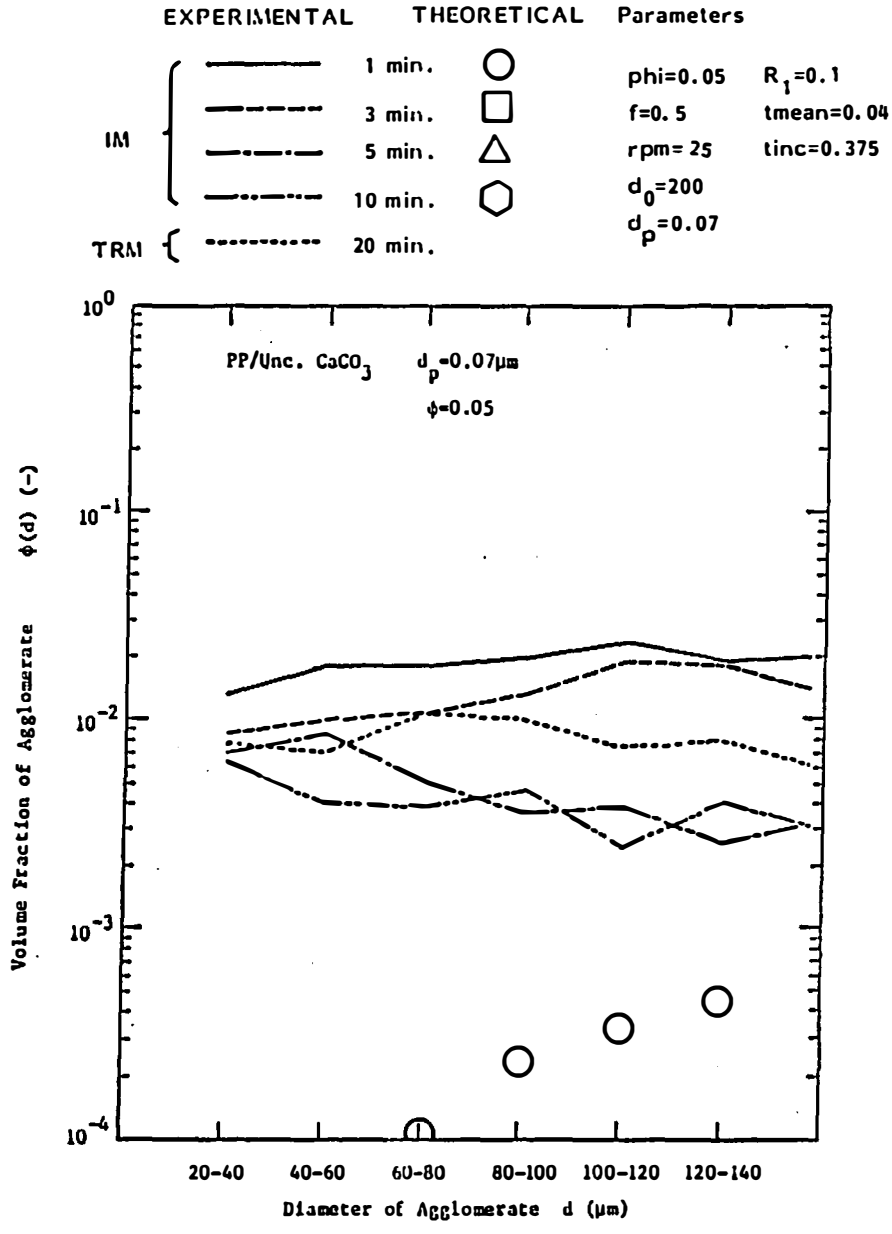

Figure XII-61. Comparison of experimental data with theoretical predictions for PP/unc. $CaCO_3$ (R_1 = 0.1, $\bar{t}$ = 0.04, t_{inc} = 0.375) with modified onion model.

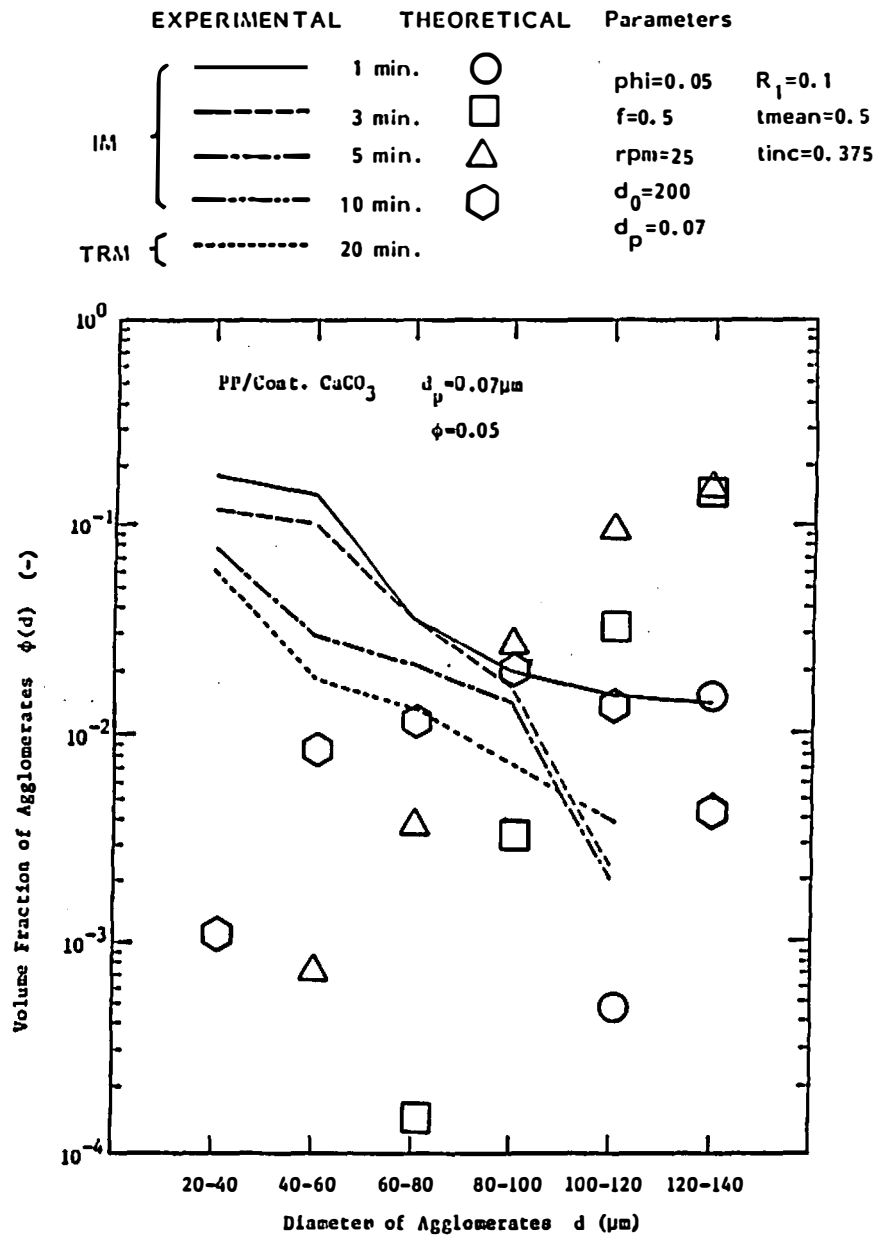

Figure XII-62. Comparison of experimental data with theoretical predictions for PP/coat. $CaCO_3$ (R_1 = 0.1, $\bar{t}$ = 0.5, t_{inc} = 0.375) with modified onion model.

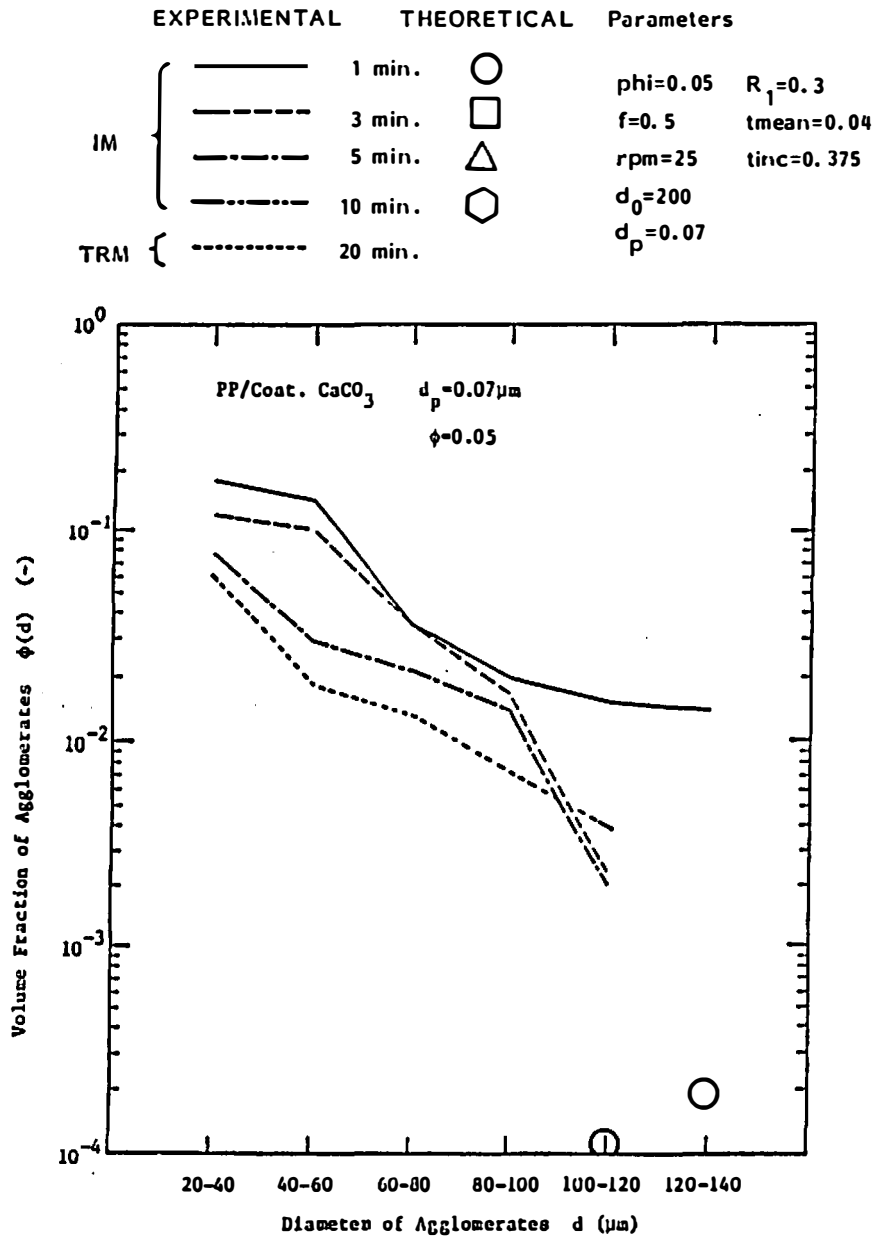

Figure XII-63. Comparison of experimental data with theoretical predictions for PP/coat. $CaCO_3$ (R_1 = 0.3, $\bar{t}$ = 0.04, t_{inc} = 0.375) with modified onion model.

Table XII-7. Models and Parameters Used for the Good Agreement with Experimental Data

Compounds	Model*	Parameters					
		d_0 (μm)	X (-)	R_1 (-)	$\bar{t}$ (min)	$\bar{t}_{inc}$ (min)	$\bar{t}_{inc}$† (mix)
PS/Unc. $CaCO_3$	MR	200	1.0	-	0.02	6.0	3.0-6.0
	MO	200	-	0.1	0.15	3.0-6.0	
PS/Coat. $CaCO_3$	MR	200	1.0	-	0.02	6.0	0.75-1.5
PP/Unc. $CaCO_3$	MR	200	1.0	-	0.10	6.0	0.375
PP/Coat. $CaCO_3$	MR	200	1.0	-	0.15	3.0	0.375

Fixed parameters: $\phi = 0.05$ (-)
$f = 0.5$ (-)
RPM = 25 (RPM)
$d_p = 0.07$ (m)

*MR: Modified Rupture
MO: Modified Onion

†Characteristic time for incorporation determined from the fraction of unincorporated filler on the chamber wall with exponential incorporation function.

Reasonable agreement was obtained with the modified rupture theory for all compounds. Fair agreement was found with the modified onion theory for the polystyrene/uncoated calcium carbonate compounds.

Initial agglomerate size d_0 of 200 μm gives good agreement for different types of compounds. The fraction of broken agglomerates during one pass through the high shear zone X of 1.0 was found for all compounds. This is equivalent to saying that all of the agglomerates which pass through the high shear zone rupture once during one revolution of rotors.

We have found the relationship that the mean residence time in the high shear zone $\bar{t}$ is greater than 0.233 when breakdown occurs only at the high shear zone.

The $\bar{t}$ values for the modified rupture model mentioned in Table XII-7 appear to be dependent upon the type of the matrix polymer. The $\bar{t}$ values are 0.02 for the polystyrene compounds and 0.10 for the polystyrene compounds and 0.10 to 0.15 for the polypropylene compounds. These values of $\bar{t}$, especially $\bar{t}$ for the polystyrene compounds, are smaller than 0.233. This denotes that the rupture of the agglomerates occurs not only in the high shear zone of the narrow gap region but also in the low shear zones of the mixer. The very small $\bar{t}$ values for the polystyrene compounds indicate that the rupture of the agglomerates might happen almost everywhere in the mixer. This may be due to the high shear viscosity of polystyrene. The shear stress level at low shear region would be large enough to cause the rupture of the agglomerates.

The characteristic times for the incorporation process $\bar{t}_{inc}$ used for the computation are generally greater than the values of $\bar{t}_{inc}$ estimated from the fraction of the unincorporated filler on the chamber walls. The reason is not clear.

Table XII-8 shows the nomenclature for Chapter XII.

Table XII-8. Nomenclature for Chapter XII

$C_n(d_j)$	volume distribution function for agglomerates
d_0	diameter of initial agglomerate
d_j	diameter of agglomerate which experienced j times of rupture or onion peel-off
d_p	diameter of ultimate particle or aggregate
$\underset{\sim}{d}_i$	deformation rate tensor at position i
i	number of rotor revolution position inside of internal mixer
I_i	incorporation rate at ith revolution
j	number of ruptures or onion peel-off
k	number of passes through the high shear rate zone
m	critical number of ruptures or onion peel-off to reach ultimate particle size
M_j	mass of agglomerate of size d_j
n	total number of rotor revolution
P(n,k),P(t,j)	probability that a fluid element passes k times through the high shear rate zone
R_j	mass reduction rate
t	total mixing time ($t = t_{dis} + t_{mix}$)
Δt	period of one rotor revolution
$\bar{t}$	mean residence time at high shear rate zone
t*	dimensionless mixing time
t_{dis}	period of filler disappears from the top of the mixing chamber
t^*_{ei}	dimensionless effective mixing time
$\bar{t}_i$	mean residence time at position i

Table XII-8 (continued)

t_{inc}	period of all filler incorporated
$\bar{t}_{inc}$	characteristic time for incorporation process
t_{mix}	mixing time counted after all filler disappeared from the top of the mixing chamber
$u(d_j)$	volume fraction of agglomerates of size d_j in the fluid elements
v_i	volume of compound passes position i during one revolution of rotor
V	total volume of compound
X	fraction of broken agglomerates during one pass through the high shear rate
$Y(n,d_j)$,$Y(t,d_j)$	volume fraction of agglomerates of size d_j
$Y_i)n,d_j)$	volume fraction of agglomerates of size d_j due to the incorporated filler in ith revolution of rotor
α	constant
$\dot{\gamma}_i$	shear rate at position i
η	viscosity of fluid
ρ	density of agglomerates
ϕ_{uni}	fraction of unincorporated filler

CHAPTER XIII

CONCLUSIONS AND RECOMMENDATIONS

A. CONCLUSIONS

The interparticulate structure of small particle filled plastic compounds has been investigated by various methods.

A.1. Sedimentation Volume Experiment

The sedimentation volume has been measured for various types of the fillers in toluene and hexane.

1. The sedimentation volume significantly increases with decreasing particle size. Small particulates presumably form a porous network structure.

2. Stearic acid surface treatment of calcium carbonates reduces sedimentation volume. This is presumably due to the reduction of the electric dipoles on the surface of the calcium carbonates.

3. The fillers which give large sedimentation volumes result in large yield stresses in the melt state after compounding.

4. Fillers which have large sedimentation volumes tend to form agglomerates in the compounds.

A.2. Optical Microscopy

The series of compounds prepared with a two roll mill and an internal mixer have been observed using a transmission light microscope.

1. Fillers which have ultimate particle sizes less than 1 μm tend to form agglomerates in the compounds.

2. The number of agglomerates increases exponentially with decreasing agglomerate size.

3. The number of agglomerates generally decreases with mixing time.

4. The polypropylene/calcium carbonate compounds have a greater number of agglomerates than the polystyrene/calcium carbonate compounds. This seems primarily to be due to the higher viscosity of polystyrene at the mixing temperature.

5. Stearic acid surface coated calcium carbonates form greater numbers of agglomerates than uncoated ones both in polypropylene and polystyrene. The number of large agglomerates (greater than 100 μm) are, however, reduced by surface coating in both systems.

6. The elongation at break decreases with increasing total volume fraction of large agglomerates.

A.3. Scanning Electron Microscopy

The fracture surface of compounds have been observed with scanning electron microscopy.

1. The particulates come into contact for volume fractions from between 0.10 to 0.30.

2. The stearic acid coated calcium carbonate particulates appear more often on the fracture surface of compounds compared with the uncoated calcium carbonates. Debonding may occur at the polymer-particle interface in the case of the coated calcium carbonates.

3. Anisotropic particulates of disk shape are oriented parallel to the surfaces of the molds.

A.4. Small Angle Light Scattering

Thin films of the polypropylene and polystyrene compounds have been investigated with the small angle light scattering technique. Intensity profiles have been obtained at elevated temperature in the case of polypropylene compounds to eliminate scattering from crystalline phases. An apparatus was designed and built in our laboratory at the University of Akron.

1. Polypropylene/calcium carbonate compounds reduce the intensity of the scattered light drastically at elevated temperatures. The reduction is greater at the lower volume fraction. This is due to the disappearance of the crystalline phase in the matrix phase.

2. Debye-Bueche and Guinier correlation distances have been determined for a wide range of calcium carbonate compounds.

3. Both Debye-Bueche and Guinier correlation distances, in general, decrease as mixing progresses. This indicates that the fraction of large agglomerates decreases with increasing mixing time.

4. Debye-Bueche correlation distances for the polypropylene/calcium carbonate compounds are greater than those for the polystyrene/calcium carbonate compounds. This indicates that the agglomerate size distributions are broader in the polypropylene compounds. This seems primarily due to the lower viscosity of polypropylene during mixing.

A.5. Electrical Conductivity Measurements

The electrical conductivities for typical carbon black compounds have been measured. The compounds were prepared both on a two roll mill and in an internal mixer. An apparatus has been developed in our laboratory.

1. The electrical conductivity increases with increasing volume fraction of carbon black and with decreasing particle size of carbon black.

2. The electrical conductivity, in general, decreases as mixing progresses. A significant decrease of the electrical conductivity with mixing time has been observed in a limited range of volume fractions of carbon black.

3. The polypropylene/carbon black compounds possess much greater electrical conductivity than the polystyrene/carbon black compounds. This is mainly due to the low viscosity of the polypropylene during mixing.

4. The heat treatment of the polypropylene/carbon black compounds increases the electrical conductivity drastically. Carbon black aggregates are presumably squeezed out from the crystalline phase and the local volume fraction of the carbon black increases in the amorphous phase.

5. The behavior of the electrical conductivity has been interpreted using percolation theory. A three-dimensional network structure of carbon black particulates was assumed.

6. A dispersion index and an average network distance have been proposed. These are based on the fraction of the carbon black which is a part of the three-dimensional network structure. High conductivity denotes a large fraction of carbon black particulates associated with the network structure.

7. A dispersion index and average network distances were defined and determined for the various carbon black compounds.

8. The dispersion indices and the average network distances of the polypropylene/carbon black compounds have been related to the elongation to break. The elongation to break increases as the average network distance increases.

A.6. Mixing Mechanism

The mechanism of mixing has been studied both experimentally and theoretically for an internal mixer.

1. Two types of the incorporation processes have been proposed. These are simultaneous incorporation and thin layer incorporation. A thin layer of unincorporated filler on the mixing chamber was often observed with the polystyrene compounds. This appears to be gradually incorporated.

2. The fraction of unincorporated filler appears to decrease roughly exponentially with mixing time.

3. Various theories of dispersion, i.e., rupture and onion theories, have been redeveloped with an incorporation rate function of the exponential form.

4. The theoretical predictions were compared with the volume fraction of agglomerates obtained by optical microscopy. The rupture and onion theories with and without the incorporation rate function have been used for the computations. Good agreement between the experimental data and the predictions has been obtained with the rupture theory with the incorporation rate function.

5. The process of incorporation of filler into the matrix phase seems to play an important role in the level of dispersion.

B. RECOMMENDATIONS

The following studies of the determination of the dispersion and mixing mechanisms are recommended for future investigators.

1. The levels of dispersion ought to be determined for a wide range of compounds prepared by various mixing methods and conditions. These include various types of mixers (single and twin screw extruders, etc.), methods of filler feeding, processing conditions (temperature, flow rate, etc.).

2. A consistent and uniform interpretation of dispersion ought to be developed based on all instruments. This must report determining the distribution function of the agglomerates through the size range and most specifically from the light scattering experiments.

3. A better theory of mixing needs to be developed. The developments required include the consideration of the distribution of the initial agglomerate size, modifications of the theory for the mixing process in extruders, proper analysis of flow patterns in mixers including free boundary effects.

LIST OF REFERENCES

LIST OF REFERENCES

A-1. Aoki, Y., J. Rheol. Japan, 7, 20 (1979).

A-2. Aoki, Y. J. Rheol., 24, 755 (1980).

A-3. Aoki, Y., and K. Nakayama, J. Rheol. Japan, 9, 39 (1981).

B-1. Biscoe, J., and B. E. Warren, J. Appl. Phys., 13, 364 (1942).

B-2. Bohn, D., Quantum Theory (Prentice-Hall, Inc., Englewood Cliffs, New Jersey, 1951), p. 275.

B-3. Bolen, W. R., and R. E. Colwell, Soc. Plastics Eng. J., 14, 24 (1958).

B-4. Boonstra, B. B., and A. I. Medalia, Rubber Age, 92, 892 (1963).

B-5. Boonstra, B. B., and A. I. Medalia, Rubber Chem. Tech., 36, 115 (1963).

B-6. Bowden, F. P., and D. Tabor, The Friction and Lubrication of Solids (Oxford Unv. Press, London, 1950).

B-7. Broadbent, S. R., and J. M. Hammersley, Proc. Camb. Phil. Soc., 53, 629 (1957).

C-1. Capman, F. M., and T. S. Lee, SPE J., 26, 37 (1970).

C-2. Casson, N., Rheology of Disperse Systems, C. C. Mill (ed.), (Pergamon Press, London, 1959), p. 84.

C-3. Cembrola, R. J., Rubber Chem. Tech., 56, 233 (1983).

C-4. Cohan, L. H., and H. H. L. Watson, Rubber Age, 68, 687 (1951).

C-5. Czarnecki, L., and J. L. White, J. Appl. Polym. Sci., 25, 1217 (1980).

D-1. Dannenberg, E. M., Ind. Eng. Chem., 44, 813 (1952).

D-2. Dean, P., and N. F. Bird, Mathematics Division Report Ma. 61 (1966) of the National Physical Laboratory, Teddington, Middlesex, England.

D-3. Dean, P., and N. F. Bird, Proc. Camb. Phil. Soc. Math. Phys. Sci., 63, 477 (1967).

D-4. Debye, P., Ann. Phys., 46, 809 (1915).

D-5. Debye, P., R. Anderson, Jr., and H. Brumberger, 28, 679 (1957).

D-6. Debye, P., and A. M. J. Bueche, Appl. Phys., 20, 518 (1949).

D-7. Debye, P., and M. Fortschr. Roeutgenforch, 2, 1 (1931).

D-8. De Waele, A. J., Oil Colour Chem. Soc., 6, 33 (1923).

D-9. Dizon, E. S., and L. A. Papazian, Rubber Chem. Tech., 50, 765 (1977).

D-10. Domb, C., Nature, 184, 509 (1959).

D-11. Domb, C., and M. F. Sykes, Phys. Rev. 122, 77 (1961).

D-12. Donnet, ., and Voet, Carbon Black

E-1. Ebell, P. C., and D. A. Hemsley, Rubber Chem. Tech., 54, 698 (1981).

E-2. Elliot, R. J., B. R. Heap, D. J. Morgan, and G. S. Rushbrooke, Phys. Rev. Letters, 5, 336 (1960).

E-3. Endo, Y., Jap., 13991 (Feb. 3, 1976).

F-1. Fisher, J. C., and Giaerer, J. Appl.. Phys., 32, 172 (1961).

F-2. Folkes, M. J., and A. Keller, Polym., 12, 222 (1971).

F-3. Freakley, P. K., and S. R. Patel, Proc. Intern. Rubber Conf., III-5 (1982).

F-4. Freakley, P. K., and W. Y. Wan Idris, Rubber Chem. Tech., 52, 134 (1979).

F-5. Freindlich, H., and D. Jones, J. Phys. Chem., 40, 1217 (1936).

F-6. Freundlich, H., and F. Juliusberger, Trans. Farad. Soc., 30, 333 (1934).

F-7. Freundlich, H., and F. Juliusberger, Trans. Farad. Soc., 31, 920 (1935).

F-8. Frisch, H. L., J. H. Hammersley, and D. J. A. Welsh, Phys. Rev., 126, 949 (1962).

F-9. Frisch, H. L., E. Sonnenblich, V. A. Vyssotsky, and J. H. Hammersley, Phys. Rev., 124, 1021 (1961).

G-1. Galanti, A. V., and L. H. Sperling, J. Appl. Polym. Sci., 14, 2785 (1970).

G-2. Gans, R., Ann. Phys., 76, 29 (1925).

G-3. Guinier, A., Ann. Phys., 12, 161 (1936); J. Chem. Phys., 40, 133 (1943).

G-4. Guinier, A., Ann. Phys., 12, 161 (1939).

G-5. Guinier, A., and G. Fournet, Small Angle Scattering of X-rays (John Wiley & Sons, New York, 1955).

H-1. Halmann, and I. Laulicht, J. Chem. Phys., 43, 1503 (1965).

H-2. Han, C. D., J. Appl. Polym. Sci., 15, 2591 (1971).

H-3. Han, C. D., C. Stanford, and H. J. Yoo, Polym. Eng. Sci., 18, 850 (1978).

H-4. Han, C. D., van den Weghe, P. Shete, and R. Haw., Polym. Eng. Sci., 21, 196 (1981).

H-5. Hashimoto, T., K. Sasaki, and H. Kawai, Macromolecules, 17, 2812 (1984).

H-6. Heckman, F. A., and D. F. Harling, Rubber Chem. Tech., 39, 1 (1966).

H-7. Heller, W., M. Nakagami, and M. L. Wallach, J. Chem. Phys., 30, 444 (1959).

H-8. Hendus, H., K. Illers, and E. Ropte, Kolloid-Zeit., 216-217, 110 (1967).

H-9. Henneka, T. A., and C. A. Rotz, SPE ANTEC, 27, 223 (1981).

H-10. Holm, R., J. Appl. Phys., 22, 569 (1951).

H-11. Holm, R., and B. Kirschstein, Z. Tech. Phsik, 16, 488 (1935).

H-12. Holland, A. C., and G. Gagne, Appl. Opt., 9, 113 (1970).

H-13. Holliday, L., and G. Thackray, Nature, 201, 270 (1964).

J-1. Jansen, J., and G. Kraus, Rubber Chem. Tech., 53, 48 (1980).

J-2. Jellinek, M. H., E. Solomon, and I. Fankuchen, Ind. Eng. Chem., 18, 172 (1946).

K-1. Kanno, T., H. Igarashi, and K. Uemeya, J. Soc. Rheol., Japan, 4, 39 (1976).

K-2. Keller, A., E. Pedemonte, and F. M. Willmouth, Kolloid-Zeit., 238, 25 (1970).

K-3. Kerker, M., The Scattering of Light and Other Electromagnetic Radiation (Academic Press, New York, 1969).

K-4. Kirkpatrick, S., Phys. Rev. Letters, 27, 1722 (1971).

K-5. Kirkpatrick, S., Rev. Mod. Phys., 45, 574 (1973).

K-6. Kirkpatrick, S., Solid State Comm., 12, 1279 (1973).

K-7. Klasen, G., and J. Kubat, J. Appl. Polym. Sci., 19, 831 (1978).

K-8. Kohler, F., U.S. Patent 3,243,753 (March 29, 1966).

K-9. Kotaka, T., T. Kitano, Y. Oyanagi, and M. Sasahara, Rheol. Acta, 18, 635 (1979).

K-10. Kusy, R. P. and D. T. Turner, Nature

L-1. Lee, T. S., Proc. 5th Int. Rheol. Cong., 4, 421 (1970).

L-2. Leigh-Dugmore, C. H., Rubber Chem. Tech., 29, 1303 (1956).

L-3. Lennard-Jones, J. E., Chapter X of R. H. Fowler's Statistical Mechanics (Cambridge, 2nd Ed., 1936).

L-4. Lips, A., C. Smart, E. Willis, Trans. Farad. Soc., 67, 2979 (1971).

L-5. Lips, A., and E. Willis, J. Chem. Soc. Farad. Trans., 69, 1 (1973).

L-6. Lobe, V. M., and J. L. White, Polym. Eng. Sci., 19, 617 (1979).

L-7. Lorentz, L., Oeuvres Scientifiques

L-8. Lorentz, L., Videnskab Selskab. Skrifter, 6 (1890).

M-1. Malliaris, A., and D. T. Turner, J. Appl. Phys., 42, 614 (1971).

M-2. Manas-Zloczower, I., A. Nir, and Z. Tadmor, Rubber Chem. Tech., 55, 1250 (1982).

M-3. Matsumoto, T., S. Okumura, S. Yao., and S. Onogi, J. Rheol. Japan, 9, 116 (1981).

M-4. Maxwell, J. C., A Treatise on Electricity and Magnetism, 2nd Ed., Vol. 1 (Clarendon Press, Oxford, 1881), p. 435.

M-5. McKelvey, J. M., Polymer Processing (John Wiley & Sons, Inc., New York, 1962).

M-6. Medalia, A. I., Rubber Age, 97, 82 (1965. ASTM D2663.

M-7. Medalia, A. I., J. Colloid Interface Sci., 32, 115 (1970).

M-8. Meder, A., and W. May, Rubber J., 146, 39 (1964).

M-9. Meyer, J., Quarterly Reports, Texas Instruments Co., 1967, 1970.

M-10. Meyer, J., Polym. Eng. Sci., 13, 462 (1973).

M-11. Meyer, J., Polym. Eng. Sci., 14, 706 (1974).

M-12. Mie, G., Ann. Physik, 11, 657 (1903).

M-13. Mie, G., Ann. Phys., 25, 377 (1908).

M-14. Mihira, K., T. Ohsawa, and A. Nakayama, Kolloid Z. Z. Polym., 222, 135 (1968).

M-15. Min, K., and J. L. White, Rubber Chem. Tech., 58, 1024 (1985).

M-16. Min, K., to be published.

M-17. Min, K., and J. L. White, to be published.

M-18. Minagawa, N., and J. L. White, J. Appl. Polym. Sci., 20, 501 (1976).

M-19. Montes, A., and J. L. White, Rubber Chem. Tech., 55, 1354 (1982).

M-20. Moritani, M., T. Inoue, M. Motegi, and H. Kawai, Macromolecules, 3, 434 (1970).

M-21. Münstedt, H., Proc. 7th Int. Rheol. Cong., 496 (1976).

M-22. Münstedt, H., Polym. Eng. Sci., 21, 259 (1981).

M-23. Münstedt, H., Paper presented at International Conference on Toughing Plastics, London.

N-1. Nakajima, N., Rubber Chem. Tech., 55, 931 (1982).

N-2. Napper, D. H., and R. H. Ottewill, Trans. Farad. Soc., 60, 1466 (1963).

N-3. Nishikido, N., M. Shinozaki, G. Sugihara, and M. Tanaka, J. Colloid Inter. Sci., 74, 474 (1980).

O-1. Ohno, R., Nihon Gom Kyokaishi, 57, 72 (1984).

O-2. Omotoso, M. A. A., J. L. White, and J. F. Fellers, J. Appl. Polym. Sci., 25, 1573 (1980).

O-3. Oster, G., and D. P. Rilley, Acta Cryst., 5, 1 (1952).

O-4. Otsuki, K., and K. Eguchi, Japan Patent 113562 (October 2, 1974).

P-1. Parfitt, G. D., and J. A. Wood, Kolloid-Zeit., 229, 55 (1968).

P-2. Payne, A. R., J. Appl. Polym. Sci., 3, 127 (1960).

P-3. Payne, A. R., J. Appl. Polym. Sci., 6, 57 (1962).

P-4. Pike, G. E., and C. H. Seager, Phys. Rev. B, 10, 1421 (1974).

P-5. Polley, M., and B. Boonstra, Rubber Chem. Tech., 30, 170 (1957).

R-1. Rayleigh, Lord, Phil. Mag., 12, 81 (1881).

R-2. Rayleigh, Lord, Proc. Roy. Soc. (London), A84, 25 (1811).

R-3. Rayleigh, Lord, Proc. Roy. Soc. (London), A90, 219 (1914).

R-4. Riley, D. P., Brit. Coal Utilization Research Association Conference, London, 1944.

R-5. Rudd, W. G., and H. L. Frish, Phys. Rev. B, 2, 162 (1970).

R-6. Rushbrooke, G. S., and D. J. Morgan, Mol. Phys., 4, 1 (1961).

S-1. Saito, Y., J. Rheol. Japan, 10, 135 (1982).

S-2. Scher, H., and R. Zallen, Chem. Phys., 53, 3759 (1970).

S-3. Sheng, P., Phys. Rev. B, 21, 2180 (1980).

S-4. Shiga, S., and M. Furnta, Nippon Gomu Kyokaishi, 55, 491 (1982).

S-5. Simmons, J. G., J. Appl. Phys., 34, 1793 (1963).

S-6. Sitcar, A. K., and T. G. Lamond, Rubber Chem. Tech., 51, 126 (1978).

S-7. Spencer, R. S., and R. N. Wiley, J. Colloid Sci., 6, 133 (1951).

S-8. Straley, J., Phys. Rev. B, 15, 5733 (1977).

S-9. Stump, N. A., and H. E. Railsback, Rubber World, 151, 41 (1964).

S-10. Suetsugu, Y., M. S. Thesis, Polymer Engineering, The University of Tennessee, Knoxville, 1982.

S-11. Suetsugu, Y., and J. L. White, J. Appl. Polym. Sci, 28, 1481 (1983).

S-12. Suetsugu, Y., and J. L. White, J. Non-Newtonian Fluid Mech., 14, 121 (1984).

S-13. Sumita, M., E. Kijima, H. Aida, and K. Ishikawa, Kobunshi Ronbunshu, 40, 203 (1983).

S-14. Sweitzer, C. W., W. H. Hess, and J. E. Callan, Rubber World, 138, 869 (1958).

S-15. Sweitzer, C. W., W. H. Hess, and J. E. Callan, Rubber World, 139, 74 (1958).

S-16. Sweitzer, C. W., and P. A. Marsh, Rubber Age, 92, 251 (1963).

S-17. Sykes, M. F., and J. W. Essam, J. Math. Phys., 5, 1117 (1964).

S-18. Sykes, M. F., and J. W. Essam, Phys. Rev., 133, A130 (1964).

T-1. Tabar, R. J., S. R. Hu, and R. S. Stein, J. Appl. Polym. Sci., 28, 1409 (1983).

T-2. Tanaka, H., and J. L. White, Polym. Eng. Sci., 20, 949 (1980).

T-3. Tanaka, H., and J. L. White, Polym. Eng. Rev., 1, 89 (1981).

T-4. Tang, I. N., and H. R. Munkelwitz, J. Colloid Int. Sci., 63, 297 (1978).

T-5. Thomson, J. J., Recent Researches in Electricity and Magnetism (Oxford Univ. Press, London and New York, 1893).

T-6. Tidmus, L. S., and D. Parkinson, Trans. Inst. Rubber Ind., 13, 152 (1937).

T-7. Toki, S., M. Takeshita, Y. Morimoto, and M. Okuyama, Paper presented at American Chemical Society Rubber Division Meeting, Houston, 1983.

T-8. Toki, S., and J. L. White, J. Appl. Polym. Sci., 27, 3171 (1982).

T-9. Tokita, N., and I. Pliskin, Rubber Chem. Tech., 46, 1166 (1973).

T-10. Tokita, N., and J. L. White, J. Appl. Polym. Sci., 10, 1011 (1966).

T-11. Tokita, N., and J. L. White, J. Appl. Polym. Sci., 12, 1589 (1968).

T-12. Trapenznikov, A. A., and E. A. Frolova, Kolloid. Zhurnal, 43, 85 (1981).

U-1. Uemura, Y., M. Fujimura., T. Hashimoto, and H. Kawai, Polym. J., 10, 341 (1978).

U-2. Uemura, Y., T. Hashimoto, and H. Kawai, Polym. J., 11, 413 (1979).

V-1. Vegvari, P. C., W. M. Hess, and V. E. Chirico, Rubber Chem. Tech., 51, 817 (1978).

V-2. Verhelst, W. F., K. G. Walthuis, A. Voet., P. Ehrburger, and J. B. Donnet, Rubber Chem. Tech., 50, 735 (1977).

V-3. Vinogradov, G. A., A. Ya. Malkin, E. P. Plotonikova., O. Yu Sabsai, and N. E. Nikolayeva, Int. J. Polym. Mater., 2, 1 (1972).

V-4. Voet, A., and P. Aboytes, Rubber Chem. Tech., 43, 1359 (1970).

V-5. Voet, A., and F. R. Cook, Rubber Chem. Tech., 41, 1207 (1968).

V-6. Voet, A., and F. R. Cook, Rubber Chem. Tech., 41, 1215 (1968).

V-7. Voet, A., and W. N. Whitten, Jr., Rubber World, 146, 771 (1962).

V-8. Vyssotsky, V. A., S. B. Gordon, H. L. Frish, and J. M. Hammersley, Phys. Rev., 123, 1566 (1961).

W-1. White, J. L., and J. W. Crowder, J. Appl. Polym. Sci., 18, 1013 (1974).

W-2. White, J. L., F. Dibachi, Y. Suetsugu, and D. Christopher, Polym. Eng. Rev., (1985).

W-3. White, J. L., and H. Tanaka, J. Appl. Polym. Sci., 26, 579 (1981).

W-4. Wiegand, W. B., Canadian Chem. Met., 10, 251 (1926).

W-5. Williams, J. A., Ph.D. Dissertation, Pennsylvania State University, March, 1970.

W-6. Wolfer, D., Eur. Rubber J., 17 (April 1977).

W-7. Wu, S., Polymer Interface and Adhesion (Marcel Dekker, Inc., New York).

Y-1. Yamane, M., Yogyo-Kyokai-shi, 589, 88 (1980).

Z-1. Zakharenko, N. V., F. S. Tolstukhina., and G. M. Bartenev, Rubber Chem. Tech., 35, 326 (1962).

Z-2. Zerull, R., Forschungsbericht W73-18, Bundesministerium für Forschungund Technologie (1973).

Z-3. Zosel, A., Rheol. Acta, 11, 229 (1972).

APPENDICES

APPENDIX A

THE VOLUME FRACTION OF AGGLOMERATES OF SIZE d_j IN THE FLUID ELEMENT WHICH HAS PASSED k TIMES THROUGH THE HIGH SHEAR ZONE FOR THE ONION MODEL

One of the characteristics of onion mechanism of dispersion is that the number of agglomerates N maintain constant during the mixing process. We assume that all agglomerates which passed high shear zone are peeled-off.

The volume fraction of agglomerates of size j is given by

$$u(d_j) = \frac{N \cdot (\frac{\pi}{6}) \cdot d_j^3}{N \cdot (\frac{\pi}{6}) \cdot d_0^3} = (\frac{d_j}{d_0})^3 \qquad \text{(A-1)}$$

where d_0 is the diameter of initial agglomerates.

The volume fraction of agglomerates of size d_j in the fluid element which has passed k times through the high shear zone $u_k(d_j)$ may be derived as follows. $^*u_k(d_j)$ for the fluid element which has passed 0 time through the high shear zone is

$$u_0(d_j) = (\frac{d_j}{d_0})^3 = 1 \qquad \text{for } j = 0$$

$$= 0 \qquad \text{for } j \neq 0$$

$$u_0(d_m) = 0$$

$^*u_k(d_j)$ for the fluid element which has passed 1 time through the high shear zone is

$$u_1(d_j) = (\frac{d_j}{d_0})^3 \qquad \text{for } j = 1 \qquad \text{(A-2)}$$

$$= 0 \qquad \text{for } j \neq 1, m$$

$$u_1(d_m) = 1 - \left(\frac{d_1}{d_0}\right)^3 \tag{A-3}$$

*$u_k(d_j)$ for the fluid element which has passed 2 times through the high shear zone is

$$u_2(d_j) = \left(\frac{d_j}{d_0}\right)^3 \qquad \text{for } j = 2 \tag{A-4}$$

$$= 0 \qquad \text{for } j \neq 1, m$$

$$u_2(d_m) = 1 - \left(\frac{d_2}{d_0}\right)^3 \tag{A-5}$$

.

.

.

*$u_k(d_j)$ for the fluid element which has passed k times through the high shear zone is

$$u_k(d_j) = \left(\frac{d_j}{d_0}\right)^3 \qquad \text{for } k = j < m \tag{A-6}$$

$$= 0 \qquad \text{for } k \neq j, m$$

$$u_k(d_m) = 1 - \left(\frac{d_k}{d_0}\right)^3 \qquad \text{for } k < m \tag{A-7}$$

$$= 1 \qquad \text{for } k \geq m$$

APPENDIX B

THE VOLUME FRACTION OF AGGLOMERATES OF SIZE d_j IN THE MIXER AFTER THE TOTAL MIXING PERIOD OF t FOR THE ONION MODEL

Suppose that the number of revolutions of the rotor is n in the total mixing time of t. The fluid in the mixer may experience 0 to n times of high shear zone. P(n,k) is the probability that the fluid element passes k times through the high shear zone after n revolutions. $U_k(d_j)$ is the volume fraction of agglomerates of size d_j in the fluid element which passed k times through the high shear zone.

The volume fraction of agglomerates of size d_j in the mixer $Y(d_j)$ after n revolutions of the rotor is, in general, given by

$$Y(d_j) = \sum_{k=j}^{s} P(n,k) \cdot u_k(d_j) \qquad \text{(B-1)}$$

$$s = n \qquad \text{for } n < m$$

$$s = m-1 \qquad \text{for } n \geq m$$

$$j = 0,1,2, \ldots , s$$

In the onion model, however, $u_k(d_j)$ is zero for $k \neq j$ as shown in Appendix A. Equation (B-1) then reduces to

$$Y(d_j) = P(n,j) \cdot u_j(d_j) \qquad \text{(B-2)}$$

$$j = 0,1,2, \ldots n \; n \quad \text{for } n < m$$

$$j = 0,1,2, \ldots , m-1 \quad \text{for } n \geq m$$

Agglomerates of size d_j is contained only in the fluid element which has experienced j times of the high shear zone. Fraction of ultimate particles is given by

$$Y(d_m) = 1 - \sum_{j=0}^{m-1} Y(d_j) \qquad \text{for } n > 0$$

APPENDIX C

COMPUTER PROGRAM FOR RUPTURE MODEL WITH INCORPORATION RATE FUNCTION

```
C      RUPTURE MODEL WITH EXPONENTIAL INCORPORATION
       DIMENSION XX(12), D(1000), DUD(1000),DJL(1000),T(1000), YDF(1000)
       DIMENSION YDFL(1000),AN(1000),ANL(1000),YD(1000),YDL(1000),X(1000)

       DIMENSION NNN(10), DE(200), YDE(200)
C      DATA INPUT
C      ENTER VOLUME FRACTION OF FILLER (-)
       PHI=0.05
C      ENTER DIAMETER OF INITIAL AGGLOMERATES (MICRON)
       D0=200.0
C      ENTER DIAMETER OF ULTIMATE PARTICLE (MICRON)
       DP=0.07
C      ENTER FRACTION OF RUPTURED AGGLOMERATES IN ONE PASS THROUGH THE GAP
     ( 0 TO 1)
       YY=1.0
C      ENTER PARAMETER FOR AGGLOMERATE BREAK-DOWN
C      B=10.0
C      ENTER FILLING FACTOR OF AGGLOMERATE STRUCTURE (0 TO 1)
       F=0.5
C      ENTER ROTATIONAL SPEED OF THE ROTOR (RPM)
       RPM=25
C      ENTER TIME CONSTANT FOR INCORPORATION
       TINC=3.000
C      ENTER MEAN RESIDENCE TIME IN THE WELL MIXED REGION OF THE MIXER (MI
     N)
       TMEAN=0.15
       DD=ALOG(10.)
       WRITE(6,10)
    10 FORMAT(  '      <<<SAMPLE>>>     '  )
       READ(5,20) (XX(I), I=1,12)
    20 FORMAT (12A4)
       WRITE(6,30)
    30 FORMAT(  ' ENTER TOTAL MIXING TIME  (MIN)  ' )
       READ (5,*) TMIX
       DO 2000 KK=1,4
       IF (KK .EQ. 1) GOTO 41
       IF (KK .EQ. 2) GOTO 42
       IF (KK .EQ. 3) GOTO 43
       IF (KK .EQ. 4) GOTO 44
    41 TMIX=TMIX
```

```
00380         GOTO 50
00390      42 TMIX=TMIX+2.
00400         GOTO 50
00410      43 TMIX=TMIX+2.
00420         GOTO 50
00430      44 TMIX=TMIX+5.
00440      50 WRITE (6,51)
00450      51 FORMAT ('                                                                    ')
00460         WRITE (6,52)
00470      52 FORMAT ('                                                                    ')
00480         WRITE (6,53)
00490      53 FORMAT ('************* FOR TOTALMIXING TIME OF ****************')
00500         WRITE (6,55)TMIX
00510      55 FORMAT (20X,E9.3)
00520         DT=1/RPM
00530         R1=-3*(ALOG(DP/D0)/ALOG(2.))
00540         IF((R1-INT(R1)) .EQ. 0.0 .OR. (R1-INT(R1)) .GT. 0 ) GOTO 200
00550         M=INT(R1-1)
00560         GOTO 220
00570     200 M=INT(R1)
00580     220 RN=TMIX*RPM
00590         N=INT(RN)
00600         IF(N .LT. M) GOTO 400
00610         NU=M
00620         GOTO 500
00630     400 NU=N+1
00640     500 YDSUM=0
00650         WRITE (6,60)
00660      60 FORMAT ('   AGGLOMERATE DISTRIBUTION')
00670         WRITE(6,61)
00680      61 FORMAT('    J      DJ          LOG DJ      DJ/D0          YF          LOG Y

00690        1F        Y           LOGY         N          LOGN ' )
00700         J=1
00710         DO 800 L=1,NU
00720         J=L-1
00730         D(J)=D0*2.0**(-J/3.)
00740         DOD(J)=D(J)/D0
00750         DJL(J)=ALOG(D(J))/DD
00760 C       X(J)=EXP(-J/B)
```

```
00770          X(J)=YY
00780          SUM=0
00790          DO 600 I=1,N
00800          T(I)=I*DT
00810          CC=I*DT/TINC+X(J)*(N+1-I)*DT/TMEAN
00820          IF(CC .GT. 150 ) GOTO 580
00830          AA=EXP(-CC)
00840          GOTO 590
00850     580  AA=0.
00860     590  FY1=AA*((X(J)**J)*(((N+1-I)*DT)**J))/(TMEAN**J)
00870  C  590  FY1=AA*((X(J)*(N+1-I)/TMEAN)**J)*(DT**J)
00880  C  590  FY1=AA*((X(J)*(N+1-I)*DT/TMEAN))**J
00890     600  SUM=SUM+FY1
00900          IF(J .EQ. 0 .OR. J .EQ. 1) GOTO 770
00910          FAC=1
00920          DO 750 K=2,J
00930     750  FAC=FAC*K
00940          GOTO 780
00950     770  FAC=1
00960     780  YDF(J)=(EXP(DT/TINC)-1)*SUM/(F*FAC)
00970          YD(J)=YDF(J)*F
00980          YDSUM=YDSUM+YD(J)
00990          IF (YDF(J) .LE. 1E-30) GOTO 101
01000          YDFL(J)=ALOG(YDF(J))/DD
01010          GOTO 102
01020     101  YDFL(J)=- 20.
01030     102  IF (YD(J) .LE. 1E-30) GOTO 103
01040          YDL(J)=ALOG(YD(J))/DD
01050          GOTO 104
01060     103  YDL(J)=-20.
01070     104  AN(J)=YDF(J)*PHI*6/(3.14159*((D(J)*1E-4)**3))
01080          IF (AN(J) .LE. 1E-30)GOTO 105
01090          ANL(J)=ALOG(AN(J))/DD
01100          GOTO 106
01110     105  ANL(J)=-20.
01120  C  106  CONTINUE
01130     106  WRITE(6,62) J,D(J),DJL(J),DOD(J),YDF(J),YDFL(J),YD(J),YDL(J),AN(J
01140       1),ANL(J)
01150      62  FORMAT(2X,I2,9(2X,E9.3))
01160     600  CONTINUE
```

```
01170          QQ=N*DT/TINC
01180          IF (QQ .GT.70) GOTO 801
01190          YM=1-EXP(-QQ)-YDSUM
01200          GOTO 802
01210    801   YM =1-YDSUM
01220    802   IF (YM .LE. 0.0)  GOTO 710
01230          YML=ALOG(YM)/DD
01240    710   DM=D0*2.0**(-M/3)
01250          DMOD=DM/D0
01260          DML=ALOG(DM)/DD
01270          WRITE(6,70)
01280     70   FORMAT('  ' ULTIMATE PARTICLE ')
01290          WRITE(6,90)
01300     90   FORMAT('       DM        DM/DO       LOGDM          YM          LOGYM    '
01310         1)
01320          WRITE(6,110) DM, DMOD, DML, YM, YML
01330    110   FORMAT(5(2X,E9.3))
01340          WRITE(6,900)
01350    900   FORMAT('  SUMMED AGGLOMERATE SIZE DISTRIBUTION')
01360          WRITE (6,910)
01370    910   FORMAT('       D(J)      AGGLOMERATE RANGE      SUM YDF     SUM AN')

01380          DO 1500 NN=1,9
01390          TI=200.-20.*NN
01400          TF=180.-20.*NN
01410          SUMY=0
01420          SUMA=0
01430          DO 1200 L=1,NU
01440          J=L-1
01450          IF (D(J) .GE. TI) GOTO 1200
01460          IF (D(J) .GE. TF. AND. D(J) .LT. TI )GOTO 1100
01470          GOTO 1300
01480   1100   SUMY=SUMY+YDF(J)
01490          SUMA=SUMA+AN(J)
01500   1200   CONTINUE
01510   1300   WRITE (6,920) D(J-1), TI, TF, SUMY, SUMA
01520    920   FORMAT (2X,E9.3,2(2X,E9.3),2(2X,E9.3))
01530   1500   CONTINUE
01540   2000   CONTINUE
01550   4000   STOP
01560          END
 END OF WORKSPACE
```

APPENDIX D

COMPUTER PROGRAM FOR ONION MODEL WITH INCORPORATION RATE FUNCTION

```
00010 C      AGGLOMERATE SIZE DISTRIBUTION
00020 C      ONION MODEL WITH INCORPORATION FUNCTION
00030        DIMENSION XX(12), D(1000), DDD(1000),DJL(1000),T(1000), YDF(1000)
00040        DIMENSION YDFL(1000),AN(1000),ANL(1000),YD(1000),YDL(1000)

00050        DIMENSION EE(1000)
00060 C      DATA INPUT
00070 C      ENTER VOLUME FRACTION OF FILLER (-)
00080        PHI=0.05
00090 C      ENTER DIAMETER OF INITIAL AGGLOMERATES (MICRON)
00100        D0=200.00
00110 C      ENTER DIAMETER OF ULTIMATE PARTICLE (MICRON)
00120        DP=0.07
00130 C      ENTER MASS RATIO FOR ONION BREAKDOWN ( 0 TO 1 )
00140        R1=0.100
00150 C      ENTER FILLING FACTOR OF AGGLOMERATE STRUCTURE (0 TO 1)
00160        F=0.5
00170 C      ENTER ROTATIONAL SPEED OF THE ROTOR (RPM)
00180        RPM=25.0
00190 C      ENTER TIME CONSTANT FOR INCORPORATION
00200        TINC=0.375
00210 C      ENTER MEAN RESIDENCE TIME IN THE WELL MIXED REGION OF THE MIXER (MI
             N)
00220        TMEAN=0.04
00230        DD=ALOG(10.)
00240        WRITE(6,10)
00250     10 FORMAT(    '      (((SAMPLE)))      '  )
00260        READ(5,20) (XX(I), I=1,12)
00270     20 FORMAT (12A4)
00280        WRITE(6,30)
00290     30 FORMAT(    ' ENTER TOTAL MIXING TIME  (MIN)  ' )
00300        READ (5,*) TMIX
00310        DO 2000 KK=1,4
00320        IF (KK .EQ. 1) GOTO 41
00330        IF (KK .EQ. 2) GOTO 42
00340        IF (KK .EQ. 3) GOTO 43
00350        IF (KK .EQ. 4) GOTO 44
00360     41 TMIX=TMIX
00370        GOTO 50
00380     42 TMIX=TMIX+2
```

```
00390       GOTO 50
00400    43 TMIX=TMIX+2
00410       GOTO 50
00420    44 TMIX=TMIX+5
00430    50 WRITE (6,51)
00440    51 FORMAT ('          ')
00450       WRITE (6,52)
00460    52 FORMAT ('          ')
00470       WRITE (6,53)
00480    53 FORMAT ('********** FOR TOTAL MIXING TIME OF **********')
00490       WRITE (6,55)TMIX
00500    55 FORMAT (20X,E9.4)
00510       DT=1/RPM
00520       RN=TMIX*RPM
00530       N=INT(RN)
00540       NU=N+1
00550       YDSUM=0
00560       WRITE (6,58)
00570    58 FORMAT (' AGGLOMORATE SIZE DISTRIBUTION ')
00580       WRITE(6,60)
00590    60 FORMAT('    J      DJ          LOG DJ      DJ/D0          YF          LOG Y

00600      1F          Y            LOGY         N          LOGN ' )
00610       DO 800 L=1,NU
00620       J=L-1
00630       IF (J .EQ. 0) GOTO 100
00640       EE(J)=R1*D0/D(J-1)
00650       IF (EE(J) .GE. 1.0 ) GOTO 850
00660       D(J)=((1-EE(J))**(1./3.))*D(J-1)
00670       IF ( D(J) .LT. DP) GOTO 850
00680       GOTO 120
00690   100 D(J)=D0
00700   120 DOD(J)=D(J)/D0
00710       DJL(J)=ALOG(D(J))/DD
00720       SUM=0
00730       DO 600 I=1,N
00740       T(I)=I*DT
00750       CC=I*DT/TINC+(N+1-I)*DT/TMEAN
00760       IF(CC .GT. 150 ) GOTO 580
00770       AA=EXP(-CC)
```

```
00780          GOTO 590
00790      580 AA=0
00800      590 FY1=AA*((N+1-I)*DT/TMEAN)**J
00810    C 590 FY1=AA*(((N+1-I)/TMEAN)**J)*(DT**J)
00820    C 590 FY1=AA*(((N+1-I)*DT)**J)/(TMEAN**J)
00830      600 SUM=SUM+FY1
00840          IF(J .EQ. 0 .OR. J .EQ. 1) GOTO 770
00850          FAC=1
00860          DO 750 K=2,J
00870      750 FAC=FAC*K
00880          GOTO 780
00890      770 FAC=1
00900      780 YDF(J)=((D(J)/D0)**3)*(EXP(DT/TINC)-1)*SUM/(F*FAC)
00910          YD(J)=YDF(J)*F
00920          YDSUM=YDSUM+YD(J)
00930          YDFL(J)=ALOG(YDF(J))/DD
00940          YDL(J)=ALOG(YD(J))/DD
00950          AN(J)=YDF(J)*PHI*6/(3.14159*((D(J)*1E-4)**3))
00960          ANL(J)=ALOG(AN(J))/DD
00970          WRITE(6,62) J,D(J),DJL(J),DOD(J),YDF(J),YDFL(J),YD(J),YDL(J
00980         1),ANL(J)
00990       62 FORMAT(2X,I2,9(2X,E9.3))
01000      800 CONTINUE
01010          IF (D(J) .GT. DP) GOTO 870
01020      850 M=J-1
01030      870 YM=1-EXP(-(N*DT)/TINC)-YDSUM
01040          YML=ALOG(YM)/DD
01050          DM=DP
01060          DMOD=DM/D0
01070          DML=ALOG(DM)/DD
01080          WRITE(6,70)
01090       70 FORMAT(' ' ULTIMATE PARTICLE ')
01100          WRITE(6,90)
01110       90 FORMAT(' '       DM        DM/DO       LOGDM          YM          LOGYM    '
01120         1)
01130          WRITE(6,110) DM, DMOD, DML, YM, YML
01140      110 FORMAT(5(2X,E9.3))
01150          WRITE (6,900)
01160      900 FORMAT (' SUMMARIZED AGGLOMERATE DISTRIBUTION')
01170          WRITE (6,910)
```

```
01180    910 FORMAT ('       D(J)      AGGLOMERATE RANGE      SUM YDF     SUM AN')
01190        DO 1500 NN=1,9
01200        TI=200.-20.*NN
01210        TF=180.-20.*NN
01220        SUMY=0
01230        SUMA=0
01240        DO 1200 L=1,NU
01250        J=L-1
01260        IF (D(J) .GT. TI ) GOTO 1200
01270        IF (D(J) .GE. TF .AND. D(J) .LT. TI) GOTO 1100
01280        GOTO 1300
01290   1100 SUMY=SUMY+YDF(J)
01300        SUMA=SUMA+AN(J)
01310   1200 CONTINUE
01320   1300 WRITE (6,920) D(J-1), TI, TF, SUMY, SUMA
01330    920 FORMAT (2X,E9.3,2(2X,E9.3),2(2X,E9.3))
01340   1500 CONTINUE
01350   2000 CONTINUE
01360        STOP
01370        END
```

APPENDIX E

COMPUTER PROGRAM FOR RUPTURE MODEL WITH INCORPORATION RATE FUNCTION (COMPUTER GRAPHICS)

```
00010 C      AGGLOMERATE SIZE DISTRIBUTION: COMPUTER GRAPHICS
00020 C      ROTOR MODEL WITH EXPONENTIAL INCORPORATION
00030        DIMENSION XX(12), D(1000), DOD(1000),DJL(1000),T(1000), YDF(1000),
00040        DIMENSION YDFL(1000),AN(1000),ANL(1000),YD(1000),YDL(1000),X(1000)

00050        DIMENSION NNN(10), DE(200), YDE(200)
00060 C      ********************************************************************
00070 C              SET THE PARAMETERS
00080 C
00090 C      ENTER VOLUME FRACTION OF FILLER (-)
00100        PHI=0.05
00110 C      ENTER DIAMETER OF INITIAL AGGLOMERATES (MICRON)
00120        D0=1.00
00130 C      ENTER DIAMETER OF ULTIMATE PARTICLE (MICRON)
00140        DF=0.01
00150 C      ENTER FRACTION OF RUPTURED AGGLOMERATES

00160 C      IN ONE PASS THROUGH THE GAP ( 0 TO 1 )
00170 C      YY=1.00
00180 C      ENTER PARAMETER FOR AGGLOMERATE BREAK-DOWN
00190        B=5.00
00200 C      ENTER FILLING FACTOR OF AGGLOMERATE STRUCTURE (0 TO 1)
00210        F=0.5
00220 C      ENTER ROTATIONAL SPEED OF THE ROTOR (RPM)
00230        RPM=50.
00240 C      ENTER TIME CONSTANT FOR INCORPORATION
00250        TINC=6.00
00260 C      ENTER MEAN RESIDENCE TIME IN THE WELL MIXED REGION

00270 C      OF THE MIXER
00280        TMEAN=0.20
00290 C      ENTER THE FIRST MIXING TIME
00300        TMIX=1.00
00310 C
00320 C      ********************************************************************
00330        DD=ALOG(10.)
00340        DO 2000 KK=1,4
00350        IF (KK .EQ. 1) GOTO 11
00360        IF (KK .EQ. 2) GOTO 12
00370        IF (KK .EQ. 3) GOTO 13
```

```
00380          IF (KK .EQ. 4) GOTO 44
00390       41 TMIX=TMIX
00400          NPS=1
00410          GOTO 50
00420       42 TMIX=TMIX+2.
00430          NPS=0
00440          GOTO 50
00450       43 TMIX=TMIX+2.
00460          NPS=3
00470          GOTO 50
00480       44 TMIX=TMIX+5.
00490          NPS=4
00500       50 DT=1/RPM
00510          R1=-3*(ALOG(DP/D0)/ALOG(2.))
00520          IF((R1-INT(R1)) .EQ. 0.0 .OR. (R1-INT(R1)) .GT. 0 ) GOTO 200
00530          M=INT(R1-1)
00540          GOTO 220
00550      200 M=INT(R1)
00560      220 RN=TMIX*RPM
00570          N=INT(RN)
00580          IF(N .LT. M) GOTO 400
00590          NU=M
00600          GOTO 500
00610      400 NU=N+1
00620      500 YDSUM=0
00630          DO 800 L=1,NU
00640          J=L-1
00650          D(L)=D0*2.0**(-J/3.)
00660          DOD(L)=D(L)/D0
00670          DJL(L)=ALOG(D(L))/DD
00680          X(L)=EXP(-J/B)
00690 C        X(L)=YY
00700          SUM=0
00710          DO 600 I=1,N
00720          T(I)=I*DT
00730          CC=I*DT/TINC+X(L)*(N+1-I)*DT/TMEAN
00740          IF(CC .GT. 150 ) GOTO 580
00750          AA=EXP(-CC)
00760          GOTO 590
00770      580 AA=0.
```

```
00780 C  590 FY1=AA*((X(L)**J)*(((N+1-I)*DT)**J))/(TMEAN**J)
00790    590 FY1=AA*((X(L)*(N+1-I)/TMEAN)**J)*(DT**J)
00800    600 SUM=SUM+FY1
00810        IF(J .EQ. 0 .OR. J .EQ. 1) GOTO 770
00820        FAC=1
00830        DO 750 K=2,J
 0840    750 FAC=FAC*K
00850        GOTO 780
00860    770 FAC=1
00870    780 YDF(L)=(EXP(DT/TINC)-1)*SUM/(F*FAC)
00880        YD(L)=YDF(J)*F
00890        YDSUM=YDSUM+YD(L)
00900        IF (YDF(L) .LE. 1E-30)  GOTO 101
00910        YDFL(L)=ALOG(YDF(L))/DD
00920        GOTO 102
00930    101 YDFL(L)=-20.
00940    102 IF (YDFL(L) .GT. -5.0) GOTO 112
00950        YDFL(L)=-4.9
00960    112 IF (YD(L) .LE. 1E-30)  GOTO 103
00970        YDL(L)=ALOG(YD(L))/DD
00980        GOTO 104
00990    103 YDL(L)=-20.
01000    104 AN(L)=YDF(L)*PHI*6/(3.14159*((D(L)*1E-4)**3))
01010        IF (AN(L) .LE. 1E-30) GOTO 105
01020        ANL(L)=ALOG(AN(L))/DD
01030        GOTO 800
01040    105 ANL(L)=-20.
01050     62 FORMAT(2X,I2,9(2X,E9.3))
01060    800 CONTINUE
01070        QQ=N*DT/TINC
01080        IF (QQ .GT. 70) GOTO 107
01090        YM=1.-EXP(-QQ)-YDSUM
01100        GOTO 108
01110    107 YM=1.-YDSUM
01120    108 IF (YM .LE. 0.0)  GOTO 710
01130        YML=ALOG(YM)/DD
01140    710 DM=D0*2.0**(-M/3)
01150        DMOD=DM/D0
01160        DML=ALOG(DM)/DD
01170 C      ******     SUMMED AGGLOMERATE SIZE DISTRIBUTION    ******
```

```
01180        DO 1500 NN=1,9
01190        TI=200.-20.*NN
01200        TF=180.-20.*NN
01210        SUMY=0
01220        SUMA=0
01230        DO 1200 L=1,NU
01240 C      J=L-1
01250        IF (D(L) .GE. TI) GOTO 1200
01260        IF (D(L) .GE. TF. AND. D(L) .LT. TI )GOTO 1100
01270  1100  SUMY=SUMY+YDF(L)
01280        SUMA=SUMA+AN(L)
01290  1200  CONTINUE
01300  1500  CONTINUE
01310 C      NU=100
01320 C      DO 5000 J=1,NU
01330 C      D(J)=0.01*J
01340 C      YDFL(J)=-5.+5*D(J)
01350 C5000  CONTINUE
01360        IF (KK .EQ. 1) GOTO 2810
01370        IF (KK .GT. 1) GOTO 2820
01380  2810  DO 2910  JJ=1,111
01390        DE(JJ)= 0.01*(JJ-1.)
01400  .     YDE(JJ)=-5.+5.*DE(JJ)
01410  2910  CONTINUE
01420        NUU=111
01430        DE(NUU+1)=0.
01440        YDE(NUU+1)=-5.
01450        DE(NUU+2)= 0.2
01460        YDE(NUU+2)= 1.0
01470  3000  CALL PLOTS
01480        CALL PLOT (2.0, 2.0, -3)
01490        D(NU+1)=0.0
01500        YDFL(NU+1)=-5.
01510        D(NU+2)= 0.2
01520        YDFL(NU+2)= 1.0
01530 C2820  CALL LINE (D, YDFL, NU, 1, 1, NPS)
01540        CALL AXIS (0.0, 0.0, 36HRELATIVE AGGLOMERATE SIZE  D(J)/D(0),
01550       1 -36, 5.0, 0.0, DE(NUU+1), DE(NUU+2))
01560        CALL AXIS (0.0, 0.0, 41HVOLUME FRACTION OF AGGLOMERATE  LOG (Y/F),
01570       1 41, 5.0, 90.0, YDE(NUU+1), YDE(NUU+2))
```

```
01580   3100 CONTINUE
01590 C2820 CALL LINE (D, YDFL, NU, 1, 1, NPS)
01600       CALL SYMBOL (0.2, 5.4, 0.13, 40HPHI=0.05 DO=1.00 DP=0.01 F=0.50, R
01610      1PM=50., 0.0, 40)
01620       CALL SYMBOL (0.2, 5.2, 0.13, 30HB=5.00  TINC=0.001  TMEAN=0.20,
01630      1 0.0, 30)
01640   2820 CALL LINE (D, YDFL, NU, 1, 1, NPS)
01650   2000 CONTINUE
01660       CALL PLOT(10.0,0.0,999)
01670   4000 STOP
01680       END
 END OF WORKSPACE
```

APPENDIX F

COMPUTER PROGRAM FOR ONION MODEL WITH INCORPORATION RATE FUNCTION (COMPUTER GRAPHICS)

```
00010 C      AGGLOMERATE SIZE DISTRIBUTION: COMPUTER GRAPHICS
00020 C      ONION MODEL WITH INCORPORATION FUNCTION
00030        DIMENSION XX(12), D(1000), DOD(1000),DOL(1000),T(1000), YDF(1000)
00040        DIMENSION YDFL(1000),AN(1000),ANL(1000),YD(1000),YDL(1000)

00050        DIMENSION EE(1000),DE(200),YDE(200)
00060 C
00070 C      ********************************************************************
00080 C                  SET THE PARAMETERS
00090 C
00100 C      ENTER VOLUME FRACTION OF FILLER (-)
00110        PHI=0.05
00120 C      ENTER DIAMETER OF INITIAL AGGLOMERATES (MICRON)
00130        D0=1.00
00140 C      ENTER DIAMETER OF ULTIMATE PARTICLE (MICRON)
00150        DP=0.01
00160 C      ENTER MASS RATIO FOR ONION BREAKDOWN ( 0 TO 1 )
00170        Ri=0.100
00180 C      ENTER FILLING FACTOR OF AGGLOMERATE STRUCTURE (0 TO 1)
00190        F=0.5
00200 C      ENTER ROTATIONAL SPEED OF THE ROTOR (RPM)
00210        RPM=50.0
00220 C      ENTER TIME CONSTANT FOR INCORPORATION
00230        TINC=10.0
00240 C      ENTER MEAN RESIDENCE TIME IN THE WELL MIXED REGION OF THE MIXER
00250        TMEAN=0.04
00260 C      ENTER THE FIRST MIXING TIME
00270        TMIX=1.00
00280 C
00290 C      ********************************************************************
00300        DD=ALOG(10.)
00310        DO 2000 KK=1,4
00320        IF (KK .EQ. 1) GOTO 41
00330        IF (KK .EQ. 2) GOTO 42
00340        IF (KK .EQ. 3) GOTO 43
00350        IF (KK .EQ. 4) GOTO 44
00360     41 TMIX=TMIX
00370        NPS=1
00380        GOTO 50
00390     42 TMIX=TMIX+2
```

```
00400          NPS=0
00410          GOTO 50
00420       43 TMIX=TMIX+2
00430          NPS=3
00440          GOTO 50
00450       44 TMIX=TMIX+5
00460          NPS=4
00470       50 DT=1/RPM
00480          RN=TMIX*RPM
00490          N=INT(RN)
00500          NU=N+1
00510          YDSUM=0
00520 C        *****    AGGLOMERATE SIZE DISTRIBUTION *****
00530          DO 800 L=1,NU
00540          J=L-1
00550          IF (L .EQ. 1) GOTO 100
00560          EE(L)=R1*D0/D(L-1)
00570          IF (EE(L) .GE. 1.0 ) GOTO 850
00580          D(L)=((1-EE(L))**(1./3.))*D(L-1)
00590          IF ( D(L) .LT. DP) GOTO 850
00600          GOTO 120
00610     100  D(L)=D0
00620     120  DOD(L)=D(L)/D0
00630          DJL(L)=ALOG(D(L))/DD
00640          SUM=0
00650          DO 600 I=1,N
00660          T(I)=I*DT
00670          CC=I*DT/TINC+(N+1-I)*DT/TMEAN
00680          IF(CC .GT. 150 ) GOTO 580
00690          AA=EXP(-CC)
00700          GOTO 590
00710     580  AA=0.0
00720 C   590  FY1=AA*((N+1-I)*DT/TMEAN)**J
00730     590  FY1=AA*(((N+1-I)*DT)**J)/(TMEAN**J)
00740 C   590  FY1=AA*(((N+1-I)/TMEAN)**J)*(DT**J)
00750     600  SUM=SUM+FY1
00760          IF(J .EQ. 0 .OR. J .EQ. 1) GOTO 770
00770          FAC=1
00780          DO 750 K=2,J
00790     750  FAC=FAC*K
```

```
00800          GOTO 780
00810     770  FAC=1
00820     780  YDF(L)=((D(L)/D0)**3)*(EXP(DT/TINC)-1)*SUM/(F*FAC)
00830          YD(L)=YDF(L)*F
00840          YDSUM=YDSUM+YD(L)
00850          IF (YDF(L) .LE. 1E-30)  GOTO 101
00860          YDFL(L)=ALOG(YDF(L))/DD
00870          GOTO 102
00880     101  YDFL(L)=-20.
00890     102  IF (YDFL(L) .GT. -5.0) GOTO 112
00900          YDFL(L)=-4.9
00910     112  IF (YD(L) .LE. 1E-30) GOTO 103
00920          YDL(L)=ALOG(YD(L))/DD
00930          GOTO 104
00940     103  YDL(L)=-20.
00950     104  AN(L)=YDF(L)*PHI*6/(3.14159*((D(L)*1E-4)**3))
00960          IF (AN(L) .LE.1E-30) GOTO 105
00970          ANL(L)=ALOG(AN(L))/DD
00980          GOTO 800
00990     105  ANL(L)=-20.
01000     800  CONTINUE
01010          IF (D(L) .GT. DP) GOTO 870
01020     850  M=J-1
01030          NV=L-1
01040     870  Q=N*DT/TINC
01050          IF (QQ .GT. 70.) GOTO 107
01060          YM=1-EXP(-QQ)-YDSUM
01070          GOTO 108
01080     107  YM=1.-YDSUM
01090     108  IF (YM .LE. 0.0) GOTO 710
01100          YML=ALOG(YM)/DD
01110     710  DM=DP
01120          DMOD=DM/D0
01130          DML=ALOG(DM)/DD
01140 C        *****     SUMMARIZED AGGLOMERATE DISTRIBUTION     *****
01150          DO 1500 NN=1,9
01160          TI=200.-20.*NN
01170          TF=180.-20.*NN
01180          SUMY=0
01190          SUMA=0
```

```
01200          DO 1200 L=1,NU
01210          J=L-1
01220          IF (D(L) .GT. TI ) GOTO 1200
01230          IF (D(L) .GE. TF .AND. D(L) .LT. TI) GOTO 1100
01240   1100   SUMY=SUMY+YDF(L)
01250          SUMA=SUMA+AN(L)
01260   1200   CONTINUE
01270   1500   CONTINUE
01280  C       NU=100
01290  C       DO 5000 J=1,NU
01300  C       D(J)=0.01*J
01310  C       YDFL(J)=-5.+5*D(J)
01320  C5000   CONTINUE
01330          IF (KK .EQ. 1) GOTO 2810
01340          IF (KK .GT. 1) GOTO 2820
01350   2810   DO 2910  JJ=1,111
01360          DE(JJ)= 0.01*(JJ-1)
01370          YDE(JJ)=-5.+5.*DE(JJ)
01380   2910   CONTINUE
01390          NUU=111
01400          DE(NUU+1)=0.
01410          YDE(NUU+1)=-5.
01420          DE(NUU+2)= 0.2
01430          YDE(NUU+2)= 1.0
01440   3000   CALL PLOTS
01450          CALL PLOT (2.0, 2.0, -3)
01460          D(NV+1)=0.0
01470          YDFL(NV+1)=-5.
01480          D(NV+2)= 0.2
01490          YDFL(NV+2)= 1.0
01500  C2820   CALL LINE (D, YDFL, NV, 1, 1, NPS)
01510          CALL AXIS (0.0, 0.0, 36HRELATIVE AGGLOMERATE SIZE  D(J)/D(0),
01520         1 -36, 5.0, 0.0, DE(NUU+1), DE(NUU+2))
01530          CALL AXIS (0.0, 0.0, 41HVOLUME FRACTION OF AGGLOMERATE  LOG (Y/F),
01540         1 41, 5.0, 90.0, YDE(NUU+1), YDE(NUU+2))
01550   3100   CONTINUE
01560  C2820   CALL LINE (D, YDFL, NV, 1, 1, NPS)
01570          CALL SYMBOL (0.2, 5.4, 0.13, 40HPHI=0.05 DO=1.00 DP=0.01 F=0.50, R
01580         1PM=50., 0.0, 40)
01590          CALL SYMBOL (0.2, 5.2, 0.13, 30HR=0.075 TINC=0.001
01600         10.0, 30)
01610   2820   CALL LINE (D, YDFL, NV, 1, 1, NPS)
01620   2500   CONTINUE
01630          CALL PLOT(10.0,0.0,999)
01640   4000   STOP
01650          END
```

VITA

Yoshiyuki Suetsugu (末次義幸) was born in Ube City, Japan, on September 19, 1956, as the oldest son of Mr. and Mrs. Yoshinori Suetsugu. After completing his basic education, he was admitted to Kyushu University in April 1975. He studied Nuclear Engineering and received a Bachelor of Science degree in March 1979. He entered The University of Tennessee, Knoxville, in September 1979 and received a Master of Science degree in Polymer Engineering in August 1982 under the direction of Professor James L. White. He moved to The University of Akron following Professor J. L. White in July 1983. In Akron, he initiated research. He received the Doctor of Philosophy degree in Polymer Engineering in June 1986.